Development and Appraisal of the Pyridazinedione Scaffold to Form Next-Generation Bioconjugates

Calise Bahou

Department of Chemistry (UCL)

Primary Supervisor: Prof. Vijay Chudasama

Secondary Supervisor: Prof. Tom Sheppard

Declaration

I, Calise James Bahou confirm that the work presented in this thesis is my own. Where information has been derived from other sources, I confirm that this has been indicated in the thesis.

28/10/2020

Acknowledgements

The last four years have been some of the most enjoyable of my life, and whilst there have been ups and downs along the way, there is no place I would rather have been, and nobody else I would rather have taken this journey with. There have been so many faces come and go throughout my time as a PhD student, and everybody has had an impact on my experience at UCL in such a positive way, and so I apologise to anybody that is not explicitly mentioned below.

Firstly, to my captain, the head honcho, Prof. Vijay Chudasama. It seems like a lifetime ago that we had that meeting in your office and I couldn't breathe because of all the stairs. I am an inconceivably different person now, and you have played such a large role in helping me become who I am today. I hope you know that I will always be grateful for the opportunities you have given me. I am NOT a whale, I am NOT a human flubber and I am NOT stuck in slow motion.

I would like to thank Dr Jamie Baker as well as Dr Elizabeth Love, Dr Andy Merritt, Dr David Matthews (and everybody else at LifeArc), for their invaluable help and support throughout my PhD. It has been an absolute pleasure working with each of you, and I hope that our paths will cross again someday. To Jamie and Liz, thank you especially for all the advice, input and one-to one support you have given me over the years.

Next, a special mention for Dr Antoine Maruani. You have been there for me since the start, and what a standard you set both academically and personally! You are the sort of guy that listens to my worries about presenting in a group meeting when you are about to go into a viva. Thank you, Antoine, for everything you put up with and for everything you have done.

To Dr Maximillian Lee and Dr Daniel Richards, you both played such a role during my early PhD years. The atmosphere you both brought to the lab was infectious and this atmosphere played a large role in my decision to apply for this PhD. I'm jealous that now other people get to experience Max's impressions and Dan's laugh on a daily basis.

To Dr Andrê Shamsabadi, Dr João Nogueira and Dr Marcos Fernandez. The four amigos. We all started this PhD together, and I guess I'm the only one left. Having you three to take this journey with has been an absolute pleasure, and you have all given me so much help and inspiration along the way. João, you really know how to get the most out of life, which is surprising considering how hard you work. Andrë, it wouldn't be fair to say that you were just "helpful" during my PhD, we have been through a lot together, even as master's students and I will forever be grateful for everything my better half has done for me.

To Dr Richard Spears, Peter Sjizz, Faiza Javaid, Nehaal Ahmed, Alex Furby, Archie Wall – the current workforce. I do not know how the PIs do it, but time and time again they pick such lovely people that add so much to the current atmosphere in the KLB. Richard, your lunches always look really good and hanging out with you in the lab is often the best part of my day. Peter, I don't know what you're still doing as a PhD student, don't have your own group by now? Faiza, you brighten up the lab with your visits, our chats over tea/coffee really have meant a lot to me over the years. Nehaal, always relaxed and level-headed, it's probably because of the shoes? Furby, always have fun hanging out with you, we are similar so many ways, except I don't frequently quiz or drop things. Archie you're a villager, that's all.

To Dr Fabien Thoreau, Dr Nafsika Forte, Dr Marco Sabatini other members of the KLB, past and present, you have all contributed to an amazing atmosphere in the lab and have made the KLB one of the most exciting, fun and collaborative environments I have had the pleasure of working in.

To Emily Leonidou, thank you for your caring and loving support, as well as a logical and level-headed answer when I needed one.

To my family – Nan, Grandad, Mum, Dad, Adam, Kimmy, Jack and Luna. I couldn't ask for a more supportive, kind and funny group of people to support me with my PhD and for everything in life. Thanks to each of you for acting as an inspiration for me on a daily basis.

Finally, I would like to thank Prof. David Spring and Dr Bob Schroeder for agreeing to read through this work and carry out my viva examination.

Abstract

Over the last two decades, the functionalisation of proteins through bioconjugation reactions (often in a therapeutic setting) has been of great interest in the field of chemical biology and within the pharmaceutical industry. Novel strategies for the modification of cysteine residues are of major relevance to the field of protein bioconjugation due to the pharmacokinetically superior nature of the homogenous products that can be formed through site-selective methodologies. Researchers have strived to enable stable, covalent modification of cysteine residues, which has been the driver behind forming leading biologics (*e.g.* in the formation of antibody-drug conjugates (ADCs)). In recent years, the cysteine reactive pyridazinedione (PD) scaffold has been developed to facilitate the efficient formation of stable, homogenous and multi-functional bioconjugates. However, whilst the PD scaffold is a highly promising reagent for bioconjugation (especially when modifying antibodies and antibody derived proteins), this is still considered an early technology; the full potential of this scaffold as a next generation bioconjugation reagent has yet to be unlocked.

This work aimed to provide greater accessibility and deepen current knowledge surrounding the PD functionalisation technology. This was achieved through the optimisation of synthetic routes to form PDs as well as providing an assessment of the extent of PD modification on native antibody function. Furthermore, novel applications that stemmed from novel fundamental PD-based chemistry were developed to provide a platform for site-selective tri-functionalisation of proteins, as well as dynamic reversible cysteine modification.

Impact Statement

This work sets out to improve upon current bioconjugation methods for the formation of next-generation chemically enhanced proteins for therapeutics. One significant breakthrough achieved through the chemical enhancement of proteins comes in the form of antibody-drug conjugates (ADCs) for cancer therapy. Cancer is currently the second leading cause of death globally and was responsible for nearly 10 million deaths in 2018. The current treatments for most cancer patients involve surgery, radiotherapy or chemotherapy. ADCs provide a targeted approach to chemotherapy consequently avoiding the toxic off-target side effects associated with traditional treatments (*e.g.* a suppressed immune system) that stem from the targeting of all rapidly dividing cells. However, ADCs still present a certain level of toxicity as current linkers employed to attach highly potent cytotoxic cargo can break down in blood and so premature release of payload is observed in unwanted areas.

The work presented in this thesis aims to further develop the pyridazinedione (PD) technology to facilitate the chemical enhancement of therapeutically relevant proteins (*e.g.* antibodies), which would aid in forming "next-generation" standard therapies. By optimising and appraising PD technology in the field of ADC synthesis, and adding to the "tool-kit" of strategies available to modify proteins, this work aims to influence how future bioconjugates are synthesised within academia and the pharmaceutical industry, thus ultimately impacting the wider community of patients that rely on higher quality therapeutics. The work from this thesis has been published across 3 reputable peer-reviewed scientific journals (*Org. Biomol. Chem., Bioconjugate Chem., Chem. Commun.*) with an additional manuscript in preparation, demonstrating acceptance from the scientific community and impacting the readership of these journals.

Contents

Abbreviations

AcOH	Acetic acid
ADC	Antibody–drug conjugate
ADCC	Antibody-dependant cell-mediated cytotoxicity
BBS	Borate buffered saline
BCN	Bicyclo[6.1.0]nonyne
BLI	Bio-layer interferometry
BME	2-Mercaptoethanol
Boc	*tert*-Butoxycarbonyl
BrPD	Bromopyridazinedione
CDC	Complement dependent cytotoxicity
CDI	Carbonyldiimidazole
CPP	Cell-penetrating peptide
CuAAC	Copper-catalysed azide–alkyne cycloaddition
DAR	Drug-to antibody ratio
DBCO	Dibenzocyclooctynol
DCC	Dicyclohexylcarbodiimide
DiBrPD	Dibromopyridazinedione
DiClPD	Dichloropyridazinedione
DiEt	Diethyl
DMF	Dimethylformamide
DTNB	5,5-Dithio-bis-2-nitrobenzoic acid
EDC	1-Ethyl-3-(3-dimethylaminopropyl)carbodiimide
EDTA	Ethylenediaminetetraacetic acid
ELISA	Enzyme-linked immunosorbant assay
Fab	Fragment antigen binding
Fc	Fragment crystallisable
FcRn	Neonatal Fc receptor
FDA	US food and drug administration
FGE	Formylglycine-generating enzyme
FRET	Förster resonance energy transfer

GFP	Green fluorescent protein
GSH	Glutathione
HATU	Hexafluorophosphate azabenzotriazole tetramethyl uronium
HER2	Human epidermal growth factor receptor 2
HIV	Human immunodeficiency virus
HPLC	High-performance liquid chromatography
HSA	Human serum albumin
IED	Inverse-electron demand
IgG1	Immunoglobulin G1
KD	Equilibrium dissociation constant
LCMS	Liquid chromatography–mass spectrometry
mAb	Monoclonal antibody
MAR	Maleimide-to-antibody ratio
MeOH	Methanol
MMAE	Monomethyl auristatin E
MTG	*Streptoverticillium mobaraense*
NAA	Natural amino acid
NHS	*N* Hydroxysuccinimide
NK	Natural killer
NMR	Nuclear magnetic resonance
NSB	Non-specific binding
PBS	Phosphate-buffered saline
PD	Pyridazinedione
PEG	Polyethylene glycol
PK	Pharmacokinetic
PyBOP	Benzotriazol-1-yl-oxytripyrrolidinophosphonium hexafluorophosphate
sdAb	Single domain antibodies
SEC MALS	Size-exclusion chromatography multi-angle light scattering
SPAAC	Strain-promoted azide-alkyne cycloaddition
SPI	Selective pressure incorporation
SPR	Surface plasmon resonance
TCEP	Tris(2-carboxyethyl)phosphine

TFA	Trifluoroacetic acid
TG	Transglutaminase
THF	Tetrahydrofuran
TNB	5-Thio-2-nitrobenzoic acid
TNF	Tumour necrosis factor
tRNA	Transfer ribonucleic acid
TSTU	Tetramethyl-O-(*N*-succinimidyl)uronium tetrafluoroborate
TTL	*Thermoanaerobacter ther-mohydrosulfuricus*
UAA	Unnatural amino acid
UV-Vis	Ultraviolet–visible

Chapter 1 Introduction

1.1 Introduction to Protein Modification

The human genome contains *ca.* 20,000 protein-encoding genes; after post-translational modifications and splicing etc. the human proteome consists of more than 1 million proteins.[1] It is clear that after years of evolution, these highly specialised biomolecules are integral to human biological systems. Over the past few decades biologists, biochemists, and chemical biologists have collaborated to explore the potential associated with the chemical modification of these biological systems.

For proteins to be highly specialised for their role, their structure is considered highly intricate and complicated to modify. Proteins are formed from 20 essential amino acids, each harbouring different functional groups (hydrophobic, hydrophilic, nucleophilic etc.) with different reactivities. Proteins have also evolved to function under certain physiological conditions (*i.e.* aqueous media, pH, temperature,).[2] Protein modification is the process of taking these highly specialised systems, and exploiting unique chemistries (through bioconjugation reactions) to insert functional modalities covalently into the protein structure – to form bioconjugates. It is therefore essential that developing technology be reactive towards certain amino acids whilst also being biocompatible with the conditions described above. Additionally, modalities installed into the protein structure must have limited impact on the base function of the protein. Developing new technology for forming bioconjugates is a complex task, with debate as to which is the most effective approach to protein modification.[3]

1.2 Protein Modification for Therapeutics

There is a great amount of interest in modifying proteins, for medicinal development in particular. There are many applications of chemically modified proteins including *in vivo* tracking of protein-fluorophore conjugates[4], polyethylene glycol (PEG)ylation of proteins[5], malaria treatments[6] and targeted cancer therapy.[7,8] It should be noted that many non-therapeutic applications may also stem from chemical modification of biomolecules (*e.g.*

rapid diagnostics through *ex vivo* testing).[9] Two exciting areas of research that exploit proteins for therapeutic benefit *in vivo* are: i) blood half-life extension;[10] and ii) targeted drug-delivery[11] (exploiting a protein of interest within a biochemical pathway to deliver a drug to a desired site in the body).

1.2.1 Blood Half-Life Extension

Extending the blood half-life of an existing therapeutic is a common goal in drug design. For many drugs that are administered intravenously the aim is to reduce dosing frequency for patient convenience (and subsequently increase patient compliance) but additionally this can help to maintain an effective blood concentration of the therapeutic for an extended period of time.[10] Human serum albumin (HSA) and the fragment crystallisable (Fc) region of antibodies have been exploited on numerous occasions to increase the blood half-life of drugs.[12,13] Both platforms significantly increase the size of the therapeutic which aids in blood retention as the bioconjugate surpasses the renal threshold (*ca.* 70 kDa).[14] In addition, these proteins are specialised to remain in the blood through cell recycling pathways (neonatal Fc receptor (FcRn) recycling prevents uptake from cells).[15]

One highly successful approach to drug design comes in the form of Fc-based fusion proteins, with at least 10 currently approved for use by the US food and drug administration (FDA).[16] Fc-fusion proteins can be expressed directly in cells, or through chemical ligation of the Fc region.[17] The longest standing Fc-fusion protein to date is Etanercept™ used to treat rheumatoid arthritis, which comprises a human tumour necrosis factor (TNF) receptor fused to a human immunoglobulin G1 (IgG1) Fc. It was found that by prolonging the half-life of the TNF receptor by fusing it to an Fc protein, an extended and a more profound biological effect could be observed.[18] In 2018 Etanercept™ was reported as the 7th bestselling pharmaceutical, grossing $7.1 billion worldwide.[19]

1.2.2 Targeted Drug-Delivery

The “magic bullet” was a concept proposed by Paul Ehrlich in the early 20th century that explores the idea of a therapeutic whereby diseased tissues are destroyed and healthy tissues are unaffected by the drug administered.[20] Antibodies produced by our immune

system (that show selectivity toward invading pathogens over healthy cells) were the original inspiration for the "magic bullet". Whilst antibodies sometimes fail to kill invading cells/microbes and so do not satisfy the idealistic concept in full, they do provide a rare opportunity for targeting diseased cells over health tissues. For this reason, antibodies have been exploited as a platform for delivery of chemically attached cargo to diseased cells. Antibody-based bioconjugates have been used for the treatment of many diseases including HIV[21], malaria[6] and cancer.[7,8] In addition, other targeting ligands (not-antibody-based) have been exploited for the use of targeted drug-delivery (*e.g.* folic acid against the folate receptor for cancer therapy).[22]

However, it should be noted that targeted delivery systems cannot be considered totally safe and selective for diseased tissues in all cases. Many factors are involved in designing a receptor-targeted drug delivery pathway that will determine the success of the therapeutic.[23,24] A typical antibody-based bioconjugate will consist of a targeting ligand, bound *via* a linker to a therapeutic cargo (Figure 1).[24] The factors that will affect the safety and efficacy of the bioconjugate are:

i) Selection of receptor – Ratio of target receptor expression on diseased cells compared to healthy cells (high expression in diseased cells, low expression in healthy cells) determines specificity. A high specificity reduces the number of off-target effects and ultimately determines the safety of the therapeutic.

ii) Selection of ligand – Binding affinity and the selectivity towards the protein of interest determines the potency and efficacy of the bioconjugate.

iii) Selection of linker and payload – Chemical properties of attached payload and linker (*e.g.* hydrophobicity) may affect the pharmacokinetic profile of the bioconjugate. Linker stability is also crucial to allow the payload to reach the desired target without premature release in circulation, ensuring safety of the bioconjugate.

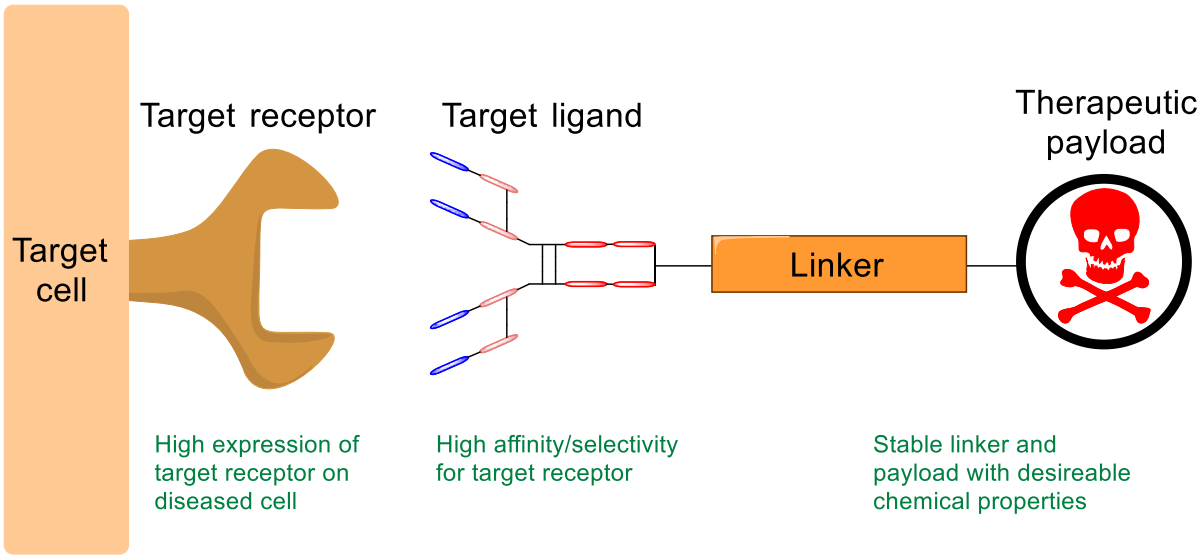

Figure 1 – Design of an ideal therapeutic capable of targeted drug-delivery.[23,24]

1.3 Current Protein Modification Methods

To date, a plethora of bioconjugation strategies exist to modify proteins, each providing a novel platform to modify chemical moieties on the protein surface.[8] Over the past two decades, novel bioconjugation chemistries have become of great interest to a large community of scientists working in a multidisciplinary field, resulting in a large number of bioconjugation strategies available to choose from.[25] Whilst the chemical biologist's "tool-kit" is vast, when working in the field of therapeutics, certain criteria must be met to provide the best prospect of developing a successful therapeutic.[3]

1.3.1 Selecting a Bioconjugation Strategy

Whilst the definition of an "optimal" conjugation strategy is likely to differ between bioconjugates with different functions, conjugation strategies that develop therapeutic products that perform *in vivo* must consider the following:

1) *Is the conjugation regioselective and chemo-selective (homogenous)?* – extensive studies have shown that bioconjugates that exhibit high levels of homogeneity often exhibit increased efficacy.[26–28] In the event of heterogenous modification, where many isomers of the same product exist (each with a unique pharmacokinetic (PK) profile) the resultant product exhibits a narrow therapeutic window, relative to homogenous

bioconjugates. Two main factors may contribute to a product's homogeneity: i) number of payloads attached; and ii) the number of sites on the protein surface that are conjugated. A conjugation strategy that enables site-specific controlled loading of a payload may subsequently allow for higher doses and more effective treatment.[26–28]

2) *Is the linker stable towards physiological conditions?* – with a targeted therapeutic approach, potent chemical payloads must ideally not degrade or be released before reaching the intended target.[29] Biodistribution of the therapeutic in targeted therapy is crucial (*i.e.* as much of the therapeutic should reach the intended target as possible). For example, commonly used linkers harbouring thiol-succinimide groups (*i.e.* from cysteine modification with maleimides) are known to partially degrade in blood through retro-Michael deconjugation pathways, decreasing the amount of bioconjugate that will remain in blood and reach the intended target.[30]

3) *Is the bioconjugate simple to manufacture?* – it is important to consider the costs of developing technologies, as large-scale production costs for pharmaceutical use may determine which bioconjugates are economically viable.[31] Bioconjugation techniques that form products in quantitative yields and require fewer purification steps are optimal with many researchers turning towards automated synthesis of bioconjugates, to reduce manufacturing costs. Additionally, modular linkers that can provide an option for testing different combinations of protein are considered useful for developing lead therapeutics through high throughput techniques.[32]

Typically, the cheapest and simplest modification technique is to modify proteins through naturally occurring amino acids. Other promising strategies, although more generally costly, include targeting unnatural amino acids (UAAs) incorporated into the protein's primary structure; by introducing unique functionality onto a protein it is possible to obtain stable bioconjugates with extremely high levels of homogeneity.

1.3.2 Unnatural Amino Acids (UAAs)

One approach to protein modification is to express a platform with an UAA pre-installed into the protein's primary structure. This is achieved by producing a mutant tRNA synthetase that is responsible for combining UAAs with a corresponding tRNA, or through a process referred

to as selective pressure incorporation (SPI).[33] As the incorporated chemical moiety often offers unique reactivity, chemoselectivity is (generally) easily achieved in the resultant bioconjugates. There is also great selectivity over where the UAA is placed in the primary structure of the protein, resulting in a highly homogenous bioconjugate.[8,34,35]

In past decades, large steps have been achieved in the field of biocatalysis through modification of enzymes with UAAs. An increase in turnover number, catalytic efficiency and stability is observed in enzymes with chemical modification.[36] Interestingly, not all improvements in these criteria come through introducing functionality that can be subsequently modified. Studies involving a lipase enzyme from the hyperthermophilic bacterium *Thermoanaerobacter ther-mohydrosulfuricus* (TTL) found that by replacing a methionine residue (**1**) with an non-oxidisable norleucine (**2**), a fully active variant of TTL was produced, that did not require heat activation (Scheme 1).[36,37]

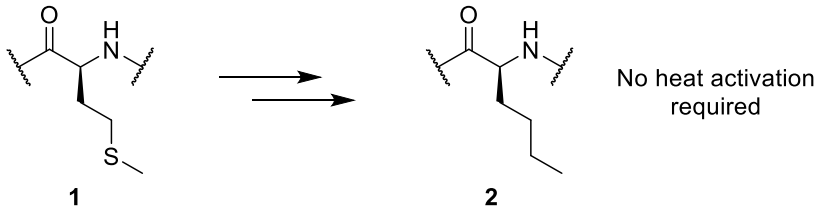

Scheme 1 – Formation of norleucine **2** from methionine **1**.

A typical example of using UAAs to add reactive functionalities to proteins was described by Rösner *et al.*[33] Here they report the incorporation of both alkyne and azide modalities into ubiquitin for the ubiquitylation of various proteins. Through Cu^{I}-catalysed azide-alkyne cycloaddition (CuAAc) it was possible to ubiquitinate various proteins, but also when incorporating both azide (**3**) and alkyne (**4**) handles on the same ubiquitin, chain formation was observed (Figure 2).

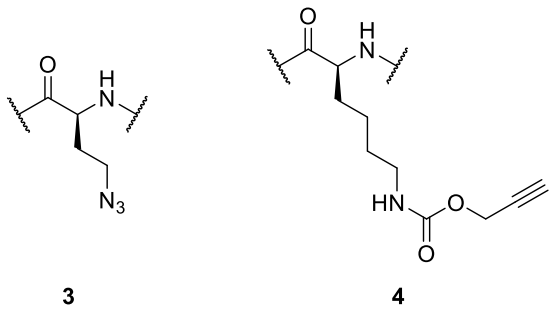

Figure 2 – Structures of unnatural amino acids incorperating azide (**3**) and alkyne (**4**) handles.

There are, however, many challenges still associated with incorporating UAA(s) into proteins. At present it is expensive to produce the mutant synthetase necessary UAA incorporation, due to stability issues.[38] This is a recurring cost issue as each UAA requires a unique mutant synthetase to be attached to the tRNA, and subsequently introduced into the protein's primary structure. Furthermore, each UAA incorporation is protein specific and this costly process must be repeated and optimised for each protein platform.

1.3.3 Natural Amino Acids (NAAs)

Due to the simplicity, scalability and low cost of natural amino acid (NAA) modification, there is great interest in developing new technologies that can achieve this. Most nucleophilic residues have been utilised for this purpose (Figure 3) although lysine **6** and cysteine **5** are the most commonly employed targets for modification.

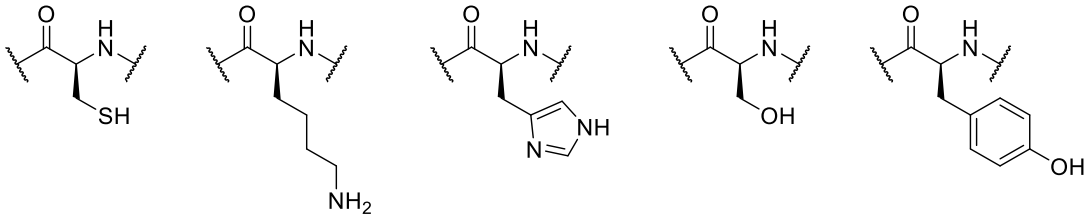

5 **6** **7** **8** **9**

Figure 3 – Structures of nucleophilic amino acid residues. From left to right: cysteine **5**, lysine **6**, histidine **7**, serine **8**, and tyrosine **9**.

1.3.3.1 Lysine Modification

Lysine is highly nucleophilic (due to the presence of an amine side-chain), high in natural abundance and has a well-defined reactivity profile. Work presented by Tanaka *et al.* highlights the extent of lysine's reactivity over other NAAs, with the exception of cysteine.[39] By subjecting biomolecules such as somatostatin and anti-green fluorescent protein (GFP) monoclonal antibody (mAb), to reactive molecules targeting lysine residues, it was found that the bioconjugates were synthesised after a time period ranging from 10-30 minutes.[39]

However, when synthesising homogenous bioconjugates, lysine residues are a sub-optimal conjugation target. Firstly, lysine is not always the most reactive centre on a protein; therefore, in the presence of amino acids with a higher nucleophilicity, unexpected modification can occur

(*e.g.* at cysteine).[40] Furthermore, the abundance of solvent accessible lysine is very high in many proteins, resulting in non-site selective modification.[41,42] This is evident in the research reported by Kim *et al.* with regards to the synthesis of trastuzumab-emtansine (Kadcyla™). It was calculated that the resulting bioconjugates likely form across 65 different lysine residues, out of a potential 92, forming a high number of regioisomers.[43] Lysine modification is also typically reported as a "degree of conjugation" due to the large distribution of drug loading observed (Figure 4).[43] For these reasons, the pharmacokinetic profile of conjugates formed by lysine conjugation is typically poor, which can lead to a decrease in efficacy during treatments.[44]

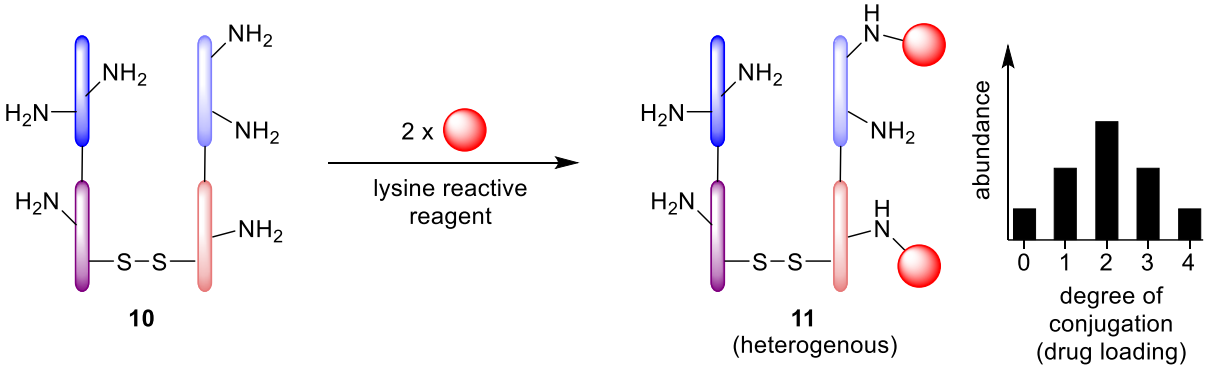

Figure 4 – Depiction of typical lysine modification forming heterogenous conjugates with varied drug loading.

However, it should be noted that whilst site-selective modification is renowned for producing pharmacokinetically superior bioconjugates, with a more predictable *in vivo* profile, this does not always result in an increase in efficacy of the therapeutic. Recent work by Yoder *et al.* surprisingly showed that when an antibody was modified heterogeneously with lysine modification, an increase in efficacy may be observed when compared to analogous homogenous bioconjugates. Whilst an overwhelming number of reports suggest homogenous conjugates should perform better *in vivo,* this work highlights many other factors that may ultimately contribute to the success of the therapeutic (*e.g.* drug loading and linker stability).[45]

1.3.3.2 Cysteine Modification

Free cysteines are extremely low in natural abundance.[46] Approximately only 1.7% of amino acids in a protein are cysteines, of which many exist as disulfide bridges (1.5%) – an integral part of a protein's tertiary structure.[47] This extremely low abundance of free cysteines has resulted in highly site-selective methodologies to targeting solvent-accessible cysteine residues,

as few exist to be modified. Furthermore, the thiol moiety is considered the most reactive centre (towards electrophiles) that can be found in naturally occurring amino acids.[40] Using site-selective cysteine modification strategies, various biomolecules have been modified to function as enzyme activity probes, protein labels as well as construct antibody–drug conjugates (ADCs).[48,49] Pioneering work by Hamblett *et al.* reported the synthesis of numerous cysteine-conjugated anti-CD30- monomethyl auristatin E (MMAE) ADCs to demonstrate the effect of drug-loading on antibody efficacy.[27] Here they find antibody loading to be a key parameter in synthesising an efficacious ADC showing conjugates with a lower drug-loading of 2 MMAE payloads per antibody to be most efficacious *in vivo* due to higher tolerated doses (compared to samples conjugated with 4 and 8 MMAE payloads). Further work by Sun *et al.* demonstrates the production of anti-CD30-MMAE conjugates *via* cysteine conjugation to produce ADCs with 60-90% homogeneity. Allowing for a somewhat controlled distribution of payload resulted in the production of highly active anti-CD30 MMAE bioconjugates both *in vitro* and *in vivo* and these were well tolerated at efficacious doses.[50]

However, complications can arise from the extremely low abundance of cysteine. Many proteins do not express a free solvent accessible cysteine, as often these exist as disulfide bonds or are buried into deep inaccessible pockets of the protein.[51] The first reported cases of cysteine modification (as showcased by Hamblett *et al*. and Sun *et al*.) utilise modification of the thiols liberated from disulfide bonds (modifying these can have great consequences on protein function) (Scheme 2a).[52] By liberating thiol moieties from disulfides, the tertiary structure of the protein becomes dependant on weaker interactions (e.g. electrostatic interactions), especially when disulfides are the only covalent attachment between protein chains. In the event that there is no free solvent accessible cysteine, one of the following two next-generation strategies can be employed:

1) Functional disulfide re-bridging: A disulfide bridge may be functionalised by insertion of a functional molecule (Scheme 2b).[53] By forming a stable functionalised bridge between two cysteine residues, the protein's tertiary structure (and function) remains intact, whilst also providing a platform for modification. However, where multiple accessible disulfides exist on a protein, these may also be subject to disulfide scrambling (*i.e.* re-bridging in a non-native conformation).

2) Site-directed mutagenesis: An amino acid sequence with no free cysteine can be mutated to include a single free, solvent accessible cysteine (Scheme 2c).[54] The advantages of this method include a high degree of site-specificity as the new single cysteine is the only free modifiable target. However, this may lead to complications during purification of the protein, as well as disulfide scrambling with disulfide bridges present on the native protein.

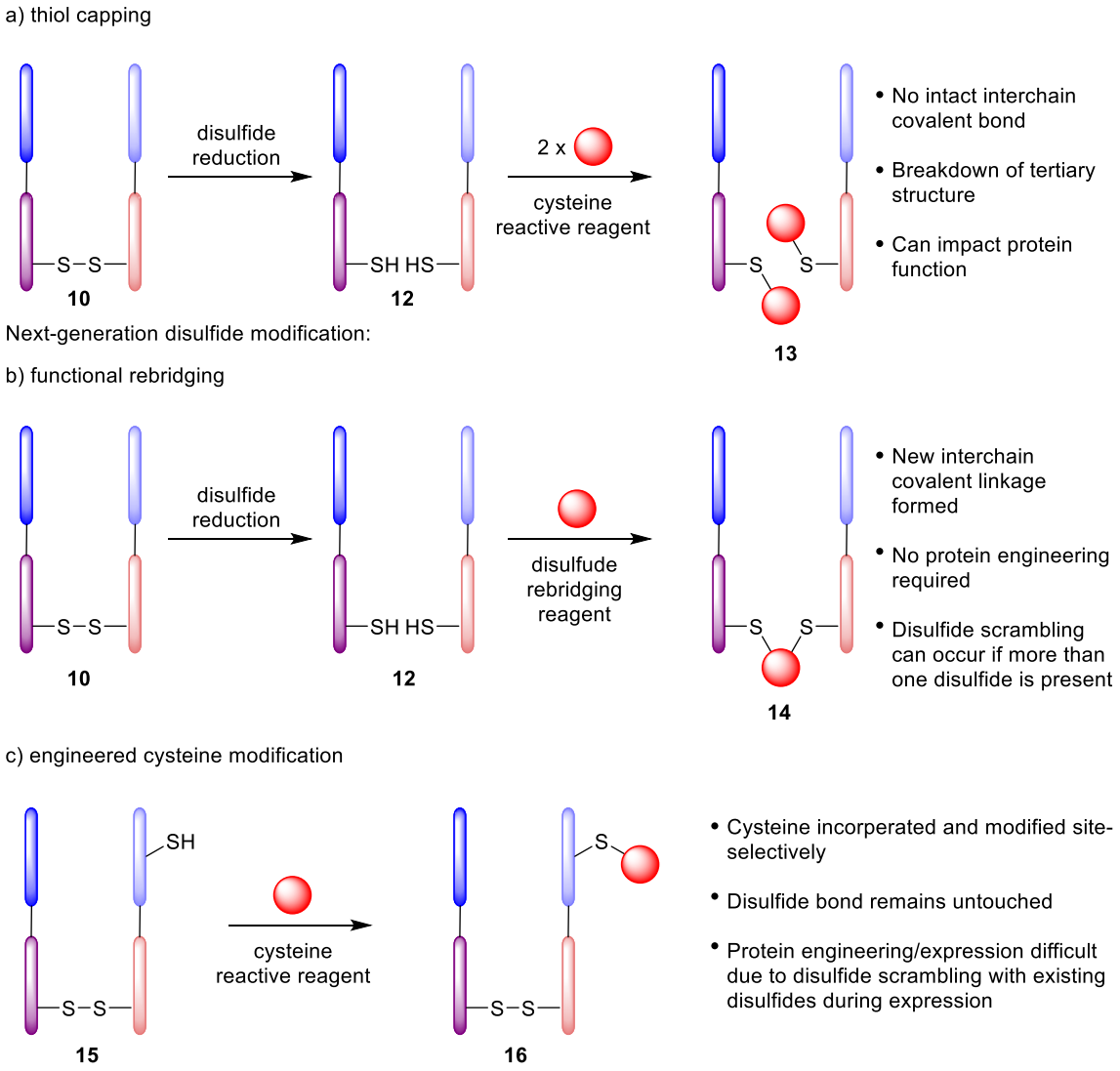

Scheme 2 – Representation of disulfide and cysteine modified conjugates and typical drug loading through a) thiol capping of reduced disulfide bonds, b) functional re-bridging of disulfide bonds and c) reaction with engineered cysteine.

1.4 Reagents for Protein Modification

For reagents to be considered for use in protein modification, they must satisfy many difficult criteria. Protein modification reagents must selectively modify an amino acid of

interest, in the presence of all other competing amino acid side chains. In addition, reagents for modification must react in conditions used to prevent protein denaturation, which include near neutral pH, aqueous conditions and the presence of buffer salts.[55] Finally, as protein bioconjugations are often carried out at low concentration (to prevent aggregation of the protein sample), the reagent must be sufficiently reactive for quantitative formation of bioconjugates.[56] In light of this challenge and the prospects that arise from chemo-selective protein modification, reagents capable of bio-orthogonal chemistry are of great interest in the field of protein modification.

1.4.1 Lysine Modification Reagents

As lysine modification has been so popular over the last few decades, many reagents exist to carry out this type of modification. Among the most popular reagents are *N*-hydroxysuccinimide (NHS) esters **17** and isothiocyanates **23** (giving rise to products **18** and **24** respectively), although there are many more small molecules that have been employed in the manufacture of lysine conjugates (Scheme 3).[57–61]

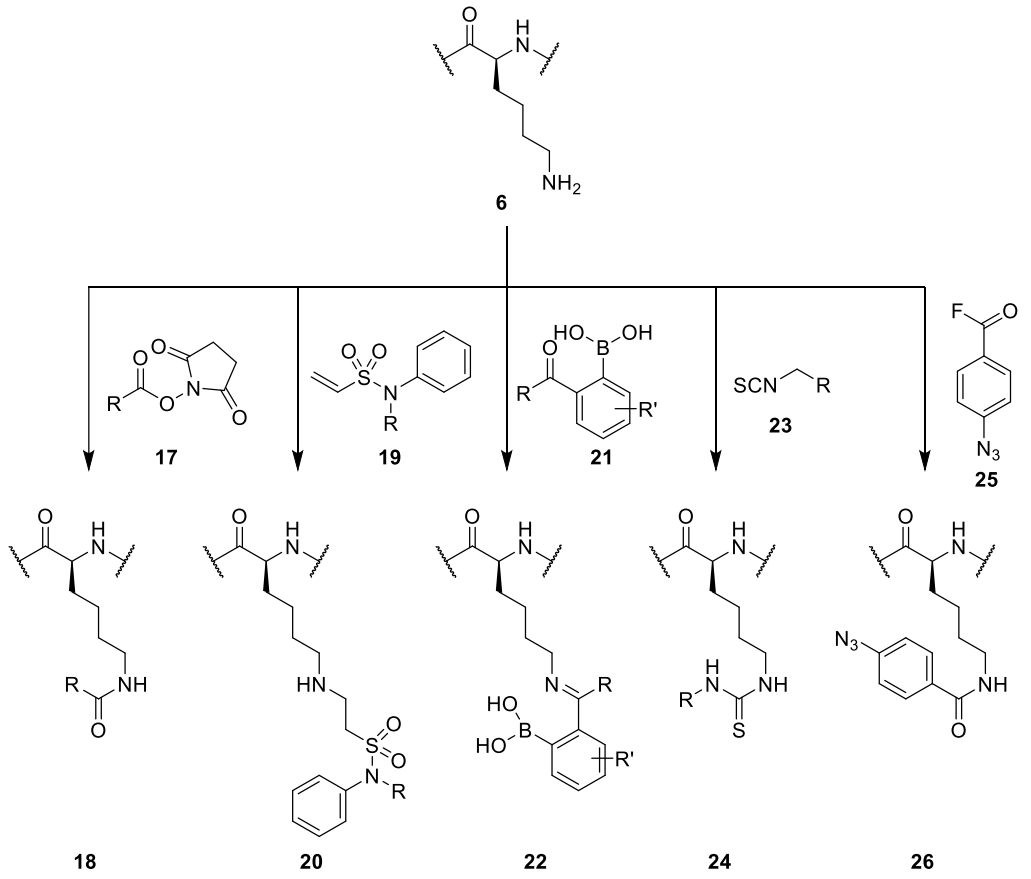

Scheme 3 – Methods for modification of lysine residues.

Recently, Matos *et al.* report an exciting development in the field of lysine conjugation, showing regioselective modification of a single lysine residue across 5 different platforms.[62] By computationally determining the lysine residue with the lowest pKa on a protein platform, they were able to selectively target this residue with a sulfonyl acrylate (**28**) reagent in mild conditions (Scheme 4). By using a mildly basic conjugation procedure they ensured only the lysine of interest to be sufficiently reactive towards the sulfonyl acrylate. They also report selective conjugation to a target lysine in the presence of a reactive cysteine thiol; the authors suggest that hydrogen bonding occurs between the lysine and sulfonyl group on the sulfonyl acrylate resulting in a significant increase in lysine reactivity over cysteine.[62] Finally, they demonstrate conjugation of the remaining acrylate through aza-Michael addition of an amine containing fluorophore (Scheme 4). However, site-selective modification in this instance can be limiting as the sulfonyl acrylate reagent allows for only one point of functionalisation per protein platform (limiting the scope for multi-functional protein conjugates). In addition, whilst this conjugation reaction is selective, there is still no

control over where the point of modification will be (*i.e.* for some proteins, the lysine with the lowest pKa may play a crucial role in the protein's function).

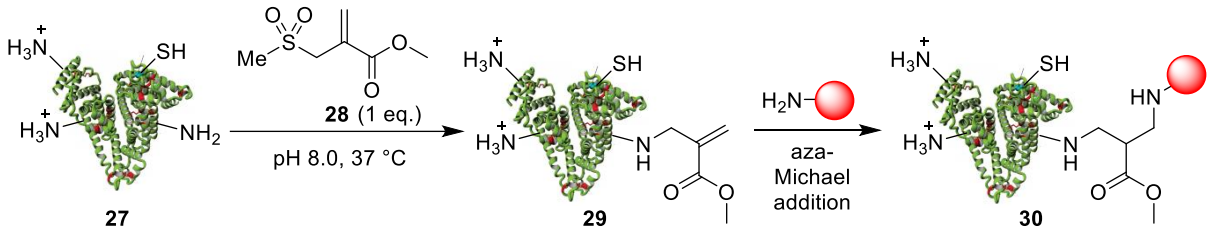

Scheme 4 – Selective lysine modification using sulfonyl acrylates.

1.4.2 Cysteine Modification Reagents

Thiol moieties present on cysteine residues provide an excellent opportunity for chemo-selective bioconjugation due to the high nucleophilicity and low pKa (*ca.* 8)[63] of the cysteine thiol. Herein, reagents capable of both single cysteine modification and functional disulfide re-bridging will be explored.

1.4.2.1 Single Cysteine Modification Reagents

As illustrated in scheme 5 there are many different small molecules that can modify a single cysteine, these reactions include oxidation, disulfide formation and alkylation (by S_N2 displacement or Michael Addition).[64–67] Michael addition in particular provides an attractive option for cysteine selective bioconjugation. Michael acceptors are considered soft electrophiles, and so promote reactions with soft nucleophiles (*e.g.* thiols). Combined with the high nucleophilicity of the thiol on cysteine, this soft-soft interaction allows for exquisite selectivity of Michael acceptors towards cysteine residues (over other nucleophilic residues *e.g.* lysine).[68] Maleimides **33**, bromomaleimides **45** and bromopyridazinediones **34** have all been applied successfully as Michael acceptors in this context.

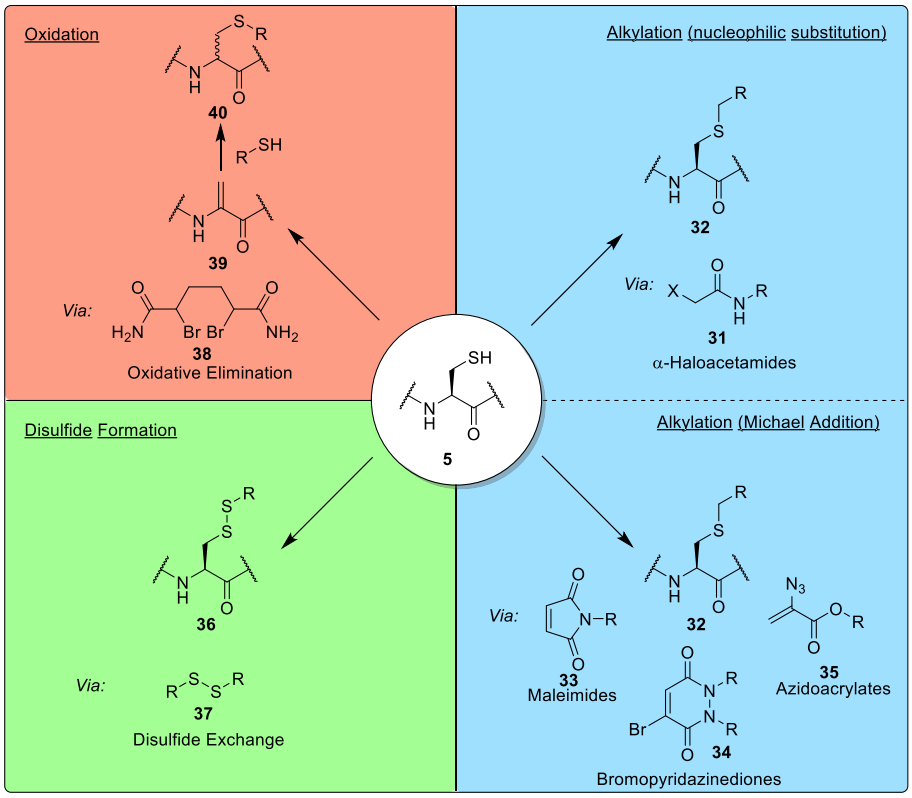

Scheme 5 – Reactions of single cysteine moiety with dibromide (oxidation), disulfides (disulfide exchange), haloacetamides, maleimides and azidoacrylates (alkylation).[64–67]

Maleimides:

Maleimides are among the most popular reagents for cysteine modification, with many functional maleimides being commercially available. However, the resultant succinimide-thiol linkage (**41**) formed when reacting maleimides with thiols is typically known to be unstable, as this moiety can undergo retro-Michael degradation (Scheme 6).[30] If this process occurs *in vivo* (*e.g.* in blood) less of the desired payload will reach the intended target (in some reported cases, only 50% of the conjugated payload was found to be attached after 7 days).[30] Furthermore, the addition of competing thiols (*e.g.* blood thiol human serum albumin (HSA) **27**) can accelerate this process, promoting deprotonation and subsequent deconjugation (k_1) and by providing an alternative reaction pathway for the liberated maleimide (k_4) (Scheme 6).

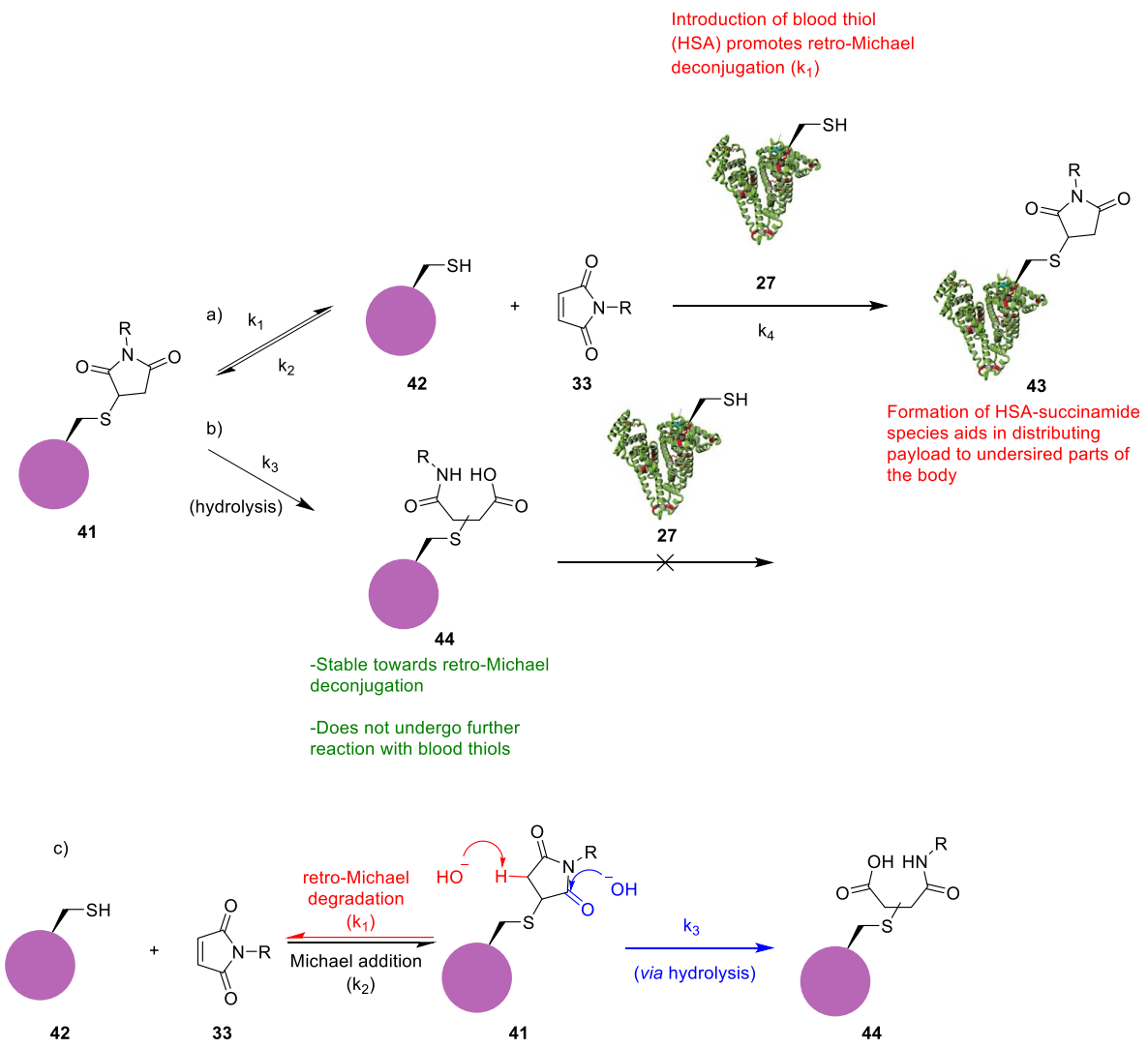

Scheme 6 – Reactions of maleimide-thiol conjugates.

A number of researchers have tried to exploit hydrolysis of cysteine-succinimide harbouring conjugates as a means of irreversible thiol modification (*i.e.* inducing serum stability) to circumvent this issue (Scheme 6b).[69,70] Many cases of thiol-succinimide hydrolysis have been reported to produce stable hydrolysed thiol-maleimide conjugates, however their yield is typically low as the conditions for hydrolysis also promote retro-Michael deconjugation (Scheme 6c). Michael acceptors that have addressed this issue of bioconjugate instability are therefore of great interest to the wider field of site-selective cysteine conjugation and have been termed “next-generation Michael acceptors”.

Bromomaleimides:

Bromomaleimides **45** are a reported class of Michael acceptor that undergo Michael addition, followed by elimination of a bromine to afford an unsaturated thiol-maleimide scaffold (**46**) (Scheme 7).[69] Smith *et al.* were first to successfully introduce bromomaleimides to form the unsaturated HSA–maleimide conjugate **46** (Scheme 5b).[69] In this report, the authors show hydrolysis of the HSA-maleimide species was achieved to form the hydrolysed HSA-maleimide species **47** in quantitative yield, without observing retro-Michael deconjugation. It should be noted that hydrolysis in the case of maleimide conjugation is considered necessary, as the highly reactive unsaturated thiol-maleimide scaffold **46** is capable of undergoing thiol exchange (*e.g.* with blood thiols). Analagous to traditional maleimides the hydrolysed unsaturated thiol-maleimide scaffold (**47**) quenches further reactions with thiols.

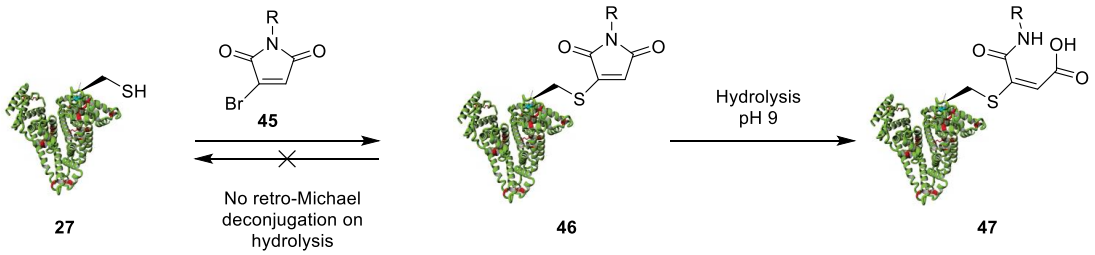

Scheme 7 – Formation of irreversible cysteine-maleamic acid conjugates.[69]

Bromopyridazinediones:

Similarly to bromomaleimides, bromopyridazinediones (BrPDs) also act as a Michael acceptors towards cysteine thiols and proceed in an analogous fashion to eliminate bromine to form an unsaturated thiol-PD linkage. Over the past decade many research groups (Caddick, Baker, Chudasama etc.) have reported exciting conjugation strategies involving derivatives of BrPDs and dibromopyridazinediones (DiBrPDs) for the quantitative formation of single cysteine and disulfide modified conjugates respectively.[71]

In a direct comparison between BrPDs and bromomaleimides, it can be seen that the PD scaffold is considerably less reactive requiring a conjugation time of 1 h (100 eq. of PD, pH 8.0, 37 °C) to quantitatively form PD conjugates, compared to just 10 minutes (2 eq. of bromomaleimide, pH 7.4, 21 °C) required for the bromomaleimide scaffold in more mild conditions.[71,72] However, due to this decrease in reactivity, reports suggest that BrPDs have a greater stability towards thiol exchange and do not require a hydrolysis step to confer serum

stability. Furthermore, the PD moiety harbours two *N*-directed functional handles, leading to conjugation strategies such as 'dual-click' chemistry as well as irreversible thiol conjugation.[73,74]

Chudasama *et al.* first exemplified the PD technology on the cysteine containing mutant SH2 domain of the Grb2 adaptor protein.[71] It was found that this 6-membered scaffold was stable to hydrolysis, in addition to participating in reversible thiol addition, in a high concentration of 2-mercaptoethanol (BME), owing to a hypothesised release mechanism in intracellular conditions.

Reports by Maruani *et al.* have also explored the suitability of PDs as irreversible thiol conjugates, in a high concentration of glutathione (*i.e.* representative of cellular conditions).[73] This was achieved through use of the second available *N*-directed handle. A single cysteine green fluorescent protein (GFP) mutant (**48**) was modified using a difunctionalised PD harbouring a cleavable *para*-azidobenzyl substituent (**49**). The resultant PD-protein conjugate **51** can then undergo further reaction with tris(2-carboxyethyl)phosphine (TCEP) **52** yielding an irreversible enol tautomer **53**, which is stable towards thiol exchange (even when excess thiol is present *e.g.* in early endosomal conditions). This strategy therefore offers great control over reversible or irreversible single cysteine modification using PDs in a high concentration of thiol (Scheme 8). It should be noted that both molecules, although reversible and irreversible in a high intracellular concentration of thiol, are stable in serum-like conditions (*i.e.* in blood mimicking conditions).

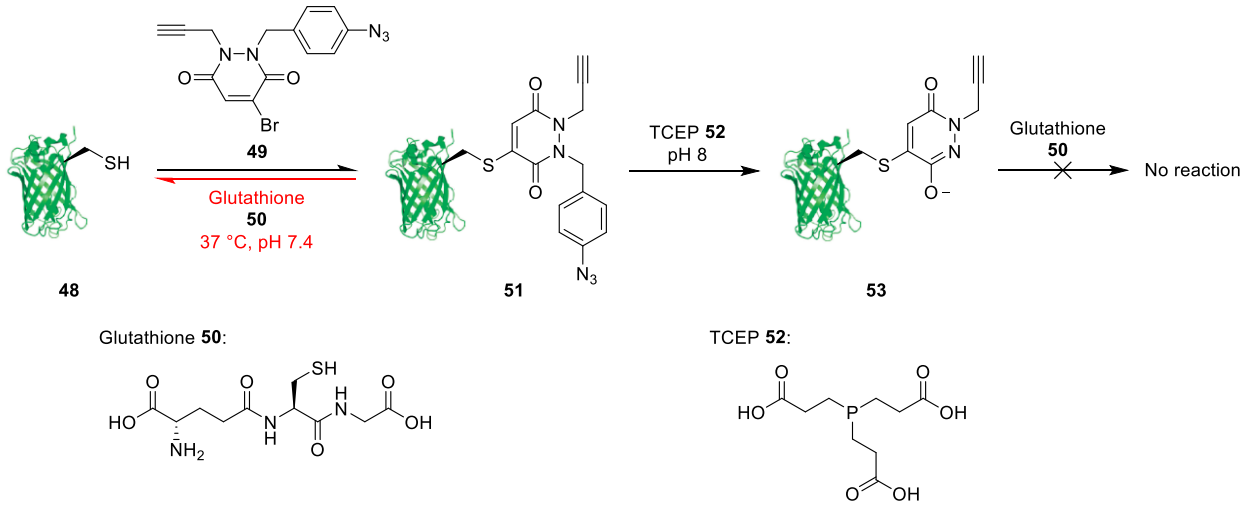

Scheme 8 – Irreversible modification of GFP using difunctionalised PDs.[73]

1.4.2.2 Disulfide Modification Reagents

Functional disulfide re-bridging requires: i) the thiol moieties to be first liberated from the disulfide bond (*i.e.* through reduction with TCEP **52**; and ii) the re-bridging agent to contain two reactive centres selective for reaction with the two released cysteine thiols. Once again, there are many reagents available to achieve this type of conjugation (Scheme 9).[53,74–79] An extensive review by Kuan *et al.* analysed various disulfide re-bridging conjugates based on seven different attributes (*e.g.* multifunctional, yield and solubility). DiBr PDs **57** and dibromomaleimides **55** were included in this analysis as they were found to re-bridge a variety of different substrates in quantitative yield. Furthermore, desirable traits such as a high rate of conjugation (dibromomaleimides **55**) and multifunctionality (DiBrPDs **57**) have previously been highlighted.[80,71]

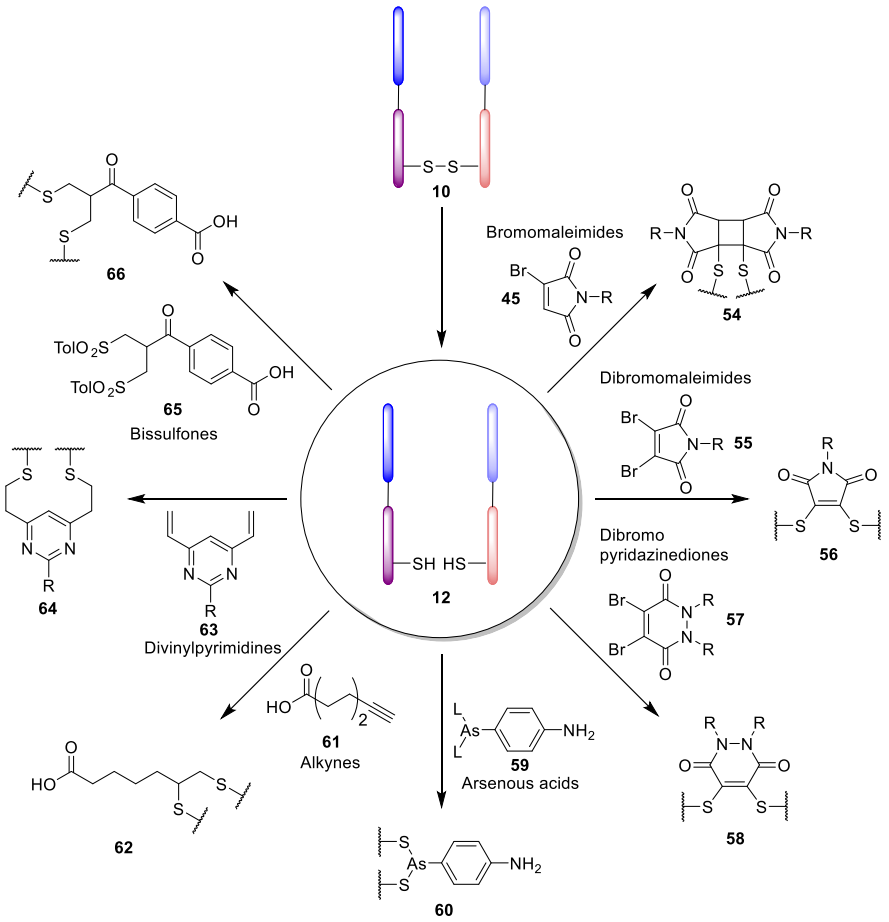

Scheme 9 – Reactions of disulfide containing proteins with a library of small molecules.[53,74–79]

Dibromomaleimides:

Adapted from bromomaleimides **45**, dibromomaleimides **55** were successfully introduced as disulfide re-bridging agents by the Baker and Caddick groups. Smith *et al.* first successfully incorporated dibromomaleimides **55** into the solvent accessible disulfide linkage found in somatostatin **67** (Scheme 10).[76] Further to this, by attaching an *N*-directed fluorescent reagent on the maleimide, a fluorescently labelled somatostatin analogue (**68**) was synthesised. However, as with the use of bromomaleimides, a hydrolysis is required to enable serum stability.

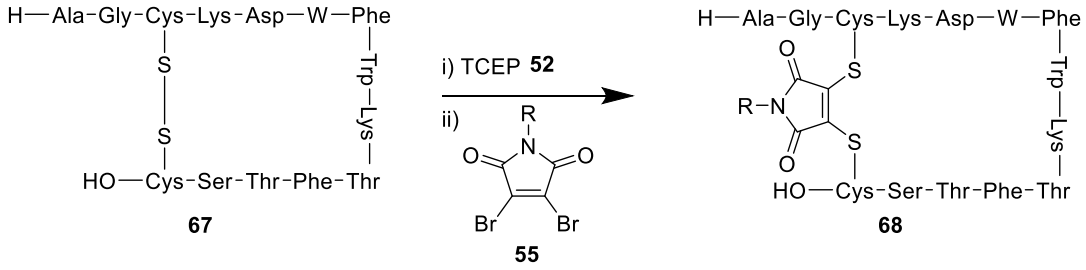

Scheme 10 – Functional re-bridging of somatostatin **67** using dibromomaleimides **55**.[76]

Dibromopyridazinediones:

Work by Maruani *et al.* introduced a "plug and play" approach to disulfide re-bridging using DiBr PDs. A PD derivative, harbouring a terminal alkyne and a strained alkyne (Astra PD **69**), was used to modify fragment antigen binding (Fab) constructs of trastuzumab, yielding dual-functionalised Fab-PD conjugates, capable of participating in dual sequential "click" reactions.[74] The "clickable" handles present on Astra-PD (**69**) can be reacted with various other moieties, such as azides, to form a vast library of site-selective, cysteine directed antibody-PD conjugates. As with the above examples, these PD-conjugates were also stable in serum-like conditions.

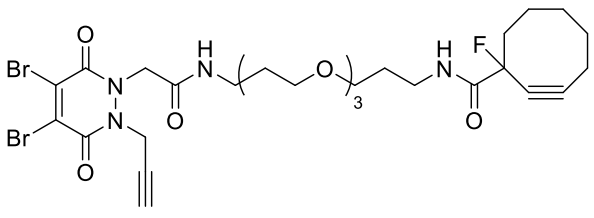

Figure 5 – Structure of Astra PD **69** harbouring strained alkyne and terminal alkyne for SPAAc and CuAAc reactions respectively.[74]

1.4.3 Reagents for "Click" Chemistry

"Click" chemistry is considered a powerful synthetic strategy and can be defined by forming a heteroatom linkage using 'spring-loaded' reactions, compatible with a narrow range of bioorthogonal conditions.[81] Due to the speed and efficiency observed with "click" reactions, particularly in the context of modular protein modification, many bioconjugation strategies aim to first install "clickable" handles so that various functional moieties may be subsequently added. Due to the increasing popularity of "click" chemistry in the context of protein modification, many functional reagents with preinstalled "clickable" moieties (azide, alkyne, strained alkyne etc.) are now commercially available. Two of the most popular reactions that undergo bioorthogonal "click" chemistry are copper-catalysed azide-alkyne cycloaddition (CuAAC) reactions and the copper free strain-promoted azide-alkyne cycloaddition (SPAAC) variant.

1.4.3.1 Copper-Catalysed Azide-Alkyne Cycloaddition (CuAAC) Reactions

CuAAC reactions between terminal (non-activated) alkynes and azides are considered bioorthogonal and highly selective as these moieties will not react at room temperature without a catalyst. This selectivity has led to the use of efficient and successful CuAAC reactions across many areas of research, some of which include protein modification,[80] enzyme activity labelling[82] and labelling of proteins in bacterial cells[83].

The reaction between terminal alkynes **72** and an azide moiety **73** is catalysed by Cu^{I}, most conveniently available through reduction of Cu^{II} (available as $CuSO_4$ **70**) through use of a reducing agent (sodium ascorbate) with an accelerating ligand (*e.g.* THTPA **71** in a 5:1 ligand:metal ratio) required to maintain the Cu^{I} in solution (Scheme 11).[84] Although still considered a useful tool for protein modification, CuAAC reactions are considered limited as the process requires the potentially toxic use of a metal which can result in oxidative damage to proteins through the formation of reactive oxygen species.[85]

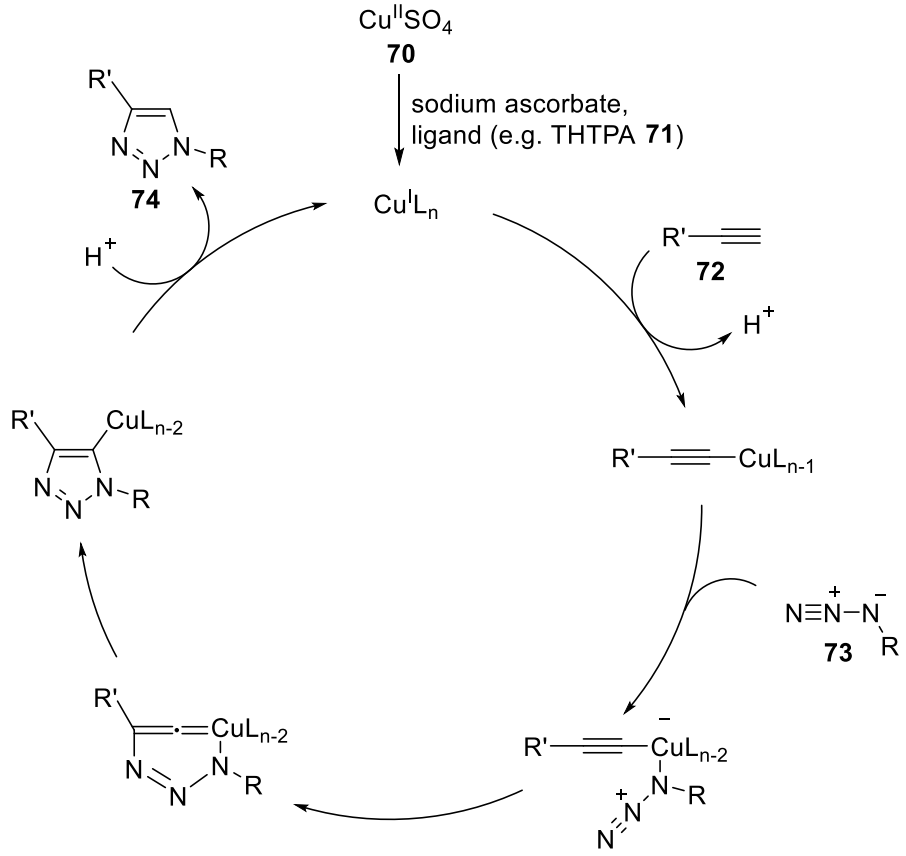

Scheme 11 – Mechanism for copper-catalysed azide–alkyne cycloaddition (CuAAC).

1.4.3.2 Strain-Promoted Azide-Alkyne Cycloaddition (SPAAC) Reactions

An elegant alternative to using metals to catalyse azide-alkyne reactions is to increase the reactivity of one of the reacting species. Work by Agard *et al.* outlined a strategy for increasing the reactivity of the alkyne by forming a strained cyctooctyne ring **75** that reportedly reacts with azides at room temperature, without requiring metal catalysis (Scheme 12a).[86] Cyclooctyne is known as the smallest stable alkyne variant that can be used for this purpose, and was found to be stable in mildly acidic (0.5 M HCl for 30 min) and mildly basic (0.8 M NaOMe for 30 min) conditions, as well as high concentrations of nucleophilic thiols (120 mM 2-mercaptoethanol for 12 h). [86]

Developments in the field of strained-alkyne mediated “click” reactions saw the introduction of more ridged and electron deficient dibenzocyclooctynol (DBCO) reagents **77** that display an increase in reactivity towards aliphatic azides (Scheme 12b).[87] Further work by Dommerholt *et al.* discovered that SPAAC proceeds *via* an inverse-electron demand (IED)

mechanism (an electron rich dienophile reacts with an electron poor diene). This further explained the increase in reactivity of DBCOs (electron poor dienes) with aliphatic azides (electron rich dienophiles). Dommerholt *et al.* found a four-fold increase in reactivity between DBCO and aliphatic azides when compared to aliphatic strained alkynes and aliphatic azides. However, DBCO reagents have occasionally been reported to react with cysteine residues as an unwanted side reaction, which is perhaps not surprising given the increase of electrophilicity of the DBCO compared to aliphatic strained alkynes.[88]

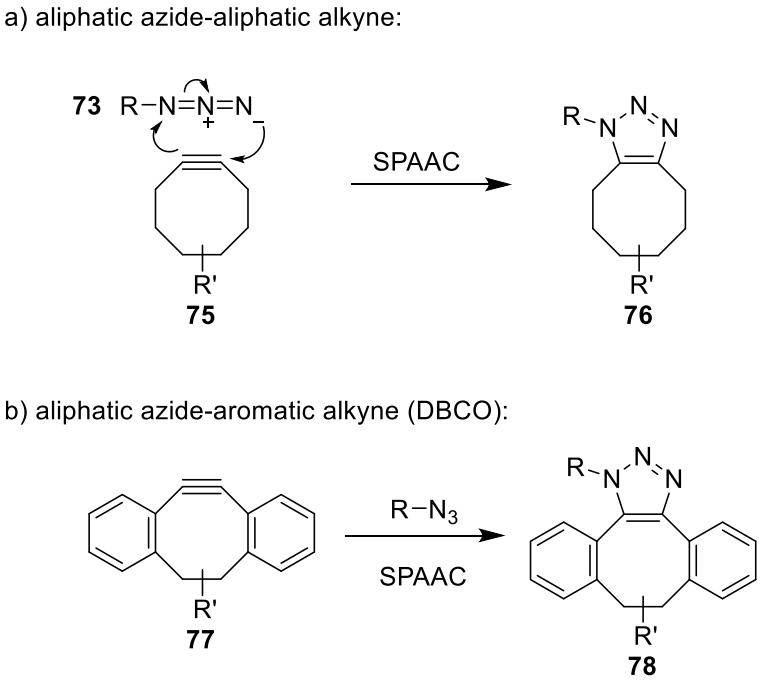

Scheme 12 – Depiction of reactions between strained alkynes and aliphatic azides. a) mechanism for reaction between aliphatic azide and aliphatic strained alkyne. b) reaction between aliphatic azide and aromatic strained alkyne (DBCO).

While many exciting strategies exist for protein modification, the context of which they can be applied should not be forgotten. Protein selection is considered integral in the process of therapeutic bioconjugate design, and a key aim of many developing bioconjugation strategies is to avoid negatively affecting the biological profile of the selected platform.

1.5 Protein Modification Platforms

Protein conjugation is a highly impactful multidisciplinary approach to treatment. However, it is only through extensive work carried out on researching and designing biological platforms that allows protein-conjugates to exist. Some biomolecules have been previously highlighted for their involvement in many diseases (*e.g.* antibodies in cancer treatment); understanding the structure and function of these proteins can be considered critical to the progression of future protein conjugates.

1.5.1 Antibodies

Antibodies are among the most popular proteins for bioengineering, with forty-seven monoclonal antibodies approved for use in the US and Europe, by 2015, for treatments of various diseases (*e.g.* cancer).[89] As recently as 2018, 7 of the top 10 bestselling pharmaceuticals were antibody derived.[19] Antibodies are large Y-shaped biomolecules produced by the B cells of the immune system and act to defend against many harmful diseases.[44]

Antibodies produced by the mammalian immune system come in the form of 5 classes (IgA, IgD, IgE, IgG and IgM) and each class plays a specific role within the immune system (Table 1). IgA and IgG isotypes can be differentiated further as they contain subclasses (2 and 4 for IgA and IgG respectively). The majority of therapeutics approved for use by the FDA are IgG based; This is perhaps not surprising considering IgG antibodies in their 4 subclasses provide the majority of antibody-based immunity within mammals.[90] For protein modification one of the most extensively explored platforms of the antibody classes and subclasses available, are IgG1 derived antibodies (*e.g.* trastuzumab which targets HER2 receptors for the treatment of breast cancer).[91]

Table 1 – Summary of mammalian antibody classes.[92]

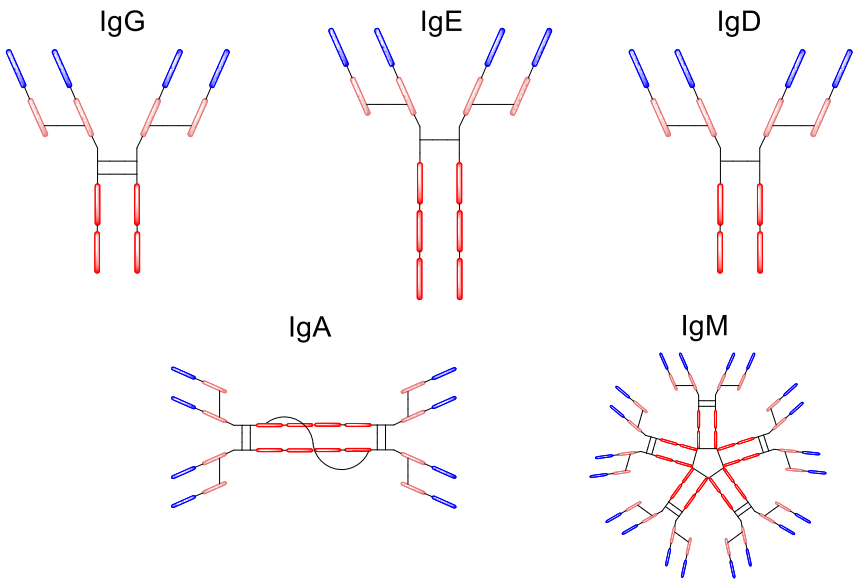

Isotype	Subclasses	General Function
A	2	Found in mucosal areas (*e.g.* respiratory tract).[93]
D	1	Recruits B cells of the immune system.[94]
E	1	Binds to allergens to trigger histamine release from mast cells.[95]
G	4	Provides blood-based antibody immunity against invading pathogens.[90]
M	1	Destroys invading pathogens as a first line of defence (before a sufficient amount of IgGs are produced).[96]

Understanding how antibodies achieve their targeted nature is key to synthesising an effective antibody-based pharmaceutical. This becomes more apparent when observing the antibody's tertiary structure in closer detail (Figure 6). The variable region (also referred to as the fragment antigen binding (Fab) region), contains regions that are produced in a complementary form to a specific antigen-binding partner, expressed by pathogens or foreign cells.[44] This allows antibodies to be engineered to bind specifically to an antigen, over-expressed by certain cell types. The non-variable region (also referred to as the Fc region) remains constant among many humanised antibodies to allow one type of cell in the immune system to bind many different types of antibody.[97] IgG antibodies (as well as many other antibody classes) are made up of light and heavy chains covalently bound by interchain disulfide bonds. Many disulfide bonds are present within the secondary structure of the antibody, however interchain disulfide

bonds are often solvent accessible, and act as a potential site-selective target for modification. Additionally, IgG1 antibodies contain *N*-glycans which serve to regulate Fc effector function.[98,99]

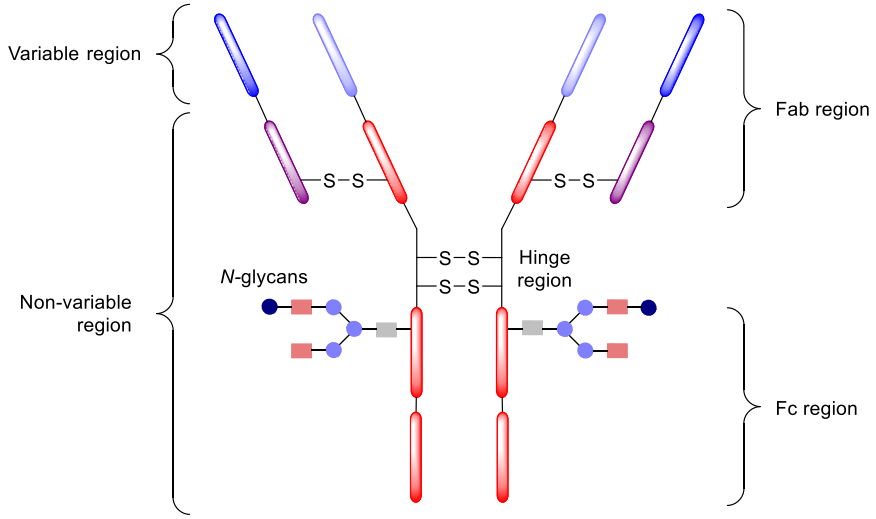

Figure 6 – General structure and terminology of an IgG1 antibody.

There are several mechanisms by which antibodies can induce an immune response, including neutralisation, aggregation, and antibody-dependant cell-mediated cytotoxicity (ADCC).[100] However each antibody in a specific role will not carry out all of these functions; using the clinically relevant trastuzumab as an example, only the ADCC mechanism is applicable.[91] ADCC is induced by the Fc region binding the CD16a receptor on the surface of natural killer (NK) cells, after the antibody has bound target antigen. Once in proximity, NK cells initiate lysis of the diseased cell (Figure 7).[97]

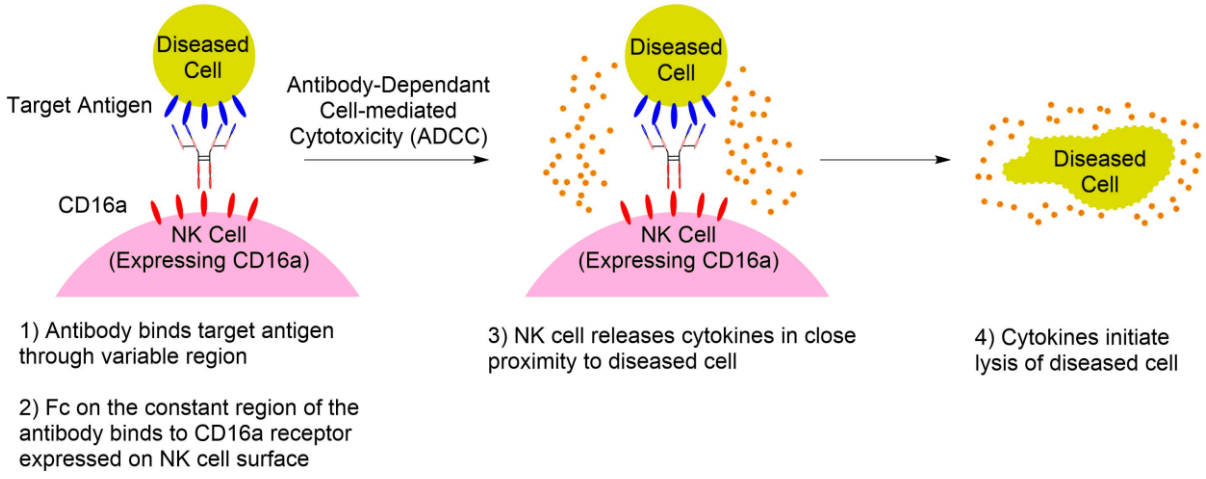

Figure 7 – General ADCC mechanism applied to multiple targets.[97]

1.5.2 Antibody Fragments

Through prokaryotic expression and enzymatic digestion of full antibodies it is possible to obtain many clinically relevant antibody fragments, with a variety of different physiochemical properties (Table 2).

Table 2 – Structure of an IgG1 antibody with obtainable antibody fragments highlighted.[101,102]

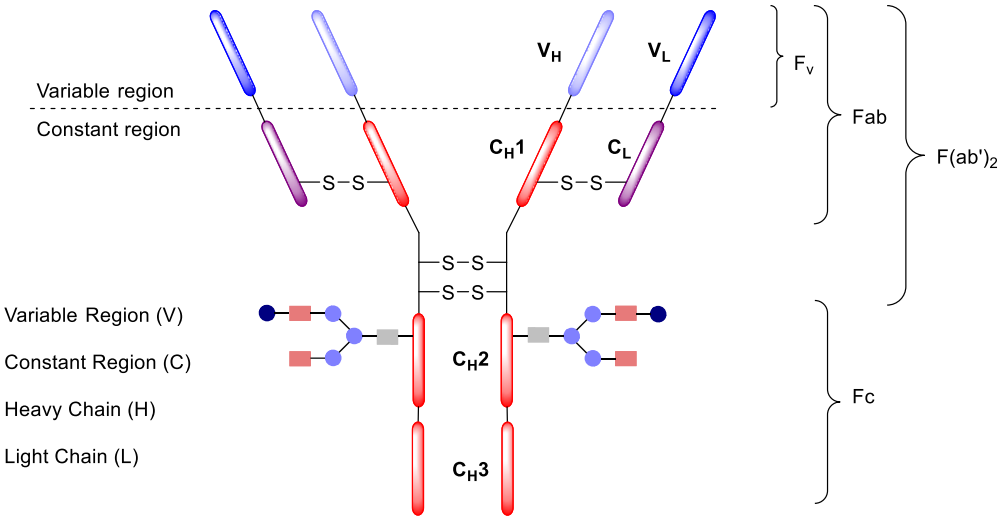

Fragment	Regions	Weight (Da)	Description
Fv	V_H/V_L	~15,000	Smallest fragments available, responsible for binding properties of antibody.
scFv	$V_H + V_L$	~28,000	Single chain variable fragment (scFv). Both Fv fragments attached by a flexible linker, optimised for stability and binding.
Fab	$V_H + C_H1 + V_L + C_L$	~50,000	Contains portions of constant region. Disulfide covalently binds $V_H + C_H1$ with $V_L + C_L$.
Fc	$2(C_H1 + C_H2)$	~50,000	Contains all Fc binding regions, also contains *N*-glycans (at N^{297}) of antibody and associated properties.
F(ab')$_2$	$2(V_H + C_H1 + V_L + C_L)$	~110,000	Two Fab fragments joined by hinge region disulfides.

The use of antibody fragments in targeted therapy (*e.g.* Fab fragments) pose many advantages over the use of full antibodies, due to their smaller size and ability to penetrate tissues, which full size antibodies cannot.[103,104] Moreover, antibody fragments that do not harbour an Fc region may be expressed by prokaryotic cells. This poses an economical advantage over monoclonal antibodies (mAbs) which are expressed in more expensive eukaryotic systems.[105]

However, the Fc domain in mAbs serves to stabilise the antibody as well as participate in FcRn-mediated recycling. Without this stabilisation factor, many antibody fragments have short circulating half-lives.[106] In an attempt to increase the *in vivo* stability of antibody fragments, work has been explored using antibody fragment-albumin and antibody fragment-PEG conjugates.[14,107–109] This technology has been successfully applied to the FDA approved anti-TNFα Fab, certolizumab pegol.

1.5.3 Single Domain Antibodies (sdAbs)/ Nanobodies

Work presented by Hamers-Casterman *et al.* first discovered an IgG like biomolecule in the camel (*camelus dromedaries*) which distinctly lacked the light chain associated with typical IgG antbodies.[110] Subsequently, it has been possible to create a new class of engineered single domain antibodies (sdAb) and nanobodies with highly robust physiochemical properties (Figure 8).

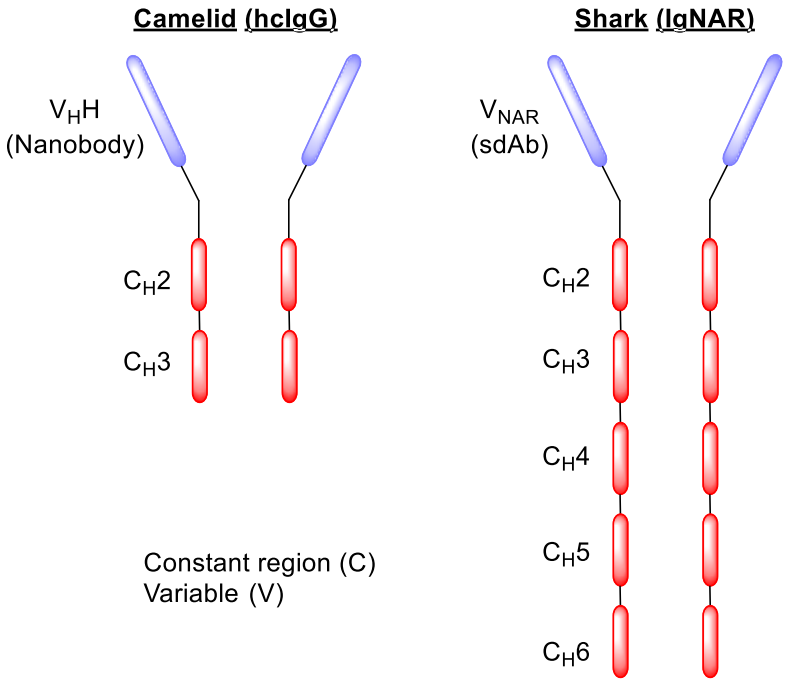

Figure 8 – General structure of camelid (hcIgG) and Shark (IgNAR)

Single-domain antibodies (sdAb) were first derived from the aforementioned camelid hcIgG antibody (sdAbs derived from hcIgG antibodies are also referred to as nanobodies). No light chain or C_H1 region is attached to the variable binding region of the antibody (V_HH and V_{NAR} for hcIgG and IgNAR antibodies respectively). Nanobodies are small in size (~15 kDa) and

have comparatively very high binding affinity towards target antigens - allowing for great stability, permeability and solubility. Furthermore, it is possible to reversibly refold these proteins and their expression is generally high yielding in a wide range of expression systems.[111–113]

The size of these biomolecules has drawn much attention in therapeutic and diagnostic fields, as these proteins can enter many places of interest that mAbs and some antibody fragments cannot. This technology has proven useful in cell imaging through gaining access to new parts of the cell, and targeted cancer therapy through deep tissue penetration.[114,115] It is also thought these proteins may be able to cross the blood-brain barrier in an attempt to treat brain tumours in a similar targeted fashion.[116]

Similar to Fv, scFv, Fab and F(ab')$_2$ fragments, the small size and lack of Fc region results in a short blood half-life of sdAbs. Additionally, the small size of sdAbs results in partial renal clearance, further diminishing the blood half-life of sdAb-conjugates.[112]

1.6 Antibody–Drug Conjugates (ADCs)

Whilst antibodies possess an ability to selectively target some cancers, the induced immune response is often not as efficacious as many current chemotherapies in killing diseased cells.[117] In the last two decades research has turned towards the synthesis of antibody–drug conjugates (ADCs).[118] ADCs consist of an antibody attached to a cytotoxic drug, using linker technology. Therefore, by exploiting the targeted therapy achieved through complementary antibody-target binding, and internalisation pathways, highly potent payloads can be delivered directly and selectively to the cancer cell for increased efficacy (Figure 9).[119,120]

It is important to understand which mechanisms are applied to ADCs for effective drug design. For example, internalisation of target receptors initiated through antibody-antigen binding are considered crucial to ADCs as this is the favoured and most common mechanism for release of the cytotoxic payload into the cell (Figure 9).[120] Once again, using the clinically relevant antibody trastuzumab as an example, for ADCs derived from trastuzumab conjugates ADCC and internalisation mechanisms may play a role in the collective induced immune response, and overall efficacy of the treatment.

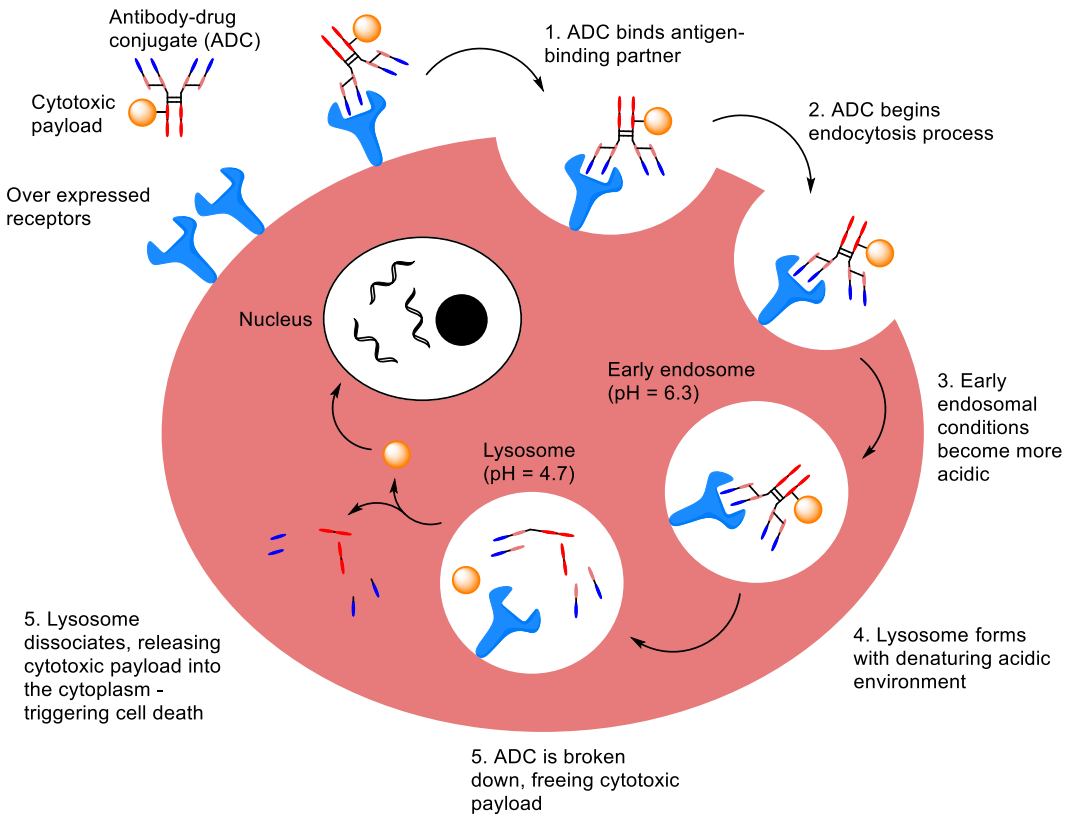

Figure 9 – General internalisation mechanism of ADCs.

There have been many successful approaches towards synthesising effective ADCs. By analysing previously reported bioconjugation strategies, it is possible to gain insight on which conjugation methods are the most successful, and why.

1.6.1 Current Antibody–Drug Conjugates

To date there are currently eight ADCs derived from full antibodies that have been approved by the FDA. The systematic names and trade names are listed below. A short summary on ADC approval date, antibody platform, payload/conjugation method, linker type and ADC treatments is provided in table 3.

i) Gemtuzumab Ozogamicin (Mylotarg™)
ii) Brentuximab Vedotin (Adcetris™)
iii) Trastuzumab Emtansine (Kadcyla)
iv) Inotuzumab Ozogamicin (Besponsa™)
v) Polatuzumab Vedotin (Polivy™)
vi) Enfortumab Vedotin (Padcev™)

vii) Trastuzumab Deruxtecan (Enhurtu)

viii) Sacituzumab Govitecan (Trodelvy)

Modification of native antibody scaffolds at cysteine and lysine residues features in many ADCs approved by the FDA thus far (*e.g.* Kadcyla and Adcetris shown in figure 10). This is understandable from a manufacturing perspective, as these routes to synthesising an ADC are among the cheapest and most convenient (requiring only chemical modifications of an easily expressed antibody platform). However, it should be noted that the conjugation strategies used in the synthesis of the FDA approved ADCs were first-in-class and developed well before the first approval of Mylotarg™ in 2000. Currently there are over 80 ADCs in clinical development, many of which utilise next-generation conjugation strategies for an enhanced *in vivo* efficacy.

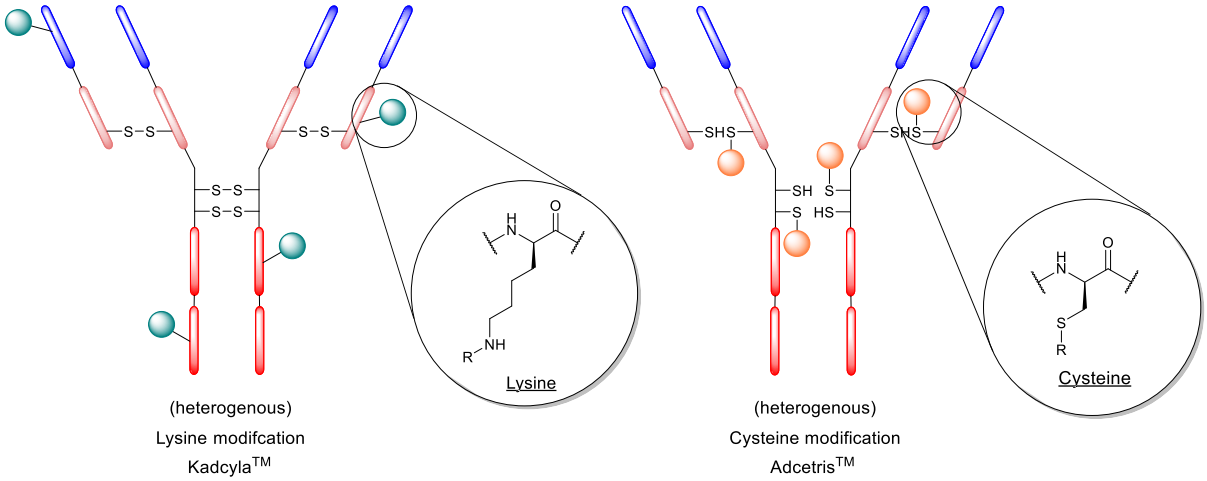

Figure 10 – Illustrations of IgG1 antibodies modified at lysine (*e.g.* Kadcyla™) and cysteine (*e.g.* Adcetris™) residues.

Table 3 – Summary of FDA approved ADCs to date

ADC	Approval Date	Antibody (Subtype-Target)	Drug (Conjugation Method)	Cleavable Linker (Type)	Treatment
Gemtuzumab Ozogamicin (Mylotarg™) [121,122]	2000/ 2017*	Gemtuzumab (IgG4-CD33)	Calicheamicin (Lysine Modified)	Acid-Cleavable (Hydrazone)	Acute Myeloid Leukaemia
Brentuximab Vedotin (Adcetris™) [123]	2011	Brentuximab (IgG1-CD30)	Monomethyl Auristatin E (Cysteine Modified)	Protease Cleavable (Val-Cit-PABC)	Hodgkin's Lymphoma/ systemic anaplasmic large cell lymphoma (ALCL)
Trastuzumab Emtansine (Kadcyla™) [124]	2013	Trastuzumab (IgG1-HER2)	DM-1 – Mertansine (Lysine Modified)	Non-Cleavable	HER2+ Breast Cancer
Inotuzumab Ozogamicin (Besponsa™) [125]	2017	Inotuxumab (IgG4-CD22)	Calicheamicin (Lysine Modified)	Acid-Cleavable (Hydrazone)	Acute Lymophblastic Leukemia (ALL)
Polatuzumab Vedotin (Polivy™) [126]	2019	Polatuzumab (IgG1-CD79b)	Monomethyl Auristatin E (Cysteine Modified)[#]	Protease Cleavable (Val-Cit-PABC)	Diffuse Large B-Cell Lymphoma (DLBCL)
Enfortumab Vedotin (Padcev™)[127]	2019	Enfortumab (IgG1-Nectin-4)	Monomethyl Auristatin E (Cysteine Modified)	Protease Cleavable (Val-Cit-PABC)	Advanced or Metastatic Urothelial Cancer
Trastuzumab Deruxtecan (Enhurtu)[128]	2019	Trastuzumab (IgG1-HER2)	DX-8951 (Exatecan Derivative) (Cysteine Modified)	Protease Cleavable (Gly-Gly-Phe-Gly)	HER2+ Breast Cancer
Sacituzumab Govitecan (Trodelvy)[129]	2020	Sacituzumab (IgG1-Trop-2)	SN-38 (Cysteine Modified)	Acid Cleavable (Carbonate)	Triple Negative Breast Cancer

*Mylotarg withdrawn from the market 2010-2017
[#]Engineered cysteines provide platform for modification
Data provided current as of August 2020

1.6.2 Site-Selective Antibody–Drug Conjugate Synthesis

In the last 20 years or more, many researchers have worked on exciting new strategies to synthesise ADCs with superior homogeneity and controlled drug-loading. There are three main approaches to site-selective antibody modification: i) chemical modification of engineered antibodies; ii) enzymatic assisted modification; and ii) chemical modification of native antibodies.

1.6.2.1 Engineered Antibodies

With rapid advances in protein engineering in recent years, the amino acid sequence of antibodies can now be manipulated to express of both naturally occurring and non-naturally occurring amino acids of choice on a protein surface.[44] By introducing reactive moieties on the antibody surface at specific sites, the resultant bioconjugate formed through chemical modification can be highly homogenous.

The thiol moiety present on cysteine residues has the highest nucleophilicity of any naturally occurring amino acid. Moreover, the presence of a solvent accessible reactive cysteine residue is rarely found in naturally occurring systems, as cysteine tends to oxidise to form disulfide bonds either intramolecularly (to form a disulfide bridge) or intermolecularly (to form a protein dimer). Thus, by engineering a cysteine residue onto the antibody surface *via* site-directed mutagenesis, a single point for chemical attachment may be possible. However, incorporation of an engineered cysteine residue can be complicated as the newly introduced thiol is also prone to forming disulfide bonds either intramolecularly (resulting in disulfide scrambling) or intermolecularly (resulting in protein dimerisation) which could reduce or remove activity.[130] Despite this challenge, Junutula *et al.* report the synthesis of the first thio-antibody (THIOMAB^{TM} **79**) with two additional cysteines expressed on the protein surface.[54] To achieve this, numerous conjugation sites on the antibody were tested in a screen against MUC16 (an antigen expressed by ovarian cancer cells). Although the cysteines were engineered correctly, expression in cells that contain a high concentration of thiol containing compounds glutathione and cysteine, resulted in capping the newly expressed thiols (Scheme 13). Therefore, in the synthesis of ADCs from THIOMABs^{TM} **79**, all disulfides present on the antibody must be reduced and selectively reoxidised in mild conditions (*i.e.*

all but the newly engineered cysteines) prior to antibody modification (Scheme 13). Nonetheless, anti-MUC16- auristatin conjugates were synthesised with 90% homogeneity with a reported drug-to antibody ratio (DAR) of 1.9.[131]

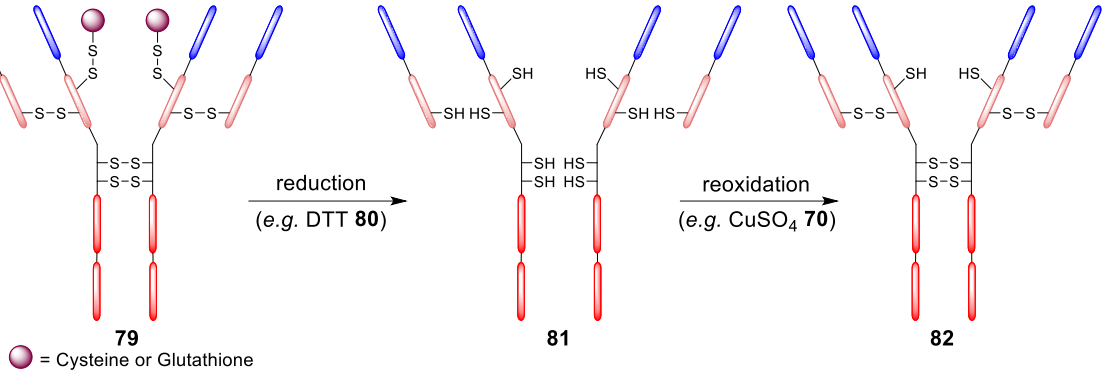

Scheme 13 – Synthesis of THIOMAB™ **79** with incorporation of two accessible and reactive cysteines

Incorporation of unnatural amino acids bearing unique chemical modalities, site-selectively is also achievable through protein engineering.[132] Using the clinically relevant trastuzumab as an example, unnatural amino acids *p*-acetylphenylanaline **84** and *p*-azidomethyl-phenylanaline **88** have been incorporated and reacted successfully. Axup *et al.* successfully demonstrate the incorporation of 2 ketone moieties (through expression of *p*-acetylphenylanaline **84**) into the structure of trastuzumab that facilitate site-selective oxime-ligation chemistry to afford near homogenous trastuzumab-aurastatin conjugates with a DAR of 2 (Scheme 14a).[132] The resulting conjugates performed well in *in vitro* assays, demonstrated a superior pharmacokinetic profile and resulted in tumour regression *in vivo*. Zimmerman *et al.* more recently engineered an azide moiety onto trastuzumab (through expression of *p*-azidomethyl-phenylaniline **88**) and found that subsequent SPAAC chemistry can provide another method towards forming highly homogenous trastuzumab-auristatin conjugates (Scheme 14b).[133]

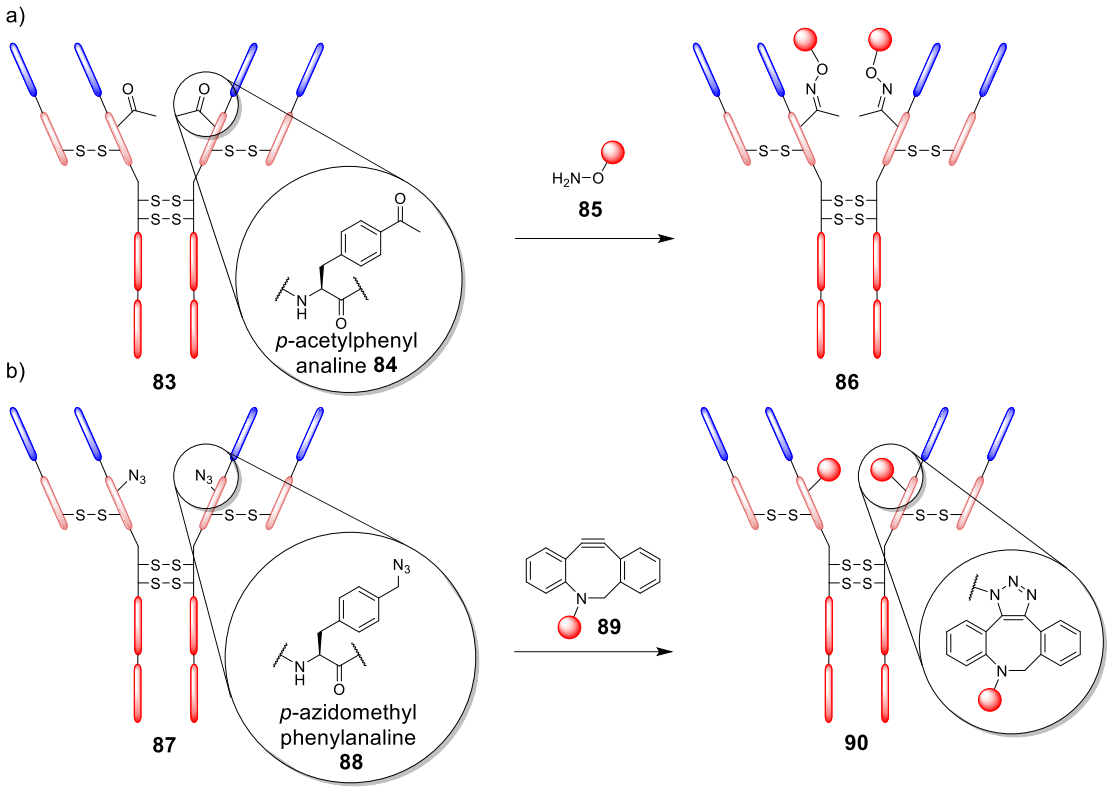

Scheme 14 – Formation of site-selective homogenous conjugates through unnatural amino acid incorporation. a) incorporation of *p*-acetylphenylanaline **84** and modification through oxime ligation. b) incorporation of *p*-azidomethyl-phenylaniline **88** and modification through SPAAC (DBCO) chemistry [132,133]

1.6.2.2 Enzymatic Antibody Modification

Many naturally occurring enzymes are already capable of carrying out selective and efficient functionalisation of proteins, as shown by enzymes that carry out post-translational protein modifications that are required for many biological processes.[134] Enzymes in the context of ADC synthesis can target specific *N*-glycans of native antibodies or recognise a specific amino acid sequence intentionally placed in the primary structure of engineered antibodies.

As many antibodies contain *N*-glycans in their constant region at the Asn-297 residue, this site serves as an interesting and potentially universal route to homogenous antibody modification. Carbohydrates present in *N*-glycans can be functionalised directly through oxidation of a primary alcohol present on sugars to form a reactive aldehyde moiety.[135] Whilst this functionalisation can be done chemically, these conditions (*e.g.* sodium periodate) are considered harsh and can result in undesirable oxidation of off-target amino

acids (*e.g.* methionine) that is known to affect FcRn binding and reduce serum half-life.[136] An alternative route to forming the aldehyde was reported by Stan *et al.* where the authors combined neuraminidases to cleave glycosidic linkages of neuraminic acids and galactose oxidase to form the reactive aldehyde moiety **95** from galactose (that has remained attached to the antibody) (Scheme 15a).[28] Stan *et al.* then proceeded to functionalise this aldehyde *via* reductive amination, to form a homogenous anti-CEA-doxorubicin conjugate with a DAR of 3.7.[28] This conjugate showed a 4-fold increase in potency *in vitro* when compared to an analogous heterogenous DAR 8 conjugate.[28] More recently, reports by Li *et al.* utilise glycosyltransferases to incorporate an azide harbouring sialic acid derivative into the glycan chain of an anti-C22 antibody (Scheme 15b).[137] Galactosyltransferase and sialyltransferase were used sequentially to add galactose **98** and the azido-sialic acid derivative **101** respectively. The incorporated azide was clicked through SPAAC chemistry to yield a near homogenous anti-CD22-doxorubicin ADC, shown to selectively target and kill lymphoma cells *in vitro*.[137]

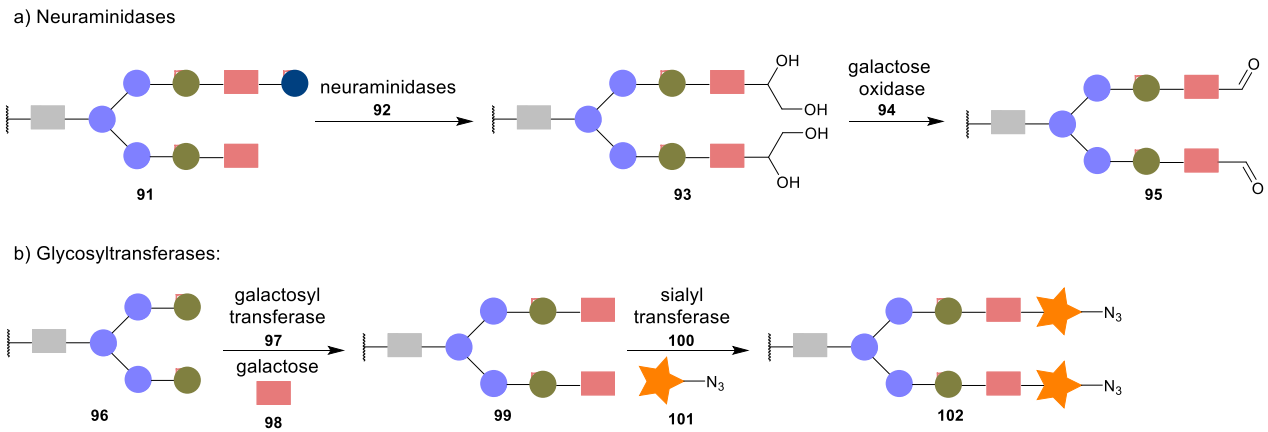

Scheme 15 – Enzymatic modification of *N*-glycans.[28,137]

Some enzymes can also identify a certain sequence of amino acids which may then initiate a chemical modification. Two key examples of such enzymes are transglutaminases (TGs) and formylglycine-generating enzymes (FGEs).[138] TGs may catalyse an acyl-transfer reaction on the amide present on the side chain of glutamine residues, and TGs derived from *Streptoverticillium mobaraense* (MTG) **104** will only recognise the sequence LLQGA referred to as the "glutamine tag" (Scheme 16a).[139–141] Strop *et al.* report the use of MTG **104** to synthesise anti-M1S1-auristatin ADCs **106**.[26] By forming a library of anti-M1S1 antibodies with a glutamine tag at 12 surface accessible regions, two possible combinations were

selected and MTG **104** was used to install the auristatin site-selectively to yield a DAR of 1.9.[26] FGEs are capable of converting cysteine residues to formylglycine in a site-selective manner (Scheme 16b). Formylglycine presents an aldehyde that does not naturally occur in proteins and is suitable for bio-orthogonal coupling reactions.[142] FGEs recognise the sequence CXPXR (where X can be serine, threonine, alanine or glycine). Drake *et al.* have reported the use of FGEs to form a library of trastuzumab conjugates harbouring the aldehyde tag.[143] Subsequent hydrazine-*iso*-Pictet-Spengler (HIPS) reactions were conducted to add a maytansinoid at three different positions. However, a general limitation associated with FGEs stems from the hydration of the formylglycine aldehyde in water to form a gem-diol incapable of further reaction, thus lowering yield of the bioconjugate.[144]

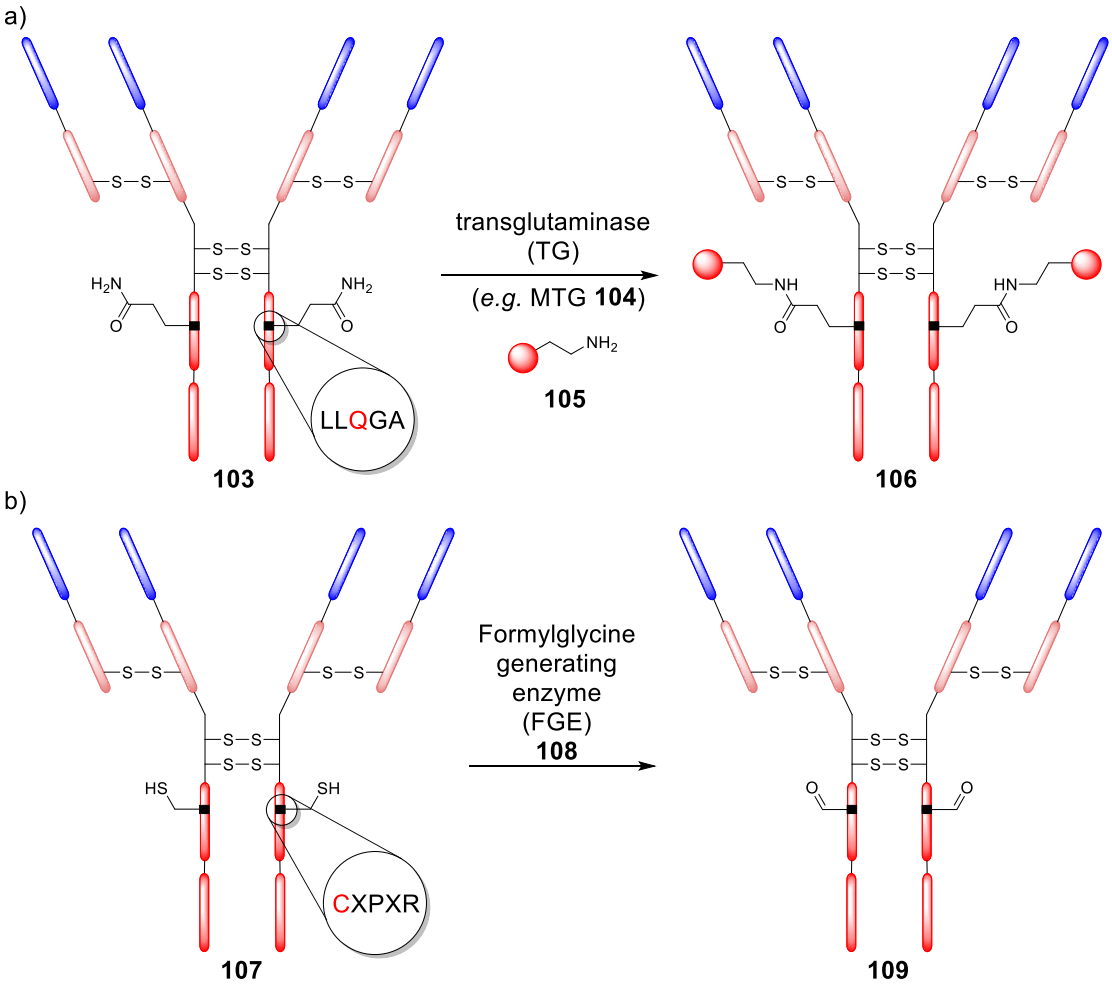

Scheme 16 – Enzymatic modification of engineered antibodies. a) transglutaminase reaction to convert gluatamine into a functional amide bioconjugate. b) formylglycine generating enzyme reaction with cysteine to form a reactive aldehyde moiety.

1.6.2.3 Native Antibody Modification

Whilst the aforementioned methods to synthesise ADCs offer incredible control over homogeneity and drug loading, manufacturability of these conjugates is a limitation. Generally, engineering antibodies, and utilising enzymes for modification require optimisation between platforms, increasing overall manufacturing costs. Therefore, combining modification of native antibody scaffolds (as utilised by the FDA approved ADCs) with site-selective homogeneous bioconjugation methods (for increased efficacy *in vivo*) may provide the most appealing route to synthesising ADCs.

One promising solution to the above utilises reagents that are capable of functionally re-bridging the cysteine residues liberated from reduction of the disulfide bonds of native antibodies.[145] This provides site-selectivity, a generally tolerated drug loading of 4 (as IgG1s contain only 4 solvent accessible disulfide bonds) and allows retention of the covalent stabilising bridge. Some of the most commonly employed disulfide bridging reagents include dibromomaleimides, bis-sulfones and DiBr PDs.[76,145–151] Work reported by Morais *et al*. explored the use of dibromomaleimides in the formation of irreversible antibody re-bridging agents. By varying the linker connecting the functional alkyne handle, a change in rate of hydrolysis was observed (Scheme 17).[80] The end result was an irreversible thiomaleic acid, bearing a terminal alkyne handle **110b**. Subsequent "click" reactions yielded an irreversibly modified antibody, in just over 1 h. However, this study is also representative of a general limitation surrounding maleimides in that hydrolysis is essential for serum stability. This study also highlights a more general limitation surrounding disulfide re-bridging which is that, in a multi-disulfide system, the disulfides may re-bridge in a non-native fashion (Scheme 17). The main by-product of this phenomenon is referred to as "half-antibody" (**112**) where the hinge region disulfides of the antibody are re-bridged in the intra-chain conformation (Scheme 17).

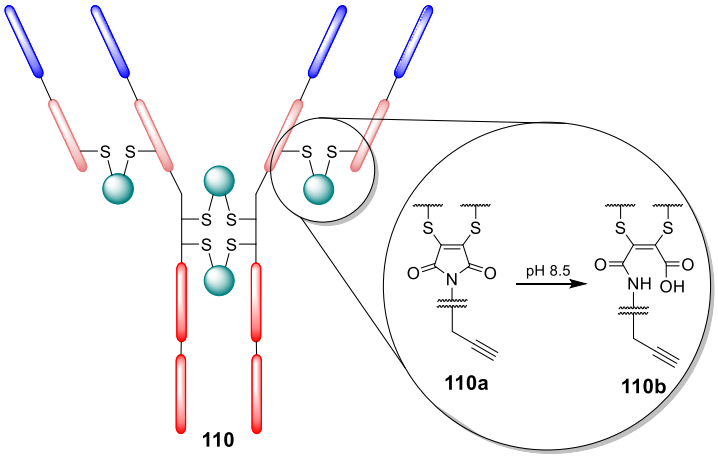

Scheme 17 – Hydrolysis of dithiomaleimide to dithiomaleic acid.[80]

DiBrPDs have shown a lot of promise as disulfide re-bridging agents; in addition to harbouring two functional handles for additional modularity and an increase hydrolytic stability, DiBrPDs have provided solutions to 2 main limitations associated with functional disulfide re-bridging: i) formation of the half-antibody isomer; and ii) limited scope for drug loading.[152] Antibodies that are functionally re-bridged with DiBr PDs generally display high levels of homogeneity (>80%) showing little disulfide scrambling.[74] This finding likely stems from reported *in situ* protocols where the re-bridging agent and the reducing agent are added instantaneously, achievable only through the PDs increased stability towards certain reducing agents.[153]

The two functional handles present on the PD scaffold have also been used to a great extent with regards to controlled drug loading, a rare feature associated with disulfide re-bridging agents. On a typical IgG1 antibody, for complete homogeneity, all 4 disulfide bonds must be

re-bridged, and with singularly functional re-bridging agents, this allows for convenient synthesis of ADCs with a DAR of 4 (**113**) (Figure 11). Indeed, DiBrPDs have also been used in this context to produce MMAE–trastuzumab conjugates, with a controlled drug to antibody ratio of 4. The resultant MMAE-trastuzumab conjugate was found to be stable in serum, and efficacious against cancer both *in vitro* and *in vivo*.[152] However, the scope for developing functionally re-bridged ADCs with an alternative to a DAR of 4 is somewhat limited. In light of this, work by Maruani *et al.* utilises DiBrPDs as dually functional re-bridging reagents **114a**, and so offer the option for a DAR of 8 (**114**) (2 drugs per conjugated PD, Figure 11).[74] Further work by Lee *et al.* has shown that a DAR of 2 is also achievable through re-bridging mechanisms.[154] By fully modifying the 4 disulfides of the IgG1 antibody trastuzumab with a bis-DiBr PD **115a** harbouring just one functional handle for every 2 DiBrPDs, synthesis of trastuzumab-fluorophore conjugates with a loading of 2 was achieved (**115**) (Figure 11). Thus, DiBr PDs to date have offered strategies for the formation of ADCs with a DAR of 2, 4 and 8.

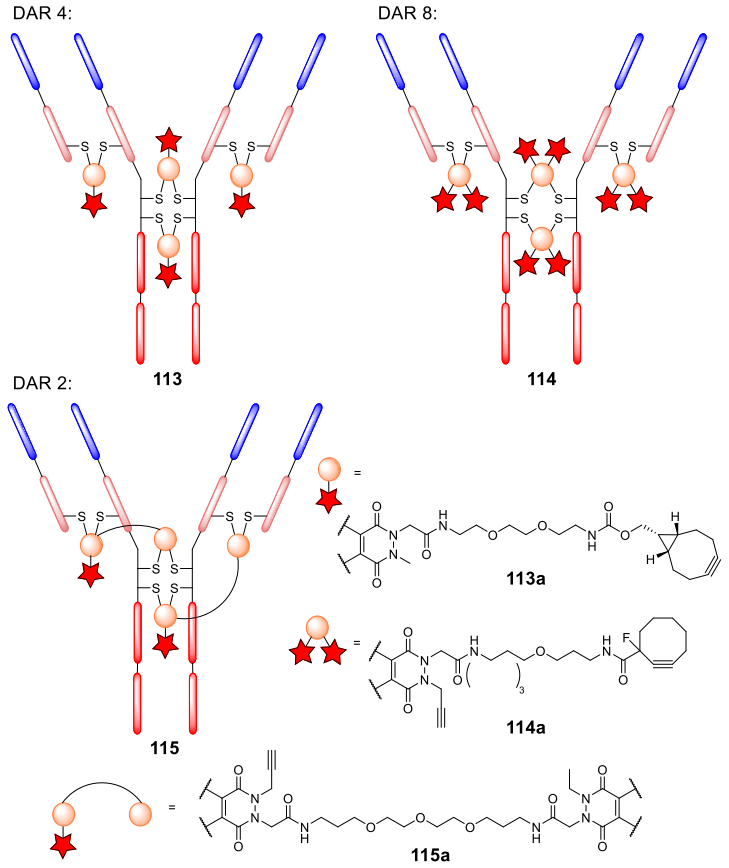

Figure 11 – Formation of IgG1 ADCs with DiBr PDs obtaining a DAR or 2, 4 and 8.[74,152,154] For DAR 2 species, functional moiety (red star) is independently interchangeable, and other and other disulfide pairs (*e.g.* Fab-Fab, Hinge-Hinge) may be functionally re-bridged.

More recently in the field of disulfide modification, work by Forte *et al.* shows that it is possible to use the disulfide residues of antibody fragments to anchor a lysine reactive group and promote a proximity induced cysteine to lysine transfer.[155] By reacting the thioester **117** with the cysteines liberated from the disulfide of trastuzumab fab **116**, a cysteine-thioester bridge **118** was formed (Scheme 18). Once the intermediate conjugate was subject to a pH switch (pH 8.4) to promote lysine attack of the thioester, transfer was observed to a single lysine in close proximity to the disulfide (K^{136}) (Scheme 18).[155] However, due to competing hydrolysis of the thio-ester bond prior to the proximity induced reaction with lysine, full transfer was not observed. Depending on the reagent employed, a loading of 1.5 (*i.e.* through modifying both cysteines individually) or 0.8 (*i.e.* through functional disulfide re-bridging) was obtained, resulting in conjugation yields of 75% and 80%, respectively.

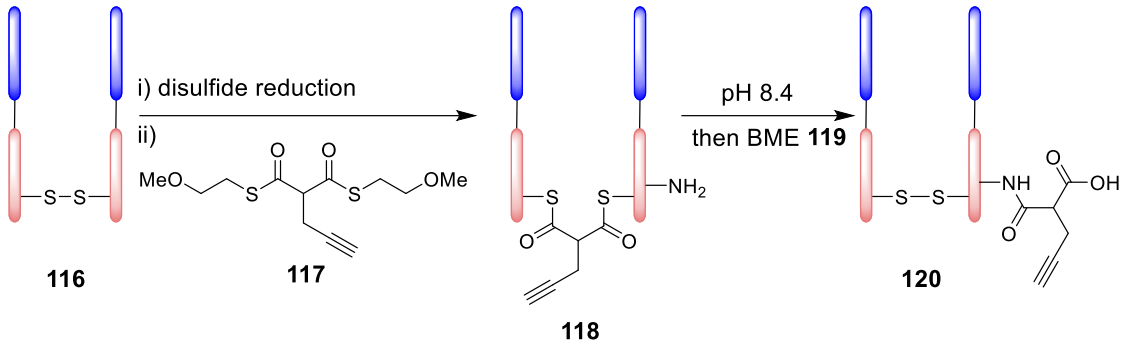

Scheme 18 – Cysteine to lysine transfer using a thioester bridge.[155]

1.7 Project Aims

This work aims to explore the development of next-generation chemical modification strategies aimed at synthesising superior bioconjugates, with particular focus on protein platforms that are derived from antibodies. The pyridazinedione (PD) motif proves to be a key component in the synthesis of next-generation antibody conjugates but is still considered to be an early technology. This thesis will explore four projects that surround the use of PDs in the context of protein modification:

1) Optimisation of current PD synthesis and bioconjugation - PD synthesis is often overlooked due to the small quantity of product required for protein modification. The formation of functionalised PD molecules in good yields is required for downstream large-scale reactions, and to make the technology more accessible to the research community. Furthermore, the conjugation protocol for reacting PDs with IgG1 antibodies will be addressed to maximise homogeneity of the resultant bioconjugates.

2) Appraisal of disulfide modified IgG1 antibodies in the context of secondary antibody function (Fc effector functions) – The full effect that disulfide modification has on base antibody functions is not yet understood. While the effect of disulfide modification on antigen binding and antibody affinity has been well defined in literature, little has been published on Fc interactions and secondary mechanisms that stem from these (*e.g.* ADCC and FcRn recycling). To this end, a library of disulfide modified conjugates will be synthesised and appraised in terms of Fc function and other key pharmacokinetic attributes.

3) Development of novel PD linker capable of tri-functionalisation – A novel PD linker will be developed with the aim of producing a modular platform for single cysteine tri-functionalisation. Adding three functions in combination *via* a single site on a protein would prove useful in the fields of combination therapies and theranostics. Further work will also be conducted to assess the effect that this novel functionalisation strategy has on the stability of this scaffold towards physiological thiols found in blood and early endosomal conditions.

4) Exploiting non-bromo PDs as reversible cysteine modification reagents – The Michael addition/ retro-Michael deconjugation equilibrium can be employed for a wide range of applications including kinase inhibition and cleavable linkers for targeted bio-therapeutics. Non-bromo (Br) PDs will be explored as reversible bioconjugation reagents to synthesise saturated PD-linked bioconjugates. Retro-Michael deconjugation of the saturated PD linker, and subsequent release of non-Br PD will be investigated to appraise the timescale of release, and how this moiety would likely behave in a therapeutic scenario (*i.e.* in the presence of blood thiols, or in the acidic tumour environment).

Chapter 2 Optimisation of Pyridazinedione (PD) Synthesis

2.1 Synthesis of Core Pyridazinedione Scaffold

To date, there are three popular synthetic techniques for synthesis of a dibromo PD moiety. The original technique, reported by the Caddick group, involved bromination of unsubstituted PD scaffold **123** (Scheme 19a).[71] Whilst this method is inexpensive and high yielding, the conditions are unfortunately incompatible with many potential *N*-situated orthogonal handles (*e.g.* alkynes). Consequently, attention turned towards the synthesis of a brominated species prior to addition of the functional hydrazines, to form the brominated PD scaffold **57**. Castañeda *et al.* reported a mild synthetic approach to PDs where a commercially available hydrazine **130** was reacted with a dibrominated carbamate group **129** (Scheme 19b).[156] This mild synthesis is employed when incorporating acid-sensitive groups into the PD scaffold. However, the most commonly utilised synthetic strategy is the reaction of dibromomaleic anhydride **133** with a deprotected difunctional hydrazine **130**, under acidic conditions (Scheme 19c).[153] By *bis*-protecting the hydrazine prior to alkylation, numerous hydrazine derivatives can be synthesised, enabling a diverse library of PD molecules to be synthesised. The use of the *tert*-butoxycarbonyl (Boc) protecting group, prior to acidic procedures, is desirable as this group is also removed under acidic conditions.

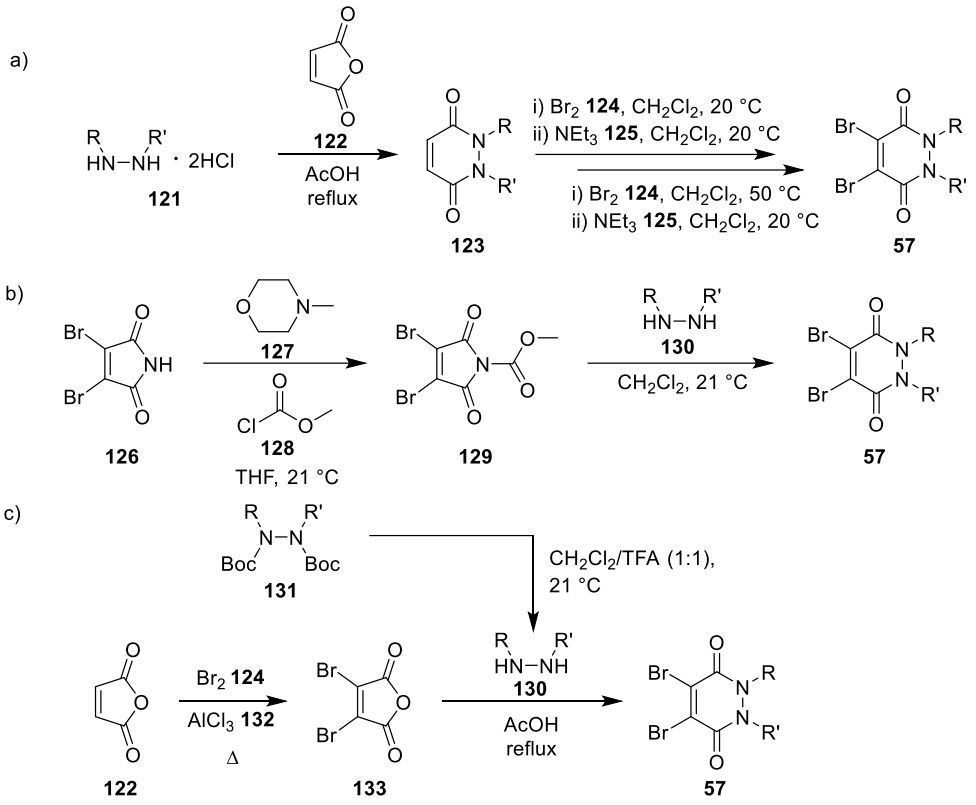

Scheme 19 – Current syntheses of the PD core scaffold **57**.[71,153,156]

The most popular synthetic route requires pre-formation of dibromomaleic anhydride **133** *via* bromination of maleic anhydride **122**, a dangerous reaction that requires high temperature and high pressure. Whilst dibromomaleic anhydride **133** may be purchased, it has very limited availability with suppliers and can be prohibitively expensive (£908/g through Sigma Aldrich). These routes also employ trifluoroacetic acid (TFA) deprotection of the hydrazine prior to the dehydration step with dibromomaleic anhydride, increasing costs and environmental impact, and decreasing overall atom efficiency (Scheme 19c).

2.1.1 Proposed Novel Synthesis of Pyridazinedione Core Scaffold

It was to be determined which synthetic route (basic or acidic) to a model dibromo diethyl PD **136** was best in terms of convenience, cost and yield. To investigate, modified conditions from the aforementioned syntheses were appraised with modifications summarised below:

a) Novel basic synthesis - Modified from the conditions reported by Castañeda *et al.*,[156] the commercially available diethyl hydrazine HCl salt **134** was desalted using A26 OH resin, and reacted with dibromo carbamate **129** (Scheme 20a).

b) Novel acidic synthesis - Adapted from the most current synthesis proposed by Lee *et al.*,[154] protected diethyl diboc hydrazine **137** was reacted with dibromomaleic anhydride **133** by refluxing in acetic acid (AcOH) (Scheme 20b). While traditionally the diethyl diboc hydrazine **137** is deprotected with TFA, it was found that the same acidic conditions required for PD condensation sufficed to form the diethyl hydrazine *in situ*.

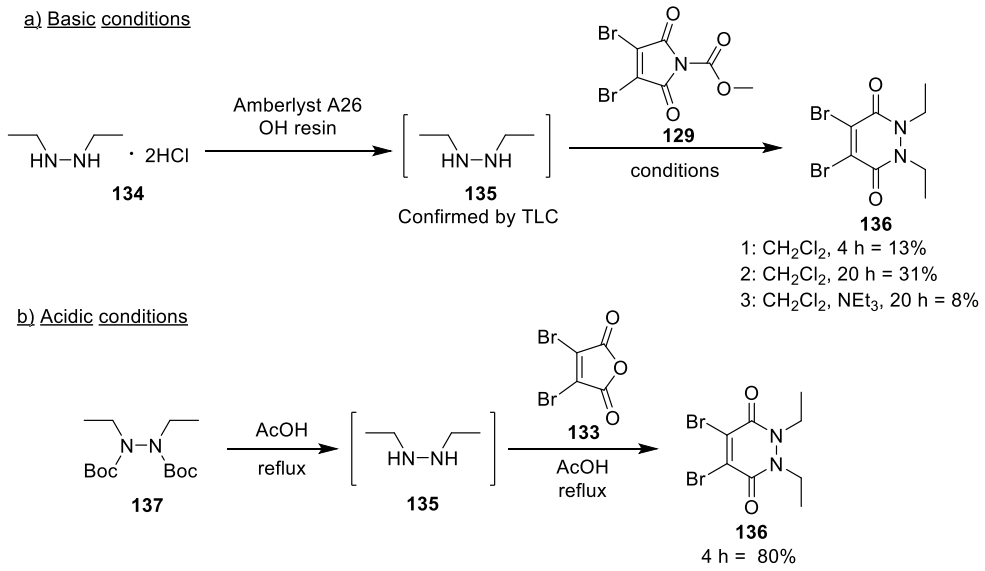

Scheme 20 – Comparison of mild and acidic PD synthetic procedures.

Acidic conditions were shown to provide the highest yields (Scheme 20). Furthermore, with the Boc deprotection step now accomplished *in situ,* step economy and overall yield was higher than previously reported (73% in literature).[154] The basic conditions tested provided lower yields than previously reported (57 % in literature).[156] This could possibly be explained by incomplete removal of HCl from the diethyl hydrazine salt, resulting in premature acid-mediated hydrolysis of dibromo carbamate **129**.

Synthesis of the core PD scaffold was then attempted from commercially available starting material dibromomaleic acid **138**. While this initially proceeded with a moderate yield of 65%, by avoiding synthesis of the dibromomaleic anhydride **133**, the reaction was preferred in terms of step economy and safety (Scheme 21). It was hypothesised that a 5-membered anhydride may be essential in the initial amide bond forming reaction required for pyridazinedione synthesis, and the dibromomaleic acid **138** may have been partially forming from the anhydride **133** under acid conditions *in situ*. To confirm, an analogous reaction was

carried out with dibromomaleic acid **138**, but where it was refluxed for 1 h in acetic acid prior to addition of the protected hydrazine **137**, *i.e.* theoretically forming dibromomaleic anhydride **133** *in situ* (Scheme 21b) This alteration provided diethyl dibromo PD **136** in a good yield of 82%, parallel to yields observed when using dibromomaleic anhydride (Scheme 20b).

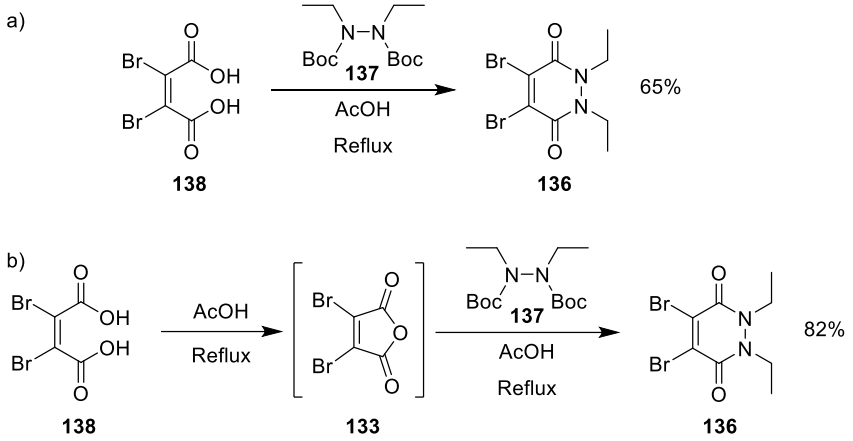

Scheme 21 – Comparison of acidic PD synthetic procedures, from dibromomaleic acid.

To confirm the *in situ* formation of dibromo maleic anhydride, a ^{13}C NMR study (in deuterated acetic acid) was attempted. This experiment showed almost full conversion of dibromomaleic acid **138** to dibromomaleic anhydride **133** after *ca.* 30 min under reflux (Figure 12). It can be assumed that for highest yields, preformation is required prior to addition of the protected hydrazine. As the deprotected hydrazine is exposed to acidic refluxing conditions for the first 30 minutes of the reaction, this may give rise to unexpected stability/volatility issues.

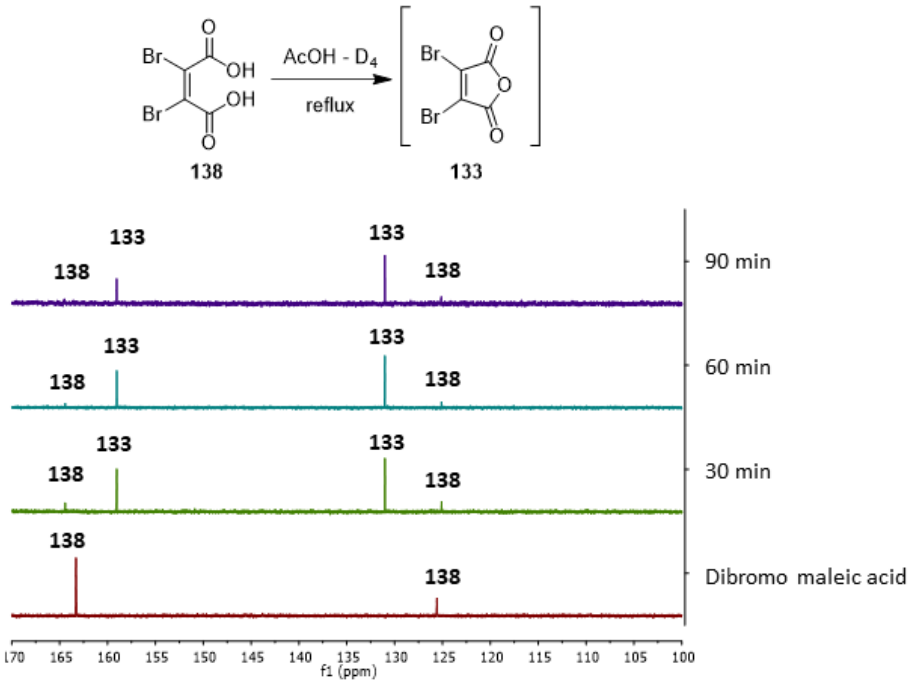

Figure 12 – *In situ* formation of dibromomaleic anhydride **133** tracked by ^{13}C NMR.

Through the findings reported above, a one-pot procedure is presented with an increase in step economy, safety, and overall yield (Scheme 22). This procedure was also shown to be reproducible (average yield of 82% from 5 experiments (80%, 80%, 86%, 84% and 82%)) and scalable (up to 15 mmol tested).

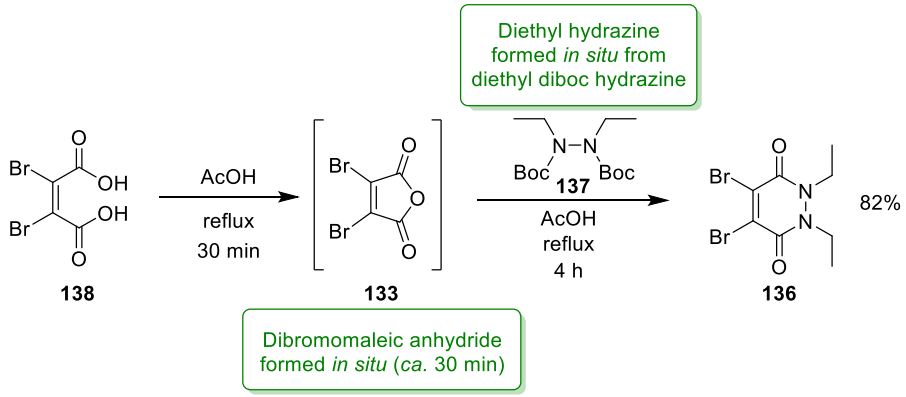

Scheme 22 – Optimal one-pot synthesis of core PD scaffold (dibromo diethyl PD **136**).

2.2 Synthesis of Pyridazinedione (PD)–Amide products

One of the most utilised reactions for adding functionality to functional re-bridging reagents is the reaction of an amine with an activated carboxylic acid.[74,152–154,157,158] The resultant

amide bond shows excellent stability *in vivo*, and a great deal of toxic payloads, fluorescent dyes, and imaging agents are commercially available as amine derivatives. Previously, carboxylic acid functionalised dibromo PDs **139** have been coupled with amines using a variety of activating reagents (Scheme 23).[74,152–154,157,158] Whilst this demonstrates a broad scope for forming functionalised dibromo PD reagents, it is also indicative of how capricious the amide formation is, *i.e.* for each new amine a different activating reagent was employed and specific reaction conditions developed. Therefore, the aim was to provide a synthesis that could be applied across a wide range of different functional amines for use in PD-amide synthesis.

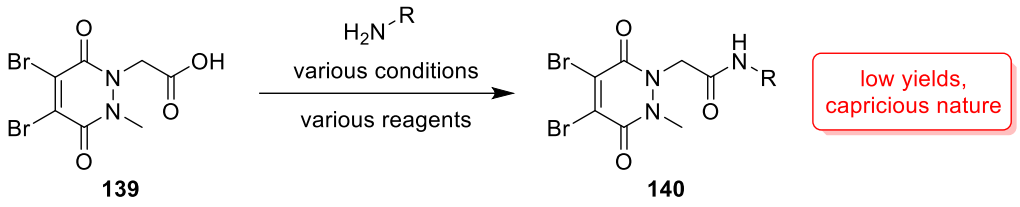

Scheme 23 – Typical coupling reaction using dibromo methyl acid (MetAc) PD **139**.

2.2.1 Development of Pyridazinedione-N-hydroxysuccinamide activated ester

To date, within the Chudasama group, methyl acid (MetAc) PD **139** has been favoured as a platform to synthesise amide coupling products **140** (Scheme 23).[74,152–154,157,158] Propargyl harbouring PDs have been previously very difficult to synthesise and are highly desired due to their use in copper "click" reactions to selectively add function to a protein, post-conjugation. MetAc PD **139** and propargyl amine **141** were subject to various coupling conditions to find a high yielding coupling reagent, that may produce high yields with other amines also. Despite using numerous industrially popular coupling reagents (DCC, CDI, PyBOP, HATU, EDC and TSTU) the PD-propargyl amide species **142** was not isolated. An *in situ* ^{1}H NMR study (in deuterated DMF) was designed to analyse: i) the activation and ii) the subsequent amide-coupling reaction of activated MetAc PD **139** with propargyl amine over time (Scheme 24). Whilst this NMR data was difficult to quantify due to overlapping ^{1}H NMR signals, it was evident that the MetAc PD **139** was being fully consumed during the activation step and many novel species were being formed instead of the expected activated acid species. These experiments therefore highlight an inherent issue stemming from the

activation of the MetAc PD **139**. It was hypothesised that intramolecular degradation may be arising from the reaction of the activated acid, with the carbonyl of the PD (*via.* a 5-membered cyclic intermediate).

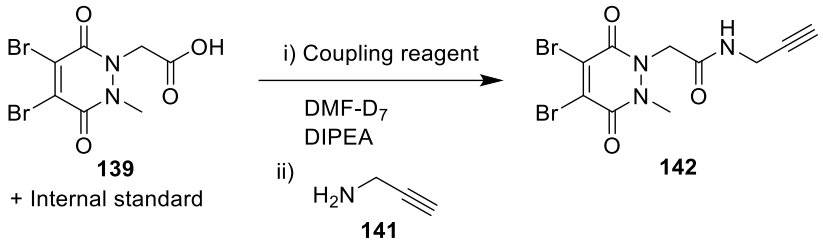

Scheme 24 – Reaction of dibromo MetAc PD **139** with various coupling reagents in the formation of a propargyl-harbouring PD **142**.

Synthesis of a PD *N*-hydroxysuccinimide activated ester **145**, was then attempted on the basis that it may provide a more stable and isolatable species that could participate in subsequent amide couplings. This reaction was also unsuccessful with all starting material PD **139** being consumed, again suggesting degradation of an activated species (Scheme 25).

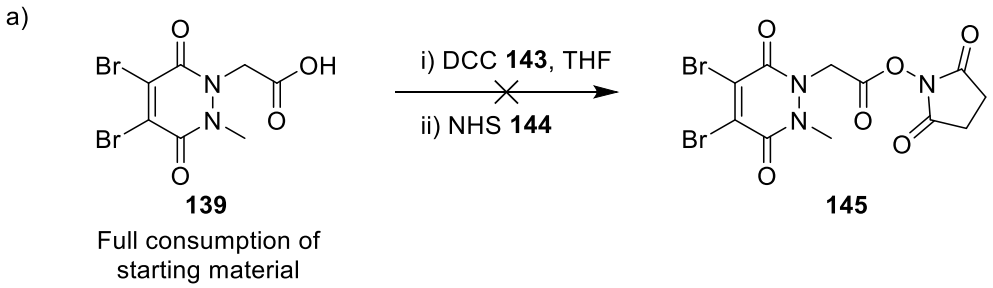

Scheme 25 – Coupling reaction of dibromo MetAc PD **139** with NHS **144** using DCC **143**.

In response, a methyl acid PD with a longer (propionic) acid chain was synthesised, to increase the distance between the reactive activated acid, and the PD core. The optimised synthesis for the core PD scaffold was applied to yield a dibromo methyl propionic acid (MetPAc) PD **151** with a good yield of 84% (Scheme 26a) Pleasingly, when applying analogous coupling conditions to the propionic derivative **151**, the propionic-NHS PD species **152** was isolated in a good yield of 72% (Scheme 26b). Additionally, the monobromo derivative of the MetPAc NHS ester PD **155** (for potential use in single cysteine modification) was synthesised in equally good yield (Scheme 26c).

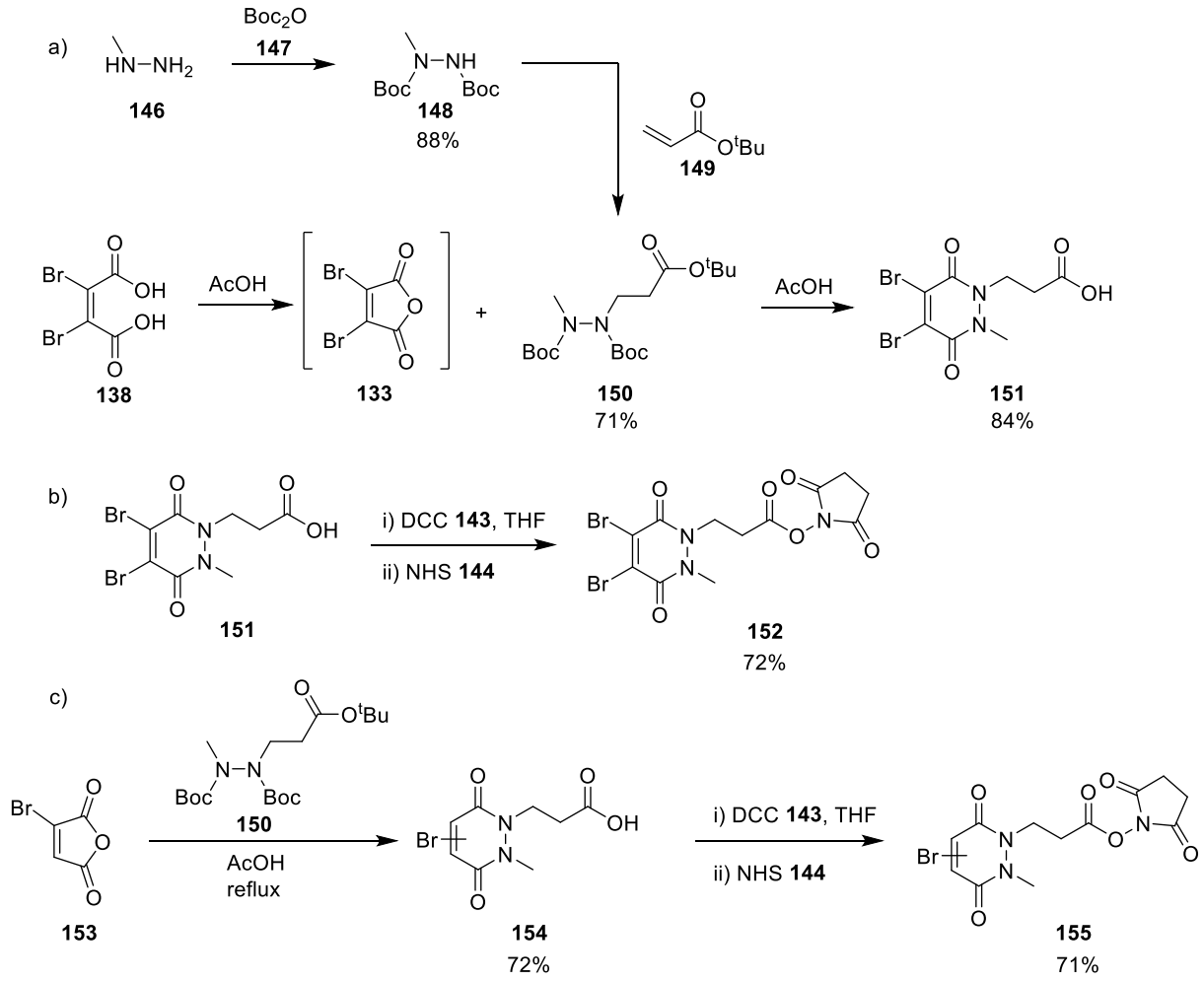

Scheme 26 – a) Overall synthesis and yield for methyl propionic acid (MetPAc) PD (**151**. b) Synthesis of activated dibromo PD-NHS ester **152**. c) Synthesis of activated monobromo PD-NHS ester **155**.

As expected, the activated MetPAc-NHS PDs (**152** and **155**) reacted well with many amines with varied functionality to form a library of amide containing functional PDs (**156a-f** and **157a-d**), in good yields (Table 4). As the most expensive reagent in functional PD synthesis is often the amine, this strategy offers a cheap and convenient alternative to current methods. A typical example of how this improved method is particularly useful is in the synthesis of dibromo PD **157f**. The published synthesis regarding the equivalent ethanoic acid PD is 8% compared to 78% when using the NHS ester.[154] Furthermore, the synthesis of the NHS ester PDs **152** and **155** were scalable (up to 1 g with similar yields) and were found to be stable for a minimum of 3 months when stored under argon and at 4˚C.

Table 4 – Yields obtained for functional amide-PDs from MetPAc NHS ester PD

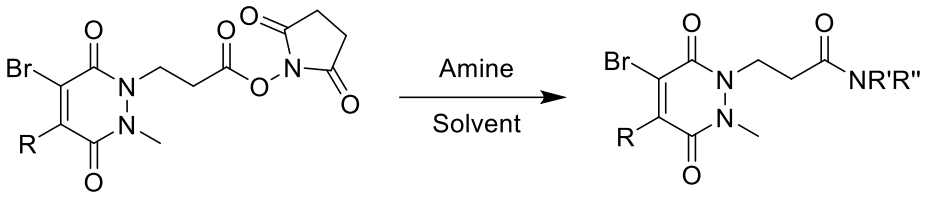

R	Solvent	Amine	Product No.	Yield
Br	CH_2Cl_2	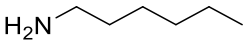	**156a**	78%
Br	CH_2Cl_2	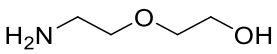	**156b**	71%
Br	MeCN	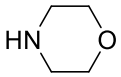	**156c**	76%
Br	MeCN	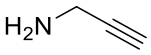	**156d**	87%
Br	MeCN	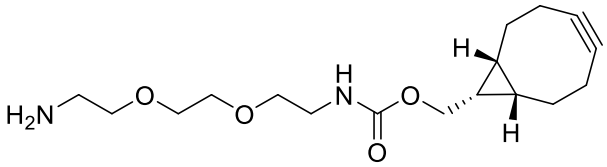	**156e**	72%
Br	MeCN	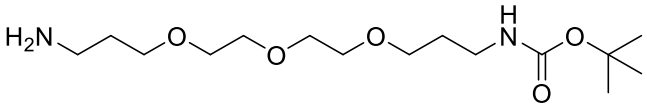	**156f**	78%
H	MeCN	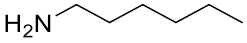	**157a**	99%
H	MeCN	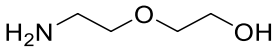	**157b**	64%
H	MeCN	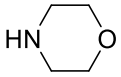	**157c**	77%
H	MeCN	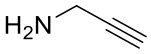	**157d**	95%

2.2.2 Testing Biocompatibility of Novel Amide-Pyridazinediones

Due to the complexity surrounding proteins, the slightest change to a small molecule may lead to consequences in bioconjugation reactions. This change may affect the stability of the

bioconjugate or the selectivity of the small molecule for a particular amino acid. One particular concern was the stability of the 3-carbon linker towards basic conditions, potentially producing the elimination products as illustrated in scheme 27.

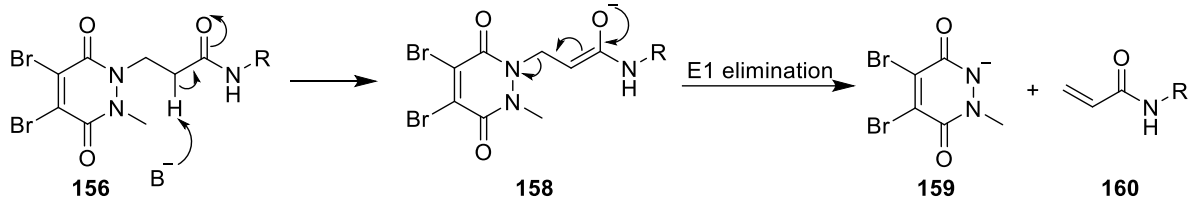

Scheme 27 – Proposed degradation mechanism of propionic acid PDs under basic conditions.

The elimination product containing the PD scaffold (**159**) is likely to be unreactive towards cysteine molecules, as this will likely form the enol tautomer (previously shown by Maruani *et al.*);[73] therefore, a study involving conjugation to the clinically relevant IgG1 antibody trastuzumab was carried out to highlight any discrepancies with the novel amide PDs. Here, after reducing the disulfides with TCEP **52**, the liberated thiols were re-bridged using PD **157e**. Bioconjugations were repeated at pH 8.0 at a range of temperatures (4 ˚C, 8 ˚C, 21 ˚C and 37 ˚C) and pH 9.0 also (at 4 ˚C). Reaction completion was confirmed by measuring UV absorption at 350 nm (unique to the PD scaffold). Pleasingly, all reactions yielded a fully modified conjugate with a PD to antibody ratio (PDAR) of 4, providing evidence of the stability of these conjugates in varied physiological conditions. Furthermore, these results aided in forming an optimised procedure for synthesising homogenous PD-trastuzumab conjugates.

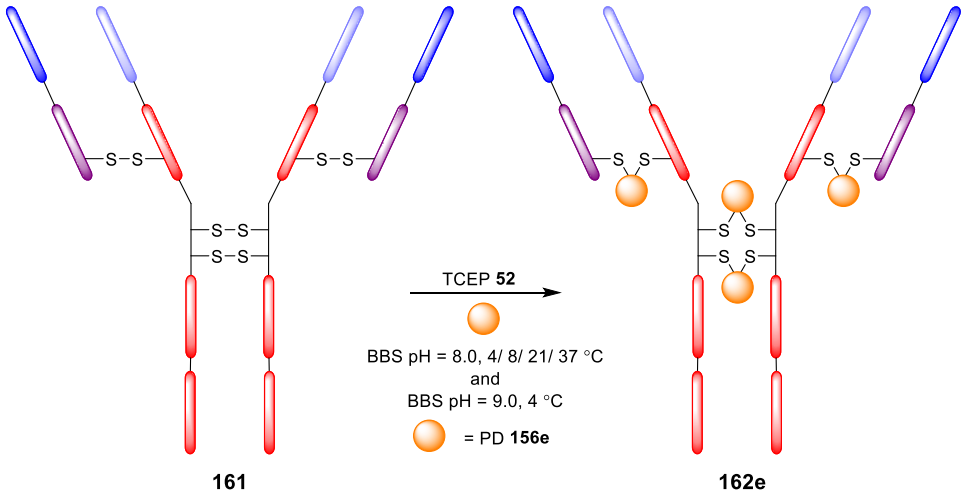

Scheme 28 – Reaction of trastuzumab **161** with PD **156e** under varying temperature and pH

Finally, the PDs **156a-e** were conjugated to trastuzumab under optimised conjugation conditions (developed by Dr. Daniel A. Richards.), to yield a range of functional PD-trastuzumab conjugates with an extremely high level of homogeneity with native re-bridging (>90 % by densitometry, see experimental for chapter 2) (Scheme 29).

Enzyme-linked immunosorbant assays (ELISAs) were carried out on the five novel PD-trastuzumab conjugates to assess any impact on trastuzumab-HER2 binding. This data suggests that modification using these conjugates has no effect on the ability of trastuzumab to bind its target antigen (see experimental for chapter 2).

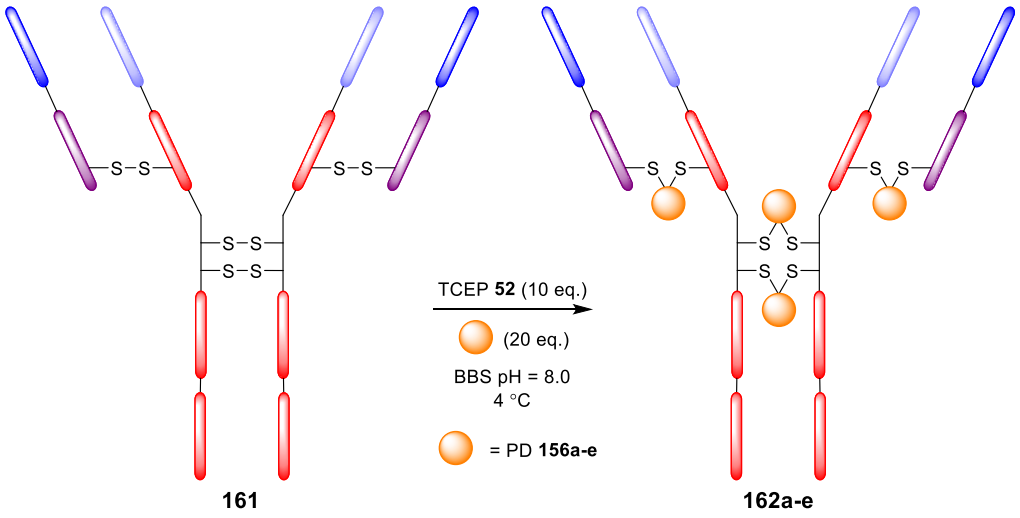

Scheme 29 – Optimised conditions for reaction of trastuzumab with PDs **156a-e**.

2.3 Conclusions

To conclude, this work describes several novel protocols that have been developed to improve the synthesis and subsequent application of functionalised DiBr PDs, a promising class of disulfide functional re-bridging reagents. During this work two pressing challenges have been addressed in their synthesis; the formation of the core scaffold, and subsequent amide-coupling reactions of this scaffold to enable chemical functionalisation. A one-pot synthesis of the core scaffold from readily available starting materials provides a safer and more efficient alternative to reported routes. Furthermore, a novel isolable NHS-ester enables a more general protocol for the derivatisation of this scaffold with a variety of amines. As the NHS ester PD has shown stability for many months under storage, it is envisaged that this synthetic route may provide a convenient branch point for the synthesis

of numerous amide-harbouring PDs. The capacity of these reagents to functionally re-bridge disulfide bonds was optimised on the humanised IgG trastuzumab, and a protocol was developed which grants high levels of homogeneity (>90 %) and a pyridazinedione-to-antibody ratio of 4.

Chapter 3 Influence of Disulfide Modification on Antibody Fc Activity

Bioengineering antibodies for effective human clinical use is a highly intricate process. Therefore, modifying antibodies with small molecules may have large consequences on protein function. Studies have already shown the importance of fully intact disulfide bonds on antibody stability.[159] Also, by using site-directed mutagenesis to replace a disulfide at the hinge and Fab regions of IgG1 antibodies, complement dependent cytotoxicity (CDC) and antibody-dependent cell mediated cytotoxicity (ADCC) can be reduced significantly.[160] For these reasons, many consider modifying the disulfide bonds of IgG1 antibodies high risk, as the full extent on antibody function is as yet unknown.

In the case of trastuzumab-HER2 binding, it has been shown that re-bridging the disulfides on full IgG1 antibodies has little to no impact on variable region binding to a target antigen.[74] Efforts to understand variable region binding of ADCs is crucial for two reasons: i) affinity towards a target antigen will likely determine the selectivity and efficacy of the ADC (*i.e.* a decrease in affinity may result in more off-target effects of the therapeutic); ii) variable region binding of the target antigen often initiates internalisation of the ADC, which is crucial for delivery of the cytotoxic payload into target cells. However, it should be noted that antibodies are complex immunoproteins that host a range of useful functions initiated by constant region-antigen binding. More specifically, the Fc region of the antibody has numerous binding sites that are responsible for binding many different antigens (Table 5). It is clear that these functions would be highly regarded within ADC therapy, however little is known about how disulfide modification impacts clinically relevant Fc region interactions.

Table 5 – Summary of Fc receptors and associated function.[89–91]

Fc receptor	Affinity	Expressed by	Effect of binding
FcγRI (CD64)	High	Monocytes, macrophages, neutrophils	Phagocytosis, cell activation
FcγRIIA (CD32)	Low	Platelets	Phagocytosis
FcγRIIB1 (CD32)	Low	B cells Mast cells	Inhibition of: phagocytosis, cell activation
FcγRIIB2 (CD32)	Low	Macrophages dendritic cells	Phagocytosis, inhibition of cell activity
FcγRIIIA (CD16a)	Low	NK cells	Initiates ADCC
FcγRIIIB (CD16b)	Low	Neutrophils	Ca^{2+} mobilisation
FcRn	High	Neutrophils Dendritic cells	Stabilisation of IgG (increased half-life), Neonatal function

This work explores the influence of disulfide modification on IgG1 Fc activity/interactions. A comparison will be made between the two main proposed strategies for disulfide modification (*i.e.* cysteine capping vs. cysteine re-bridging) to appraise what is a more optimal conjugation strategy for retaining IgG1 Fc interactions. To quantify any observable effect of disulfide modification on Fc activity, a range of trastuzumab conjugates will be synthesised to display a range of inter-chain disulfide integrity. These conjugates will then be appraised to quantify the effect on Fc-specific interactions (*i.e.* FcRn and CD16a binding) and non Fc-specific attributes (*e.g.* thermal stability/aggregation).

3.1 Synthesis of Disulfide Modified Trastuzumab Conjugates

For a comparative model, the IgG1 antibody trastuzumab **161** was selected as a good representation of an IgG1 platform that has been chemically modified for increased clinical benefit (*e.g.* as observed in the FDA-approved ADCs Kadcyla™ and Enhertu™).[164,165] Trastuzumab is well defined in terms of reactivity and exhibits both internalisation (through HER2 binding) and ADCC cell killing mechanisms.[166] Conjugation reagents DiBr PDs and

dibromo maleimides were employed as re-bridging agents as there are already several reported cases of quantitative modification of trastuzumab using these moieties.[80,152] The maleimide scaffold was employed for single cysteine modification as this is the well-defined conjugation strategy currently employed in the synthesis of FDA approved ADCs Adcetris™, Polivy™, Padcev™ and Enhertu™.[127,165,167,168] For fair comparison between antibody conjugates, all cysteine and disulfide reactive reagents were designed to harbour similar *N*-functionalities (*i.e.* a terminal alkyne to allow for subsequent modification, if required).

To highlight the importance of the interchain disulfide linkage in IgG1 antibodies, a range of trastuzumab conjugates were designed, each with differing levels of interchain disulfide integrity and homogeneity (Figure 13):

1) Natively re-bridged trastuzumab (**163**) – Antibody re-bridged in a native conformation to provide highly homogenous antibody conjugates with near fully intact interchain disulfide connectivity (Figure 13a).

2) Disulfide scrambled trastuzumab (**164**) – Antibody re-bridged in a non-native conformation to provide heterogenous antibody conjugates with an abundance of "half-antibody". This model represents intact light chain-heavy chain disulfides, but the absence of many heavy chain-heavy chain disulfide linkages (Figure 13b).

3) Thiol capped trastuzumab with maleimide-to-antibody ratio of 4 (MAR 4) **165** – Partial interchain disulfide bond reduction (average of 2) and subsequent cysteine residue capping provides heterogenous antibody conjugates with an average of 2 native interchain disulfide linkages intact. As reducing agents cannot distinguish between hinge region or Fab region disulfides, the 2 intact linkages can exist as light chain-heavy chain or heavy chain-heavy chain cross links (Figure 13c).

4) Thiol capped trastuzumab with maleimide-to-antibody ratio of 8 (MAR 8) **166** – Full interchain disulfide reduction and subsequent cysteine residue capping provides antibody conjugates with no interchain disulfide linkages intact (heavy and light chain only) (Figure 13d).

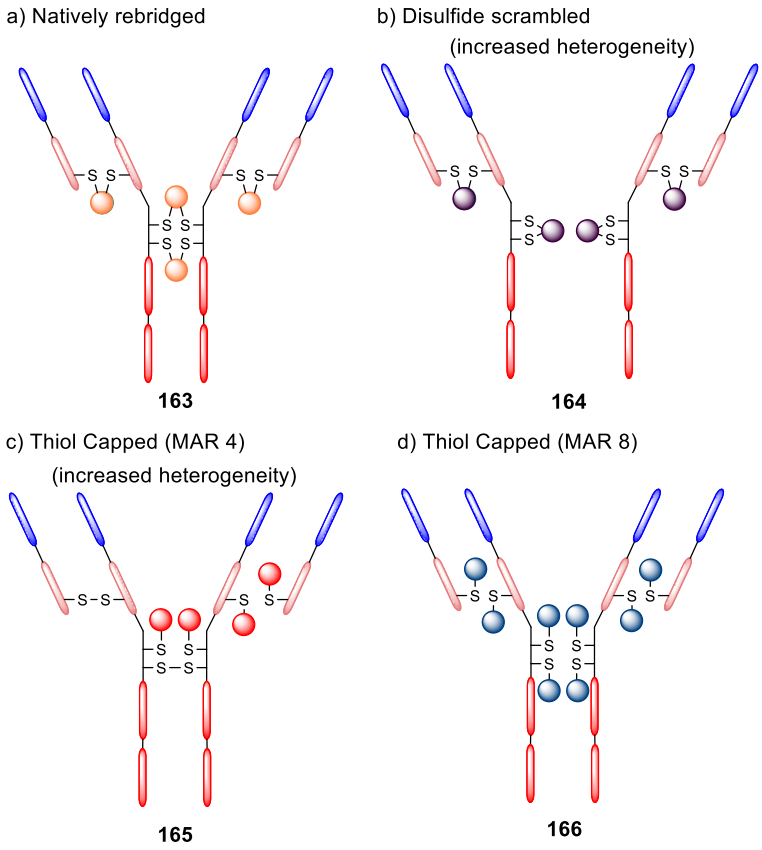

Figure 13 – Ideal structures of trastuzumab bioconjugates for Fc binding analysis.

For the natively re-bridged species **163**, DiBr PDs **167** and **174** were selected as suitable inexpensive candidates to form alkyne-bearing antibody conjugates. DiBr PDs **167** and **174** also provide an option to install an amide group within the *N*-directed linker for fair comparison between antibody conjugates. Conjugation with DiBr PDs has previously been reported to achieve consistently high levels of homogeneity.[169] It was found that an *in situ* protocol (TCEP and PD added at once) at 4 ˚C overnight provided the antibody conjugate **168** with high levels of homogeneity (~90% by densitometry) (Figure 14ai and 14b).

To form a heterogenous re-bridged trastuzumab conjugate **164**, a dibromo maleimide **175** and a novel PD derivative – dichloropyridazinedione (DiClPD) **169** were tested. Next generation maleimides have previously been shown to consistently provide DAR 4 conjugates, but on occasion, provide low levels of homogeneity depending on the functional handle. Whilst antibody-conjugates synthesised using the dibromo maleimide **175** provided more half-antibody than the DiBr PD equivalent **174**, the novel DiCl PD (**169**) along with a newly adapted conjugation protocol provided the antibody conjugate **170** that showed an exceptional level of "half-antibody" (~55% by densitometry) (Figure 14aii and 14b). In

previous reports, it has been hypothesised that the liberated cysteines from disulfides could have a greater tendency to re-bridge in a non-native conformation if fully reduced prior to addition of the re-bridging reagent.[153] Therefore, the interchain disulfides of trastuzumab were reduced for 2 h prior to the addition of a re-bridging agent. In addition, a less reactive re-bridging agent was sought, to increase the thiol residency times after reaction of one thiol (Figure 14aii).

For the formation of the thiol capped (MAR 8) conjugate **166**, an excess of reducing agent TCEP **52** (25 eq.) was added followed by an excess of *N*-propargyl maleimide **171** (25 eq.) which successfully formed the trastuzumab-maleimide species **173** (Figure 14aiv). For the synthesis of the thiol capped (MAR 4) species **165**, only 2 eq. of reducing agent were added and left to react until completion overnight, before addition of excess maleimide (25 eq.) to form the trastuzumab-maleimide species **172** (Figure 14aiii). To confirm a MAR of 4 (in addition to reduced MS analysis), a copper assisted azide−alkyne cycloaddition (CuAAC) reaction with AlexaFluor^{TM}-488 azide was carried out on the resultant conjugate to confirm an average fluorescent loading of 4 (AlexaFluor-488) by UV−vis spectroscopy (Figure 14c).

For further analysis, it is important to compare only chemically similar bioconjugates. Where more than one conjugate was made, only bioconjugates harbouring the propargyl group linked directly to the maleimide/PD handle were compared in the K_D analysis (*i.e.* conjugates synthesised using PDs **167** and **169,** and maleimide **171**).

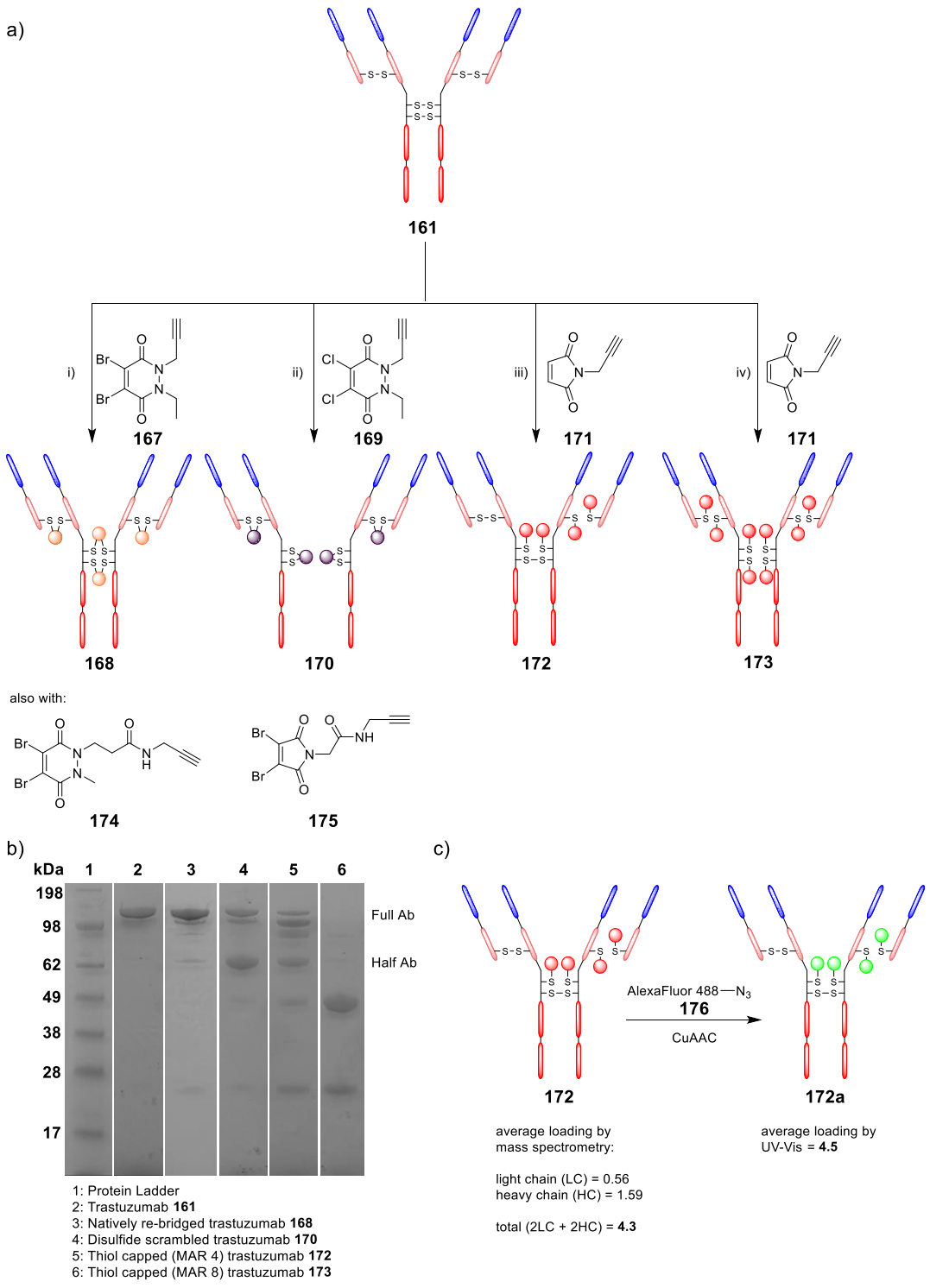

Figure 14 – a) Synthesis of trastuzumab conjugates, structures of most abundant species shown. All steps carried out in BBS pH 8.0, 0.25 mM EDTA: i) ethyl alkyne DiBr PD **167** (20 eq.), TCEP **52** (12 eq.), 4 °C, 16 h; ii) step i) TCEP **52** (25 eq.), 37 °C, 2 h., step ii) ethyl alkyne DiCl PD **169** (25 eq.), 37 °C, 4 h; iii) step i) TCEP **52** (2 eq.), 37 °C, 16 h., step ii) propargyl maleimide **171** (25 eq.) 21 °C, 16 h; iv) step i) TCEP **52** (25 eq.), 37 °C, 2 h. ii) propargyl maleimide **171** (25 eq.) 21 °C, 16 h.; b) SDS PAGE analysis of trastuzumab **161** and trastuzumab conjugates **168, 170, 172** and **173**; c) loading analysis of thiol capped (MAR 4) trastuzumab conjugate **172** by mass spectrometry and UV-Vis.

3.2 Developing a Platform for FcRn and CD16a appraisal

To obtain quantitative data on the Fc interactions of trastuzumab conjugates, bio-layer interferometry (BLI) experiments were conducted using Octet™ equipment. BLI is an optical tool used for real-time molecular interaction analysis and can be used to obtain real-time kinetic measurements.[170] By passing white light through a sensor, and analysing continuous interference patterns as proteins associate/dissociate (*i.e.* extending or shortening the bio-layer), it is possible to obtain data regarding the amount of substance bound. Kinetic measurements can then be determined by analysing the precise amount of time taken for a substance to bind a receptor.

In the case of CD16a binding, there were many complications in selecting a comprehensive binding assay to provide a K_D value for the trastuzumab control. These issues mainly stemmed from the presence of non-specific binding (NSB) resulting from the antibody/antigen binding to the BLI sensor as well as the respective antigen/antibody. As summarised in table 6, a variety of BLI sensors, buffers and blocking agents were employed to obtain a platform which provided a K_D value for trastuzumab. Finally, using a biotinylated CD16a, streptavidin sensor and HBS-EP+ buffer (containing EDTA to prevent oxidation) a K_D value of 1.75×10^{-7} M was obtained for trastuzumab which matched literature values obtained using surface plasmon resonance (SPR) (lit. 2.27×10^{-7} M).[171]

Table 6 – Conditions and results for Octet™ binding analysis.

Sensor	Buffer	Loading	Binding	Blocking (BSA/Tween)	Result
Ni-NTA	HBS-P+	CD16a	Herceptin	No	× NSB
Ni-NTA	HBS-P+	CD16a	Herceptin	Yes	× NSB
Protein L	HBS-P+	Herceptin	CD16a	No	× NSB
Anti-Fab	HBS-P+	Herceptin	CD16a	No	× NSB
Streptavidin	HBS-P+	Herceptin	CD16a	No	× NSB
Streptavidin	HBS-EP+	Blank	Herceptin/ CD16a	No	✓ No NSB
Streptavidin	HBS-EP+	CD16a (biotinylated)	Herceptin	No	✓ Positive result

*NSB = non-specific binding

As the BLI analysis between trastuzumab and CD16a is a novel assay without prior validation, experiments were conducted using a range of concentrations (666–5.02 nM) and a global analysis was used accounting for a minimum of 4 concentrations. Additionally, most consistent results were obtained when loading sensors with 0.5 µg/mL of biotinylated CD16a. K_D values were calculated assuming a 1:1 antibody-antigen interaction, allowing for a 60 sec. association and a 5 sec. dissociation (Figure 15).

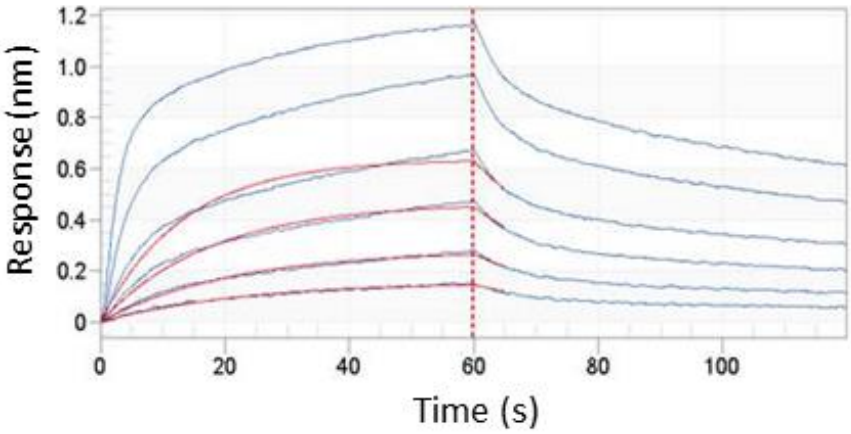

Figure 15 – BLI results of CD16a (0.5 µg/mL with trastuzumab (666 – 5.02 nM) using global (1:1) fit with 60 sec. association and 5 sec. dissociation.

Adopting a similar strategy, FcRn assay data was obtained by loading 1.0 µg/mL biotinylated FcRn onto a streptavidin sensor. However, due to the complex physiology behind FcRn binding there were many deviations from the previously developed assay. Firstly, as FcRn binding occurs in the early endosome (pH 6.0) and release occurs in pH 7.4, the binding assay allowed for K_{on}/K_{off} at pH 6.0 and K_{off} at pH 7.4. In addition, as more than one FcRn can bind to an antibody, global analysis using a range of concentrations was not feasible (*i.e*. leaving a suitable concentration range results in a change in K_D). FcRn receptors, as observed *in vivo*, are capable of being regenerated – post binding. Therefore, by using Tris-based buffer (pH 8.0) and neutralisation buffer (pH 7.4) the FcRn was regenerated 3 times before discarding.

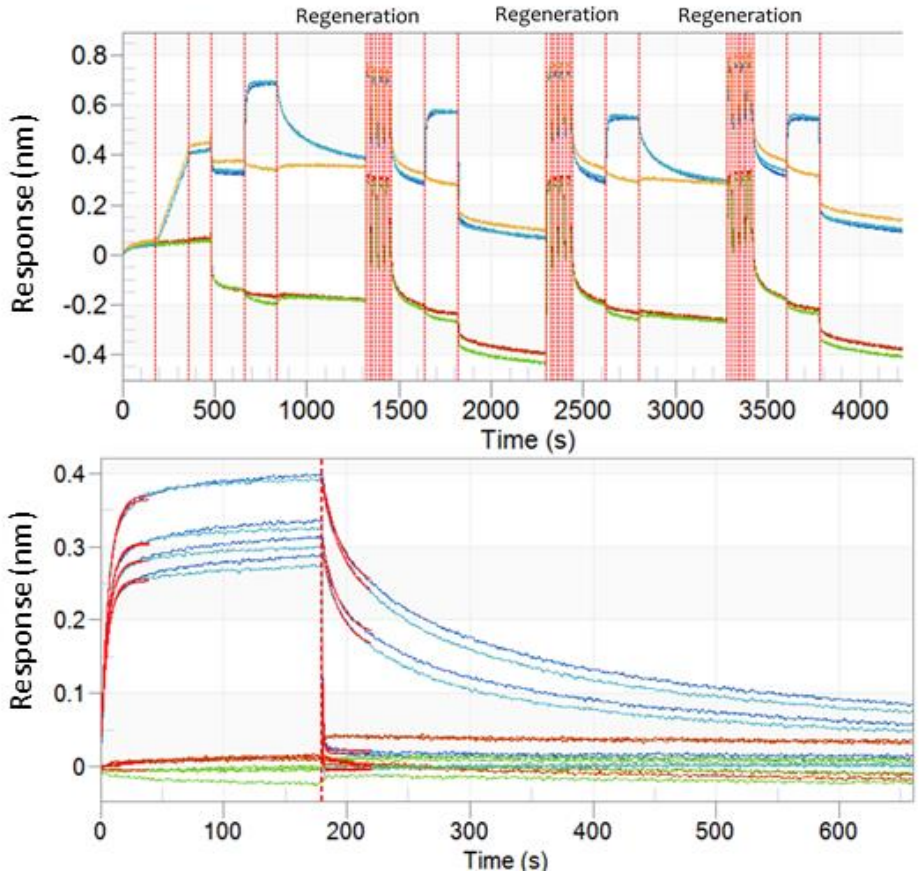

Figure 16 – BLI results of FcRn (1.0 µg/mL) with trastuzumab (200 nM) and using a partial fit with 60 sec. association and 60 sec. dissociation.

3.3 CD16a Appraisal of Trastuzumab Conjugates

3.3.1 Trastuzumab – CD16a BLI Assays

Pleasingly, K_D binding analysis showed that there was no significant difference in CD16a-trastuzumab binding affinity when all disulfides are re-bridged natively (K_D = 175 nM and 278 nM for trastuzumab **161** and natively re-bridged trastuzumab **168** respectively (Figure 17)). Surprisingly, the thiol capped (MAR 8) trastuzumab conjugate **173** exhibited a K_D of 1.84 µM – a factor of 10 higher than native trastuzumab, showing a significant decrease in binding affinity towards CD16a. The disulfide scrambled conjugate **170** also appeared to yield a similar K_D to the natively re-bridged trastuzumab **168**, while the partially capped trastuzumab **172** afforded a marginally higher, yet reproducible, K_D (Figure 17). These results highlight the native disulfide re-bridging strategy to have little to no effect on CD16a K_D

values. Furthermore, the general trend observed between these conjugates suggests intact IgG1 interchain covalent links may play a significant role in IgG1-CD16a kinetics.

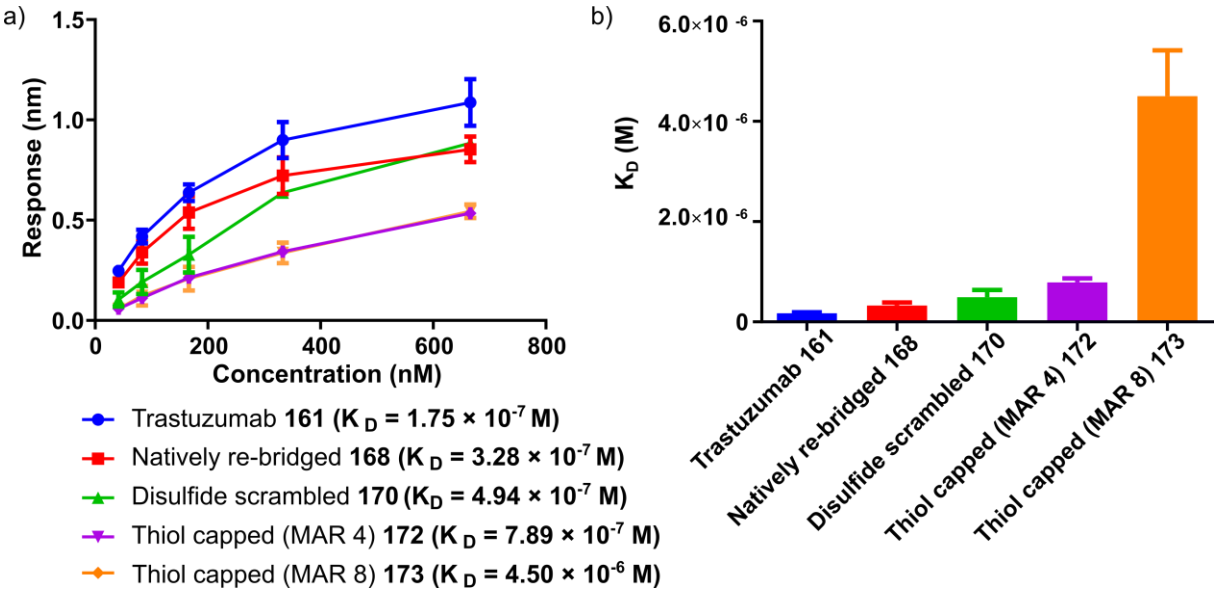

Figure 17 – Trastuzumab – CD16a BLI kinetics and ADCC cell kill assay summary. a) Maximum response at varying concentrations of trastuzumab (**161**)/trastuzumab conjugates (**168, 170, 172** and **173**). b) Average trastuzumab (**161**)/trastuzumab conjugates (**168, 170, 172** and **173**)– CD16a K_D values.

3.3.2 Antibody-Dependant Cell-Mediated Cytotoxicity (ADCC) Assays

To confirm whether the observable difference in CD16a K_D values would reflect a change in the effector function of trastuzumab, the synthesised conjugates were also subjected to an ADCC cell-kill assay (conducted by Dr Siobhán Leonard). HER2 expressing BT-474 cells (*i.e.* complementary to trastuzumab) were first incubated in labelling buffer (to allow uptake of Eu^{3+}) and were then incubated with each of the synthesised conjugates at 4 °C to allow for antigen binding but prevent internalisation of the construct. NK-92 cells mutated to stably express CD16a on the cell surface (NK-92 CD16a+) were then added to the solution of trastuzumab conjugates and BT-474 cells. After 30 minutes of incubation, cell death was calculated by analysing Eu^{3+} release from cells. Surprisingly, the conjugate repeatedly showing the least cell kill was the disulfide scrambled species **170**. As this did not align with the trends observed in CD16a kinetics, it was anticipated that this type of modification confers an unfavourable change in IgG1 interactions outside of the tested kinetic model

(immobilised CD16a-trastuzumab). Despite a significant increase in K_D for thiol capped (MAR 8) trastuzumab **173**, this conjugate and other tested species showed little decrease in ADCC activity (Figure 18). While kinetic data is not always a good representation of what to expect in ADCC assays,[172] it is evident that all types of disulfide modification affected either trastuzumab CD16a kinetics (thiol capped conjugates **172** and **173**), or ADCC activity (disulfide scrambled conjugate **170**) with the exception of the natively re-bridged species **168**.

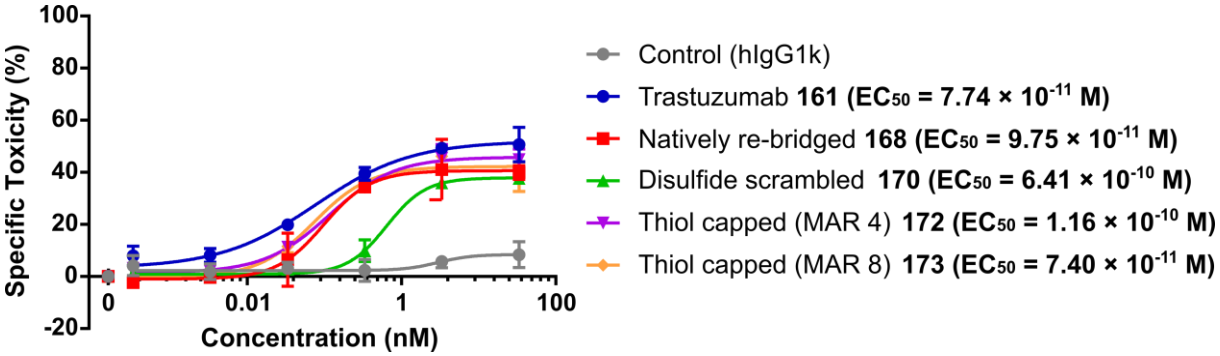

Figure 18 – ADCC dose response curves for trastuzumab (**161**)/trastuzumab conjugates (**168, 170, 172** and **173**) with EC_{50} values.

3.4 FcRn Appraisal of Trastuzumab Conjugates

The library of trastuzumab conjugates were subject to the aforementioned FcRn binding assay. However, all conjugates seemed to provide similar K_D values suggesting disulfide modification does not affect FcRn binding of trastuzumab across the conjugation methods tested (Figure 19). While it is acknowledged that the thiol capped conjugate is marginally higher the other tested conjugates, this change is not considered significant enough to justify further *in vivo* experiments to further investigate the effects associated with FcRn binding.

However, this data helps to conclude that disulfide interactions are not integral to all Fc binding regions. This suggests the results indicating a disulfide–CD16a relationship is likely to be attributed to a specific interaction between disulfides and the residues localised to the CD16a binding region. This therefore disproves that the general tertiary structure of the Fc

region is affected by disulfide modification, in which a global effect to all Fc binding sites would be observed.

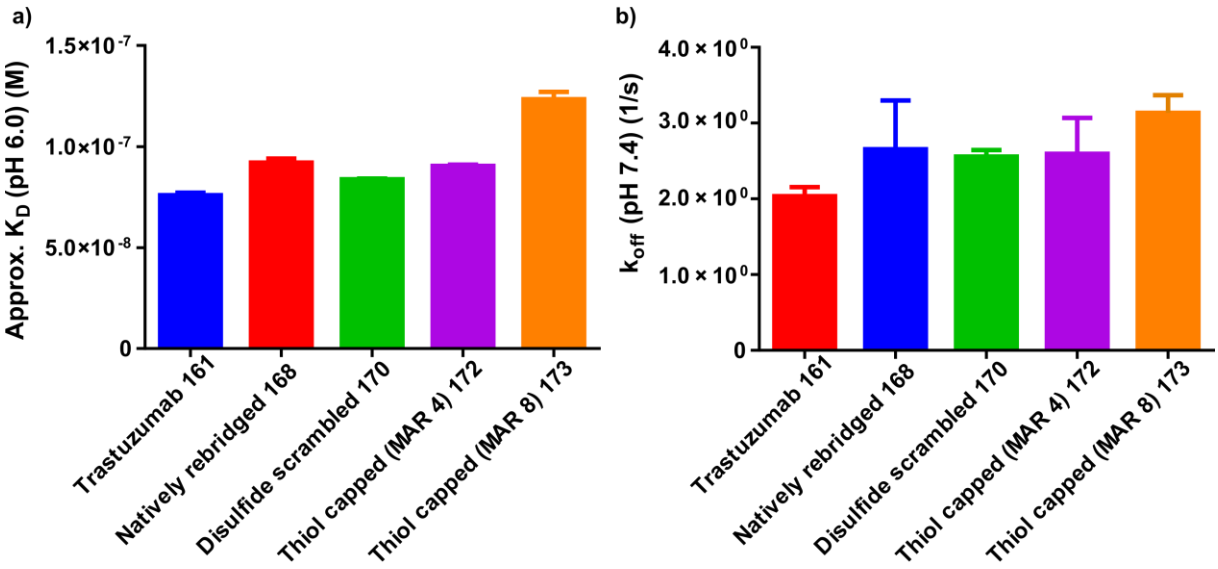

Figure 19 – Trastuzumab–FcRn BLI assay results summary. (a) Average approximate K_D values obtained at pH 6.0. (b) Average k_{off} values obtained at pH 7.4.

3.5 General Biophysical Appraisal of Trastuzumab Conjugates

In addition to the results on IgG1 Fc function, a general biophysical profile was sought for each of the synthesised conjugates. In addition to native trastuzumab **161**, the disulfide modified conjugates (**168, 170, 172** and **173**) were compared in terms of antigen-binding, thermal stability, and aggregation. These experiments were designed to provide a deeper understanding of the total influence that interchain covalent linkage integrity may have on other relevant antibody characteristics.

3.5.1 Thermal Stability Analysis of Trastuzumab Conjugates

In a comparative experiment, melting temperatures (*i.e.* T_m values) were calculated for each of the trastuzumab conjugates by conducting a thermal shift assay. Trastuzumab conjugates were incubated with SYPRO™ orange, a dye that is used to track the denaturation of proteins.[173] The fluorescence of SYPRO™ orange is strongly quenched by water and the

compound binds non-specifically to hydrophobic surfaces. When a protein is denatured, SYPRO™ orange binds the newly exposed hydrophobic regions resulting in an increase in fluorescence due to the exclusion of water.

Generally, a trend in intact interchain covalent links was established as the thiol capped conjugates **172** and **173** showed a linear decrease in T_m. Pleasingly, the natively re-bridged conjugate **168** had minimal change to the T_m, when compared with the native antibody **161** (Table 7). Unexpectedly, the disulfide scrambled conjugate **168** had a comparable T_m to the thiol capped conjugate (MAR 4) **172** despite having a large proportion of the interchain disulfides correctly re-bridged (as **170** exists as a mixture of conjugates). This may be indicative of an unstable conformation adopted by re-bridging the IgG1 disulfides in a non-native conformation.

Table 7 – Summary of thermal shift assays melting temperature (T_m) values.

Trastuzumab Conjugates	**Total T_m (51–92 ˚C) (˚C)**
Trastuzumab 161	85.3 ± 0.06
Natively re-bridged trastuzumab 168	84.6 ± 0.62
Disulfide scrambled trastuzumab 170	81.8 ± 0.24
Thiol capped (MAR 4) trastuzumab 172	81.7 ± 0.08
Thiol capped (MAR 8) trastuzumab 172	78.5 ± 0.49

3.5.2 Aggregation Analysis of Trastuzumab Conjugates

Approximate masses and polydispersity of the conjugate samples were compared with the intention of quantifying the amount of aggregate present, after bioconjugate synthesis. Size-exclusion chromatography multi-angle light scattering (SEC MALS) analysis was employed for this purpose. By separating species based on size and subsequently determining approximate masses/polydispersity through light scattering, it is possible to identify a proportion of the bioconjugate sample that is considered to have aggregated. All tested conjugates yielded an insignificant percentage of aggregate (Figure 20). The disulfide scrambled conjugate **170** showed the most aggregation, with 2% of the mass being polydisperse, although this level of aggregate is not thought to be significant enough to

affect antibody function (Table 8). Notably, natively re-bridging the disulfide residues showed no impact in terms of tendency to aggregate (Table 8).

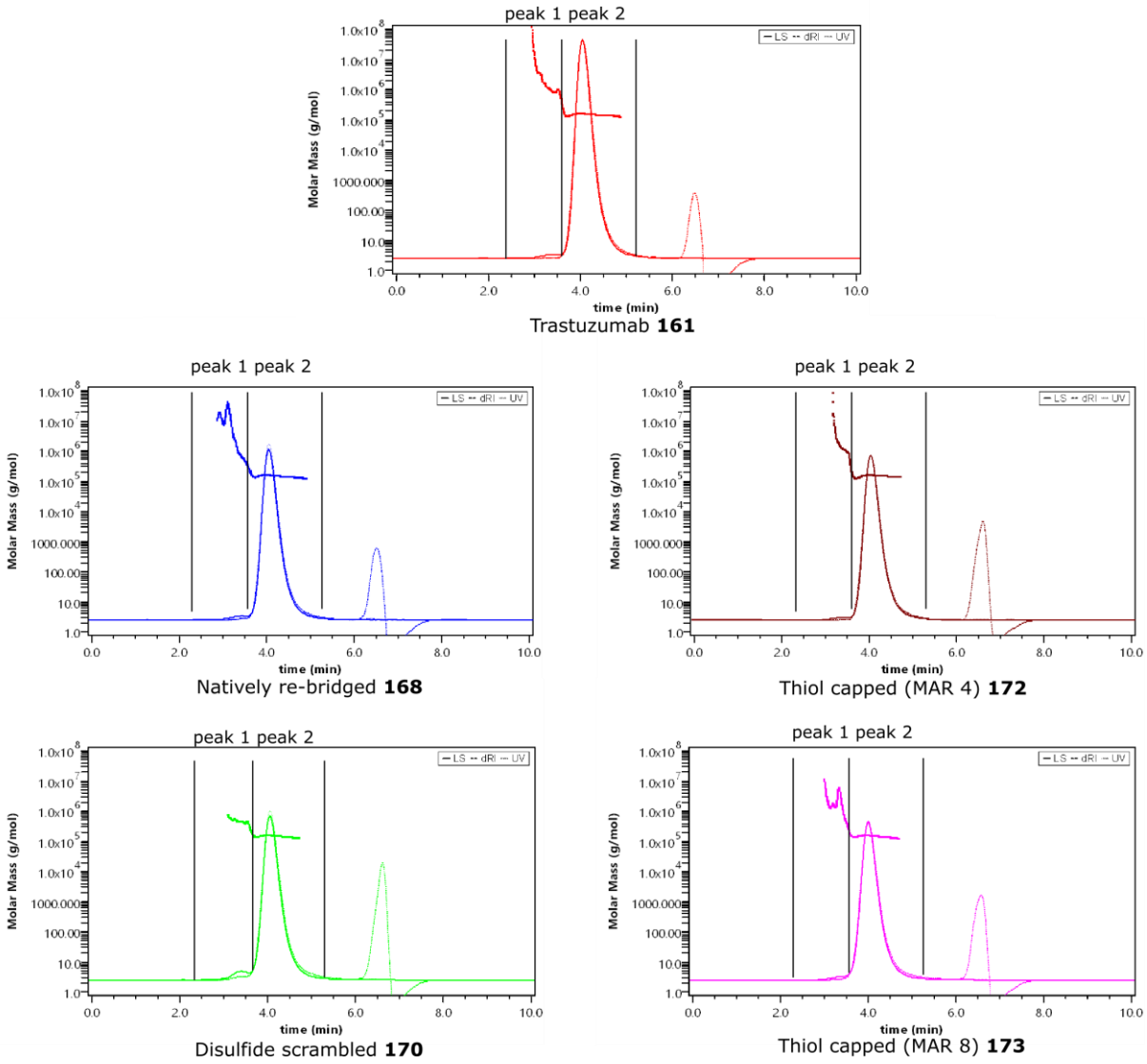

Figure 20 – SEC MALS trace of trastuzumab (**161**) and trastuzumab conjugates (**168, 170, 172** and **173**)

Table 8 – Summary for SEC-MALS analysis of trastuzumab (**161**)/ trastuzumab conjugates (**168, 170, 172** and **173**)

Conjugate	**Peak 1**			**Peak 2**		
	Mw (kDa)	Polydispersity (Mw/Mn)	Mass fraction (%)	Mw (kDa)	Polydispersity (Mw/Mn)	Mass fraction (%)
Trastuzumab **161**	1316.98	1.54	0.5	149.46	1	99.5
Natively re-bridged **168**	3040.32	5.44	0.9	149.86	1	99.1
Disulfide scrambled **170**	428.85	1.06	2.2	149.69	1	97.8
Thiol capped (MAR 4) **172**	1110.80	1.85	0.2	149.88	1	99.8
Thiol capped (MAR 8) **173**	1598.13	2.06	0.7	149.53	1	99.3

3.5.3 Antigen-Binding Analysis of Trastuzumab Conjugates

Finally, all synthesised conjugates were also subject to ELISA to test affinity towards HER2. Previous reports have shown that modifying the cysteine residues from interchain IgG1 disulfide residues has little to no impact on antigen binding, and so originally was not considered essential for this investigation. However, the disulfide scrambled conjugate **170** was synthesised using a novel DiCl PD derivative; while the resultant antibody-PD species was identical to the natively re-bridged trastuzumab **168** it was thought forming such a large proportion of “half antibody” could be impacting antigen binding, and subsequently ADCC activity. However, disulfide scrambled trastuzumab **170** and all other trastuzumab conjugates showed little deviation from the native trastuzumab control **161**, confirming that any amount of IgG1 interchain disulfide deconstruction will not affect antigen binding.

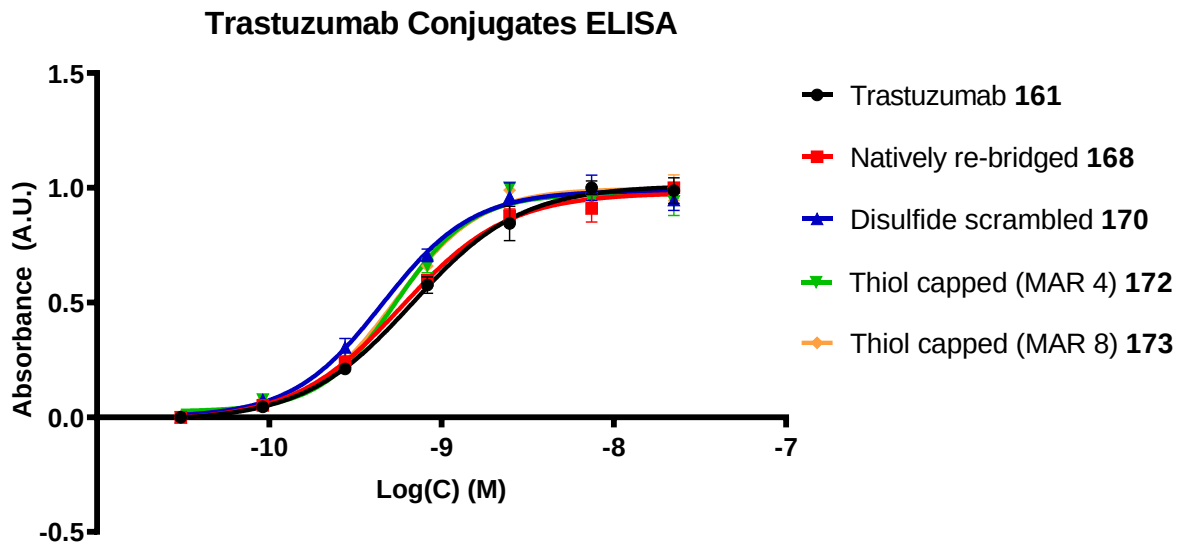

Figure 21 – Binding activity to HER 2 of trastuzumab (**161**)/ trastuzumab conjugates (**168, 170, 172** and **173**) over concentration ranges from 23.3–0.003 nM, Abs measured at 650 nm.

3.6 Conclusions

This work aimed to appraise the influence of disulfide modification on Fc interactions. Two disulfide modification strategies were compared (thiol capping and disulfide re-bridging) to highlight any subsequent effect that an intact covalent interaction may have on the Fc interactions of the IgG1 model antibody – trastuzumab. CD16a and FcRn interactions were chosen to quantify effects of disulfide modification on trastuzumab, which was achieved by use of BLI assays, and subsequent in vitro assays (ADCC) where applicable. The natively re-bridged conjugate performed exceedingly well with no apparent decrease in CD16a or FcRn binding affinity, as well as no decrease in ADCC activity - suggesting re-bridging in a native conformation has minimal effect on IgG1 Fc function. It was found that by re-bridging the disulfides in a non-native conformation, whilst not affecting CD16a kinetics, did negatively influence the ADCC activity of the native IgG1 antibody. Conversely, reducing the disulfides of trastuzumab affected the CD16a kinetics, but did not yield significantly different ADCC results from the trastuzumab control. Further biophysical analysis of these conjugates (aggregation tendencies, thermal stability, HER 2 affinity) definitively showed that natively re-bridging the disulfide residues was the only modification technique to have no impact on the biophysical profile of the IgG1 antibody.

In summary, native disulfide re-bridging presents a highly attractive option for IgG1 antibody modification, yielding a highly homogenous bioconjugate with key Fc function fully retained, and a favourable biophysical profile. Unexpected novel results surrounding the disulfide scrambled IgG1 conjugate highlights exactly how intricate the disulfide modification process can be. As the biophysical profiles of almost all tested conjugates were negatively affected (with the exception of natively re-bridged trastuzumab) this work demonstrates the sensitivity of secondary IgG1 interactions towards antibody modification. It is envisaged that this work will stimulate further efforts to appraise the secondary effector functions of novel ADCs synthesised by disulfide modification and by other strategies also.

Chapter 4 Development of a Platform for Cysteine Tri-Functionalisation

It is clear that the modification of proteins in a site-selective and homogenous fashion has contributed to the synthesis of pharmacokinetically superior bioconjugates.[25,174] Synthesis of these constructs through cysteine modification has also been highly popular in recent years.[8,109,175] Whilst a large number of cysteine-directed reagents exist for use in the synthesis of bioconjugates, few of these reagents allow for modular attachment of multiple functionalities in a site-selective fashion. The concept of protein multi-functionalisation has been exceptionally useful in the synthesis of targeted theranostics, extending the blood half-lives of protein-drug conjugates and applied Förster resonance energy transfer (FRET) chemistries.[176–178]

Research published by Maruani *et al.* gave rise to a "plug and play" approach to functional disulfide re-bridging allowing for the site-selective attachment of two functional moieties, post-protein bioconjugation.[74] By utilising a DiBr PD derivative with *N,N'*- linked terminal alkyne and strained alkyne functionality, efficient site-selective dual modification of fab fragments was achieved using orthogonal click chemistries (*i.e.* using CuAAC/SPAAC reactions with azides).[74] The authors quantitatively formed doxorubicin (Dox)–PEG, Dox–AlexaFluor^{TM}-488 and AlexaFluor^{TM}-488–sulfo-Cy5 bioconjugates, clearly showing the applicability of this linker in the synthesis of multi-functional bioconjugates.[74]

This work aims to exploit an additional point of attachment to the PD scaffold, applied in the context of single cysteine modification. To date, monoBr PDs have been employed successfully to modify single cysteine-containing proteins (Scheme 30a).[71,179] Whilst this platform allows for convenient cysteine-targeted dual functionalisation, an opportunity exists to functionalise the PD further through *C*-directed modification (Scheme 30b). Ideally, *C*-functionalisation of the PD linker could occur pre-protein, or post-protein bioconjugation, to allow for the modular synthesis of a first-in-class cysteine-directed linker, capable of tri-functional attachment of modalities onto a protein (**184**, scheme 30). Promisingly, previous work has already shown the addition of a secondary nucleophile (*i.e.* thioglucose) to a

conjugated bromo-harbouring PD linker to yield *C*-functionalised bioconjugates.[71] This work looks to further expand PD-based *C*-functionalisation to allow for the efficient, modular and homogenous synthesis of tri-functional constructs as these would be of great interest to research utilising multi-functional bioconjugates.

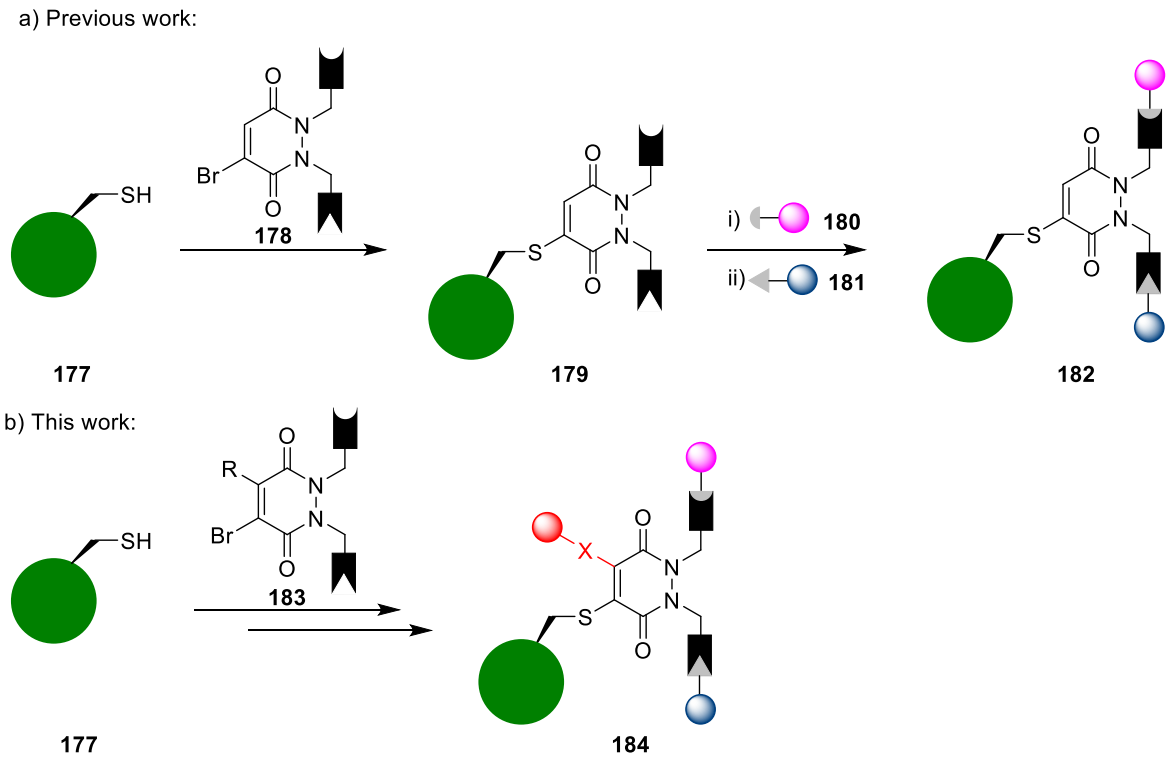

Scheme 30 – a) Previously reported work on cysteine modification using monoBr PDs. b) proposed synthesis of cysteine-linked tri-functional bioconjugates.

4.1 Synthesis of *C*-functionalised Pyridazinediones

The synthesis of a tri-functionalisation platform was investigated through two strategies: i) pre-protein bioconjugation and ii) post-protein bioconjugation (Scheme 31). For both strategies, DiBr PDs were used as a convenient synthetic branching point, as this reactive Michael acceptor can react with many commercially available nucleophiles and an optimised synthesis of DiBr PDs has been developed (see chapter 2).[169] Initially, only diethyl (DiEt) PD derivatives (lacking complex *N*-linked functionality) were synthesised to appraise reactivity of *C*-functionalised PDs.

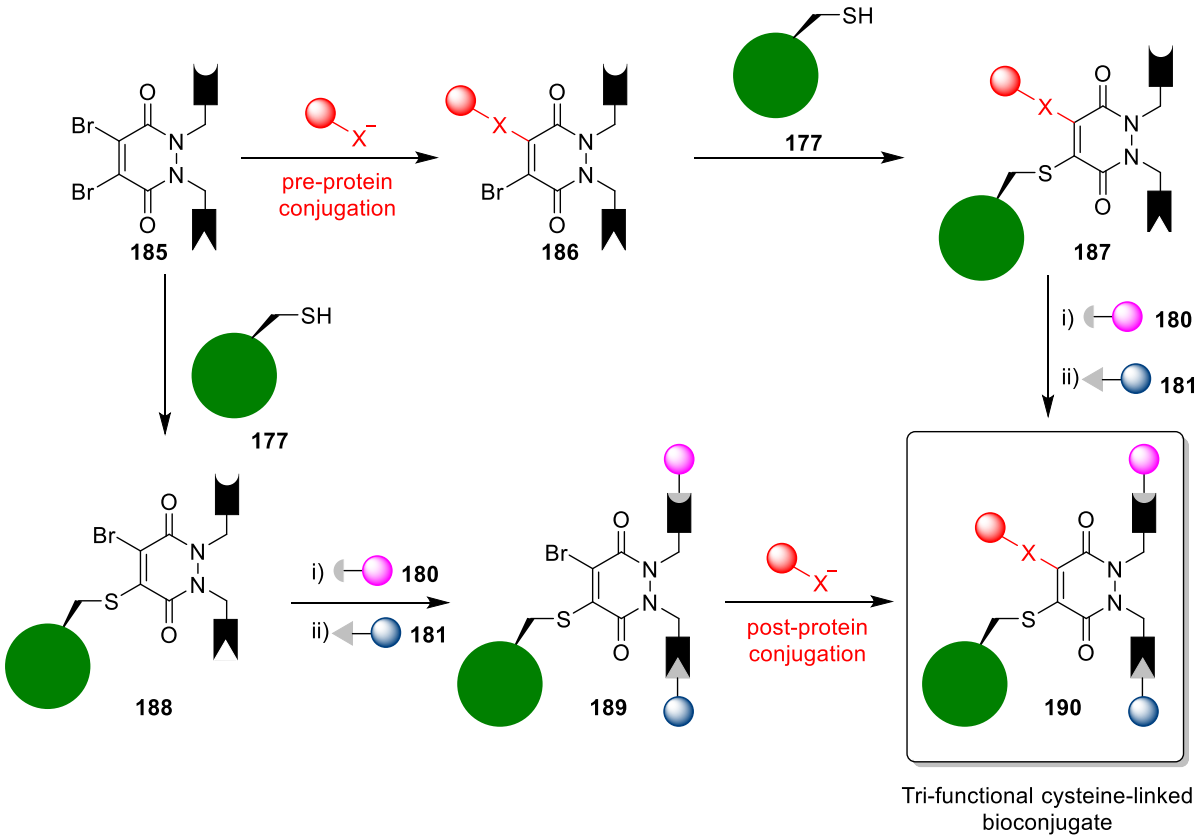

Scheme 31 – Proposed synthesis of cysteine-linked tri-functional bioconjugates through pre-protein bioconjugation or post-protein bioconjugation.

4.1.1 Reagents for Pre-Protein Bioconjugation Functionalisation

The pre-protein bioconjugation approach to protein tri-functionalisation required the synthesis of *C*-functionalised PDs which were then subsequently reacted with a cysteine-containing protein. Synthesis of tri-functional PDs with amines and thiols is an attractive strategy due to the number of commercially available small molecules harbouring these moieties. For this reason, a range of commercially available amines (*i.e. n*-hexylamine, 2-(2-aminoethoxy)ethanol and propargyl amine) and thiols (*n*-hexanethiol, 2-mercaptoethanol (BME) and 3-mercaptopropionic acid) were first selected to functionalise the vinyl position on the PD scaffold. Upon reaction with DiEt DiBr PD **136**, both 2-(2-aminoethoxy)ethanol and propargyl amine did not afford any desired product, and only starting material DiEt DiBr PD **136** was obtained. However, *n*-hexylamine did react with DiEt DiBr PD **136**, under strong basic conditions (NaOH), to form the bromo-amino PD **191** in good yield (71%). *n*-Hexanethiol, BME and 3-mercaptopropionic acid were reacted successfully with DiEt DiBr PD

136, under mildly basic conditions (NaOAc), to afford the bromo-thiol PDs **192–194** in moderate to good yields (Table 9).

Table 9 – Synthesis and yield of mono bromo mono amino/thiol PDs 191-194

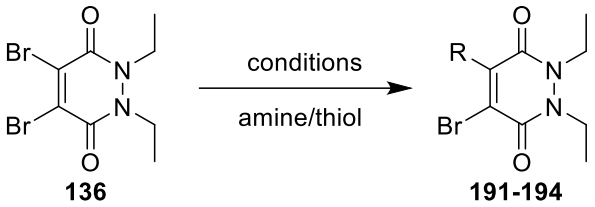

136 **191-194**

Conditions	R	Product No.	Yield
MeOH/NaOH	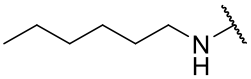	**191**	71%
MeOH/NaOAc	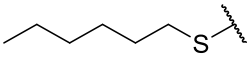	**192**	60%
MeOH/NaOAc	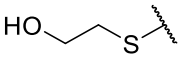	**193**	71%
MeOH/NaOAc	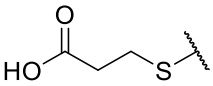	**194**	58%

4.1.2 Reagents for Post-Protein Bioconjugation Functionalisation

The post-protein bioconjugation approach to protein tri-functionalisation required the conjugation of a PD linker to a cysteine residue, and subsequent modification of a pre-installed modality at the allyl position would yield *C*-functionalised bioconjugates. However, to modify a linker post-protein bioconjugation, strict criteria must be met. The reactive moiety installed on the linker must be stable to amino acid side-chains and in aqueous conditions. Additionally, the subsequent modification must be bio-orthogonal and "click-like" in nature to allow for quantitative formation of product at low concentrations typically observed with bioconjugations.[25]

The use of azide moieties for post-conjugation functionalisation has been well-defined in literature and presents a convenient strategy to allow for the facile attachment of

functionality to proteins through “click” chemistry (*i.e.* through CuAAC and SPAAC reactions). Through installing a *C*-linked azide moiety directly onto the PD scaffold, it is thought that subsequent “click” chemistry could be performed to provide an additional handle for modification. As azide harbouring PDs are novel to the field of cysteine bioconjugation, it was not known whether the azide would eliminate preferentially to bromine when conjugating to a cysteine residue. Therefore, an azide-bromo PD **196** and a diazide PD **197** were synthesised from dibromo diethyl PD **136**, using sodium azide **195** only, in excellent yields (Scheme 32).

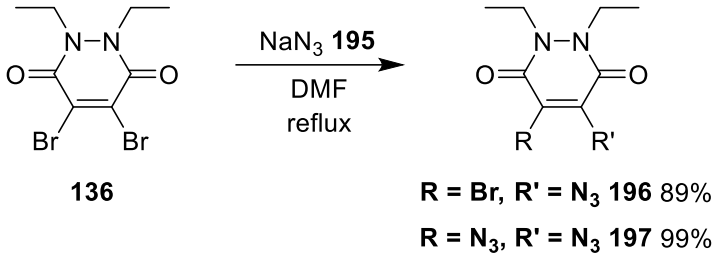

Scheme 32 – Synthesis of *C*-linked azide harbouring PDs **196** and **197**.

Finally, through reaction with a single cysteine, DiBr PDs produce a cysteine-bromo PD that may satisfy these criteria. If no other free cysteine is present, the remaining bromo-substituted position will be stable in the required conditions and can react in a “click-like” manner with nucleophiles (*e.g.* thiols) through Michael addition. For these reasons, DiBr PDs will also be considered as a route towards cysteine-tri-functionalisation.

4.2 Selection of a Single Cysteine Containing Platform

A protein harbouring a reactive solvent accessible cysteine residue was required to assess the reactivity of the synthesised PD derivatives. Introduction of a cysteine residue can result in complications, especially in the presence of a disulfide residue that can lead to disulfide scrambling. Any synthesised platforms will be tested in terms of function and cysteine reactivity to assess suitability for use in this work.

4.2.1 Mutant Anti-TNFα Nanobody

The anti-TNFα nanobody **198** (a subcomponent of ozoralizumab) was initially selected as a candidate for its robust physical properties alongside TNFα being a highly explored binding platform. The solvent accessible single cysteine was incorporated by using an expression sequence containing a His-tag followed by a spacer and cysteine residue. This His-tag aids in purification while the spacer provides extra stability and increased reactivity of the incorporated cysteine residue (Figure 22).[180]

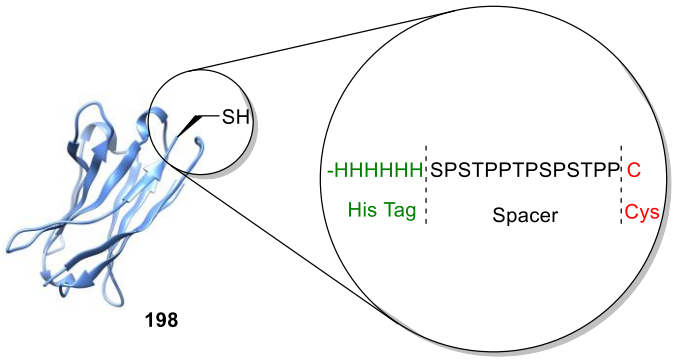

Figure 22 – Anti-TNFα nanobody **198** with incorporated construct.

After the mutated construct was prepared, it was multiplied by transfecting into TOP10 *E.Coli* cells followed a maxi-prep protocol (Promega PurePield Maxiprep System) for extraction. The mutated DNA was then sequenced (GATC), and the anti-TNFα nanobody **198** was expressed and purified (Trenzyme) to obtain a mixture of monomer and dimer. Anti-TNFα binding activity was appraised using a bio-layer interferometry assay, showing reasonable affinity towards the TNFα antigen.

Next, the reactivity of the free cysteine on the anti-TNFα nanobody **198** was tested. Due to the native nanobody scaffold existing as a partial homodimer, a reducing agent (TCEP **52**, 20 eq.) was required to fully reduce the interchain disulfide bond. Unfortunately, when reacting the anti-TNFα nanobody **198** with DiEt DiBr PD **136**, two PDs had conjugated to the nanobody (Figure 23). The observed mass indicated that, in addition to single cysteine conjugation, an exposed disulfide was also being modified, resulting in the addition two PD scaffolds to the nanobody (**200**). For this reason, the anti-TNFα nanobody **198** was not found to be suitable platform for this project.

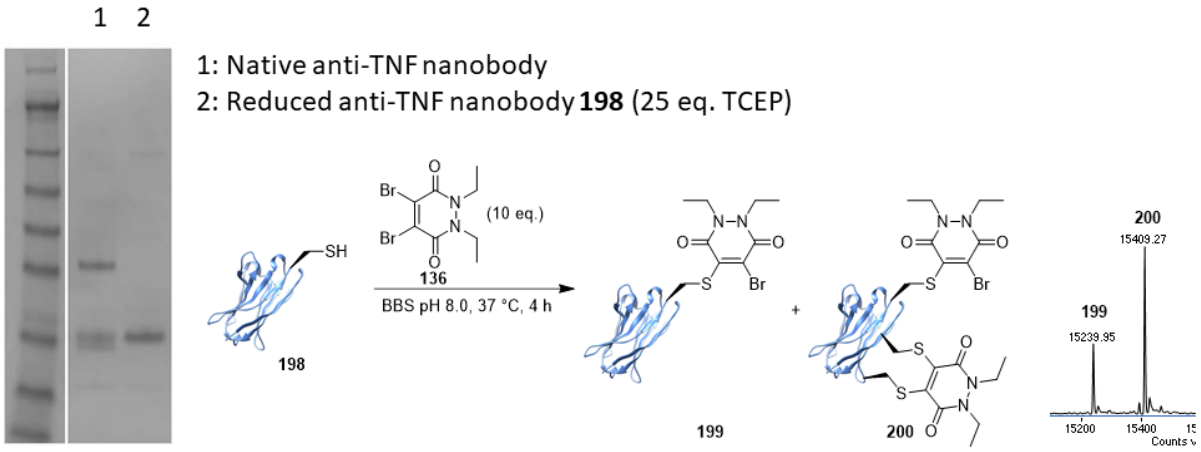

Figure 23 – SDS PAGE of native and reduced anti-TNFα nanobody **198** and mass spectra for reaction of anti-TNFα antibody **198** with DiEt DiBr PD **136**.

4.2.2 Mutant Green Fluorescent Protein (GFP) S147C

An alternative single cysteine containing platform comes in the form of GFPS147C **48**, a green fluorescent protein (GFP) with a Ser^{147} to Cys^{147} mutation. This protein, unlike the anti-TNFα nanobody **198**, has been previously synthesised and well documented in terms of bioconjugation to the engineered cysteine residue.[73] Similar to previous reports, GFPS147C **48** was expressed in competent BL21 (DE3) cells and was subject to a two-step purification process including affinity chromatography (between an engineered His_6 tag and immobilised Ni^{2+}) and subsequent size exclusion chromatography (SEC) (see experimental for chapter 4). GFPS147C **48** was analysed by SDS-PAGE and by mass spectrometry and was found to be of high quality, with the exception of a minor artefact in the mass spectrum occurring at +178 Da which is likely representative of another cysteine containing species with an additional 2 amino acids. Due to the tendency of solvent accessible cysteine of GFPS147C **48** to form interprotein disulfide bonds (forming a GFP homodimer), therefore the GFPS147C must be reduced prior to reaction with cysteine reactive reagents. The phosphine-based reducing agent TCEP **52** was employed over other thiol-containing reducing agents (*e.g.* DTT) to avoid cross reactivity towards thiol reactive conjugation reagents. An excess of TCEP **52** (25 eq.) was required for full reduction of the GFPS147C homodimer (Figure 24).

To confirm cysteine reactivity, the reduced GFPS147C **48** (50 µM, pH 7.4) was first reacted with DiEt DiBr PD **136** (20 eq., 1 mM final concentration). Pleasingly, the only species observed was the conjugated GFP-PD-bromo species **201** confirming the engineered cysteine

to be reactive. Importantly, the reaction between a PD scaffold with two cysteine reactive centres did not result in GFP dimerisation. Finally, the GFP chromophore (formed from the Ser[65], Tyr[66] and Gly[67] residues) appeared to remain functional post-protein expression which was confirmed by analysing the characteristic GFP UV absorption at 495 nm.[181]

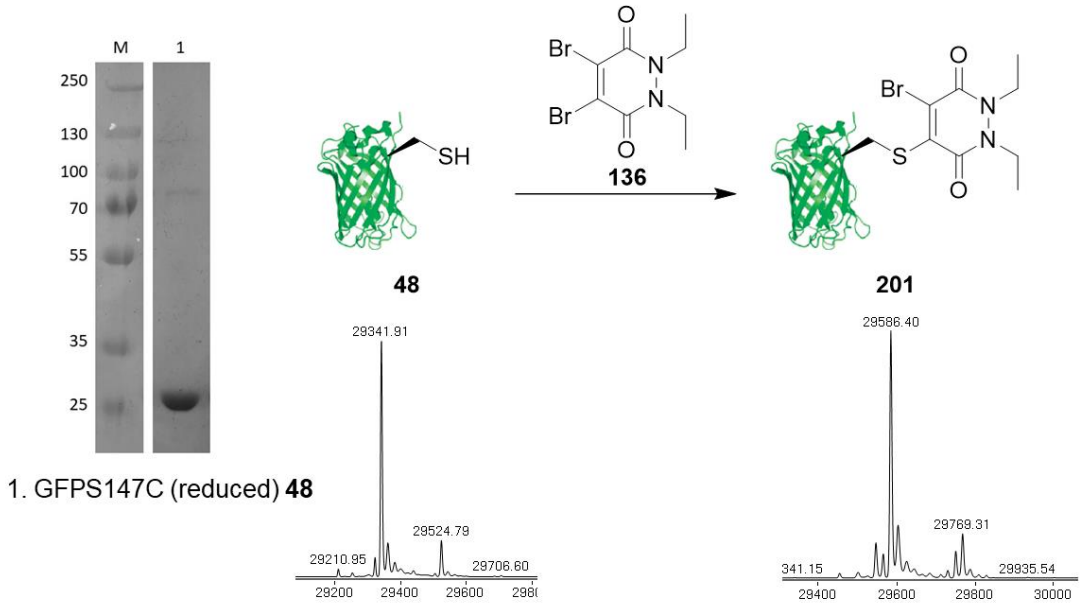

Figure 24 – SDS-PAGE and LCMS analysis of reduced GFPS147C **48** and reaction with DiBr PD **136** to form GFP-PD-Br species **201**

4.3 Novel Cysteine Functionalisation of GFPS147C

GFPS147C **48** was reacted with the small library of PDs (**191-194, 196** and **197**) to investigate two methods that could contribute towards a tri-functionalisation platform. These strategies can be referred to as: i) pre-protein conjugation functionalisation (though use of PDs **191-194**) and ii) post-protein conjugation functionalisation (through use of PDs **196** and **197**). It is thought that by providing an option for functionalisation of the platform before and after bioconjugation using the PD scaffold, this would further increase the modularity and applicability of the tri-functionalisation approach. All bioconjugation reactions were analysed by LCMS to assess the extent of any modification on GFPS147C **48**.

4.3.1 Pre-Protein Conjugation Functionalisation

Upon reaction with GFPS147C **48** (50 µM, pH 7.4) at 37 °C for 4 h, the small library of bromo-thiol PDs **192-194** (20 eq., 1 mM final concentration) afforded the GFP-PD-thiol species **202-204** only (Figure 25a). This result provides evidence to suggest full cysteine-thiol selectivity for the bromo position on the PD over competing thiol exchange *(i.e.* forming the undesired GFP-PD-Br species **201**). Interestingly, the functional moieties present on the *C-S* functionalised PDs **192-194** were well tolerated and were unaffected by the cysteine-PD bioconjugation. These results are promising as a high level of functional group tolerance would allow the addition of many diverse and commercially available thiols at this position.

Interestingly, the bromo-amino PD **191** (20 eq., 1 mM final concentration) did not show any reactivity towards GFPS147C **48** (Figure 25b). Whilst this result is initially disappointing, this does suggest that amine substitution at this position is sufficient to decrease the electrophilicity of the Michael acceptor, such that thiol reactivity is quenched. Therefore, it was envisaged that if an amine could be reacted at this position post-protein conjugation, this transformation may confer an additional level of stability towards thiol exchange (*i.e.* the resultant species may be stable to high concentrations of thiol).

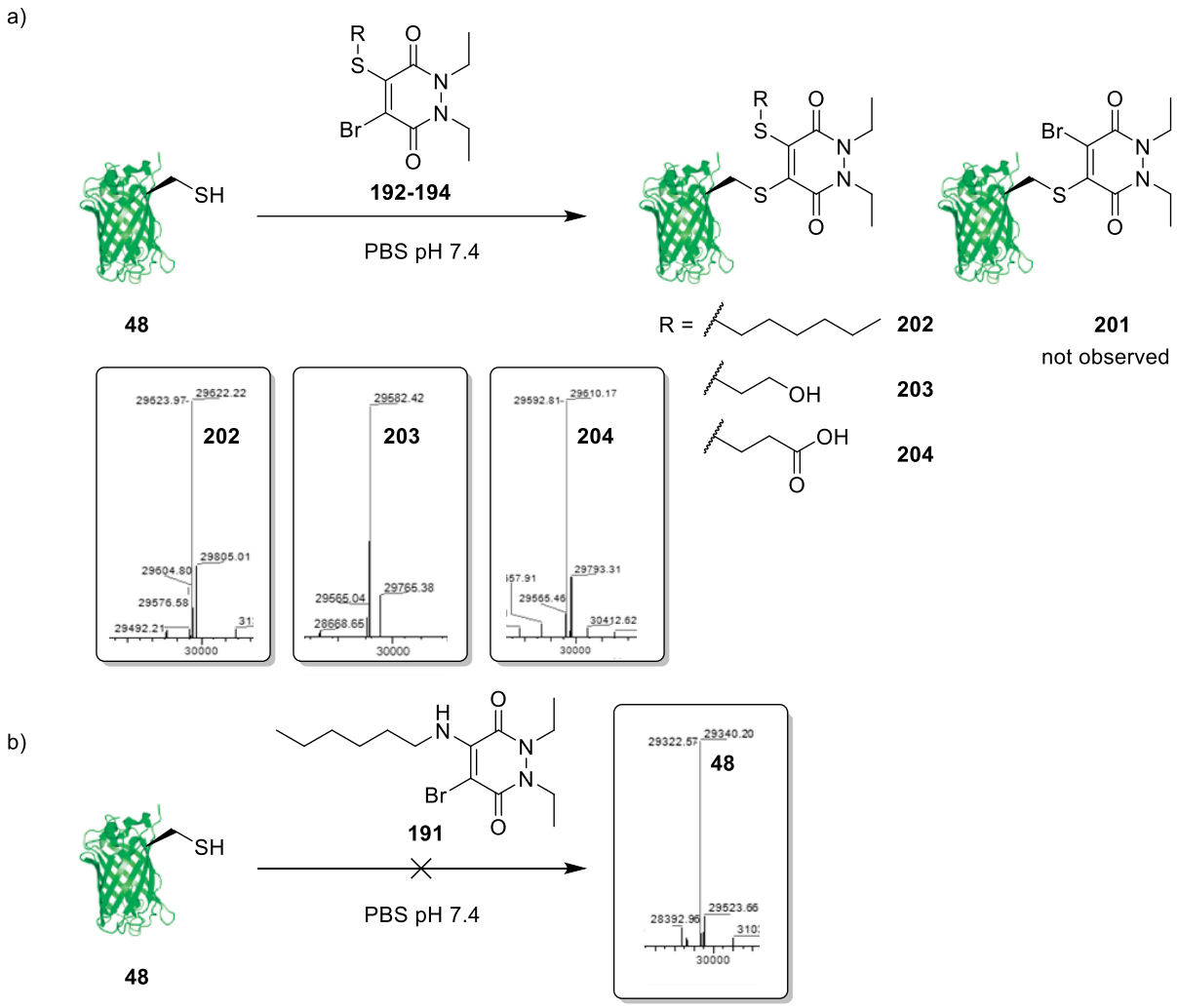

Figure 25 – a) reaction between GFPS147C **48** (50 µM, pH 7.4) and mono Br mono thiol PDs **192-194** (20 eq., 1 mM final concentration) to produce GFP-PD-thiol species **202-204**. b) Reaction between GFPS147C **48** (50 µM, pH 7.4) and mono Br mono amino PD **191** (20 eq., 1 mM final concentration) to show no observable bioconjugation.

4.3.2 Post-Protein Conjugation Functionalisation

GFPS147C **48** was first incubated with azide harbouring PD derivatives **196** and **197** in an attempt to synthesise an azide harbouring GFP-PD conjugate which may then facilitate post-protein conjugation "click" reactions. The mono Br mono azide PD **196** (20 eq., 1 mM final concentration) was reacted with the GFPS147C **48** (50 µM, pH 7.4) for 4 h at 37 °C to afford a large quantity of the GFP-PD-Br species **201** (Figure 26a). As the azide appeared to function as a leaving group in a cysteine bioconjugation scenario, the diazide PD **197** (20 eq., 1 mM final concentration) was also reacted with the GFPS147C **48** (50 µM, pH 7.4) for 4 h at 37 °C

(Figure 26b). Unfortunately, no observable mass for the GFP-PD-azide species was detected. The peaks observed by LCMS analysis correspond to unreacted GFPS147C **48** in abundance in addition to numerous unidentifiable species (Figure 26b).

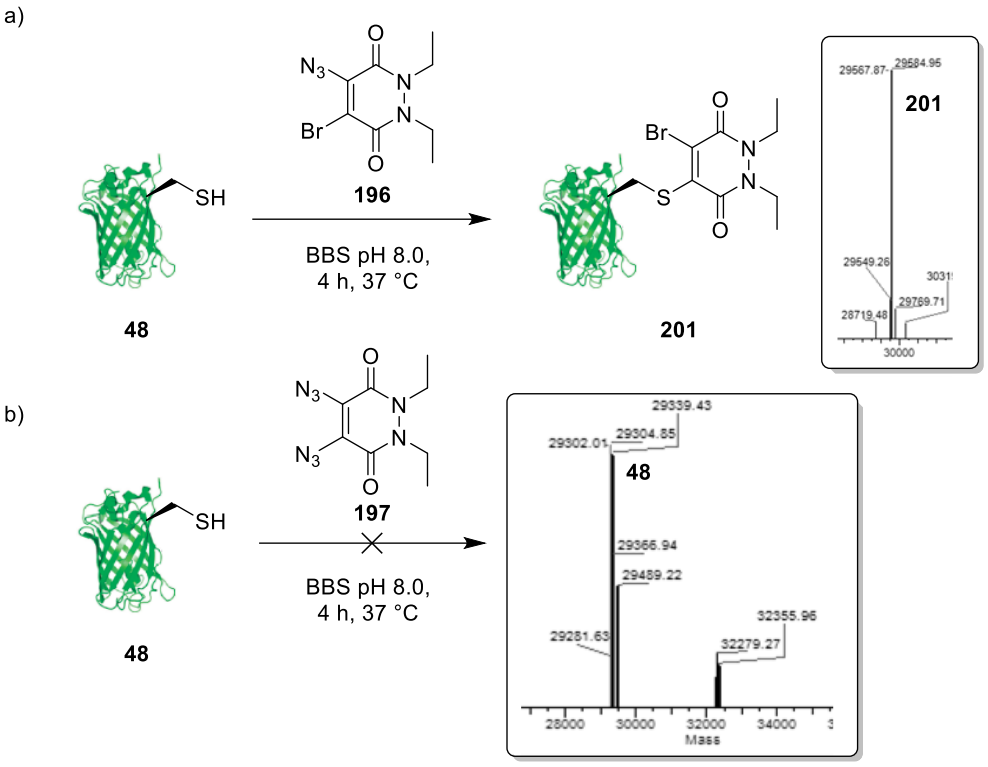

Figure 26 – a) Reaction between GFPS147C **48** and monoBr mono azide DiEt PD **196**. b) Reaction between GFPS147C **48** and diazide DiEt PD **197**.

DiEt DiBr PD **136** (20 eq., 1 mM final concentration) was reacted with GFPS147C **48** (50 µM, pH 7.4) for 4 h at 37 °C, to provide quantitative formation of the GFP-PD-Br species **201** (Figure 27a). It was then envisaged that the remaining bromine-substituted position on the PD may react further with thiol and amine groups in biorthogonal conditions, to produce *C-S* and *C-N* functionalised linkers. The GFP-PD-Br species **201** (50 µM, pH 8.0) was reacted with 1-hexanethiol (20 eq., 1 mM final concentration) at 4 °C for 16 h, to quantitatively produce the GFP-PD-thiol species **206** (Figure 27b). Nucleophilic attack of the thiol was selective for the bromo-substituted position on the PD, and undesired thiol exchange/PD cleavage (to form unconjugated GFPS147C **48**) was not observed. Notably, bioconjugations that exceeded a final concentration of 1 mM 1-hexanethiol began to result in cleavage of the PD moiety from GFPS147C **48** (*i.e.* through thiol exchange and elimination of the GFPS147C **48** from the PD).

Reaction of 1-hexylamine (1000 eq., 50 mM final concentration, pH 8.0) with the GFP-PD-Br species **201** (50 µM, pH 8.0) at 37 °C for 16 h did not yield any of the desired product, likely due to a large proportion of the aliphatic primary amine being protonated under bioconjugation conditions (*i.e.* pKa of 1-methylamine = approx. 10).[182] Following recent reports on aniline reactivity towards Michael acceptors under physiological conditions,[183] the aniline derivative *p*-anisidine (1000eq., 50 mM final concentration) was reacted with the GFP-PD-Br species **201** (50 µM, pH 8.0) at 37 °C for 16 h, and successfully produced the GFP-PD-amino species **208** with excellent conversion (Figure 27c).

Finally, the GFP-PD-Br species **201** was reacted with functional thiols and aniline derivatives using optimised conditions, to determine if complex functionality may affect amine/thiol conjugation. A cysteine containing model peptide (FEKGC) (synthesised by Dr R. J. Spears, see experimental for chapter 4) was selected as a functional thiol, representing many chemical moieties in the form of amino acid side chains. The peptide (20 eq., 1 mM final concentration) was reacted with the GFP-PD-Br species **201** (50 µM, pH 8.0) at 4 °C for 16 h, to successfully produce the *C-S* functionalised GFP-PD-peptide **207** (Figure 27b). As the number of commercially available aniline-derived functional compounds is low, an azide-harbouring aniline derivative (synthesised by Mr A. Wall, see experimental for chapter 4) was used as a platform to subsequently conjugate functionality through "click" chemistries. The aniline-azide linker (1000 eq., 50 mM final concentration) was reacted with the GFP-PD-Br species **201** (50 µM, pH 8.0) at 37 °C for 16 h, which pleasingly resulted in quantitative formation of the *C-N* functionalised GFP-PD-azide species **209** (Figure 27c).

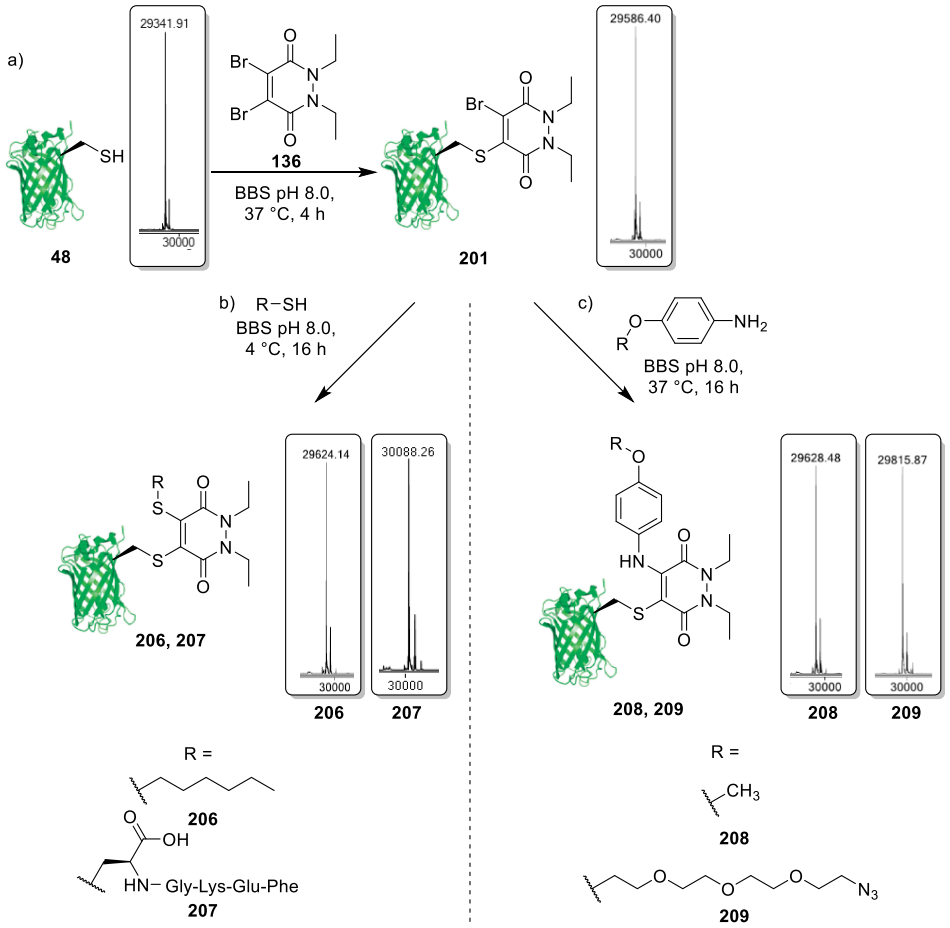

Figure 27 – a) Reaction between GFPS147C **48** (50 µM, pH 7.4) and DiBr DiEt PD **136** (20 eq., 1 mM final concentration) to produce the GFP-PD-Br species **201**. b) Reaction between GFP-PD-Br species **201** (50 µM, pH 8.0) and 1-hexane thiol (20 eq., 1 mM final concentration) and a model peptide (FEKGC) (20 eq., 1 mM final concentration) at 4 °C for 16 h to produce GFP-PD-thiol species **206** and **207**. c) Reaction between GFP-PD-Br species **201** (50 µM, pH 8.0) and aniline derivatives (1000 eq., 50 mM final concentration) at 37 °C for 16 h to produce GFP-PD-amino species **208** and **209**.

4.4 Thiol Stability Appraisal of *C-N* and *C-S* Functionalised Scaffolds

Stability towards blood thiols (*i.e.* HSA and glutathione (GSH)) remains a challenge for many linkers used in the field of *in vivo* therapeutics. When using cysteine-reactive reagents (*e.g.* maleimides) the resultant bioconjugates are often still mildly thiol reactive and highly abundant thiols in blood can facilitate premature release of cargo through thiol exchange. Biologics with applications *in vivo* are required to be stable in blood to allow for effective

delivery of chemically attached cargo to the target of interest. Due to diverse and novel nature of the synthesised GFP-PD derived constructs, the thio (*C*-*S*) and novel amino (*C*-*N*) functionalised PDs were appraised in terms of their reactivity towards thiols found in blood and cellular conditions. Understanding how these bioconjugates behave during circulation, and after uptake into cells could prove key in determining efficacy and application of the therapeutic.

In blood, the most abundant thiol reported is HSA with a concentration of around 40 g/L.[184] Although, it is known that there is a reduced reactivity of the Cys^{34} on HSA due to the placement of this residue in a hydrophobic cleft.[185] The most abundant reactive thiol in blood is glutathione (GSH) with a blood concentration of 1-10 μM.[186] For the purpose of thiol stability appraisal, the synthesised constructs would ideally be stable to the aforementioned concentrations of thiols for approximately 1 week (to account for the extended circulation half-lives of many antibody-based therapeutics).[187]

Whilst previous reports of serum stability (monitored by HPLC) have shown maleimide-derived bioconjugates to transfer payload to the Cys^{34} of HSA, PD-based bioconjugates have shown to remain stable under analogous conditions.[152] However, it should be noted that to date the only PD-based bioconjugates that have been subject to serum stability studies have been disulfide-derived. This work will aim to explore the serum stability of single cysteine-derived thio and amino functionalised PDs.

To investigate how the synthesised bioconjugates may behave after cellular uptake, early endosomal conditions should be tested. The most abundant and reactive thiol in early endosomal conditions is GSH with a concentration of 1-10 mM.[186] It should also be noted that the pH in early endosomal conditions are reported to be mildly acidic (pH = 6.5) and early endosomal conditions should reflect this also.[188] Whilst cysteine-PD and disulfide-PD derived bioconjugates have been shown to react with high concentrations of thiol (addition of BME resulted in thiol exchange and subsequent release of PD), early endosomal-mimicking conditions have yet to be applied to these constructs.[71] This work will aim to investigate how the GFP-PD derived bioconjugates behave in early endosomal-mimicking conditions.

4.4.1 Blood-Mimicking Conditions

The model DiEt *C-S* and *C-N* functionalised GFP-PD species **206** and **208** (7 μM) were first incubated with low concentrations of the reactive thiol GSH (5 μM) at pH 7.4 to determine how these constructs may behave in blood, and whether the newly formed *C-S* or *C-N* linkage would remain intact (reactions were monitored using LCMS analysis).[186] The GFP-PD-thiol species **206** and the GFP-PD-amino species **208** showed no significant reaction with blood concentrations of GSH **50** (5 μM) under the conditions tested (pH 7.4, 37 °C, 24 h) (Scheme 33).

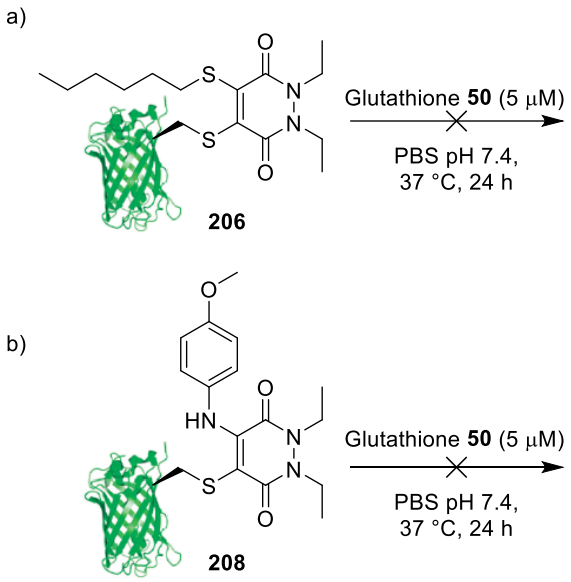

Scheme 33 – a) Incubation of GFP-PD-thiol species **206** (7 μM) in blood mimicking conditions (5 μM GSH **50**, pH 7.4). b) Incubation of GFP-PD-amino species **208** (7 μM) in blood mimicking conditions (5 μM GSH **50**, pH 7.4).

Next the stability of the *C-S* and *C-N* functionalised GFP-PD conjugates in human serum was appraised. A serum stability study was conducted (in collaboration with Ms F. Javaid) to assess whether the conjugated PD would participate in thiol exchange with the abundant blood thiol HSA. For this assay, a fluorophore-functionalised PD was required so that the PD could be traced following potential transfer to HSA. The AlexaFluor™-488 (AF-488) functionalised GFP-PD(AF-488)-thiol species **210** and GFP-PD(AF-488)-amino species **211** were successfully synthesised through use of an AF-488 azide and a strained alkyne (BCN) DiBr PD **156e** (synthesised as described in Chapter 2) (for synthesis of **210** and **211** see

experimental for chapter 4). The GFP-PD(AF-488)-thiol species **210** (7 µM) and GFP-PD(AF-488)-amino species **211** (7 µM) were then incubated in human serum for 7 days and analysed by SEC-HPLC (Figure 28b). Both *C-S* and *C-N* functionalised PDs were shown to be stable for the 7-day incubation period, showing no significant transfer of the AF-488 labelled PD to HSA during this time.

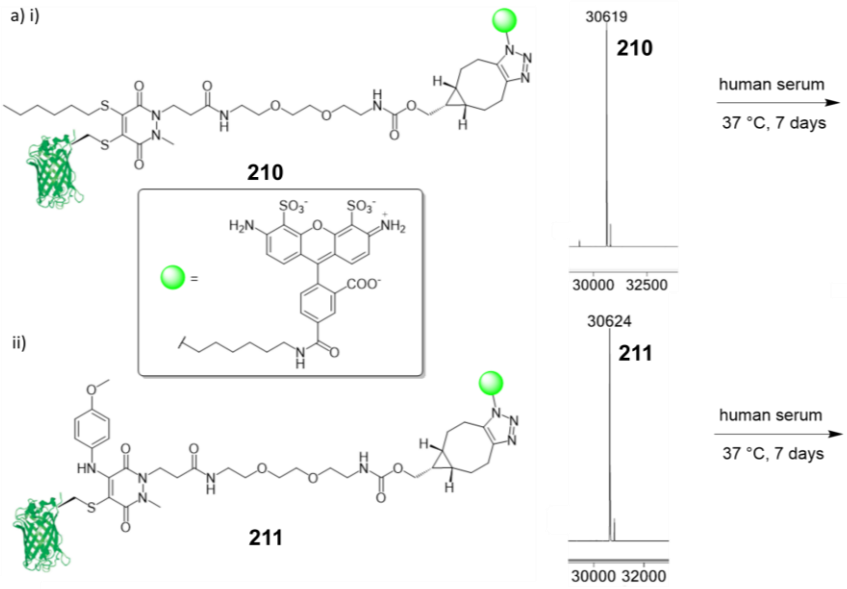

b) i) Serum stability appraisal of *C-S* functionalised species **210**

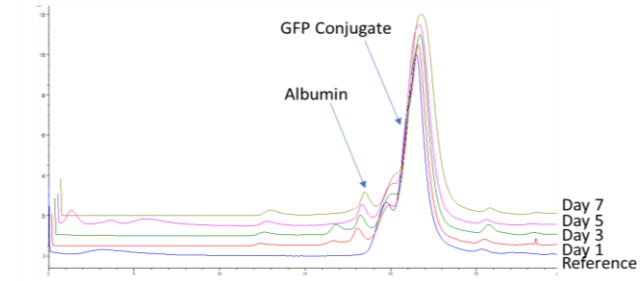

ii) Serum stability appraisal of *C-N* functionalised species **211**

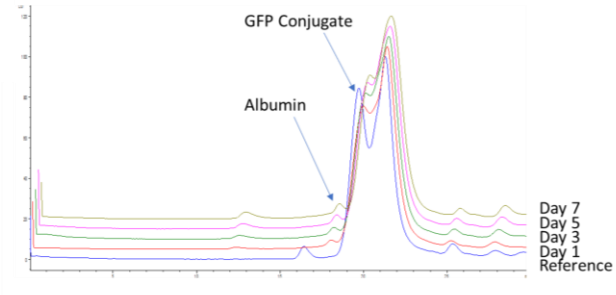

Figure 28 – a) Structure and LCMS analysis for i) GFP-PD(AF-488)-thiol species **210** and ii) GFP-PD(AF-488)-amino species **211**. b) Serum stability SEC-HPLC analysis for i) GFP-PD(AF-488)-thiol species **210** and ii) GFP-PD(AF-488)-amino species **211**.

Following incubation assays in serum and with blood concentrations of GSH, the synthesised PD-derived bioconjugates appear to be stable in blood mimicking conditions and therefore suitable for applications *in vivo.*

4.4.2 Early Endosomal-Mimicking Conditions

GFP-PD-thiol species **206** (7 µM) and GFP-PD-amino species **208** (7 µM) were incubated in early endosomal mimicking conditions (5 mM GSH, pH 6.5) for a total of 24 h. Samples were taken at 2, 4, 8 and 24 h timepoints and analysed by LCMS. When the GFP-PD-thiol species **206** was exposed to early endosomal mimicking conditions, full cleavage of the PD was observed in just 2 h (Figure 29a). GFPS147C **48**, once liberated from the PD, began to oxidise with GSH **50** to from GFP-GSH species **212** (Figure 29a). Observing the GFP-GSH species **212** after 24 h through thiol oxidation is promising evidence that the cysteine thiol was unaffected by the PD conjugation/cleavage. This finding consolidates previously published results that infer thiol-derived PD conjugates to be considered cleavable in cellular conditions.[71]

Interestingly, after incubating the GFP-PD-amino species **208** for 24 h in analogous conditions, no PD cleavage was observed over the 24 h period (Figure 29b). This observation therefore suggests that amine conjugation at this position on the PD scaffold, does indeed confer a high degree of thiol stability.

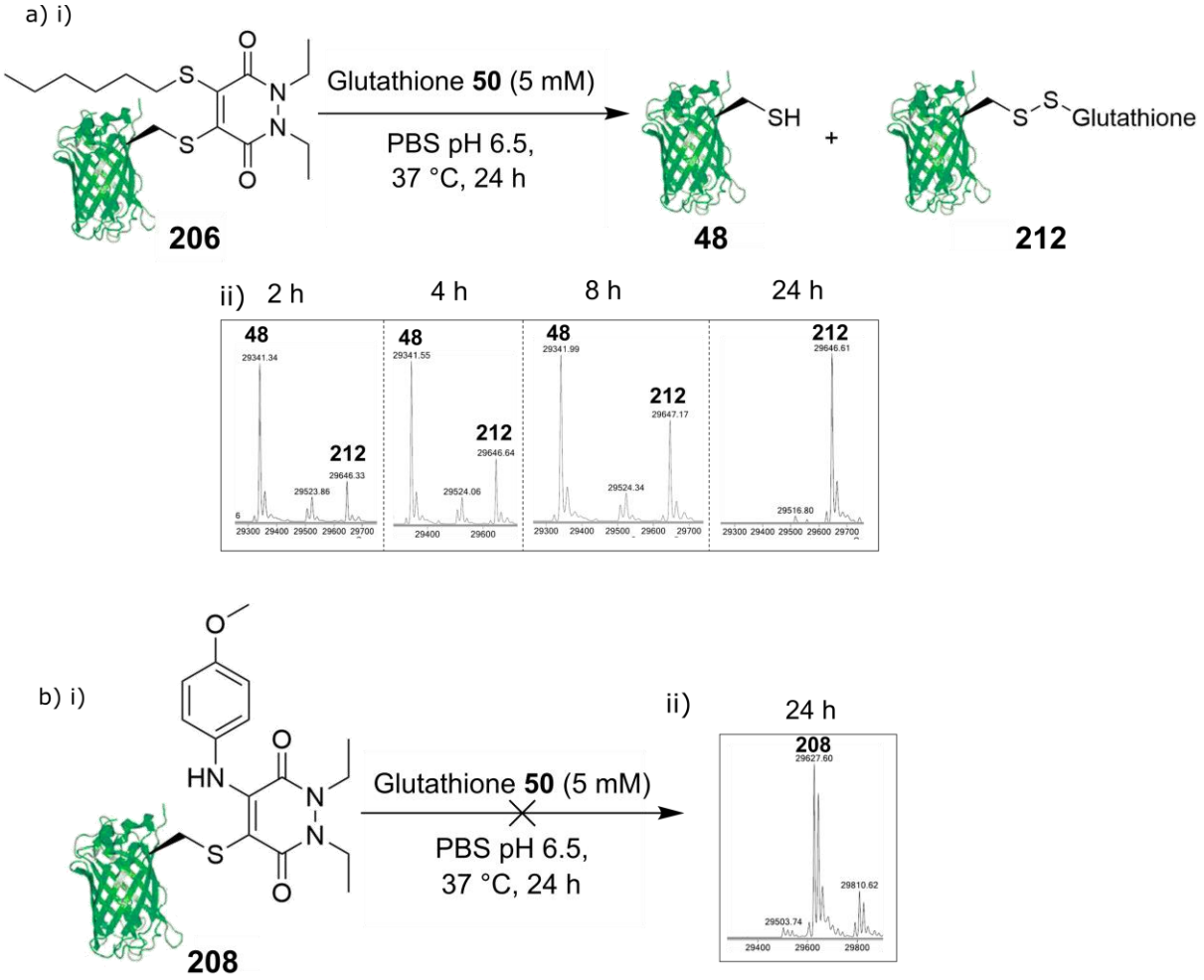

Figure 29 – a) i) Incubation of GFP-PD-thiol species **206** in early endosomal mimicking conditions (5 mM GSH, pH 6.5). ii) LCMS analysis for 2, 4, 8 and 24 h timepoints. b) i) Incubation of GFP-PD-amino species **208** in early endosomal mimicking conditions (5 mM GSH, pH 6.5). ii) LCMS analysis for the 24 h timepoint.

In tandem, these results show a unique opportunity for control over release of payload after uptake in cells. By governing cleavability of the linker employed, the resultant bioconjugates may be employed for application in a wide range of physiological conditions.

4.5 Synthesis of Tri-functional Cysteine Bioconjugates

Through design and synthesis of a dually clickable DiBr PD with *N,N'* tetrazine and azide functionality **213** the platform was expanded to allow for the attachment of three functionalities post-conjugation. GFPS147C **48** (50 µM, pH 7.4), was reacted with DiBr tetrazine azide PD **213** (20 eq., 1 mM final concentration) (synthesised by Mr P.A. Szijj, see

experimental for chapter 4) at 37 °C for 4 h to produce the GFP-PD(tetrazine-azide)-Br species **214** (Figure 30).

Dibenzocyclooctyl (DBCO)-biotin **216** and bicyclo[6.1.0]nonyne (BCN)-fluorescein **215** were selected as reagents to react with PD linked azide and tetrazine moieties respectively (*i.e.* through SPAAC chemistry). Exploiting the selectivity of DBCO-azide, and BCN-tetrazine SPAAC reactions (*i.e.* the electron deficient tetrazine reacts preferentially with electron rich strained alkynes),[189] the dual modification was attempted in a one-pot fashion to reduce the total time required for complete bioconjugate synthesis. BCN-fluorescein **215** (2 eq., 100 µM final concentration) and DBCO-biotin **216** (10 eq., 500 µM final concentration) were added *in situ* to the GFP-PD(tetrazine-azide)-Br species **214** (50 µM, pH 7.4) and were incubated for 4 h at 37 °C to produce the dually clicked GFP-PD-Br species **217** only (Figure 30). Presence of GFP-PD(biotin-biotin)-Br or GFP-PD(fluorescein- fluorescein)-Br was not detected, suggesting the *in situ* addition of BCN and DBCO was successful in selectively modifying tetrazine and azide groups respectively.

To synthesise the tri-functional *C-S* species, the model peptide (FEKGC) **218** was employed once again. The peptide **218** (20 eq., 1 mM final concentration) was reacted with the dually modified GFP-PD-Br species **217** (50 µM, pH 8.0) at 4 °C for 16 h, to successfully produce the tri-functional *C-S* modified GFP-PD (biotin-fluorescein-peptide) species **219** (Figure 30). As previously mentioned, few commercially available aniline-derived regents exist for bioconjugation, so the aniline-azide linker **220** was incorporated. The aniline-azide species **220** (1000 eq., 50 mM final concentration) was reacted with the dually modified GFP-PD-Br species **217** (50 µM, pH 8.0) at 37 °C for 16 h to produce the tri-functional *C-N* modified GFP-PD (biotin-fluorescein-azide) species **221** (Figure 30). A DBCO-PEG_{12} reagent **222** (20 eq., 1 mM final concentration) was then added to the *C-N* modified GFP-PD (biotin-fluorescein-azide) species **221** (50 µM, pH 8.0) at 37 °C and left for 4 h to produce the tri-functional *C-N* modified GFP-PD (biotin-fluorescein-PEG) species **223.** In the synthesis of both *C-S* and *C-N* tri-functionalised bioconjugates, quantitative formation of intermediates was observed, and final products were afforded with a conversion of >90% (confirmed by LCMS analysis). Furthermore, only removal of excess small molecule was required for purification, which was achieved through simple desalting or dialysis techniques.

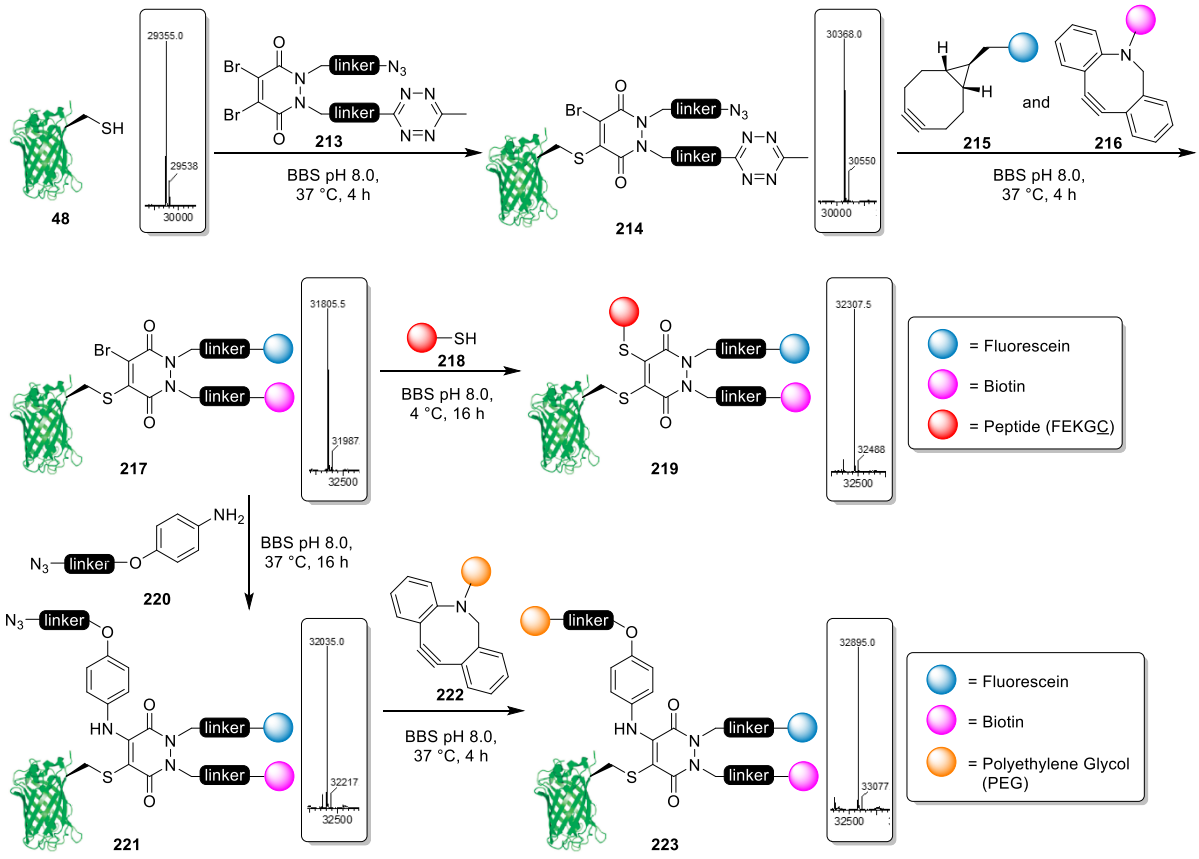

Figure 30 – Synthesis of tri-functional *C-S* GFP-PD (biotin-fluorescein-peptide) species **219** and trifunctional *C-N* (biotin-fluorescein-PEG) species **223**.

4.6 Conclusions

In this work, a library of PD derived cysteine targeting linkers were synthesised to allow for the site-selective attachment of three functionalities to a protein. The initial aim was to exploit an additional reactive centre on the PD scaffold through synthesising chemically diverse PD derivatives to react with cysteine residues. However, this approach proved limited due to the unforeseen affect that modifying the finely tuned Michael acceptor had on cysteine reactivity. The only method found to synthesise a tri-functional reagent that may participate in cysteine conjugation was through addition of a thiol moiety. In all other tested scenarios modifying the PD scaffold prior to cysteine conjugation resulted in a lack of reactivity and specificity towards cysteine.

However, through use of post-conjugation functionalisation of a conjugated bromo PD derivative, a linker that can provide a platform for the efficient synthesis of chemically

diverse bioconjugates that can host up to three functionalities is provided. This work demonstrates the process of conjugating and subsequently modifying a bromo harbouring Michael acceptor with various thiol and aniline derivatives. The resultant bioconjugates were then appraised in terms of thiol stability. Bioconjugates synthesised using thiols (*C-S* functionalised) and with aniline derivatives (*C-N* functionalised) were both shown to be stable in blood mimicking conditions. However, when these conjugates were incubated in conditions designed to mimic the early endosome, the results suggest that thiol derived bioconjugates were susceptible to cleavage in early endosomal conditions, whereas amine derived bioconjugates were stable for a minimum of 24 h. Therefore, through subsequent modification of this platform with thiols and aniline derivatives, a considerable amount of control may be achieved over cleavability in cellular conditions.

It is envisaged that this platform for site-selective tri-functionalisation may contribute to research fields where multifunctionality is required (*e.g.* theranostics, FRET, blood half-life extension). Additionally, offering control over cleavability in early endosomal conditions may allow this platform to be extended to applications for use in a range of physiological environments (*e.g.* intracellular imaging using CPPs).

Chapter 5 Reversible Covalent Modification of Cysteine Using Pyridazinediones

Over the past decade, bromo-harbouring Michael acceptors (*i.e.* BrPDs and bromomaleimides) have been successfully employed for the quantitative modification of cysteine residues on proteins.[69,71–73] These next-generation bromo-containing bioconjugation reagents form unsaturated thio-vinyl linkages that are stable to retro-Michael deconjugation, and can produce serum-stable bioconjugates.[69,152] This precludes their ability to be involved in a Michael equilibrium (Michael addition followed by subsequent retro-Michael deconjugation), which in the context of reversible cysteine modification, is an intriguing property that can be exploited for many applications such as cleavable linkers (as applied to antibody-based bioconjugates) and in reversible kinase inhibitors.[190–192]

Previous reports by Baldwin *et al.* have exploited retro-Michael deconjugation of succinimide-thiol linkages (*i.e.* formed through maleimide-thiol Michael addition) by demonstrating the cleavability of this moiety in high concentrations of glutathione (*i.e.* representative of early endosomal conditions).[193] Incubation of the succinimide-thiol species in high GSH concentrations (5 mM) resulted in the formation of a new maleimide-GSH linkage, liberating the originally conjugated thiol. The maleimide-thiol Michael equilibrium can be considered highly shifted in favour of product (thiol-succinimide **225**) formation, due to the high rate of Michael addition observed between thiols **224** and maleimides **33** (Scheme 34).[193] Furthermore, the high rate of Michael addition contributes to the rapid formation of the thiol-maleimide Michael equilibrium and thus succinimide-based bioconjugates are formed quickly and efficiently. In buffer, succinimide-based bioconjugates appear stable as any maleimide liberated through retro-Michael deconjugation will react rapidly with the cysteine thiol once again; however, a high concentration of a second thiol can outcompete the cysteine residue for reaction with the maleimide, thus liberating the protein from maleimide-linked cargo. It is important to note, however, that maleimide hydrolysis affects the efficiency of the reversible cysteine equilibrium. Once hydrolysed, the resultant maleamic acid **226** and the thio-succinamic acid derivative **227** no longer

participate in Michael addition and retro-Michael deconjugation, respectively (Scheme 34a).[193]

Another reported instance of an application based on retro-Michael deconjugation is through the use of cyanoacrylates as reversible kinase inhibitors. Serafimova *et al.* have shown cyanoacrylates **228** to reversibly inhibit the p90 ribosomal protein S6 kinase (RSK) through utilisation of a Michael equilibrium.[192] The authors show that by increasing the acidity of the α-hydrogen (though utilisation of an electron withdrawing cyano group), the retro-Michael deconjugation rate was accelerated and a dynamic equilibrium was formed (Scheme 34b). Due to an increased rate of retro-Michael deconjugation, the cyanoacrylate-thiol Michael equilibrium is not shifted in favour of product formation (as seen with maleimides), and so can be considered ideal for the purpose of rapid kinase inhibition. Furthermore, extensive efforts have been made to tune the reactivity of the various Michael acceptors (similar in structure to cyanoacrylates), for the purpose of developing a library of kinase inhibitors with a range of potencies.[194]

This work aims to explore the use of non-Br PD derivatives **123** in the context of reversible cysteine modification. It is thought that the saturated PD-thiol linkage **230** may undergo retro-Michael deconjugation in a similar manner to previously reported maleimide and cyanoacrylate derivatives (Scheme 34c). In contrast to maleimides, the PD scaffold exhibits hydrolytic stability and thus would avoid termination of the Michael equilibrium. Furthermore, through *N,N'*-functionalisation, the pyridazinedione could provide a platform for the modular synthesis of functional reversible cysteine modification reagents. This project will explore the reactivity of non-Br PD derivatives towards cysteine residues, and subsequent rates of retro-Michael deconjugation. Understanding the Michael equilibrium displayed between cysteine-thiols and PDs will be essential in determining a potential application for these bioconjugation reagents.

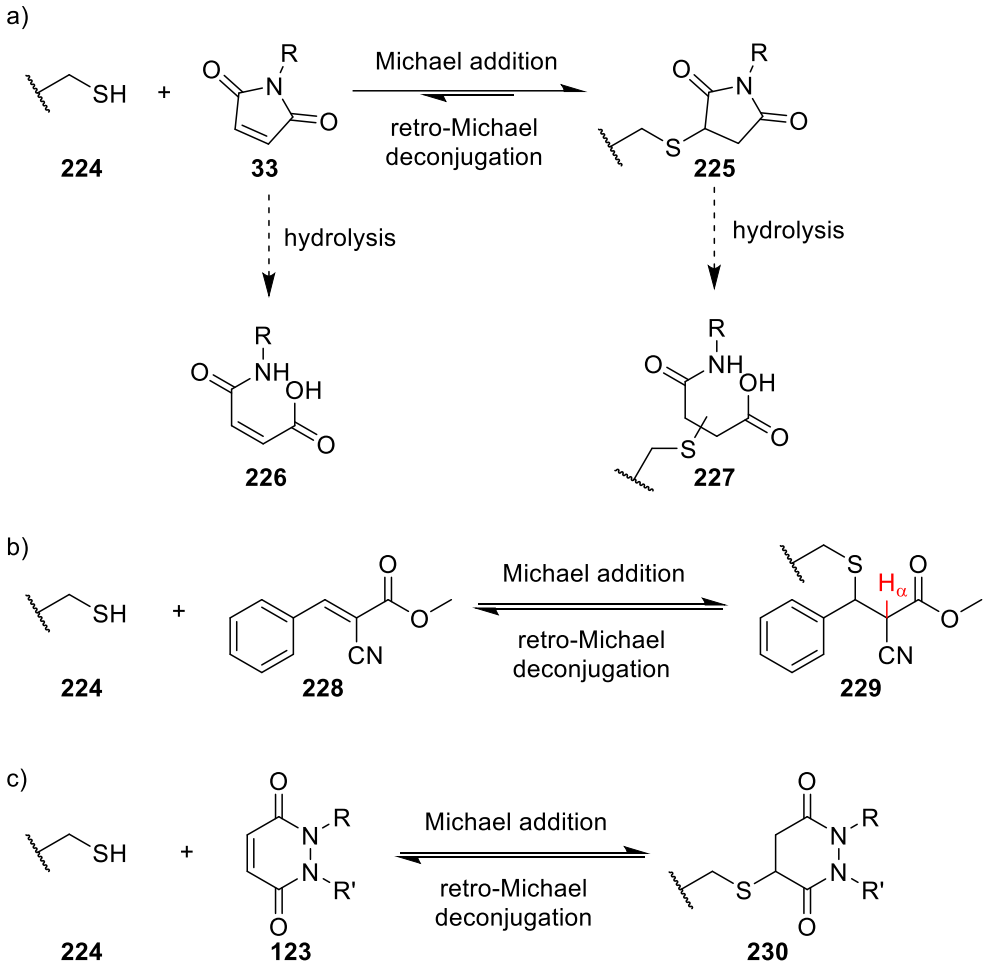

Scheme 34 – a) Reversible reaction between a thiol and a classical maleimide to produce a thio-succinimide. Ring opening hydrolysis of maleimide and succinimide groups. b) Reversible reaction between a thiol and a cyanoacrylate. c) Proposed reversible reaction between a thiol and a non-Br PD.

5.1 Reversible Cysteine Modification Using Pyridazinediones

To investigate the reaction between cysteine and non-Br PDs, initial reactivity studies were conducted on a small molecule-containing cysteine thiol (*i.e.* Boc-Cys-OMe **231**) and a cysteine containing protein GFPS147C **48**. All small molecule studies were characterised using NMR analysis and carried out by Dr R. J. Spears. Protein conjugations were monitored through LCMS analysis. Initially, PD-conjugated small molecules and proteins were synthesised to assess the reactivity of non-Br PDs towards cysteine thiols (*i.e.* through Michael addition). The PD-conjugated models were then subject to incubation in buffered

conditions to assess whether retro-Michael mediated release of PD would occur, and to obtain data regarding relevant timescales of release.

5.1.1 Reversible Modification of Boc-Cys-OMe

The commercially available Boc-Cys-OMe **231** was selected as a suitable candidate to represent a reactive small molecule cysteine thiol. The following synthesis of non-Br DiEt PD **232** and reactions with Boc-Cys-OMe **231** were carried out by Dr R. J. Spears. Boc-Cys-OMe **231** was reacted successfully with a model DiEt non-Br PD **232** in mildly basic conditions (NaOAc) to produce Boc-Cys(PD)-OMe **233** with a moderate yield of 54% (Figure 31a).

Boc-Cys(PD)-OMe **233** was then monitored to investigate whether this species would undergo retro-Michael deconjugation to afford Boc-Cys-OMe **231** and DiEt PD **232**. Boc-Cys(PD)-OMe **233** was incubated in a phosphate buffer (PB) pH 7.4:CD_3CN (7:3) solvent system at 37 °C and was analysed by ^1H NMR at 24 h intervals over the course of 96 h (Figure 31b). During the course of this experiment, new peaks in the ^1H NMR corresponding to deconjugated PD **232** emerged, with integrations of the newly appearing DiEt PD **232** vinyl CH protons (*i.e.* relative to the ethyl groups on the PD), suggesting that the PD moiety was gradually being liberated from the conjugate over time (Figure 31b).

To further confirm that the cysteine thiol (*i.e.* Boc-Cys-OMe **231**) was being released through retro-Michael deconjugation, an Ellman's test was performed to establish the concentration of free thiol generated over time. Boc-Cys(PD)-OMe **233** was incubated with 5,5-dithio-bis-2-nitrobenzoic acid (DTNB) **234** in a PB pH 7.4:CH_3CN (7:3) solvent system at 37 °C, and anticipated 5-thio-2-nitrobenzoic acid (TNB) **236** release (*i.e.* from reaction of liberated Boc-Cys-OMe **231** with DTNB **234**) was monitored by UV-Vis absorption at 412 nm at 24 h intervals over the course of 96 h (Figure 31c). Over this time course, a significant increase in the absorbance at 412 nm (A_{412}) was observed when DTNB **234** was incubated with Boc-Cys(PD)-OMe **233**, compared to a control experiment where DTNB **234** was incubated under identical conditions without the addition of Boc-Cys(PD)-OMe **233**.

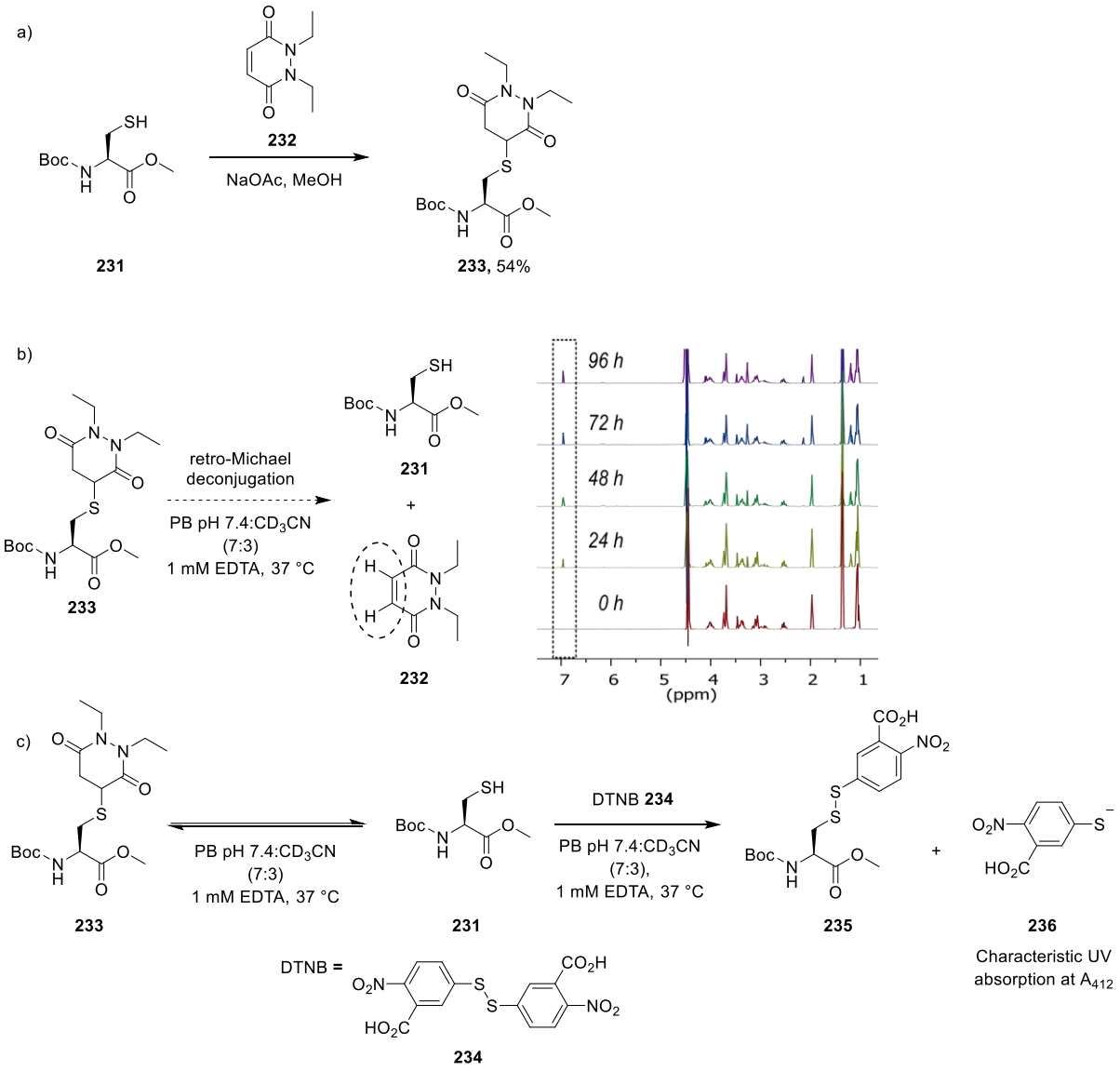

Figure 31 – a) Synthesis of Boc-Cys(PD)-OMe **233**. b) NMR analysis showing slow release of PD **232** from Boc-Cys(PD)-OMe **233** to form Boc-Cys-OMe **231** and DiEt PD **232**. c) Release of Boc-Cys-OMe **231** from Boc-Cys(PD)-OMe **233** and subsequent reaction with DTNB **234** to form Boc-Cys(TNB)-OMe **235** and TNB **236**.

5.1.2 Reversible Modification of GFPS147C

To explore the reversibility of non-Br PDs in the context of cysteine bioconjugation, reaction between non-Br PDs and the cysteine mutant GFPS147C **48** was investigated. GFPS147C **48** was selected as a suitable protein model harbouring a single solvent-accessible cysteine residue, which has been well-documented in terms of reactivity.[73] GFPS147C **48** was

expressed as described in chapter 4 and required reduction of any disulfide linked GFP-homodimer species with TCEP **52** (25 eq.) prior to bioconjugation.

GFPS147C **48** (50 µM, pH 7.4) was incubated with DiEt PD (200 eq., 10 mM final concentration) **232** for 16 h at 37 °C to quantitatively produce the GFP-PD species **237**. Concerned with the high concentration of DiEt PD **232** required to synthesise the GFP-PD species **237**, this reaction was also repeated at pH 8.0 (*i.e.* increasing the amount of cysteine thiolate present during the bioconjugation). It was found that GFPS147C **48** (50 µM) could be fully modified with just 50 molar equiv. of DiEt PD **232** (2.5 mM final concentration) at pH 8.0 (Scheme 35a). As the reactivity of maleimide Michael acceptors have been well documented, a comparative GFP-maleimide species **239** was also synthesised for comparison alongside PD-based bioconjugates. GFPS147C **48** (50 µM, pH 7.4) was modified with a slowly hydrolysing *N*-methyl maleimide **238** (5 eq., 250 µM final concentration) to quantitively produce the GFP-maleimide species **239** (Scheme 35b).[195]

GFP-PD **237** and GFP-maleimide **239** conjugates (50 µM) were incubated at 37 °C for 7 days in PBS pH 7.4 and analysed by LCMS to assess if there was any retro-Michael mediated linker release in this time (Scheme 35c and 35e). The GFP-PD conjugate **237** showed no ring hydrolysis within this time but remarkably, a significant amount of the PD species (*ca.* 40%) had been released, as confirmed by the large quantity of GFPS147C **48** and GFPS147C dimer observed by LCMS (Scheme 35c). In parallel experiments, the GFP-maleimide conjugate **239** afforded only the succinamic acid species **241**, previously shown to be stable retro-Michael deconjugation (Scheme 35e).[195] PD and maleimide GFP conjugates **237** and **239** (50 µM) were also subject to incubation with a model monoBr PD species **157d** (200 eq., 10 mM final concentration) to assess the extent of retro-Michael deconjugation displayed by these bioconjugates (Scheme 35d and 35f). The reaction between GFPS147C **48** and monoBr PD species **157d** would in theory produce an irreversible unsaturated thiol-PD GFP species **240** that would serve as a trap for any available cysteine liberated from a retro-Michael pathway (Scheme 35d and 35f). For the GFP-PD species **237**, only the newly formed unsaturated GFP-PD species **240** was obtained, indicating full release of the original PD cargo from the cysteine residue, before reaction with monoBr PD **157d** (Scheme 35d). Interestingly, when GFP-maleimide species **239** was reacted with monoBr PD **157e**, partial formation of some unsaturated PD-GFP species **240** was observed (Scheme 35f).

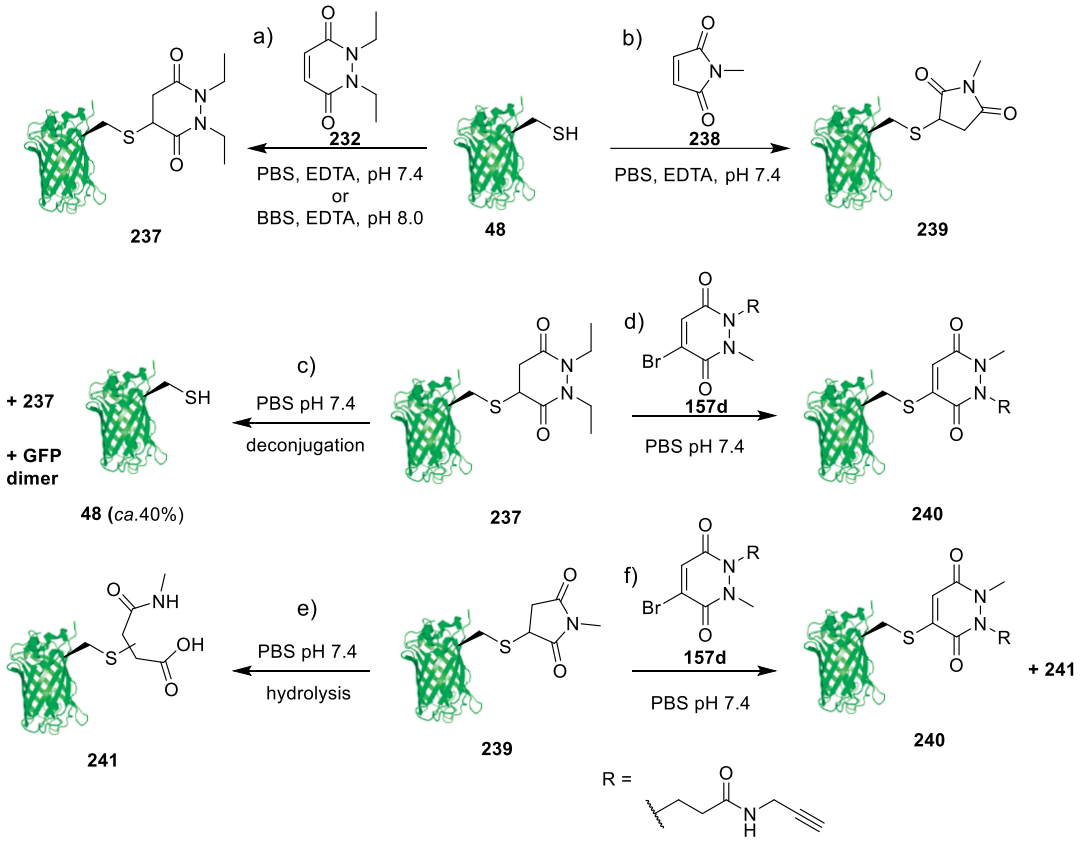

Scheme 35 – a) Bioconjugation of GFPS147C **48** (50 µM) with diethyl PD **232** (200 eq., 10 mM final concentration, at pH 7.4; 50 eq., 2.5 mM final concentration, at pH 8.0), for 16 h at 37 °C. b) Bioconjugation of GFPS147C **48** (50 µM, pH 7.4) with *N*-methyl maleimide **238** (5 eq., 250 µM final concentration) for 5 min at 21 °C. c) Incubation of GFP-PD conjugate **237** (50 µM, pH 7.4) for 7 days at 37 °C. d) Reaction of GFP-PD conjugate (50 µM, pH 7.4) **237** with monoBr PD **157d** (200 eq., 10 mM final concentration) for 7 days at 37 °C. e) Incubation of GFP-maleimide conjugate **239** (50 µM, pH 7.4) for 7 days at 37 °C. f) Reaction of GFP-maleimide conjugate (50 µM, pH 7.4) **239** with monoBr PD **157d** (200 eq., 10 mM final concentration) for 7 days.

An investigation was also conducted to assess the comparative rates of retro-Michael deconjugation displayed by these bioconjugates. By incubating GFP-PD species **237** (14 µM, pH 7.4) and GFP-maleimide species **239** (13 µM, pH 7.4) with excess DTNB **234** (250 µM final concentration) at 37 °C, any liberated cysteine was assumed to react quantitatively to form TNB **236** with a characteristic absorbance at 412 nm (Figures 32a and 32b). The value obtained for the concentration of TNB **236** was then subtracted from initial concentrations of GFP conjugates **237** and **239** to plot the change in concentration over 12 h (Figure 32c and 32d). Rate constants for the pseudo first order retro-Michael deconjugation reactions were found to be 2.34×10^{-5} s^{-1} for the GFP-maleimide species **239** and 2.29×10^{-5} s^{-1} for the GFP-

PD species **237**. When comparing rate constants for deconjugation of the maleimide and PD species, there appears to be no significant difference between these values. From these results it can be deduced that the difference in equilibrium shift between maleimides and PDs (shown by incubation in buffered conditions at pH 7.4 and with monoBr PD **157d**) is likely a consequence of the vastly different rates of Michael addition presented by these two motifs.

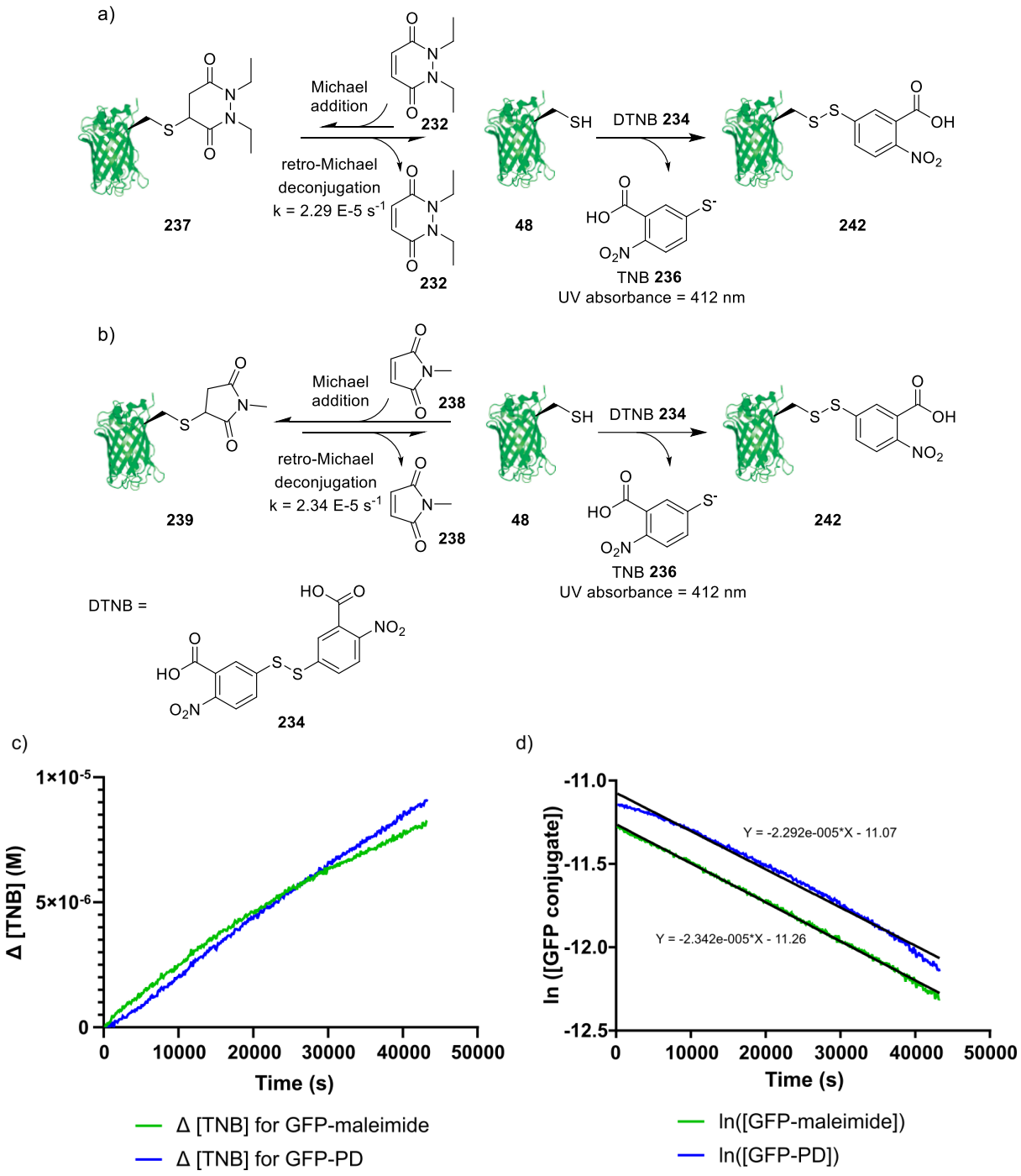

Figure 32 – a) Reaction of PD conjugate (14 µM in PBS pH 7.4) **237** with DTNB **234** (250 µM) for 12 h at 37 °C. b) Reaction of GFP-maleimide conjugate **239** (13 µM in PBS pH 7.4) with DTNB **234** (250 µM) for 12 h at 37 °C. c) Plot showing the change in TNB **236** concentration against time for GFP-PD conjugate **237** and GFP-maleimide conjugate **239**. d) Plot showing concentration logarithm of GFP conjugates against time.

These results confirm that both the GFP-PD species **237** and GFP-maleimide species **239** participate in retro-Michael deconjugation and both bioconjugates display a Michael

equilibrium. Interestingly, the rates of retro-Michael mediated release appear to be similar between these two Michael acceptors (2.34×10^{-5} s^{-1} and 2.29×10^{-5} s^{-1} for the maleimide and PD respectively (Figure 32c). However, non-Br PDs were shown to be considerably less reactive towards thiols than maleimide scaffolds (*i.e.* PDs exhibit a lower rate of Michael addition) and so display a unique Michael equilibrium in the context of reversible cysteine modification. Due to stability towards hydrolysis and a decreased reactivity towards cysteine, non-Br PDs were slowly released from saturated PD-based bioconjugates over time.

5.2 Pyridazinediones as Reversible Linkers in a Therapeutic Setting

Controlled linker release of cargo from a protein platform is an observation that may be utilised for numerous applications *in vivo,* including slow release of cargo in blood and as an extracellular cleavable linker for targeted therapies. It is envisaged that by synthesising a saturated PD-linked bioconjugate using a protein with a long blood half-life (*e.g.* Fc fragments),[13] slow and controlled release of cargo could be achieved (*i.e.* maintaining an effective blood concentration of therapeutic and decreasing dosing frequency).[10] Furthermore, targeted therapeutics harbouring linkers that undergo extracellular cleavage are in high demand (*i.e.* for ADCs that target non-internalising receptors) (Figure 33). It is thought that saturated PD-based bioconjugates could be used for this application, as long as the protein platform does not display a blood half-life in large excess of the timescale of PD release (*i.e.* resulting in significant loss of payload in blood before reaching the target cell).

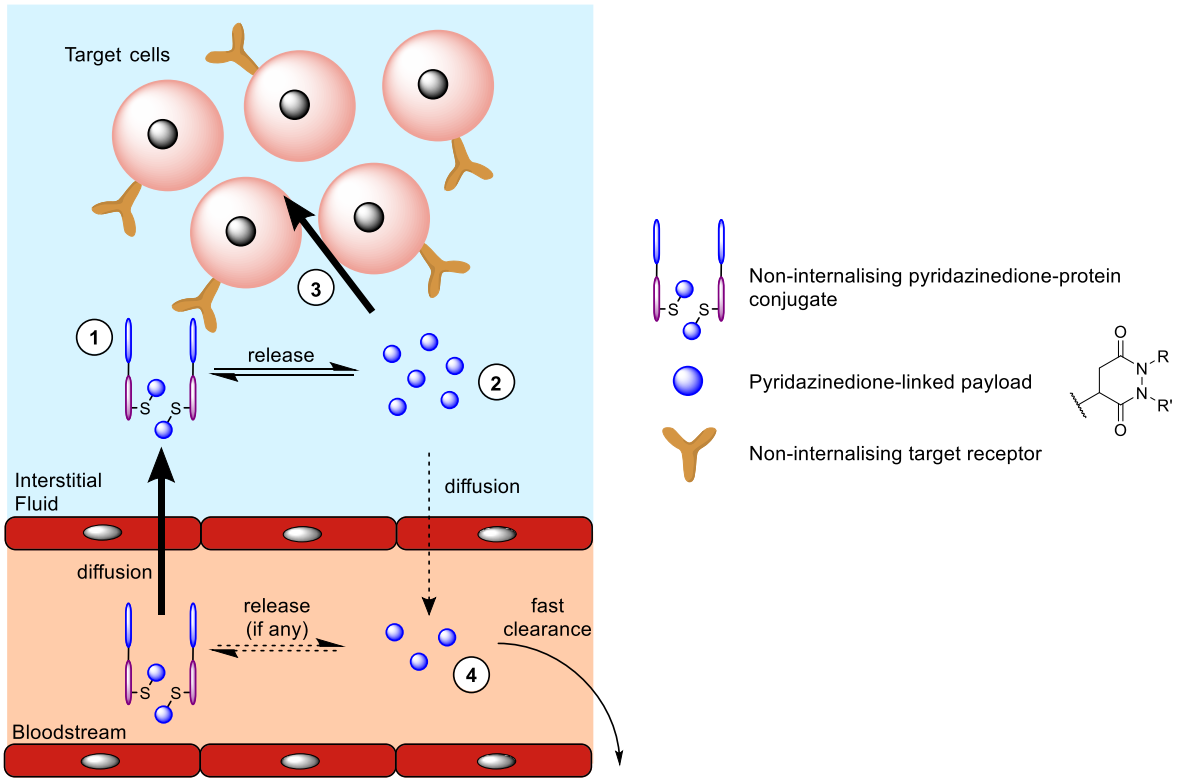

Figure 33 – Mechanism of action for non-internalising protein conjugates with cleavable PD linker. 1) Binding of protein-PD conjugate to non-internalising receptor; 2) controlled time-dependent release of PD in target area forming a high local concentration of payload; 3) Diffusion of payload into target cells; 4) If PD-payload diffuses back into the blood, or if prematurely released, a potential lack of reactivity toward blood thiols results in quicker clearance from the blood (*i.e.* no HSA-PD conjugate forms).

This work will investigate the use of non-Br PDs to modify a therapeutically relevant antibody fragment trastuzumab Fab **116**, and the stability of the resultant bioconjugates will be appraised. Trastuzumab **161** is used clinically in the treatment of breast, oesophageal and stomach cancers and is the antibody component of ADC Kadcyla.[164] Furthermore, the Fab fragment can easily be produced by digesting the readily available full antibody,[158] and there is ongoing clinical interest in the trastuzumab Fab fragment conjugates, particularly for use in imaging.[196–198] Trastuzumab Fab **116** contains a solvent accessible disulfide bond that will be reduced and the liberated cysteine residues will be modified individually. Many therapeutically relevant platforms contain a solvent accessible disulfide bond (*i.e.* antibody-derived proteins) and, if modification with non-Br PDs can be achieved, these results would vastly increase the applicability of saturated PD-linked bioconjugates in therapeutics. Once

trastuzumab Fab-PD conjugates have been synthesised, PD release will be monitored to assess whether retro-Michael deconjugation from this platform occurs on a suitable time scale for *in vivo* applications.

To appraise whether the therapeutically relevant bioconjugates synthesised using non-Br PDs would be suitable for applications *in vivo*, certain criteria must be met. Saturated PD-linked bioconjugates must be stable in blood and PD-release should be unaffected by blood thiols (*i.e.* GSH and HSA) to allow for controlled linker release. Ideally, once liberated, the non-Br PD should be unreactive towards the abundant blood thiol HSA (*i.e.* avoiding HSA-PD formation) as this would likely extend the half-life of the PD-linked cargo and would result in unwanted relocation of payload from the target site (if the PD is used as an extracellularly cleavable linker). Therefore, trastuzumab Fab-PD conjugates and non-Br PDs will be appraised in terms of reactivity towards blood thiols HSA and GSH.

5.2.1 Reversible Modification of Trastuzumab Fab Using Pyridazinediones

The cysteines available for modification on IgG1 Fab fragments exist as disulfide residues, so reduction of the disulfide bond of trastuzumab Fab **116** was required prior to addition of the PD. Reduced trastuzumab Fab **243** (20 µM, pH 8.0), was incubated with DiEt PD **232** (50 eq., 1 mM final concentration) for 16 h at 37 °C to quantitatively produce the Fab-PD species **244** (Figure 34a). Despite the presence of EDTA (added to complex metal ions in solution and prevent metal-catalysed disulfide re-oxidation), excess TCEP **52** (30 eq., 600 µM final concentration) was required to prevent competing disulfide re-oxidation over the time course of the PD conjugation (Figure 34a). A Fab-maleimide conjugate **245**, representing a chemically similar clinically relevant bioconjugate, was also synthesised for comparison with the Fab-PD conjugate **244**. Reduced trastuzumab Fab **243** (20 µM, pH 7.4), was incubated with *N*-methyl maleimide **238** (10 eq., 200 µM) for 5 min at 21 °C to quantitatively produce the Fab-maleimide species **245** (Figure 34a). Both Fab-PD species **244** Fab-maleimide species **245** were appraised in terms of binding affinity against HER2. ELISA results showed no significant difference between conjugated species **244** and **245** when compared with native trastuzumab Fab **116** (see experimental for chapter 5).

The Fab-PD conjugate **244** (20 µM, pH 7.4) and the Fab-maleimide conjugate **245** (20 µM, pH 7.4) were both incubated in PBS for 7 days at 37 °C. Surprisingly, after this time, the Fab-PD conjugate **244** had released all of the conjugated DiEt PD **232**, and only re-oxidised trastuzumab Fab **116** was observed by LCMS (Figure 34b). This observation suggests that PD release from a disulfide platform occurs in a shorter timeframe when compared with single cysteine models. This is likely due to a competing irreversible re-oxidation pathway that shifts the reversible equilibrium further in favour of retro-Michael deconjugation – releasing the PD (and potential cargo) (Figure 34b). The Fab–maleimide conjugate **245**, despite using a slowly hydrolysing *N*-methyl maleimide[199], only showed conjugate hydrolysis in the 7 day timeframe with no re-oxidsed Fab observed by LCMS (Figure 34c). This observation was expected however, due to the high reactivity of maleimides shifting the equilibrium in favour of Michael conjugation, and a competing hydrolysis that yields an irreversibly modified succinamic acid–cysteine conjugate (Figure 34c).

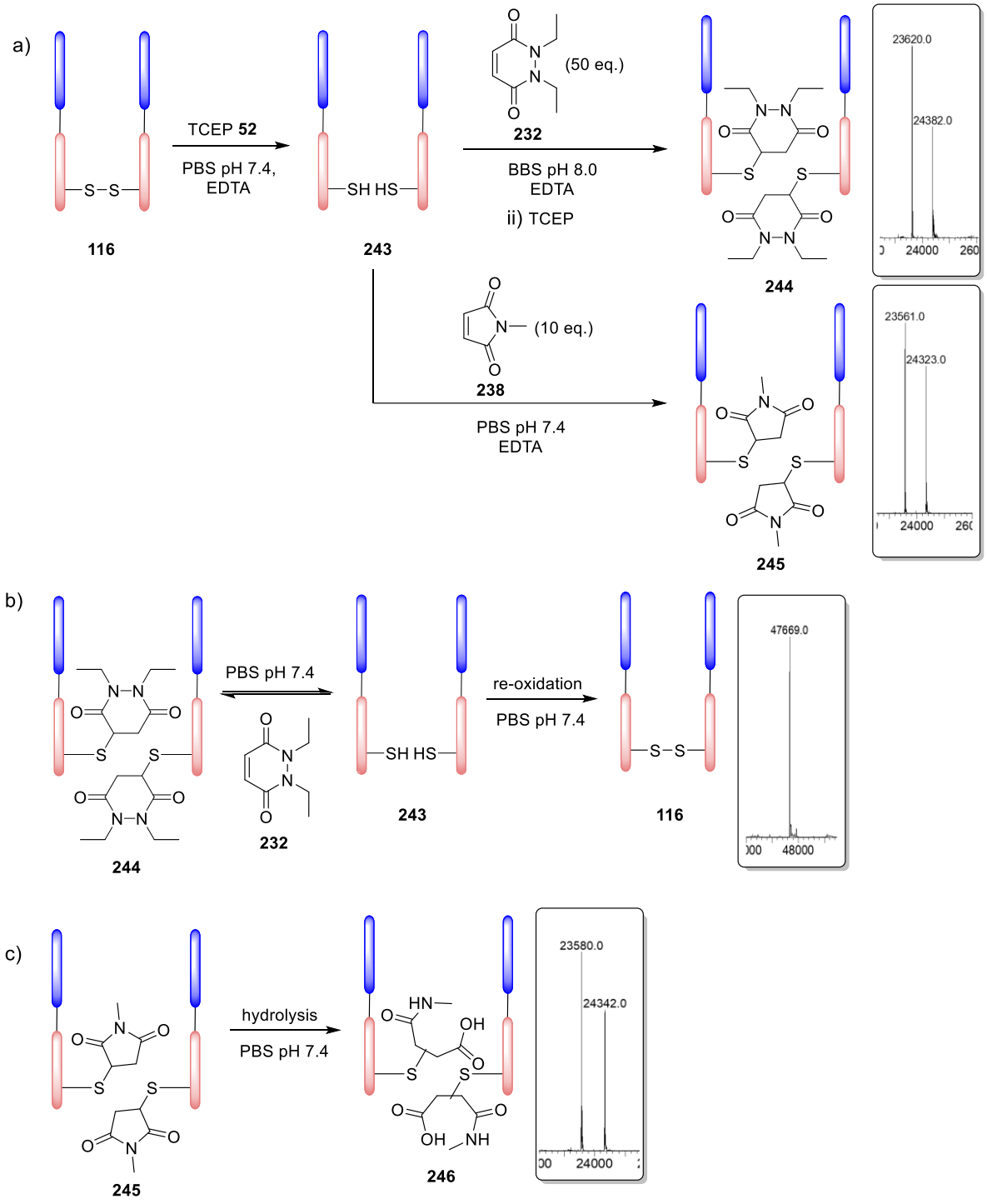

Figure 34 – a) Reduction of trastuzumab Fab **116** (20 µM, pH 7.4) reduction with TCEP **52** (20 eq., 400 µM final concentration) and subsequent reactions with DiEt PD **232** (50 eq., 1 mM final concentration, pH 8.0, 37 °C, 16 h) and *N*-methyl maleimide **238** (10 eq., 200 µM, pH 7.4, 21 °C, 5 min). Additional TCEP **52** (30 eq.) added to DiEt PD **232** reaction. b) Incubation of Fab-PD conjugate **244** (20 µM, pH 7.4, 37 °C, 7 days.). c) Incubation of Fab-maleimide conjugate **245** (20 µM, pH 7.4, 37 °C, 7 days.)

5.2.2 Stability Appraisal of PD-linked Bioconjugates Towards Blood Thiols

A general limitation associated with maleimide conjugates is the exceptional reactivity of the maleimide towards blood thiols. Once deconjugated, the free maleimide reacts with the abundant blood thiol human serum albumin (HSA), carrying cargo away from the desired parts of the body and retaining it in the blood. It was thought that the vast decrease in reactivity observed with PDs towards cysteine may provide an attractive alternative linker that is unreactive towards blood thiols.

To this end, the Fab-PD conjugate **244** and the Fab-maleimide conjugate **245** were incubated with HSA **27** and monitored by LCMS to assess whether transfer of payload to HSA **27** had occurred (Figure 35a and 35b). Incubation of the Fab-PD conjugate **244** (20 μM, pH 7.4) with HSA **27** (20 μM, 48 h), showed the saturated PD-Fab conjugate **244** to be stable and no transfer of PD was observed by LCMS (Figure 35a). In sharp contrast, when Fab-maleimide conjugate **245** (20 μM, pH 7.4) was subjected to paralleled HSA incubation conditions, significant amounts of HSA-maleimide species **247** was observed; confirming previous reports of blood instability of maleimide conjugates (Figure 35b).[200] The Fab-PD conjugate **244** (20 μM, pH 7.4) was also incubated with blood-mimicking concentrations of GSH **50** (5 μM) to assess whether the presence of a reactive thiol would accelerate PD release (Figure 35a). When compared to control experiments (*i.e.* incubation without the presence of GSH **50**), LCMS analysis showed no increase in the amount of PD released when incubating the Fab-PD conjugate **244** with GSH **50** (5 μM).

Finally, DiEt PD **232** was subjected to incubation (at pH 7.4) with GSH **50** and HSA **27** to assess the reactivity of the PD scaffold towards blood thiols at physiological pH. Incubation of each of HSA **27** (50 μM) and GSH **50** (500 μM) with diethyl PD **232** (2.5 mM and 500 μM, respectively) for 24 h at pH 7.4 led to no observable reaction in either case, even under these forcing conditions (Figure 35c).

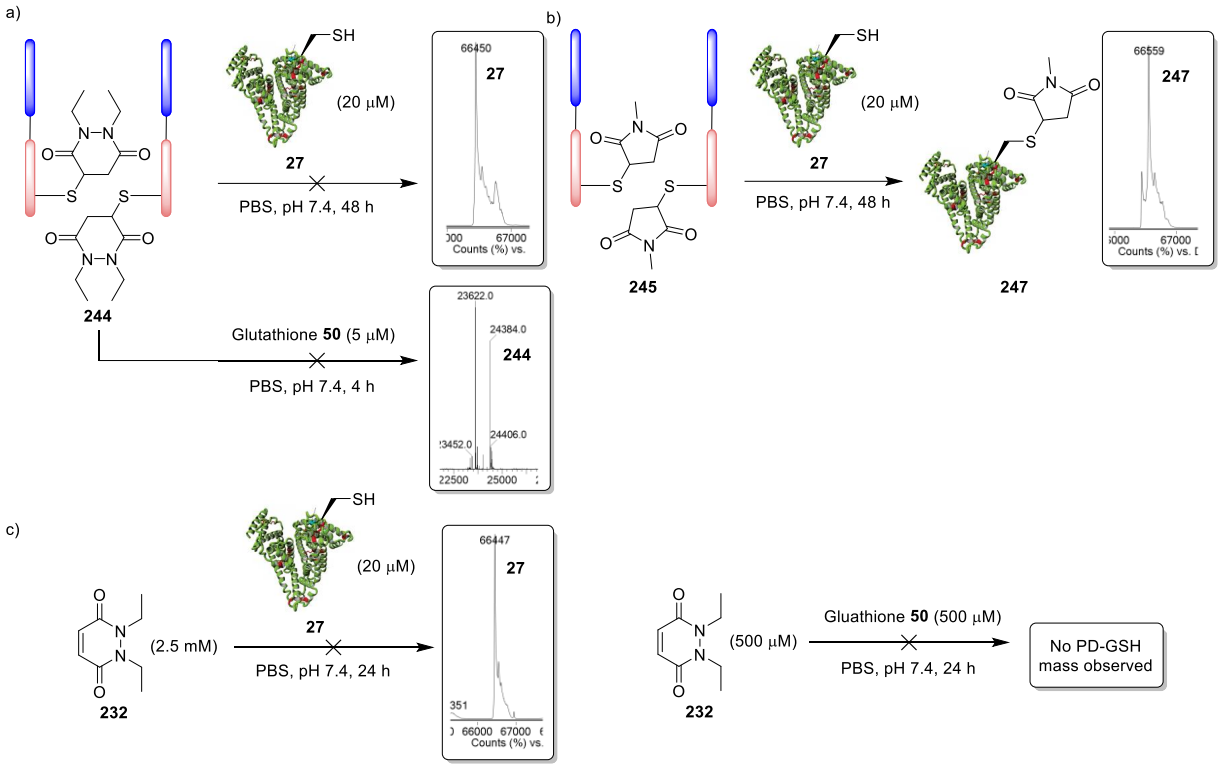

Figure 35 – a) Incubation of trastuzumab Fab-PD conjugate **244** (20 μM, pH 7.4) with HSA **27** (20 μM) for 48 h and incubation of trastuzumab Fab-PD conjugate **244** (20 μM, pH 7.4) in blood concentrations of GSH **50** (5 μM) for 4 h. b) Incubation of trastuzumab Fab-maleimide species **245** (20 μM, pH 7.4) with HSA **27** (20 μM) for 48 h. c) Incubation of non-Br DiEt PD **232** (2.5 mM) with HSA **27** (50 μM, pH 7.4) for 24 h and incubation of non-Br DiEt PD **232** (500 μM) with GSH **50** (500 μM, pH 7.4). All reactions of were carried out at 37 °C.

From these results it can be inferred that the saturated PD-linked bioconjugates are likely not affected by blood thiols, and that controlled release of PD-linked cargo could be achieved *in vivo*. Furthermore, the lack of cross-reactivity between the abundant blood thiol HSA **27** and non-Br PDs is an exciting observation. Combining a predictable time-dependent release mechanism with a high tolerance towards HSA may provide a useful cleavage mechanism, such that a PD payload could be slowly released in a target area without being carried away by blood thiols.

5.2.3 Effect of pH on Retro-Michael Mediated PD Release

Target environments for linker release such a tumour microenvironment or the intracellular early endosome have been reported to be mildly acidic in nature (*c.a.* pH 6.5).[201] Therefore, the effect of partially acidic pH on retro-Michael mediated PD release from the Fab-PD

species **244** was investigated. If PD release occurs under these conditions within a suitable timescale, saturated PD-linked bioconjugates could be used for applications that exploit linker cleavage in these environments (*e.g.* extracellular cleavable linkers for non-internalising ADCs).

Fab-PD species **244** (20 µM) was incubated under buffered conditions at pH 6.5 for 7 days. Despite acidic conditions slowing down the rate of Michael deconjugation, the majority of the DiEt PD **232** was still released from the conjugate (Figure 36b). A reduction in retro-Michael deconjugation can be expected at a lower pH as hydroxide ions likely initiate the E1cB elimination of the conjugated thiol, resulting in PD release. This concept was explored further by incubating the Fab-PD species **244** (20 µM) at pH 5.5 for 7 days, which resulted in a significant decrease in the amount of DiEt PD **232** released from the Fab PD species **244** (Figure 36c). This result shows an exciting example of how this dynamic reversible system may be controlled by varying pH to accelerate or slow PD release. PD-thiol conjugates could therefore be used for *ex* vivo applications in place of succinimide-thiol conjugates that are used as degradable systems (*e.g.* in the synthesis of hydrogels). The lack of PD release at pH 5.5 may also provide a logistical solution to long-term storage of synthesised conjugates in buffer.

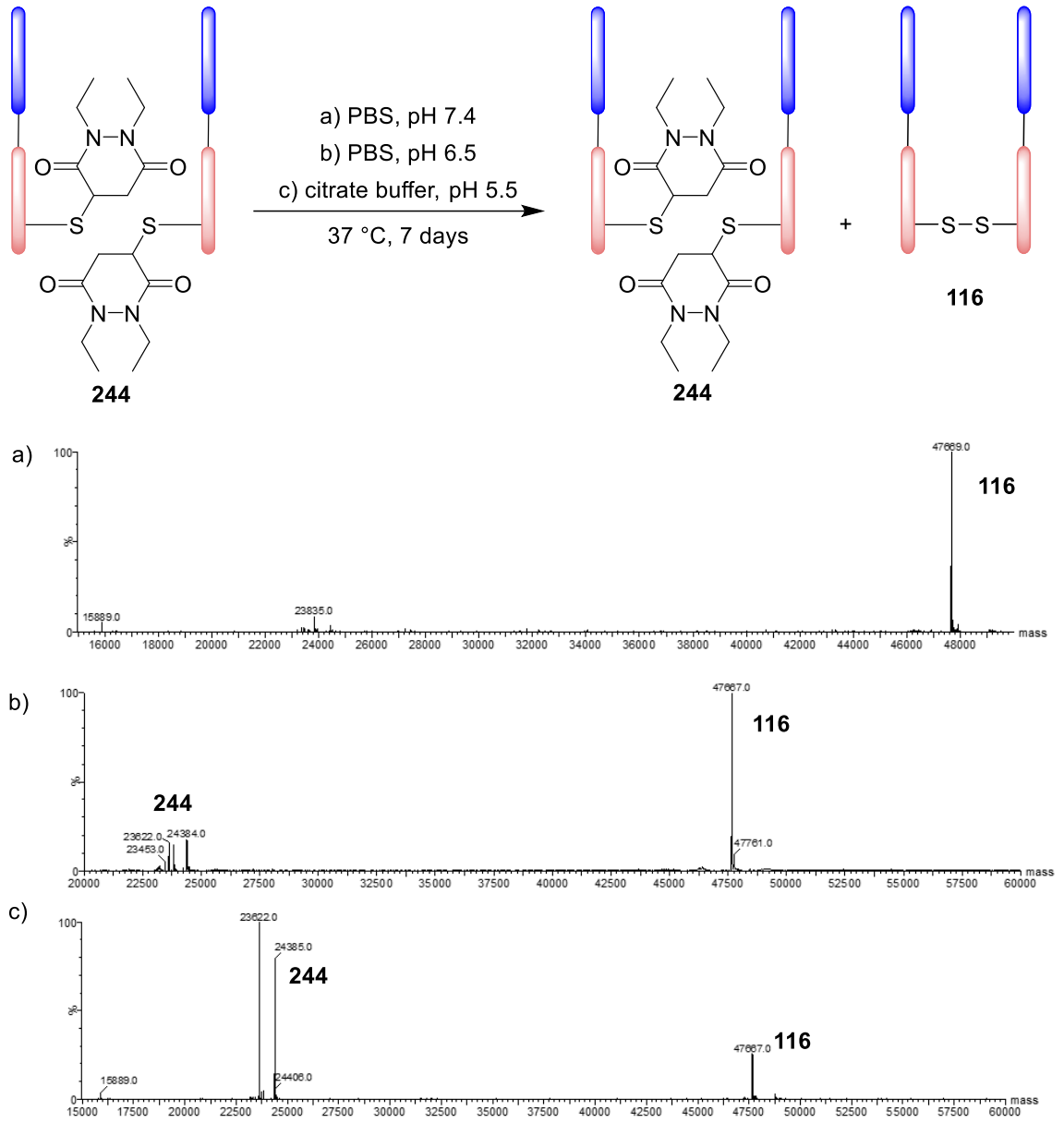

Figure 36 – Incubation of Fab-PD conjugate **244** in a) PBS pH 7.4; b) PBS pH 6.5; c) Citrate buffer pH 5.5.

5.3 Conclusions and Further Work

In this work, for the first time, the PD motif has been explored in the context of dynamic reversible cysteine modification. When comparing this motif with other Michael acceptors used in the field (e.g. highly thiol-reactive maleimides and cyanoacrylates) a slow release of PD was observed over time as well as the absence of any competing hydrolysis and a lack of reactivity between PDs and blood thiols (particularly with blood thiol serum albumin). This

non-Br PD derivative could have a unique place in the extracellular cleavable linker space by providing an opportunity for consistent slow release of cargo, which can then diffuse into cells and undergo intracellular specific cleavage, as a novel alternative to triggered cleavable linkers applied in the same context. Through rational bioconjugate design, a targeting protein with a suitable blood half-life modified with PD linkers could provide a slow release of payload without concern over cleavage in off-target areas. Alternatively, a protein with a long half-life in blood could be modified for a controlled release mechanism of PD linked cargo into blood.

This scaffold also has great potential to be developed further as a tuneable reversible system (as seen with other Michael acceptors used for reversible cysteine modification)[194]. By controlling rates of Michael addition and retro-Michael deconjugation, a reasonable level of control may be obtained over the timescale of PD release, allowing for the extensive use of this moiety in exciting aforementioned *in vivo* applications, or for a wider range of applications based on reversible cysteine modification (*e.g.* as reversible kinase inhibitors)[192].

By incorporating electron withdrawing groups (EWGs) onto the PD scaffold, the electrophilicity of this Michael acceptor is likely to increase. Therefore, PDs harbouring EWGs (*i.e.* **248** and **250**, scheme 36) would display an increased rate of Michael addition towards cysteine residues (Scheme 36). The resultant saturated-PD species containing EWGs (*i.e.* **249** and **251**, scheme 36) would also likely be more susceptible to retro-Michael deconjugation due to an increased acidity of the α-hydrogen that would in turn initiate E1cB elimination of the conjugated thiol (Scheme 36). In the context of a Michael equilibrium, an increased rate of Michael addition and retro-Michael deconjugation could result in PD-thiol reactivity at physiological pH, potentially leading to the use of PDs as reversible kinase inhibitors. Furthermore, tuning the PD scaffold and manipulating the Michael equilibrium could be used to further develop PDs for controlled linker release (*i.e.* control over the timescale of PD release could be achieved).

C-Functionalisation:

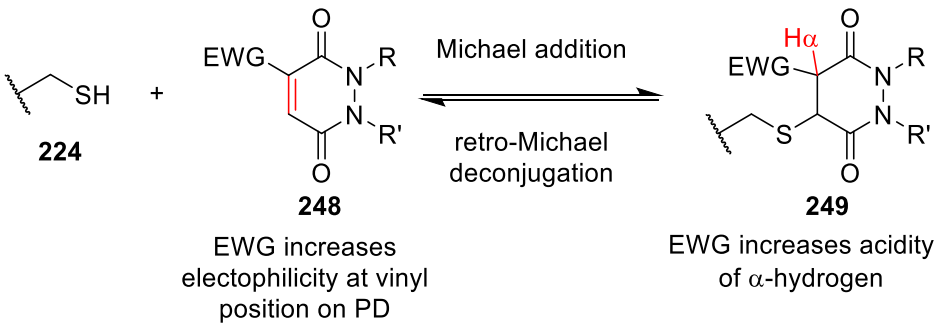

224 **248** **249**

EWG increases electophilicity at vinyl position on PD

EWG increases acidity of α-hydrogen

N-Functionalisation:

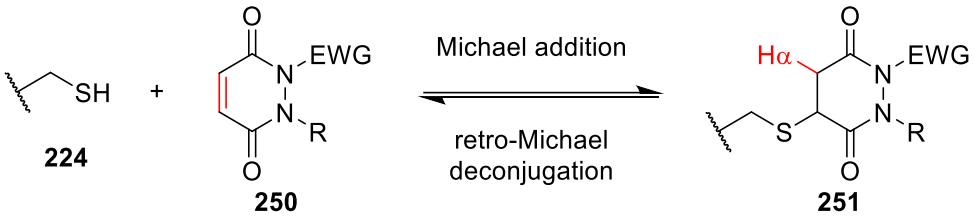

224 **250** **251**

EWG adjacent to nitrogen lone pair, increases electrophilicity of PD scaffold

Electron deficient PD increases acidity of α-hydrogen

Scheme 36– Potential Michael equilibrium shown by EWG-substituted PDs.

Conclusions and Future Outlook

In summary, this work set out to appraise and further develop the pyridazinedione (PD) scaffold in an attempt to form next-generation methodologies for the chemical enhancement of therapeutically relevant platforms. The following projects were presented:

***1) Synthesis optimisation of the core PD scaffold and functional amide derivatives*:** A one-pot synthesis of the core scaffold from readily available starting materials provides a safer and more efficient alternative to reported routes. Furthermore, a novel isolable NHS-ester enables a more general protocol for the derivatisation of this scaffold to form functional amide harbouring PDs in good to excellent yields.

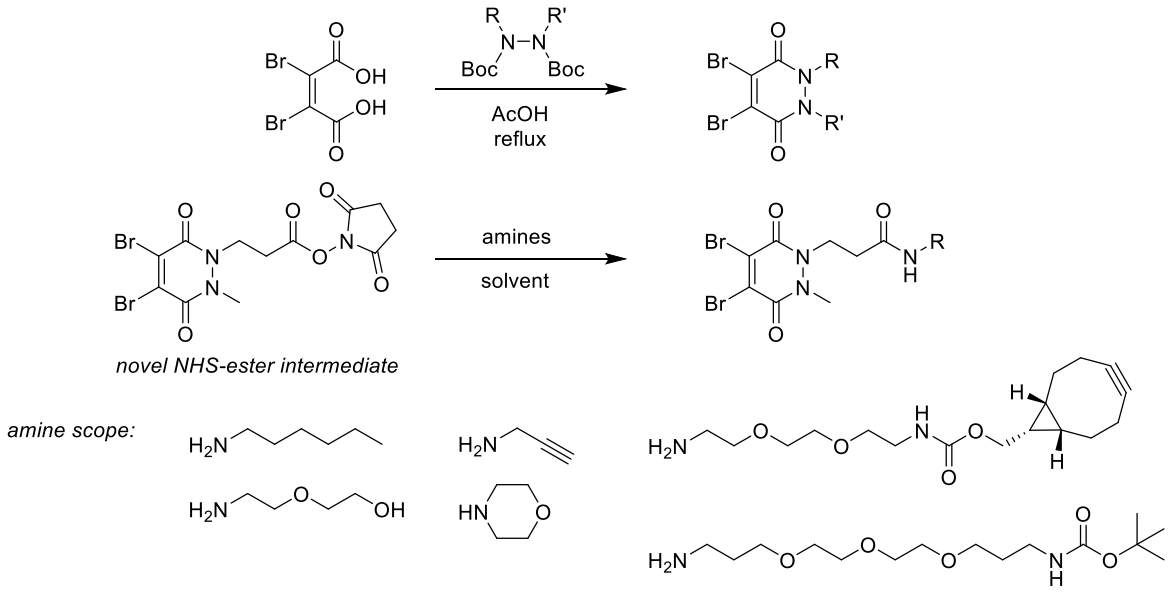

Scheme 37 – Summary of optimised synthesis to form core PD scaffold and functional amide harbouring PDs.

Future Outlook: Emerging compounds for bioconjugation often overlook synthetic yields due to the small quantity of reagent required to modify proteins on a small scale. By building on previously reported PD synthesis to provide higher overall yields and providing a synthetic intermediate that may act as a synthetic branch point, this synthesis can be considered more appealing for large scale-production. Furthermore, by providing alternative synthetic routes that avoid potentially unsafe procedures, this may further encourage use of this scaffold in the wider scientific community. With an increased number of academic/industrial

researchers adopting PD technology for use as a bioconjugation reagent, the development of this scaffold may reach an unprecedented level of use and development.

2) Appraisal of disulfide modified IgG1 antibodies in the context of secondary antibody function (Fc effector functions): The model IgG1 antibody trastuzumab was modified to provide a small library of bioconjugates each with a differing amount of interchain disulfide integrity. These bioconjugates were then compared in terms of antibody binding towards CD16a and FcRn (representative of ADCC activity and FcRn recycling respectively), and other biophysical attributes (*i.e.* antigen (HER2) binding, aggregation, thermal stability). This analysis revealed that, in most cases, modification of disulfide residues can result in a consequent effect on secondary antibody activity (confirmed through either CD16a kinetic data, or ADCC cell kill assays). However, when disulfide residues were re-bridged in a native conformation, tested secondary antibody interactions (*i.e.* CD16a and FcRn binding) were unaffected and bioconjugates remained fully active in ADCC cell kill assays. Natively re-bridged bioconjugates also provided a satisfactory biophysical profile, providing evidence that PD modification does not affect antigen binding, aggregation or thermal stability under the conditions tested.

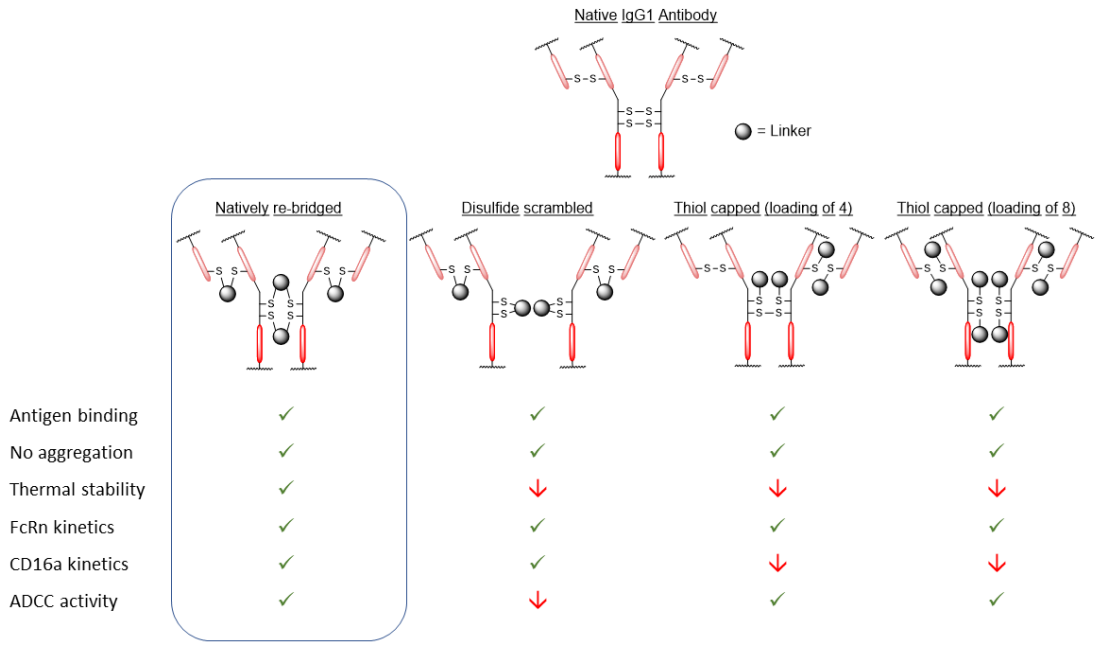

Figure 37 – Summary of results for disulfide modified trastuzumab conjugates.

Future outlook: To date, four of the ADCs that have been approved by the FDA utilise modification of interchain IgG1 disulfide bonds to attach payloads to the antibody platform. It is also expected that the linkers used for many of the ADCs in clinical development employ some form of disulfide modification. The results presented in this work that compare different methods of disulfide modification are therefore of great relevance to the expanding field of antibody conjugation. Importantly, this work provides evidence that a small change to antibody structure caused through intricate chemical modification can result in significant changes in antibody activity which may affect the efficacy of the therapeutic (*e.g.* re-bridging interchain disulfide bonds in a non-native conformation can affect ADCC activity). Consequently, researchers developing novel bioconjugation methods may benefit from similar analyses of their novel antibody conjugates, which should be straightforward to conduct following the detailed assays that have been developed in this work.

***3) Development of novel PD linker capable of tri-functionalisation*:** A general strategy for the addition of three functionalities to a single cysteine residue of a model protein (*i.e.* GFPS147C) is provided through use of post-conjugation functionalisation of a conjugated bromo PD derivative. This work demonstrates the process of conjugating and subsequently modifying a bromo harbouring Michael acceptor with various thiol and aniline derivatives. The resultant bioconjugates were then appraised in terms of thiol stability and all synthesised conjugates were shown to be stable in blood mimicking conditions. However, when these conjugates were incubated in conditions designed to mimic the early endosome, thiol derived bioconjugates were susceptible to cleavage under these conditions, whereas amine derived bioconjugates were stable for a minimum of 24 h. The results provided in this work suggest that PDs may provide an efficient platform for the addition of multiple functionalities (*i.e.* 1, 2 or 3 moieties) to single cysteine containing proteins, with significant control over thiol-stability of the resultant bioconjugates.

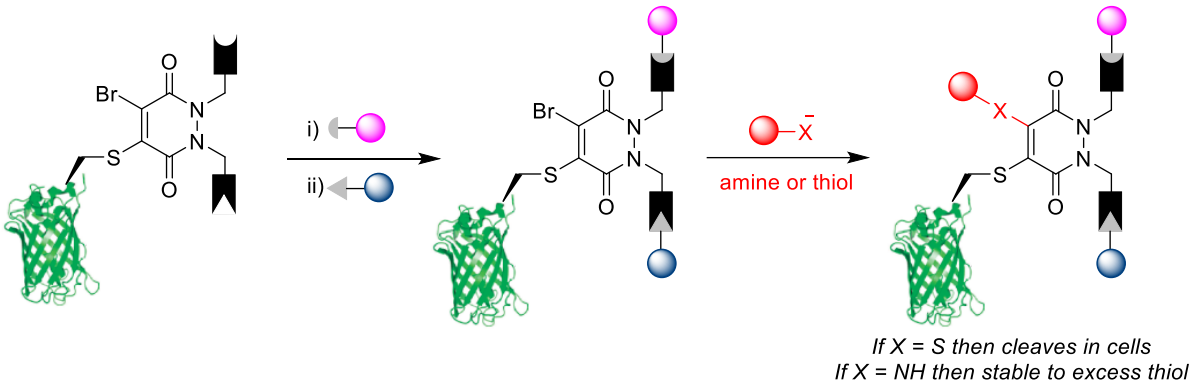

Scheme 38 – Summary showing post-conjugation functionalisation of GFP-PD-Br species as a platform for site-selective tri-functionalisation.

Future outlook: By providing a platform for the site-selective attachment of multiple commercially available functional compounds (*i.e.* DBCO, BCN and thiol containing moieties) it is envisaged that this linker may play a crucial role in research fields where multifunctionality is required (*e.g.* theranostics, FRET, blood half-life extension). Additionally, offering control over cleavability in high thiol concentrations may allow this platform to be extended to applications that use a range of physiological environments (*e.g.* intracellular imaging using CPPs).

4) Exploiting non-Br PDs as reversible cysteine modification reagents: In this work, for the first time, the PD motif was explored in the context of dynamic reversible cysteine modification. Modification of single cysteine- (*i.e.* GFPS147C) and disulfide- (*i.e.* trastuzumab Fab) containing proteins is presented, yielding saturated protein-PD species. Upon incubation in buffered conditions (pH 7.4) controlled PD-release was observed from the protein platforms over the timeframe of approximately 7 days. Through this retro-Michael based cleavage, it is thought that PDs could be exploited as cleavable linkers and applied in environments *in vivo* (*i.e.* in blood or in the extracellular space). Saturated PD-protein conjugates as well as non-Br PDs were shown to be unaffected by incubations with blood thiols human serum albumin and glutathione, suggesting they may be suitable for applications in the aforementioned thiol-containing physiological environments *in vivo*.

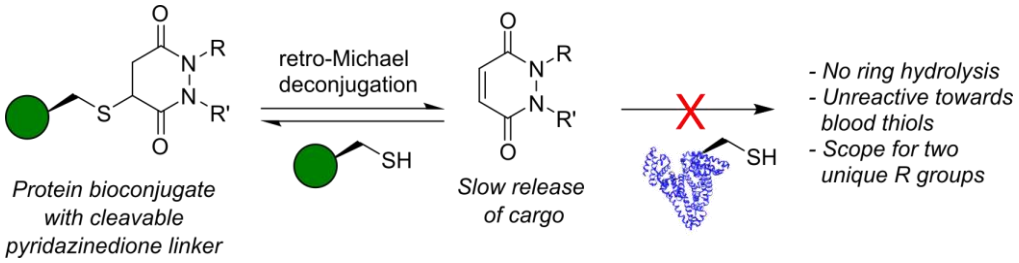

Scheme 39 – Summary showing dynamic reversible cysteine modification (*via* retro-Michael deconjugation) as a cleavable system that could potentially be applied *in vivo*.

Future outlook: This work presents a rare example of how PDs, alongside bioconjugate therapeutic design, may be used to exploit retro-Michael deconjugation for novel applications *in vivo*. In addition, the non-Br PD scaffold can also harbour up to two functionalities and could provide a multifunctional linker that can facilitate cleavage in blood or in the extracellular environment. It is also envisaged that this platform could be developed further to provide fine-tuned PD derivatives that display different rates of Michael addition and retro-Michael deconjugation. By controlling the electrophilicity of this Michael acceptor (*i.e.* by substituting the PD with EWGs/EDGs), it may be possible to achieve reasonable control over the timescale of PD release from the protein platform. These novel PD derivatives could then be functionalised and applied in physiologically relevant environments (*i.e.* in human serum or incubated with cells containing non-internalising receptors) to assess the practicality of this scaffold for the intended applications.

Experimental

General Experimental

All chemical reagents were purchased from Sigma Aldrich (Merck), Fisher Scientific, Alfa Aesar and Acros. Compounds and solvents were used as received. Petrol refers to petroleum ether (b.p. 40–60 °C). All reactions were carried out under positive pressure of argon, unless stated otherwise, and were monitored using thin layer chromatography (TLC) on pre-coated silica gel plates (254 μm). Flash column chromatography was carried out with pre-loaded FlashPure™ or GraceResolv™ flash cartridges on a Biotage® Isolera Spektra One flash chromatography system. ^{1}H NMR spectra were obtained at 300 MHz, 400 MHz, 500 MHz, 600 MHz or 700 MHz. ^{13}C NMR spectra were obtained at 125 MHz, 150 MHz or 175 MHz. All results were obtained using Bruker NMR instruments, the models are as follows: Avance Neo 700, Avance III 600, DRX 500, Avance III 400, Avance 300. All samples were run at the default number of scans and at 21 °C. Chemical shifts (δ) for ^{1}H NMR and ^{13}C NMR are quoted relative to residual signals of the solvent on a parts per million (ppm) scale. Where amide rotamers are the case, and when possible, only the major rotamer has been assigned for chemical shifts, and areas underneath all rotameric peaks have been considered for integration calculations. Coupling constants (*J* values) are reported in Hertz (Hz) and are reported as $J_{H\text{-}H}$ couplings. Infrared spectra were obtained on a Perkin Elmer Spectrum 100 FTIR spectrometer operating in ATR mode. Mass spectra were obtained for synthetic products from the Swansea EPSRC NMSF facility or the UCL mass spectroscopy service on either a LTQ Orbitrap XL (Swansea), Thermo Finnigan MAT900Xp (EI and CI, UCL) or Waters LCT Premier XE (ES, UCL) mass spectrometer. Melting points were measured with Gallenkamp apparatus and are uncorrected.

UV-Vis spectroscopy

UV-Vis spectroscopy was used to determine protein concentrations and payload to antibody ratios (PAR), using a Varian Cary 100 Bio UV-Visible spectrophotometer or a NanoDrop™ One microvolume UV-Vis spectrophotometer operating at 21 °C. Sample buffer was used as blank for baseline correction. Extinction coefficients for proteins (at A_{280}) and payloads (at

A_{max}) are listed below. A correction factor was applied in the event that the conjugated payload had a competing absorption at A_{280}, which is listed in the table below. PAR values were calculated by comparing concentrations of the payloads and the protein (calculated with corrected A_{280} values).

Protein	**Extinction Coefficient ε_{280} (M^{-1} cm^{-1})**
Trastuzumab	215,000
Trastuzumab Fab	68,590
Green Fluorescent Protein (GFPS147C)	20,500 (55,000 @ ε_{495})

Payload	**Extinction Coefficient (M^{-1} cm^{-1})**			**Correction Factor**
	ε_{280}	ε_{335}	ε_{495}	
Pyridazinedione Scaffolds	2,275	9,100	-	0.25
AlexaFluor-488	8,030	-	73,000	0.11

Corrected A_{280} = Experimental A_{280} – (A_{max} × Correction Factor)

Mass Spectrometry

LCMS analysis – Method 1

LCMS was performed on protein samples (<50 kDa) using a Waters Acquity uPLC connected to Waters Acquity Single Quad Detector (SQD). All samples were diluted to a final concentration of 1 mg/mL in deionised water and run with the following parameters. Column: Hypersil Gold C4, 1.9 µm, 2.1 µm × 50 µm. Wavelength: 254 nm. Mobile Phase: 95:5 Water (0.1% Formic Acid): MeCN (0.1% Formic Acid) Gradient over 4 min (to 5:95 Water (0.1% Formic Acid): MeCN (0.1% Formic Acid). Flow Rate: 0.6 mL/min. MS Mode: ES+. Scan Range: *m/z* = 250 – 2000. Scan time: 0.25 s. Data obtained in continuum mode. The electrospray source of the MS was operated with a capillary voltage of 3.5 kV and a cone voltage of 50 V. Nitrogen was used as the nebulizer and desolvation gas at a total flow of 600 L/h. Ion series were generated by integration of the total ion chromatogram (TIC) over the appropriate range. Total mass spectra for protein samples were reconstructed from the ion series using the MaxEnt 1 algorithm pre-installed on MassLynx software.

LCMS analysis – Method 2

Molecular masses were measured using an Agilent 6510 QTOF LC-MS system (Agilent, UK). Agilent 1200 HPLC system was equipped with an Agilent PLRP-S, 1000A, 8 µM, 150 mm x 2.1

mm column. 10 µL of a protein sample (diluted to 0.2 mg/mL in d.d. H_2O) was separated on the column using mobile phase A (water-0.1% formic acid) and B (acetonitrile-0.1% formic acid) with an eluting gradient (as shown below) at a flow rate of 0.3 mL/min. The oven temperature was maintained at 60 °C. Antibody samples (100 µL, 1.0 mg/mL, in ammonium acetate buffer, 0.2 M, pH 6.8) were deglycosylated by incubating with PNGase F (1 µL, New England BioLabs) at 37 °C for 16 h.

LCMS mobile phase gradient for A/B elution:

Time (min)	**Solvent A (%)**	**Solvent B (%)**
0	85	15
2	85	15
3	68	32
4	68	32
14	65	35
18	5	95
20	5	95
22	85	15
25	85	15

Agilent 6510 QTOF mass spectrometer was operated in a positive polarity mode, coupled with an ESI ion source. The ion source parameters were set up with a VCap of 3500 V, a gas temperature at 350 °C, a dry gas flow rate at 10 L/min and a nebulizer of 30 psig. MS Tof was acquired under conditions of a fragmentor at 350 V, a skimmer at 65 V and an acquisition rate at 0.5 spectra/s in a profile mode, within a scan range between 700 and 4500 *m/z*. The data was then analysed by deconvoluting a spectrum to a zero-charge mass spectrum using a maximum entropy deconvolution algorithm within the MassHunter software version B.07.00. Deconvoluted spectra were avoided where possible in the quantification of conjugates due to differing ionisation tendencies between species with significantly different masses.

LCMS analysis – Method 3

LC-MS was performed on a Thermo Scientific Q-Exactive Plus Orbitrap mass spectrometer coupled to Vanquish Flex UHPLC system using an Agilent PLRP-S column (1,000 Å, 5 µm, S21 2.1 mm x 50 mm). Flow rate: 0.250 ml/min; Run time: 6 min. Solvent A: 0.1% formic acid in water, Solvent B: Acetonitrile; Gradient: 15-90%. Column temperature: 80 ˚C. All mass spectrometry results were analysed using Thermo Scientific BioPharma Finder informatics platform for protein characterization.

SDS-PAGE & Densitometry Analysis

Non-reducing glycine-SDS-PAGE at 10% acrylamide running were performed following standard lab procedures. A 4% stacking gel was used and a broad-range molecular weight (MW) marker (3–198 kDa, Prestained SeeBlue™ Plus 2 protein standard, ThermoScientific) was co-run to estimate protein weights. Samples (10 µL at 7 µM) were mixed with loading buffer (2 µL, composition for 5 × SDS: 1 g SDS, 3 mL glycerol, 6 mL 0.5 M Tris buffer pH = 6.8, 2 mg bromophenol blue in 10 mL), heated at 75 °C for 5 min, and centrifuged at 16,000 RPM for 5 min. Samples were subsequently loaded into the wells in a volume of 5 µL. Gels were stained using InstantBlue™ protein stain (expedeon). Densitometry was performed using imageJ software. Background subtraction was achieved using the built-in plugin with a rolling ball radius of 30, sliding paraboloid, and smoothing. Brightness and contrast settings were auto-adjusted within the software.

Enzyme-linked immunosorbent assay (ELISA) – Trastuzumab against HER2

A Nunc MaxiSorp 384-well ELISA plate was coated with HER2 diluted to a final concentration of 1 µg/mL in PBS and incubated overnight at 4 ˚C. After emptying the wells, the plate was blocked for 1 h at 21 °C with 2% bovine serum albumin (BSA) in PBST (0.1% tween – 20). The plate was then washed 3 times with PBST, and the serially diluted test samples (22.3, 7.44, 2.48, 0.827, 0.276, 0.092, 0.031, 0.010, 0.003 nM) of trastuzumab and ADCs were added in 0.2% BSA, PBST. The plate was incubated for 1 h at 21 °C, washed 3 times with PBST, and anti-human IgG, Fab-specific-horseradish peroxidase (HRP) antibody (Sigma Aldrich, 1:5000 in 0.2% BSA, PBST) was added. After 1 h at 21 °C, the plate was washed again and 20 µL enhanced K-Blue® substrate (TMB) (Neogen) was added to each well. Once colour was observed, reaction was stopped by adding 10 µL Red Stop solution. Absorbance was immediately measured at 650 nm. Controls were included in every ELISA, in which PBS had been added to some of the wells instead of HER2 or instead of antibody sample. Each sample was tested in triplicate, and errors are shown as the standard deviation of the average.

Experimental for Chapter 2

Organic Synthesis

Di-*tert*-butyl 1,2-diethylhydrazine-1,2-dicarboxylate 137[71]

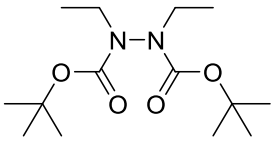

137

To a solution of di-*tert*-butyl hydrazine-1,2-dicarboxylate (1.16 g, 5.00 mmol) in DMF (20 mL) were added caesium carbonate (3.26 g, 10.0 mmol) and bromoethane (0.70 mL, 14.7 mmol). The heterogeneous mixture was stirred at 21 °C for 24 h. After this time, DMF was removed *in vacuo* with toluene co-evaporation (3 × 50 mL as an azeotrope). The crude reaction mixture was then dissolved in diethyl ether (100 mL), and then washed with water (3 × 30 mL) and saturated aq. LiCl solution (2 × 30 mL). The organic layer was dried ($MgSO_4$) and concentrated *in vacuo* to yield di-*tert*-butyl 1,2-diethylhydrazine-1,2-dicarboxylate **137** (1.21 g, 4.21 mmol, 81%) as a colourless oil: ^{1}H NMR (600 MHz, $CDCl_3$, rotamers) δ 3.47–3.40 (m, 4H), 1.47–1.42 (m, 18H), 1.15 (t, *J* = 7.2 Hz, 6H); ^{13}C NMR (150 MHz, $CDCl_3$, rotamers) δ 155.2 (C), 80.7 (C), 44.4 (CH_2), 28.4 (CH_3), 13.0 (CH_3); IR (thin film) 2976, 2934, 1702 cm^{-1}.

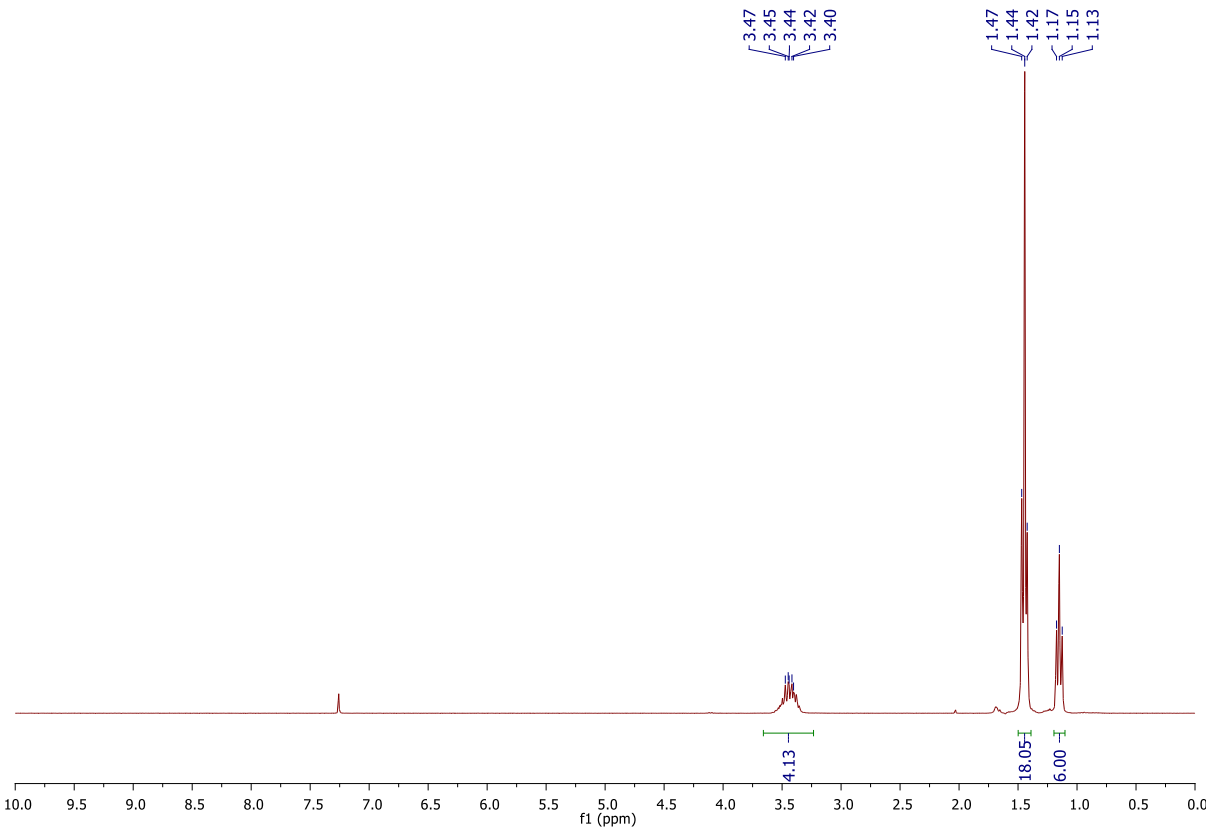
3.47
3.45
3.44
3.42
3.40
1.47
1.44
1.42
1.17
1.15
1.13
4.13
18.05
6.00
f1 (ppm)

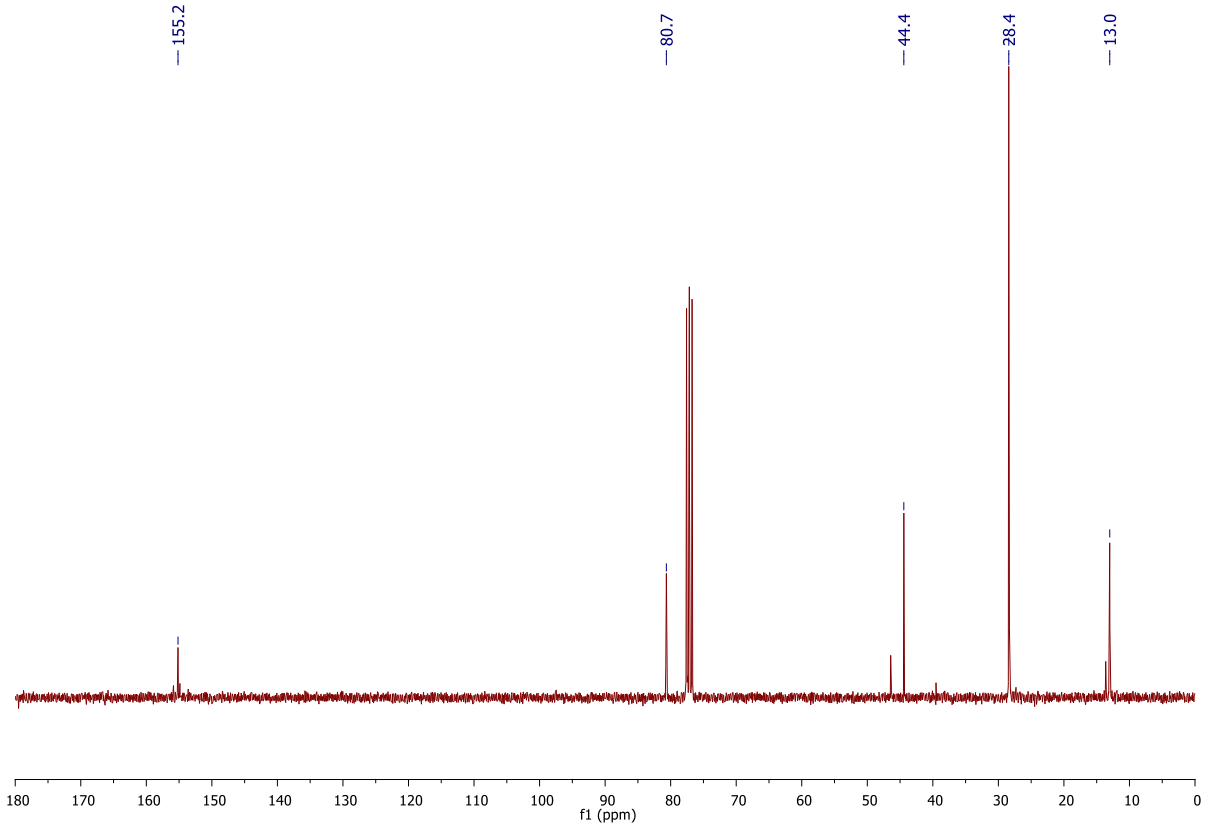
155.2
80.7
44.4
28.4
13.0
f1 (ppm)

***N*-Methoxycarbonyl-3,4-dibromomaleimide 129**[156]

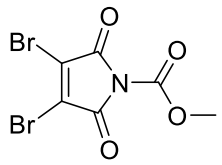

129

To a solution of 3,4-dibromo-1*H*-pyrrole-2,5-dione (500 mg, 2.00 mmol) and 4-methylmorpholine (0.21 mL, 2.00 mmol) in THF (20 mL), was added methyl chloroformate (0.15 mL, 2.00 mmol). The reaction mixture was stirred at 21 °C for 30 min. After this time, the THF was removed *in vacuo,* the crude residue dissolved in EtOAc (75 mL) and washed with water (3 × 25 mL). The organic layer was then dried ($MgSO_4$) and concentrated *in vacuo* to yield *N*-methoxycarbonyl-3,4-dibromomaleimide **129** (525 mg, 1.68 mmol, 84%) as a purple solid: m.p. 120–122 °C; ^{1}H NMR (600 MHz, $CDCl_3$) δ 4.01 (s, 3H); ^{13}C NMR (150 MHz, $CDCl_3$) δ 159.4 (C), 147.1 (C), 131.6 (C), 54.9 (CH_3); IR (solid) 2961, 2851, 1809, 1771, 1727, 1601 cm^{-1}.

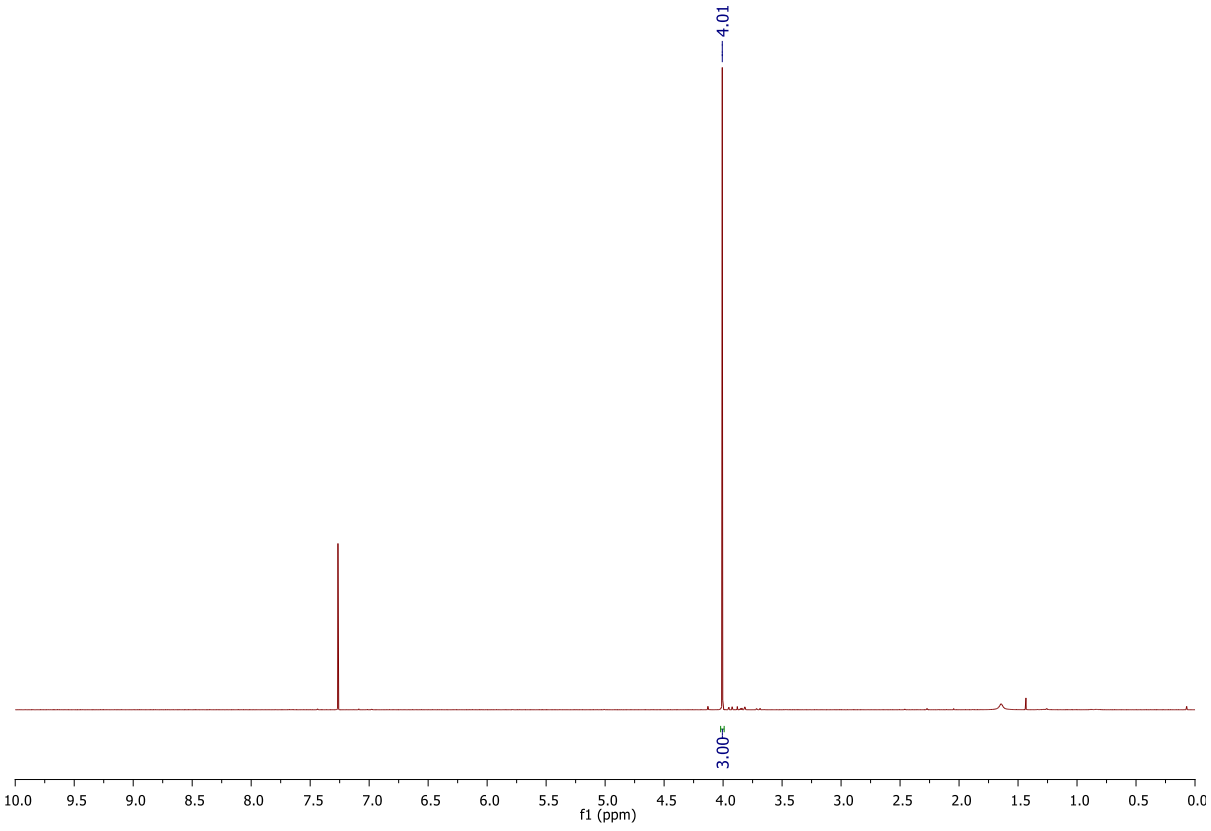

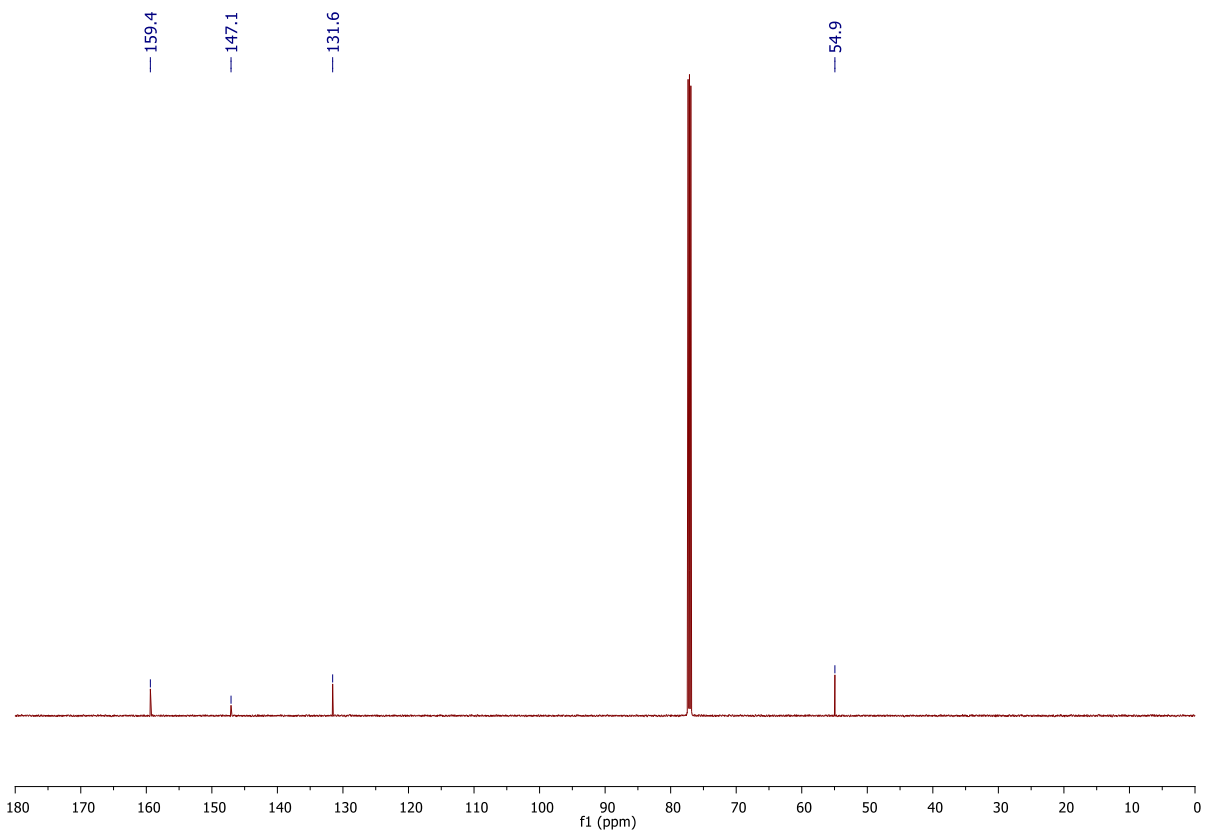
159.4
147.1
131.6
54.9
180
170
160
150
140
130
120
110
100
90
80
70
60
50
40
30
20
10
0
f1 (ppm)

4,5-Dibromo-1,2-diethyl-1,2-dihydropyridazine-3,6-dione 136[71]

Preformation of dibromo maleic anhydride in situ:

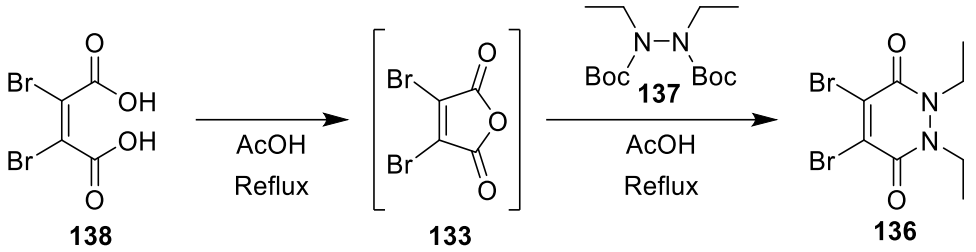

138 133 136

Dibromomaleic acid **138** (274 mg, 1.00 mmol) was dissolved in AcOH (10 mL) and heated under reflux for 2 h. After this time, di-*tert*-butyl 1,2-diethylhydrazine-1,2-dicarboxylate **137** (347 mg, 1.20 mmol) was added and the resultant mixture was heated under reflux for a further 4 h. After this time, the reaction mixture was concentrated *in vacuo* with toluene co-evaporation (3 × 20 mL, as an azeotrope). Purification of the crude residue by flash column chromatography (30% to 70% EtOAc/petrol) yielded 4,5-dibromo-1,2-diethyl-1,2-dihydropyridazine-3,6-dione **136** (267 mg, 0.819 mmol, 82%) as a yellow solid: m.p. 110–115 °C; ^{1}H NMR (600 MHz, $CDCl_3$) δ 4.17 (q, *J* = 7.1 Hz, 4H), 1.29 (t, *J* = 7.1 Hz, 6H); ^{13}C NMR (150 MHz, $CDCl_3$) δ 153.2 (C), 136.1 (C), 42.4 (CH_2), 13.1 (CH_3); IR (solid) 2979, 2937, 2873, 1629, 1574 cm^{-1}.

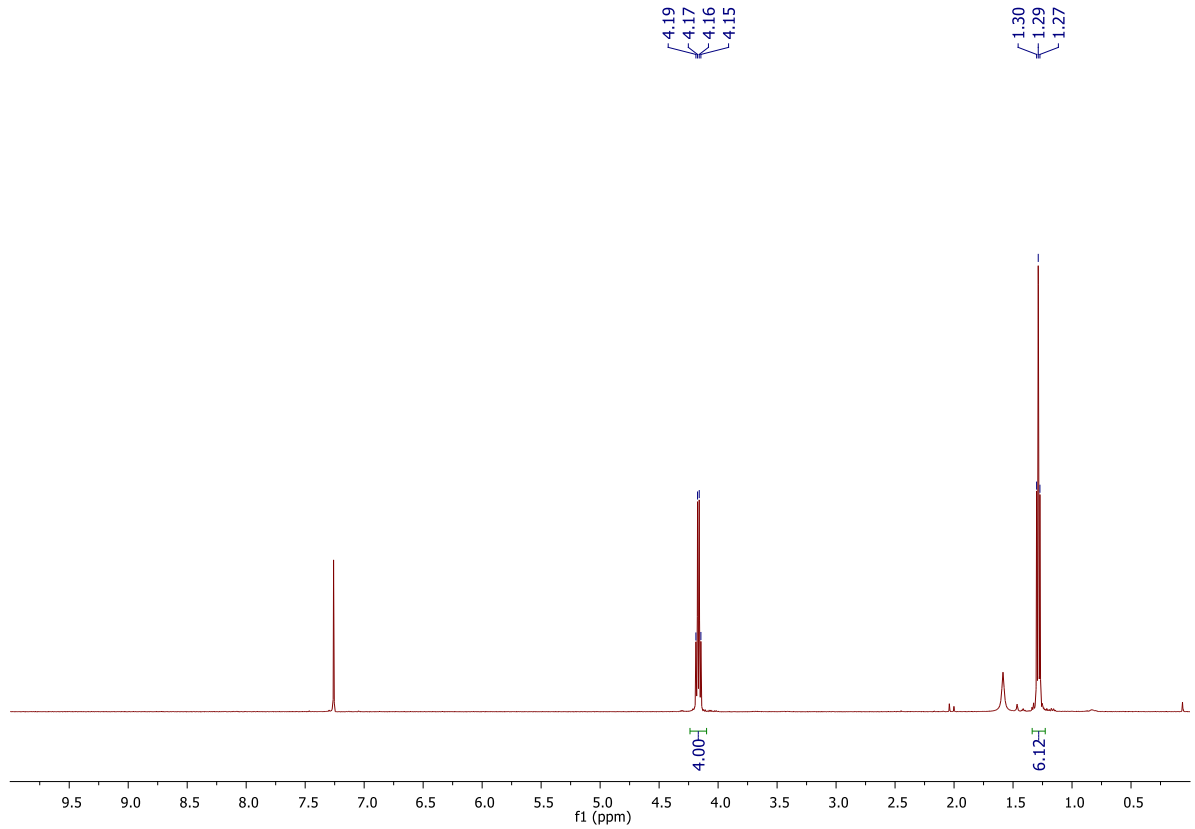
4.19
4.17
4.16
4.15
1.30
1.29
1.27
4.00
6.12
9.5 9.0 8.5 8.0 7.5 7.0 6.5 6.0 5.5 5.0 4.5 4.0 3.5 3.0 2.5 2.0 1.5 1.0 0.5
f1 (ppm)

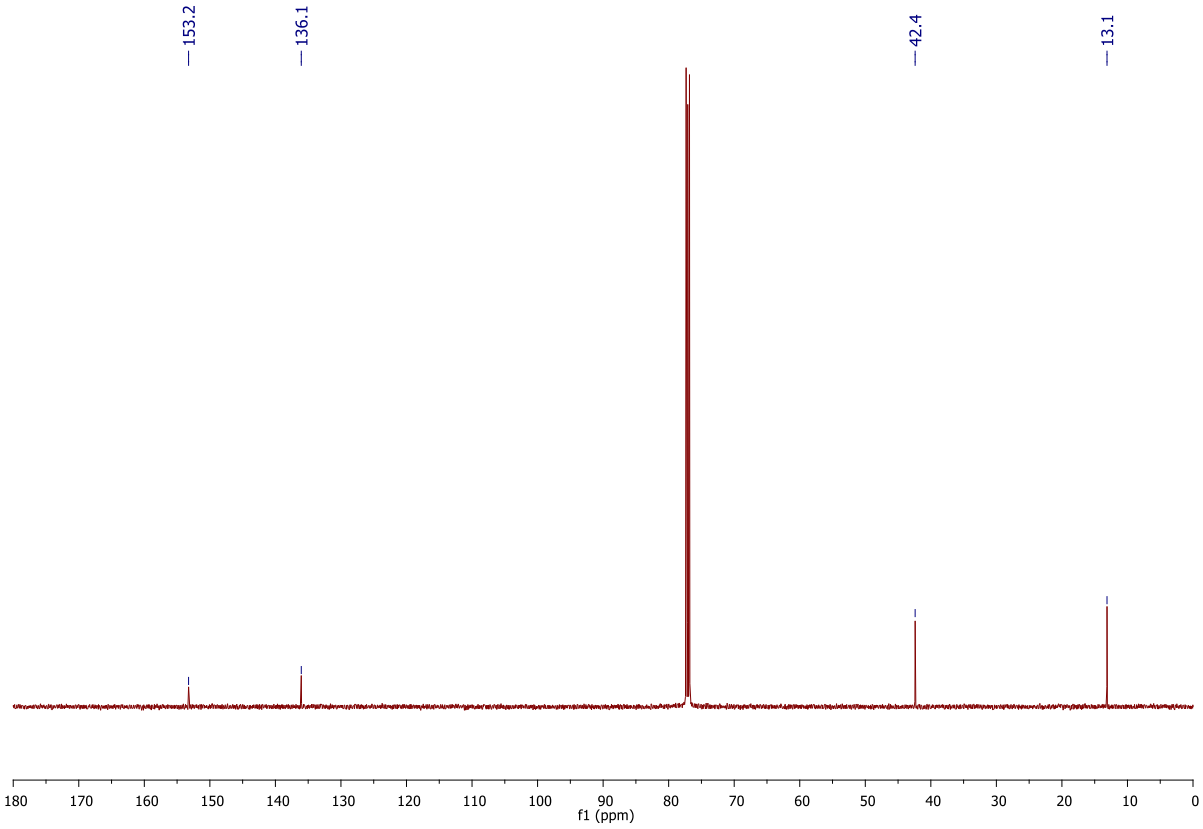
153.2
136.1
42.4
13.1
180 170 160 150 140 130 120 110 100 90 80 70 60 50 40 30 20 10 0
f1 (ppm)

No preformation of anhydride in situ:

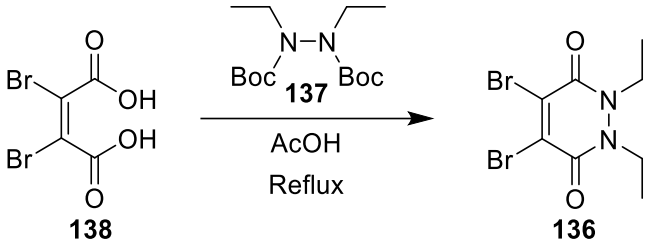

To a solution of dibromomaleic acid **138** (274 mg, 1.00 mmol) in AcOH (10 mL) was added di-*tert*-butyl 1,2-diethylhydrazine-1,2-dicarboxylate **137** (347 mg, 1.20 mmol) and the reaction mixture heated under reflux for 4 h. After this time, the reaction mixture was concentrated *in vacuo* with toluene co-evaporation (3 × 20 mL, as an azeotrope). Purification of the crude residue by flash column chromatography (30% to 70% EtOAc/petrol) yielded 4,5-dibromo-1,2-diethyl-1,2-dihydropyridazine-3,6-dione **136** (210 mg, 0.65 mmol, 65%) as a yellow solid.

From dibromo maleic anhydride:

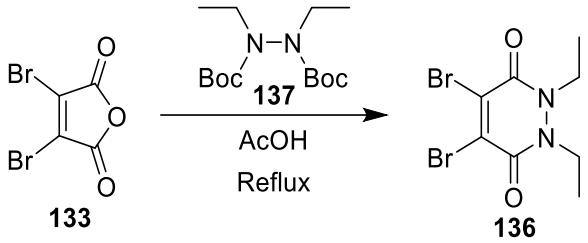

To a solution of dibromomaleic anhydride **133** (258 mg, 1.00 mmol) in AcOH (10 mL), was added di-*tert*-butyl 1,2-diethylhydrazine-1,2-dicarboxylate **137** (347 mg, 1.20 mmol) and the reaction mixture heated under reflux for 4 h. After this time, the reaction mixture was concentrated *in vacuo* with toluene co-evaporation (3 × 20 mL, as an azeotrope). Purification of the crude residue by flash column chromatography (30% to 70% EtOAc/petrol) yielded 4,5-dibromo-1,2-diethyl-1,2-dihydropyridazine-3,6-dione **136** (261 mg, 0.80 mmol, 80%) as a yellow solid.

From N-methoxycarbonyl-3,4-dibromomaleimide (24 h + Base):

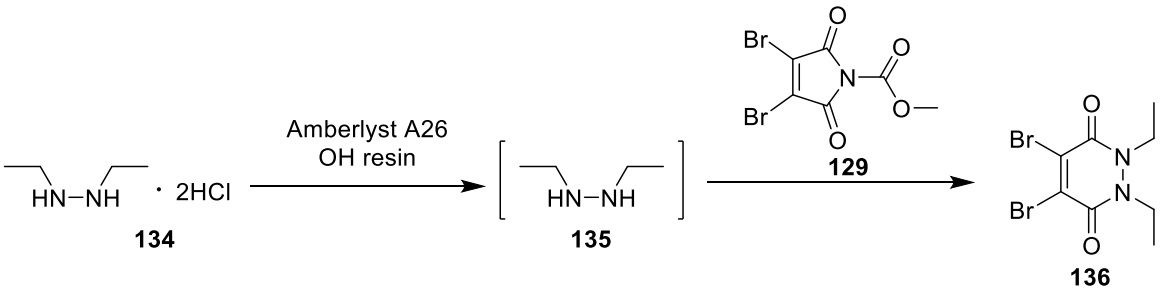

To a heterogeneous solution of amberlyst A26 OH resin (200 mg) in CH_2Cl_2 (10 mL), was added 1,2-diethylhydrazine dihydrochloride **134** (193 mg, 1.20 mmol). The reaction mixture was stirred at 21 °C for 2 h. Following this, the resin was removed by filtration and was added *N*-methoxycarbonyl-3,4-dibromomaleimide **129** (313 mg, 1.00 mmol). The reaction mixture was then stirred for a further 20 h at 21 °C. After this time, CH_2Cl_2 was removed *in vacuo* and the crude residue was purified by flash column chromatography (30% to 70% EtOAc/petrol) to yield 4,5-dibromo-1,2-diethyl-1,2-dihydropyridazine-3,6-dione **136** (101 mg, 0.31 mmol, 31%) as a yellow solid.

Dibromomaleic anhydride 133 (by NMR in AcOH-D_4)

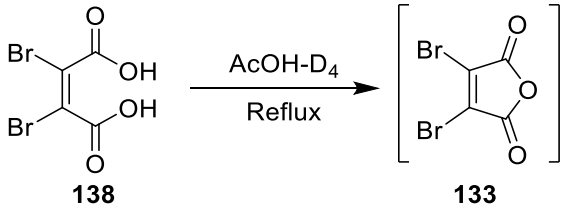

138 **133**

Dibromomaleic acid **138** (55 mg, 0.20 mmol) was dissolved in deuterated AcOH (AcOH-D_4) (2.4 mL) and the reaction heated under reflux for 90 min. The reaction mixture (0.5 mL) was cooled and analysed at 30 min intervals. Formation of dibromomaleic anhydride **133** was tracked by ^{13}C NMR. ^{13}C NMR (150 MHz, AcOH-d_4) δ 159.0 (C), 131.0 (C).

30 min:

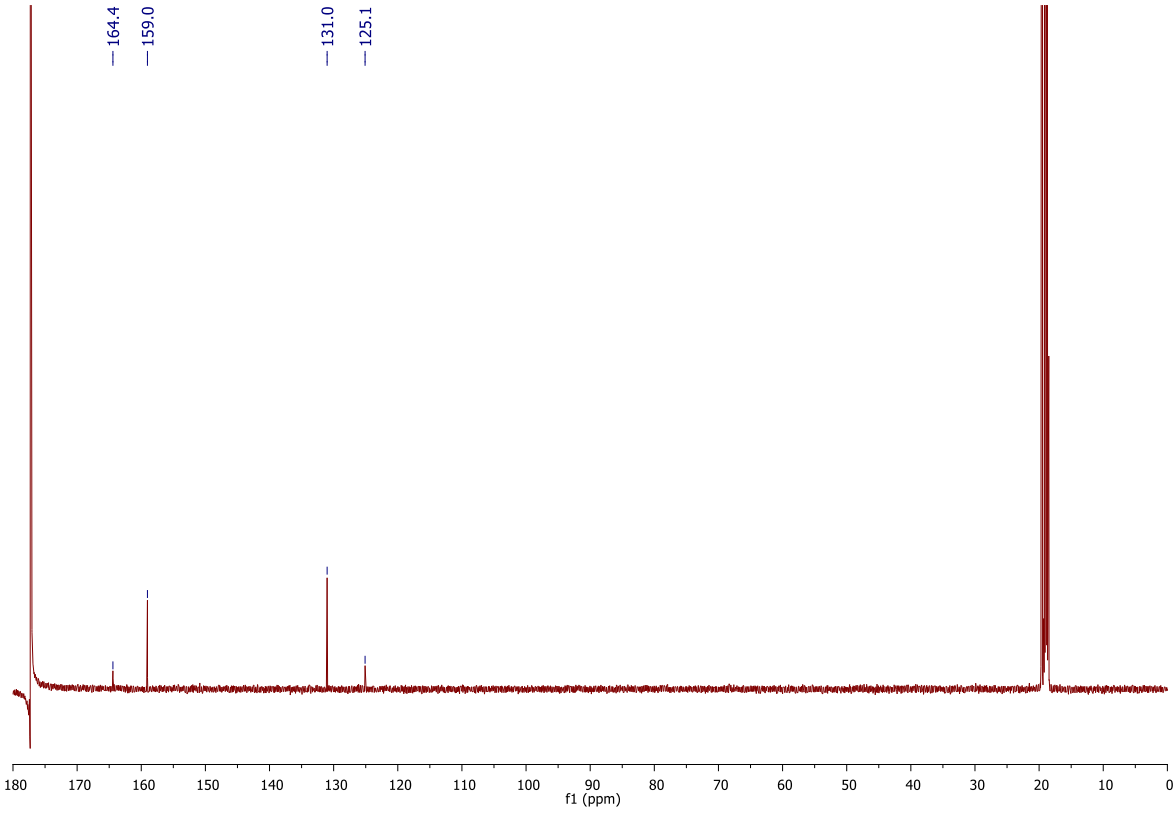

60 min:

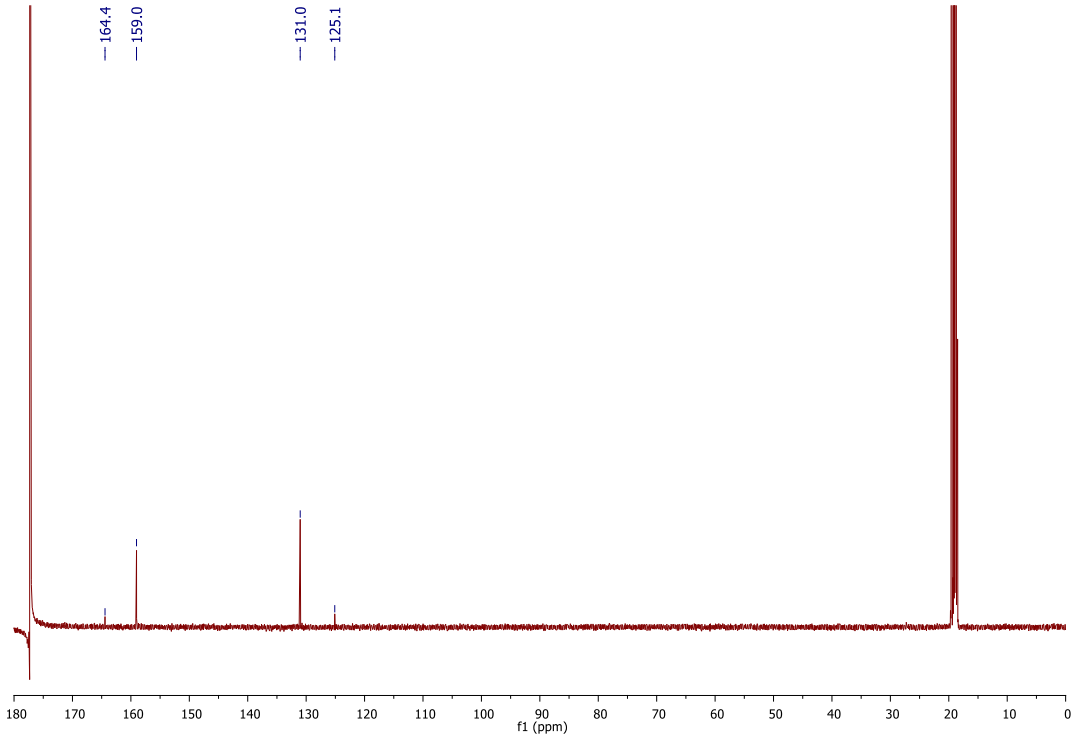
164.4
159.0
131.0
125.1
180 170 160 150 140 130 120 110 100 90 80 70 60 50 40 30 20 10 0
f1 (ppm)

90 min:

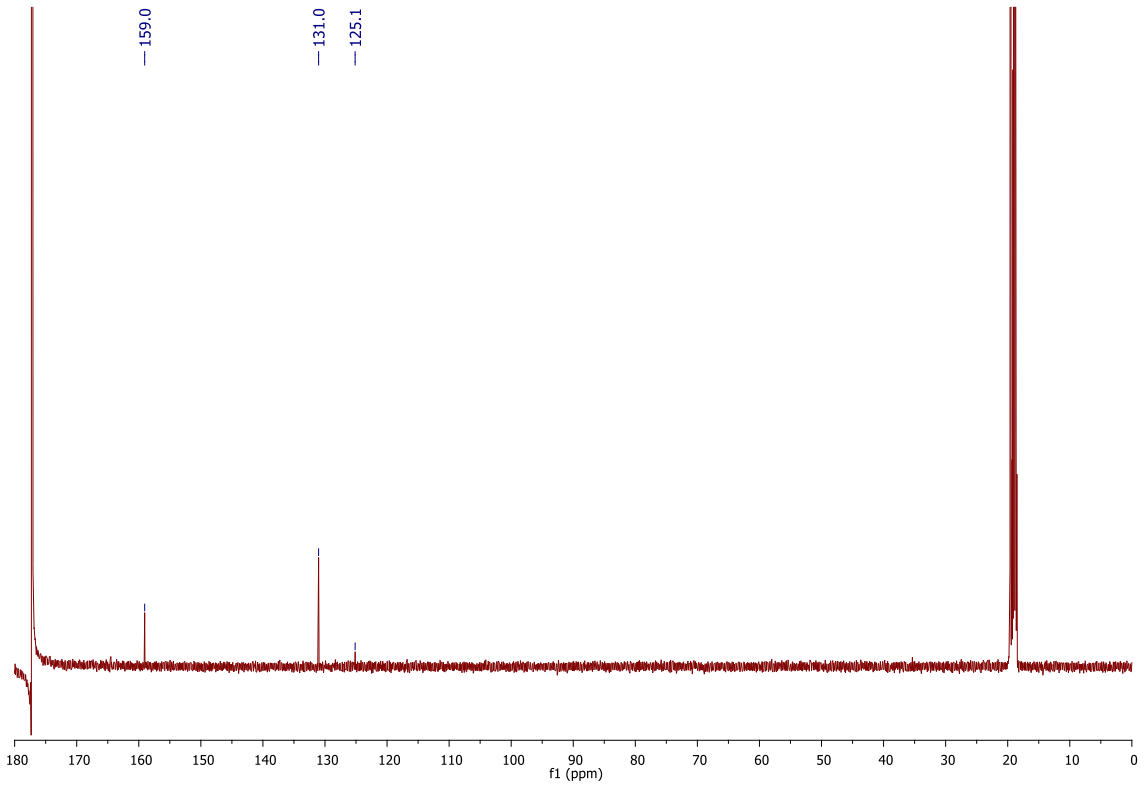
159.0
131.0
125.1
180 170 160 150 140 130 120 110 100 90 80 70 60 50 40 30 20 10 0
f1 (ppm)

Di-*tert*-butyl-1-methylhydrazine-1,2-dicarboxylate 148[154]

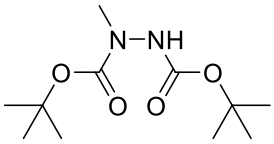

148

To a solution of methyl hydrazine (1.14 mL, 21.7 mmol) in *i*-PrOH (16 mL), was added a solution of di-*tert*-butyl dicarbonate (11.4 g, 52.1 mmol, pre-dissolved in CH_2Cl_2 (12 mL)) drop-wise over 30 min. The reaction was then stirred at 21 °C for 16 h. After this time, the solvents were then removed *in vacuo* and the crude residue purified by flash column chromatography (0% to 15% EtOAc/petrol) to afford di-*tert*-butyl-1-methylhydrazine-1,2-dicarboxylate **148** (4.67 g, 19.1 mmol, 88%) as a white solid: m.p. 58–62 °C (*lit m.p.* 54–56 °C)[1]; ^{1}H NMR (600 MHz, $CDCl_3$, rotamers) δ 6.41–6.16 (m, 1H) 3.11 (s, 3H), 1.47–1.46 (m, 18H); ^{13}C NMR (150 MHz, $CDCl_3$, rotamers) δ 155.9 (C), 81.3 (C), 37.5 (CH_3), 28.3 (CH_3); IR (solid) 3315, 2981, 1702 cm^{-1}.

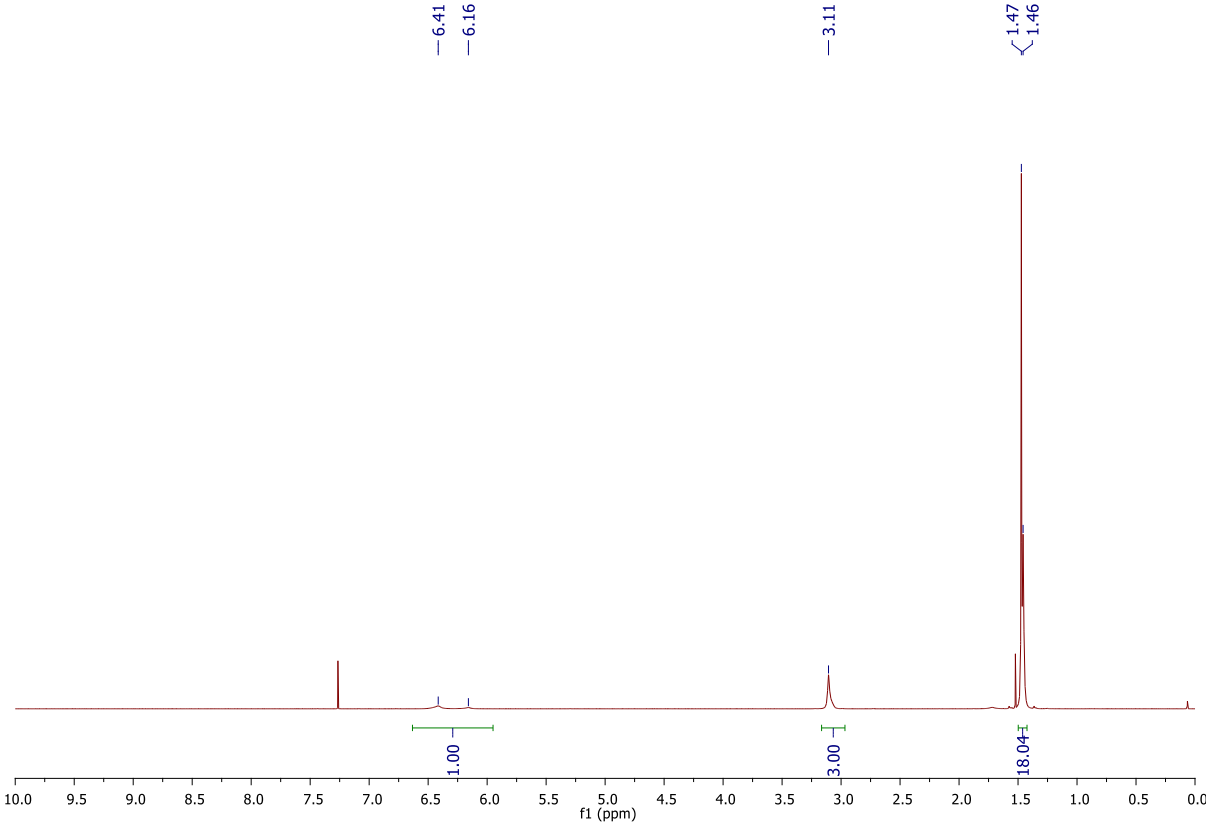

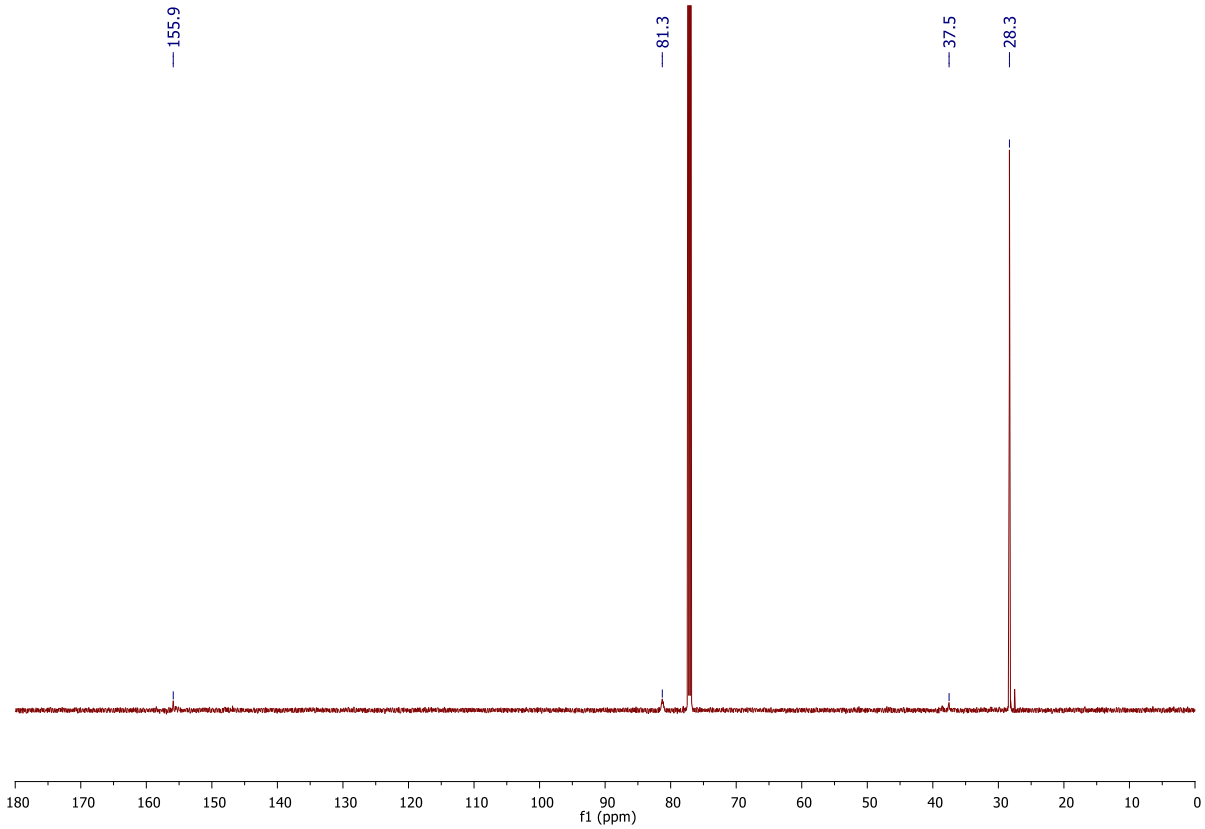
155.9
81.3
37.5
28.3
180
170
160
150
140
130
120
110
100
90
80
70
60
50
40
30
20
10
0
f1 (ppm)

Di-*tert*-butyl-1-(3-(*tert*-butoxy)-3-oxopropyl)-2-methylhydrazine-1,2-dicarboxylate 150

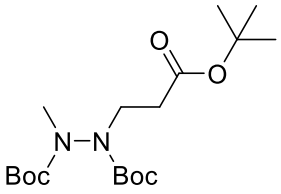

150

To a solution of di-*tert*-butyl 1-methylhydrazine-1,2-dicarboxylate **148** (3.00 g, 12.2 mmol) in *t*-BuOH (15 mL) was added 10% NaOH (0.5 mL) and the reaction mixture stirred at 21 °C for 10 min. After this, *tert*-butyl acrylate (5.31 mL, 36.6 mmol) was added to the solution and the reaction mixture was heated at 60 °C for 24 h. Following this, the solvent was removed *in vacuo* and the crude residue was dissolved in EtOAc (150 mL) and washed with water (3 × 50 mL). The organic layer was then dried ($MgSO_4$) and concentrated *in vacuo.* Purification of the crude residue by flash column chromatography (0% to 20% EtOAc/petrol) to afford di-*tert*-butyl-1-(3-(*tert*-butoxy)-3-oxopropyl)-2-methylhydrazine-1,2-dicarboxylate **150** (3.33 g, 8.66 mmol, 71 %) as a clear oil: ^{1}H NMR (600 MHz, $CDCl_3$, rotamers) δ 3.85–3.52 (m, 2H), 3.06–2.99 (m, 3H), 2.51 (t, *J* = 7.2 Hz, 2H), 1.48–1.43 (m, 27H); ^{13}C NMR (150 MHz, $CDCl_3$, rotamers) δ 171.0 (C), 155.4 (C), 154.4 (C), 81.0 (C), 44.6 (CH_3), 36.6 (CH_2), 34.1 (CH_2), 28.3 (CH_3); IR (thin film) 2976, 2933, 1709 cm^{-1}; LRMS (ESI) 375 (100, $[M+H]^+$), 319 (30, $[M-C_4H_9+2H]^+$ HRMS (ESI) calcd for $C_{18}H_{35}N_2O_6$ $[M+H]^+$ 376.2524; observed 376.2516.

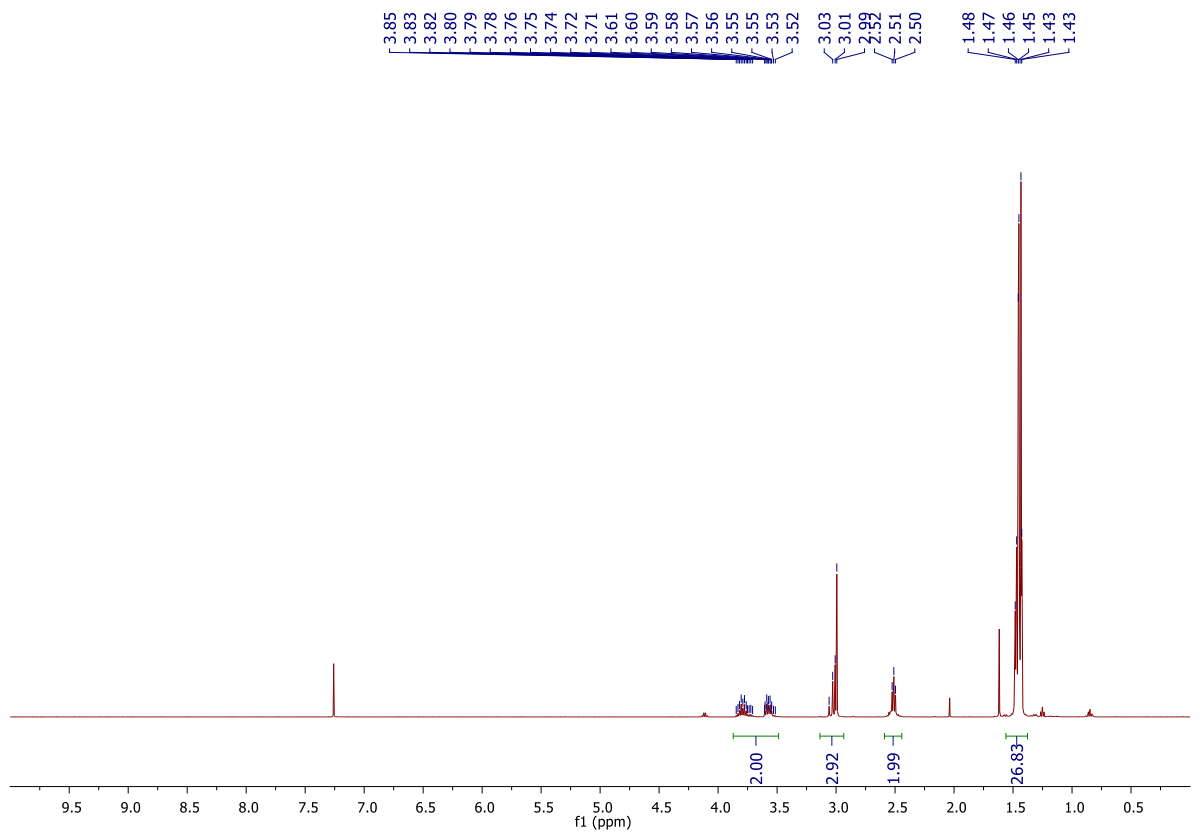
3.85
3.83
3.82
3.80
3.79
3.78
3.76
3.75
3.74
3.72
3.71
3.61
3.60
3.59
3.58
3.57
3.56
3.55
3.55
3.53
3.52
3.03
3.01
2.99
2.52
2.51
2.50
1.48
1.47
1.46
1.45
1.43
1.43
2.00
2.92
1.99
26.83
f1 (ppm)

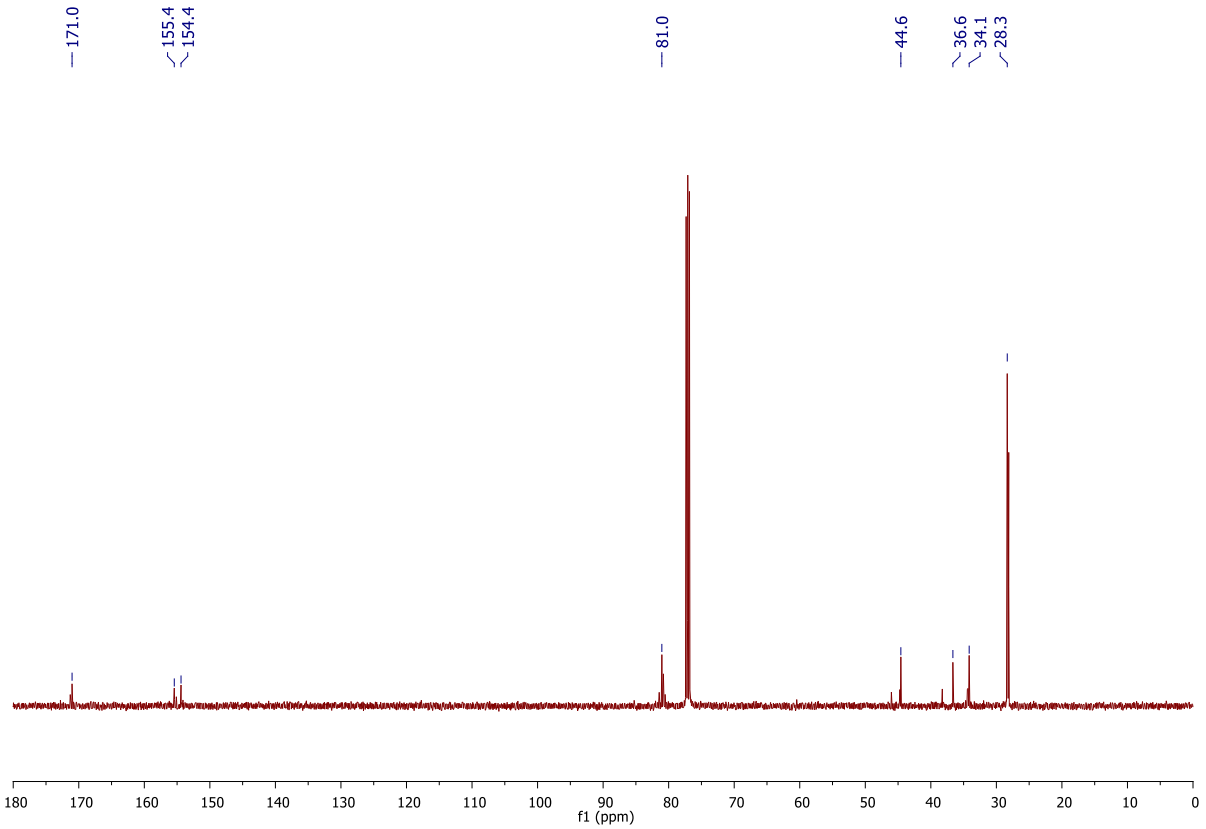
171.0
155.4
154.4
81.0
44.6
36.6
34.1
28.3
f1 (ppm)

3-(4,5-Dibromo-2-methyl-3,6-dioxo-3,6-dihydropyridazin-1(2*H*)-yl) propanoic acid 151

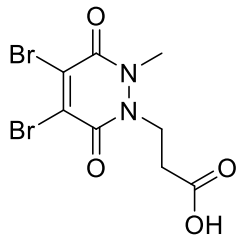

151

Dibromomaleic acid **138** (880 mg, 3.06 mmol) was dissolved in AcOH (25 mL) and heated under reflux for 30 min. To this solution, was added di-*tert*-butyl-1-(3-(*tert*-butoxy)-3-oxopropyl)-2-methylhydrazine-1,2-dicarboxylate **150** (1.00 g, 2.67 mmol) and the reaction heated under reflux for a further 4 h. After this time, the reaction mixture was concentrated *in vacuo* with toluene co-evaporation (3 × 30 mL, as an azeotrope) and the crude residue purified by flash column chromatography (50% to 100% EtOAc/petrol (1% AcOH)) to afford 3-(4,5-dibromo-2-methyl-3,6-dioxo-3,6-dihydropyridazin-1(2*H*)-yl) propanoic acid **151** (801 mg, 2.25 mmol, 84%) as a yellow solid: m.p. 140–144 °C; ^{1}H NMR (600 MHz, DMSO-d_6) δ 4.28 (t, *J* = 7.3 Hz, 2H), 3.56 (s, 3H), 2.63 (t, *J* = 7.3 Hz, 2H); ^{13}C NMR (150 MHz, DMSO-d_6) δ 171.9 (C), 152.7 (C), 152.4 (C), 135.3 (C), 135.0 (C), 43.1 (CH_3), 34.7 (CH_2), 31.7 (CH_2); IR (solid) 3044, 1725, 1606, 1570 cm^{-1} LRMS (ESI). 359 (50, $[M^{81}Br^{81}Br+H]^+$) 357 (100, $[M^{79}Br^{81}Br+H]^+$), 355 (50, $[M^{79}Br^{79}Br+H]^+$). HRMS (ESI) calcd for $C_8H_9Br_2N_2O_4$ $[M^{81}Br^{81}Br+H]^+$ 358.8883; observed 358.8882.

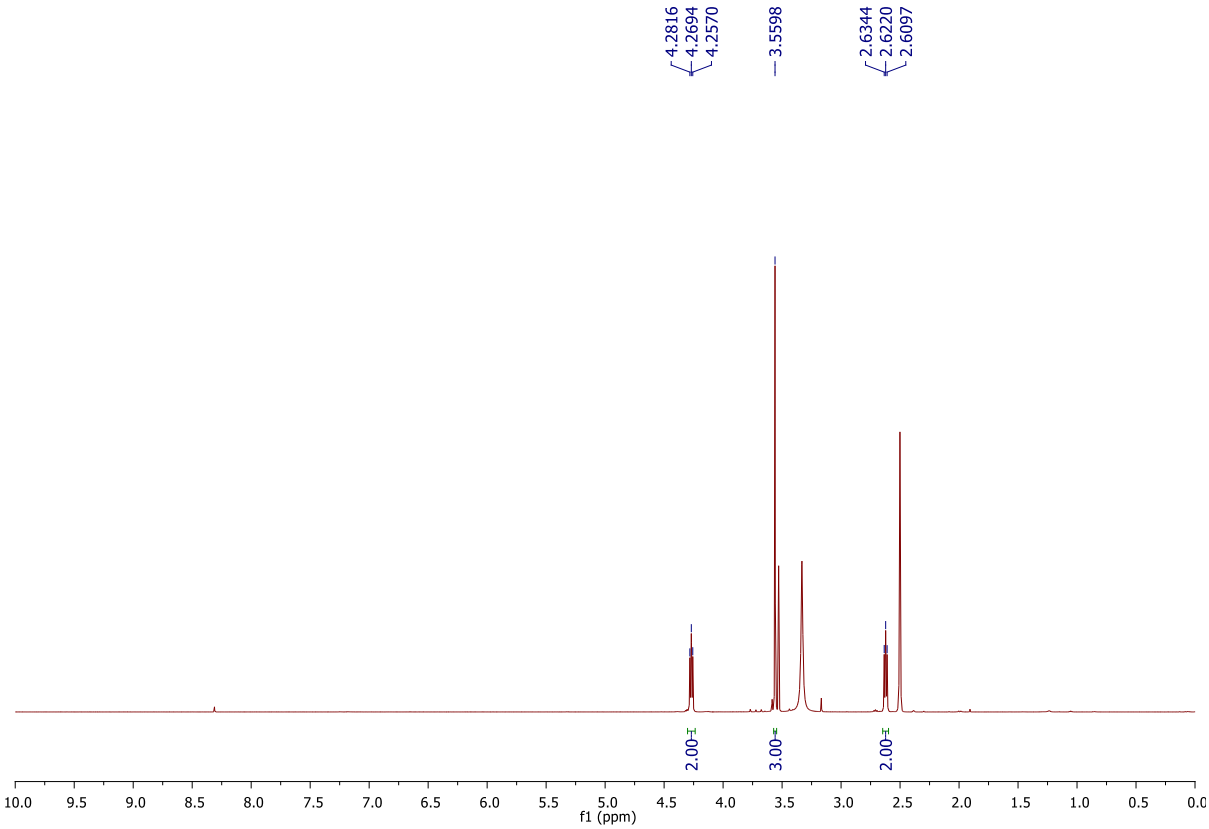
4.2816
4.2694
4.2570
3.5598
2.6344
2.6220
2.6097
2.00
3.00
2.00
10.0 9.5 9.0 8.5 8.0 7.5 7.0 6.5 6.0 5.5 5.0 4.5 4.0 3.5 3.0 2.5 2.0 1.5 1.0 0.5 0.0
f1 (ppm)

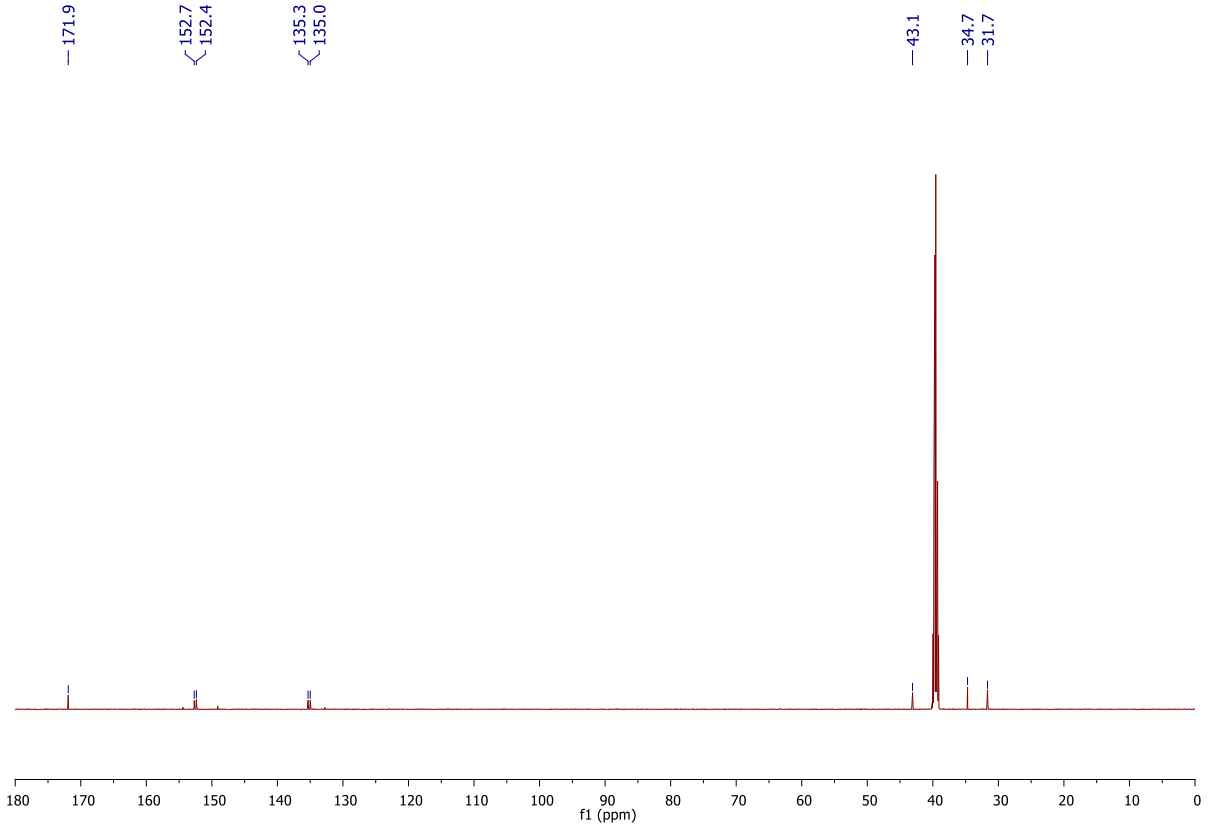
171.9
152.7
152.4
135.3
135.0
43.1
34.7
31.7
180 170 160 150 140 130 120 110 100 90 80 70 60 50 40 30 20 10 0
f1 (ppm)

2-(4,5-Dibromo-2-methyl-3,6-dioxo-3,6-dihydropyridazin-1(2*H*)-yl)acetic acid (MetAc PD 139) coupling reagent screening

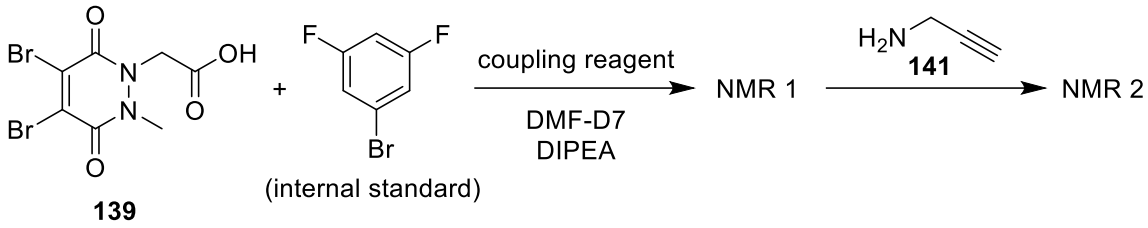

To a solution of 2-(4,5-dibromo-2-methyl-3,6-dioxo-3,6-dihydropyridazin-1(2*H*)-yl)acetic acid **139** (17 mg, 0.05 mmol) in deuterated DMF (0.5 mL) was added DIPEA (16 µL, 0.10 mmol). Following this 1-bromo-3,5-difluorobenzene (3 µL, 0.03 mmol – internal standard) and coupling reagent (0.05 mmol) were added and the homogenous solution incubated at 21 °C for 30 min. After this time the first ^{1}H NMR experiment was conducted. Propargyl amine **141** (3.8 µL, 0.06 mmol) was then added and the reaction mixture was stirred at 21 °C for a further 16 h and the second ^{1}H NMR experiment was conducted.

Reaction	Coupling reagent	PD Consumption (30 min)
A	EDC	100%
B	HATU	100%
C	PyBOP	96%
D	CDI	100%
E	TSTU	100%

2,5-Dioxopyrrolidin-1-yl 3-(4,5-dibromo-2-methyl-3,6-dioxo-3,6-dihydropyridazin-1(2*H*)-yl) propanoate 152

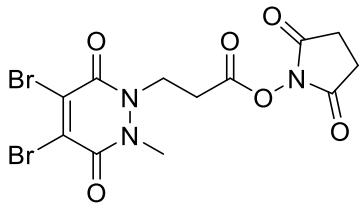

152

To a solution of 3-(4,5-dibromo-2-methyl-3,6-dioxo-3,6-dihydropyridazin-1(2*H*)-yl) propanoic acid **151** (250 mg, 0.702mmol) in THF (10 mL) cooled to 0 °C, was added *N,N'*-dicyclohexylcarbodiimide (160 mg, 0.774mmol). The homogenous solution was then stirred at 0 °C for 30 min. After this time, was added *N*-hydroxysuccinimide (89.0 mg, 0.78 mmol) and the reaction stirred at 21 °C for a further 16 h. The newly formed heterogeneous mixture was then filtered and the filtrate concentrated *in vacuo*. Purification of the crude residue by flash column chromatography (20% to 100% EtOAc/petrol) afforded 2,5-dioxopyrrolidin-1-yl 3-(4,5-dibromo-2-methyl-3,6-dioxo-3,6-dihydropyridazin-1(2*H*)-yl) propanoate **152** (230 mg, 0.507 mmol, 72%) as a yellow solid: m.p. 100–104 °C; ^{1}H NMR (600 MHz, $CDCl_3$) δ 4.48 (t, *J* = 6.9 Hz, 2H), 3.68 (s, 3H), 3.11 (t, *J* = 6.9 Hz, 2H), 2.85 (s, 4H); ^{13}C NMR (150 MHz, $CDCl_3$) δ 168.7 (C), 166.0 (C), 153.3 (C), 153.1 (C), 136.9 (C), 135.3 (C), 43.0 (CH_2), 35.3 (CH_3), 29.1 (CH_2), 25.7 (CH_2); IR (solid) 2992, 1814, 1782, 1735, 1634, 1576 cm^{-1}. LRMS (ESI) 358 (50, $[M^{81}Br^{81}Br$+H-succinimide$]^+$), 356 (100, $[M^{81}Br^{79}Br$+H-succinimide$]^+$), 354 (50, $[M^{79}Br^{79}Br$+H-succinimide$]^+$). Unable to obtain HRMS data due to decomposition of the NHS ester under mass spec conditions.

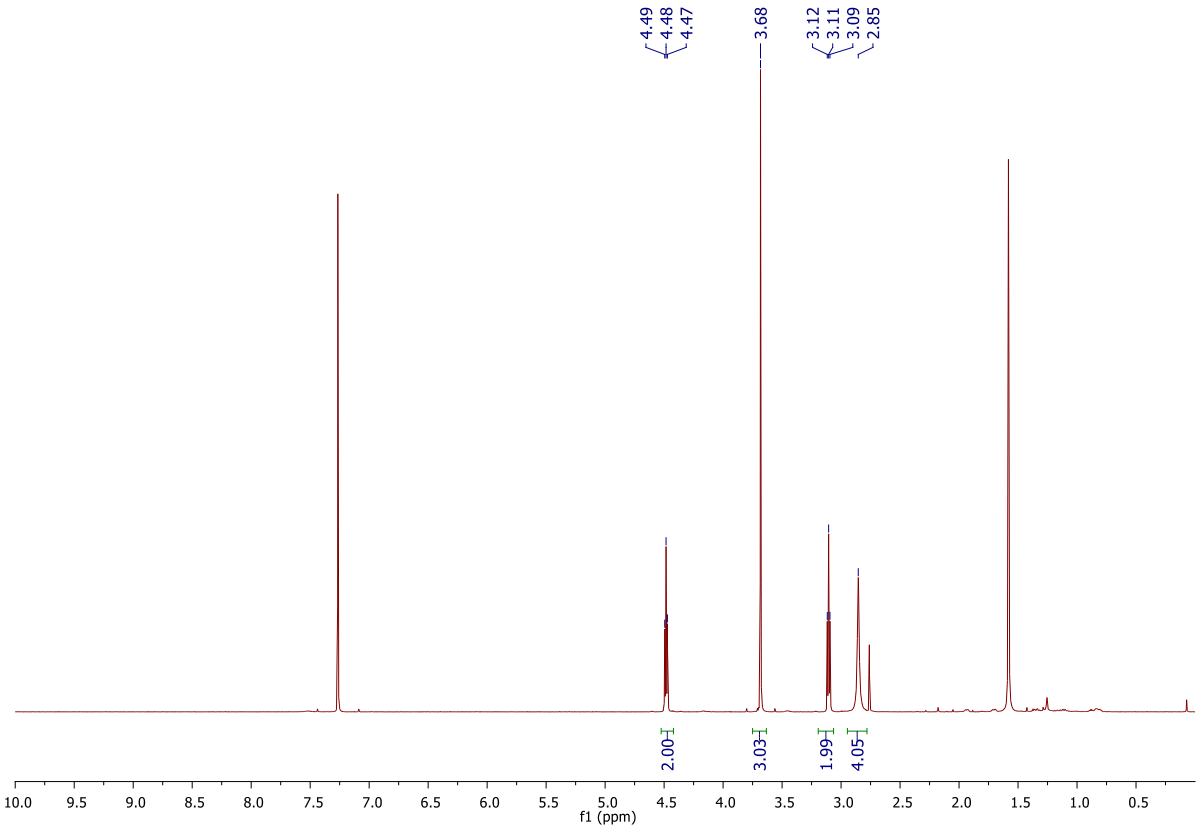
4.49
4.48
4.47
3.68
3.12
3.11
3.09
2.85
2.00
3.03
1.99
4.05
f1 (ppm)

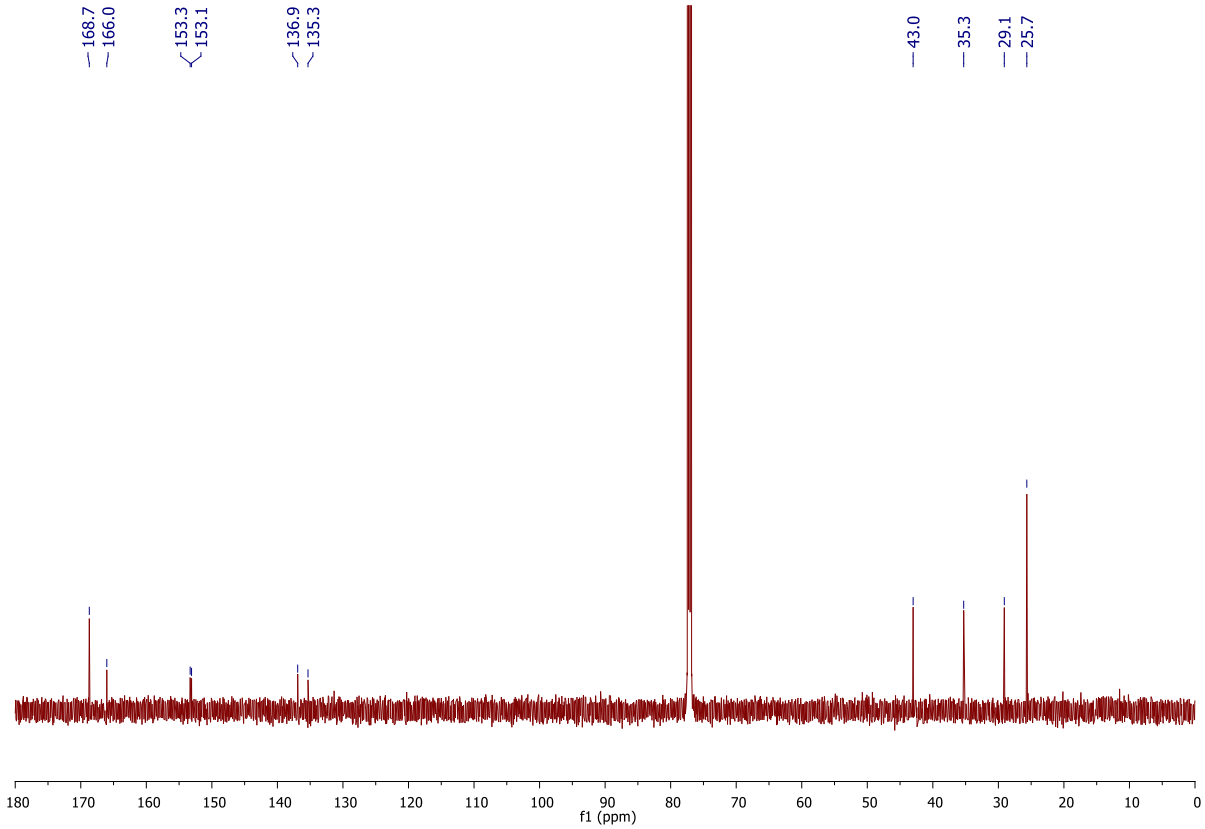
168.7
166.0
153.3
153.1
136.9
135.3
43.0
35.3
29.1
25.7
f1 (ppm)

3 months:

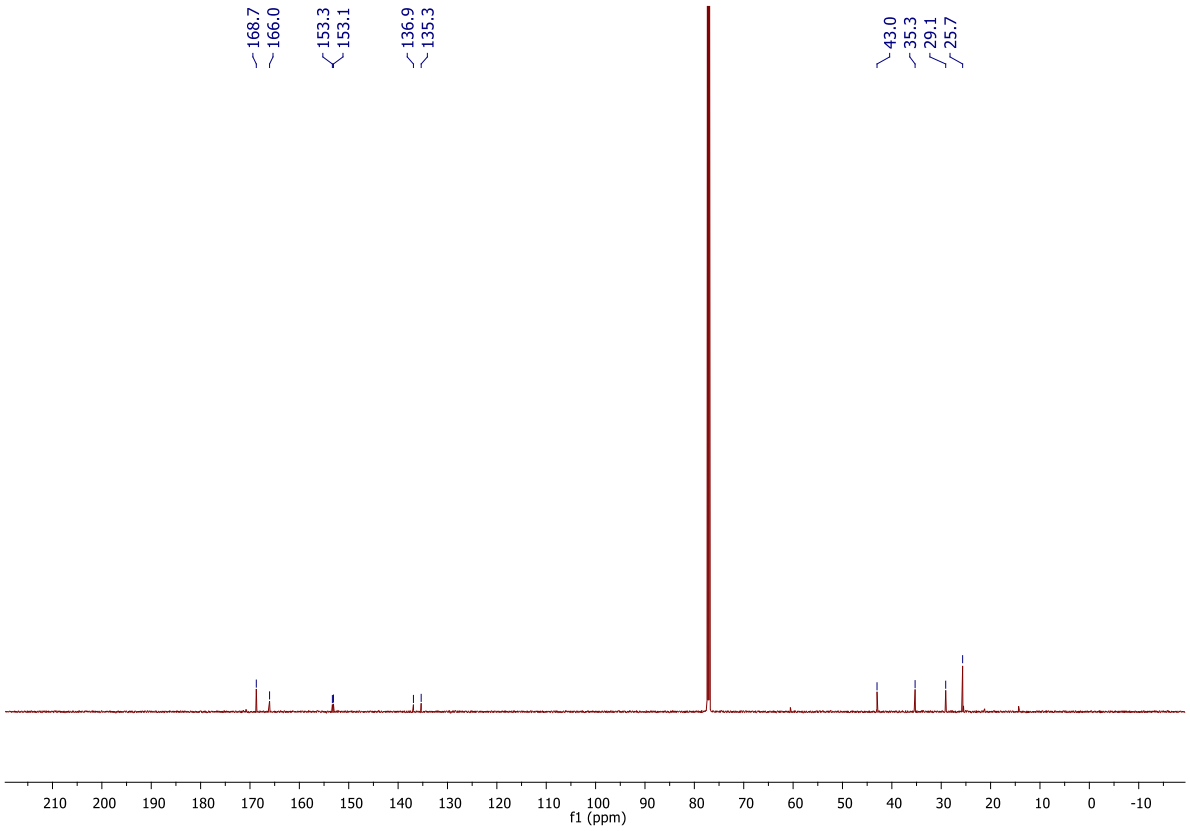
168.7
166.0
153.3
153.1
136.9
135.3
43.0
35.3
29.1
25.7
210 200 190 180 170 160 150 140 130 120 110 100 90 80 70 60 50 40 30 20 10 0 -10
f1 (ppm)

3-(Bromo-2-methyl-3,6-dioxo-3,6-dihydropyridazin-1(2*H*)-yl)propanoic acid 154

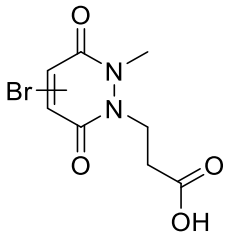

154

To a solution of di-*tert*-butyl-1-(3-(*tert*-butoxy)-3-oxopropyl)-2-methylhydrazine-1,2-dicarboxylate **150** (1.50 g, 4.01 mmol) in AcOH (20 mL) was added bromomaleic anhydride **153** (0.41 mL, 4.41 mmol) and the reaction heated under reflux for 4 h. After this time, the reaction mixture was concentrated *in vacuo* with toluene co-evaporation (3 × 30 mL, as an azeotrope). The crude residue was then purified by flash column chromatography (0% to 10% MeOH/EtOAc (1% AcOH)) to afford an inseparable mixture of regioisomers 3-(4-bromo-2-methyl-3,6-dioxo-3,6-dihydropyridazin-1(2*H*)-yl)propanoic acid and 3-(5-bromo-2-methyl-3,6-dioxo-3,6-dihydropyridazin-1(2*H*)-yl)propanoic acid **154** (804 mg, 2.90 mmol, 72%) as a white solid m.p. 142–145 °C. ^{1}H NMR (600 MHz, DMSO, regioisomers) δ 7.60 (s, 0.5H), 7.59 (s, 0.5H), 4.28 (t, *J* = 7.4 Hz, 1H), 4.21 (t, *J* = 7.4 Hz, 1H), 3.57 (s, 1.5H), 3.50 (s, 1.5H), 2.66–2.54 (m, 2H). ^{13}C NMR (150 MHz, DMSO, regioisomers) δ 172.0 (C), 171.9 (C), 155.4 (C), 155.1 (C), 153.5 (C), 153.2 (C), 135.8 (CH), 135.5 (CH), 132.8 (C), 132.3 (C) 42.7 (CH_2), 41.5 (CH_2), 34.2 (CH_3), 32.9 (CH_3), 31.8 (CH_2). IR (solid) 3058, 1722, 1619 cm^{-1}. LRMS (ESI) 279 (95, [M^{81}Br+H]$^{+}$), 277 (100, [M^{79}Br+H]$^{+}$), HRMS (ESI) calcd for $C_8H_{10}Br_1N_2O_4$ [M^{79}Br+H]$^{+}$ 276.9818; observed 276.9820.

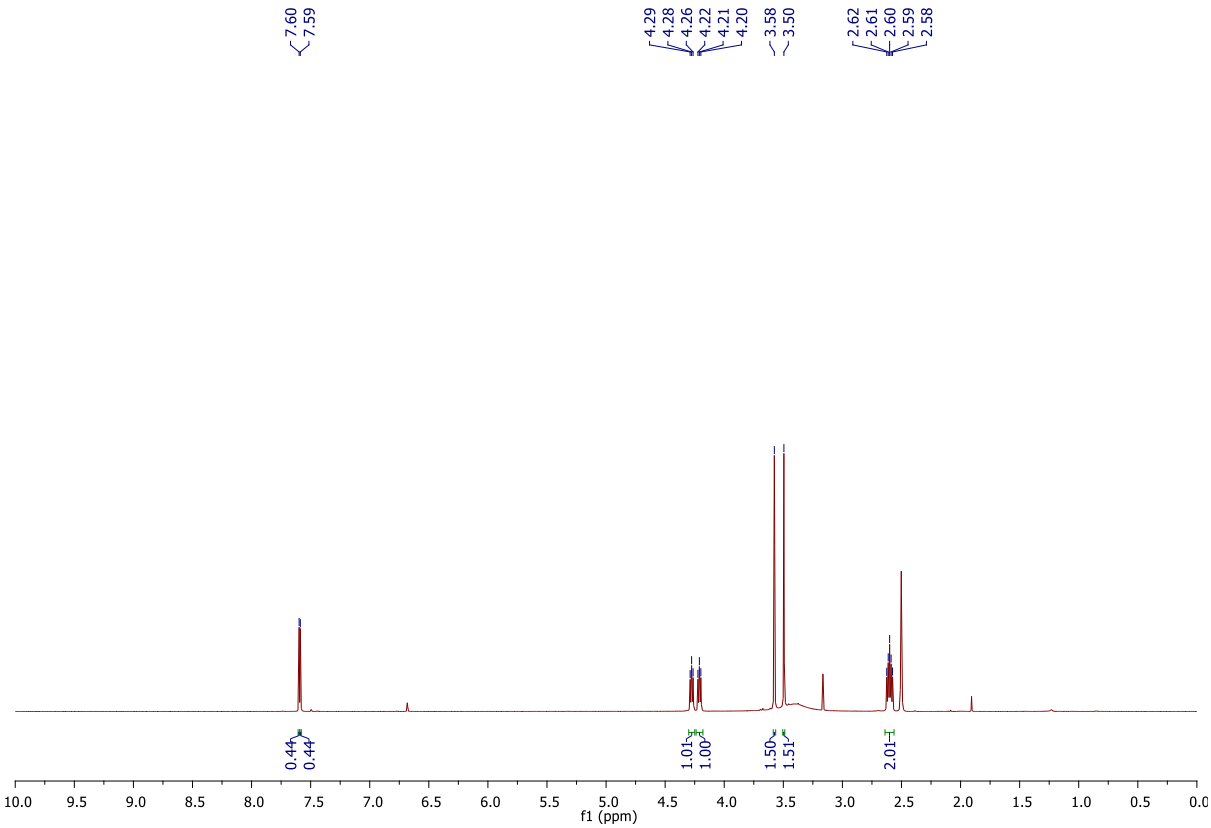
7.60
7.59
4.29
4.28
4.26
4.22
4.21
4.20
3.58
3.50
2.62
2.61
2.60
2.59
2.58
0.44
0.44
1.01
1.00
1.50
1.51
2.01
f1 (ppm)

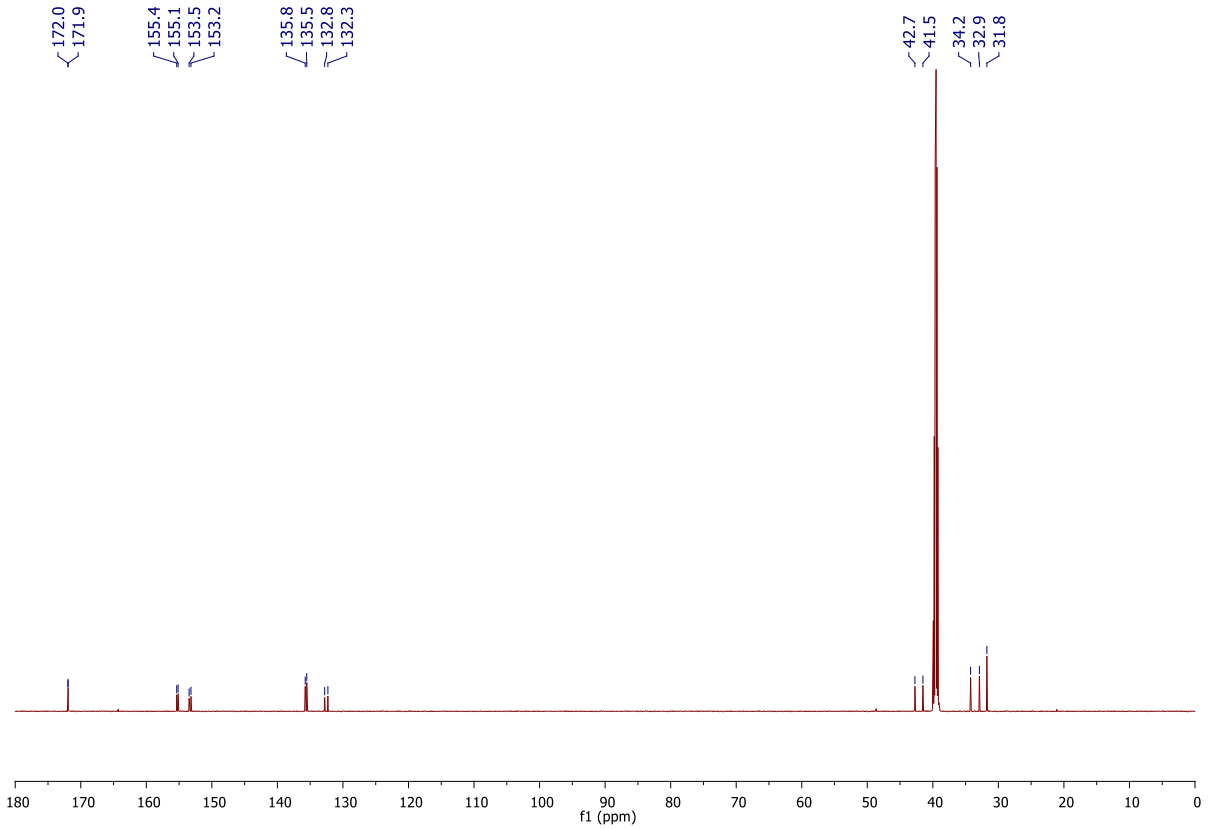
172.0
171.9
155.4
155.1
153.5
153.2
135.8
135.5
132.8
132.3
42.7
41.5
34.2
32.9
31.8
f1 (ppm)

2,5-Dioxopyrrolidin-1-yl 3-(bromo-2-methyl-3,6-dioxo-3,6-dihydropyridazin-1(2*H*)yl) propanoate 155

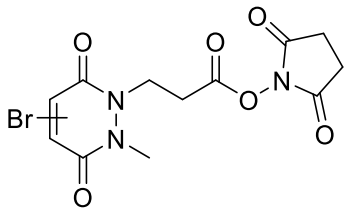

155

To a solution of 3-(bromo-2-methyl-3,6-dioxo-3,6-dihydropyridazin-1(2*H*)-yl) propanoic acid **154** (2.00 g, 7.22 mmol) in THF (10 mL) cooled to 0 °C, was added *N,N'*-dicyclohexylcarbodiimide (1.64 g, 7.95 mmol). The homogenous solution was then stirred at 0 °C for 30 min. After this time, was added *N*-hydroxysuccinimide (0.91 g, 7.95 mmol) and the reaction was stirred at 21 °C for a further 16 h. The newly formed heterogeneous mixture was then filtered and the filtrate concentrated *in vacuo*. Purification of the crude residue by flash column chromatography (50% to 100% EtOAc/petrol) afforded an inseparable 1:1 mixture of regioisomers 2,5-dioxopyrrolidin-1-yl 3-(4-bromo-2-methyl-3,6-dioxo-3,6-dihydropyridazin-1(2*H*)-yl)propanoate and 2,5-dioxopyrrolidin-1-yl 3-(5-bromo-2-methyl-3,6-dioxo-3,6-dihydropyridazin-1(2*H*)-yl)propanoate **155** (1.92 g, 5.13 mmol, 71%) as a white powder. m.p. 142–145 °C. ^{1}H NMR (500 MHz, DMSO, regioisomers) δ 7.59–7.58 (m, 1H), 4.39 (t, *J* = 7.2 Hz, 1H), 4.33 (t, *J* = 7.2 Hz, 1H), 3.58 (s, 1.5H), 3.50 (s, 1.5H), 3.17–3.14 (m, 2H), 2.80 (s, 4H). ^{13}C NMR (150 MHz, DMSO, regioisomers) δ 170.0 (C), 166.7 (C), 155.4 (C), 155.2 (C), 153.5 (C), 153.3 (C), 135.9 (CH), 135.4 (CH), 133.0 (C), 132.1 (C), 41.7 (CH_2), 40.6 (CH_2), 34.3 (CH_3), 33.0 (CH_3), 28.5 (CH_2), 25.4 (CH_2). IR (solid) 2944, 1808, 1778, 1731, 1632, 1596 cm^{-1}. LRMS (ESI) 279 (100, [M^{81}Br+H-succinimide]$^{+}$), 277 (100, [M^{79}Br+H-succinimide]$^{+}$). Unable to obtain HRMS data due to decomposition of the NHS ester under mass spec conditions.

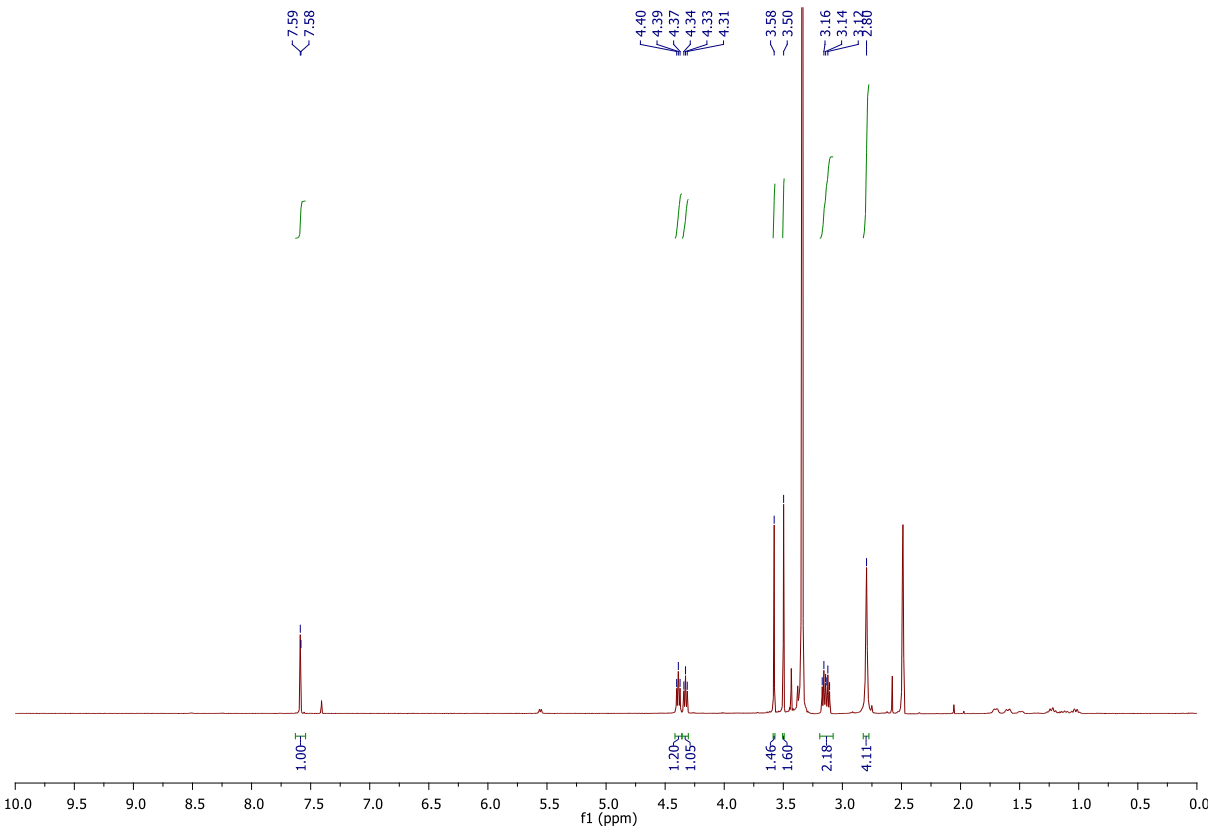
7.59
7.58
4.40
4.39
4.37
4.34
4.33
4.31
3.58
3.50
3.16
3.14
3.12
2.80
1.00
1.20
1.05
1.46
1.60
2.18
4.11
f1 (ppm)

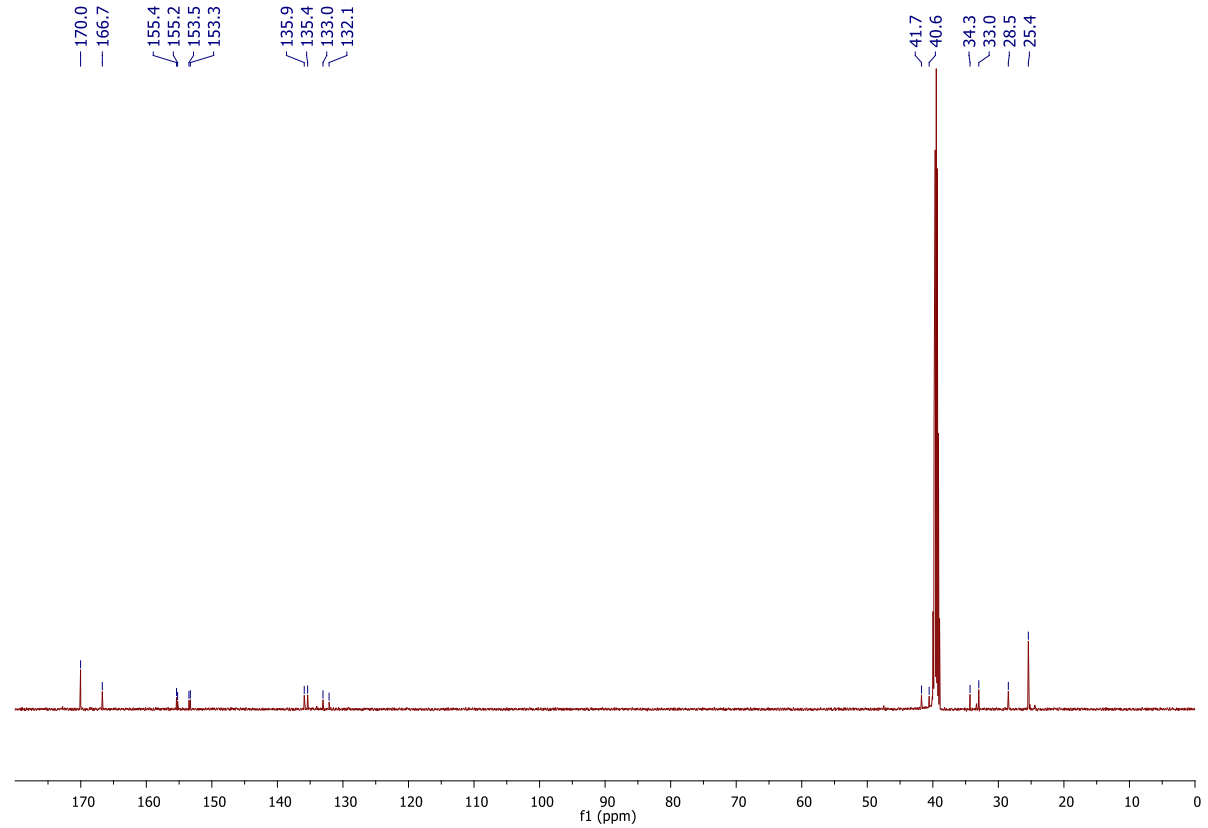
170.0
166.7
155.4
155.2
153.5
153.3
135.9
135.4
133.0
132.1
41.7
40.6
34.3
33.0
28.5
25.4
f1 (ppm)

tert-Butyl (3-(2-(2-(3-aminopropoxy)ethoxy)ethoxy)propyl)carbamate S1[202]

J. C. Slootweg, S. Van Der Wal, H. C. Quarles Van Ufford, E. Breukink, R. M. J. Liskamp and D. T. S. Rijkers, Bioconjug. Chem., 2013, 24, 2058–2066.

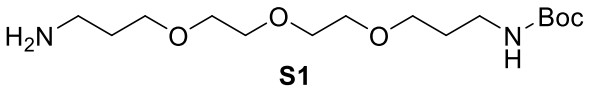

S1

To a solution of 3,3'-((oxybis(ethane-2,1-diyl))bis(oxy))bis(propan-1-amine) (8.10 g, 37.1 mmol) in 1,4-dioxane (60 mL) was added dropwise di-*tert*-butyl dicarbonate (1.00 g, 4.60 mmol, pre-dissolved in 1,4-dioxane (25 mL)) over 2 h, ensuring that the temperature did not exceed 21 °C. After this time, the reaction mixture was stirred at 21 °C for a further 30 mins. Following this, the reaction mixture was concentrated *in vacuo*, the crude residue dissolved in water (50 mL), and the organics extracted into EtOAc (5 × 30 mL). The organics were combined, dried ($MgSO_4$) and concentrated *in vacuo* to give *tert*-butyl (3-(2-(2-(3-aminopropoxy)ethoxy)ethoxy)propyl)carbamate **S1** (1.10 g, 3.45 mmol, 75%) as a yellow oil: ^{1}H NMR (600 MHz, $CDCl_3$) δ 5.16 (s, 1H), 3.62–3.50 (m, 12H), 3.20–3.18 (m, 2H), 2.76 (t, *J* = 6.7 Hz, 2H), 1.72–1.68 (m, 4H), 1.40 (s, 9H); ^{13}C NMR 150 MHz, $CDCl_3$) δ 156.2 (C), 78.9 (C), 70.7 (CH_2), 70.7 (CH_2), 70.3 (CH_2), 70.3 (CH_2), 69.7 (CH_2), 69.6 (CH_2), 39.7 (CH_2), 38.6 (CH_2), 33.4 (CH_2), 29.7 (CH_2), 28.6 (CH_3); IR (thin film) 3358, 2927, 2867, 1693, 1518 cm^{-1}.

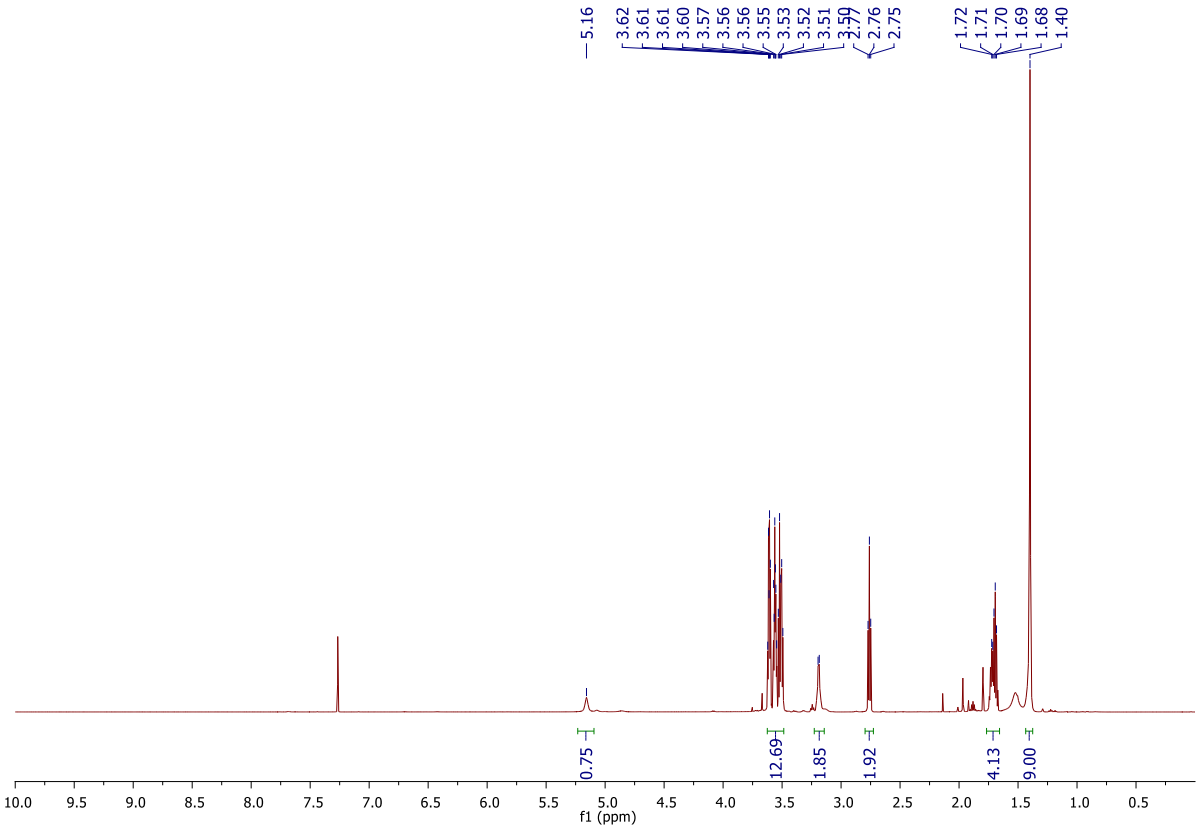
5.16
3.62
3.61
3.61
3.60
3.57
3.56
3.56
3.55
3.53
3.52
3.51
3.50
2.77
2.76
2.75
1.72
1.71
1.70
1.69
1.68
1.40
0.75
12.69
1.85
1.92
4.13
9.00
f1 (ppm)

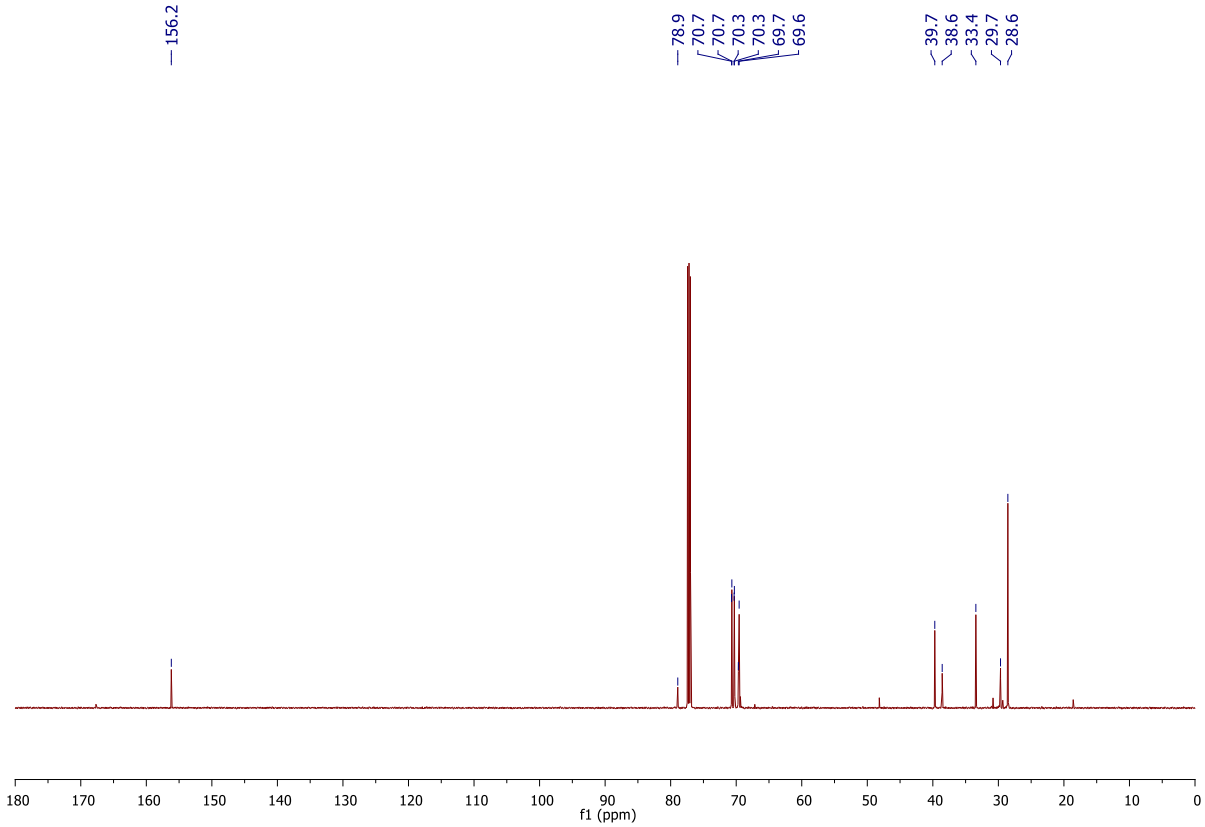
156.2
78.9
70.7
70.7
70.3
70.3
69.7
69.6
39.7
38.6
33.4
29.7
28.6
f1 (ppm)

General PD-Amide coupling protocol:

Dibromo PD-Amides (protocol A):

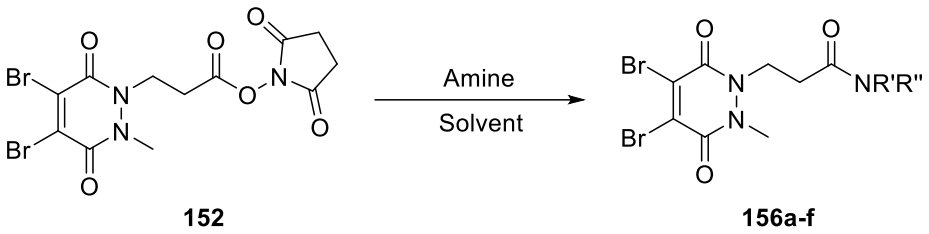

152 **156a-f**

To a solution of 2,5-dioxopyrrolidin-1-yl 3-(4,5-dibromo-2-methyl-3,6-dioxo-3,6-dihydropyridazin-1(2*H*)-yl) propanoate **152** (100 mg, 0.221 mmol, pre-dissolved in solvent (10 mL)), was added amine (0.243 mmol) and the reaction mixture was stirred at 21 °C for 16 h. After this time, the reaction was concentrated *in vacuo* and the crude residue dissolved in $CHCl_3$ (50 mL), and washed with water (2 × 30 mL) and saturated aq. K_2CO_3 (30 mL). The organic layer was then dried ($MgSO_4$) and concentrated *in vacuo.* Purification of the crude residue by flash column chromatography (0% to 10% MeOH/EtOAc) afforded amide products **156a-f** as described in the sections below. Detail of the solvent used in each synthesis is indicated below.

Monobromo PD-Amides (protocol B):

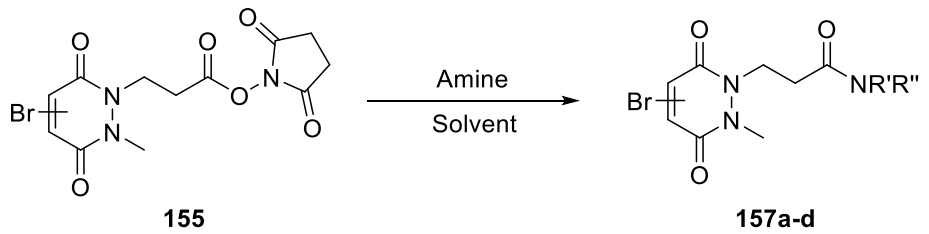

155 **157a-d**

To a solution of 2,5-dioxopyrrolidin-1-yl 3-(bromo-2-methyl-3,6-dioxo-3,6-dihydropyridazin-1(2*H*)yl) propanoate **155** (100 mg, 0.267 mmol, pre-dissolved in solvent (10 mL)), was added amine (0.294 mmol) and the reaction mixture was stirred at 21 °C for 16 h. After this time, the reaction was concentrated *in vacuo* and the crude residue dissolved in $CHCl_3$ (50 mL), and washed with water (2 × 30 mL) and saturated aq. K_2CO_3 (30 mL). The organic layer was then dried ($MgSO_4$) and concentrated *in vacuo.* Purification of the crude residue by flash column chromatography (0% to 10% MeOH/EtOAc) afforded amide products **157a-d** as described in the sections below. Detail of the solvent used in each synthesis is indicated

below.

3-(4,5-Dibromo-2-methyl-3,6-dioxo-3,6-dihydropyridazin-1(2*H*)-yl)-*N*-hexylpropanamide 156a

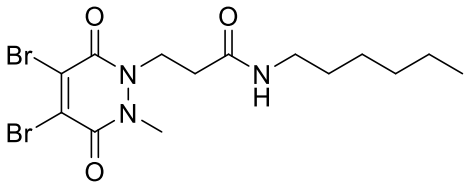

156a

General amide coupling protocol A (solvent used: CH_2Cl_2) afforded 3-(4,5-dibromo-2-methyl-3,6-dioxo-3,6-dihydropyridazin-1(2*H*)-yl)-*N*-hexylpropanamide **156a** (75.2 mg, 0.172 mmol, 78%) as a viscous oil: ^{1}H NMR (600 MHz, $CDCl_3$) δ 5.93 (s, 1H), 4.43 (t, *J* = 7.0 Hz, 2H), 3.74 (s, 3H), 3.21 (m, 2H), 2.61 (t, *J* = 7.0 Hz, 2H), 1.47–1.45 (m, 2H), 1.30–1.25 (m, 6H), 0.87 (t, *J* = 6.7 Hz, 3H); ^{13}C NMR (150 MHz, $CDCl_3$) δ 168.9 (C), 153.0 (C), 153.0 (C), 136.5 (C), 135.3 (C), 44.8 (CH_2), 39.9 (CH_2), 35.1 (CH_3), 34.30 (CH_2), 31.5 (CH_2), 29.5 (CH_2), 26.7 (CH_2), 22.7 (CH_2), 14.2 (CH_3); IR (thin film) 3317, 2924, 2854, 1736, 1627, 1572, 1545 cm^{-1}; LRMS (ESI) 442 (50, [M^{81}Br^{81}Br+H]$^+$), 440 (100, [M^{79}Br^{81}Br+H]$^+$) 438 (50, [M^{79}Br^{79}Br+H]$^+$); HRMS (ESI) calcd for $C_{14}H_{22}Br_2N_3O_3$ [M^{79}Br^{81}Br+H]$^+$ 440.0002; observed 439.9998.

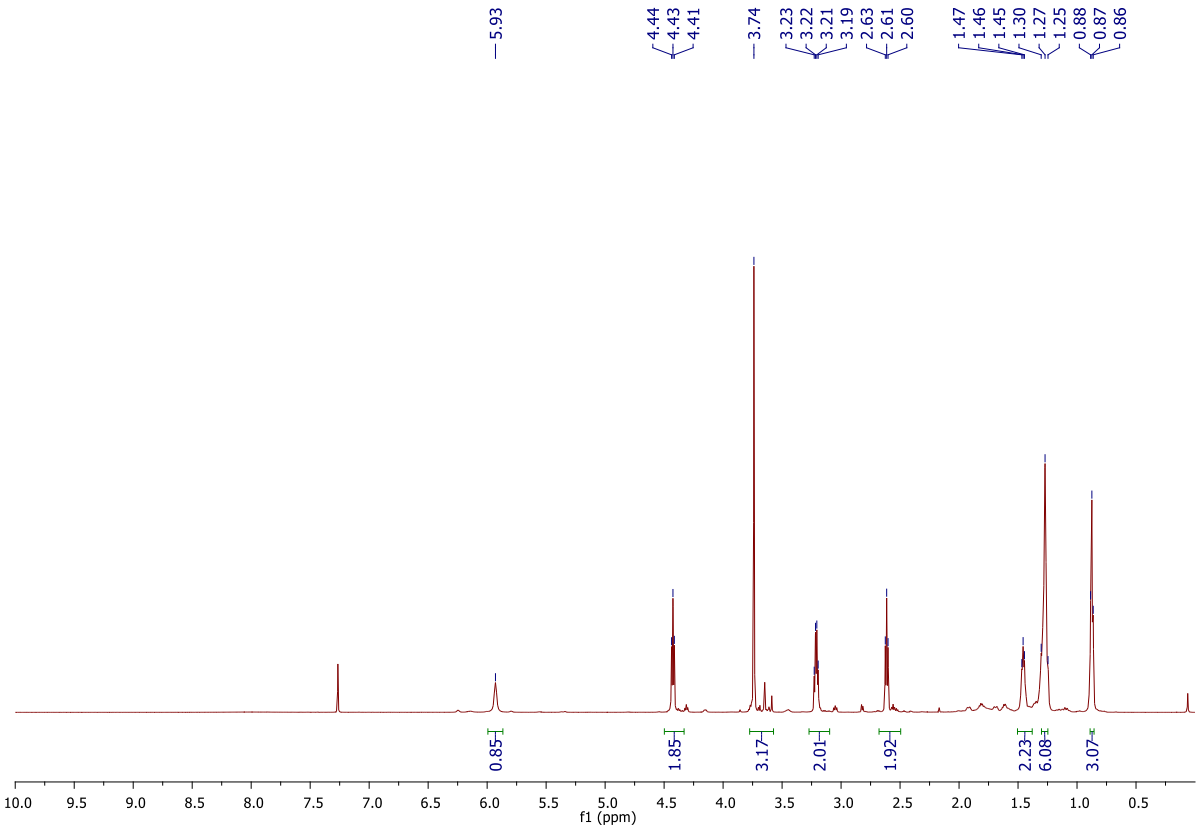

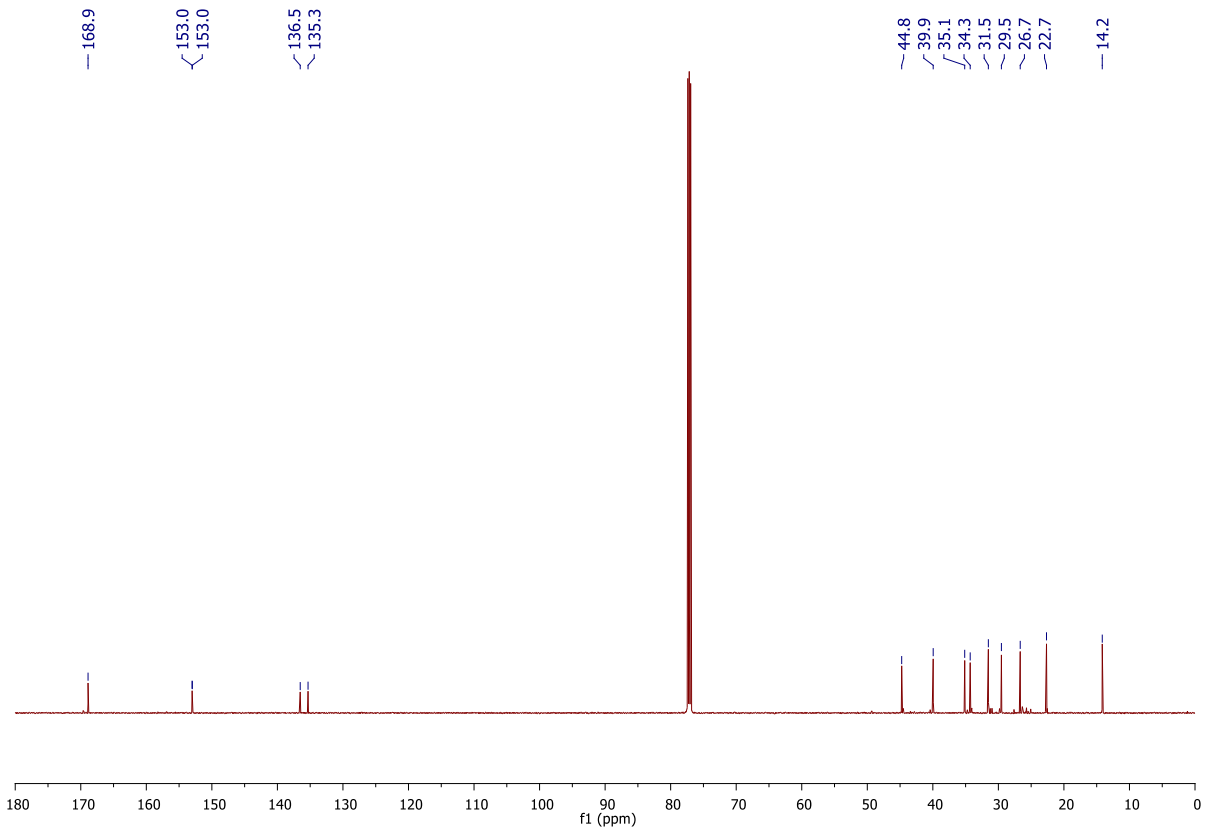
168.9
153.0
153.0
136.5
135.3
44.8
39.9
35.1
34.3
31.5
29.5
26.7
22.7
14.2
180
170
160
150
140
130
120
110
100
90
80
70
60
50
40
30
20
10
0
f1 (ppm)

3-(4,5-Dibromo-2-methyl-3,6-dioxo-3,6-dihydropyridazin-1(2*H*)-yl)-*N*-(2-(2-hydroxyethoxy)ethyl)propanamide 156b

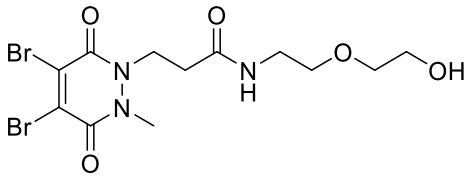

156b

General amide coupling protocol A (solvent used: CH_2Cl_2) afforded 3-(4,5-dibromo-2-methyl-3,6-dioxo-3,6-dihydropyridazin-1(2*H*)-yl)-*N*-(2-(2- hydroxyethoxy) ethyl)propanamide **156b** (69.2 mg, 0.156 mmol, 71%) as a light yellow oil: ^{1}H NMR (600 MHz, $CDCl_3$) δ 6.73–6.70 (m, 1H), 4.44 (t, *J* = 7.0 Hz, 2H), 3.75–3.74 (m, 2H), 3.74–3.73 (s, 3H), 3.58–3.54 (m, 2H), 3.55 (t, *J* = 5.2 Hz, 2H), 3.45–3.43 (m, 2H), 2.63 (t, *J* = 7.0 Hz, 2H); ^{13}C NMR (150 MHz, $CDCl_3$) δ 169.3 (C), 153.1 (C), 136.6 (C), 135.4 (C), 72.4 (CH_2), 69.6 (CH_2), 61.9 (CH_2), 44.7 (CH_2), 39.6 (CH_2), 35.2 (CH_3), 34.4 (CH_2); IR (thin film) 3323, 2922, 2854, 1733, 1628, 1571 cm^{-1}; LRMS (ESI) 465 (60, [M^{79}Br^{81}Br+Na]$^+$), 446 (50, [M^{81}Br^{81}Br+H]$^+$), 444 (100, [M^{79}Br^{81}Br+H]$^+$), 442 (50, [M^{79}Br^{79}Br+H]$^+$); HRMS (ESI) calcd for $C_{12}H_{18}Br_2N_3O_3$ [M^{79}Br^{81}Br+H]$^+$ 443.9584; observed 443.9588.

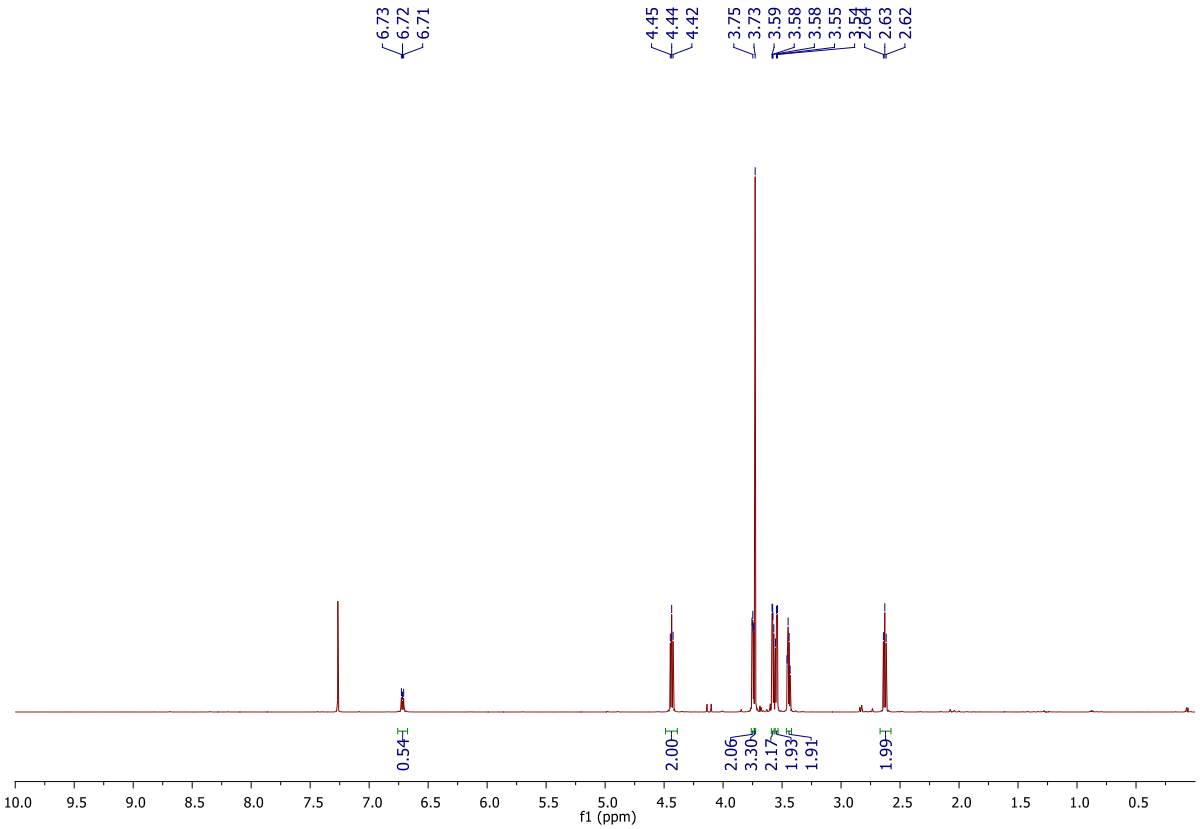
6.73
6.72
6.71
4.45
4.44
4.42
3.75
3.73
3.59
3.58
3.58
3.55
3.54
2.64
2.63
2.62
0.54
2.00
2.06
3.30
2.17
1.93
1.91
1.99
f1 (ppm)

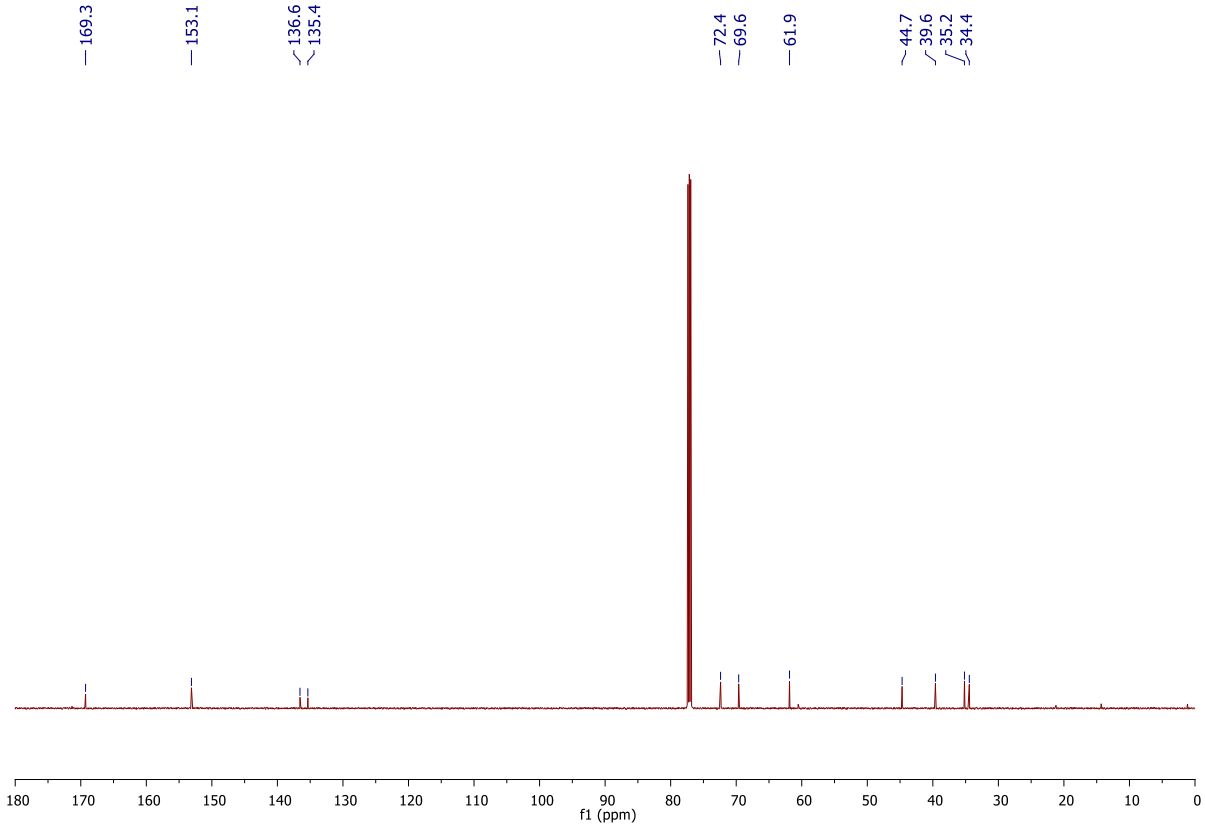
169.3
153.1
136.6
135.4
72.4
69.6
61.9
44.7
39.6
35.2
34.4
f1 (ppm)

4,5-Dibromo-1-methyl-2-(3-morpholino-3-oxopropyl)-1,2-dihydropyridazine-3,6-dione 156c

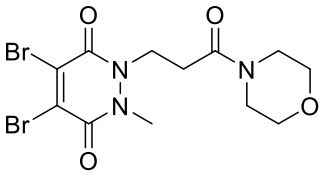

156c

General amide coupling protocol A (solvent used: MeCN) afforded 4,5-dibromo-1-methyl-2-(3-morpholino-3-oxopropyl)-1,2-dihydropyridazine-3,6-dione **156c** (71.1 mg, 0.167 mmol, 76%) as a yellow oil: ^{1}H NMR (600 MHz, $CDCl_3$, rotamers) δ 4.44 (t, *J* = 7.4 Hz, 2H), 3.74 (s, 3H), 3.69–3.65 (m, 4H), 3.63–3.57 (m, 2H), 3.45 (m, 2H), 2.75 (t, *J* = 7.4 Hz, 2H); ^{13}C NMR (150 MHz, $CDCl_3$, rotamers) δ 169.0 (C), 167.8 (C), 153.1 (C), 153.0 (C), 136.4 (C), 135.5 (C), 66.8 (CH_2), 66.6 (CH_2), 46.0 (CH_2), 44.4 (CH_2), 42.1 (CH_2), 35.1 (CH_3), 30.6 (CH_2), 25.4 (CH_2); IR (thin film) 2921, 2856, 1733, 1628, 1574 cm^{-1}; LRMS (ESI) 428 (50, $[M^{81}Br^{81}Br+H]^+$), 426 (100, $[M^{79}Br^{81}Br+H]^+$), 424 (50, $[M^{79}Br^{79}Br+H]^+$); HRMS (ESI) calcd for $C_{12}H_{16}Br_2N_3O_4$ $[M^{79}Br^{81}Br+H]^+$ 425.9482; observed 425.9474.

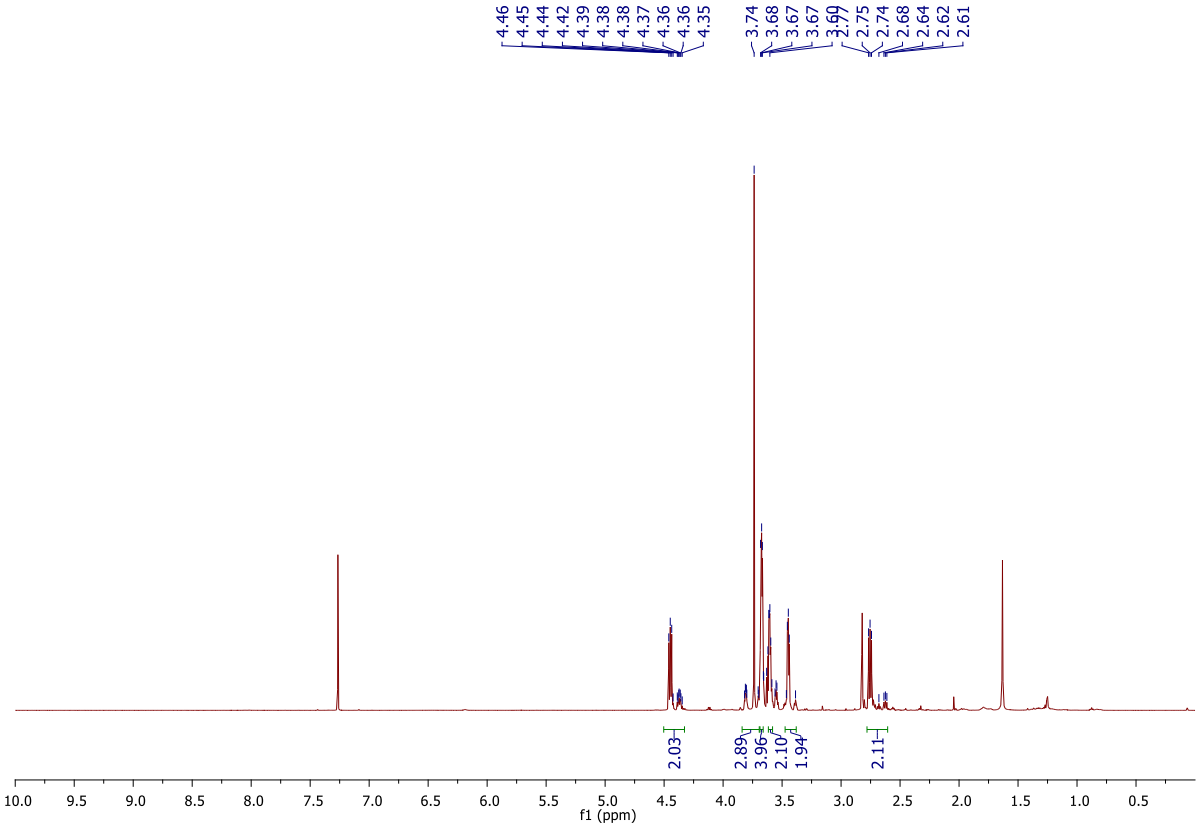

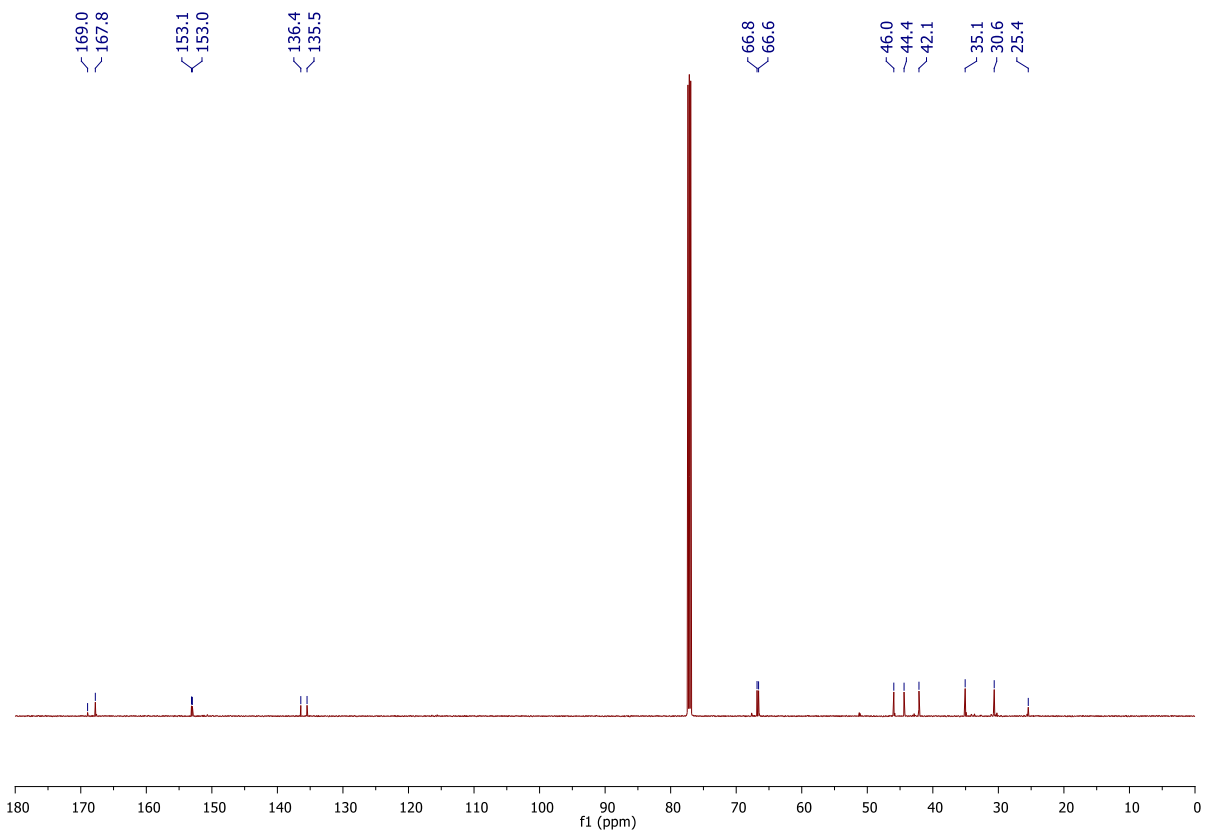
169.0
167.8
153.1
153.0
136.4
135.5
66.8
66.6
46.0
44.4
42.1
35.1
30.6
25.4
180
170
160
150
140
130
120
110
100
90
80
70
60
50
40
30
20
10
0
f1 (ppm)

3-(4,5-Dibromo-2-methyl-3,6-dioxo-3,6-dihydropyridazin-1(2*H*)-yl)-*N*-(prop-2-yn-1-yl)propanamide 156d

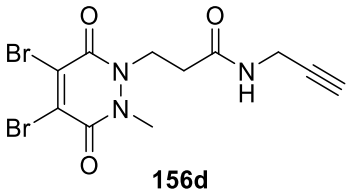

156d

General amide coupling protocol A (solvent used: MeCN) afforded 3-(4,5-dibromo-2-methyl-3,6-dioxo-3,6-dihydropyridazin-1(2*H*)-yl)-*N*-(prop-2-yn-1-yl)propenamide **156d** (75.2 mg, 0.191 mmol, 87%) as an orange oil: ^{1}H NMR (600 MHz, DMSO-d_6) δ 8.46 (t, *J* = 5.2 Hz, 1H), 4.26 (t, *J* = 7.2 Hz, 2H), 3.82 (m, 2H), 3.55 (s, 3H), 3.09 (t, *J* = 2.3 Hz, 1H), 2.48 (t, *J* = 7.2 Hz, 2H); ^{13}C NMR (150 MHz, DMSO-d_6) δ 169.0 (C), 152.6 (C), 152.3 (C), 135.3 (C), 135.0 (C), 80.8 (C), 73.2 (CH), 43.7 (CH_2), 34.7 (CH_3), 32.8 (CH_2), 27.9 (CH_2); IR (thin film) 3294, 2932, 2855, 1734, 1632, 1571, 1542 cm^{-1}; LRMS (ESI) 411 (50, [M^{79}Br^{81}Br+NH_4]$^+$), 396 (50, [M^{81}Br^{81}Br+H]$^+$), 394 (100, [M^{79}Br^{81}Br+H]$^+$), 392 (50, [M^{79}Br^{79}Br+H]$^+$); HRMS (ESI) calcd for $C_{11}H_{12}Br_2N_3O_3$ [M^{79}Br^{81}Br+H]$^+$ 393.9219; observed 393.9218.

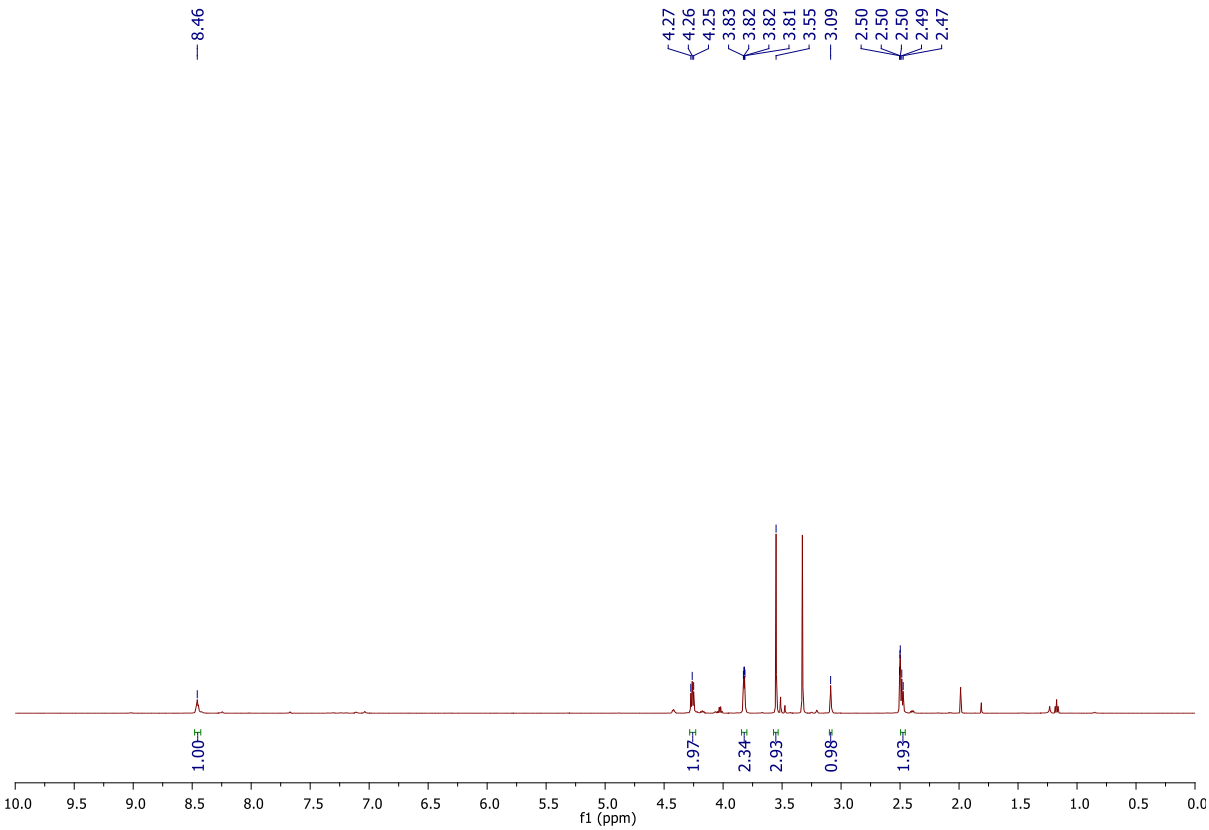

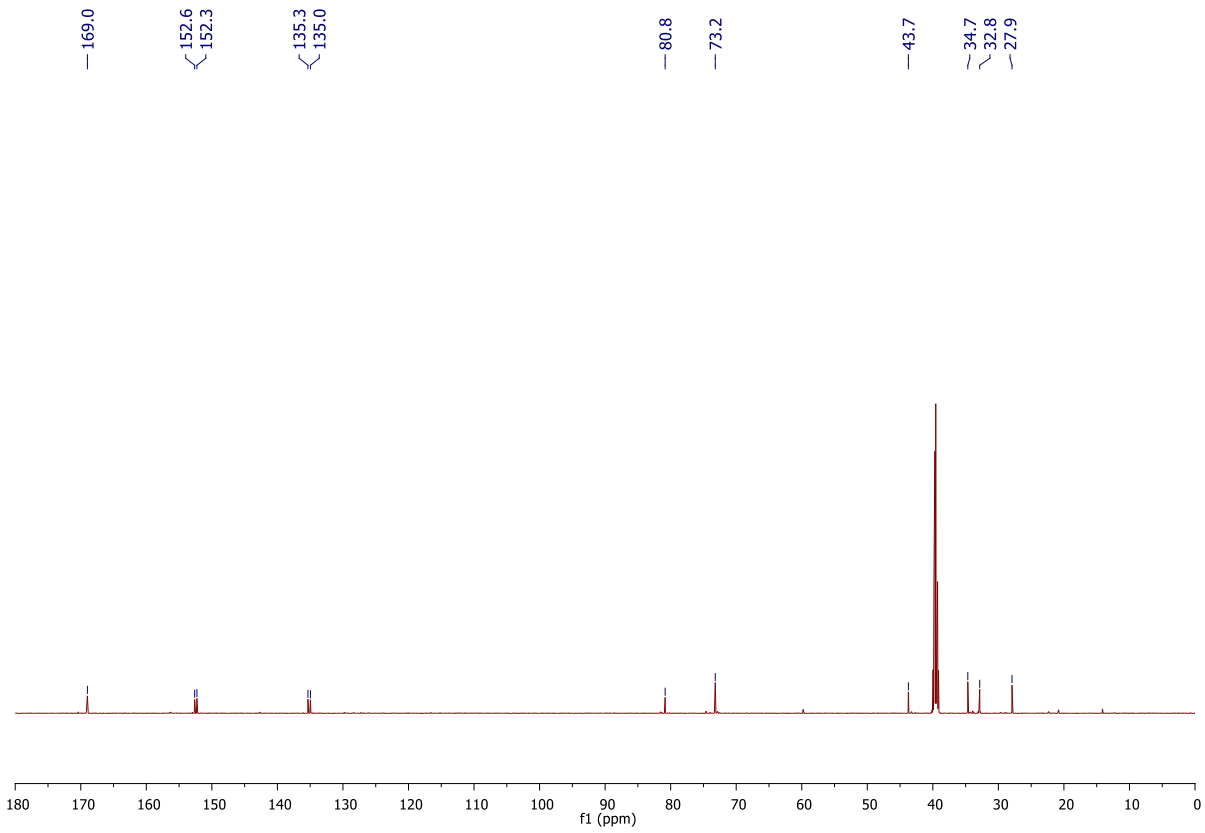
169.0
152.6
152.3
135.3
135.0
80.8
73.2
43.7
34.7
32.8
27.9
180
170
160
150
140
130
120
110
100
90
80
70
60
50
40
30
20
10
0
f1 (ppm)

((1*R*,8*S*,9*S*)-Bicyclo[6.1.0]non-4-yn-9-yl)methyl (2-(2-(2-(3-(4,5-dibromo-2-methyl-3,6-dioxo-3,6-dihydropyridazin-1(2*H*)-yl)propanamido)ethoxy)ethoxy)ethyl) carbamate 156e

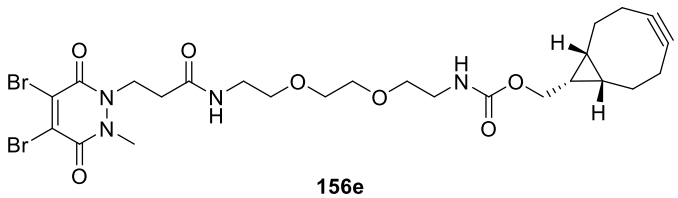

156e

General amide coupling protocol A (solvent used: MeCN) afforded ((1*R*,8*S*,9*S*)-Bicyclo[6.1.0] non-4-yn-9-yl)methyl (2-(2-(2-(3-(4,5-dibromo-2-methyl-3,6-dioxo-3,6-dihydropyridazin-1(2*H*)-yl)propanamido)ethoxy)ethoxy)ethyl) carbamate **156e** (105 mg, 0.168 mmol, 72%) as a yellow oil: ^{1}H NMR (600 MHz, $CDCl_3$, rotamers) δ 7.84 (s, 0.3H), 6.38 (s, 0.7H), 5.78 (s, 0.3H), 5.24 (s, 0.7H), 4.44 (t, *J* = 6.6 Hz, 2H), 4.14–4.12 (m, 2H), 3.73–3.71 (m, 3H), 3.60–3.57 (m, 6H), 3.53–3.52 (m, 2H), 3.45–3.43 (m, 2H), 3.39–3.35 (m, 2H), 2.62 (t, *J* = 6.6 Hz, 2H), 2.29–2.20 (m, 6H), 1.61–1.57 (m, 2H), 1.35–1.32 (m, 1H), 0.96–0.94 (m, 2H); ^{13}C NMR (150 MHz, $CDCl_3$, rotamers) δ 169.1 (C), 156.9 (C), 153.1 (C), 153.0 (C), 136.4 (C), 135.5 (C), 98.9 (C), 70.4 (CH_2), 70.3 (CH_2), 69.7 (CH_2), 63.0 (CH_2), 44.6 (CH_2), 40.8 (CH_2), 39.5 (CH_2), 35.1 (CH_3), 34.1 (CH_2), 29.3 (CH_2), 29.2 (CH_2), 21.6 (CH_2), 20.2 (CH_2), 17.9 (CH), 14.3 (CH); IR (thin film) 3329, 2920, 2858, 1708, 1630, 1572, 1534 cm^{-1}; LRMS (ESI), 687 (50, $[M^{81}Br^{81}Br+Na]^+$) 685 (100, $[M^{79}Br^{81}Br+Na]^+$), 683 (50, $[M^{79}Br^{79}Br+Na]^+$), 663 (60, $[M^{79}Br^{81}Br+H]^+$); HRMS (ESI) calcd for $C_{25}H_{35}Br_2N_4O_7$ $[M^{79}Br^{81}Br+H]^+$ 663.0847; observed 663.0846.

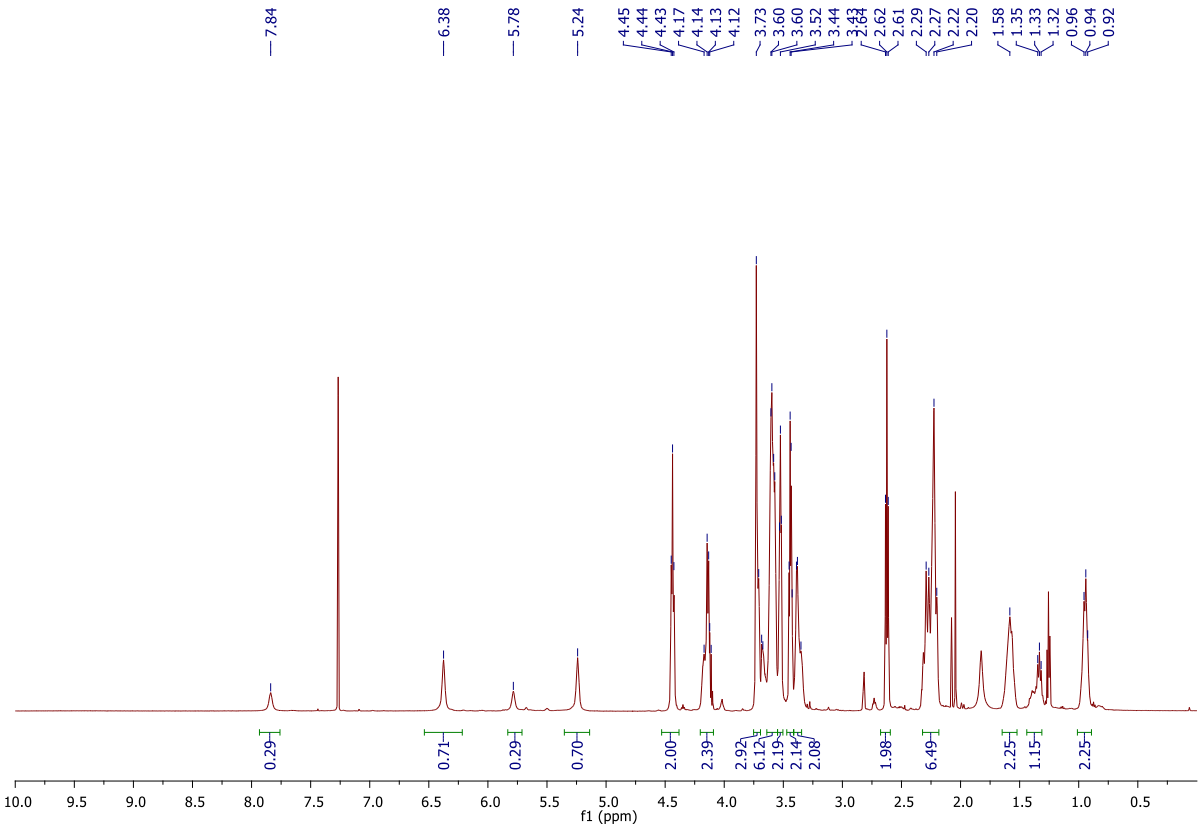
7.84
6.38
5.78
5.24
4.45
4.44
4.43
4.17
4.14
4.13
4.12
3.73
3.60
3.60
3.52
3.44
2.62
2.61
2.29
2.27
2.22
2.20
1.58
1.35
1.33
1.32
0.96
0.94
0.92
0.29
0.71
0.29
0.70
2.00
2.39
2.92
6.12
2.19
2.14
2.08
1.98
6.49
2.25
1.15
2.25
f1 (ppm)

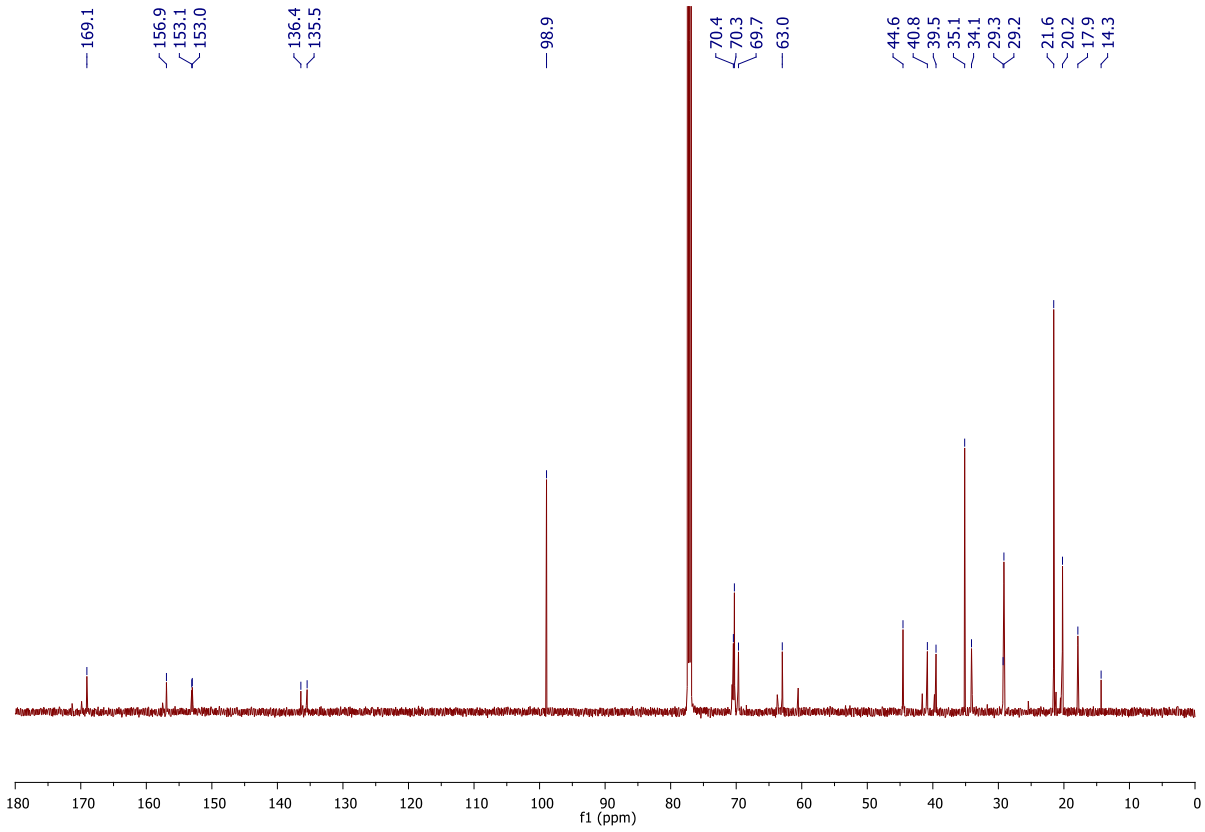
169.1
156.9
153.1
153.0
136.4
135.5
98.9
70.4
70.3
69.7
63.0
44.6
40.8
39.5
35.1
34.1
29.3
29.2
21.6
20.2
17.9
14.3
f1 (ppm)

***tert*-Butyl (17-(4,5-dibromo-2-methyl-3,6-dioxo-3,6-dihydropyridazin-1(2*H*)-yl)-15-oxo-4,7,10-trioxa-14-azaheptadecyl)carbamate 156f**

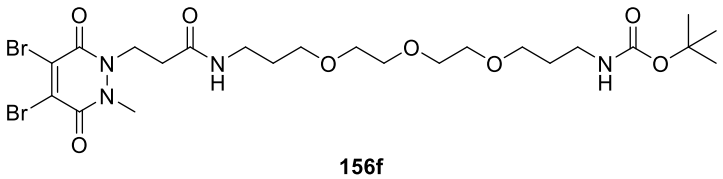

156f

General amide coupling protocol A (solvent used: MeCN) afforded *tert*-butyl (17-(4,5-dibromo-2-methyl-3,6-dioxo-3,6-dihydropyridazin-1(2*H*)-yl)-15-oxo-4,7,10-trioxa-14-azaheptadecyl)carbamate **156f** (113 mg, 0.172 mmol, 78%) as a yellow oil: ^{1}H NMR (600 MHz, $CDCl_3$) δ 6.76 (s, 1H), 4.97 (s, 1H), 4.44 (t, *J* = 6.9 Hz, 2H), 3.73 (s, 3H), 3.63–3.51 (m, 12H), 3.39–3.34 (m, 2H), 3.21–3.20 (s, 2H), 2.56 (t, *J* = 6.9 Hz, 2H), 1.75–1.71 (m, 4H), 1.43 (s, 9H); ^{13}C NMR 150 MHz, $CDCl_3$) δ 169.0 (C), 156.2 (C), 153.1 (C), 152.9 (C), 136.4 (C), 135.5 (C), 79.1 (C), 70.5 (CH_2), 70.5 (CH_2), 70.3 (CH_2), 70.2 (CH_2), 70.1 (CH_2), 69.5 (CH_2), 44.5 (CH_2), 38.7 (CH_2), 38.5 (CH_2), 38.3 (CH_2), 35.2 (CH_3), 29.8 (CH_2), 28.6 (CH_3), 25.6 (CH_2); IR (thin film) 3336, 2929, 2869, 1778, 1736, 1702, 1634 cm^{-1}; LRMS (ESI) 678 (50, $[M^{81}Br^{81}Br+NH_4]^+$), 676 (100, $[M^{79}Br^{81}Br+NH_4]^+$), 674 (50, $[M^{79}Br^{79}Br+NH_4]^+$), 659 (50, $[M^{79}Br^{81}Br+H]^+$); HRMS (ESI) calcd for $C_{23}H_{39}Br_2N_4O_8$ $[M^{79}Br^{81}Br+H]^+$ 659.1111; observed 659.1106.

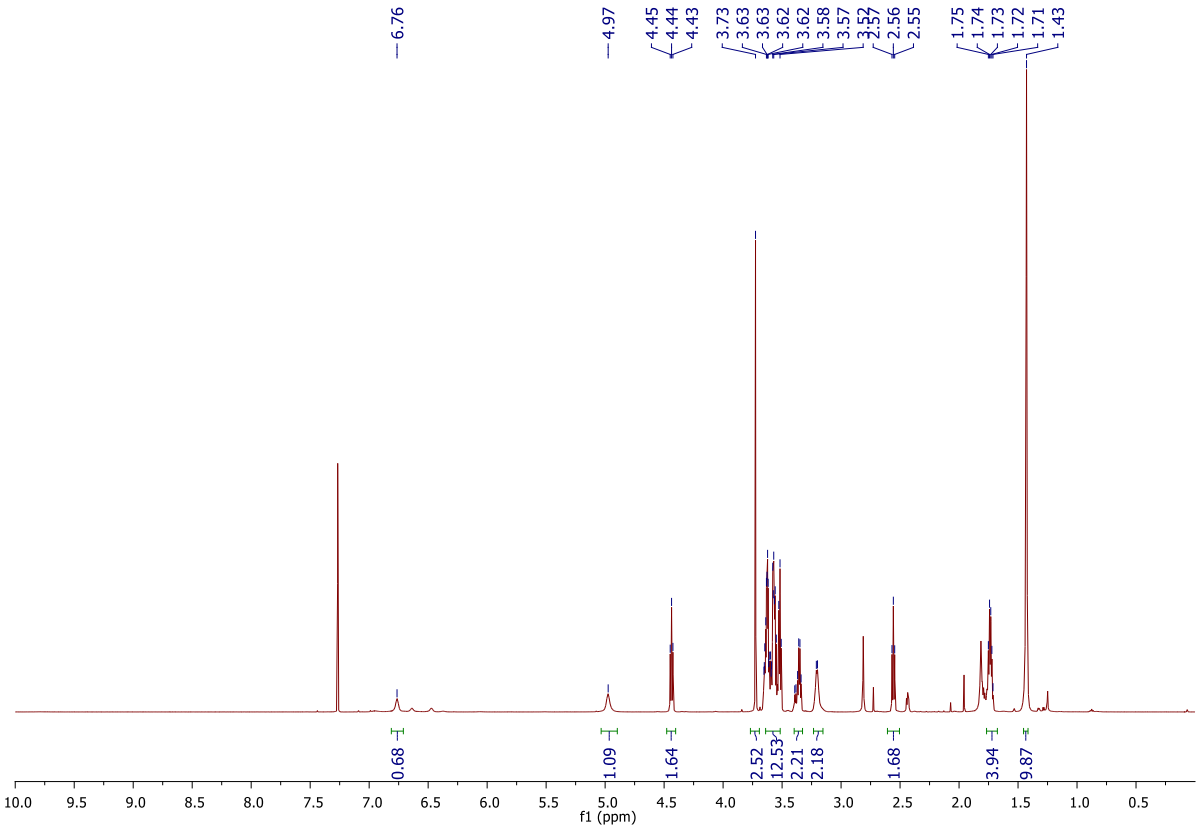
6.76
4.97
4.45
4.44
4.43
3.73
3.63
3.62
3.58
3.57
2.56
2.55
1.75
1.74
1.73
1.72
1.71
1.43
0.68
1.09
1.64
2.52
12.53
2.21
2.18
1.68
3.94
9.87
f1 (ppm)

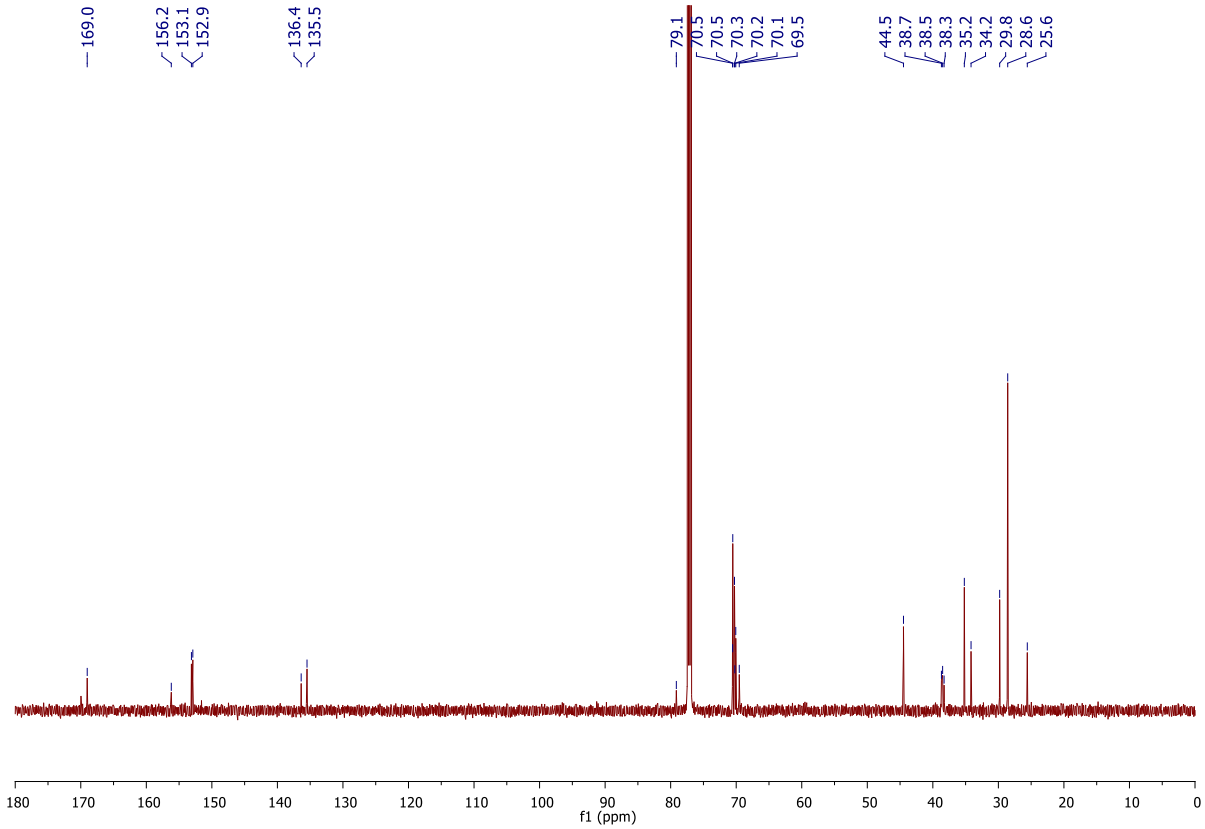
169.0
156.2
153.1
152.9
136.4
135.5
79.1
70.5
70.5
70.3
70.2
70.1
69.5
44.5
38.7
38.5
38.3
35.2
34.2
29.8
28.6
25.6
f1 (ppm)

3-(Bromo-2-methyl-3,6-dioxo-3,6-dihydropyridazin-1(2*H*)-yl)-*N*-hexyl propanamide 157a

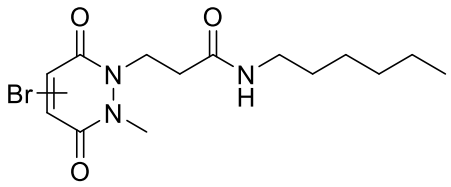

157a

General amide coupling protocol B (solvent used: MeCN) afforded an inseparable 1:1 mixture of regioisomers 3-(4-bromo-2-methyl-3,6-dioxo-3,6-dihydropyridazin-1(2*H*)-yl)-*N*-hexyl propanamide and 3-(5-bromo-2-methyl-3,6-dioxo-3,6-dihydropyridazin-1(2*H*)-yl)-*N*-hexyl propanamide **157a** (95.2 mg, 0.264 mmol, 99%) as a viscous oil. ^{1}H NMR (600 MHz, $CDCl_3$, regioisomers) δ 7.38 (s, 0.5H), 7.34 (s, 0.5H), 5.86–5.83 (m, 1H), 4.43 (t, *J* = 7.0 Hz, 1H), 4.36 (t, *J* = 7.0 Hz, 1H), 3.73 (s, 1.5H), 3.65 (s, 1.5H), 3.22–3.20 (m, 2H), 2.61–2.55 (m, 2H), 1.47–1.45 (m, 2H), 1.31–1.26 (m, 6H), 0.88 (t, *J* = 6.8 Hz, 3H). ^{13}C NMR (150 MHz, $CDCl_3$, regioisomers) δ 168.9 (C), 155.9 (C), 155.8 (C), 154.0 (C), 154.0 (C), 136.3 (CH), 135.4 (CH), 134.3 (C), 133.0 (C), 44.3 (CH_2), 43.2 (CH_2), 39.9 (CH_2), 34.7 (CH_2), 34.5 (CH_2), 34.4 (CH_3), 33.4 (CH_3), 31.5 (CH_2), 29.5 (CH_2), 29.5 (CH_2), 26.7 (CH_2), 22.7 (CH_2), 14.1 (CH_3). IR (thin film) 3305, 2924, 2854, 1739, 1624, 1545 cm^{-1}. LRMS (ESI) 382 (35, $[M^{79}Br+Na]^+$), 362 (100, $[M^{81}Br+H]^+$), 360 (100, $[M^{79}Br+H]^+$). HRMS (ESI) calcd for $C_{14}H_{23}Br_1N_3O_3$ $[M^{79}Br+H]^+$ 360.0917; observed 360.0919.

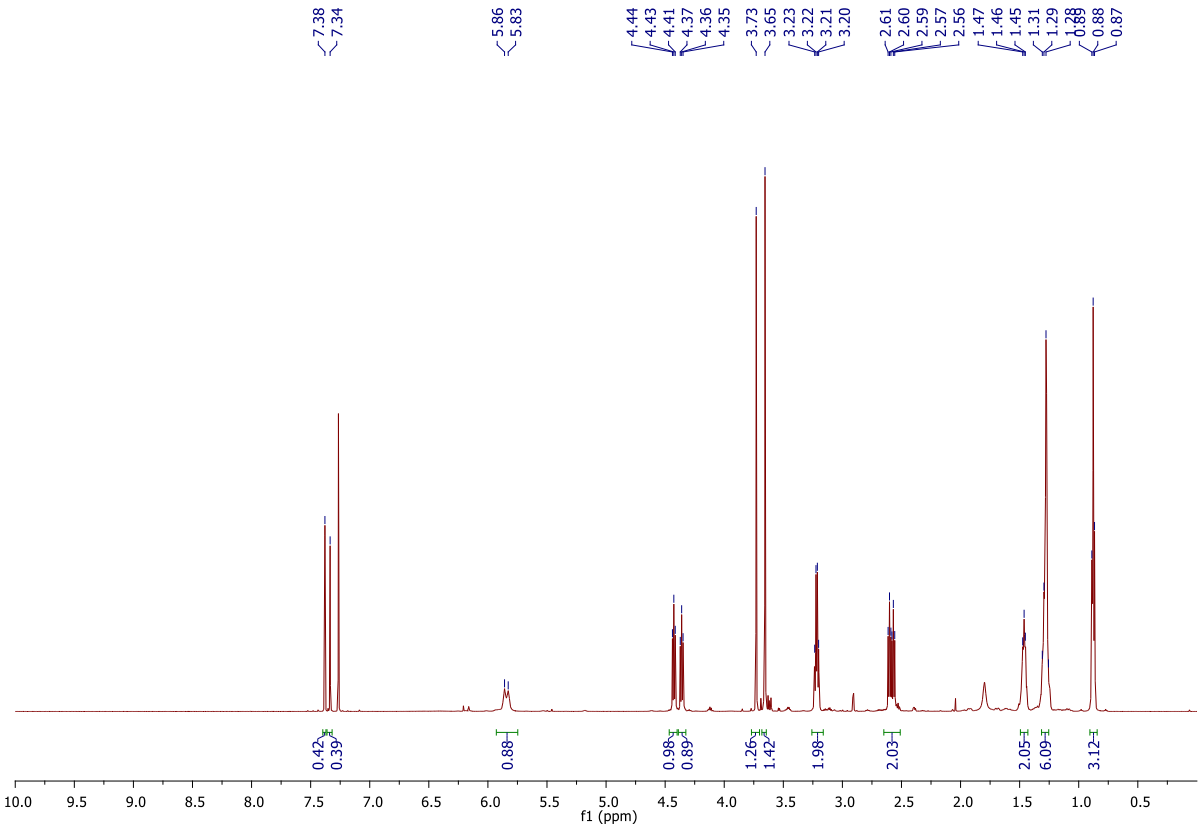
7.38
7.34
5.86
5.83
4.44
4.43
4.41
4.37
4.36
4.35
3.73
3.65
3.23
3.22
3.21
3.20
2.61
2.60
2.59
2.57
2.56
1.47
1.46
1.45
1.31
1.29
0.88
0.87
0.42
0.39
0.88
0.98
0.89
1.26
1.42
1.98
2.03
2.05
6.09
3.12
f1 (ppm)

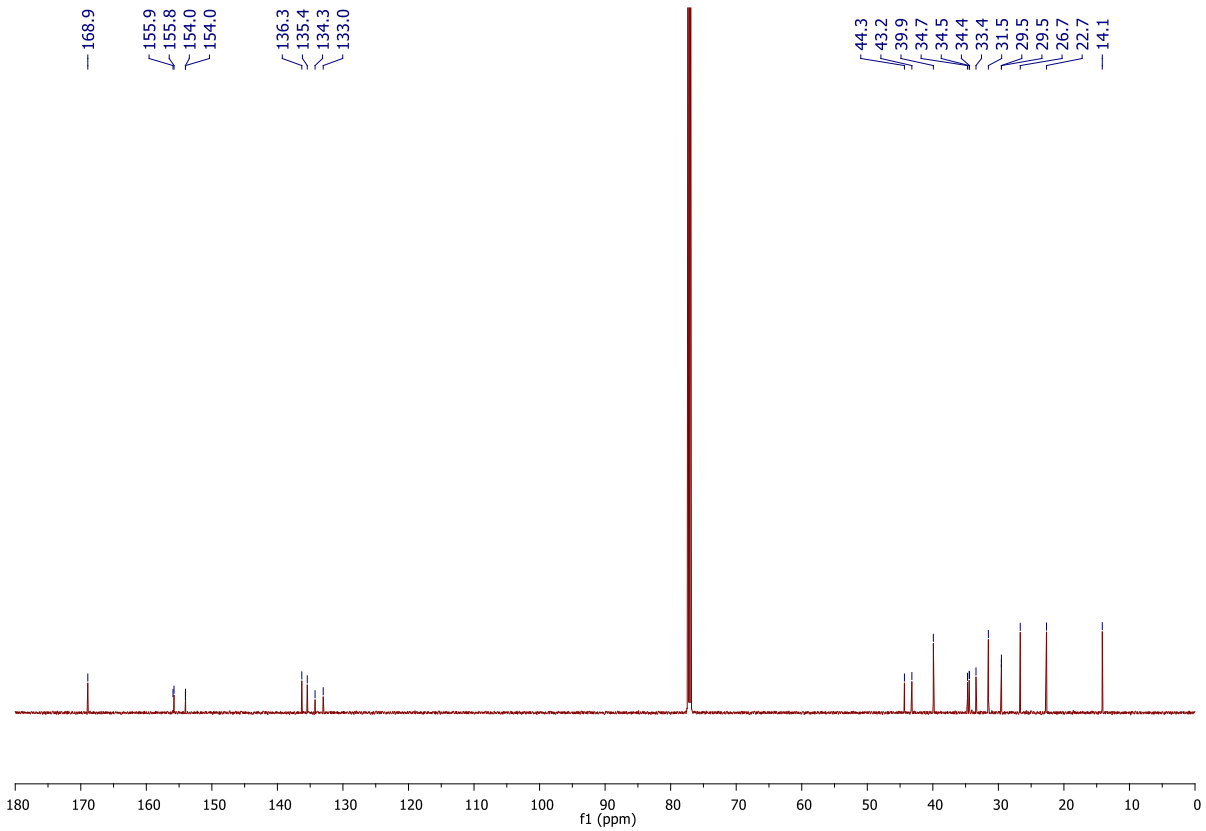
168.9
155.9
155.8
154.0
154.0
136.3
135.4
134.3
133.0
44.3
43.2
39.9
34.7
34.5
34.4
33.4
31.5
29.5
29.5
26.7
22.7
14.1
f1 (ppm)

3-(Bromo-2-methyl-3,6-dioxo-3,6-dihydropyridazin-1(2*H*)-yl)-*N*-(2-(2-hydroxyethoxy)ethyl)propanamide 157b

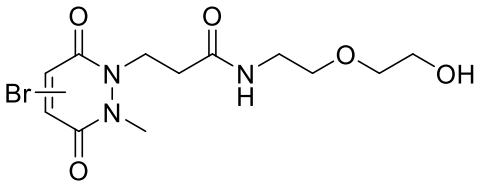

157b

General amide coupling protocol B (solvent used: MeCN) afforded an inseparable 1:1 mixture of regioisomers 3-(4-bromo-2-methyl-3,6-dioxo-3,6-dihydropyridazin-1(2*H*)-yl)-*N*-(2-(2- hydroxyethoxy)ethyl) propanamide and 3-(5-bromo-2-methyl-3,6-dioxo-3,6-dihydropyridazin-1(2*H*)-yl)-*N*-(2-(2-hydroxyethoxy)ethyl)propanamide **157b** (62.2 mg, 0.171 mmol, 64%) as a colourless oil. ^{1}H NMR (600 MHz, $CDCl_3$, regioisomers) δ 7.39 (s, 0.5H), 7.36 (s, 0.5H), 6.93 (s, 0.5H), 6.85 (s, 0.5H), 4.43 (t, *J* = 7.0 Hz, 1H), 4.37 (t, *J* = 7.0 Hz, 1H), 3.75–3.73 (m, 2H), 3.72 (s, 1.5H), 3.64 (s, 1.5H), 3.58–3.55 (m, 4H), 3.48–3.42 (m, 2H), 2.63–2.59 (m, 2H). ^{13}C NMR (150 MHz, $CDCl_3$, regioisomers) δ 169.4 (C), 169.3 (C), 156.1 (C), 155.9 (C), 154.1 (C), 136.3 (CH), 135.4 (CH), 134.4 (C), 133.0 (C), 72.5 (CH_2), 72.4 (CH_2), 69.6 (CH_2), 61.8 (CH_2), 44.3 (CH_2), 43.2 (CH_2), 39.6 (CH_2), 34.8 (CH_2), 34.7 (CH_2), 34.5 (CH_2), 34.0 (CH_3), 33.5 (CH_3). IR (thin film) 3316, 2926, 2854, 1621, 1551 cm^{-1}. LRMS (ESI) 386 (35, [M^{79}Br+Na]$^{+}$), 366 (100, [M^{81}Br+H]$^{+}$), 364 (100, [M^{79}Br+H]$^{+}$). HRMS (ESI) calcd for $C_{12}H_{19}Br_1N_3O_5$ [M^{79}Br+H]$^{+}$ 364.0503; observed 364.0503.

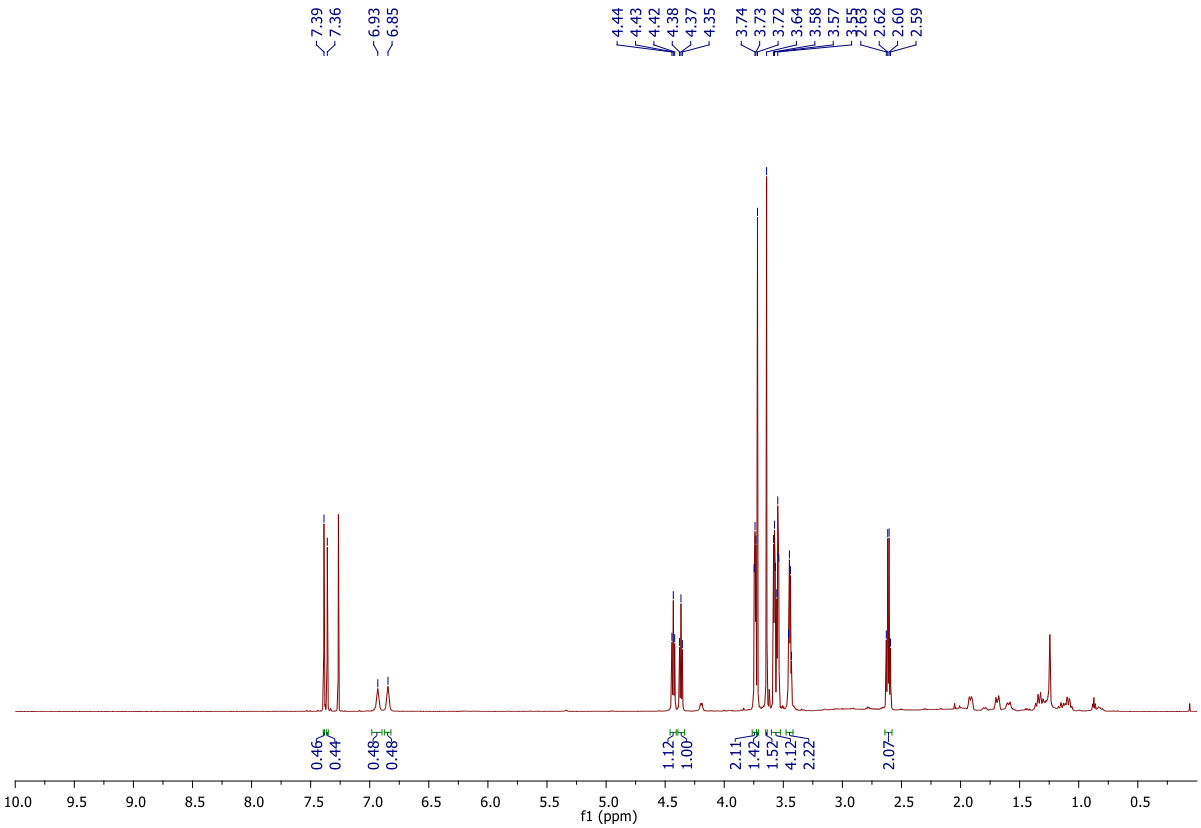
7.39
7.36
6.93
6.85
4.44
4.43
4.42
4.38
4.37
4.35
3.74
3.73
3.72
3.64
3.58
3.57
2.62
2.60
2.59
0.46
0.44
0.48
0.48
1.12
1.00
2.11
1.42
1.52
4.12
2.22
2.07
f1 (ppm)

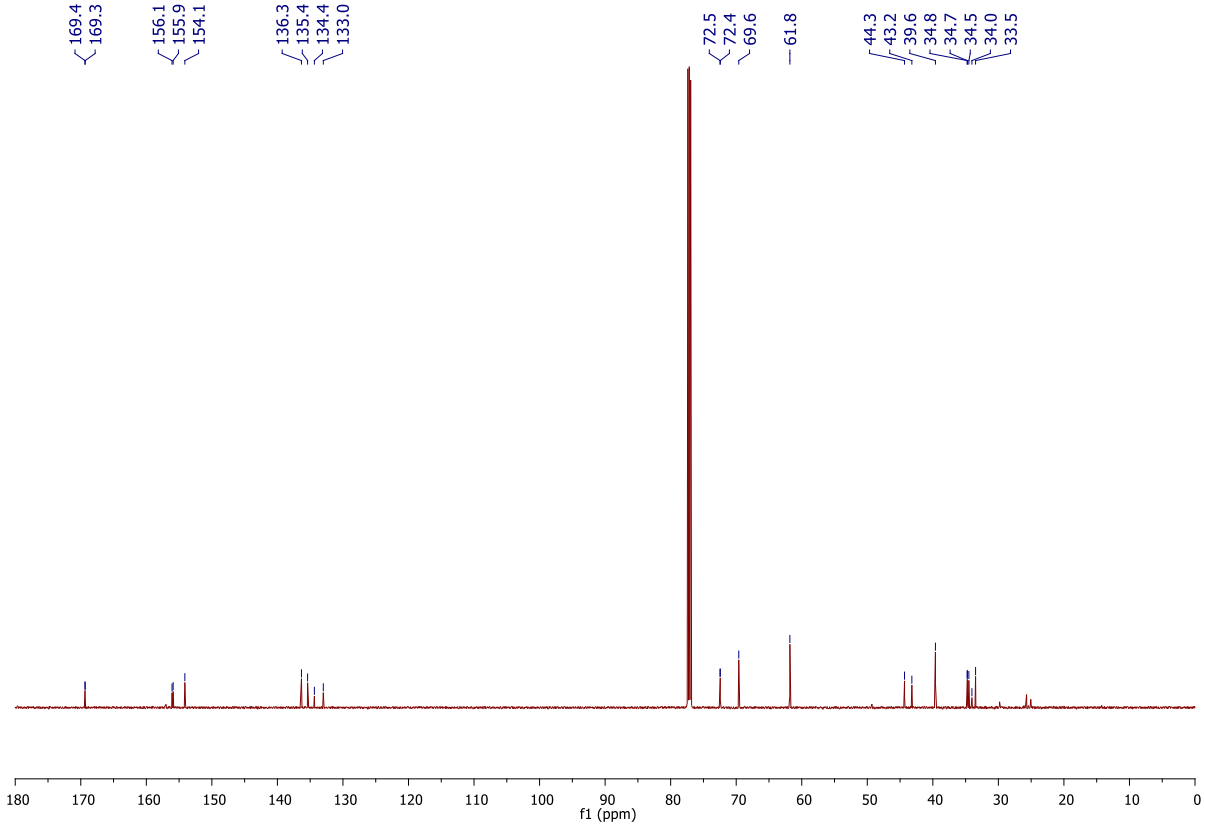
169.4
169.3
156.1
155.9
154.1
136.3
135.4
134.4
133.0
72.5
72.4
69.6
61.8
44.3
43.2
39.6
34.8
34.7
34.5
34.0
33.5
f1 (ppm)

Bromo-1-methyl-2-(3-morpholino-3-oxopropyl)-1,2-dihydropyridazine-3,6-dione 157c

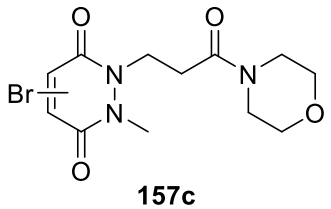

157c

General amide coupling protocol B (solvent used: MeCN) afforded an inseparable 1:1 mixture of regioisomers 4-bromo-1-methyl-2-(3-morpholino-3-oxopropyl)-1,2-dihydropyridazine-3,6-dione and 5-bromo-1-methyl-2-(3-morpholino-3-oxopropyl)-1,2-dihydropyridazine-3,6-dione **157c** (71.1 mg, 0.206 mmol, 77%) as a yellow oil. ^{1}H NMR (600 MHz, $CDCl_3$, regioisomers) δ 7.38 (s, 0.5H), 7.34 (s, 0.5H), 4.45–4.42 (m, 1H), 4.38–4.36 (m, 1H), 3.71 (s, 1.5H), 3.67–3.65 (m, 4H), 3.64 (s, 1.5H), 3.60–3.58 (m, 2H), 3.45–3.43 (m, 2H), 2.75–2.69 (m, 2H). ^{13}C NMR (150 MHz, $CDCl_3$, rotamers) δ 167.9 (C), 167.9 (C), 155.9 (C), 155.9 (C), 154.1 (C), 154.0 (C), 136.2 (C), 135.5 (C), 134.2 (C), 133.2 (C), 66.8 (CH_2), 66.6 (CH_2), 66.6 (CH_2), 46.0 (CH_2), 45.9 (CH_2), 44.0 (CH_2), 42.9 (CH_2), 42.1 (CH_2), 42.1 (CH_2), 34.7 (CH_2), 34.1 (CH_3), 33.4 (CH_3), 30.7 (CH_2), 30.7 (CH_2). IR (thin film) 2924, 2852, 1739, 1627 cm^{-1}. LRMS (ESI) 348 (95, $[M^{81}Br+H]^+$), 346 (100, $[M^{79}Br+H]^+$). HRMS (ESI) calcd for $C_{12}H_{17}Br_1N_3O_4$ $[M^{79}Br+H]^+$ 346.0397; observed 346.0399.

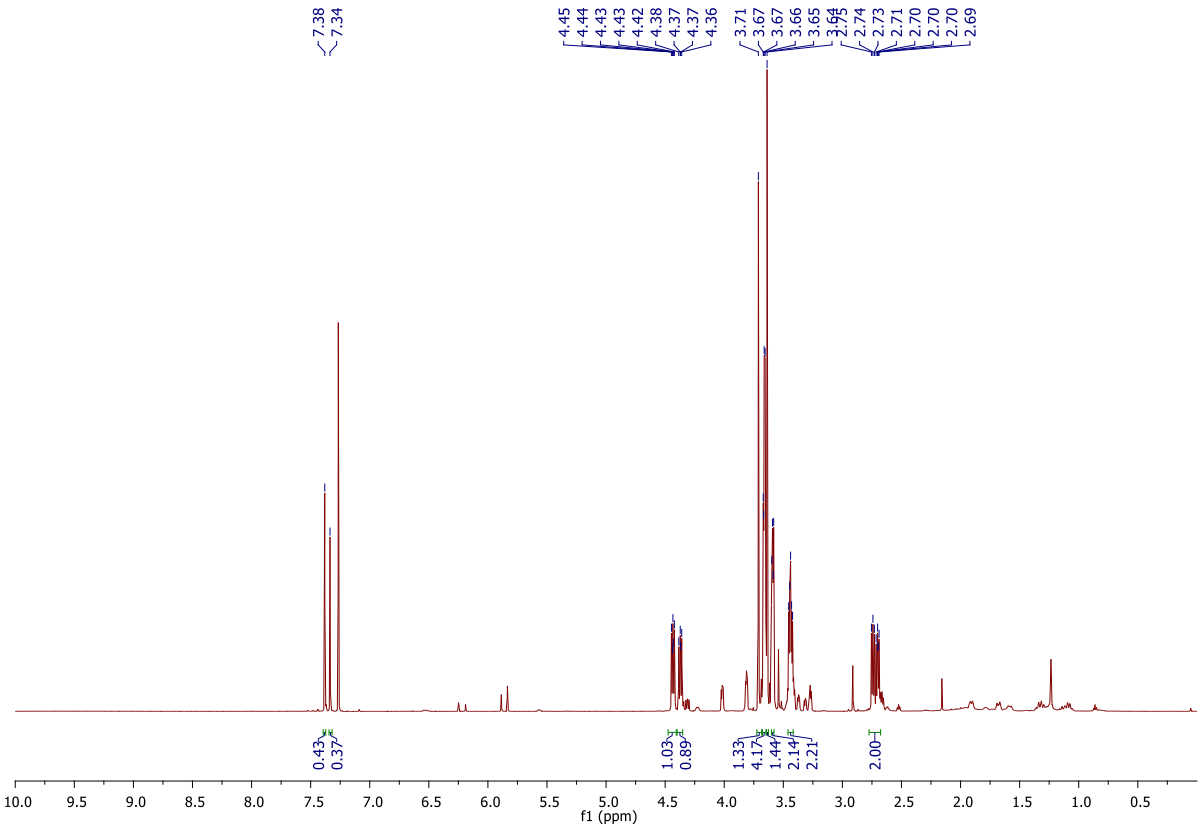
7.38
7.34
4.45
4.44
4.43
4.43
4.42
4.38
4.37
4.37
4.36
3.71
3.67
3.67
3.66
3.65
2.74
2.73
2.71
2.70
2.70
2.69
0.43
0.37
1.03
0.89
1.33
4.17
1.44
2.14
2.21
2.00
f1 (ppm)

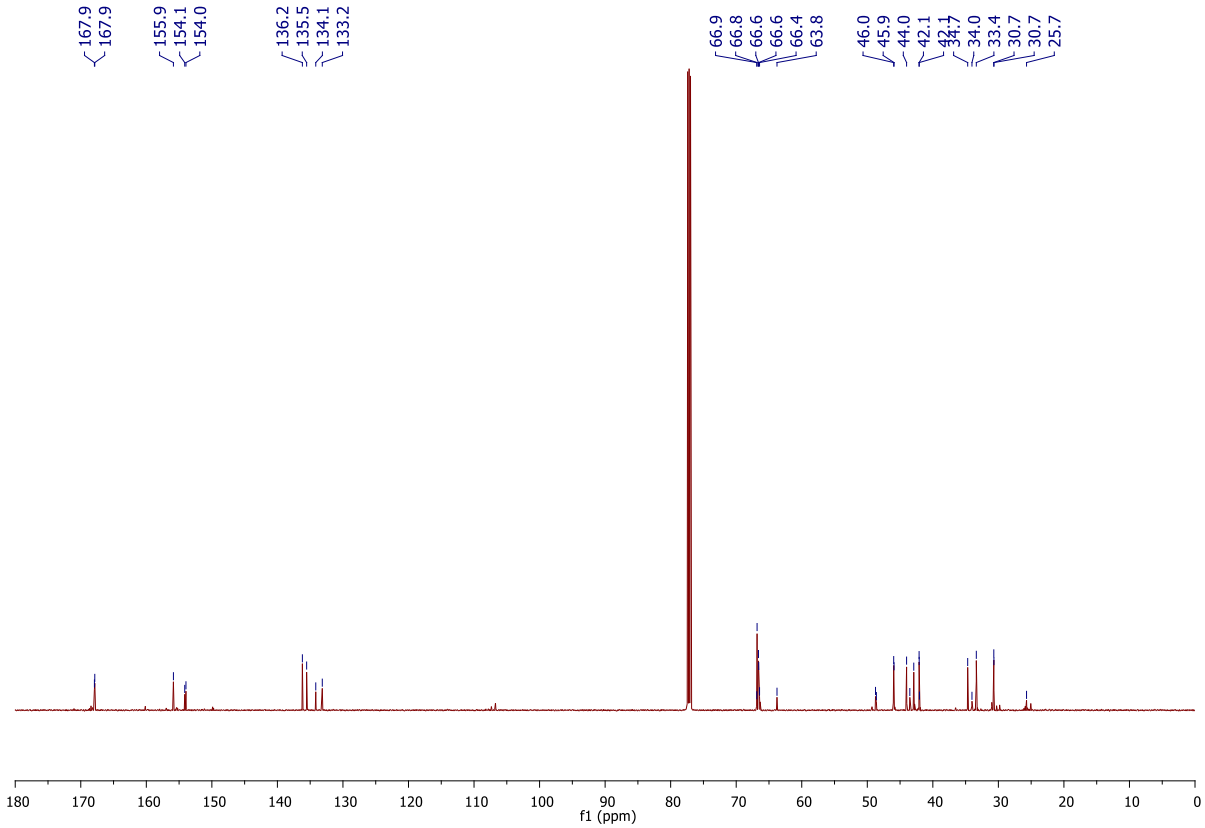
167.9
167.9
155.9
154.1
154.0
136.2
135.5
134.1
133.2
66.9
66.8
66.6
66.6
66.4
63.8
46.0
45.9
44.0
42.1
34.0
33.4
30.7
30.7
25.7
f1 (ppm)

3-(Bromo-2-methyl-3,6-dioxo-3,6-dihydropyridazin-1(2*H*)-yl)-*N*-(prop-2-yn-1-yl)propanamide 157d

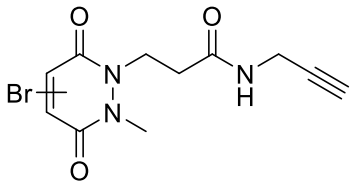

157d

General amide coupling protocol B (solvent used: MeCN) afforded an inseparable 1:1 mixture of regioisomers 3-(4-bromo-2-methyl-3,6-dioxo-3,6-dihydropyridazin-1(2*H*)-yl)-*N*-(prop-2-yn-1-yl)propanamide and 3-(5-bromo-2-methyl-3,6-dioxo-3,6-dihydropyridazin-1(2*H*)-yl)-*N*-(prop-2-yn-1-yl)propanamide **157d** (79.6 mg, 0.254 mmol, 95%) as a light yellow oil. ^{1}H NMR (600 MHz, $CDCl_3$, regioisomers) δ 7.39 (s, 0.5H), 7.35 (s, 0.5H), 6.25–6.03 (m, 1H), 4.44 (t, *J* = 7.0 Hz, 1H), 4.37 (t, *J* = 7.0 Hz, 1H), 4.04–4.03 (m, 2H), 3.73 (s, 1.5H), 3.65 (s, 1.5H), 2.67–2.62 (m, 2H), 2.25–2.24 (m, 1H). ^{13}C NMR (150 MHz, $CDCl_3$, regioisomers) δ 168.8 (C), 156.0 (C), 155.8 (C), 154.1 (C), 154.1 (C), 136.4 (CH), 135.4 (CH), 134.4 (C), 133.0 (C), 79.1 (C), 79.0 (C), 72.1 (CH), 44.1 (CH_2), 43.0 (CH_2), 34.7 (CH_2), 34.1 (CH_3), 34.0 (CH_2), 33.5 (CH_3), 29.5 (CH_2). IR (thin film) 3290, 3058, 2924, 2849, 1623, 1540 cm^{-1}. LRMS (ESI) 336 (30, $[M^{79}Br+Na]^+$), 316 (99, $[M^{81}Br+H]^+$), 314 (100, $[M^{79}Br+H]^+$). HRMS (ESI) calcd for $C_{11}H_{13}Br_1N_3O_3$ $[M^{79}Br+H]^+$ 314.0135; observed 314.0137.

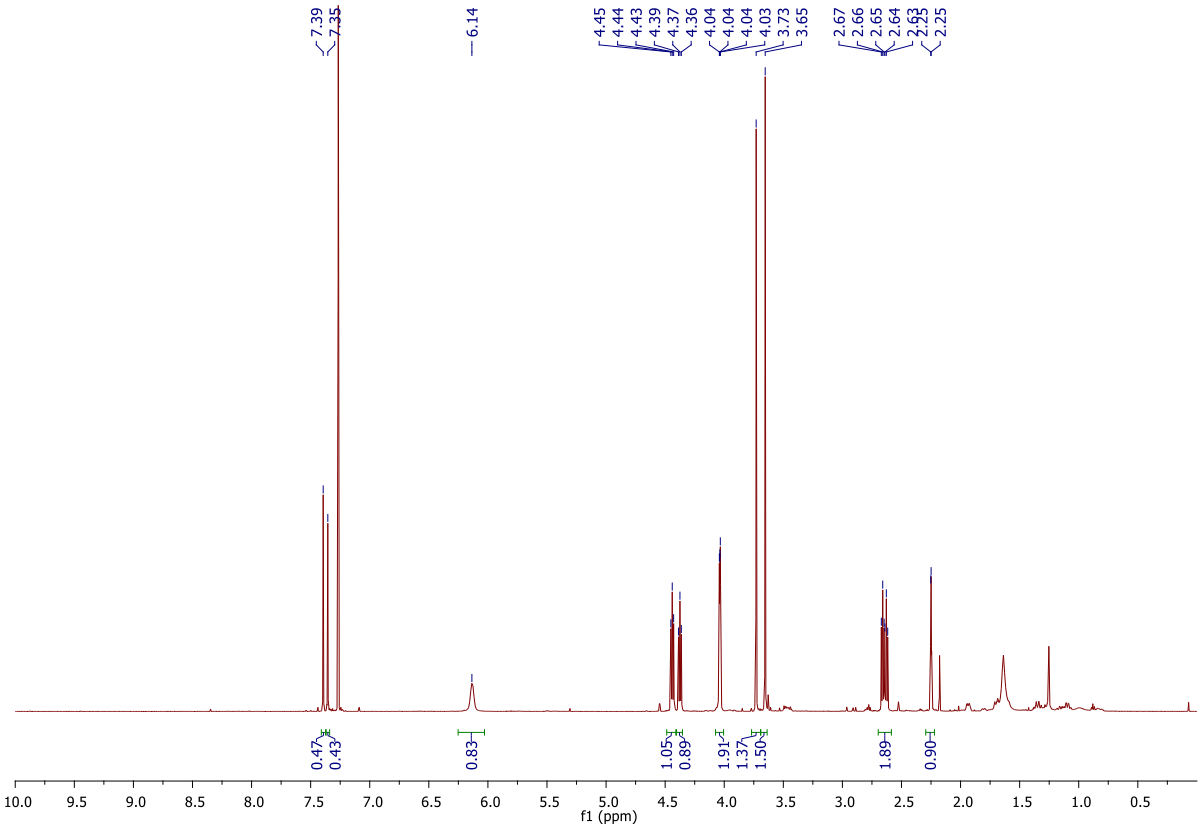
7.39
7.35
6.14
4.45
4.44
4.43
4.39
4.37
4.36
4.04
4.04
4.04
4.03
3.73
3.65
2.67
2.66
2.65
2.64
2.63
2.25
2.25
0.47
0.43
0.83
1.05
0.89
1.91
1.37
1.50
1.89
0.90
f1 (ppm)

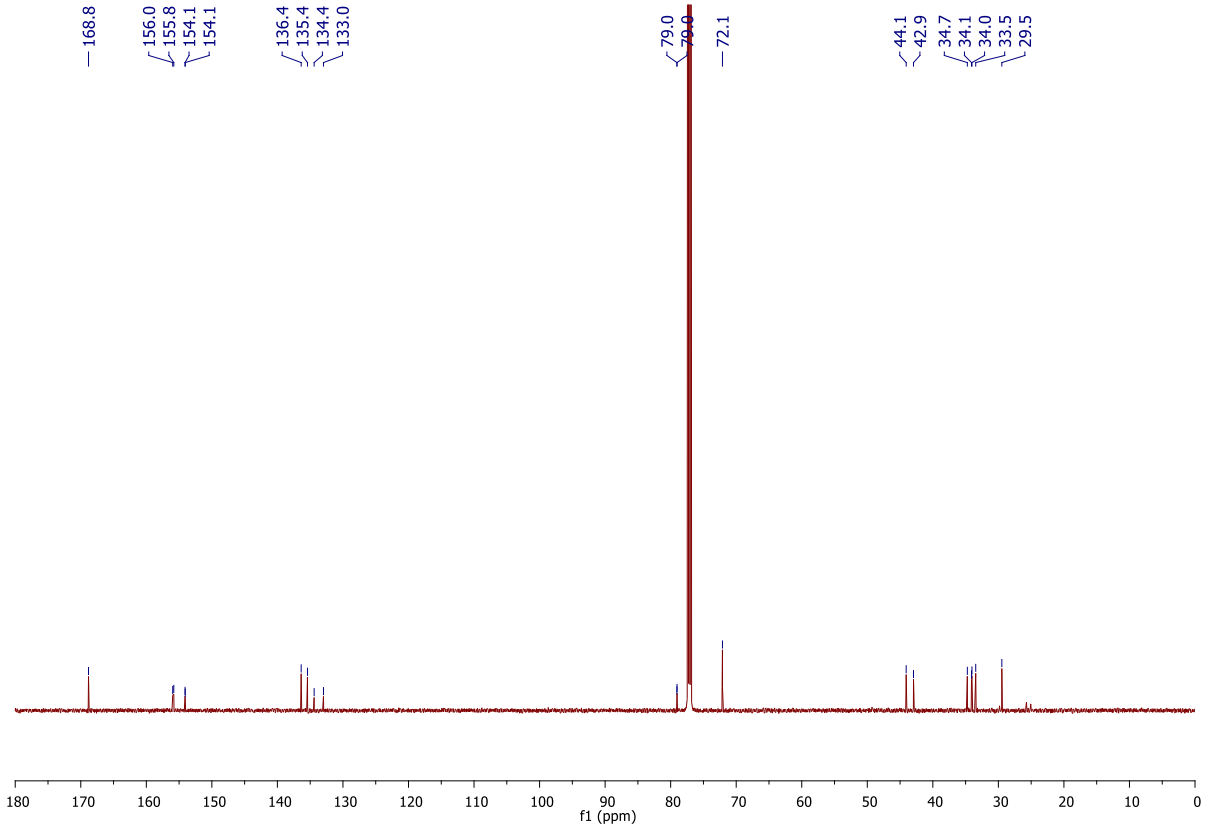
168.8
156.0
155.8
154.1
154.1
136.4
135.4
134.4
133.0
79.0
79.0
72.1
44.1
42.9
34.7
34.1
34.0
33.5
29.5
f1 (ppm)

Chemical Biology

Temperature comparison for the functional bridging of trastuzumab 161 with diBrPD 156e

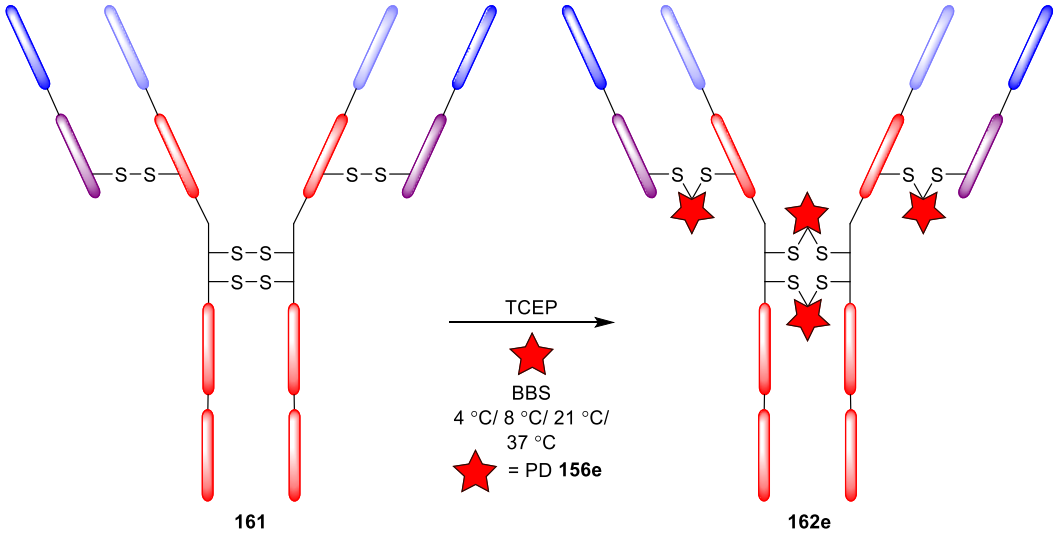

DiBrPD **156e** (2.0, µL, 10 mM in DMSO, 20 eq.) was added to a solution of trastuzumab **161** (50 µL, 20 µM) in BBS (25 mM sodium borate, 25 mM NaCl, 0.5 mM EDTA, 2% DMSO, pH 8.0) and the solution incubated at 4 °C, 8 °C, 21 °C or 37 °C for 1 h. TCEP·HCl (1.0 µL, 10 mM in deionised water at 4 °C, 8 °C, 21 °C, or 37 °C, 10 eq.) was added and the solution incubated at 4 °C, 8 °C, 21 °C or 37 °C for 16 h. Excess reagents were removed by ultrafiltration (6 × 10000 MWCO, VivaSpin®¸ GE Healthcare) into PBS (pH = 7.4).

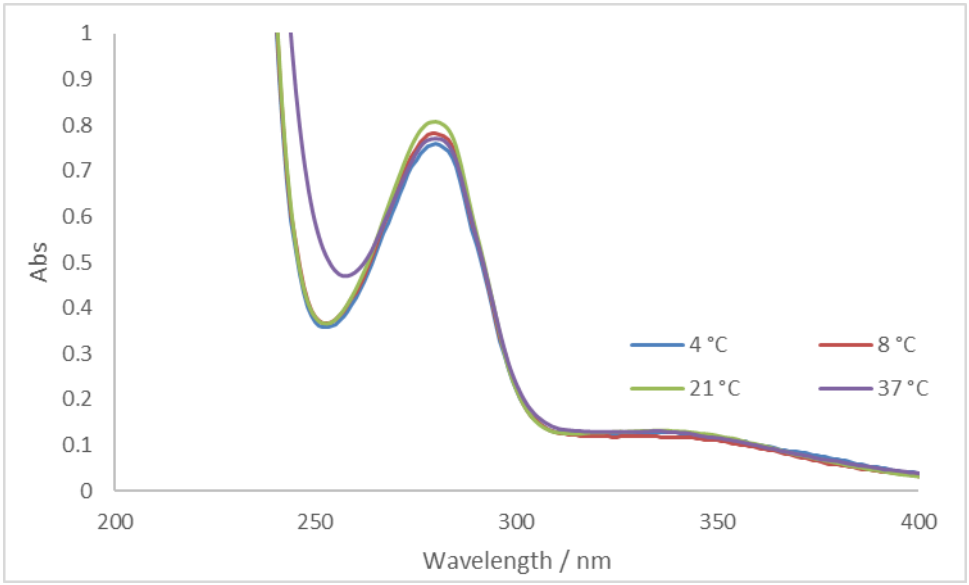

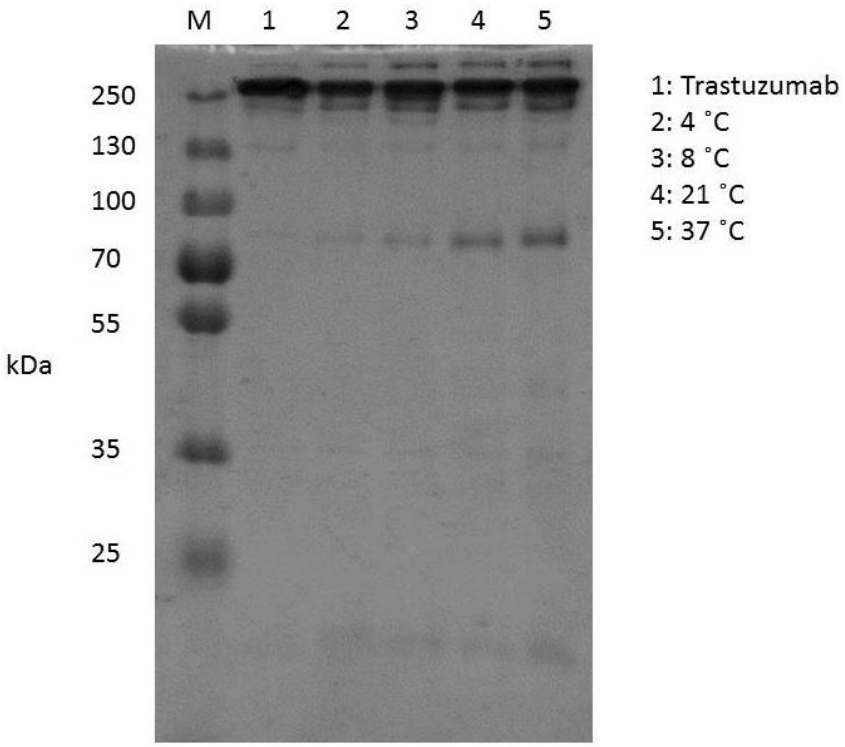
M
1
2
3
4
5
250
130
100
70
55
kDa
35
25
1: Trastuzumab
2: 4 ˚C
3: 8 ˚C
4: 21 ˚C
5: 37 ˚C

Functional bridging of trastuzumab 161 with diBrPD 156e at pH 9

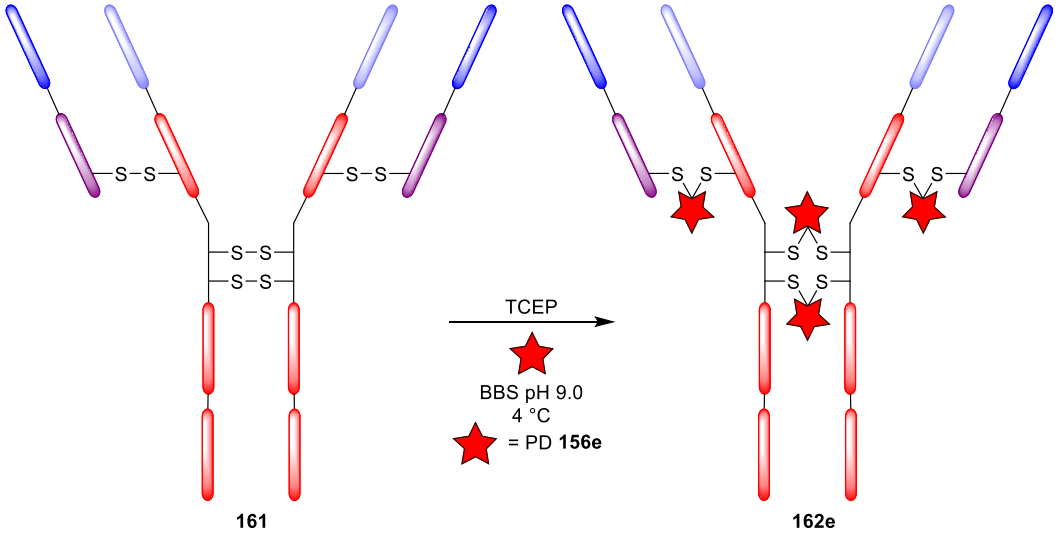

DiBrPD **156e** (2.0, µL, 10 mM in DMSO, 20 eq.) was added to a solution of trastuzumab **161** (50 µL, 20 µM) in BBS (25 mM sodium borate, 25 mM NaCl, 0.5 mM EDTA, 2% DMSO, pH 9.0) and the solution cooled to 4 °C for 2 h. TCEP·HCl (1.0 µL, 10 mM in deionised water at 4 °C, 10 eq.) was added and the solution incubated at 4 °C for 16 h. Excess reagents were removed by ultrafiltration (6 × 10000 MWCO, VivaSpin®, GE Healthcare) into PBS (pH = 7.4).

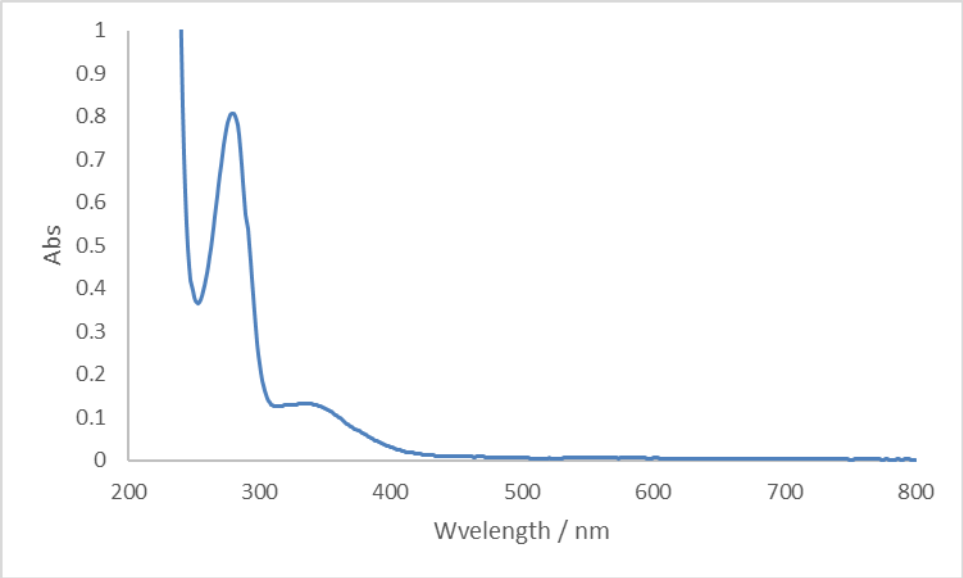

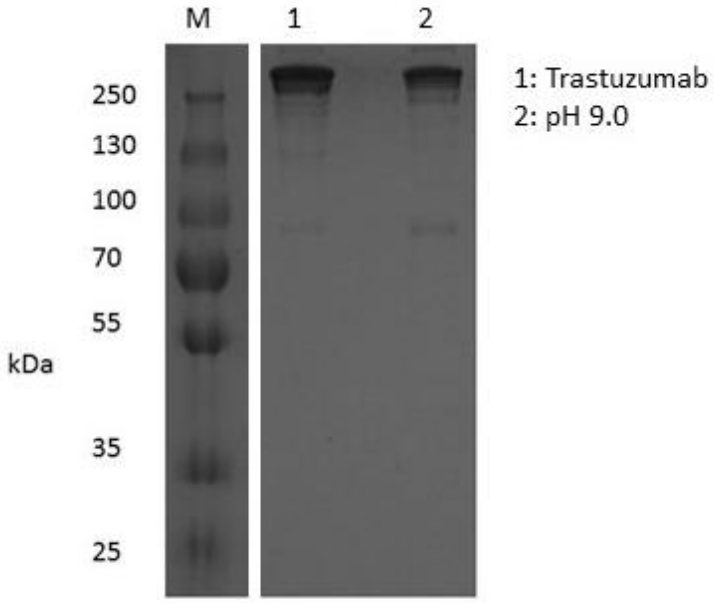
M
1
2
250
130
100
70
55
kDa
35
25
1: Trastuzumab
2: pH 9.0

Optimised protocol for the functional bridging of trastuzumab 161 with diBrPDs 156a-e.

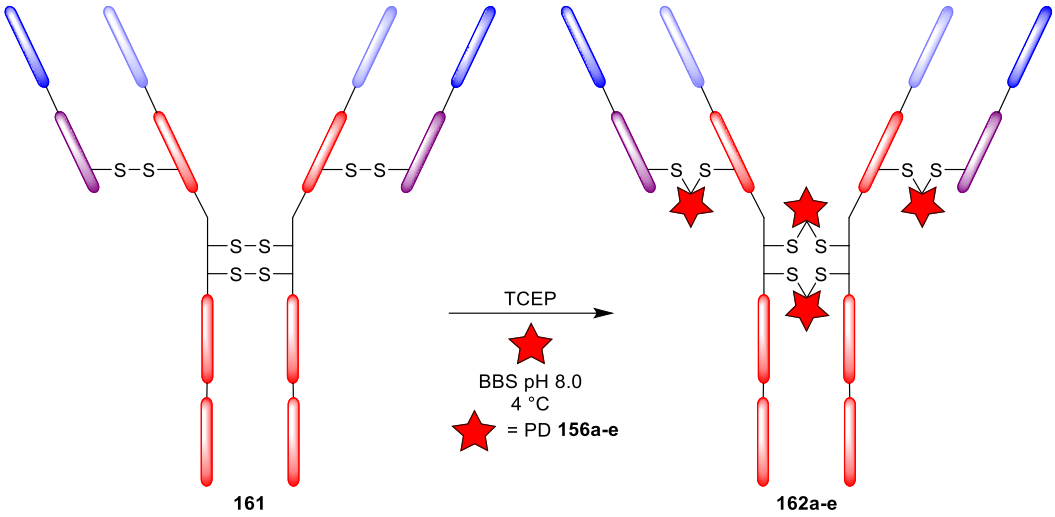

Below is a general protocol which was repeated for diBrPDs **156a-e**.

DiBrPD **156a-e** (2.0, µL, 20 mM in DMSO, 20 eq.) was added to a solution of trastuzumab **161** (50 µL, 40 µM) in BBS (25 mM sodium borate, 25 mM NaCl, 0.5 mM EDTA, 2% DMSO, pH 8.0) and the solution incubated at 4 °C for 1 h. TCEP·HCl (1.0 µL, 20 mM in deionised water at 4 °C, 10 eq.) was added and the solution incubated at 4 °C for 16 h. Excess reagents were removed by ultrafiltration (6 × 10000 MWCO, VivaSpin®, GE Healthcare) into PBS (pH = 7.4). All samples were analysed by SDS-PAGE, densitometry and UV-vis spectrometry.

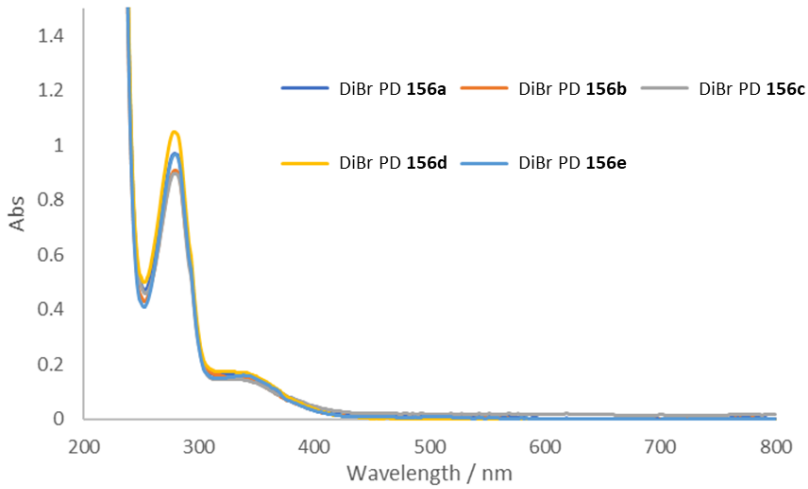

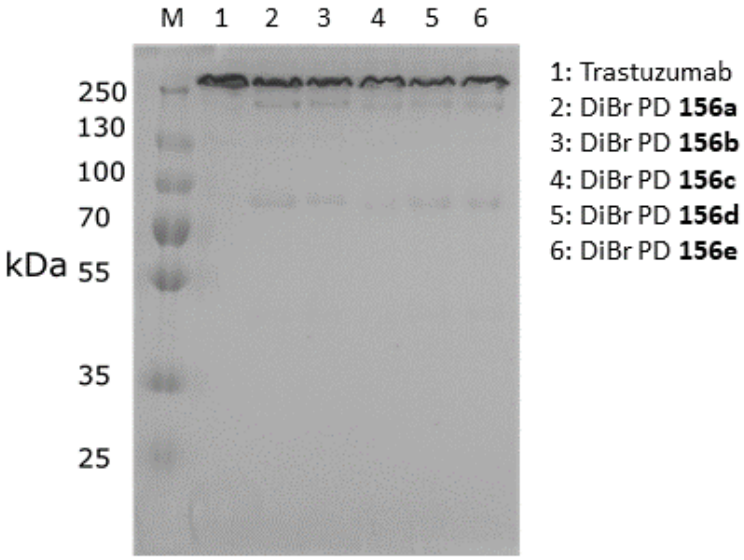
M 1 2 3 4 5 6
250
130
100
70
kDa 55
35
25
1: Trastuzumab
2: DiBr PD **156a**
3: DiBr PD **156b**
4: DiBr PD **156c**
5: DiBr PD **156d**
6: DiBr PD **156e**

HER2 ELISA for trastuzumab 161 and trastuzumab-PD conjugates 162a-e

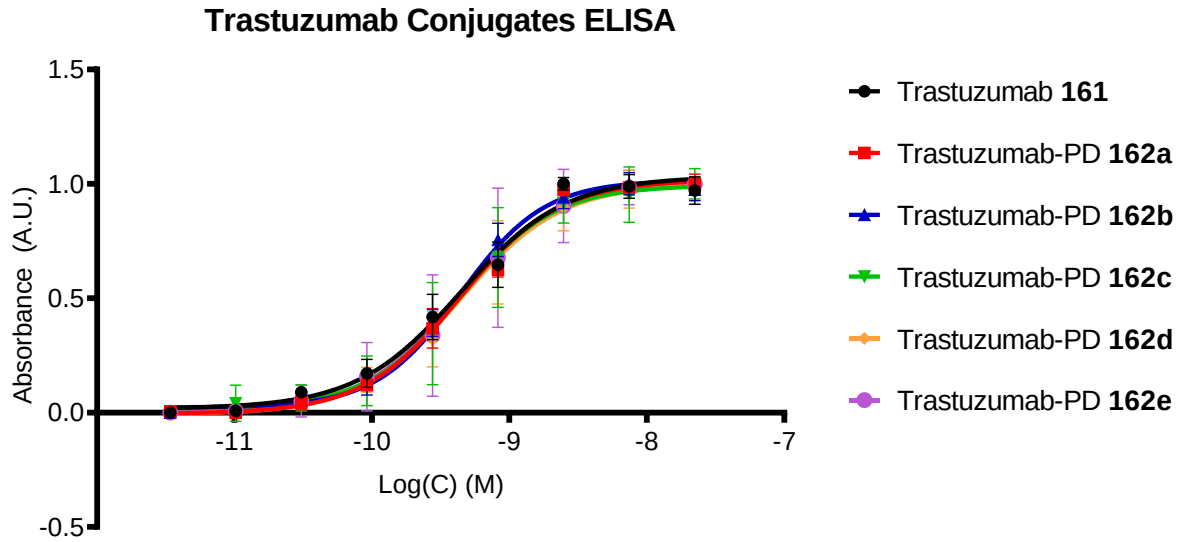

Conjugate	IC_{50} (M) Values
Trastuzumab **161**	4.1×10^{-10}
Trastuzumab-PD **162a**	4.9×10^{-10}
Trastuzumab-PD **162b**	3.8×10^{-10}
Trastuzumab-PD **162c**	4.7×10^{-10}
Trastuzumab-PD **162d**	5.0×10^{-10}
Trastuzumab-PD **162e**	4.7×10^{-10}

Experimental for Chapter 3

Organic Synthesis

Di-*tert*-butyl 1-ethyl-2-(prop-2-yn-1-yl)hydrazine-1,2-dicarboxylate S2[153]

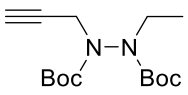

S2

To a solution of di-*tert*-butyl 1-(prop-2-yn-1-yl)hydrazine-1,2-dicarboxylate (2.08 g, 7.69 mmol) and caesium carbonate (3.75 g, 11.5 mmol) in DMF (25 mL) was added bromoethane (1.00 mL, 14 mmol) and the reaction mixture stirred at 21 °C for 24 h. The reaction mixture was then diluted with EtOAc (50 mL) and washed with water (3 × 25 mL) and brine (3 × 25 mL). The organic phase was then dried ($MgSO_4$) and concentrated *in vacuo.* Purification of the crude residue by flash column chromatography (5% to 15% EtOAc/petrol) yielded di-*tert*-butyl 1-ethyl-2-(prop-2-yn-1-yl)hydrazine-1,2-dicarboxylate **S2** (1.47 g, 4.92 mmol, 64%) as a colourless oil. ^{1}H NMR (600 MHz, $CDCl_3$, rotamers) δ 4.64–4.44 (m, 1H), 3.99–3.95 (m, 1H), 3.62–3.45 (m, 2H), 2.24–2.22 (m, 1H), 1.49–1.43 (m, 18H), 1.22–1.15 (m, 3H); ^{13}C NMR (150 MHz, $CDCl_3$, rotamers) δ 154.9 (C), 154.5 (C), 154.5 (C), 81.7 (C), 81.1 (C), 78.7 (C), 72.7 (CH), 44.7 (CH_2), 39.6 (CH_2), 28.4 (CH_3), 28.3 (CH_3), 13.0 (CH_3); IR (thin film) 3260, 2975, 2935, 2126, 1710 cm^{-1}.

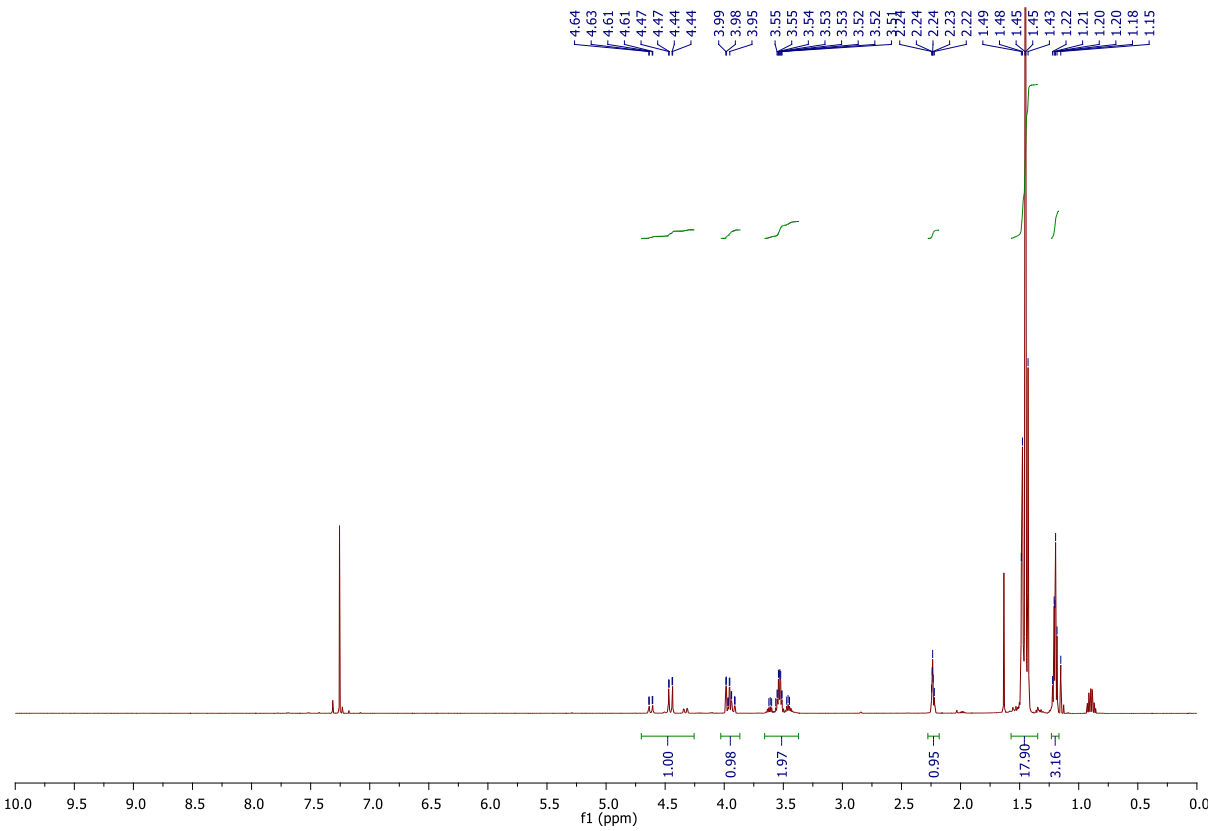
4.64
4.63
4.61
4.61
4.47
4.47
4.44
4.44
3.99
3.98
3.95
3.55
3.55
3.54
3.53
3.52
3.52
2.24
2.24
2.24
2.23
2.22
1.49
1.48
1.45
1.45
1.43
1.22
1.21
1.20
1.20
1.18
1.15
1.00
0.98
1.97
0.95
17.90
3.16
10.0
9.5
9.0
8.5
8.0
7.5
7.0
6.5
6.0
5.5
5.0
4.5
4.0
3.5
3.0
2.5
2.0
1.5
1.0
0.5
0.0
f1 (ppm)

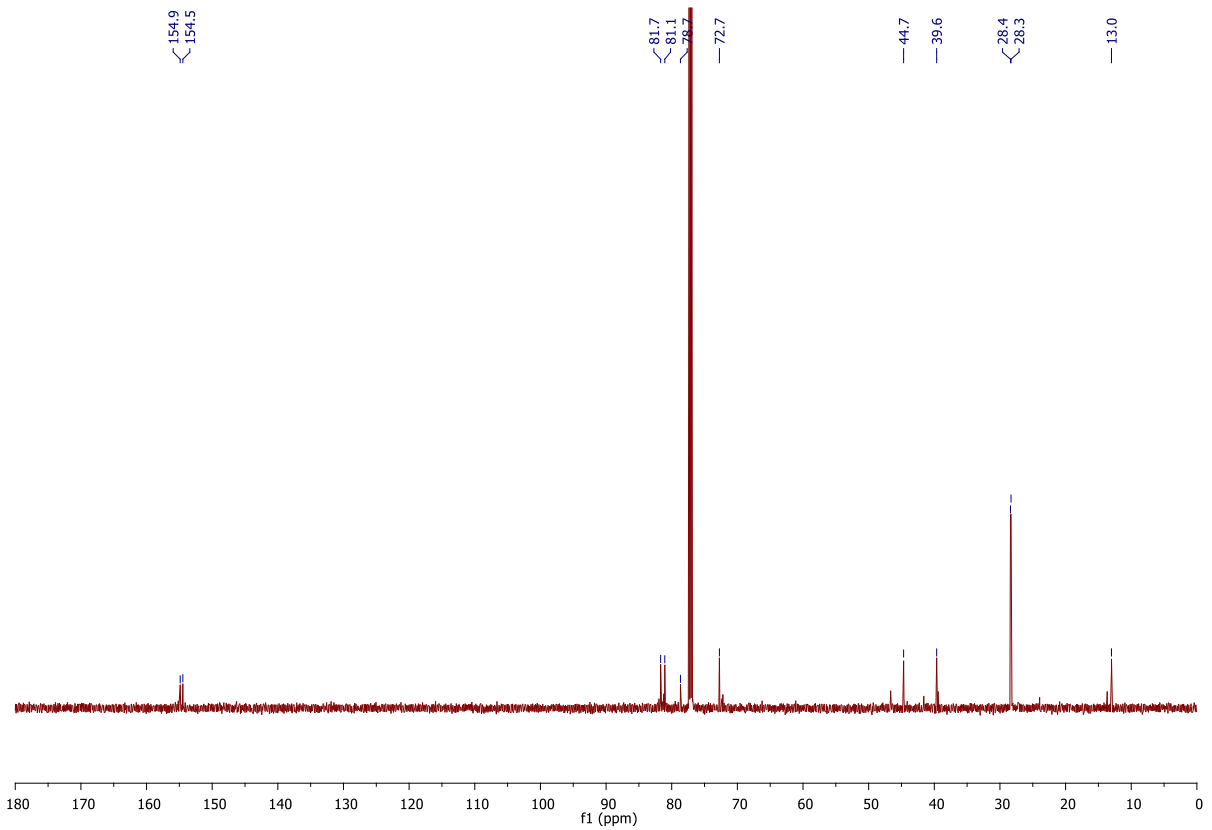
154.9
154.5
81.7
81.1
78.7
72.7
44.7
39.6
28.4
28.3
13.0
180
170
160
150
140
130
120
110
100
90
80
70
60
50
40
30
20
10
0
f1 (ppm)

4,5-Dibromo-1-ethyl-2-(prop-2-yn-1-yl)-1,2-dihydropyridazine-3,6-dione 167[153]

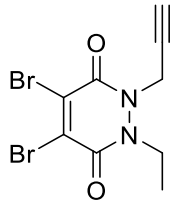

167

Dibromomaleic acid **138** (274 mg, 1.00 mmol) was dissolved in AcOH (10 mL) and heated under reflux for 30 min. After this time, di-*tert*-butyl 1-ethyl-2-(prop-2-yn-1-yl)hydrazine-1,2-dicarboxylate **S2** (347 mg, 1.20 mmol) was added and the resultant mixture was heated under reflux for a further 4 h. After this time, the reaction mixture was concentrated *in vacuo* with toluene co-evaporation (3 × 20 mL, as an azeotrope). Purification of the crude residue by flash column chromatography (30% to 70% EtOAc/petrol) yielded 4,5-dibromo-1-ethyl-2-(prop-2-yn-1-yl)-1,2-dihydropyridazine-3,6-dione **167** (195 mg, 0.580 mmol, 58%) as a yellow solid: m.p. 95-100 °C; ^{1}H NMR (600 MHz, $CDCl_3$) δ 4.89 (d, *J* = 2.4 Hz, 2H), 4.29 (q, *J* = 7.1 Hz, 2H), 2.42 (t, *J* = 2.4 Hz, 1H), 1.32 (t, *J* = 7.1 Hz, 3H); ^{13}C NMR (125 MHz, $CDCl_3$) δ 153.7 (C), 152.9 (C), 137.3 (C), 135.2 (C), 75.7 (C), 75.0 (CH) 43.0 (CH_2), 37.1 (CH_2), 13.2 (CH_3); IR (solid) 3246, 2983, 2127, 1636, 1575 cm^{-1}.

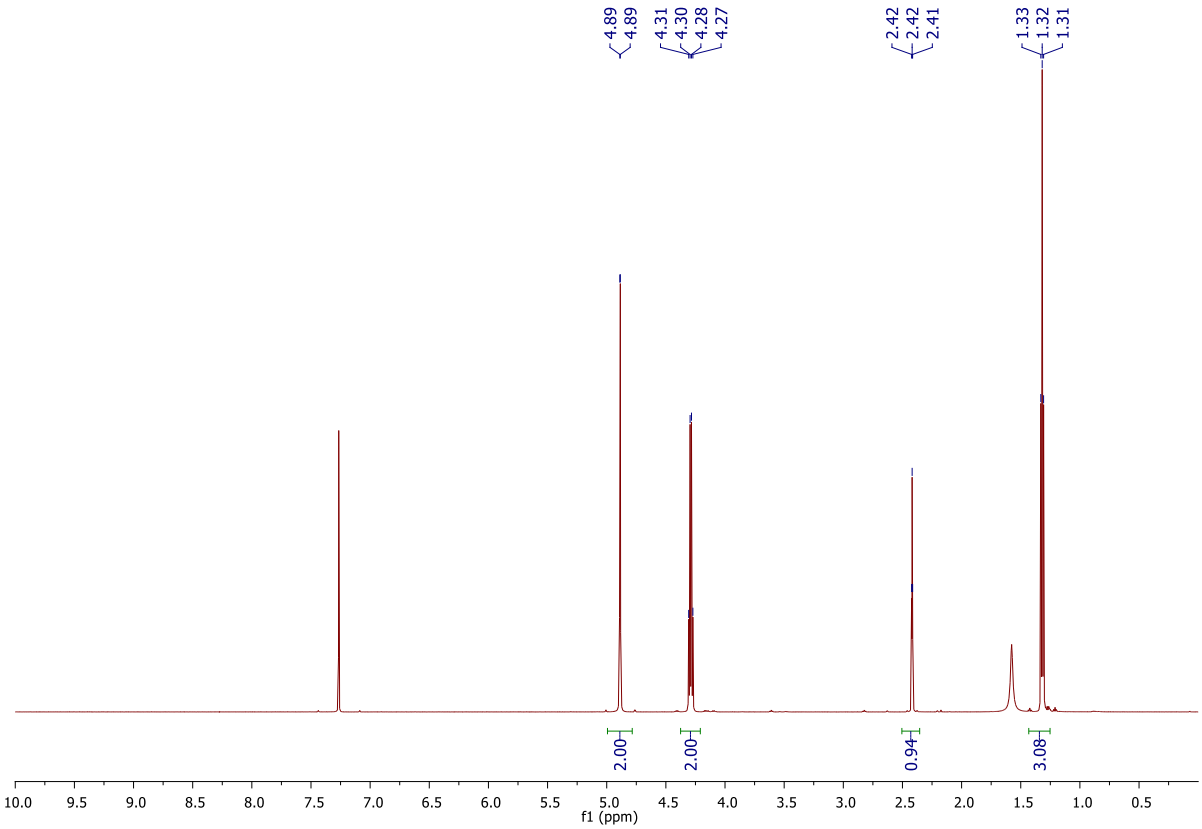
4.89
4.89
4.31
4.30
4.28
4.27
2.42
2.42
2.41
1.33
1.32
1.31
2.00
2.00
0.94
3.08
f1 (ppm)

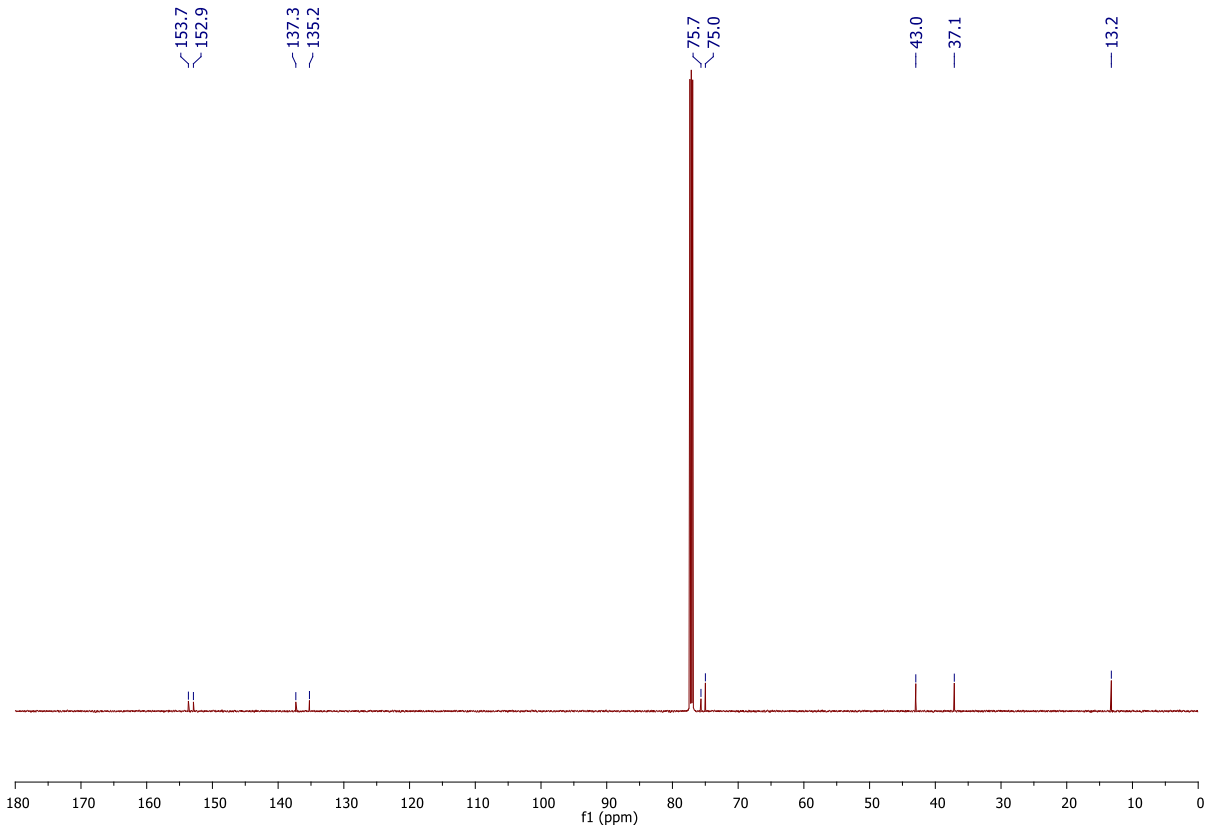
153.7
152.9
137.3
135.2
75.7
75.0
43.0
37.1
13.2
f1 (ppm)

4,5-Dichloro-1-ethyl-2-(prop-2-yn-1-yl)-1,2-dihydropyridazine-3,6-dione 169

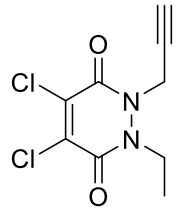

169

Dichloromaleic anhydride (167 mg, 1.00 mmol) and di-*tert*-butyl 1-ethyl-2-(prop-2-yn-1-yl)hydrazine-1,2-dicarboxylate **S2** (347 mg, 1.20 mmol) were dissolved in AcOH (10 mL) and the resultant mixture was refluxed for 4 h. After this time, the reaction mixture was concentrated *in vacuo* with toluene co-evaporation (3 × 20 mL, as an azeotrope). Purification of the crude residue by flash column chromatography (30% to 70% EtOAc/petrol) yielded 4,5-dichloro-1-ethyl-2-(prop-2-yn-1-yl)-1,2-dihydropyridazine-3,6-dione **169** (167 mg, 0.704 mmol, 70%) as an orange solid: m.p. 102-105 °C; ^{1}H NMR (600 MHz, $CDCl_3$) δ 4.89 (d, *J* = 2.5 Hz, 2H), 4.29 (q, *J* = 7.1 Hz, 2H), 2.42 (t, *J* = 2.5 Hz, 1H), 1.32 (t, *J* = 7.1 Hz, 3H); ^{13}C NMR (125 MHz, $CDCl_3$) 153.7 (C), 152.9 (C), 139.6 (C), 138.0 (C), 75.6 (C), 75.0 (CH), 42.6 (CH_2), 36.7 (CH_2), 13.3 (CH_3); IR (solid) 3245, 2983, 2127, 1639, 1589 cm^{-1}. LCMS (ESI): 252 (10, $[M^{37}Cl^{37}Cl+H]^+$), 249 (70, $[M^{35}Cl^{37}Cl+H]^+$), 247 (100, $[M^{35}Cl^{35}Cl+H]^+$). HRMS (ESI) calcd for $C_9H_8Cl_2N_2O_2$ $[M^{35}Cl^{35}Cl+H]^+$ 247.0041; observed 247.0039.

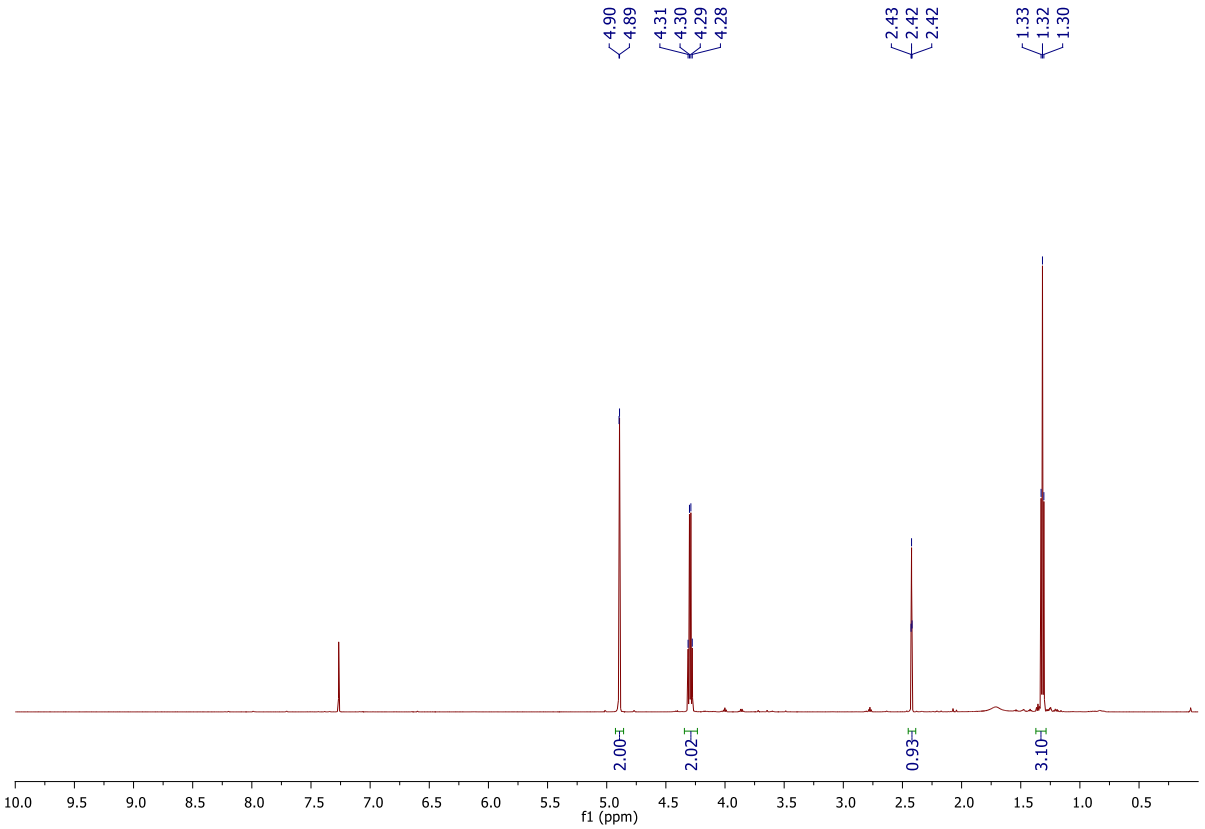
4.90
4.89
4.31
4.30
4.29
4.28
2.43
2.42
2.42
1.33
1.32
1.30
2.00
2.02
0.93
3.10
f1 (ppm)

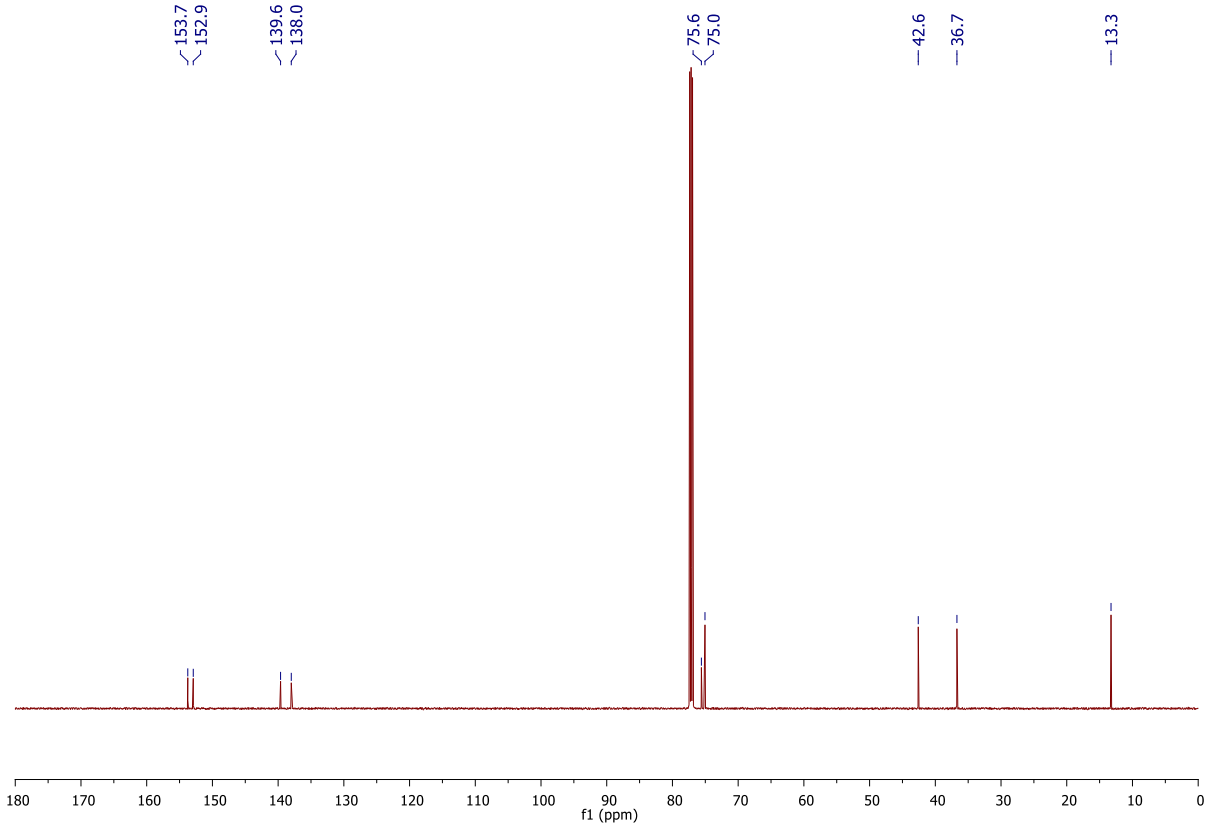
153.7
152.9
139.6
138.0
75.6
75.0
42.6
36.7
13.3
f1 (ppm)

1-(Prop-2-yn-1-yl)-1*H*-pyrrole-2,5-dione 171[203]

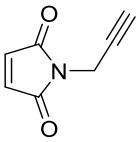

171

Maleic anhydride (300 mg, 3.06 mmol) and propargyl amine (0.22 mL, 3.37 mmol) were dissolved in AcOH (15 mL) and the resultant mixture was heated under reflux for 2 h. After this time, the reaction mixture was concentrated *in vacuo* with toluene co-evaporation (3 × 20 mL, as an azeotrope). Purification of the crude residue by flash column chromatography (0% to 50% EtOAc/petrol) yielded 1-(prop-2-yn-1-yl)-1*H*-pyrrole-2,5-dione **171** (173 mg, 1.29 mmol, 42%) as a yellow gum: ^{1}H NMR (600 MHz, $CDCl_3$) δ 6.75 (s, 2H), 4.28 (d, *J* = 2.5 Hz, 2H), 2.21 (t, *J* = 2.5 Hz, 1H); ^{13}C NMR (150 MHz, $CDCl_3$) δ 169.4 (C), 134.7 (C), 71.7 (C), 71.6 (CH), 27.0 (CH_2); IR (thin-film) 3051, 2120, 1720 cm^{-1}.

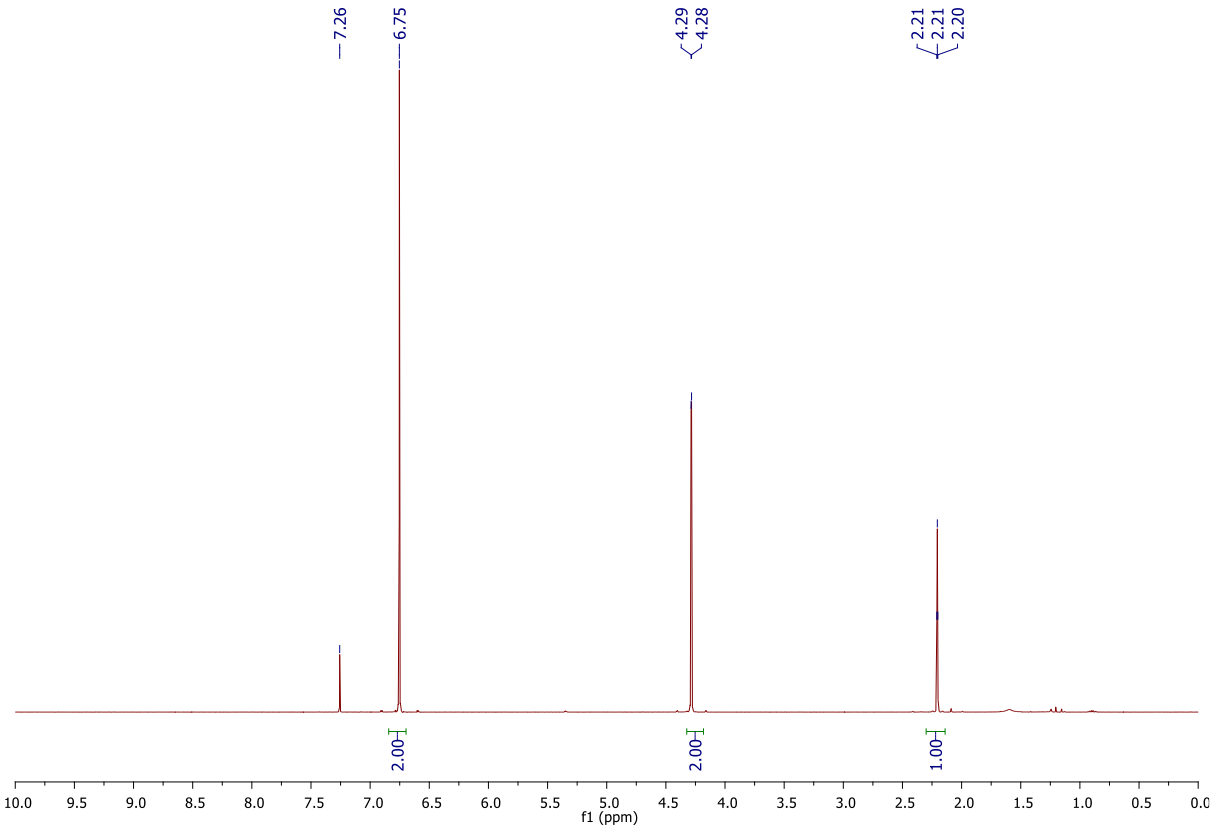

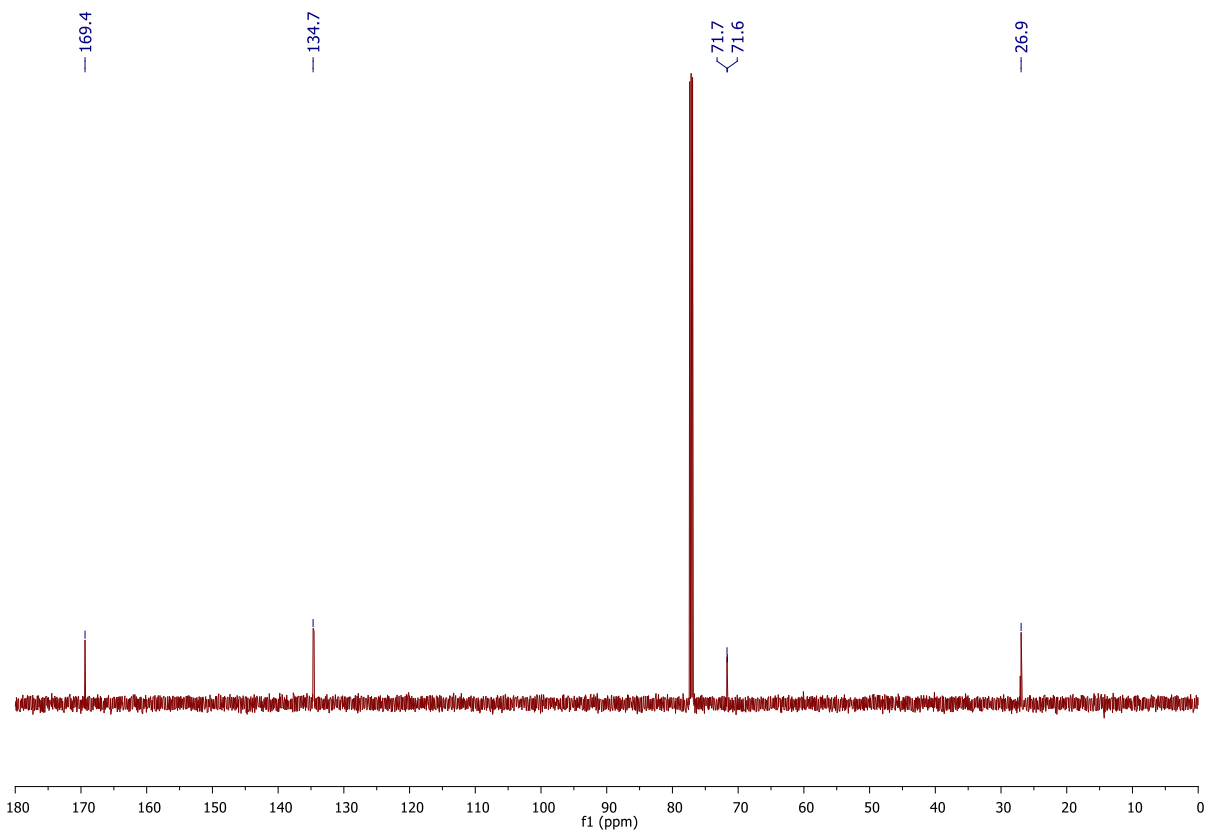
169.4
134.7
71.7
71.6
26.9
180
170
160
150
140
130
120
110
100
90
80
70
60
50
40
30
20
10
0
f1 (ppm)

Chemical Biology

Natively re-bridged trastuzumab 168

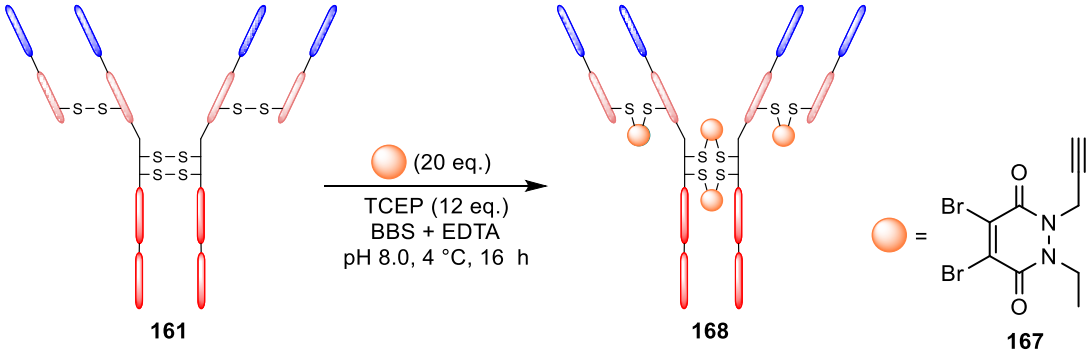

Dibromo ethyl alkyne PD **167** (4.0, µL, 20 mM in DMSO, 20 eq.) was added to a solution of trastuzumab **161** (100 µL, 40 µM) in BBS (25 mM sodium borate, 25 mM NaCl, 0.5 mM EDTA, 2% DMSO, pH 8.0) and the solution incubated at 4 °C for 1 h. TCEP·HCl (2.4 µL, 20 mM in deionised water at 21 °C, 12 eq.) was added and the solution incubated at 4 °C for 16 h. Excess reagents were removed by ultrafiltration (6 × 10000 MWCO, VivaSpin®, GE Healthcare) into PBS (pH = 7.4). Conjugate **168** was analysed by SDS-PAGE, densitometry and LCMS (Method 2): expected mass: 145,886 Da, observed mass: 145,887 Da.

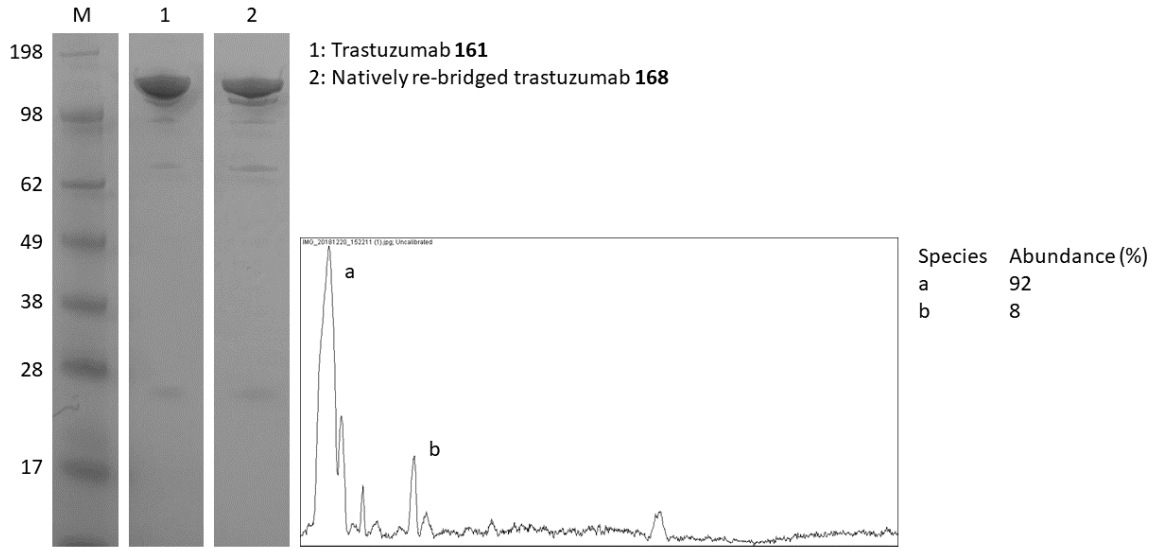

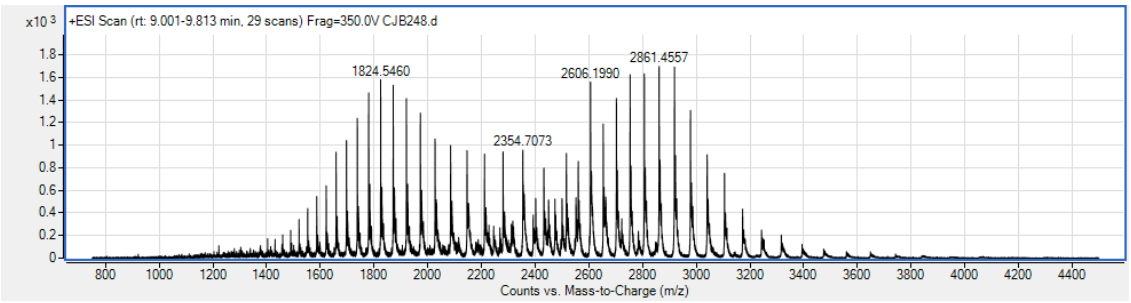
x10 3
+ESI Scan (rt: 9.001-9.813 min, 29 scans) Frag=350.0V CJB248.d
1824.5460
2606.1990
2861.4557
2354.7073
Counts vs. Mass-to-Charge (m/z)

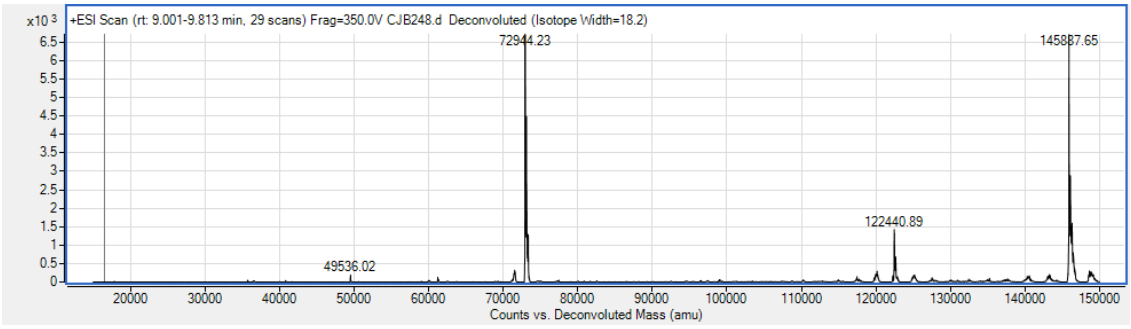
x10 3
+ESI Scan (rt: 9.001-9.813 min, 29 scans) Frag=350.0V CJB248.d Deconvoluted (Isotope Width=18.2)
72944.23
145887.65
122440.89
49536.02
Counts vs. Deconvoluted Mass (amu)

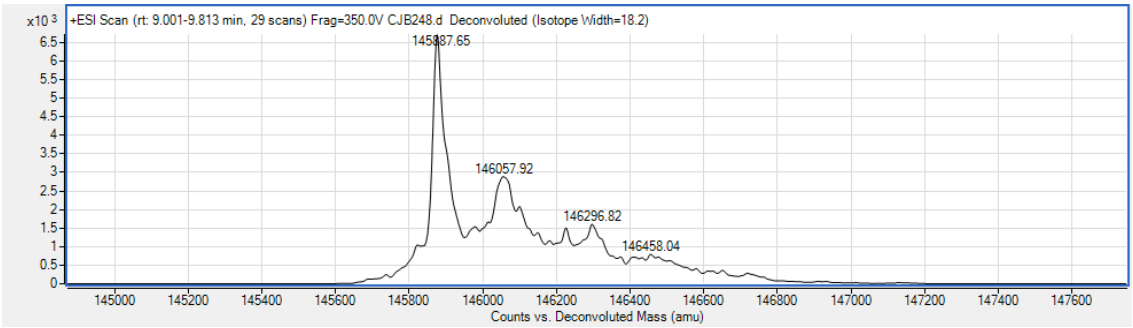
x10 3
+ESI Scan (rt: 9.001-9.813 min, 29 scans) Frag=350.0V CJB248.d Deconvoluted (Isotope Width=18.2)
145887.65
146057.92
146296.82
146458.04
Counts vs. Deconvoluted Mass (amu)

Disulfide scrambled trastuzumab 170

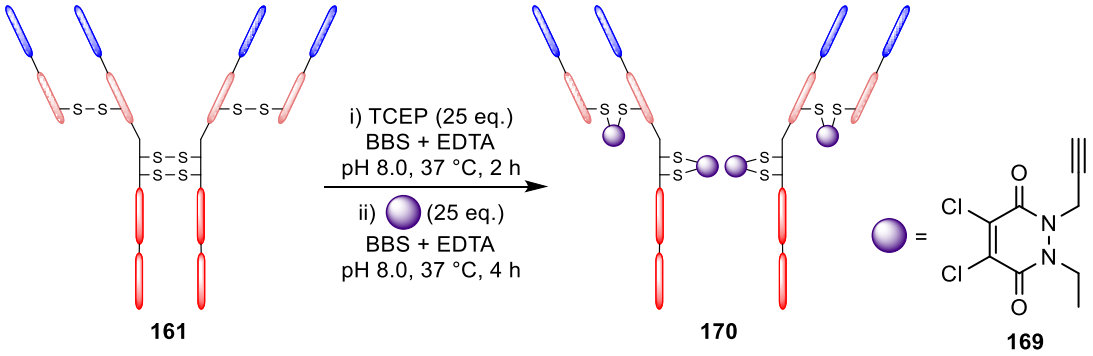

TCEP·HCl (5.0 µL, 20 mM in deionised water, 25 eq.) was added to a solution of trastuzumab **161** (100 µL, 40 µM) in BBS (25 mM sodium borate, 25 mM NaCl, 0.5 mM EDTA, 2% DMSO, pH 8.0) and the solution incubated at 37 °C for 2 h. Dichloro ethyl alkyne PD **169** (5.0, µL, 20 mM in DMSO, 25 eq.) was added and the solution incubated for a further 4 h at 37 °C. Excess reagents were removed by ultrafiltration (6 × 10000 MWCO, VivaSpin®, GE Healthcare) into PBS (pH = 7.4). Conjugate **170** was analysed by SDS-PAGE, densitometry and LCMS (Method 2): expected mass: 145,886 Da, observed mass: 145,887 Da.

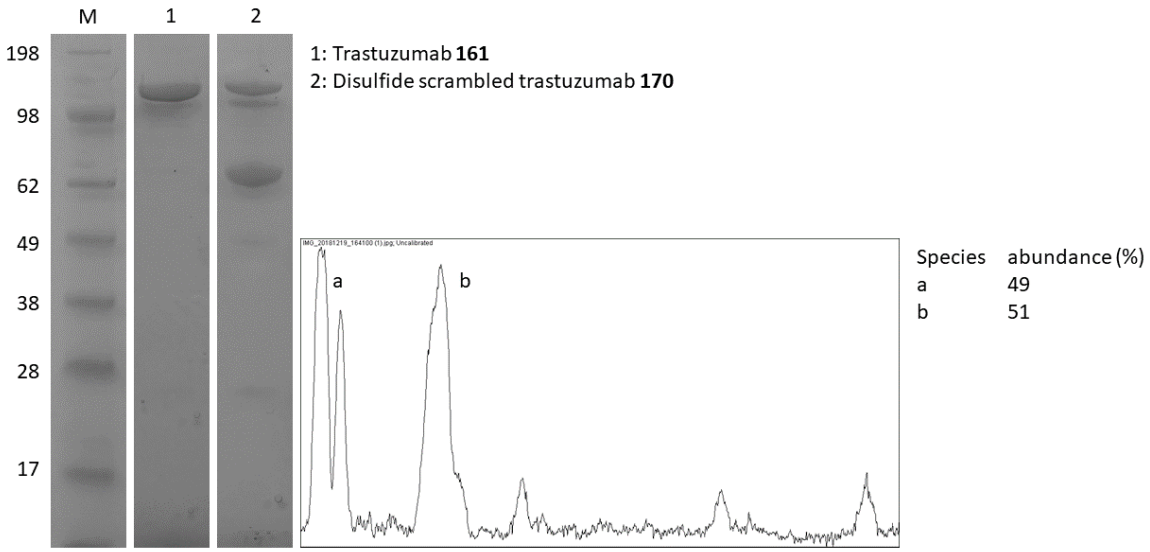

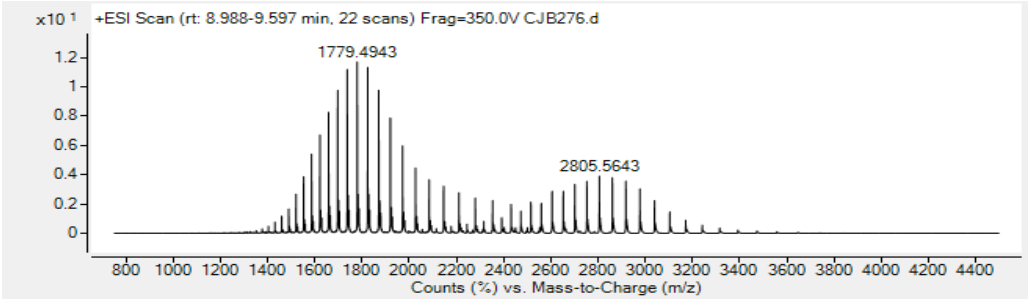
x10 1
+ESI Scan (rt: 8.988-9.597 min, 22 scans) Frag=350.0V CJB276.d
1779.4943
2805.5643
Counts (%) vs. Mass-to-Charge (m/z)

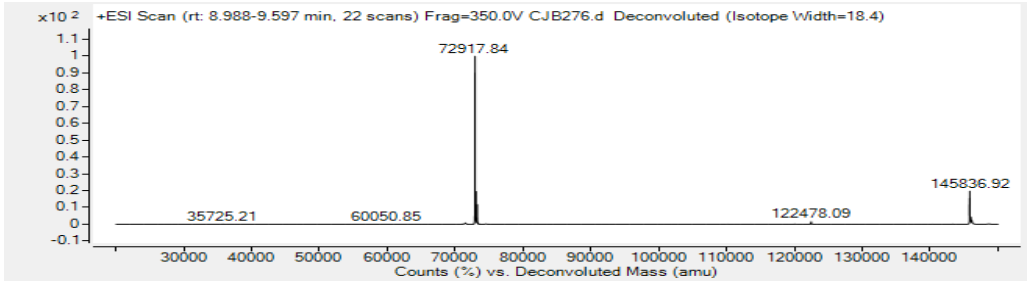
x10 2
+ESI Scan (rt: 8.988-9.597 min, 22 scans) Frag=350.0V CJB276.d Deconvoluted (Isotope Width=18.4)
72917.84
35725.21
60050.85
122478.09
145836.92
Counts (%) vs. Deconvoluted Mass (amu)

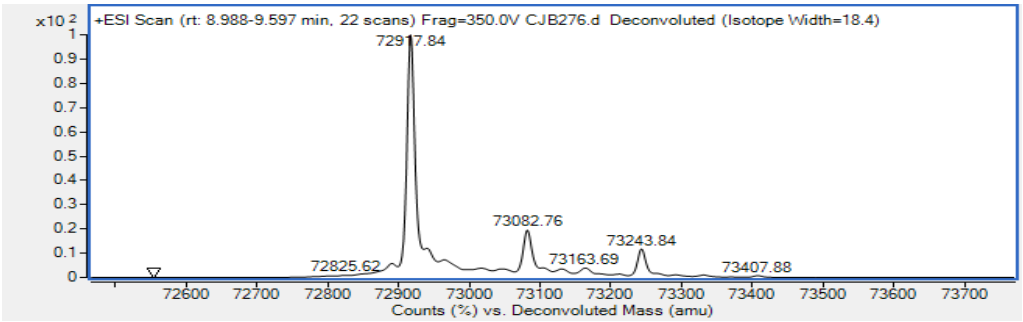
x10 2
+ESI Scan (rt: 8.988-9.597 min, 22 scans) Frag=350.0V CJB276.d Deconvoluted (Isotope Width=18.4)
72917.84
73082.76
73243.84
72825.62
73163.69
73407.88
Counts (%) vs. Deconvoluted Mass (amu)

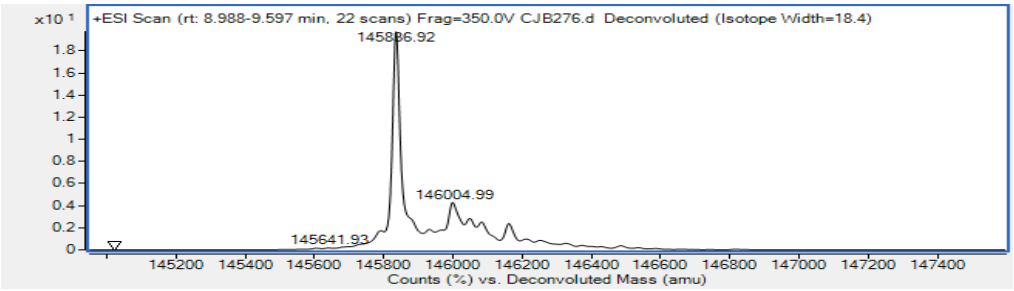
x10 1
+ESI Scan (rt: 8.988-9.597 min, 22 scans) Frag=350.0V CJB276.d Deconvoluted (Isotope Width=18.4)
145836.92
146004.99
145641.93
Counts (%) vs. Deconvoluted Mass (amu)

Thiol capped (MAR 4) trastuzumab 172

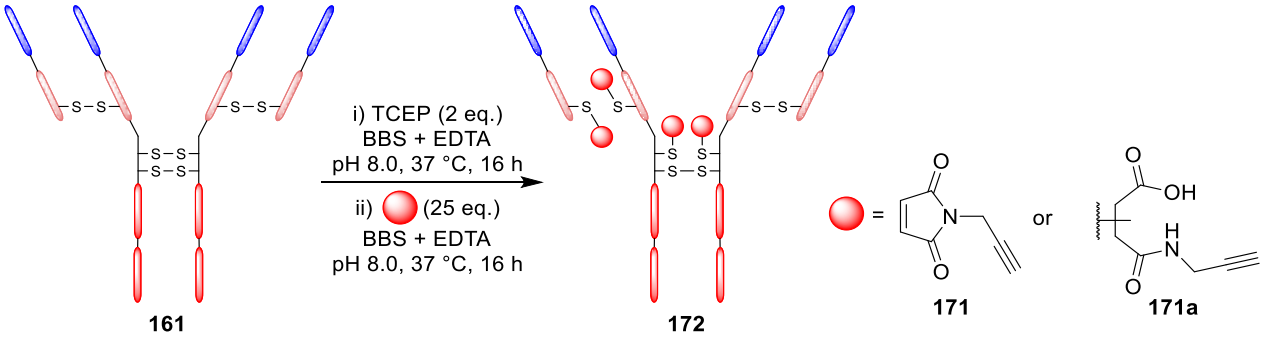

TCEP·HCl (1.6 µL, 5 mM in deionised water, 2 eq.) was added to a solution of trastuzumab **161** (100 µL, 40 µM) in BBS (25 mM sodium borate, 25 mM NaCl, 0.5 mM EDTA, 2% DMSO, pH 8.0) and the solution incubated at 37 °C for 16 h. The solution was cooled to 21 °C, propargyl maleimide **171** (5.0, µL, 20 mM in DMSO, 25 eq.) was added and the solution incubated for a further 16 h. Excess reagents were removed by ultrafiltration (6 × 10000 MWCO, VivaSpin®, GE Healthcare) into PBS (pH = 7.4). Conjugate **172** was analysed by SDS-PAGE, densitometry and LCMS (Method 2) (reduced):

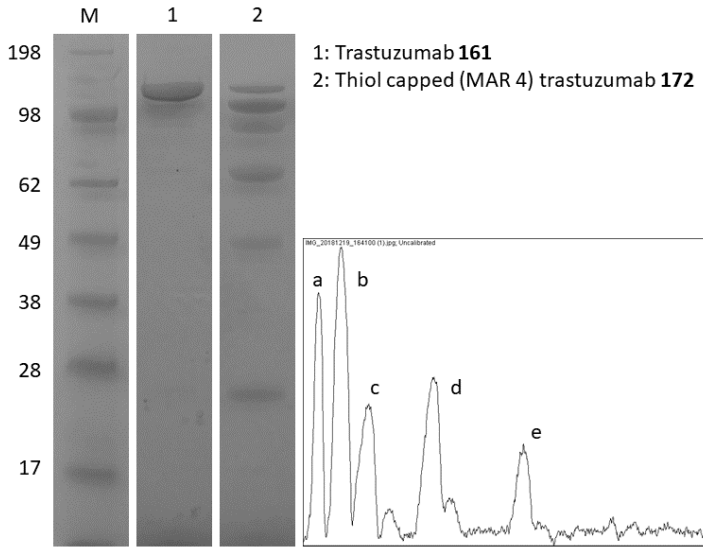

1: Trastuzumab **161**
2: Thiol capped (MAR 4) trastuzumab **172**

Species	Abundance (%)
a	15
b	27
c	14
d	21
e	8
f	15

Table 10 – Table of LC-MS values obtained and calculation of maleimide loading for thiol capped (MAR 4) trastuzumab **172**

Species	Expected mass	Observed mass	Peak Height	Relative peak height	Number of Maleimides per species	Relative loading per species
Trastuzumab Light Chain (LC)	23438	23438	28530	0.441231055	0	0
LC + propargyl maleimide	23574	23573	36130	0.558768945	1	0.56
Trastuzumab Heavy Chain (HC)	49148	49148	5387	0.172009707	0	0
HC + 1 propargyl maleimide	49284	49283	9314	0.297400856	1	0.30
HC + 2 propargyl maleimide	49420	49419	9310	0.297273134	2	0.59
HC + 3 propargyl maleimide	49556	49554	7307	0.233316304	3	0.70
Total loading for LC	0.56					
Total loading for HC	1.59					
Total loading for LC and HC	2.15					
Projected loading for full Ab	4.30					

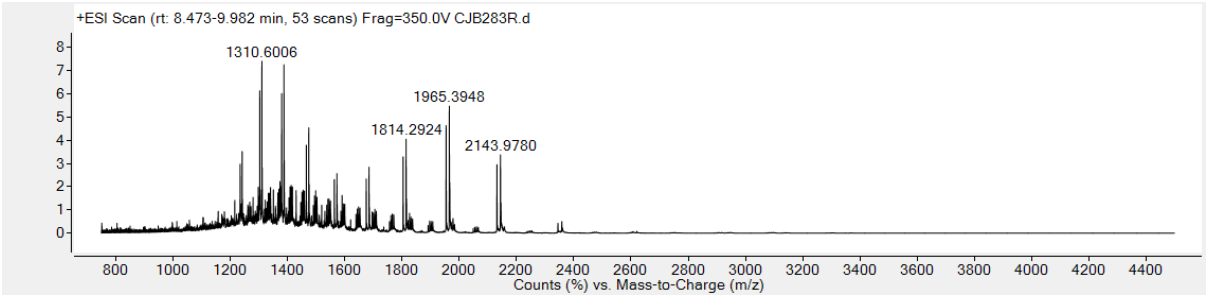

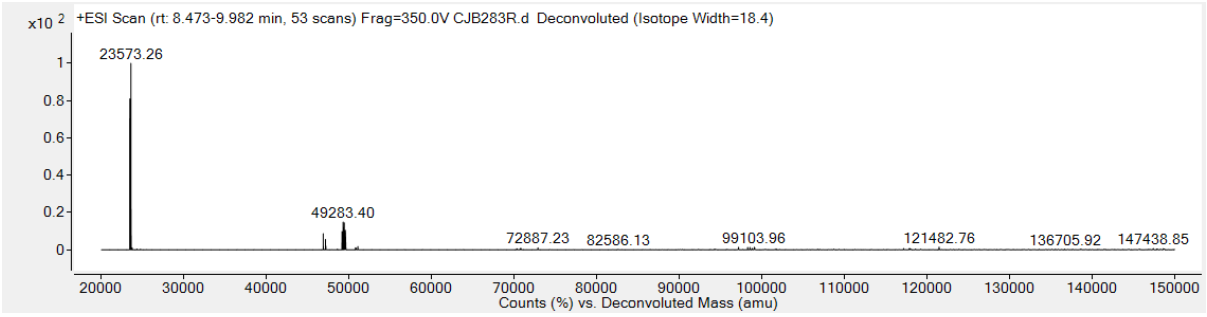

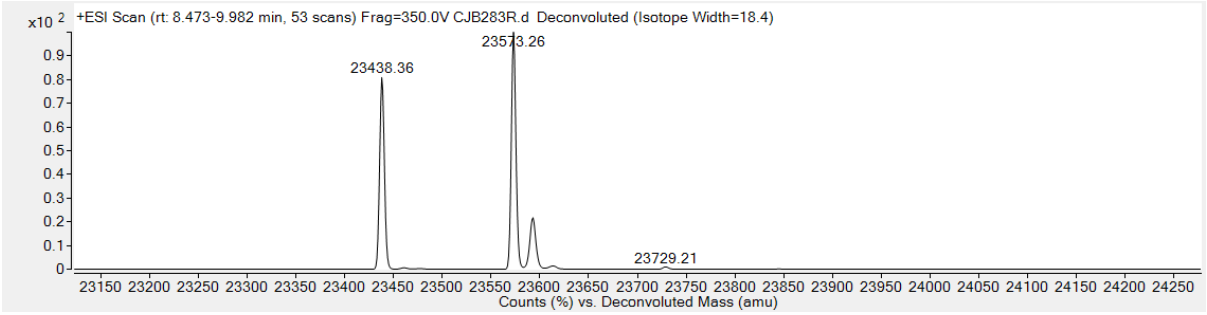

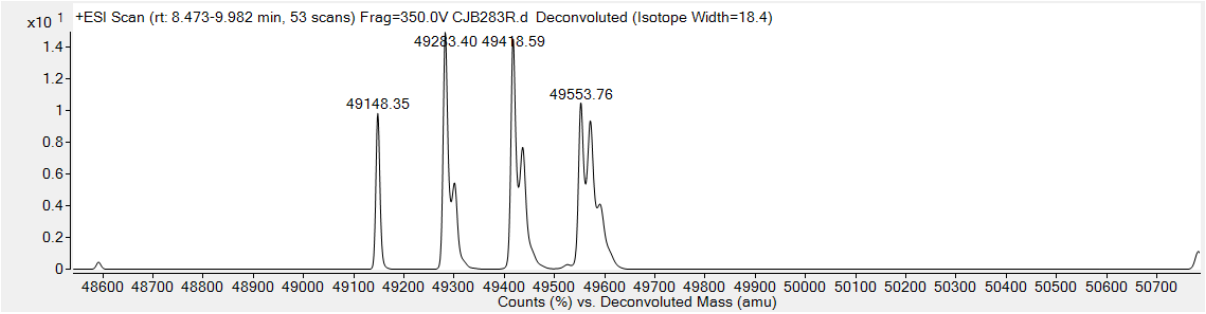
x10 1
+ESI Scan (rt: 8.473-9.982 min, 53 scans) Frag=350.0V CJB283R.d Deconvoluted (Isotope Width=18.4)
49283.40
49418.59
49148.35
49553.76
1.4
1.2
1
0.8
0.6
0.4
0.2
0
48600 48700 48800 48900 49000 49100 49200 49300 49400 49500 49600 49700 49800 49900 50000 50100 50200 50300 50400 50500 50600 50700
Counts (%) vs. Deconvoluted Mass (amu)

Thiol capped (MAR 4) trastuzumab - AlexaFluor™-488 172a

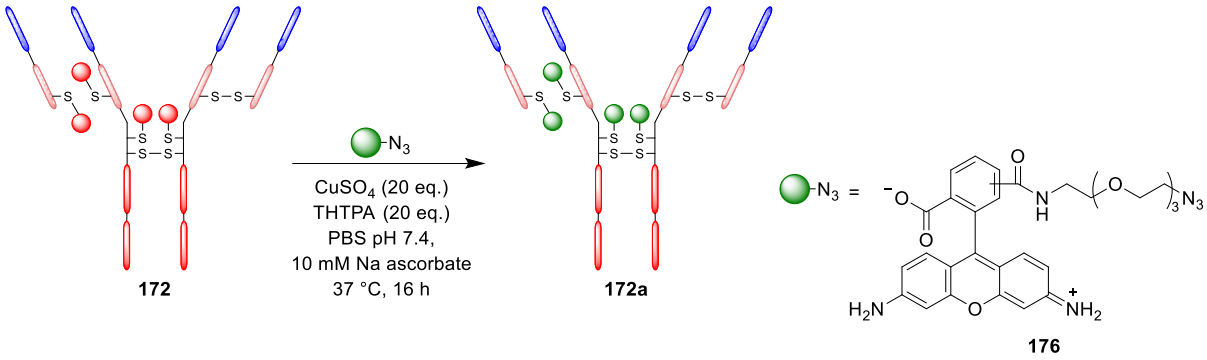

THTPA (2.0 µL, 20 mM in deionised water, 20 eq.) and $CuSO_4$ (2.0 µL, 20 mM in deionised water, 20 eq.) was added to a solution of thiol capped (loading of 4) trastuzumab **172** (50 µL, 40 µM) in PBS (10 mM phosphate, 150 mM NaCl, 10 mM Na ascorbate, pH 7.4). AlexaFluor™-488 azide (4.0 µL, 5 mM in DMSO, 10 eq., Life Technologies-Thermo Scientific) was added and the solution incubated at 37 °C for 16 h. Excess reagents were removed by ultrafiltration (6 × 10000 MWCO, VivaSpin®, GE Healthcare) into PBS (pH = 7.4). Conjugate **172a** was analysed by UV-Vis spectroscopy.

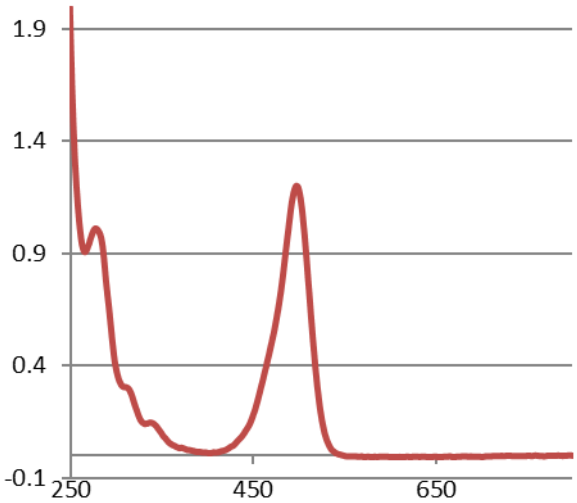

Thiol capped (MAR 8) trastuzumab 173

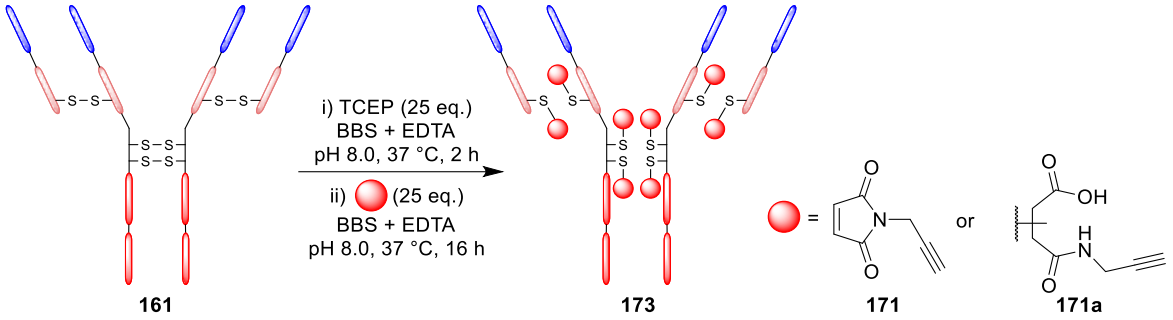

TCEP·HCl (5 µL, 20 mM in deionised water, 25 eq.) was added to a solution of trastuzumab **161** (100 µL, 40 µM) in BBS (25 mM sodium borate, 25 mM NaCl, 0.5 mM EDTA, 2% DMSO, pH 8.0) and the solution incubated at 37 °C for 2 h. The solution was cooled to 21 °C, propargyl maleimide **171** (5.0, µL, 20 mM in DMSO, 25 eq.) was added and the solution incubated for a further 16 h. Excess reagents were removed by ultrafiltration (6 × 10000 MWCO, VivaSpin®, GE Healthcare) into PBS (pH = 7.4). Conjugate **173** was analysed by SDS-PAGE, densitometry and LCMS (Method 2): expected mass (hydrolysed maleimide): 23,592 Da, 49,612 Da; observed mass: 23,593 Da, 49,610 Da.

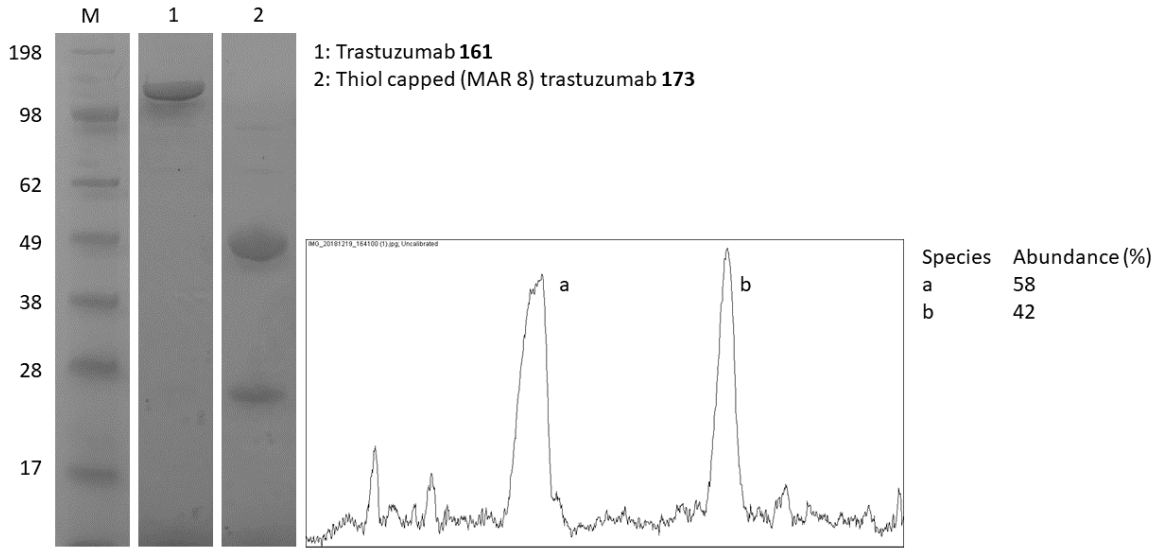

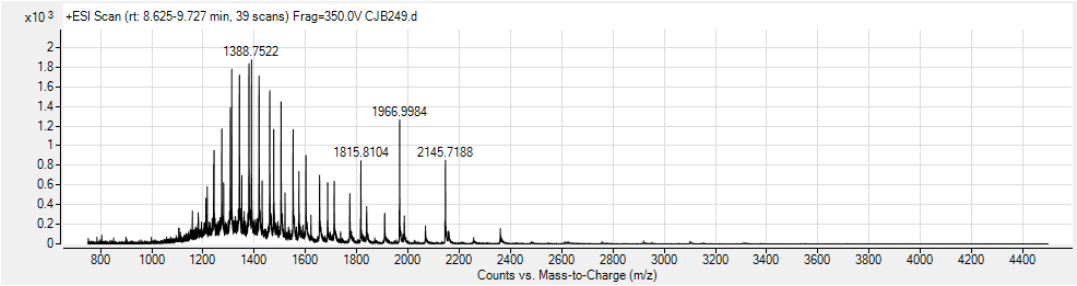
x10 3
+ESI Scan (rt: 8.625-9.727 min, 39 scans) Frag=350.0V CJB249.d
1388.7522
1966.9984
1815.8104
2145.7188
Counts vs. Mass-to-Charge (m/z)

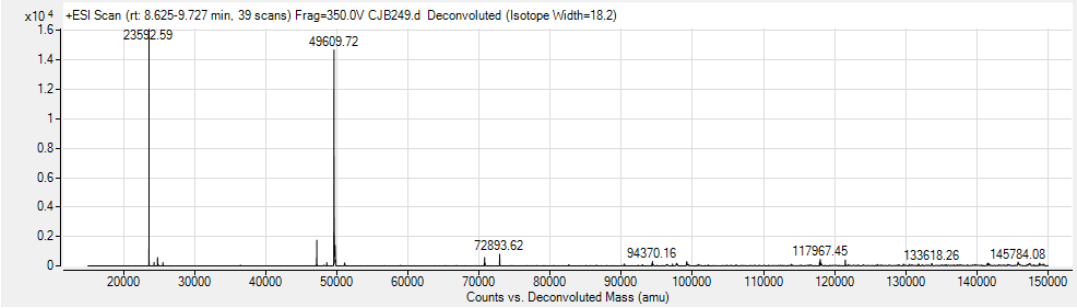
x10 4
+ESI Scan (rt: 8.625-9.727 min, 39 scans) Frag=350.0V CJB249.d Deconvoluted (Isotope Width=18.2)
23592.59
49609.72
72893.62
94370.16
117967.45
133618.26
145784.08
Counts vs. Deconvoluted Mass (amu)

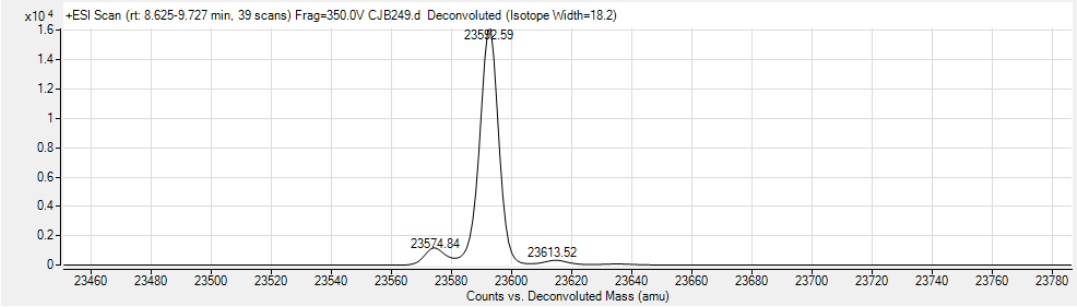
x10 4
+ESI Scan (rt: 8.625-9.727 min, 39 scans) Frag=350.0V CJB249.d Deconvoluted (Isotope Width=18.2)
23592.59
23574.84
23613.52
Counts vs. Deconvoluted Mass (amu)

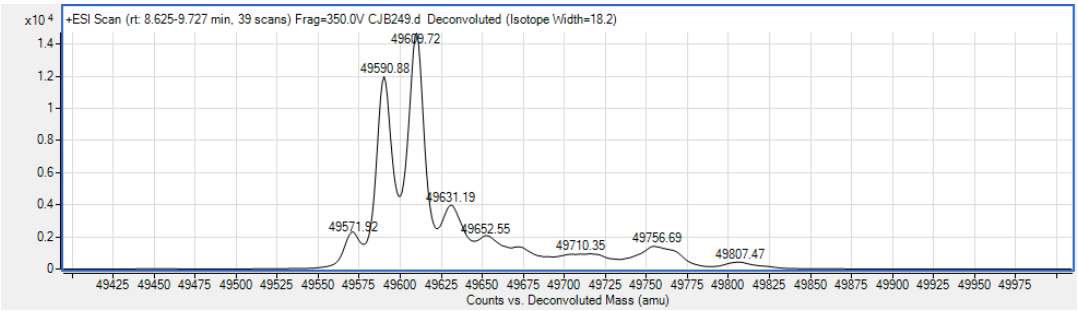
x10 4
+ESI Scan (rt: 8.625-9.727 min, 39 scans) Frag=350.0V CJB249.d Deconvoluted (Isotope Width=18.2)
49609.72
49590.88
49631.19
49571.92
49652.55
49710.35
49756.69
49807.47
Counts vs. Deconvoluted Mass (amu)

Trastuzumab-FcRn bio-layer interferometry (BLI) analysis

All K_D values were obtained on Octet^{RED} 384 (Forte Bio/PALL) equipment. Streptavidin (SA) dip and read biosensors (Forte Bio/ PALL) were first soaked in HBS-EP+ buffer for 15 min. On a non-binding tilted-bottom 384 well plate from left to right, columns were filled with: 1) HBS-P+ buffer (baseline 1), 2) 0.1 µg/mL of biotinylated FcRn (AviTag^{TM}, AMS Biotechnology) (loading), 3) HBS-P+ buffer (baseline 2), 4) PBS (pH 6.0) (baseline 3/dissociation 1), 5) trastuzumab/trastuzumab conjugates diluted to 200 nM in PBS (pH 6.0) (association), 6) PBS (pH 7.4) (dissociation 2), 7) Tris based buffer (50 mM Tris HCl, 200 mM NaCl, 0.1% tween-20, pH 8.0) (activation), 8) PBS (pH 6.0) (quenching). The assay was run in 3 steps: Loading of biotinylated FcRn (baseline 1, loading, baseline 2); association/dissociation of IgG1 (baseline 3, association, dissociation 1/dissociation 2), regeneration of biotinylated FcRn (activation, quenching, repeated 4 times). Each phase was equilibrated for the following times: baseline 1 = 180 s, loading = 180 s, baseline 2 = 120 s, baseline 3 = 180 s, association = 180 s, dissociation 1 = 480 s, dissociation 2 = 480 s, activation = 20 s, quenching = 15 s. The data was then processed as described in the ForteBio/PALL application note. A 1:1 model and a partial fit (encompassing 60 s of association/ 60 s of dissociation) was used.

Table 11 – Summary of kinetic values (k_{on}, k_{off}, K_D) and associated X^2 and R^2 obtained at pH 6.0 for trastuzumab (**161**)/ trastuzumab conjugates (**168, 170, 172, 173**).

Conjugate	**K_D (M)**	**k_{on} (1/Ms)**	**k_{off} (1/s)**	**Assoc X^2**	**Assoc R^2**
Trastuzumab **161**	**7.68×10^{-8}**	4.83×10^{5}	3.70×10^{-2}	0.001897	0.996230
Trastuzumab **161**	**7.50×10^{-8}**	5.73×10^{5}	4.30×10^{-2}	0.000831	0.995549
Natively re-bridged trastuzumab **168**	**9.35×10^{-8}**	3.82×10^{5}	3.57×10^{-2}	0.001331	0.997251
Natively re-bridged trastuzumab **168**	**9.07×10^{-8}**	4.56×10^{5}	4.13×10^{-2}	0.000636	0.996208
Disulfide scrambled trastuzumab **170**	**8.44×10^{-8}**	4.50×10^{5}	3.79×10^{-2}	0.001469	0.996411
Disulfide scrambled trastuzumab **170**	**8.36×10^{-8}**	5.16×10^{5}	4.31×10^{-2}	0.000948	0.993802
Thiol capped (MAR 4) trastuzumab **172**	**9.09×10^{-8}**	2.77×10^{5}	3.48×10^{-2}	0.001153	0.997185
Thiol capped (MAR 4) trastuzumab **172**	**9.01×10^{-8}**	3.19×10^{5}	3.85×10^{-2}	0.000573	0.996291
Thiol capped (MAR 8) trastuzumab **173**	**1.26×10^{-7}**	4.10×10^{5}	3.72×10^{-2}	0.001508	0.996807
Thiol capped (MAR 8) trastuzumab **173**	**1.21×10^{-7}**	4.71×10^{5}	4.24×10^{-2}	0.001016	0.994202

Table 12 – Summary of kinetic values (k_{off}) and associated X^2 and R^2 obtained at pH 7.4 for trastuzumab (**161**)/ trastuzumab conjugates (**168, 170, 172, 173**).

Conjugate	**K_D (M)**	**k_{on} (1/Ms)**	**k_{off} (1/s)**	**Assoc X^2**	**Assoc R^2**
Trastuzumab **161**	–	–	**1.95**	0.000953	0.996475
Trastuzumab **161**	–	–	**2.12**	0.000739	0.994731
Natively re-bridged trastuzumab **168**	–	–	**2.20**	0.000660	0.997298
Natively re-bridged trastuzumab **168**	–	–	**3.11**	0.000589	0.995432
Disulfide scrambled trastuzumab **170**	–	–	**2.62**	0.000814	0.996222
Disulfide scrambled trastuzumab **170**	–	–	**2.50**	0.000829	0.993082
Thiol capped (MAR 4) trastuzumab **172**	–	–	**2.26**	0.000755	0.997000
Thiol capped (MAR 4) trastuzumab **172**	–	–	**2.93**	0.001176	0.991714
Thiol capped (MAR 8) trastuzumab **173**	–	–	**2.97**	0.000522	0.997544
Thiol capped (MAR 8) trastuzumab **173**	–	–	**3.30**	0.000646	0.994808

Trastuzumab-CD16a bio-layer interferometry (BLI) analysis

All K_D values were obtained on Octet^{RED} 384 (Forte Bio/PALL) equipment. Streptavidin (SA) dip and read biosensors (Forte Bio/ PALL) were first soaked in HBS-EP+ buffer for 15 min. On a non-binding tilted-bottom 384 well plate from left to right, columns were filled with: 1) HBS-EP+ buffer (baseline 1), 2) 0.5 µg/mL of biotinylated CD16a (Avitag^{TM}, V176, (loading), 3) HBS-EP+ buffer (baseline 2), 4) trastuzumab/trastuzumab conjugates (association) and 5) HBS-EP+ buffer (dissociation). trastuzumab/trastuzumab conjugates were diluted 2-fold covering to concentration ranges 666 – 3.13 nM (666.0, 333.0, 166.5, 83.25, 41.63, 20.81 nM) while leaving one row with only HBS-EP+ buffer as a control. The streptavidin sensors were left to equilibrate for each phase for the following times: baseline 1 = 120 s, loading = 150 s, baseline 2 = 180 s, association = 60 s, dissociation = 60 s. The data was then processed as described in the ForteBio/PALL application note. A 1:1 model and a global fit (encompassing 60 s of association/5 s of dissociation) was employed over a minimum of 4 concentrations to calculate all K_D values.

Table 13 – Summary of kinetic values (k_{on}, k_{off}, K_D) and full X^2 and R^2 obtained for trastuzumab (**161**)/ trastuzumab conjugates (**168, 170, 172, 173**)

Conjugate	K_D (M)	k_{on} (1/Ms)	k_{off} (1/s)	Full X^2	Full R^2
Trastuzumab **161**	$\mathbf{1.800 \times 10^{-7}}$	2.17×10^5	3.90×10^{-2}	0.1203	0.9931
Trastuzumab **161**	$\mathbf{1.905 \times 10^{-7}}$	1.99×10^5	3.79×10^{-2}	0.1126	0.9943
Trastuzumab **161**	$\mathbf{1.533 \times 10^{-7}}$	2.43×10^5	3.73×10^{-2}	0.1182	0.9915
Natively re-bridged trastuzumab **168**	$\mathbf{3.615 \times 10^{-7}}$	1.34×10^5	4.85×10^{-2}	0.1041	0.9905
Natively re-bridged trastuzumab **168**	$\mathbf{2.592 \times 10^{-7}}$	1.71×10^5	4.44×10^{-2}	0.0802	0.9908
Natively re-bridged trastuzumab **168**	$\mathbf{3.646 \times 10^{-7}}$	1.29×10^5	4.71×10^{-2}	0.1343	0.9920
Disulfide scrambled trastuzumab **170**	$\mathbf{3.797 \times 10^{-7}}$	9.96×10^4	3.78×10^{-2}	0.0436	0.9923
Disulfide scrambled trastuzumab **170**	$\mathbf{6.517 \times 10^{-7}}$	6.69×10^4	4.36×10^{-2}	0.0443	0.9938
Disulfide scrambled trastuzumab **170**	$\mathbf{4.496 \times 10^{-7}}$	9.14×10^4	4.11×10^{-2}	0.0468	0.9924
Thiol capped (MAR 4) trastuzumab **172**	$\mathbf{7.272 \times 10^{-7}}$	5.81×10^4	4.22×10^{-2}	0.0272	0.9946
Thiol capped (MAR 4) trastuzumab **172**	$\mathbf{7.618 \times 10^{-7}}$	5.95×10^4	4.53×10^{-2}	0.0113	0.9939
Thiol capped (MAR 4) trastuzumab **172**	$\mathbf{8.770 \times 10^{-7}}$	5.15×10^4	4.51×10^{-2}	0.0253	0.9953
Thiol capped (MAR 8) trastuzumab **173**	$\mathbf{4.153 \times 10^{-6}}$	1.38×10^4	5.71×10^{-2}	0.0218	0.9928
Thiol capped (MAR 8) trastuzumab **173**	$\mathbf{5.540 \times 10^{-6}}$	9.62×10^3	5.33×10^{-2}	0.0081	0.9945
Thiol capped (MAR 8) trastuzumab **173**	$\mathbf{3.480 \times 10^{-6}}$	1.55×10^4	5.40×10^{-2}	0.0090	0.9937

Table 14 – Summary of maximum response per concentration for trastuzumab (**161**)/ trastuzumab conjugates (**168, 170, 172, 173**).

Conjugate	**Response (nm)**				
	666 nM	333 nM	166.5 nM	83.3 nM	41.6 nM
Trastuzumab **161**	1.1444	0.9415	0.6427	0.4514	0.2607
Trastuzumab **161**	1.1638	0.9623	0.6741	0.4179	0.2385
Trastuzumab **161**	0.9528	0.7957	0.5926	0.385	0.2428
Natively re-bridged trastuzumab **168**	0.8890	0.7276	0.5282	0.326	0.1907
Natively re-bridged trastuzumab **168**	0.7785	0.6262	0.4619	0.2913	0.1691
Natively re-bridged trastuzumab **168**	0.8913	0.8104	0.6240	0.4008	0.2097
Disulfide scrambled trastuzumab **170**	0.9029	0.6489	0.3718	0.2332	0.1286
Disulfide scrambled trastuzumab **170**	0.8896	0.6438	0.2263	0.1223	0.0649
Disulfide scrambled trastuzumab **170**	0.8598	0.6184	0.3862	0.2199	0.1195
Thiol capped (MAR 4) trastuzumab **172**	0.5250	0.3339	0.2000	0.1050	0.0526
Thiol capped (MAR 4) trastuzumab **172**	0.5494	0.3541	0.2337	0.1208	0.0657
Thiol capped (MAR 4) trastuzumab **172**	0.5270	0.3413	0.2070	0.1109	0.0549
Thiol capped (MAR 8) trastuzumab **173**	0.5626	0.3958	0.2761	0.1800	0.0900
Thiol capped (MAR 8) trastuzumab **173**	0.5646	0.3078	0.0948	0.0445	0.0179
Thiol capped (MAR 8) trastuzumab **173**	0.5041	0.3070	0.1704	0.0929	0.0403

Antibody-Dependent Cellular Cytotoxicity (ADCC) Assay[204]

Target cells, BT-474 (ATCC), were maintained in Dulbecco's Modified Eagle's Medium (DMEM)/F12 (Gibco) supplemented with 10% (v/v) Foetal Bovine Serum (FBS) (Gibco) and 5 µg/mL insulin (Gibco, 1285-014). Cells were in the log phase of growth when used in cytotoxicity assays. Effector NK-92 cells (ATCC), were maintained in Minimum Essential Medium (MEM)α GlutaMAX (Gibco) supplemented with 12.5% (v/v) FBS, 12.5% (v/v) horse serum (Sigma, H1138) 200 µM myo-inositol, 20 µM folic acid, 100 µM 2-mercaptoethanol, 25 U/mL human interleukin-2 (Sigma) and 4 µg/mL blasticidin.

BT-474 target cells were washed once with labelling buffer (50 mM HEPES, 83 mM NaCl, 5 mM KCl, $MgCl_2$, pH 7.4) before 1×10^7 viable cells were resuspended in 1 mL labelling buffer supplemented with 600 µM $EuCl_3$, 3 mM diethylenetriamine pentaacetate (DTPA) and 25 mg/L dextran sulfate. The cell suspension was incubated on ice for 30 min with occasional shaking. 10 ml of repair buffer (labelling buffer supplemented with 2 mM $CaCl_2.2H_2O$ and 10 mM D-glucose) was then added to stop the labelling process. After a further 10 min incubation on ice, cells were washed three times with 10 mL repair buffer then resuspended in unsupplemented Roswell Park Memorial Institute (RPMI) 1640 medium (Gibco) at a density of 3.5×10^5 cells/mL. In a round bottom 96-well plate (Corning, 3799), 100 µL of the cell suspension was incubated with 50 µL of trastuzumab (**161**), trastuzumab conjugates (**168, 170, 172, 173**) or an isotype control (Sigma) (diluted 10-fold in unsupplemented RPMI 1640, covering the following concentrations: 33.0, 3.30, 0.33, 3.30×10^{-2}, 3.30×10^{-3}, 3.30×10^{-4}, 3.30×10^{-5} nM). Cells were incubated for 30 min at 4 °C. Effector cells were washed once with unsupplemented RPMI 1640 then diluted to a density of 3.5×10^6 cells/mL. 50 µL of the $CD16^+$ NK-92 cell suspension was added to give a 5:1 effector to target ratio. The microplate was centrifuged briefly to bring effector and target cells in contact with each other and then incubated for 4 h at 37 °C in a humidified atmosphere of 5% CO_2 in air. To determine Eu^{3+} release, 20 µL aliquots of the supernatants were transferred to a white opaque 96-well plate (Corning) containing 200 µL of enhancer solution (Perkin Elmer, 1244). After mixing at 600 rpm for 30 min at RT, time-resolved fluorescence was measured using a CLARIOstar microplate reader (excitation filter: TR, emission filter: 615-18). The percentage of specific cytotoxicity was calculated as: 100 × (antibody dependent release - spontaneous

release)/(maximum release - minimum release). Spontaneous release was determined by incubating target cells with 50 µL of RPMI 1640 instead of antibody before the addition of effector cells, maximum release was determined by incubating target cells with 1% (v/v) Triton-X100 for 45 min, and minimum release was determined by incubating target cells alone with 200 µl RPMI 1640.

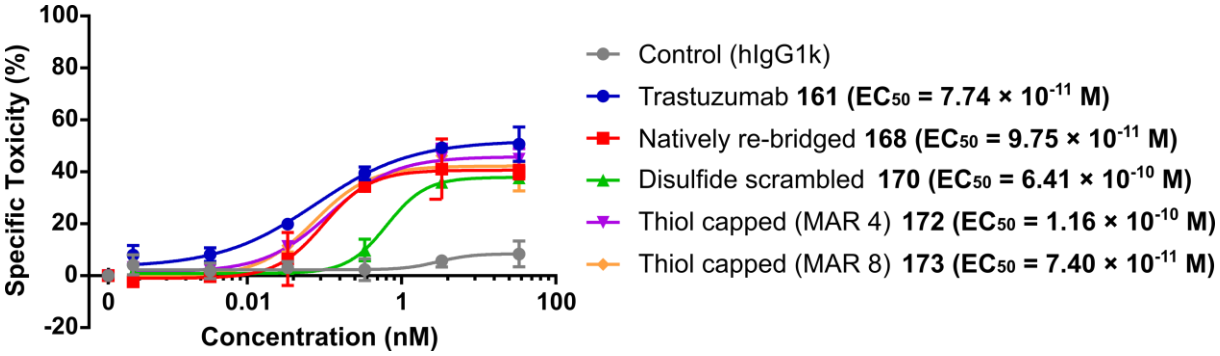

Thermal shift assay

Melting temperature (T_m) of trastuzumab/trastuzumab conjugates was determined by thermal melt using Stratagene qPCR equipment and MxPro software. Trastuzumab/trastuzumab conjugates were diluted to 1 µM in PBS pH 7.4 to give a final volume of 25 µL. SYPRO^{TM} orange (Thermo Fischer) (2.5 µl, diluted 1:100 in PBS pH 7.4) was added to each sample before transferring to a 96-well PCR plate (Fischer Sci). Samples were heated in the range of 25–95 ˚C with ramping temperature at 1 ˚C/min. Thermal shift curves were analysed using Edexcel-XLfit software to determine T_m (midpoint) values. For comparison between biphasic curves, T_{m1} (62–76 ˚C) and T_{m2} (77–92 ˚C) were calculated. For global comparison, total T_m values (51–92 ˚C) were calculated.

Table 15 – Summary of melting temperatures (T_m, T_{m1} and T_{m2}) for trastuzumab (**161**)/ trastuzumab conjugates (**168, 170, 172, 173**)

Conjugate	**Total T_m (51–92 ˚C) (˚C)**	**T_{m1} (62–76 ˚C) (˚C)**	**T_{m2} (77–92 ˚C) (˚C)**
Trastuzumab **161**	**85.3**	71.9	88.7
Trastuzumab **161**	**85.4**	72.3	88.6
Natively re-bridged trastuzumab **168**	**83.9**	71.4	88.9
Natively re-bridged trastuzumab **168**	**85.2**	72.0	88.2
Disulfide scrambled trastuzumab **170**	**81.6**	70.1	87.1
Disulfide scrambled trastuzumab **170**	**82.9**	70.6	87.9
Thiol capped (MAR 4) trastuzumab **172**	**81.6**	71.2	86.5
Thiol capped (MAR 4) trastuzumab **172**	**81.8**	71.7	87.3
Thiol capped (MAR 8) trastuzumab **173**	**78.0**	70.6	84.9
Thiol capped (MAR 8) trastuzumab **173**	**79.0**	70.7	86.5

Size Exclusion Chromatography – Multi angle light angle scattering (SEC MALS)

Antibody samples (1.0 mg/mL, PBS buffer pH 7.4) were analysed by SEC-HPLC on a Superdex^{TM} 200 Increase 5/150 GL (GE healthcare) column connected to an Agilent 1260 infinity HPLC equipped with a thermostated column compartment, DAWN^{TM} HELEOS^{TM} (Wyatt Technology) light scattering detector and an Optilab^{TM} T-rEX refractometer (Wyatt Technology). Samples were eluted using PBS (pH 7.4) as mobile phase at a flow rate of 0.4 mL/min. over 10 min. The data was then analysed to calculate approximate mass and polydispersity of each eluted species using Astra^{TM} 7.1.4 luminary software.

Table 16 – Summary for SEC-MALS analysis of trastuzumab (**161**)/ trastuzumab conjugates (**168, 170, 172, 173**)

Conjugate	**Peak 1**			**Peak 2**		
	Mw (kDa)	Polydispersity (Mw/Mn)	Mass fraction (%)	Mw (kDa)	Polydispersity (Mw/Mn)	Mass fraction (%)
Trastuzumab **161**	1316.98	1.54	0.5	149.46	1	99.5
Natively re-bridged **168**	3040.32	5.44	0.9	149.86	1	99.1
Disulfide scrambled **170**	428.85	1.06	2.2	149.69	1	97.8
Thiol capped (MAR 4) **172**	1110.80	1.85	0.2	149.88	1	99.8
Thiol capped (MAR 8) **173**	1598.13	2.06	0.7	149.53	1	99.3

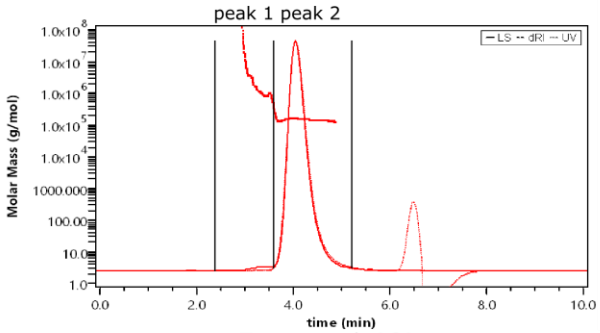

Trastuzumab **161**

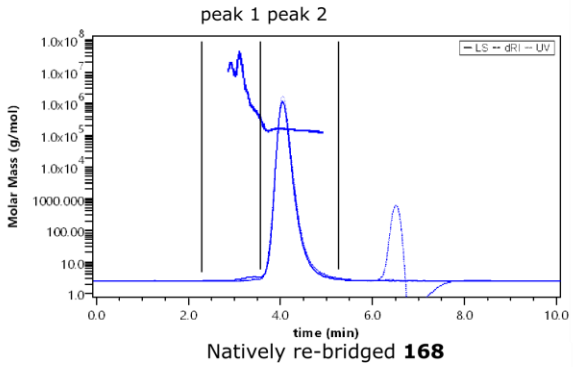

Natively re-bridged **168**

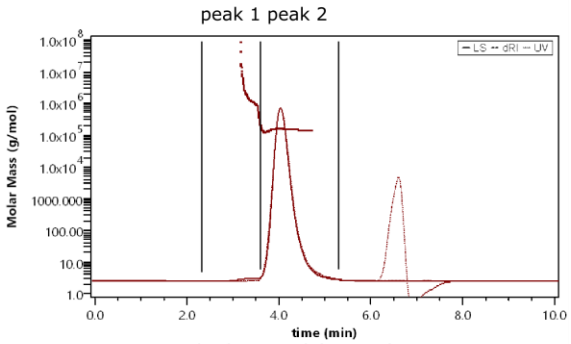

Thiol capped (MAR 4) **172**

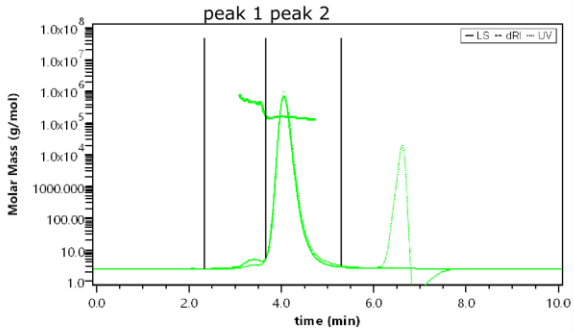

Disulfide scrambled **170**

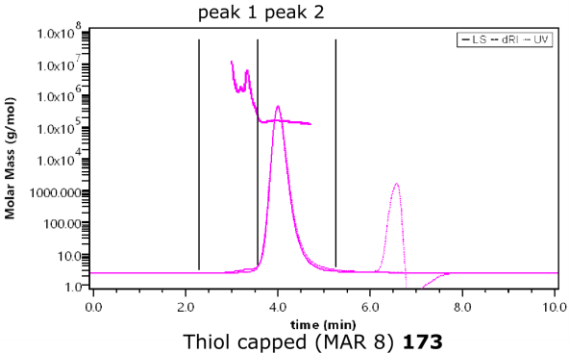

Thiol capped (MAR 8) **173**

HER2 ELISA for trastuzumab 161 and trastuzumab conjugates 168, 170, 172, 173

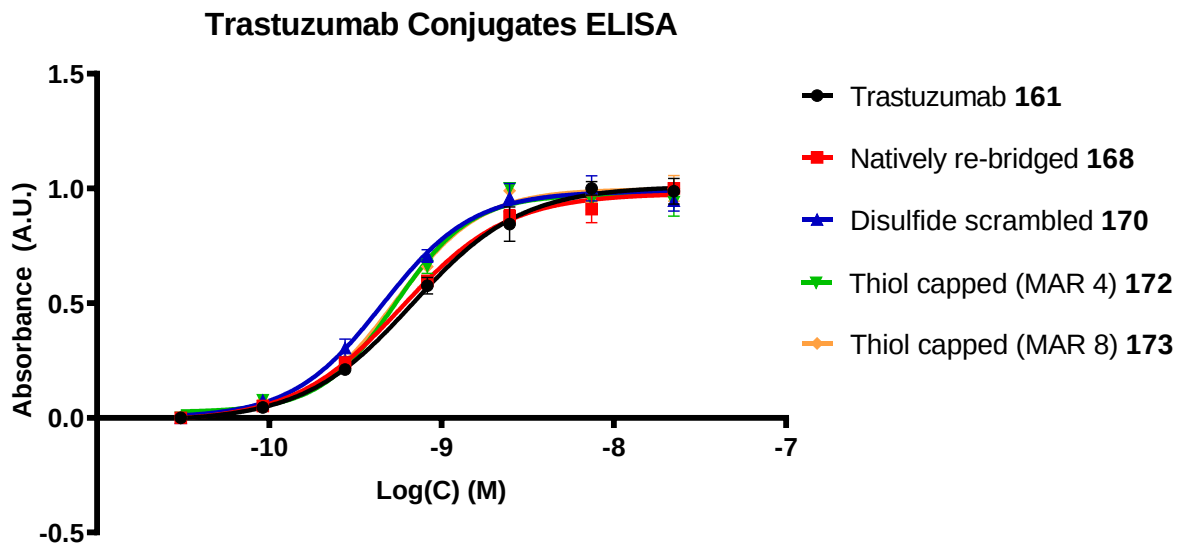

Conjugate	IC_{50} Values
Trastuzumab **161**	6.8×10^{-10}
Natively re-bridged trastuzumab **168**	5.8×10^{-10}
Disulfide scrambled trastuzumab **170**	4.5×10^{-10}
Thiol capped (MAR 4) trastuzumab **172**	5.4×10^{-10}
Thiol capped (MAR 8) trastuzumab **173**	5.4×10^{-10}

Experimental for Chapter 4

Organic Synthesis

4,5-Dibromo-1,2-diethyl-1,2-dihydropyridazine-3,6-dione 136[71]

4,5-Dibromo-1,2-diethyl-1,2-dihydropyridazine-3,6-dione **136** was synthesised as described in experimental for chapter 2 using the preformation of dibromo maleic anhydride strategy shown below:

Preformation of dibromo maleic anhydride in situ:

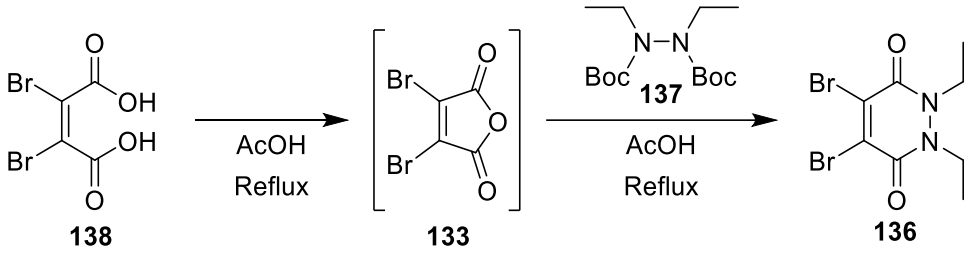

4-Bromo-1,2-diethyl-5-(hexylamino)-1,2-dihydropyridazine-3,6-dione 191

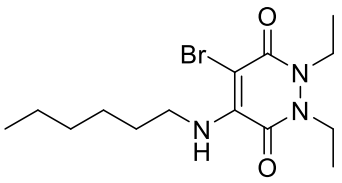

191

To a solution of NaOH (60 mg, 1.50 mmol, pre-dissolved in MeOH (10 mL)), was added a solution of hexan-1-amine (144 µL, 1.1 mmol) and the reaction stirred at 21 °C for 10 min. 4,5-Dibromo-1,2-diethyl-1,2-dihydropyridazine-3,6-dione **136** (326 mg, 1.00 mmol) was then added and the reaction stirred at 21 °C for a further 16 h. After this time, MeOH was removed *in vacuo*, the crude residue dissolved in EtOAc (30 mL) and then washed with water (3 × 10 mL). The organic layer was then dried ($MgSO_4$) and concentrated *in vacuo*. Purification of the crude residue by flash column chromatography (50% to 100% EtOAc/petrol) afforded 4-bromo-1,2-diethyl-5-(hexylamino)-1,2-dihydropyridazine-3,6-dione **191** (246 mg, 0.71 mmol, 71%) as a yellow oil. ^{1}H NMR (600 MHz, $CDCl_3$) δ 6.02 (s, 1H), 4.10–4.05 (m, 4H), 3.74–3.77 (m, 2H), 1.64–1.59 (m, 2H), 1.38–1.34 (m, 2H), 1.32–1.27 (m, 4H), 1.24 (t, *J* = 7.1 Hz, 3H), 1.15 (t, *J* = 7.1 Hz, 3H), 0.88 (t, *J* = 7.0 Hz, 3H).; ^{13}C NMR (150 MHz, $CDCl_3$) δ 158.6 (C), 154.4 (C), 142.8 (C), 44.5 (CH_2), 41.9 (CH_2), 41.5 (CH_2), 31.5 (CH_2), 31.0 (CH_2), 26.4 (CH_2), 22.7 (CH_2), 14.1 (CH_3), 12.9 (CH_3), 12.8 (CH_3); IR (thin-film) 3303, 2955, 2929, 2856, 1599, 1509 cm^{-1}. LRMS (ESI) 348 (100, $[M^{81}Br+H]^+$), 346 (100, $[M^{79}Br+H]^+$). HRMS (ESI) calcd for $C_{14}H_{25}Br_1N_3O_2$ $[M^{79}Br+H]^+$ 346.1125; observed 345.1124.

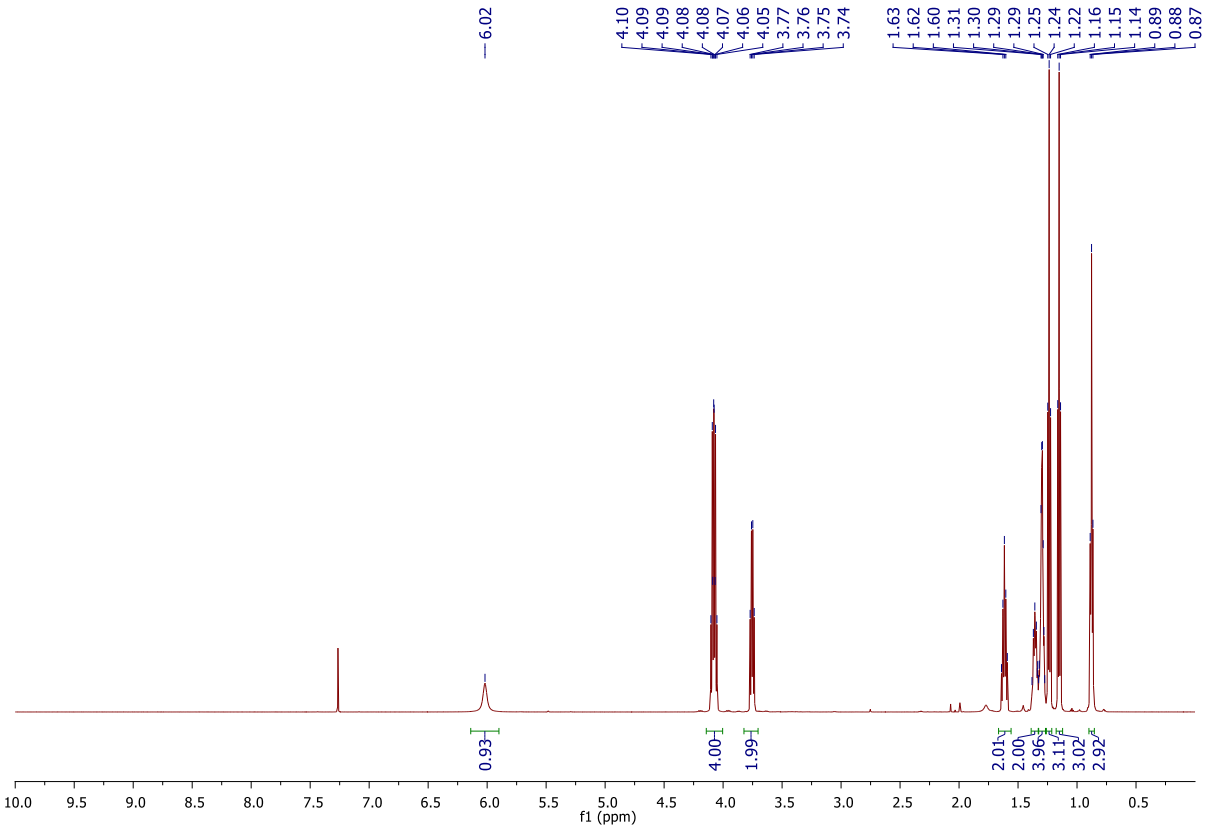
6.02
4.10
4.09
4.09
4.08
4.08
4.07
4.06
4.05
3.77
3.76
3.75
3.74
1.63
1.62
1.60
1.31
1.30
1.29
1.29
1.25
1.24
1.22
1.16
1.15
1.14
0.89
0.88
0.87
0.93
4.00
1.99
2.01
2.00
3.96
3.11
3.02
2.92
f1 (ppm)

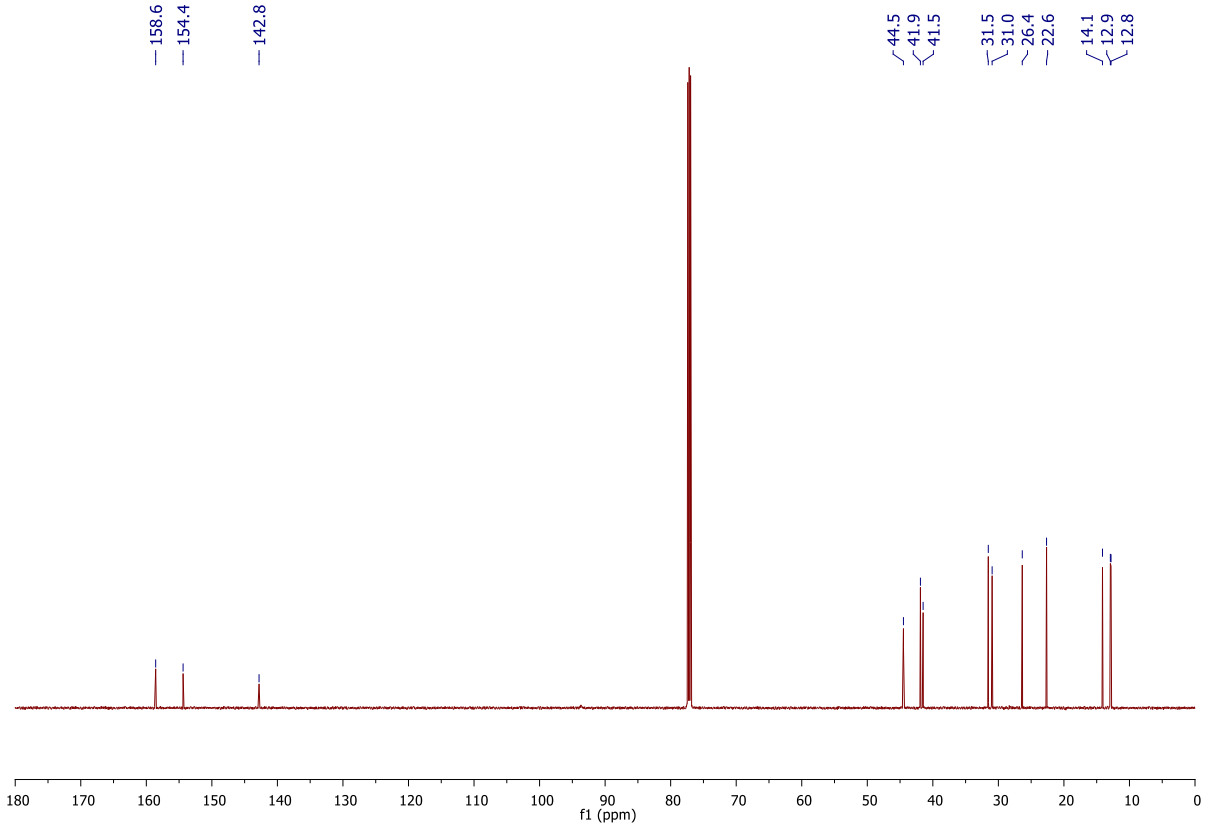
158.6
154.4
142.8
44.5
41.9
41.5
31.5
31.0
26.4
22.6
14.1
12.9
12.8
f1 (ppm)

4-Bromo-1,2-diethyl-5-(hexylthio)-1,2-dihydropyridazine-3,6-dione 192

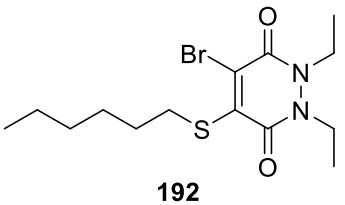

192

To a solution of NaOAc (123 mg, 1.50 mmol, pre-dissolved in MeOH (10 mL)) was added a solution of hexane-1-thiol (156 µL, 1.1 mmol) and the reaction stirred at 21 °C for 10 min. 4,5-Dibromo-1,2-diethyl-1,2-dihydropyridazine-3,6-dione **136** (326 mg, 1.00 mmol) was then added and the reaction stirred at 21 °C for a further 16 h. After this time, MeOH was removed *in vacuo,* the crude residue was dissolved in EtOAc (30 mL) and then washed with water (3 × 10 mL). The organic layer was then dried ($MgSO_4$) and concentrated *in vacuo*. Purification of the crude residue by flash column chromatography (30% to 80% EtOAc/petrol) afforded 4-bromo-1,2-diethyl-5-(hexylthio)-1,2-dihydropyridazine-3,6-dione **192** (218 mg, 0.60 mmol, 60%) as a yellow oil. ^{1}H NMR (600 MHz, $CDCl_3$) δ 4.13 (q, *J* = 7.1 Hz, 2H), 4.08 (q, *J* = 7.1 Hz, 2H), 3.38 (t, *J* = 7.5 Hz, 2H), 1.63–1.59 (m, 2H), 1.42–1.40 (m, 2H), 1.30–1.23 (m, 10H), 0.87 (t, *J* = 7.0 Hz, 3H).; ^{13}C NMR (150 MHz, $CDCl_3$) δ 154.7 (C), 154.0 (C), 147.0 (C), 129.2 (C), 42.2 (CH_2), 41.3 (CH_2), 34.4 (CH_2), 31.4 (CH_2), 30.4 (CH_2), 28.4 (CH_2), 22.6 (CH_2), 14.1 (CH_3), 13.1 (CH_3), 12.8 (CH_3); IR (thin film) 2955, 2927, 2856, 1628, 1537 cm^{-1}. LRMS (ESI) 365 (100, $[M^{81}Br+H]^+$), 363 (100, $[M^{79}Br+H]^+$). HRMS (ESI) calcd for $C_{14}H_{24}Br_1N_2O_2S$ $[M^{79}Br+H]^+$ 363.0742; observed 363.0741.

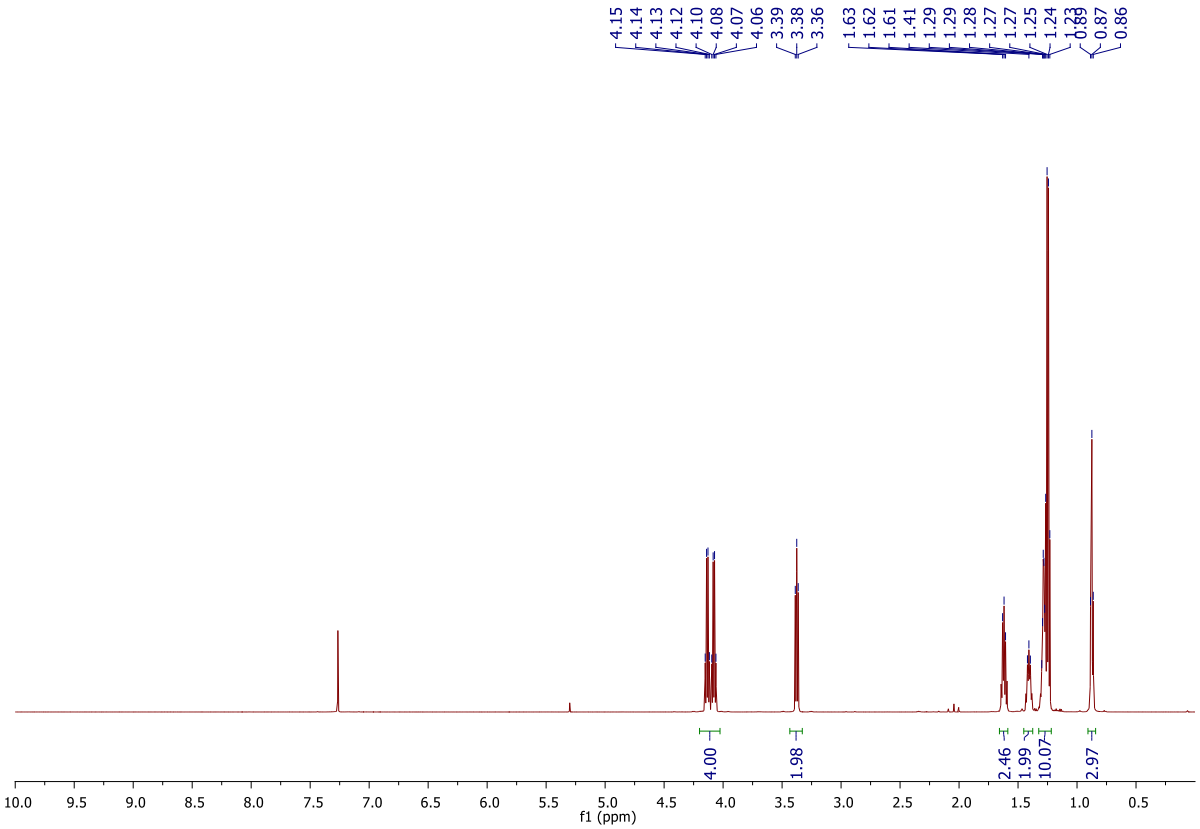
4.15
4.14
4.13
4.12
4.10
4.08
4.07
4.06
3.39
3.38
3.36
1.63
1.62
1.61
1.41
1.29
1.29
1.28
1.27
1.27
1.25
1.24
1.23
0.89
0.87
0.86
4.00
1.98
2.46
1.99
10.07
2.97
f1 (ppm)

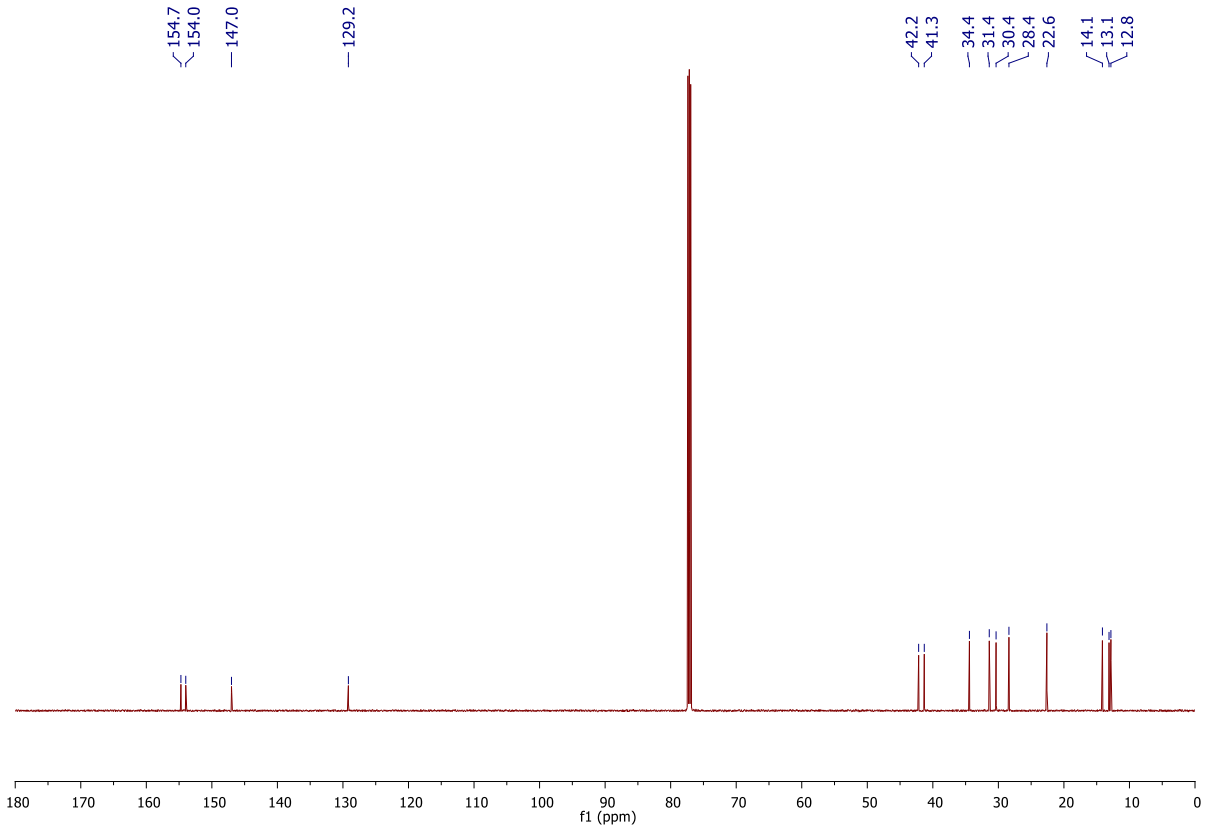
154.7
154.0
147.0
129.2
42.2
41.3
34.4
31.4
30.4
28.4
22.6
14.1
13.1
12.8
f1 (ppm)

4-Bromo-1,2-diethyl-5-((2-hydroxyethyl)thio)-1,2-dihydropyridazine-3,6-dione 193

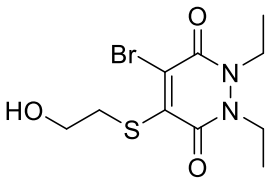

193

To a solution of NaOAc (123 mg, 1.50 mmol) pre-dissolved in MeOH (10 mL), was added 2-mercaptoethan-1-ol (77 µL, 1.1 mmol) and the reaction was stirred at 21 °C for 10 min. 4,5-Dibromo-1,2-diethyl-1,2-dihydropyridazine-3,6-dione **136** (326 mg, 1.00 mmol) was then added and the reaction stirred at 21 °C for a further 16 h. After this time, MeOH was removed *in vacuo,* the crude residue was dissolved in EtOAc (30 mL) and then washed with water (3 × 10 mL). The organic layer was then dried ($MgSO_4$) and concentrated *in vacuo*. Purification of the crude residue by flash column chromatography (30% to 80% EtOAc/petrol) afforded 4-bromo-1,2-diethyl-5-((2-hydroxyethyl)thio)-1,2-dihydropyridazine-3,6-dione **193** (229 mg, 0.71 mmol, 71%) as a yellow solid. m.p. 90–94 °C. ^{1}H NMR (600 MHz, $CDCl_3$) δ 4.14 (q, *J* = 7.1 Hz, 2H), 4.09 (q, *J* = 7.1 Hz, 2H), 3.84 (t, *J* = 5.6 Hz, 2H), 3.53 (t, *J* = 5.7 Hz, 2H), 1.28–1.24 (m, 6H); ^{13}C NMR (150 MHz, $CDCl_3$) δ 154.8 (C), 153.7 (C), 145.7 (C), 131.1 (C), 62.2 (CH_2), 42.3 (CH_2), 41.6 (CH_2), 37.0 (CH_2), 13.2 (CH_3), 12.9 (CH_2); IR (solid) 3418, 2976, 2935, 2873, 1608, 1536 cm^{-1}. LRMS (ESI) 325 (100, $[M^{81}Br+H]^+$), 323 (100, $[M^{79}Br+H]^+$). HRMS (ESI) calcd for $C_{10}H_{16}Br_1N_2O_3S$ $[M^{79}Br+H]^+$ 323.0065; observed 323.0066.

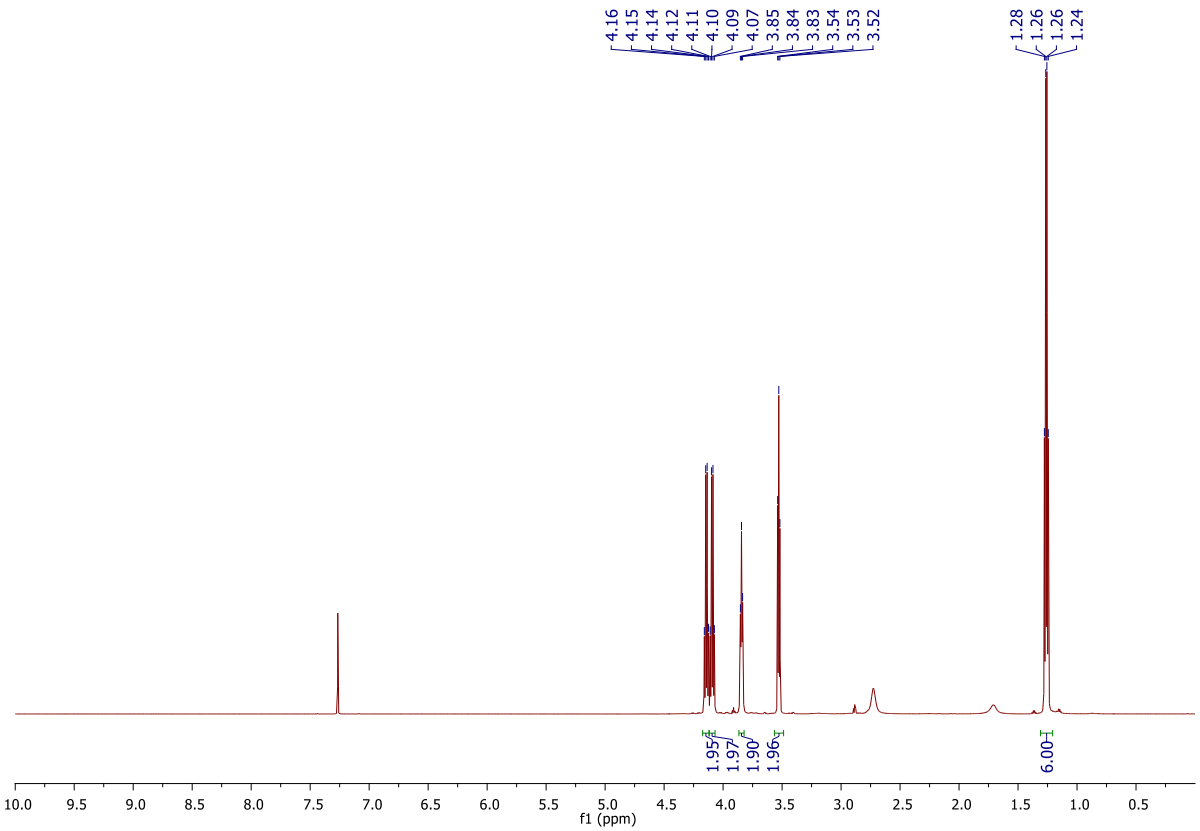
4.16
4.15
4.14
4.12
4.11
4.10
4.09
4.07
3.85
3.84
3.83
3.54
3.53
3.52
1.28
1.26
1.26
1.24
1.95
1.97
1.90
1.96
6.00
f1 (ppm)

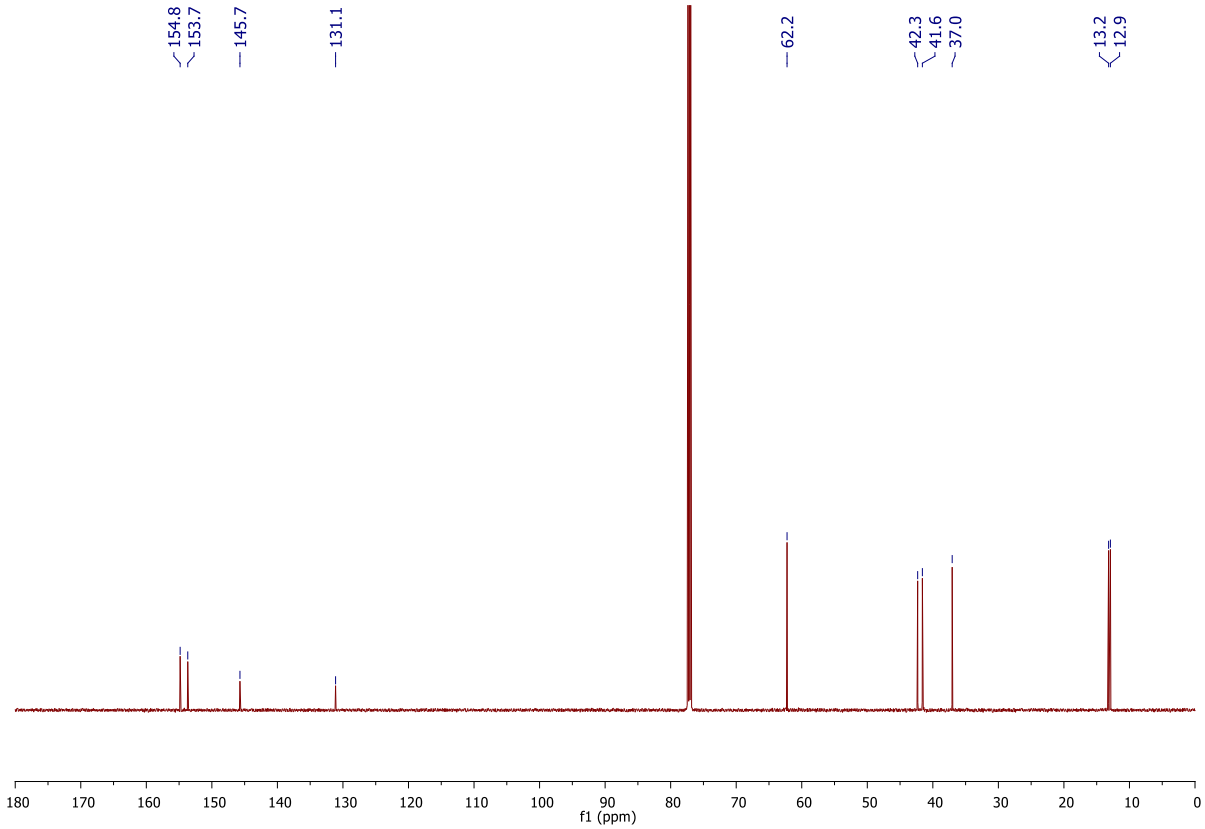
154.8
153.7
145.7
131.1
62.2
42.3
41.6
37.0
13.2
12.9
f1 (ppm)

3-((5-Bromo-1,2-diethyl-3,6-dioxo-1,2,3,6-tetrahydropyridazin-4-yl)thio)propanoic acid 194

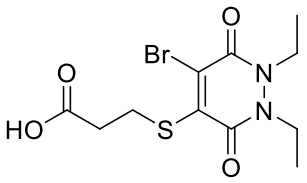

194

To a solution of NaOAc (123 mg, 1.50 mmol, pre-dissolved in MeOH (10 mL)) was added a solution of 10% 3-mercaptopropanoic acid (96 µL, 1.1 mmol) and the reaction was stirred at 21 °C for 10 min. 4,5-Dibromo-1,2-diethyl-1,2-dihydropyridazine-3,6-dione **136** (326 mg, 1.00 mmol) was then added and the reaction stirred at 21 °C for a further 16 h. After this time, MeOH was removed *in vacuo,* the crude residue was dissolved in EtOAc (30 mL) and then washed with water (3 × 10 mL). The organic layer was then dried ($MgSO_4$) and concentrated *in vacuo*. Purification of the crude residue by flash column chromatography (30% to 80% EtOAc/petrol) afforded 3-((5-bromo-1,2-diethyl-3,6-dioxo-1,2,3,6-tetrahydropyridazin-4-yl)thio)propanoic acid **194** (204 mg, 0.58 mmol, 58%) as a yellow solid. m.p. 143–145 °C; ^{1}H NMR (600 MHz, $CDCl_3$) δ 4.15 (q, *J* = 7.1 Hz, 2H), 4.10 (q, *J* = 7.1 Hz, 2H), 3.60 (t, *J* = 7.0 Hz, 2H), 2.82 (t, *J* = 7.0 Hz, 2H), 1.29–1.25 (m, 6H); ^{13}C NMR (150 MHz, $CDCl_3$) δ 176.0 (C), 154.5 (C), 153.7 (C), 145.8 (C), 129.7 (C), 42.3 (CH_2), 41.5 (CH_2), 35.4 (CH_2), 28.8 (CH_2), 13.2 (CH_3), 12.9 (CH_3); IR (solid) 3445, 2978, 2937, 1729, 1607 cm^{-1}. LRMS (ESI) 353 (100, $[M^{81}Br+H]^+$), 351 (100, $[M^{79}Br+H]^+$). HRMS (ESI) calcd for $C_{11}H_{16}Br_1N_2O_4$ $[M^{79}Br+H]^+$ 351.0014; observed 351.0013.

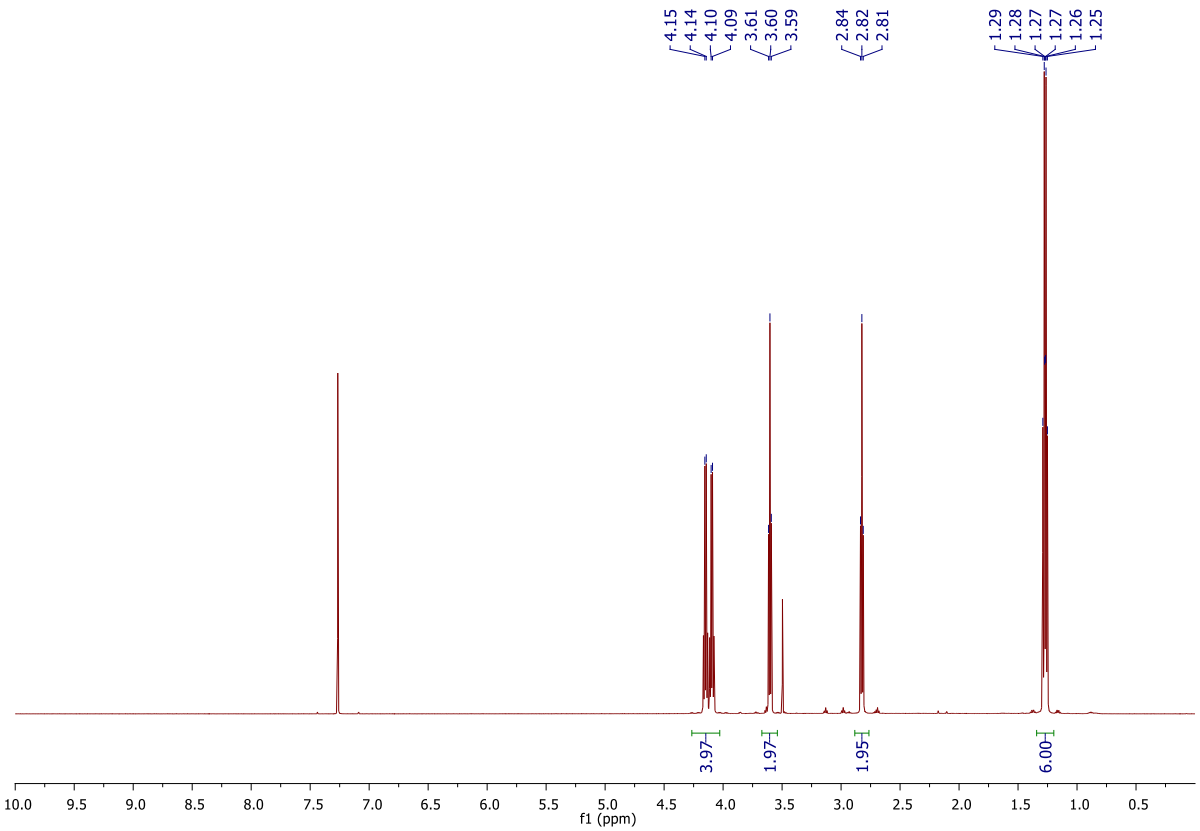
4.15
4.14
4.10
4.09
3.61
3.60
3.59
2.84
2.82
2.81
1.29
1.28
1.27
1.27
1.26
1.25
3.97
1.97
1.95
6.00
10.0 9.5 9.0 8.5 8.0 7.5 7.0 6.5 6.0 5.5 5.0 4.5 4.0 3.5 3.0 2.5 2.0 1.5 1.0 0.5
f1 (ppm)

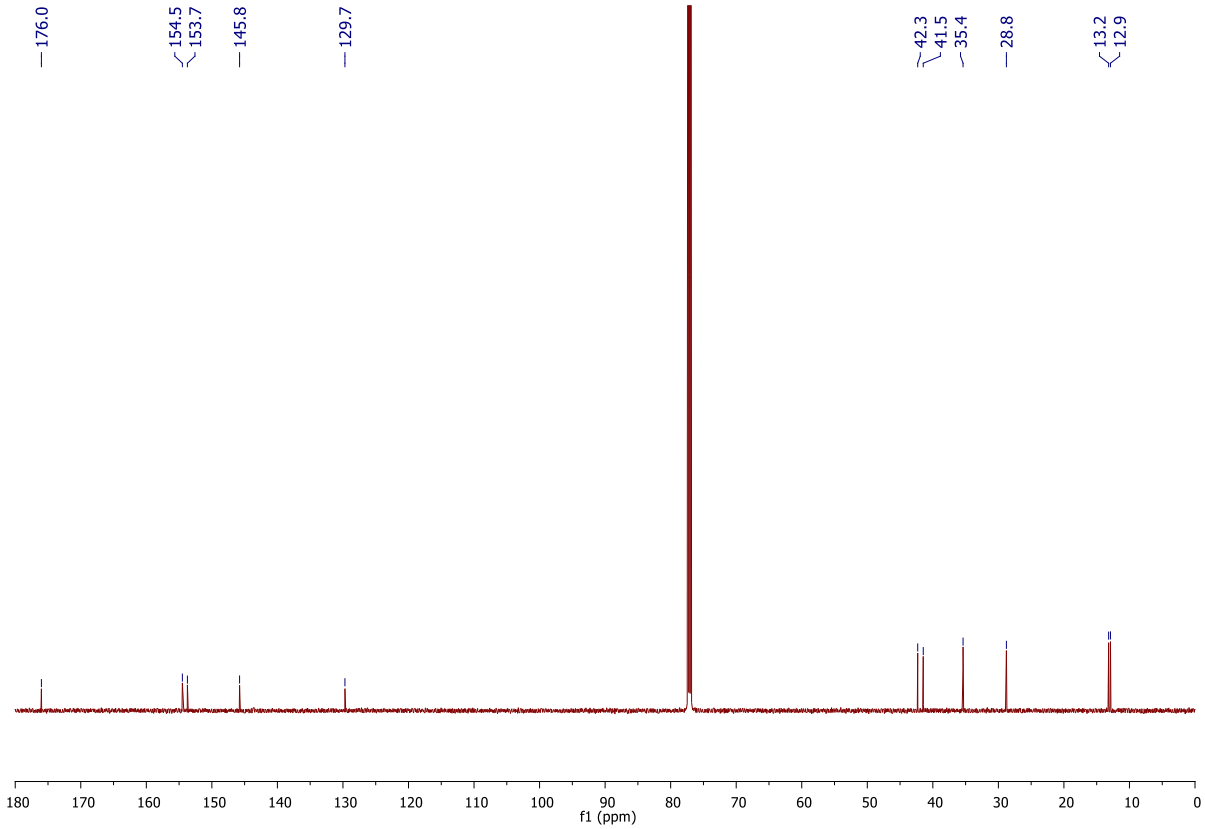
176.0
154.5
153.7
145.8
129.7
42.3
41.5
35.4
28.8
13.2
12.9
180 170 160 150 140 130 120 110 100 90 80 70 60 50 40 30 20 10 0
f1 (ppm)

4-Azido-5-bromo-1,2-diethyl-1,2-dihydropyridazine-3,6-dione 196

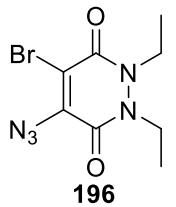

196

To a solution of 4,5-dibromo-1,2-diethyl-1,2-dihydropyridazine-3,6-dione **136** (326 mg, 1.00 mmol) in DMF (15 mL) was added dropwise a pre-dissolved solution of sodium azide (72 mg, 1.10 mmol) in DMF (5 mL) and the reaction stirred at 21 °C for 16 h. After this time, the DMF was removed *in vacuo* with toluene co-evaporation (3 × 20 mL, as an azeotrope) and the crude residue dissolved in EtOAc (50 mL), and washed with water (2 × 30 mL) followed by saturated aq. LiCl solution (2 × 30 mL). The organic layer was dried ($MgSO_4$) and concentrated *in vacuo* to afford afforded 4-azido-5-bromo-1,2-diethyl-1,2-dihydropyridazine-3,6-dione **196** (256 mg, 0.89 mmol, 89%) as an orange solid. ^{1}H NMR (600 MHz, $CDCl_3$) δ 4.18–4.12 (m, 4H), 1.30 (t, *J* = 7.1 Hz, 3H), 1.25 (t, *J* = 7.1 Hz, 3H). ^{13}C NMR (150 MHz, $CDCl_3$) δ 155.4 (C), 153.2 (C), 141.5 (C), 113.2 (C), 42.0 (CH_2), 41.5 (CH_2), 13.2 (CH_3), 13.1 (CH_3). IR (solid) 2979, 2936, 2874, 2130, 1626, 1591 cm^{-1} LRMS (ESI) 290 (100, $[M^{81}Br+H]^+$), 288 (100, $[M^{79}Br+H]^+$); HRMS (ESI) calcd for $C_8H_{11}Br_1N_5O_2$ $[M^{79}Br+H]^+$ 288.0091; observed 288.0092.

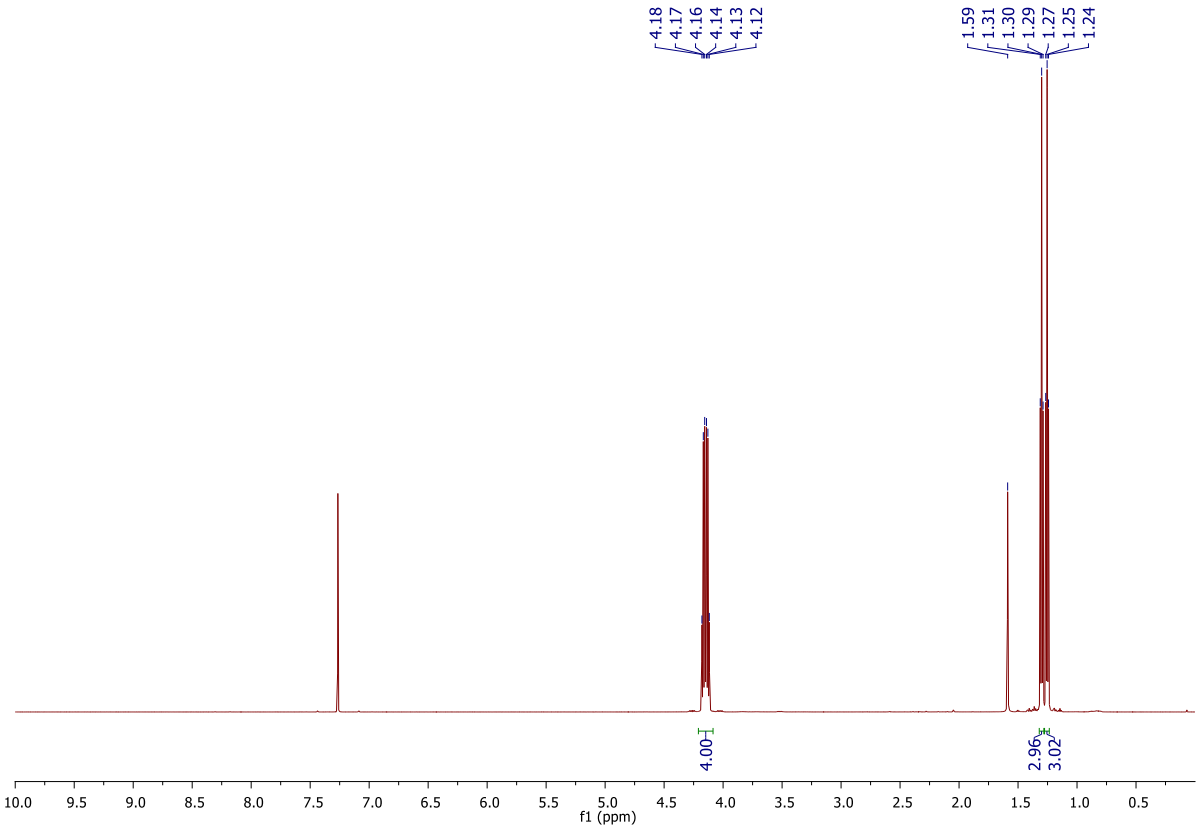
4.18
4.17
4.16
4.14
4.13
4.12
1.59
1.31
1.30
1.29
1.27
1.25
1.24
4.00
2.96
3.02
f1 (ppm)

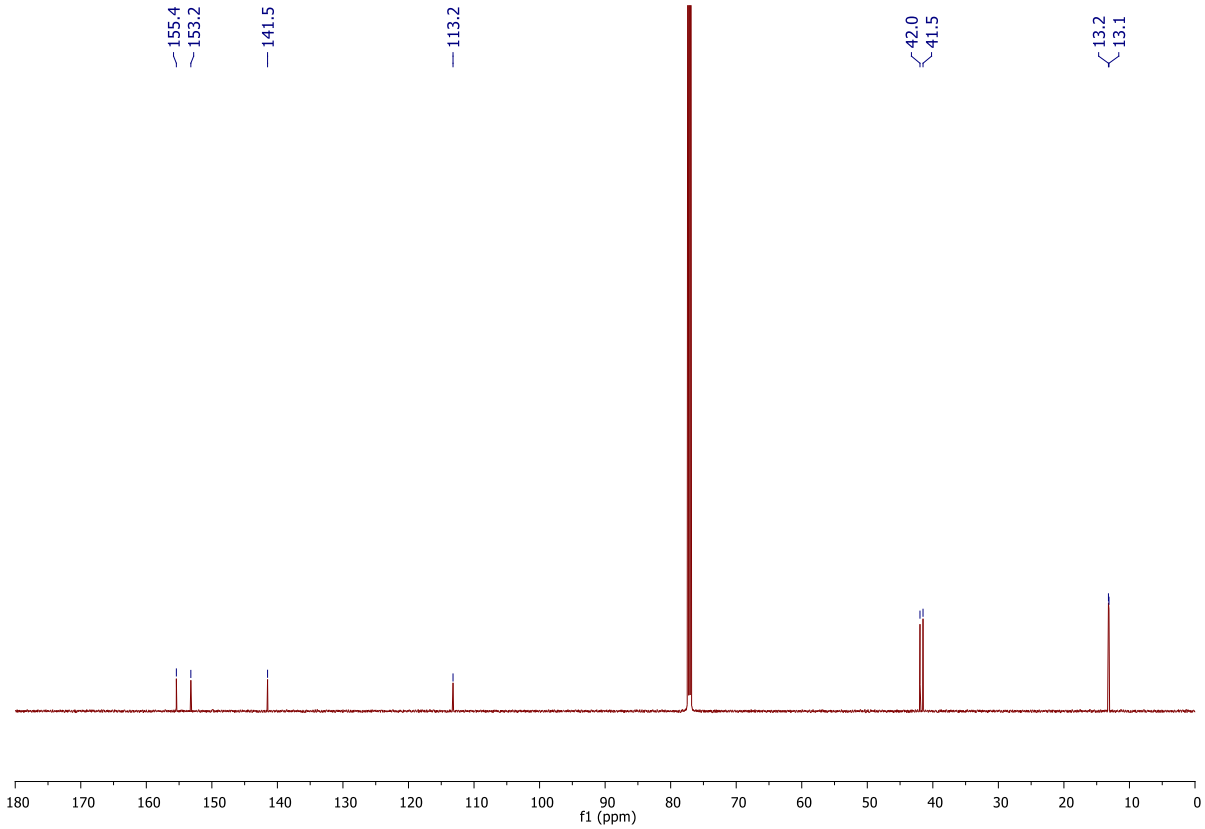
155.4
153.2
141.5
113.2
42.0
41.5
13.2
13.1
f1 (ppm)

4,5-Diazido-1,2-diethyl-1,2-dihydropyridazine-3,6-dione 197

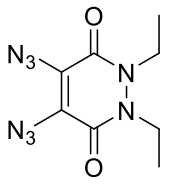

197

To a solution of sodium azide (390 mg, 6.0 mmol) in DMF (15 mL) was added 4,5-dibromo-1,2-diethyl-1,2-dihydropyridazine-3,6-dione **136** (652 mg, 2.0 mmol) the reaction was stirred at 21 °C and for 16 h. After this time, the DMF was removed *in vacuo* with toluene co-evaporation (3 × 20 mL, as an azeotrope) and purification of the crude residue by flash column chromatography (50% to 100% EtOAc/Petrol) afforded 4,5-diazido-1,2-diethyl-1,2-dihydropyridazine-3,6-dione **197** (495 mg, 1.98 mmol, 99%) as a yellow solid. ^{1}H NMR (600 MHz, $CDCl_3$) δ 4.11 (q, *J* = 7.1 Hz, 4H), 1.26 (t, *J* = 7.1 Hz, 6H). ^{13}C NMR (150 MHz, $CDCl_3$) δ 155.4 (C), 125.1 (C), 41.1 (CH_2), 13.1 (CH_3). IR (solid) 2985, 2942, 2233, 2115, 1691, 1624 cm^{-1}; LRMS (ESI) 523 (30, $[2M+Na]^+$), 251 (100, $[M+H]^+$); HRMS (ESI) calcd for $C_8H_{11}N_8O_2$ $[M+H]^+$ 251.0999; observed 251.0999.

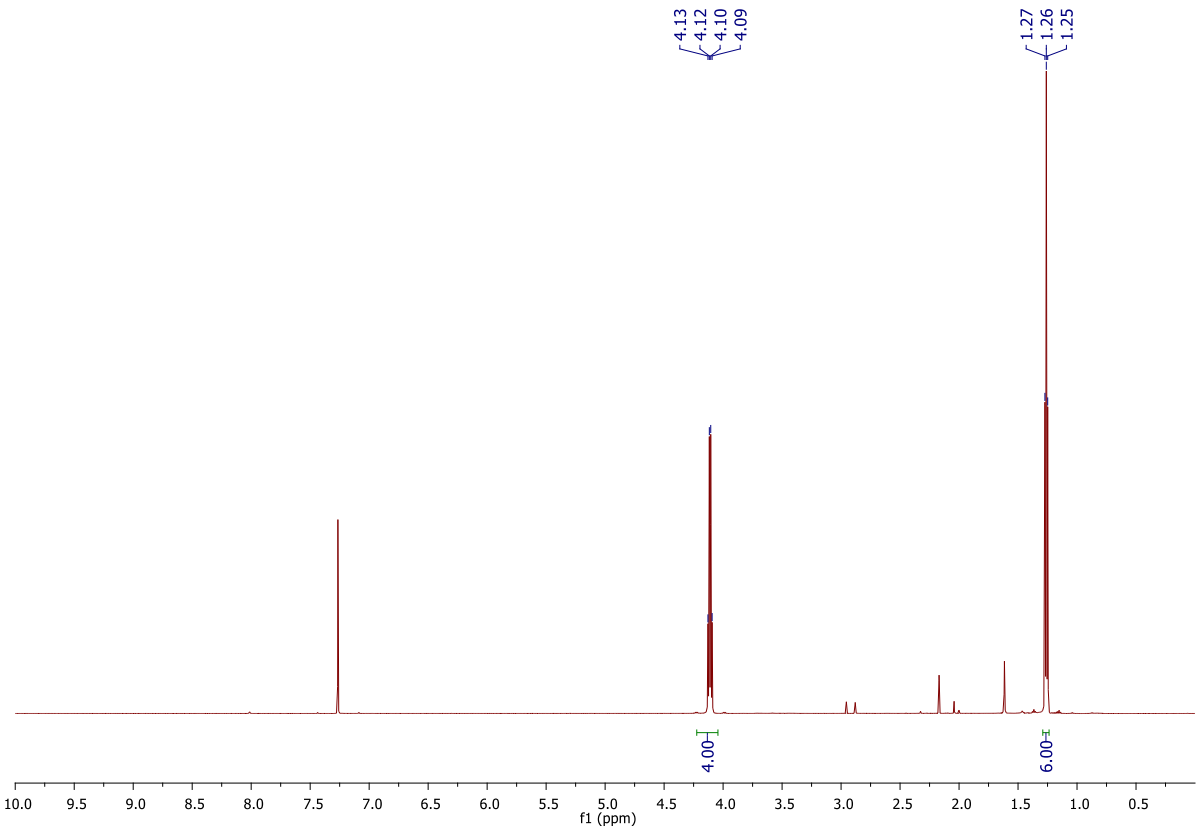

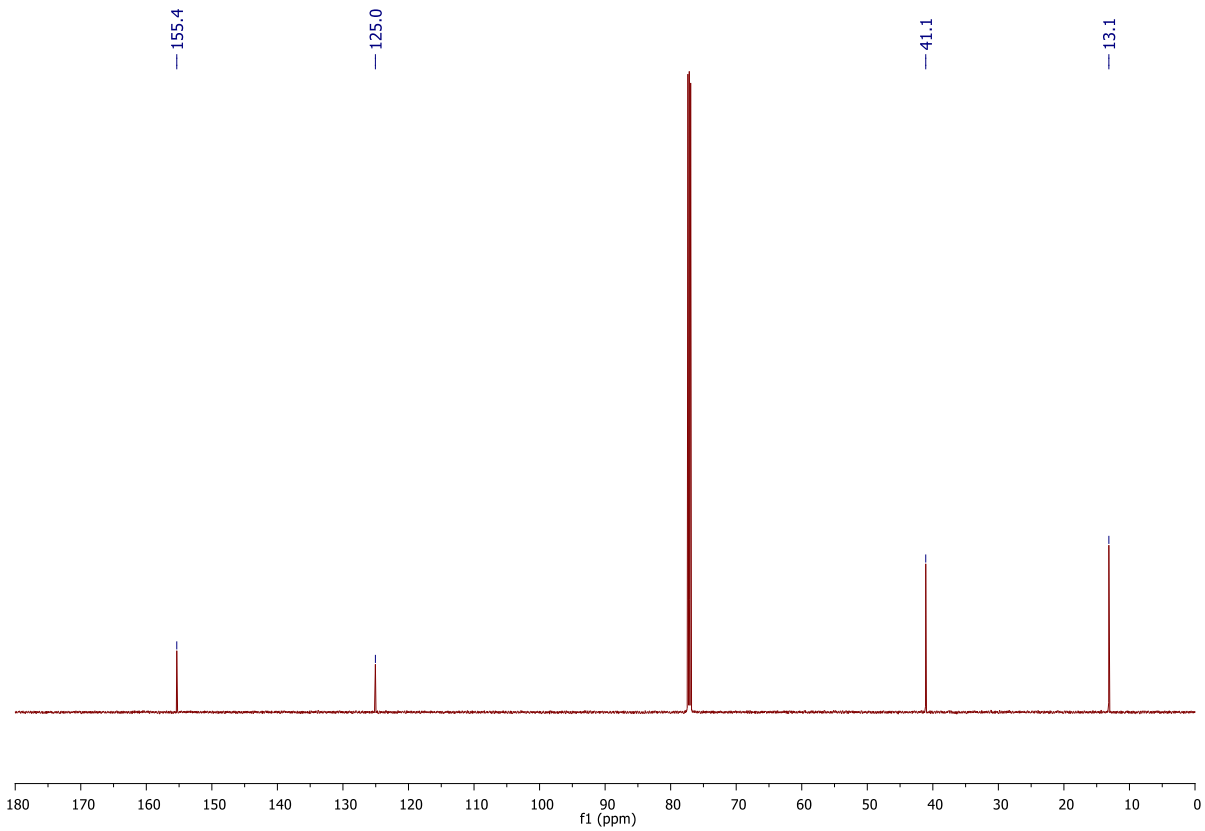
155.4
125.0
41.1
13.1
180
170
160
150
140
130
120
110
100
90
80
70
60
50
40
30
20
10
0
f1 (ppm)

((1*R*,8*S*,9*S*)-Bicyclo[6.1.0]non-4-yn-9-yl)methyl (2-(2-(2-(3-(4,5-dibromo-2-methyl-3,6-dioxo-3,6-dihydropyridazin-1(2*H*)-yl)propanamido)ethoxy)ethoxy)ethyl) carbamate 156e

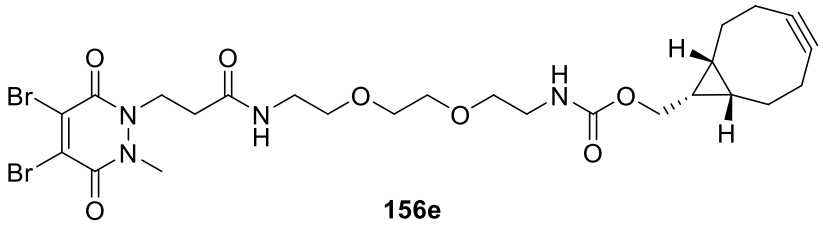

156e

((1R,8S,9s)-Bicyclo[6.1.0]non-4-yn-9-yl)methyl (2-(2-(2-(3-(4,5-dibromo-2-methyl-3,6-dioxo-3,6-dihydropyridazin-1(2*H*)-yl)propanamido)ethoxy)ethoxy)ethyl) carbamate **156e** was synthesised as described in experimental for chapter 2.

***tert*-Butyl (4-cyanobenzyl)carbamate S3[205] – Procedure provided by Mr P. A. Szijj**

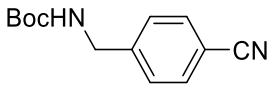

S3

To a solution of 4-(aminomethyl)benzonitrile (5.0 g, 29.7 mmol) in water (30 mL) was added a pre-dissolved solution of NaOH (3.6 g, 89.1 mmol) and di-*tert*-butyl dicarbonate (7.1 g, 32.6 mmol) in water (30 mL). The solution was stirred for 16 h at 21 °C, to form a heterogenous solution. After this time, the resulting solid was isolated, washed with water (100 mL), and dried solid to afford *tert*-butyl (4-cyanobenzyl)carbamate **S3** as a white solid (6.09 g, 26.2 mmol, 88%). ^{1}H NMR (400 MHz, $CDCl_3$) δ 7.62 (d, *J* = 8.3 Hz, 2H), 7.38 (d, *J* = 8.3 Hz, 2H), 4.96 (br s, 1H), 4.37 (d, *J* = 5.9 Hz, 2H), 1.46 (s, 9H); ^{13}C NMR (100 MHz, $CDCl_3$) δ 144.7 (C), 132.5 (C), 127.9 (C), 118.8 (C), 111.2 (C), 80.8 (C), 44.3 (CH_2), 28.4 (CH_3); IR (solid) 3350, 2974, 2927, 2226, 1692 cm^{-1}.

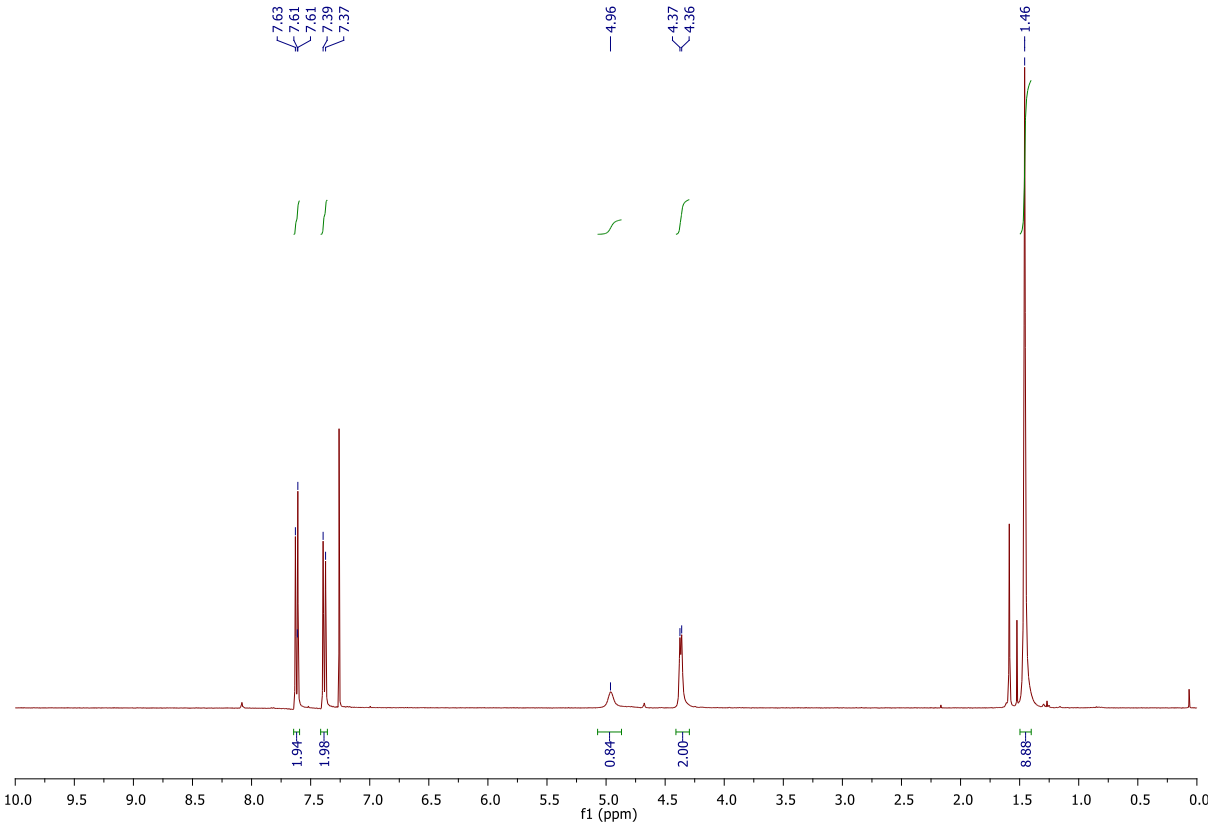

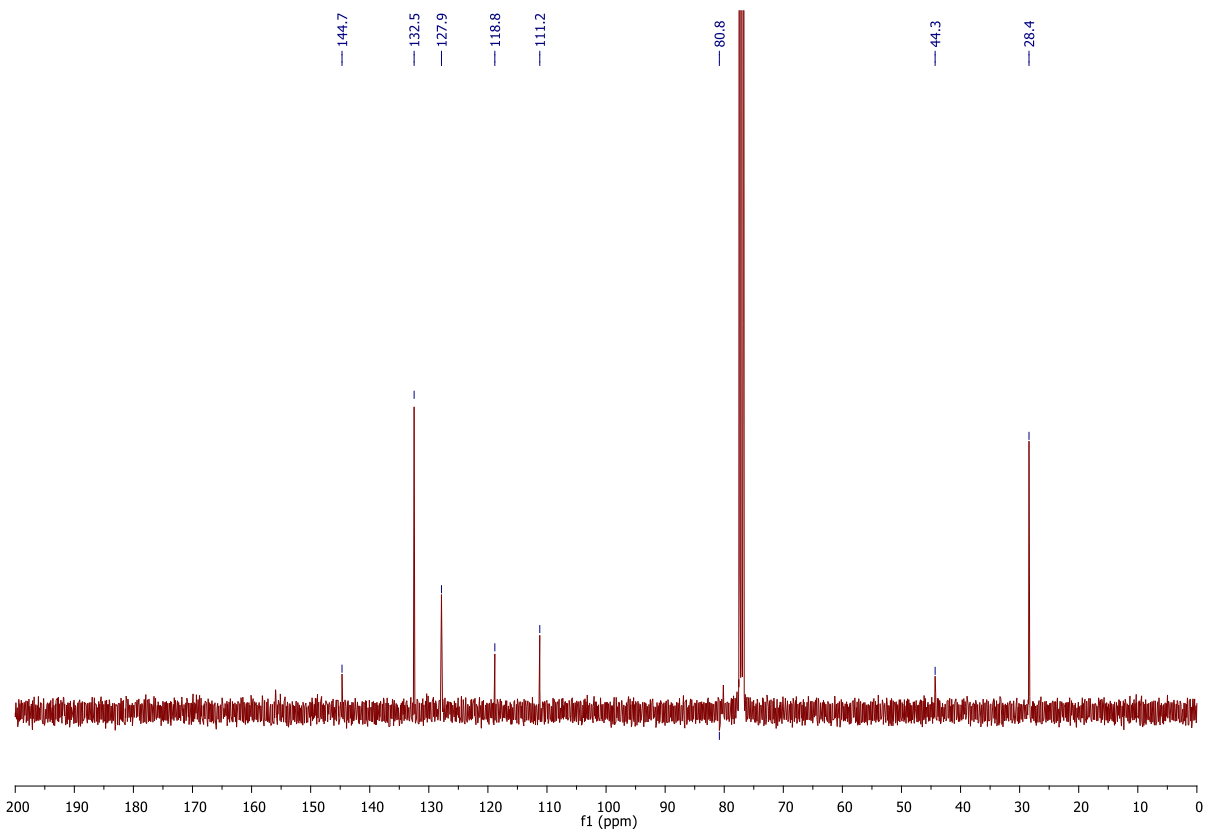
144.7
132.5
127.9
118.8
111.2
80.8
44.3
28.4
200 190 180 170 160 150 140 130 120 110 100 90 80 70 60 50 40 30 20 10 0
f1 (ppm)

***tert*-Butyl (4-(6-methyl-1,2,4,5-tetrazin-3-yl)benzyl)carbamate S4[205] – Procedure provided by Mr P. A. Szijj**

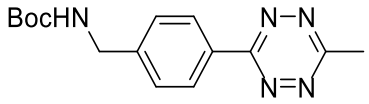

S4

To a solution of *tert*-butyl (4-cyanobenzyl)carbamate **S3** (3.0 g, 12.9 mmol), acetonitrile (6.72 mL, 12.9 mmol), and $Zn(OTf)_2$ (2.34 g, 6.46 mmol) in 1,4-dioxane (6 mL), was added hydrazine hydrate (80% w/w, 39.5 mL, 646 mmol) and the reaction was and stirred at 65 °C for 72 h. After this time the reaction was diluted with EtOAc (50 mL), washed with 1 M HCl (50 mL) and the aqueous phase extracted with EtOAc (2 × 30 mL). The organic phase was dried ($MgSO_4$), and EtOAc was removed *in vacuo*. The resulting crude residue was dissolved in CH_2Cl_2 and AcOH (1:1, 200 mL), and $NaNO_2$ (17.8 g, 258 mmol) was added portion-wise over 15 min. The reaction was then diluted in CH_2Cl_2 (200 mL) and washed with sat. aqueous $NaHCO_3$ (200 mL). The product was extracted with CH_2Cl_2 (2 × 100 mL), dried ($MgSO_4$), and CH_2Cl_2 was removed *in vacuo*. The crude residue was purified by silica gel chromatography (20% EtOAc/petrol) to afford *tert*-butyl (4-(6-methyl-1,2,4,5-tetrazin-3-yl)benzyl)carbamate **S4** as a pink solid (1.07 g, 3.55 mmol, 28%). ^{1}H NMR (400 MHz, $CDCl_3$) δ 8.55 (d, *J* = 8.4 Hz, 2H), 7.50 (d, *J* = 8.3 Hz, 2H), 4.97 (br s, 1H), 4.44 (d, *J* = 5.8 Hz, 2H), 3.09 (s, 3H), 1.48 (s, 9H); ^{13}C NMR (100 MHz, $CDCl_3$) δ 167.3 (C), 164.0 (C), 144.0 (C), 130.9 (C), 128.3 (C), 128.1 (C), 80.1 (C), 28.5 (CH_3), 21.2 (CH_3); IR (solid) 3339, 2974, 2928, 1696, 1516 cm^{-1}.

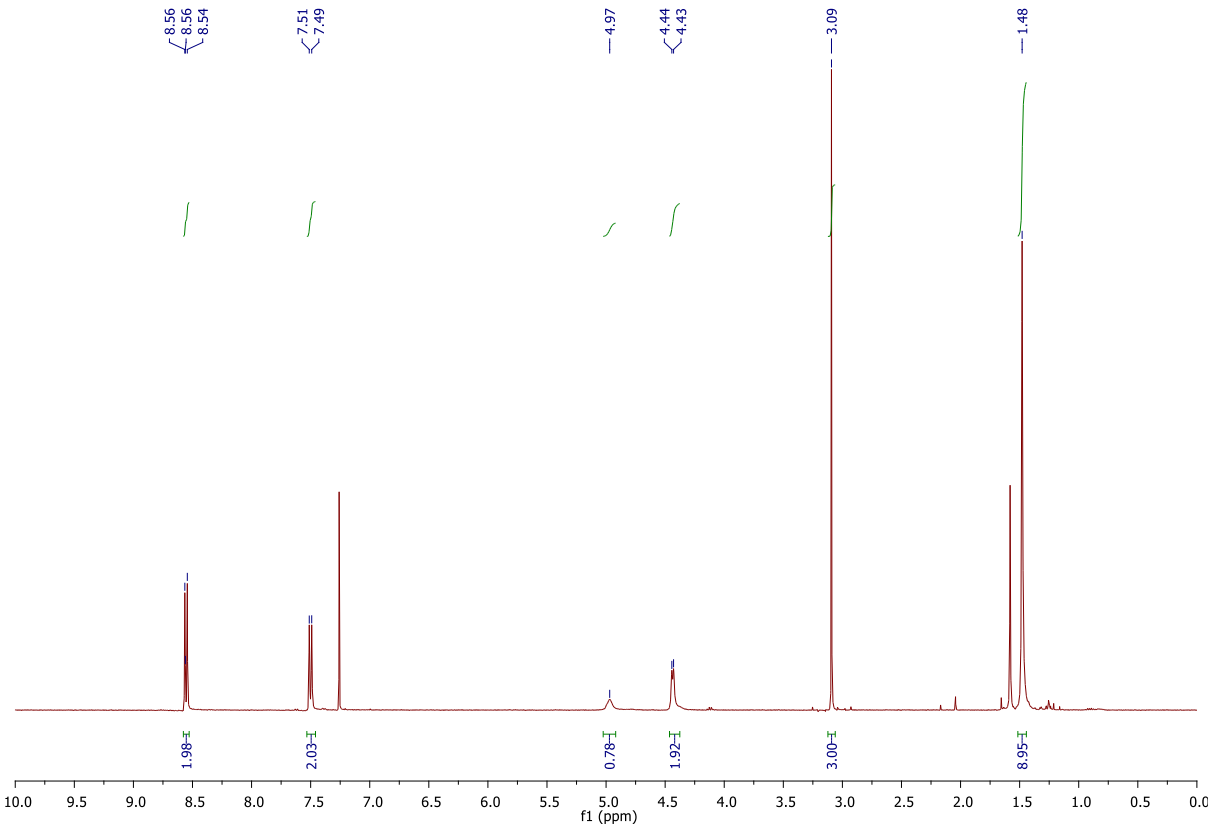
8.56
8.56
8.54
7.51
7.49
4.97
4.44
4.43
3.09
1.48
1.98
2.03
0.78
1.92
3.00
8.95
f1 (ppm)

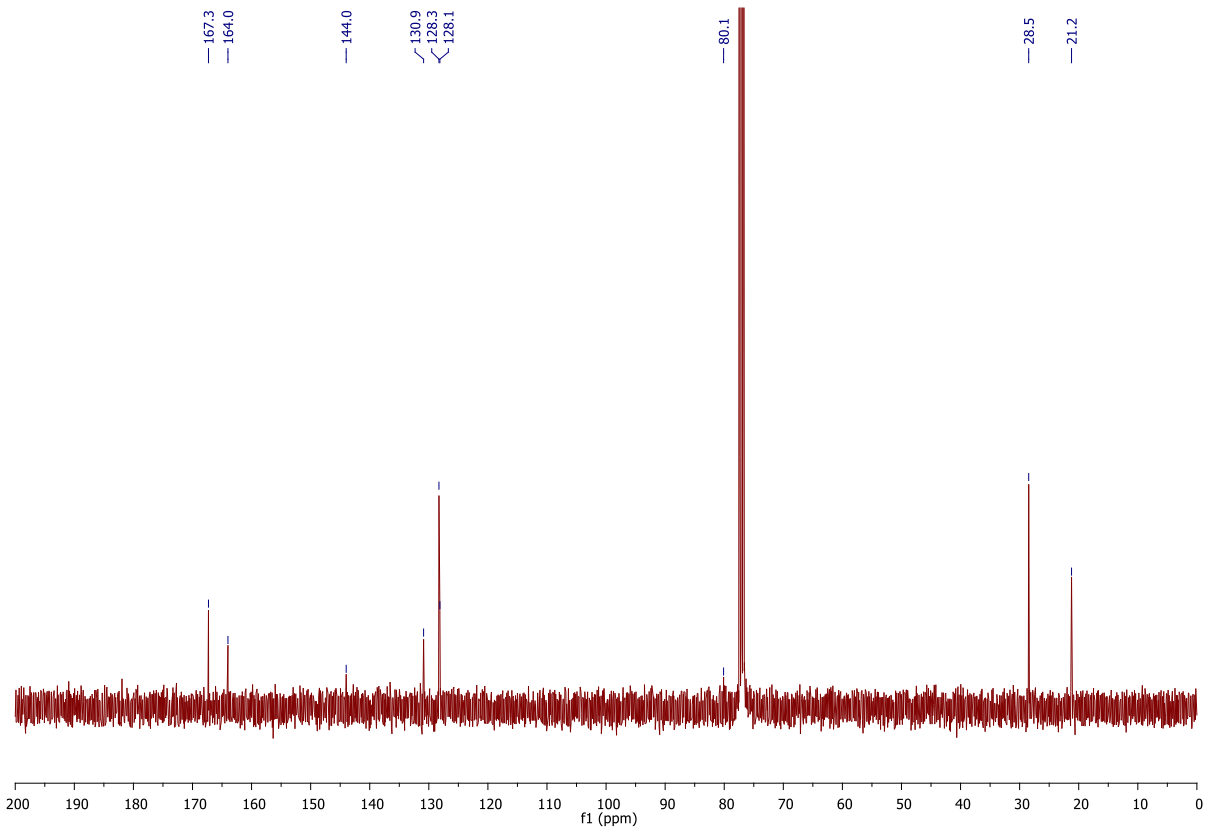
167.3
164.0
144.0
130.9
128.3
128.1
80.1
28.5
21.2
f1 (ppm)

5-((4-(6-Methyl-1,2,4,5-tetrazin-3-yl)benzyl)amino)-5-oxopentanoic acid S5[206] **– Procedure provided by Mr P. A. Szijj**

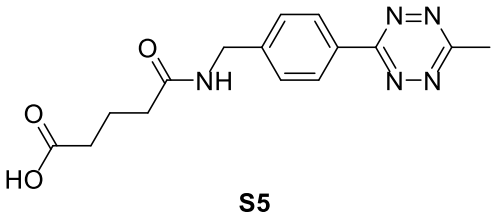

S5

To a solution of TFA and CH_2Cl_2 (1:4, 20 mL), was added *tert*-butyl (4-(6-methyl-1,2,4,5-tetrazin-3-yl)benzyl)carbamate **S4** (800 mg, 2.65 mmol) and the reaction was stirred at 21 °C for 2 h. After this time the TFA and CH_2Cl_2 was removed *in vacuo.* The crude residue was dissolved in THF (50 mL), was added glutaric anhydride (605 mg, 5.31 mmol) and the reaction was stirred at 55 °C for a further 16 h. THF was removed *in vacuo* and crude residue was dissolved in sat. aqueous K_2CO_3 solution (100 mL). The product was then acidified with 15% HCl (20 mL), and extracted with EtOAc (3 × 50 mL). The product was then washed with water (4 × 30 mL) and brine (30 mL), dried ($MgSO_4$) and the EtOAc removed *in vacuo* to afford 5-((4-(6-methyl-1,2,4,5-tetrazin-3-yl)benzyl)amino)-5-oxopentanoic acid **S5** as a purple solid (691 mg, 2.2 mmol, 83%). ^{1}H NMR (400 MHz, $CDCl_3$) δ 8.41 (d, *J* = 8.4, 2H), 7.51 (d, *J* = 8.5 Hz, 2H), 4.38 (d, *J* = 6.0 Hz, 2H), 2.98 (s, 3H), 2.22 (q, *J* = 7.4 Hz, 4H), 1.76 (p, *J* = 7.4 Hz, 2 H); ^{13}C NMR (100 MHz, $CDCl_3$) δ 174.2 (C), 171.9 (C), 167.1 (C), 163.2 (C), 144.5 (C), 130.4 (C), 128.1 (C), 127.5 (C), 41.9 (CH_2), 34.4 (CH_2), 33.1 (CH_2), 20.8 (CH_3), 20.7 (CH_2); IR (solid) 3271, 3025, 2973, 2923, 2880, 1694, 1630, 1523 cm^{-1}.

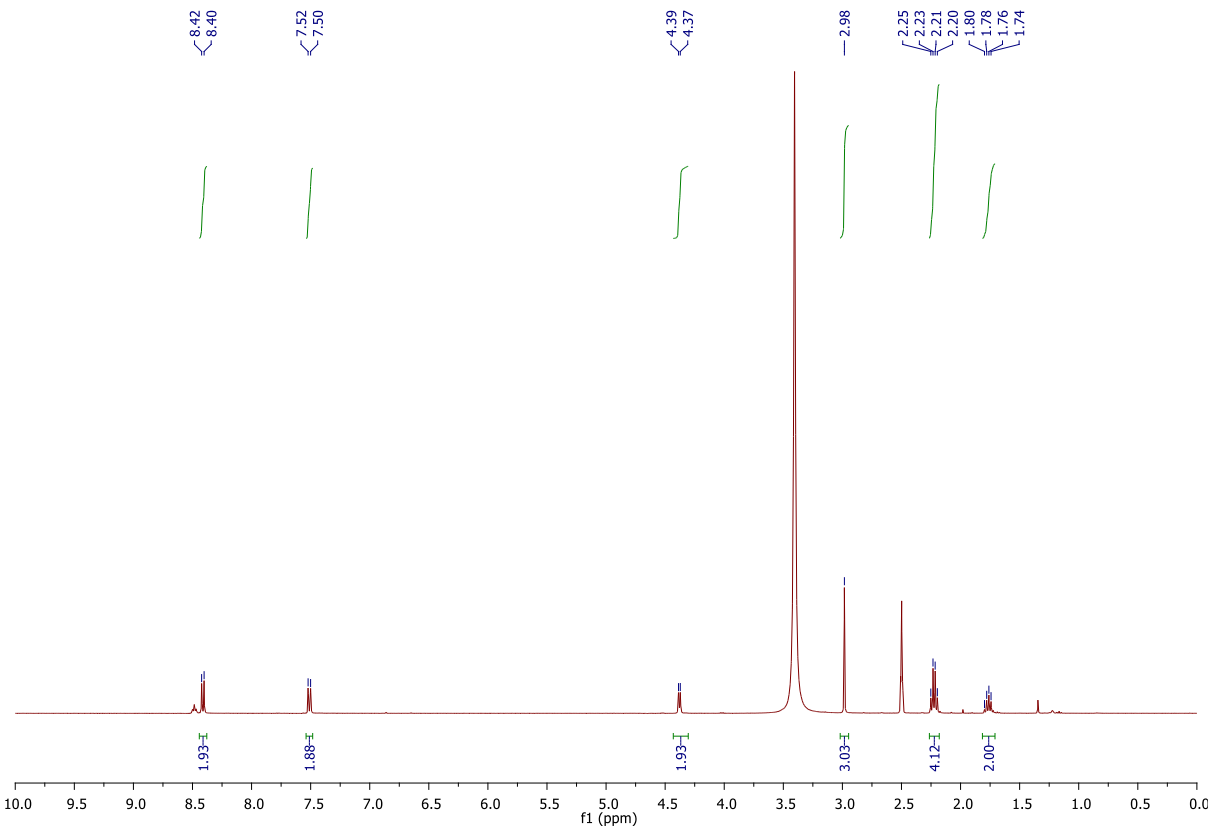
8.42
8.40
7.52
7.50
4.39
4.37
2.98
2.25
2.23
2.21
2.20
1.80
1.78
1.76
1.74
1.93
1.88
1.93
3.03
4.12
2.00
f1 (ppm)

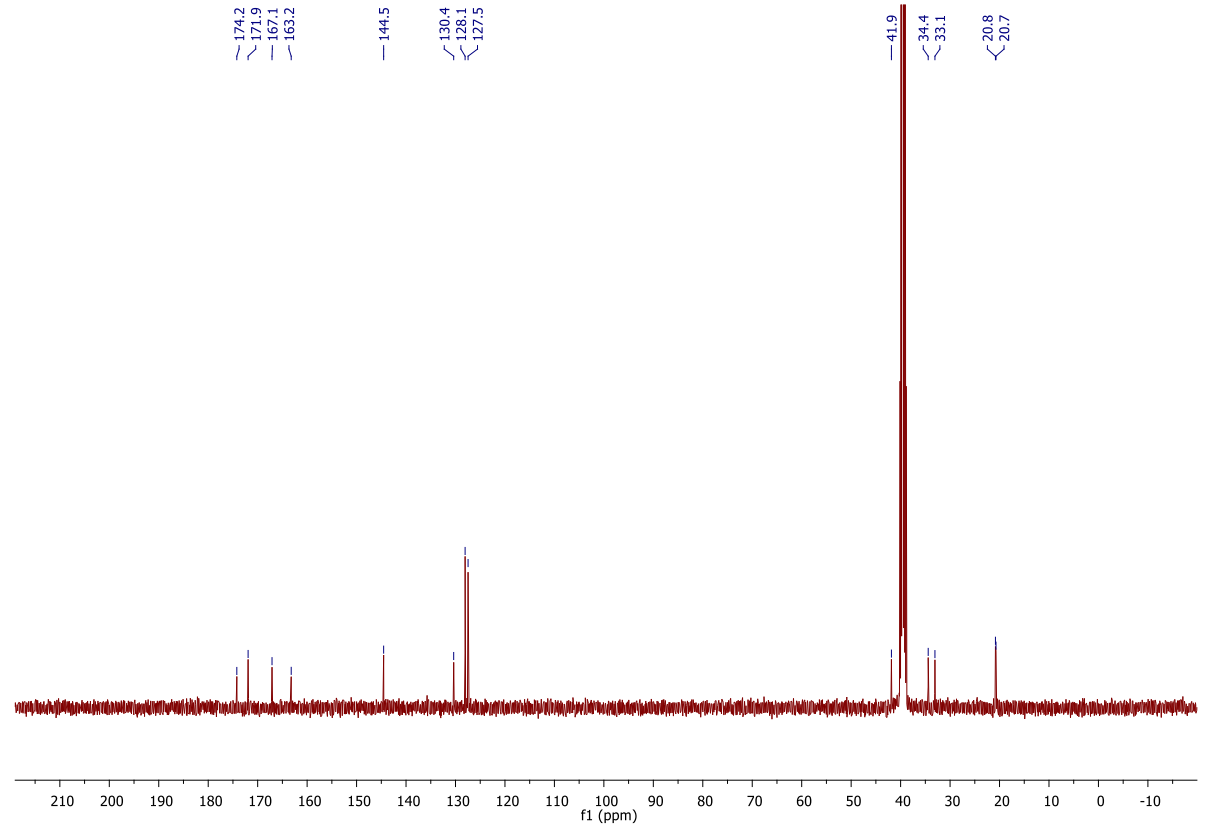
174.2
171.9
167.1
163.2
144.5
130.4
128.1
127.5
41.9
34.4
33.1
20.8
20.7
f1 (ppm)

Di-*tert*-butyl 1-(prop-2-yn-1-yl)hydrazine-1,2-dicarboxylate S6[207]

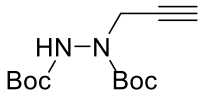

S6

To a solution of di-*tert*-butyl hydrazine-1,2-dicarboxylate (3.00 g, 12.9 mmol) in a mixture of toluene (15 mL) and 5% aq. NaOH (15mL) were added tetra-*n*-butylammonium bromide (104 mg, 0.32 mmol) and propargyl bromide (5.76 g, 38.7 mmol). The reaction mixture was stirred at 21 °C for 16 h. After this time, water (20 mL) was added and the mixture was extracted with EtOAc (3 × 30 mL). The combined organic layers were washed with brine (30 mL), dried ($MgSO_4$), and concentrated *in vacuo*. Purification by flash column chromatography (20 % EtOAc/petrol) afforded di-*tert*-butyl 1-(prop-2-yn-1-yl)hydrazine-1,2-dicarboxylate **S6** (2.04 g, 7.56 mmol, 59%) as a white solid. ^{1}H NMR (400 MHz, $CDCl_3$, rotamers) δ 6.48-6.17 (br s, 1H), 4.27 (s, 2H), 2.24 (t, *J* = 2.4 Hz, 1H), 1.47 (s, 18H); ^{13}C NMR (125 MHz, $CDCl_3$, rotamers) δ 154.9 (C), 154.7 (C), 82.1 (C), 81.6 (C), 78.8 (C), 72.1 (CH), 39.3 (CH_2), 28.3 (CH_3), 28.2 (CH_3); IR (solid) 3310, 3290, 2982, 1729, 1688, 1512 cm^{-1}.

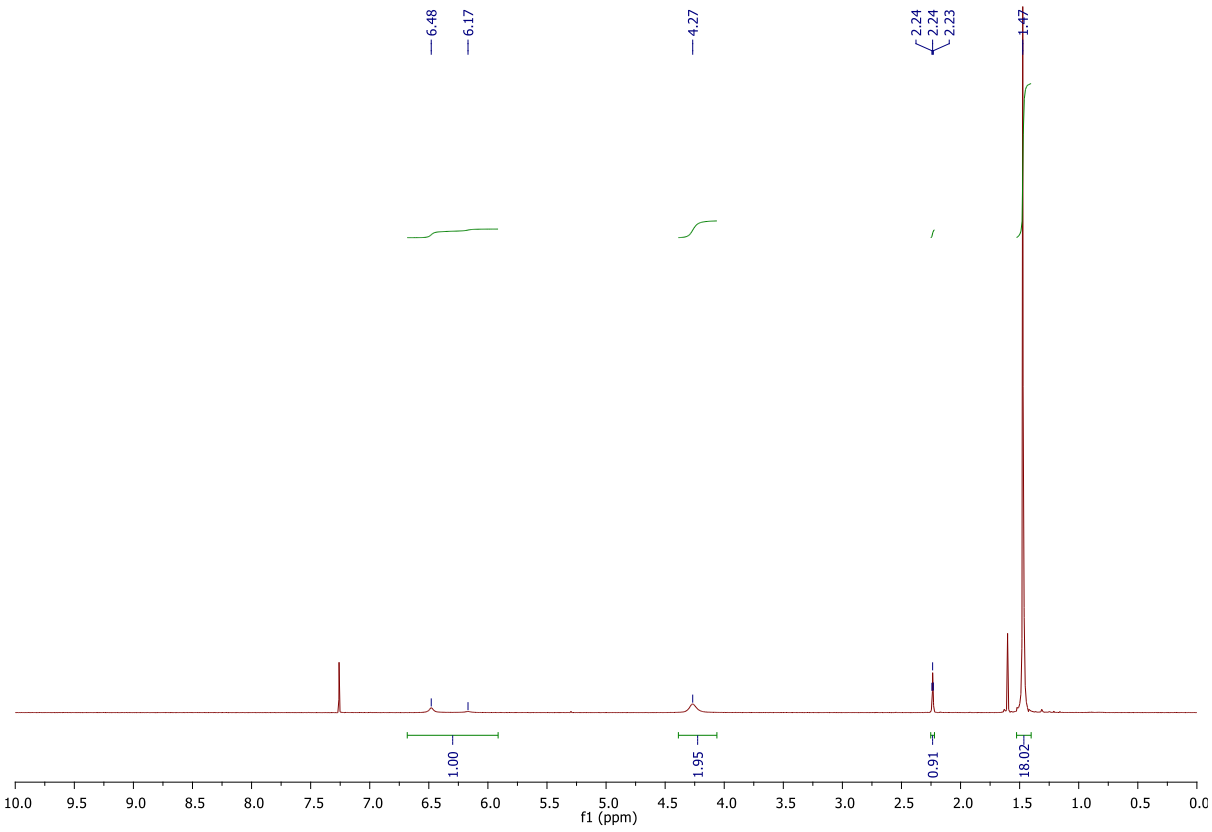

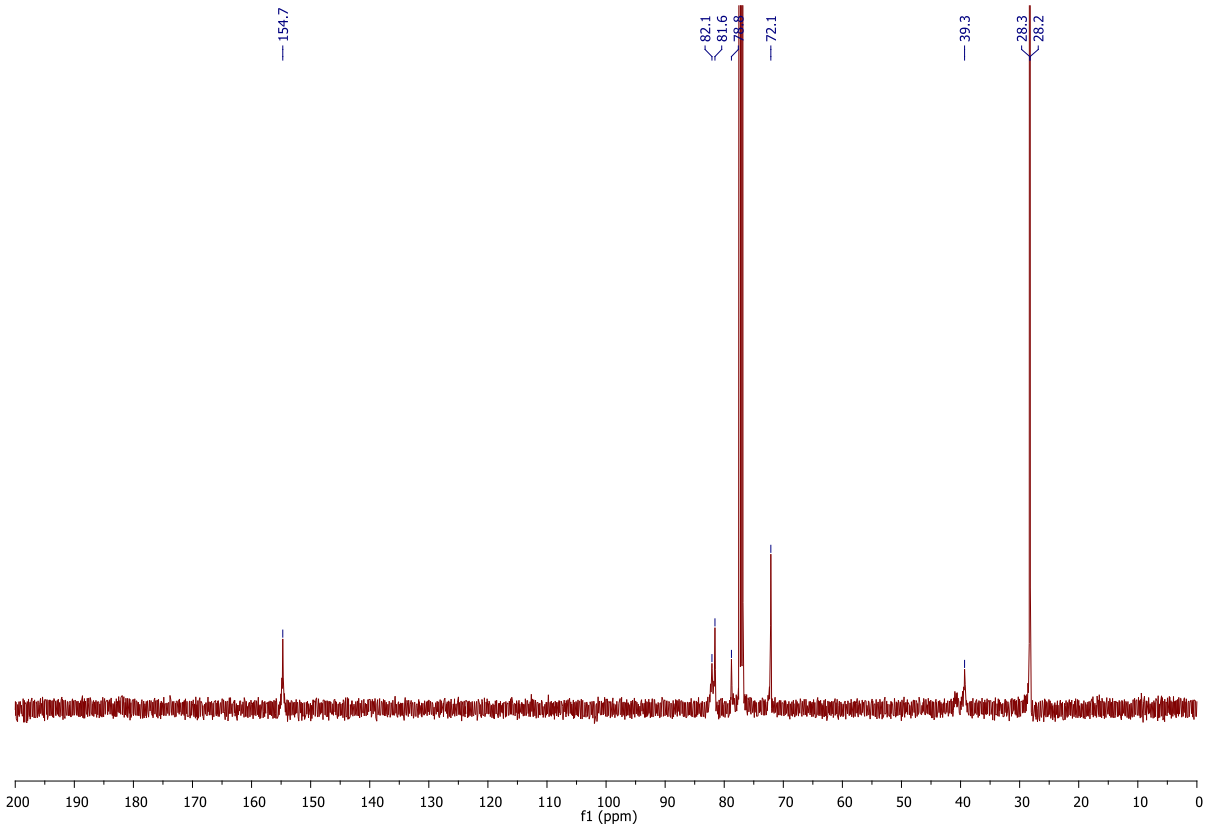
154.7
82.1
81.6
78.8
72.1
39.3
28.3
28.2
200
190
180
170
160
150
140
130
120
110
100
90
80
70
60
50
40
30
20
10
0
f1 (ppm)

Di-*tert*-butyl 1-(3-(tert-butoxy)-3-oxopropyl)-2-(prop-2-yn-1-yl)hydrazine-1,2-dicarboxylate S7

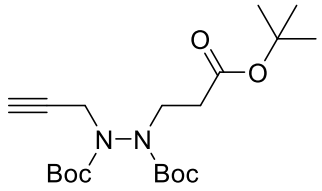

S7

To a solution of di-*tert*-butyl 1-(prop-2-yn-1-yl)hydrazine-1,2-dicarboxylate **S6** (2.05 g, 7.60 mmol) in *t*-BuOH (15 mL) was added 10% NaOH (0.17 mL), and the reaction mixture stirred at 21 °C for 10 min. After this, *tert*-butyl acrylate (1.47 mL, 15.2 mmol) was added to the solution and the reaction mixture was heated at 60 °C for 24 h. Following this, the solvent was removed *in vacuo* and the crude residue was dissolved in EtOAc (150 mL) and washed with water (3 × 50 mL). The organic layer was then dried ($MgSO_4$) and concentrated *in vacuo.* Purification of the crude residue by flash column chromatography (0% to 20% EtOAc/petrol) to afford di-*tert*-butyl 1-(3-(tert-butoxy)-3-oxopropyl)-2-(prop-2-yn-1-yl)hydrazine-1,2-dicarboxylate **S7** (2.20 g, 5.52 mmol, 73%) as a clear oil: ^{1}H NMR (600 MHz, $CDCl_3$, rotamers) δ 4.61–4.00 (m, 2H), 3.83–3.68 (m, 2H), 2.64 (t, *J* = 7.6 Hz, 2H), 2.27 (t, *J* = 2.5 Hz, 1H), 1.50–1.43 (m, 27H); ^{13}C NMR (150 MHz, $CDCl_3$, rotamers) δ 171.1 (C), 155.5 (C), 154.4 (C), 82.0 (C), 81.5 (C), 80.7 (C), 78.5 (C), 73.0 (CH), 46.2 (CH_2), 39.5 (CH_2), 34.2 (CH_2), 28.3 (CH_3), 28.2 (CH_3), 28.2 (CH_3); IR (thin film) 3265, 2978, 2934, 1710 cm^{-1}; LRMS (ESI) 343 (60, $[M\text{-}C_4H_9+2H]^+$, 399 (100, $[M+H]^+$). HRMS (ESI) calcd for $C_{20}H_{34}N_2O_6$ $[M+H]^+$ 399.2490; observed 399.2487.

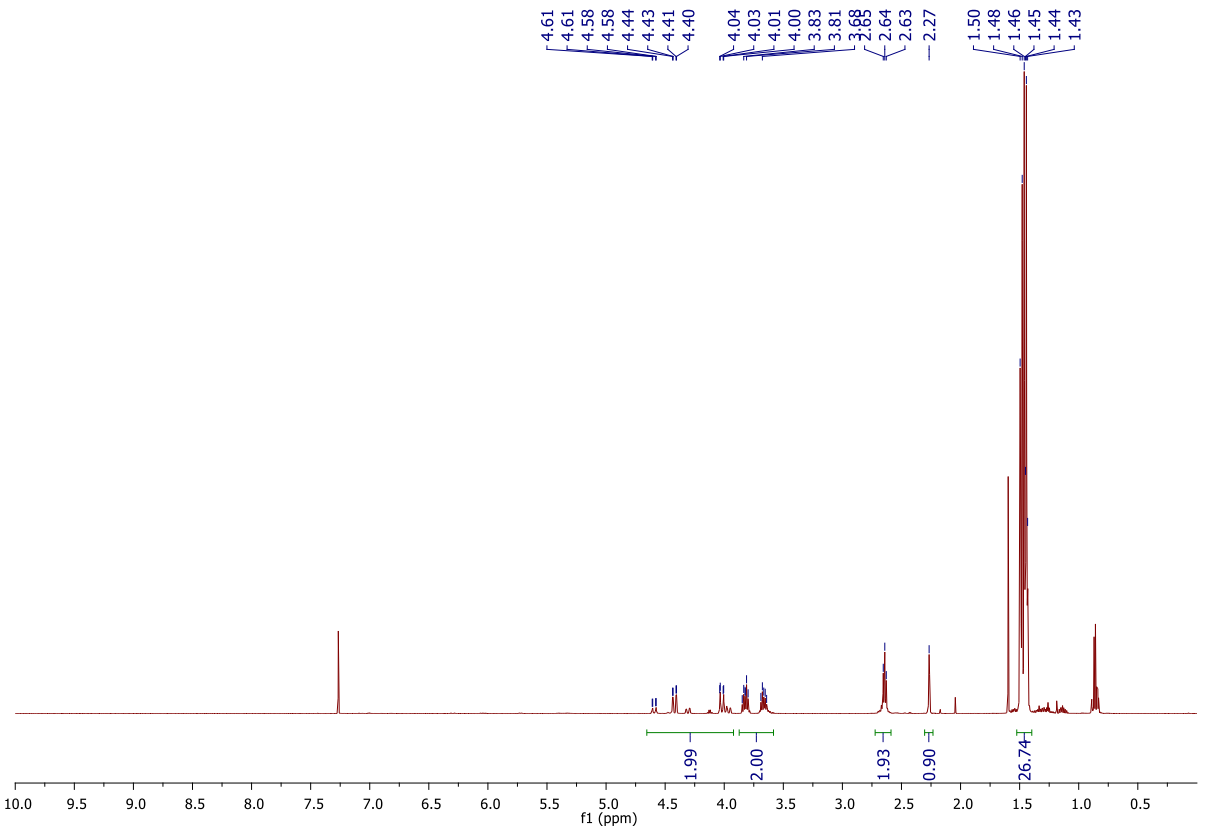
4.61
4.61
4.58
4.58
4.44
4.43
4.41
4.40
4.04
4.03
4.01
4.00
3.83
3.81
2.64
2.63
2.27
1.50
1.48
1.46
1.45
1.44
1.43
1.99
2.00
1.93
0.90
26.74
f1 (ppm)

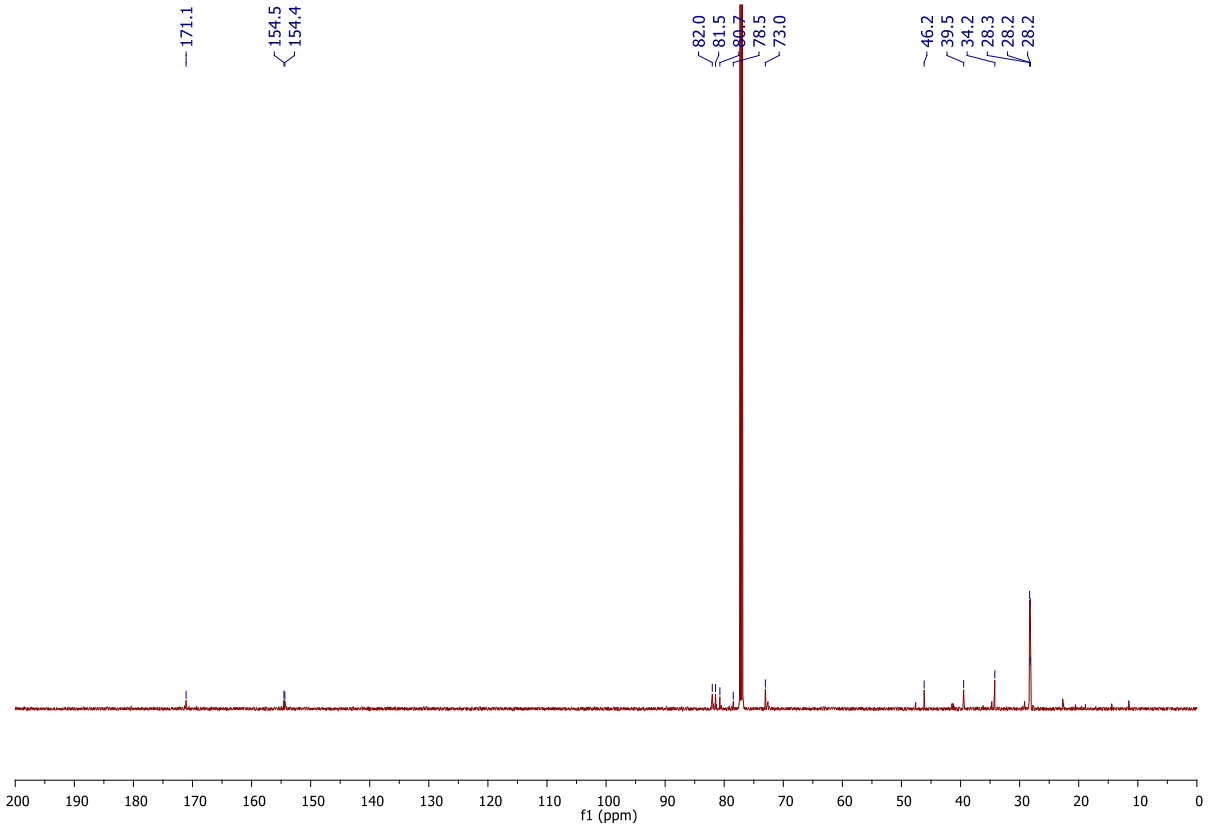
171.1
154.5
154.4
82.0
81.5
80.7
78.5
73.0
46.2
39.5
34.2
28.3
28.2
28.2
f1 (ppm)

3-(4,5-Dibromo-3,6-dioxo-2-(prop-2-yn-1-yl)-2,3-dihydropyridazin-1(6*H*)-yl)propanoic acid S8

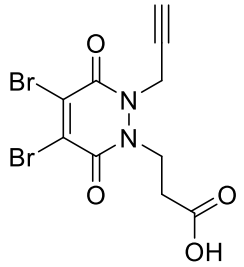

S8

Dibromomaleic acid **138** (1.66 g, 6.06 mmol) was dissolved in AcOH (25 mL) and heated under reflux for 30 min. To this solution, was added di-*tert*-butyl 1-(3-(*tert*-butoxy)-3-oxopropyl)-2-(prop-2-yn-1-yl)hydrazine-1,2-dicarboxylate **S7** (2.20 g, 5.51 mmol) and the reaction heated under reflux for a further 4 h. After this time, the reaction mixture was concentrated *in vacuo* with toluene co-evaporation (3 × 30 mL, as an azeotrope) and the crude residue purified by flash column chromatography (50% to 100% EtOAc/petrol (1% AcOH)) to afford 3-(4,5-dibromo-3,6-dioxo-2-(prop-2-yn-1-yl)-2,3-dihydropyridazin-1(6*H*)-yl)propanoic acid **S8** (801 mg, 2.25 mmol, 77%) as a yellow solid: m.p. 136–140 °C; ^{1}H NMR (600 MHz, DMSO-D_6) δ 4.91 (d, *J* = 2.4 Hz, 2H), 4.27 (t, *J* = 7.5 Hz, 2H), 3.77 (s, 1H), 3.52 (t, *J* = 2.4 Hz, 1H), 2.66 (t, *J* = 7.5 Hz, 2H); ^{13}C NMR (150 MHz, DMSO-d_6) δ 171.9 (C), 153.4 (C), 153.0 (C), 136.2 (C), 135.1 (C), 77.2 (C), 76.7 (CH), 43.5 (CH_2), 37.6 (CH_2), 31.5 (CH_2); IR (solid) 3216, 2979, 1723 cm^{-1} LRMS (ESI). 379 (5k0, $[M^{81}Br^{81}Br+H]^+$), 381 (100, $[M^{79}Br^{81}Br+H]^+$), 383 (50, $[M^{79}Br^{79}Br+H]^+$). HRMS (ESI) calcd for $C_{10}H_8Br_2N_2O_4$ $[M^{79}Br^{81}Br+H]^+$ 380.8904; observed 380.8906.

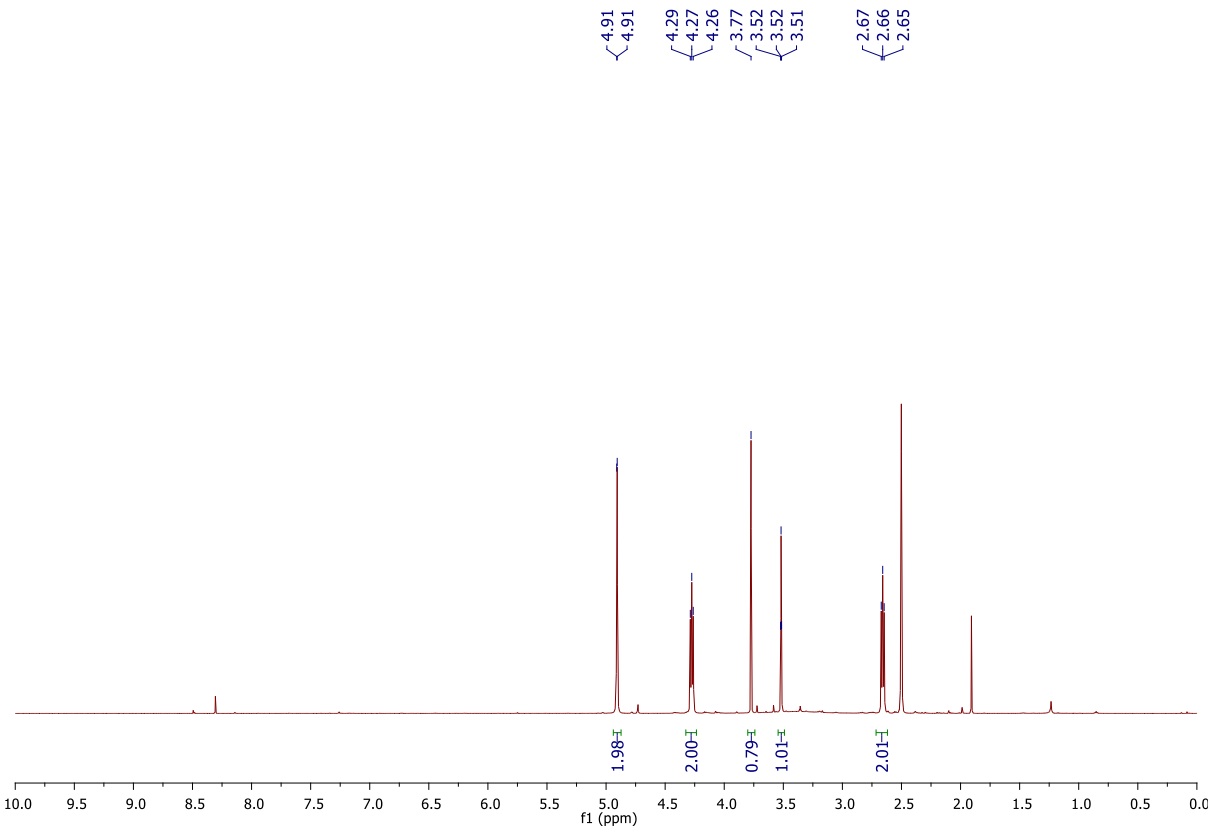
4.91
4.91
4.29
4.27
4.26
3.77
3.52
3.52
3.51
2.67
2.66
2.65
1.98
2.00
0.79
1.01
2.01
f1 (ppm)

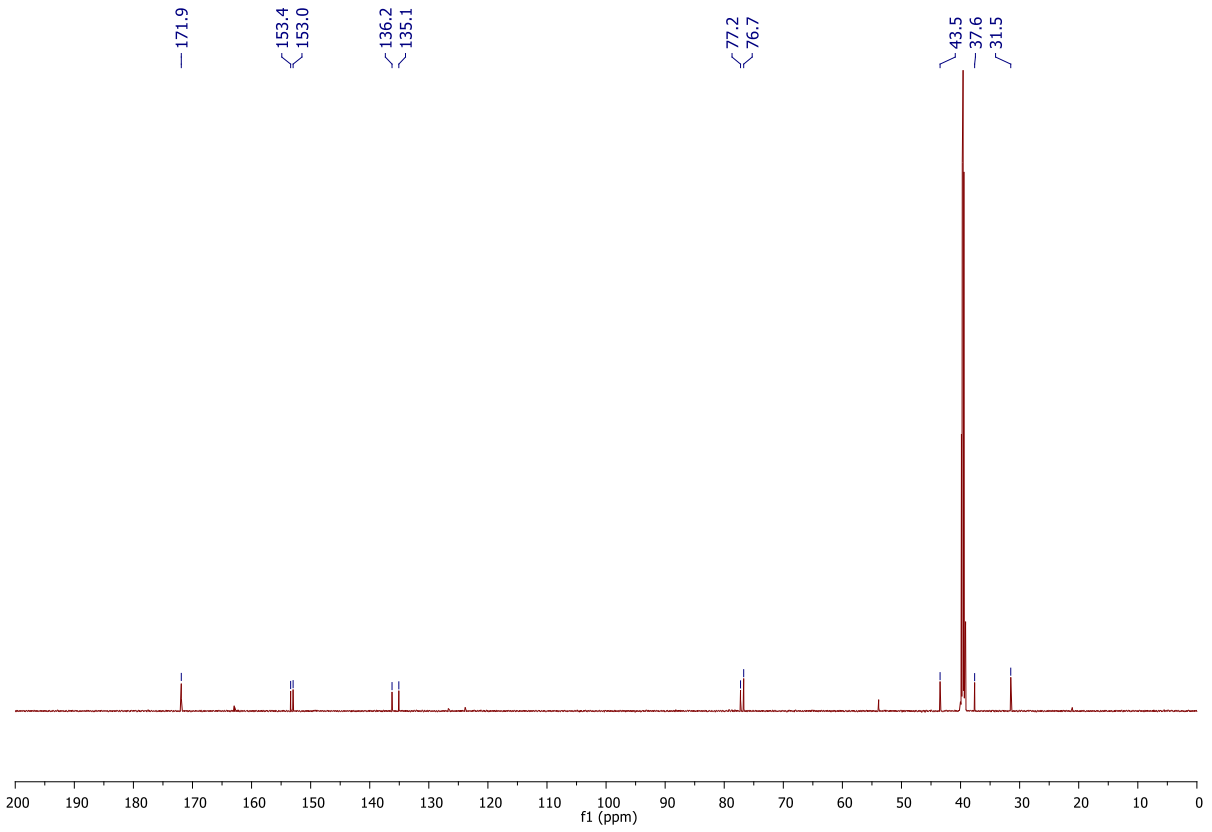
171.9
153.4
153.0
136.2
135.1
77.2
76.7
43.5
37.6
31.5
f1 (ppm)

N^1-(2-(2-(2-(2-Azidoethoxy)ethoxy)ethoxy)ethyl)-N^5-(4-(6-methyl-1,2,4,5-tetrazin-3-yl)benzyl)glutaramide S9 – Procedure provided by Mr P. A. Szijj

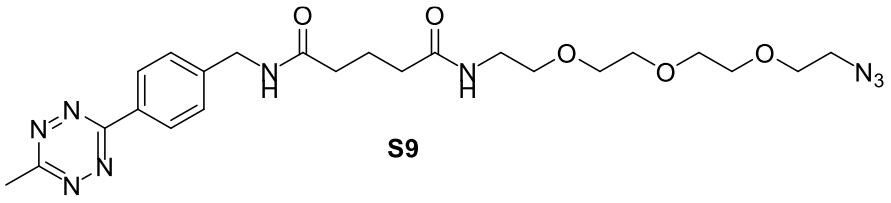

S9

To a solution of 5-((4-(6-methyl-1,2,4,5-tetrazin-3-yl)benzyl)amino)-5-oxopentanoic acid **S6** (200 mg, 0.63 mmol) in CH_2Cl_2 (5 mL) was added HATU (240 mg, 0.63 mmol), and NEt_3 (87.8 µL, 0.63 mmol) and the reaction stirred for 5 min at 21 °C. To this solution was added a solution of 2-(2-(2-(2-azidoethoxy)ethoxy)ethoxy)ethan-1-amine (387.5 µL, 1.96 mmol) in CH_2Cl_2 (5 mL), and the resulting solution was stirred at 21 °C for 16 h. The reaction was diluted with EtOAc (25 mL) and water (25 mL) and the phases separated. The aqueous phase was extracted with EtOAc (3 × 25 mL) and the combined organic phases were washed with water (3 × 25 mL), brine (20 mL), dried ($MgSO_4$) and the solvent removed *in vacuo*. The crude residue was purified by flash column chromatography (0-10% MeOH in CH_2Cl_2) to afford N^1-(2-(2-(2-(2-azidoethoxy)ethoxy)ethoxy)ethyl)-N^5-(4-(6-methyl-1,2,4,5-tetrazin-3-yl)benzyl)glutaramide **S9** (209.5 mg, 0.51 mmol, 64%) as a purple solid: ^{1}H NMR (400 MHz, $CDCl_3$) δ 8.55 (d, *J* = 8.4 Hz, 2H), 7.51 (d, *J* = 8.5 Hz, 2H), 6.61 (br s, 1H), 6.16 (br s, 1H), 4.55 (d, *J* = 6.0 Hz, 2H), 3.67–3.60 (m, 10 H), 3.55–3.53 (m, 2H), 3.44–3.36 (m, 4H), 3.09 (s, 3H), 2.35 (t, *J* = 7.1 Hz, 2H), 2.26 (t, *J* = 6.9 Hz, 2H), 2.01 (p, *J* = 6.9 Hz, 2H); ^{13}C NMR (100 MHz, $CDCl_3$) δ 172.7 (C), 172.7 (C), 167.3 (C), 163.9 (C), 143.6 (C), 131.0 (C), 128.5 (CH), 128.3 (CH), 70.8 (CH_2), 70.7 (CH_2), 70.6 (CH_2), 70.3 (CH_2), 70.1(CH_2), 69.8 (CH_2), 50.7 (CH_2), 43.2 (CH_2), 39.3 (CH_2), 35.3 (CH_2), 35.2 (CH_2), 22.0 (CH_2), 21.2 (CH_3). IR (solid) 3298, 3076, 2868, 2101, 1637, 1541 cm^{-1}. HRMS (ESI) calcd for $C_{23}H_{34}N_9O_5$ $[M+H]^+$ 516.2677; observed 516.2677.

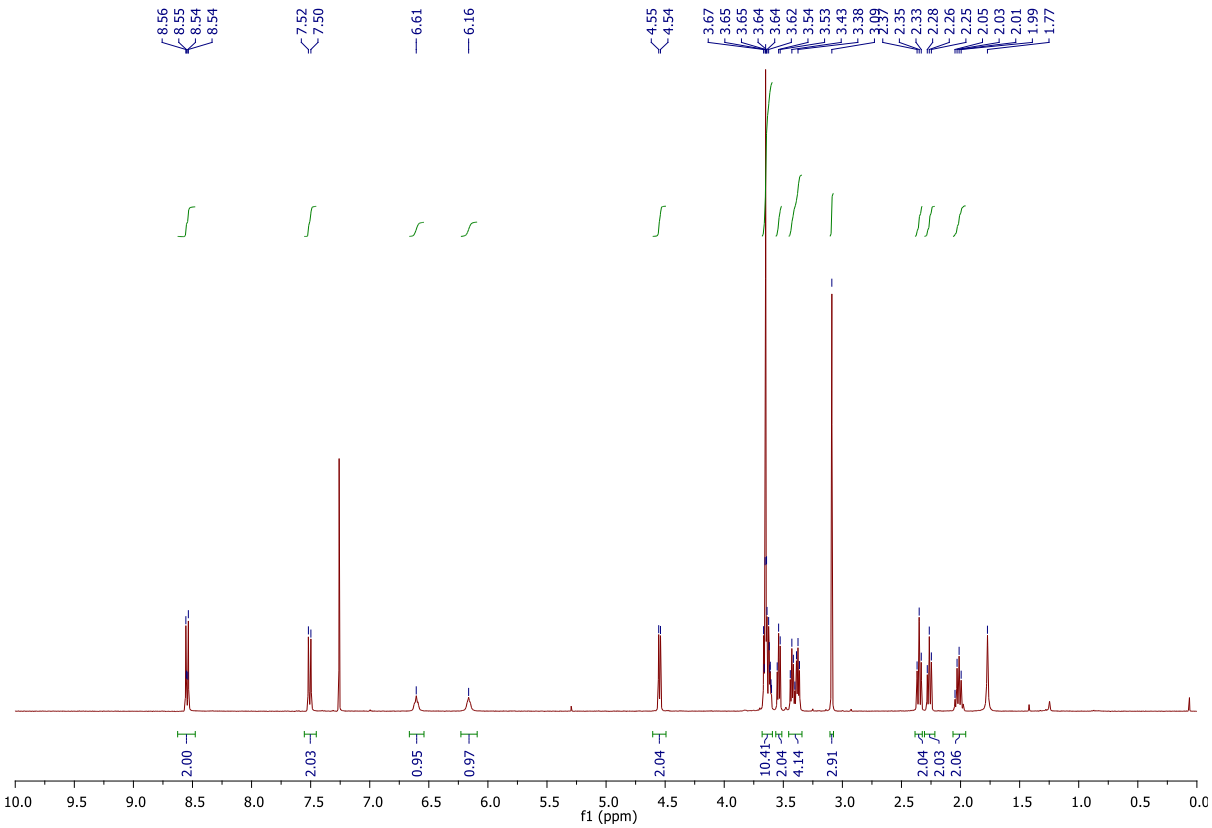
8.56
8.55
8.54
8.54
7.52
7.50
6.61
6.16
4.55
4.54
3.67
3.65
3.65
3.64
3.64
3.62
3.54
3.53
3.43
3.38
3.09
2.37
2.35
2.33
2.28
2.26
2.25
2.05
2.03
2.01
1.99
1.77
2.00
2.03
0.95
0.97
2.04
10.41
2.04
4.14
2.91
2.04
2.03
2.06
f1 (ppm)

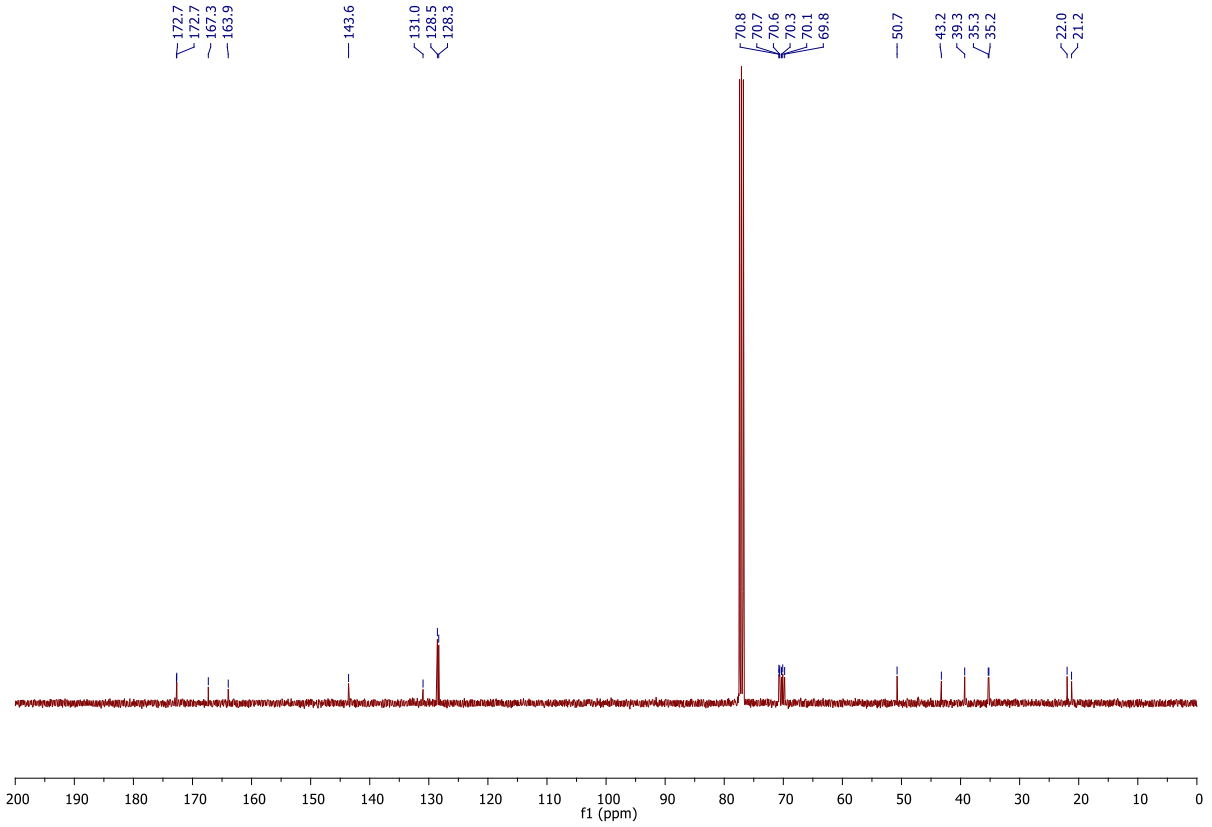
172.7
172.7
167.3
163.9
143.6
131.0
128.5
128.3
70.8
70.7
70.6
70.3
70.1
69.8
50.7
43.2
39.3
35.3
35.2
22.0
21.2
f1 (ppm)

3-(4,5-Dibromo-2-((1-(1-(4-(6-methyl-1,2,4,5-tetrazin-3-yl)phenyl)-3,7-dioxo-11,14,17-trioxa-2,8-diazanonadecan-19-yl)-1*H*-1,2,3-triazol-4-yl)methyl)-3,6-dioxo-3,6-dihydropyridazin-1(2*H*)-yl)propanoic acid S10 – Procedure provided by Mr P. A. Szijj

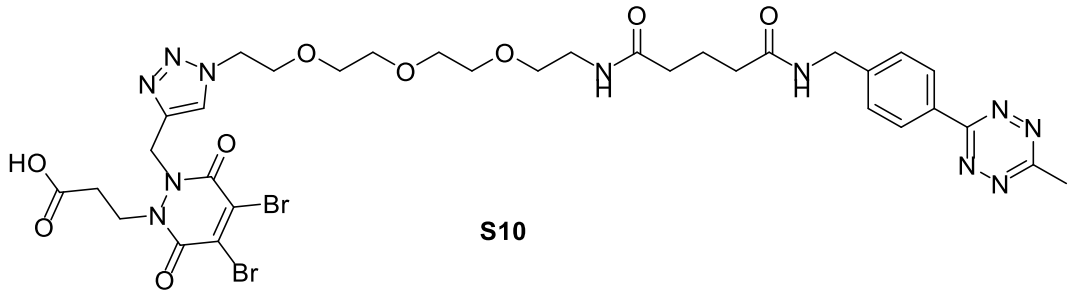

S10

To a solution of N^1-(2-(2-(2-(2-azidoethoxy)ethoxy)ethoxy)ethyl)-N^5-(4-(6-methyl-1,2,4,5-tetrazin-3-yl)benzyl)glutaramide **S9** (50 mg, 97.0 µmol) and 3-(4,5-dibromo-3,6-dioxo-2-(prop-2-yn-1-yl)-3,6-dihydropyridazin-1(2*H*)-yl)propanoic acid **S8** (44.3 mg, 116.6 µmol) in THF (10 mL) was added DIPEA (16.8 µL, 97.0 µmol) and CuI (9.35 mg, 48.5 µmol) and the mixture stirred at 21 °C for 5 h. The mixture was then filtered, and the solvent removed *in vacuo*. The mixture was dissolved in water (10 mL), basified with sat. aq. $NaHCO_3$, and washed with CH_2Cl_2 (3 × 10 mL). CH_2Cl_2 (10 mL) was then added to the aqueous phase. The aqueous phase was then acidified with 4 M HCl until the purple product visibly transferred to the organic phase. The aqueous phase was then extracted with further CH_2Cl_2 (3 × 10 mL). The combined organic phases were washed with brine, dried ($MgSO_4$), filtered and the solvent removed *in vacuo*. The crude residue was purified by column chromatography (0% to 20% MeOH/CH_2Cl_2, 1% AcOH) to yield 3-(4,5-dibromo-2-((1-(1-(4-(6-methyl-1,2,4,5-tetrazin-3-yl)phenyl)-3,7-dioxo-11,14,17-trioxa-2,8-diazanonadecan-19-yl)-1*H*-1,2,3-triazol-4-yl)methyl)-3,6-dioxo-3,6-dihydropyridazin-1(2*H*)-yl)propanoic acid **S10** (67.2 mg, 75.0 µmol, 77%) as a purple solid: ^{1}H NMR (400 MHz, DMSO-d_6) δ 8.42 (d, *J* = 8.3 Hz, 2H), 8.10 (s, 1H), 7.88 (s, 1H), 7.51 (d, *J* = 8.3 Hz, 2H), 5.35 (br s, 2H), 4.5 (t, *J* = 5.1 Hz, 2H), 4.38 (d, *J* = 6.0 Hz, 2H), 4.30 (s 2H), 3.78 (t, *J* = 5.3 Hz, 2H), 3.48–3.44 (m, 9 H), 3.39 (t, *J* = 6.0 Hz, 3H), 3.18 (q, *J* = 5.9 Hz, 2H), 2.99 (s, 3H), 2.18 (t, *J* = 7.5 Hz, 2H), 2.10 (t, *J* = 7.4 Hz, 2H), 1.76 (p, *J* = 7.7 Hz, 2 H); ^{13}C NMR (125 MHz, DMSO-d_6) δ 172.0 (C), 171.8 (C), 167.1 (C), 163.2 (C), 153.5 (C), 152.9 (C), 144.6 (C), 135.9 (C), 135.2 (C), 130.3 (C), 128.1 (CH), 127.5 (CH), 124.5 (CH), 69.7 (CH_2), 69.6 (CH_2), 69.6 (CH_2), 69.2 (CH_2), 68.6 (CH_2), 54.9 (CH_2), 49.6 (CH_2), 41.8 (CH_2), 34.8 (CH_2),

34.7 (CH_2), 21.5 (CH_2), 20.8 (CH_3). IR (thin film) 3335, 2924, 1721, 1630, 1545 cm^{-1}. HRMS (ESI) calcd for $C_{33}H_{42}Br_2N_{11}O_9$ $[M^{79}Br^{81}Br+H]^+$ 896.1435; observed 896.1503.

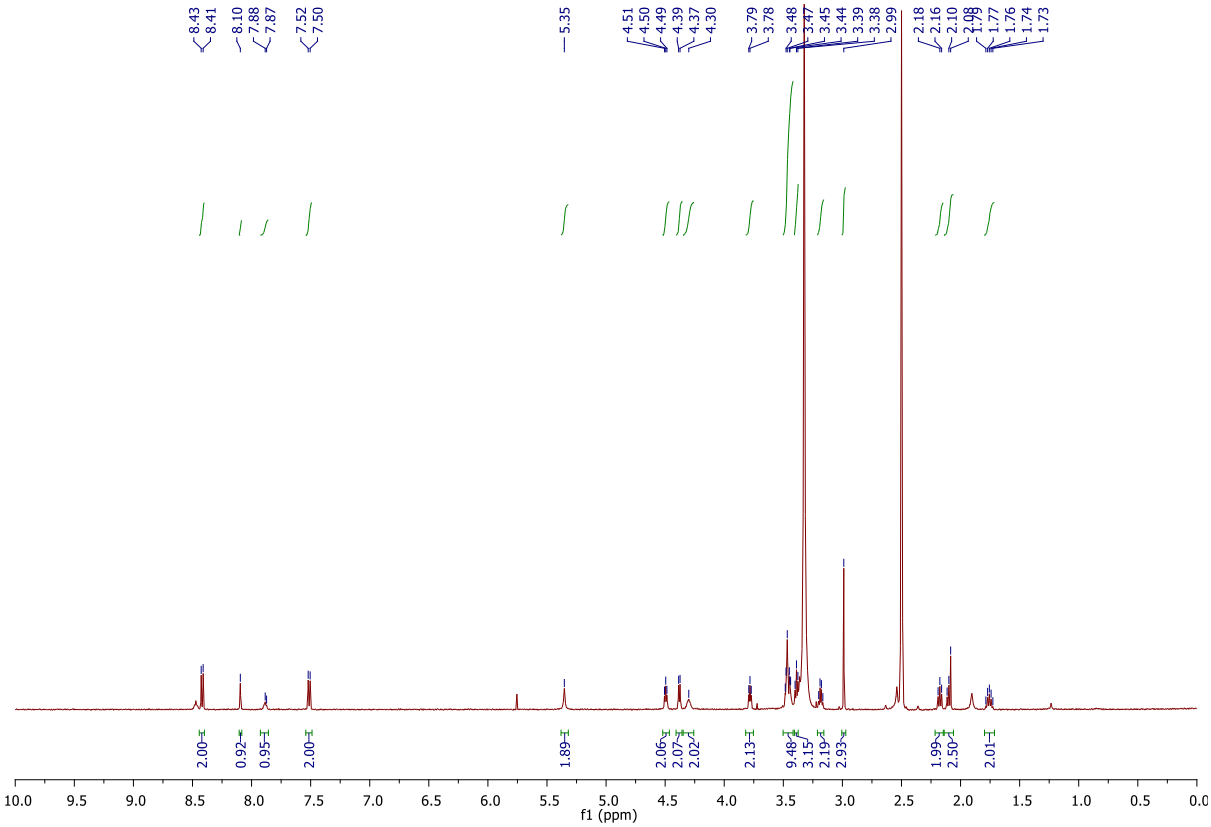

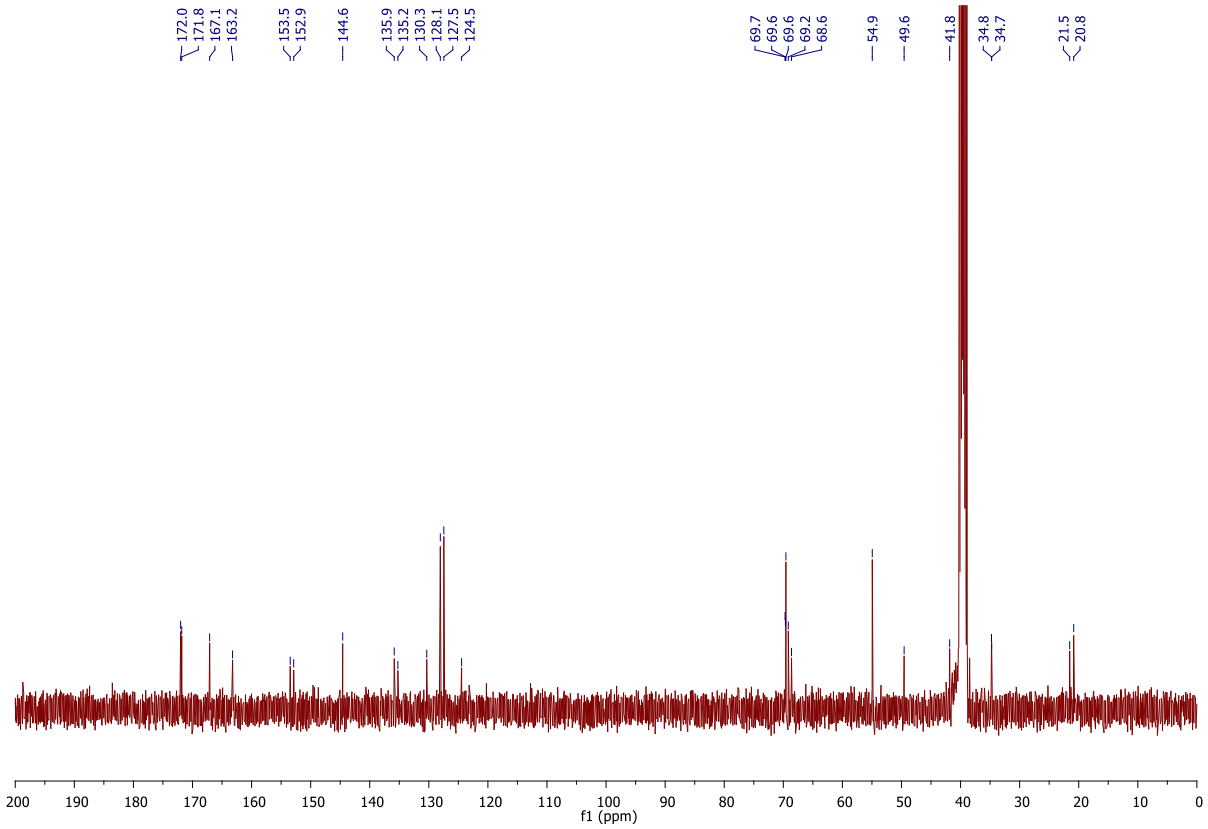
172.0
171.8
167.1
163.2
153.5
152.9
144.6
135.9
135.2
130.3
128.1
127.5
124.5
69.7
69.6
69.6
69.2
68.6
54.9
49.6
41.8
34.8
34.7
21.5
20.8
200 190 180 170 160 150 140 130 120 110 100 90 80 70 60 50 40 30 20 10 0
f1 (ppm)

N^1-(2-(2-(2-(2-(4-((2-(1-Azido-13-oxo-3,6,9-trioxa-12-azapentadecan-15-yl)-4,5-dibromo-3,6-dioxo-3,6-dihydropyridazin-1(2*H*)-yl)methyl)-1*H*-1,2,3-triazol-1-yl)ethoxy)ethoxy)ethoxy)ethyl)-N^5-(4-(6-methyl-1,2,4,5-tetrazin-3-yl)benzyl)glutaramide

213 – Procedure provided by Mr P. A. Szijj

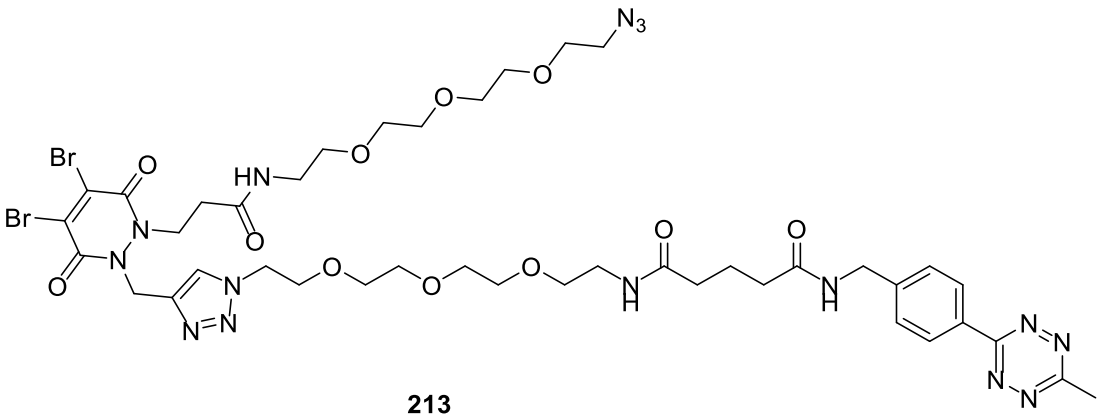

213

To a solution of 3-(4,5-dibromo-2-((1-(1-(4-(6-methyl-1,2,4,5-tetrazin-3-yl)phenyl)-3,7-dioxo-11,14,17-trioxa-2,8-diazanonadecan-19-yl)-1*H*-1,2,3-triazol-4-yl)methyl)-3,6-dioxo-3,6-dihydropyridazin-1(2*H*)-yl)propanoic acid **S10** (40 mg, 45 µmol) in CH_2Cl_2 (2.5 mL) was added HATU (28.1 mg, 74 µmol), and DIPEA (5.78 mg, 45 µmol) and the reaction stirred for 5 min at 21 °C. To this solution was added 2-(2-(2-(2-azidoethoxy)ethoxy)ethoxy)ethan-1-amine (14.6 mg, 67 µmol) in CH_2Cl_2 (2.5 mL), and the resulting mixture was stirred at 21 °C for a further 16 h. The reaction was diluted with EtOAc (10 mL) and washed with sat. aq. $NaHCO_3$ (3 × 10 mL), 1 M HCl (3 × 10 mL), water (10 mL), brine (10 mL), dried ($MgSO_4$), filtered and the solvent removed *in vacuo*. The crude residue was purified by flash column chromatography (0% to 10% MeOH/CH_2Cl_2) to afford N^1-(2-(2-(2-(2-(4-((2-(1-azido-13-oxo-3,6,9-trioxa-12-azapentadecan-15-yl)-4,5-dibromo-3,6-dioxo-3,6-dihydropyridazin-1(2*H*)-yl)methyl)-1*H*-1,2,3-triazol-1-yl)ethoxy)ethoxy)ethoxy)ethyl)-N^5-(4-(6-methyl-1,2,4,5-tetrazin-3-yl)benzyl)glutaramide **213** (16.7 mg, 15 µmol, 34%) as a purple solid: ^{1}H NMR (500 MHz, $CDCl_3$) δ 8.52 (d, *J* = 8.4 Hz, 2H), 7.84 (s, 1H), 7.50 (d, *J* = 8.5 Hz, 2H), 6.74 (br s, 1H), 6.65 (br s, 1H), 6.43 (br s, 1H), 4.65 (t, *J* = 6.8 Hz, 2H), 4.54 (d, *J* = 5.9 Hz, 2H), 4.50 (t, *J* = 4.9 Hz, 2H), 3.85 (t, *J* = 5.1 Hz, 2H), 3.68–3.51 (m, 24 H), 3.43–3.38 (m, 6H), 3.09 (s, 3H), 2.66 (t, *J* = 6.8 Hz, 2H), 2.35 (t, *J* = 7.1 Hz, 2H), 2.38 (t, *J* = 7.0 Hz, 2H), 2.01 (p, *J* = 7.0 Hz, 2 H); ^{13}C NMR (125 MHz, $CDCl_3$) δ 172.9 (C), 172.8 (C), 169.5 (C), 167.4 (C), 164.0 (C), 153.4 (C), 153.1 (C), 143.7 (C), 141.0 (C), 136.5 (C), 135.7 (C), 131.0 (C), 128.6 (CH), 128.3 (CH), 125.1

(CH), 70.8 (CH_2), 70.7 (CH_2), 70.7 (CH_2), 70.6 (CH_2), 70.6 (CH_2), 70.6 (CH_2), 70.4 (CH_2), 70.3 (CH_2), 70.1(CH_2), 69.9 (CH_2), 69.6 (CH_2), 69.3 (CH_2), 50.8 (CH_2), 50.5 (CH_2), 45.2 (CH_2), 43.3 (CH_2), 42.7 (CH_2), 39.5 (CH_2), 39.3 (CH_2), 35.5 (CH_2), 35.3 (CH_2), 34.0 (CH_2), 29.8 (CH_2), 22.0 (CH_2), 21.3 (CH_3). IR (thin film) 3306, 2919, 2101, 1722, 1634, 1543 cm^{-1}. HRMS (ESI) calcd for $C_{41}H_{58}Br_2N_{15}O_{11}$ $[M^{79}Br^{81}Br+H]^+$ 1096.2708; observed 1096.2782.

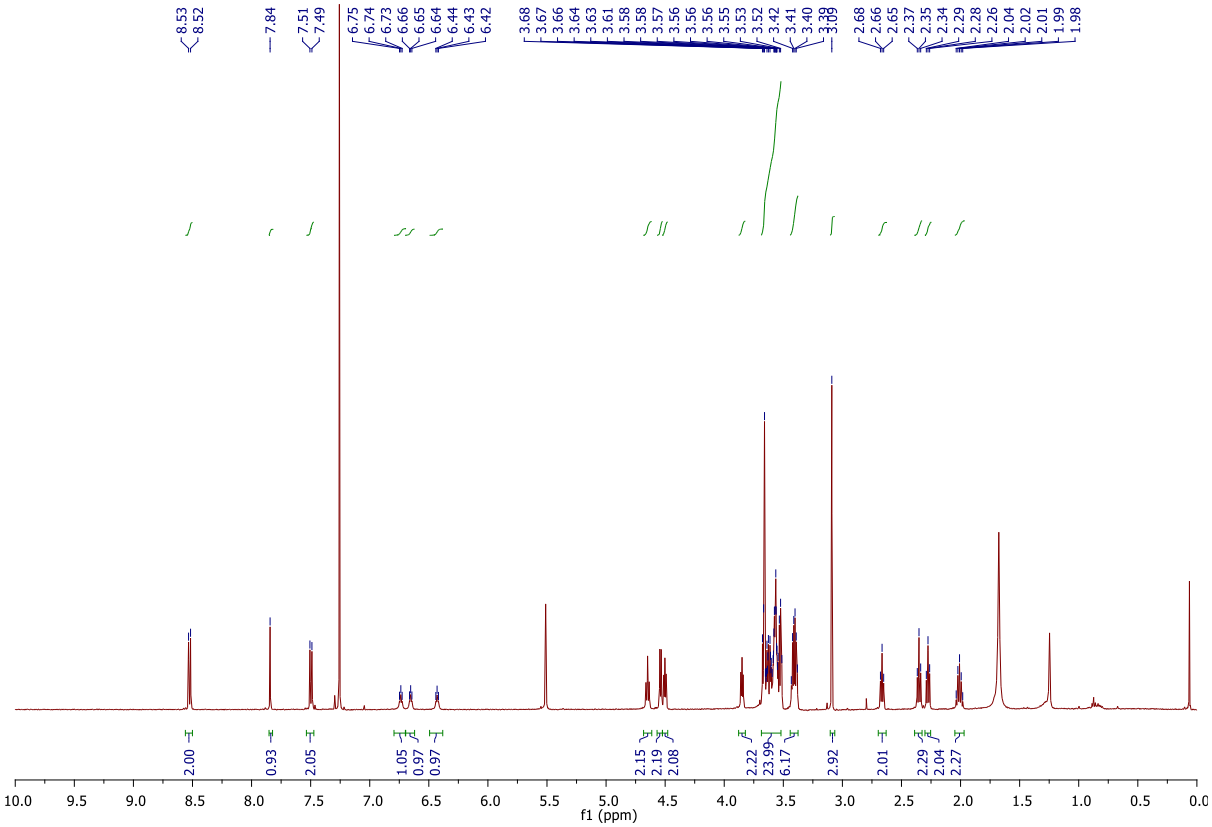

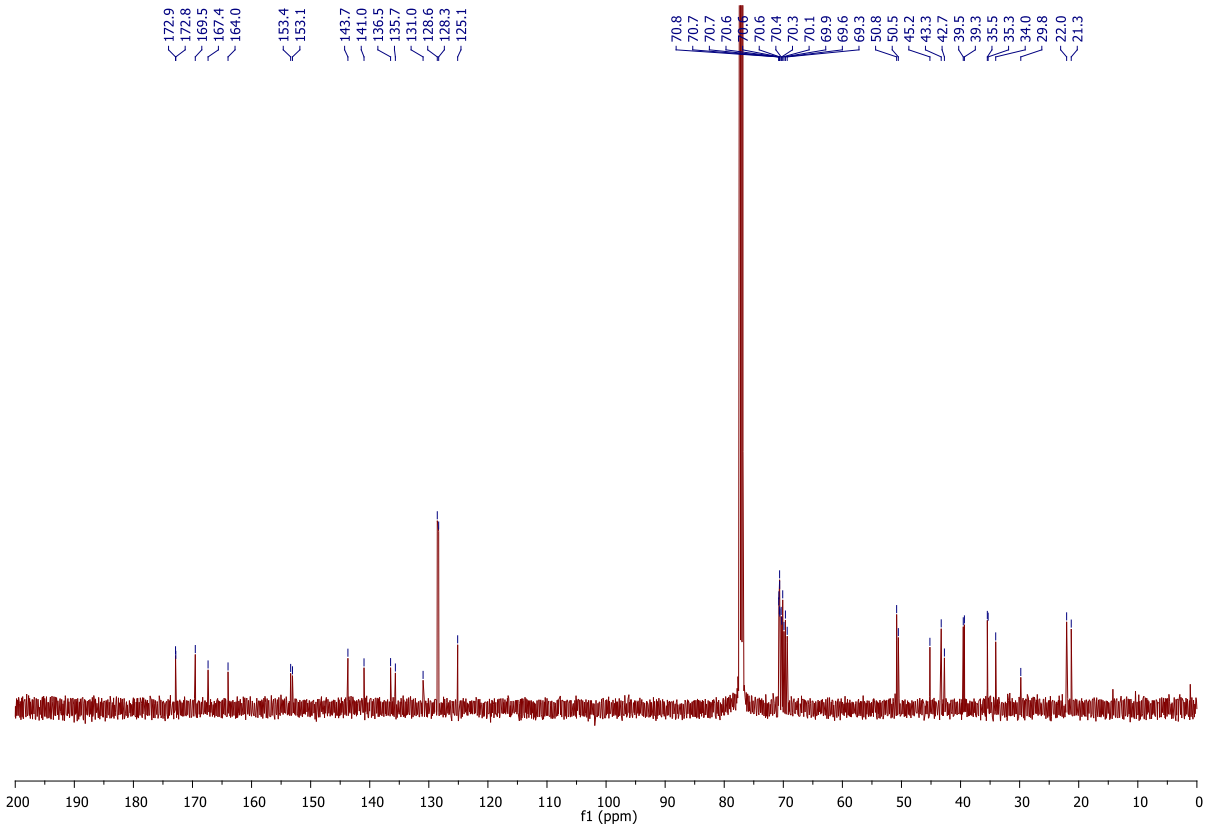
172.9
172.8
169.5
167.4
164.0
153.4
153.1
143.7
141.0
136.5
135.7
131.0
128.6
128.3
125.1
70.8
70.7
70.7
70.6
70.6
70.6
70.4
70.3
70.1
69.9
69.6
69.3
50.8
50.5
45.2
43.3
42.7
39.5
39.3
35.5
35.3
34.0
29.8
22.0
21.3
200
190
180
170
160
150
140
130
120
110
100
90
80
70
60
50
40
30
20
10
0
f1 (ppm)

2-(4-Hydroxyphenyl)isoindoline-1,3-dione S11[208] – Procedure provided by Mr A. Wall

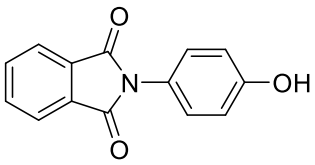

S11

p-Aminophenol (275 mg, 2.52 mmol) was added to phthalic anhydride (0.373 g, 2.52 mmol) dissolved AcOH (10 mL). The mixture was heated under reflux for 16 h. After cooling to room temperature, the precipitate was filtered and washed with MeOH (10 mL). The solvent was removed *in vacuo* to afford 2-(4-hydroxyphenyl)isoindoline-1,3-dione **S11** as a white solid (0.391 g, 1.64 mmol, 65%). ^{1}H NMR (600 MHz, DMSO-D_6); δ 9.75 (s, 1H), 7.95–7.93 (m, 2H), 7.90–7.88 (m, 2H), 7.21–7.20 (m, 2H), 6.88–6.86 (m, 2H); ^{13}C NMR (150 MHz, DMSO-D_6); δ 167.4 (C), 157.3 (C), 134.6 (CH), 131.6 (C), 128.8 (CH), 123.3 (CH), 122.9 (C), 115.4 (CH). IR (solid) 3412, 1787, 1712, cm^{-1}.

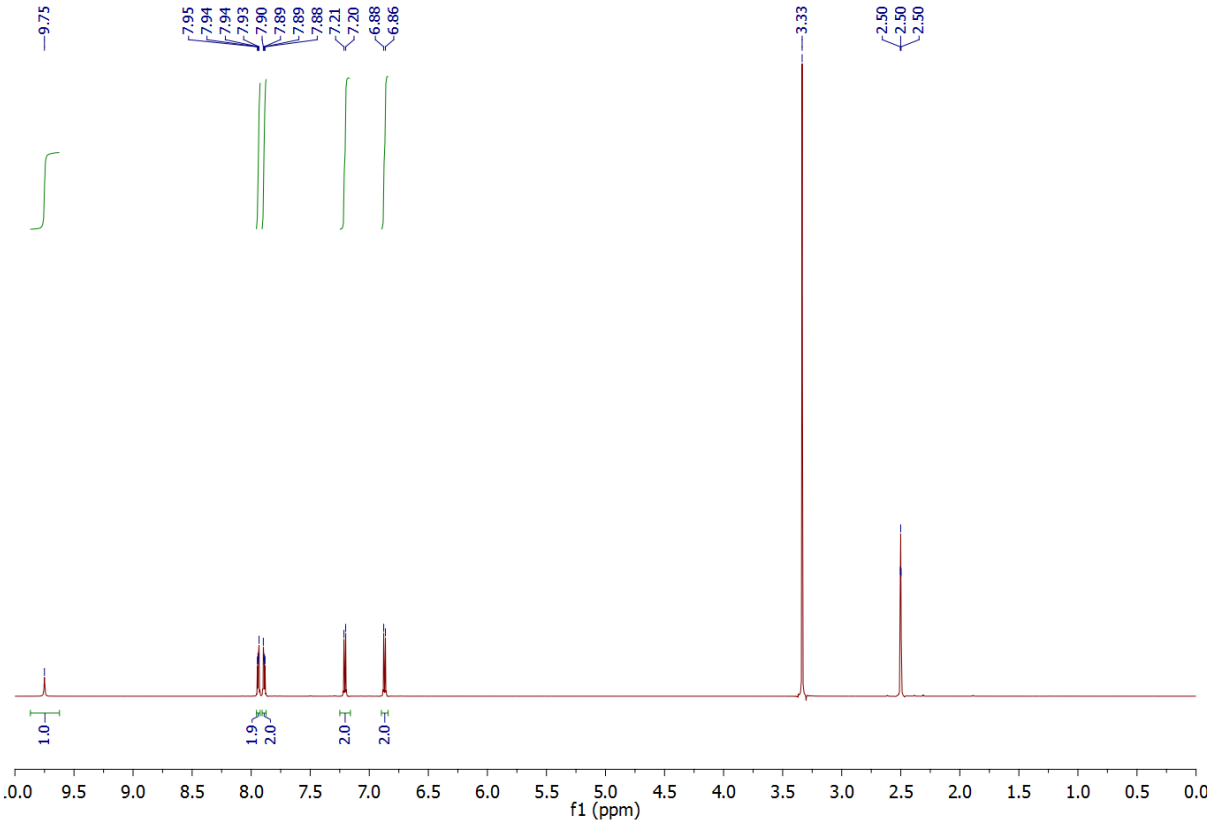

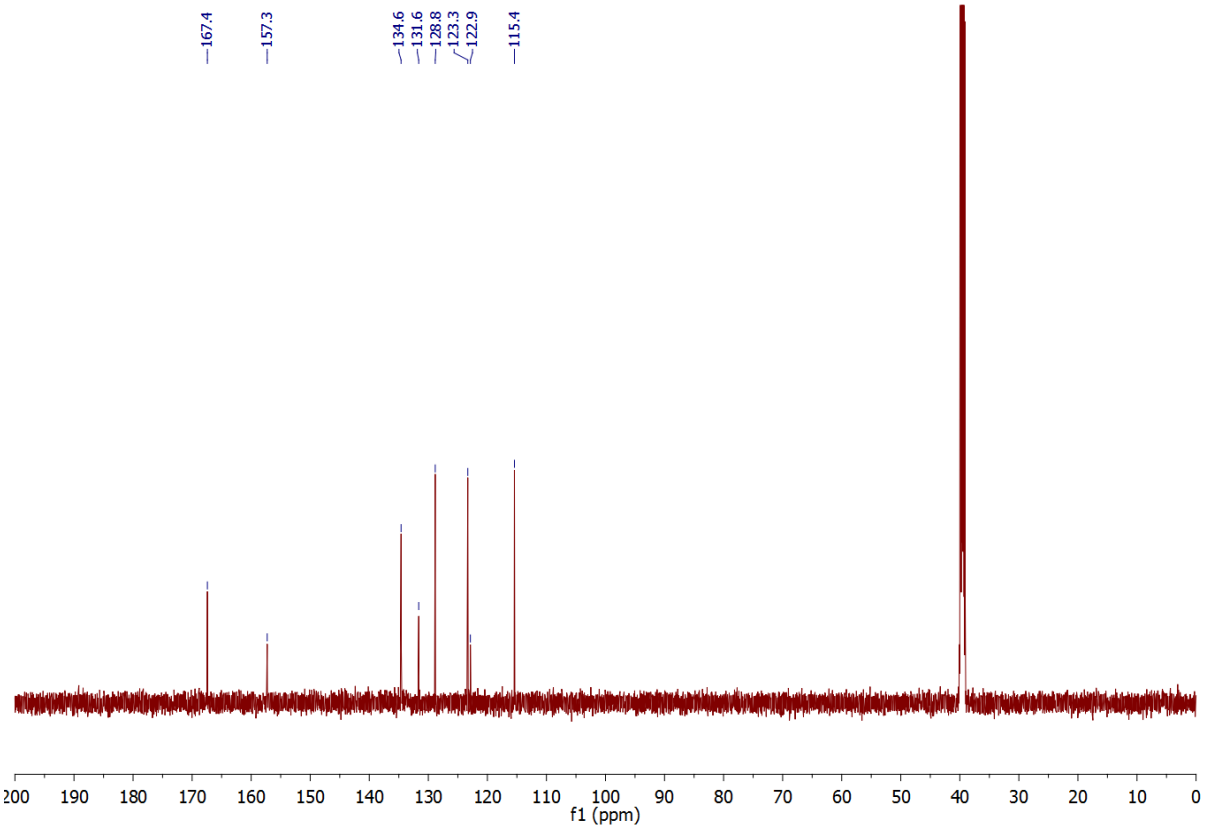
167.4
157.3
134.6
131.6
128.8
123.3
122.9
115.4
200 190 180 170 160 150 140 130 120 110 100 90 80 70 60 50 40 30 20 10 0
f1 (ppm)

((Oxybis(ethane-2,1-diyl))bis(oxy))bis(ethane-2,1-diyl) bis(4-methylbenzenesulfonate) S12[209] **– Procedure provided by Mr A. Wall**

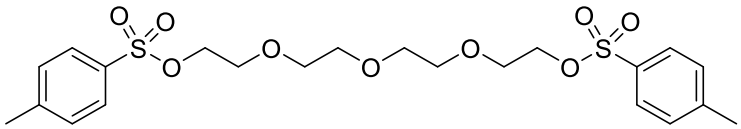

S12

To a stirred solution of tetra ethylene glycol (1.08 g, 5.56 mmol) in pyridine (3.6 mL) at 0 °C was added dropwise over 30 min tosyl chloride (2.33 g, 12.23 mmol, pre-dissolved in CH_2Cl_2 (5 mL)). The mixture was stirred for 6 h at 0 °C. Ice water (30 mL) was added to the reaction mixture and crude product extracted with EtOAc (3 x 30 mL). The organic layer was washed with HCl (2 M, 2 × 13 mL). The organic layer was then dried ($MgSO_4$), filtered and the solvent removed *in vacuo* to afford ((oxybis(ethane-2,1-diyl))bis(oxy))bis(ethane-2,1-diyl) bis(4-methylbenzenesulfonate) **S12** as a colourless oil (1.74 g, 3.45 mmol, 62%). ^{1}H NMR (600 MHz, $CDCl_3$) δ 7.80–7.78 (m, 4H), 7.34–7.33 (m, 4H), 4.16–4.14 (m, 4H), 3.68–3.67 (m, 4H), 3.58–3.54 (m, 8H), 2.44 (s, 6H); ^{13}C NMR (150 MHz, $CDCl_3$) δ 145.0 (C), 133.0 (C), 130.0 (CH), 128.1 (CH), 70.9 (CH_2), 70.7 (CH_2), 69.4 (CH_2), 68.8 (CH_2), 21.8 (CH_3). IR (thin film); 2913, 2870, 1550.

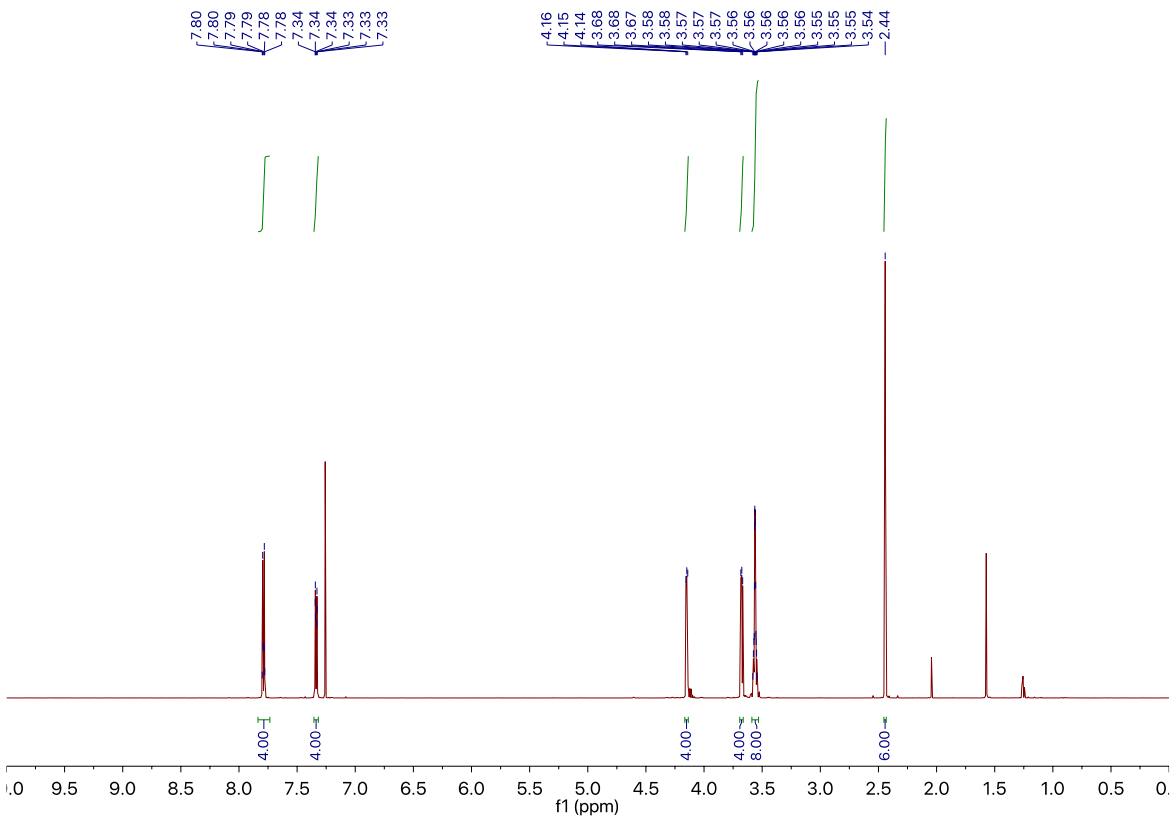
7.80
7.80
7.79
7.79
7.78
7.78
7.34
7.34
7.33
7.33
7.33
4.16
4.15
4.14
3.68
3.68
3.67
3.58
3.58
3.57
3.57
3.57
3.56
3.56
3.56
3.56
3.56
3.55
3.55
3.54
2.44
4.00
4.00
4.00
4.00
8.00
6.00
f1 (ppm)

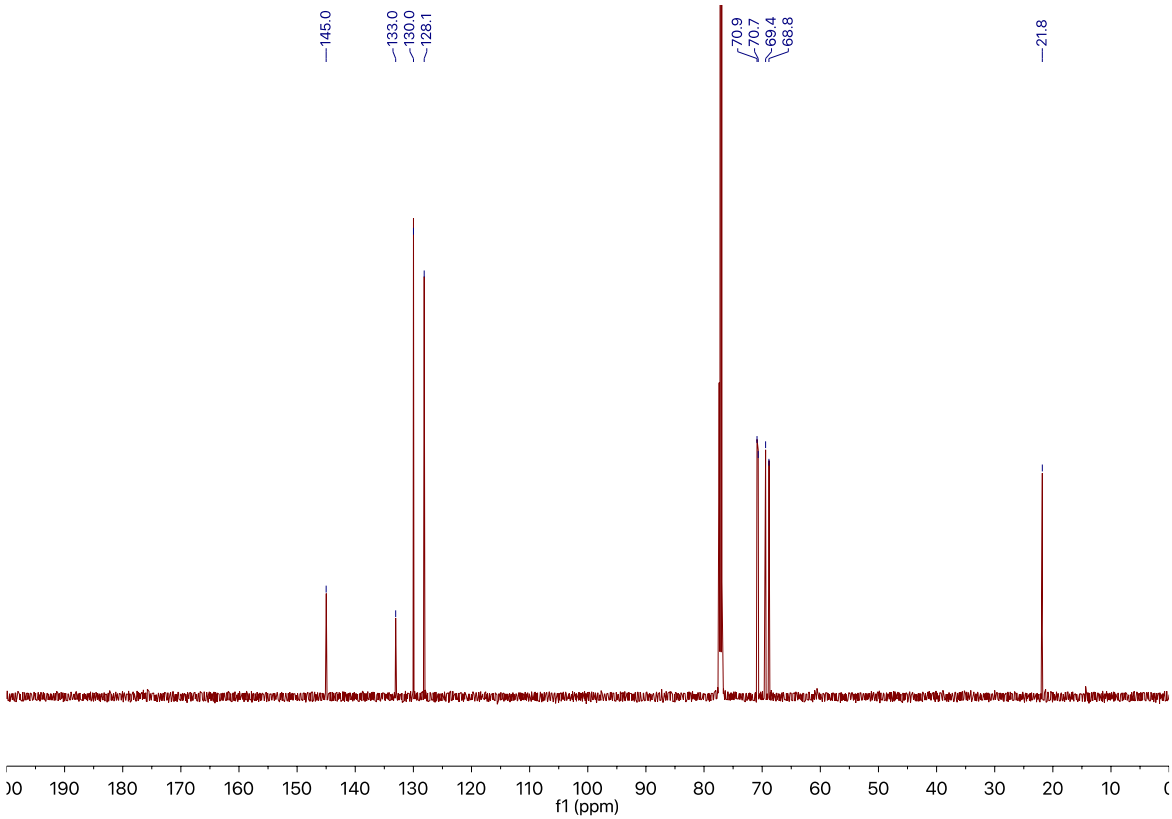
145.0
133.0
130.0
128.1
70.9
70.7
69.4
68.8
21.8
f1 (ppm)

2-(2-(2-(2-Azidoethoxy)ethoxy)ethoxy)ethyl 4-methylbenzenesulfonate S13[210] **– Procedure provided by Mr A. Wall**

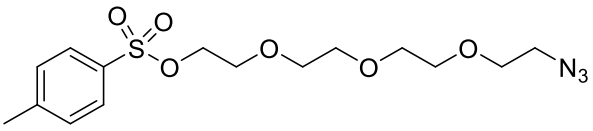

S13

To a solution of ((oxybis(ethane-2,1-diyl))bis(oxy))bis(ethane-2,1-diyl) bis(4-methylbenzenesulfonate) **S12** (0.24 g, 0.48 mmol) in ethanol (5 mL) was added sodium azide (0.033 g, 0.51 mmol). The resulting solution was heated at 80 ^{o}C for 16 h. The reaction was then poured into ice water (15 mL) and the product was extracted with ethyl acetate (3 x 15 mL). The organic extracts were washed with water (15 mL), brine (15 mL) and dried ($MgSO_4$), the resulting mixture was filtered and the solvent removed *in vacuo.* The crude residue was purified by flash column chromatography (25% to 80% EtOAc/petrol) to afford 2-(2-(2-(2-azidoethoxy)ethoxy)ethoxy)ethyl 4-methylbenzenesulfonate **S13** as a light brown oil (0.062 g, 0.168 mmol, 35%). ^{1}H NMR (600 MHz, $CDCl_3$) δ 7.79–7.77 (m, 2H), 7.33–7.32 (m, 2H), 4.15– 4.13 (m, 2H), 3.66–3.57 (m, 12H), 3.34 (t, *J* = 5.3 Hz, 2H), 2.41 (s, 3H, CH_3); ^{13}C NMR (150 MHz, $CDCl_3$) δ 144.9 (C), 133.1 (C), 129.9 (CH), 128.1 (CH), 70.9 (CH_2), 70.8 (CH_2), 70.8 (CH_2), 70.7 (CH_2), 70.1 (CH_2), 69.4 (CH_2), 68.8 (CH_2), 50.8 (CH_2), 21.8 (CH_3); IR (thin film); 2100, 2869 cm^{-1}.

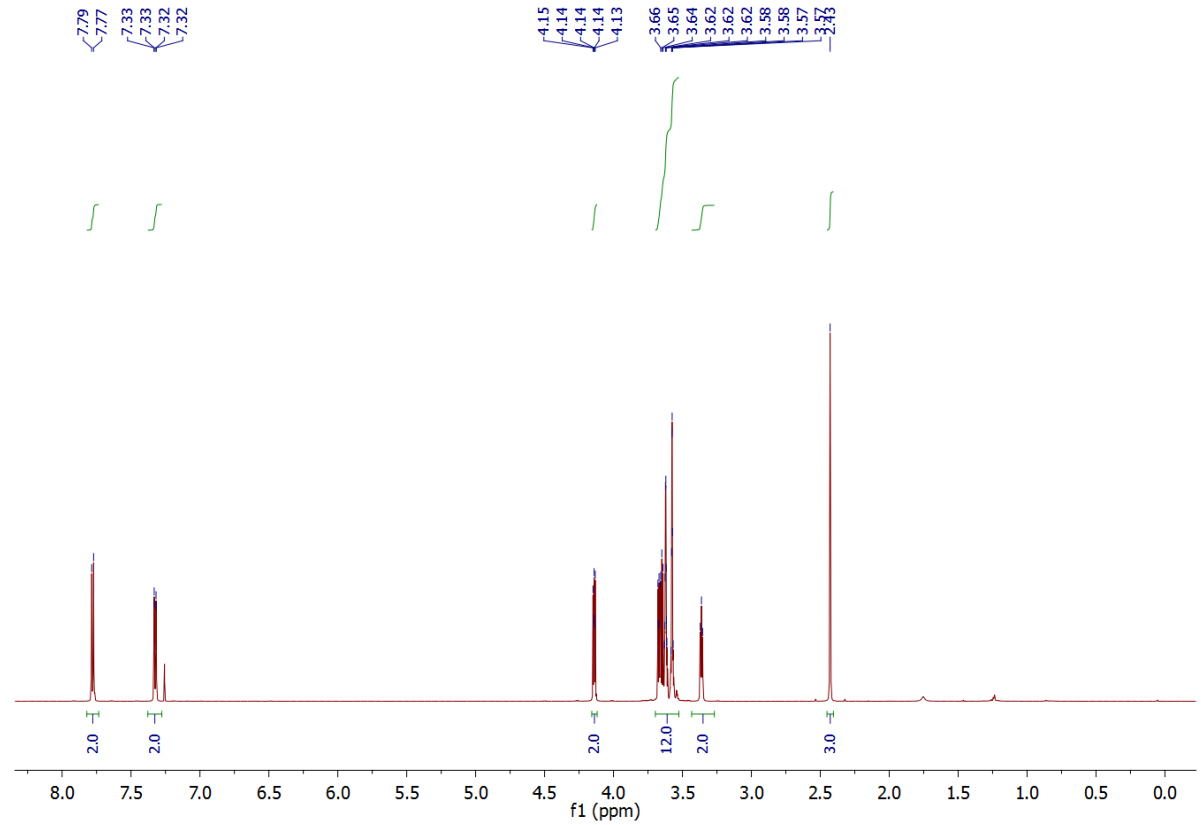
7.79
7.77
7.33
7.33
7.32
7.32
4.15
4.14
4.14
4.14
4.13
3.66
3.65
3.64
3.62
3.62
3.58
3.58
3.57
3.57
2.43
2.0
2.0
2.0
12.0
2.0
3.0
f1 (ppm)

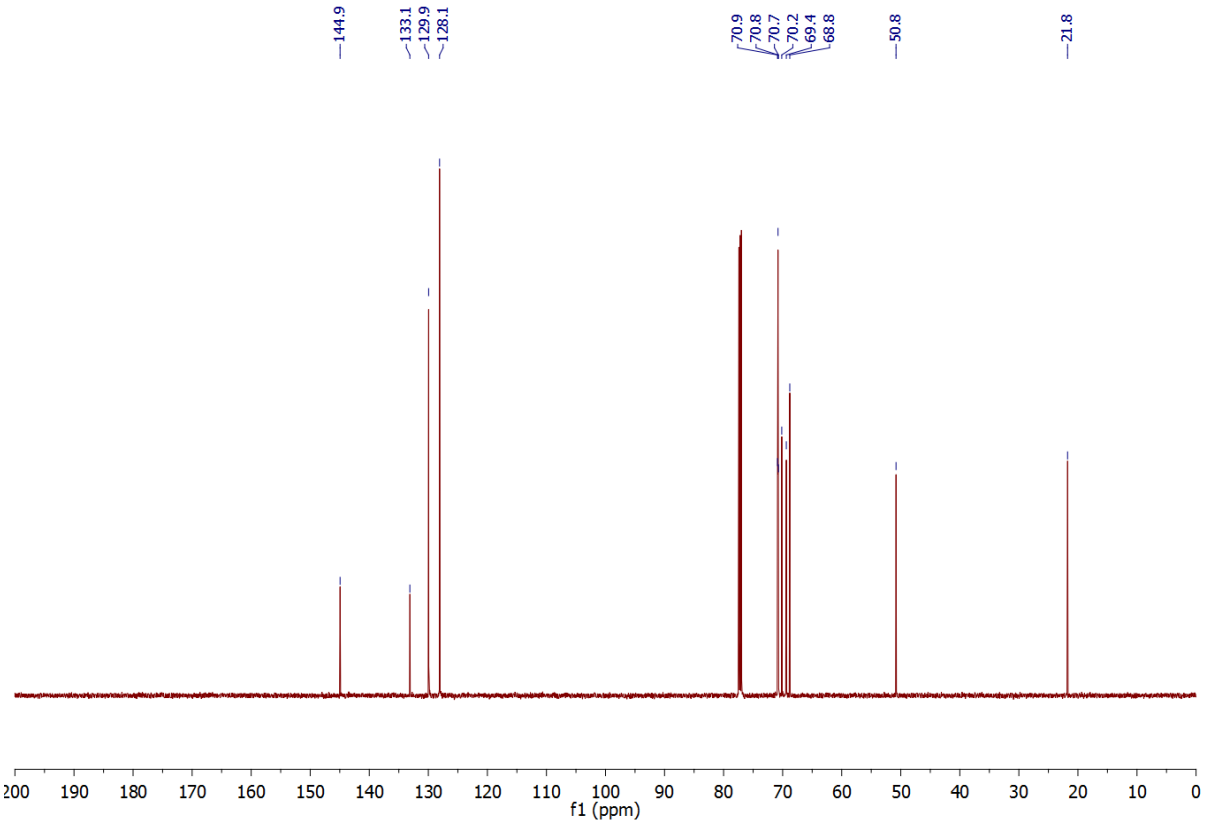
144.9
133.1
129.9
128.1
70.9
70.8
70.7
70.2
69.4
68.8
50.8
21.8
f1 (ppm)

2-(4-(2-(2-(2-(2-Azidoethoxy)ethoxy)ethoxy)ethoxy)phenyl)isoindoline-1,3-dione S14 – Procedure provided by Mr A. Wall

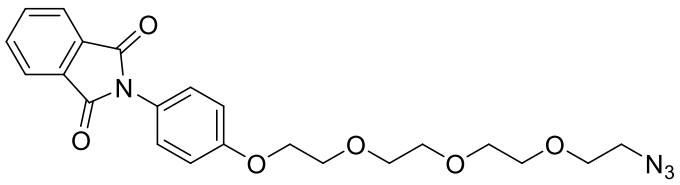

S14

To solution of potassium *tert*-butoxide (725 µL, 1M in THF) in DMF (20 mL), was added 2-(4-hydroxyphenyl)isoindoline-1,3-dione **S11** (189 mg, 0.79 mmol) and the reaction was stirred at 21 °C for 5 min. 2-(2-(2-(2-Azidoethoxy)ethoxy)ethoxy)ethyl 4-methylbenzenesulfonate **S13** (245 mg, 0.66 mmol) was then added, and the reaction mixture was stirred at 90 °C for 16 h. The reaction was diluted with water (100 mL), and the crude product was extracted with EtOAc (3 × 30 mL). The organic extracts were combined and washed with saturated lithium chloride solution (2 × 30 mL) and then dried ($MgSO_4$). The solvent was *in vacuo* and the crude residue was purified by flash column chromatography (25% to 80% EtOAc/petrol) to afford 2-(4-(2-(2-(2-(2-azidoethoxy)ethoxy)ethoxy)ethoxy)phenyl)isoindoline-1,3-dione **S14** as a clear yellow oil (202 mg, 0.46 mmol, 70%). ^{1}H NMR (600 MHz, $CDCl_3$) δ 7.89–7.88 (m, 2H), 7.74–7.69 (m, 2H), 7.30–7.28 (m, 2H), 7.00–6.99 (m, 2H), 4.14–4.13 (m, 2H), 3.86–3.82 (m, 2H), 3.72–3.69 (m, 2H), 3.64–3.61 (m, 8H), 3.35–3.33 (m, 2H); ^{13}C NMR (150 MHz, $CDCl_3$) δ 167.6 (C), 158.6 (C), 134.4 (CH), 131.9 (C), 128.0 (CH), 124.6 (C), 123.7 (CH), 115.2 (CH), 71.0 (CH_2), 70.8 (CH_2), 70.8 (CH_2), 70.8 (CH_2), 70.1 (CH_2), 69.7 (CH_2), 67.8 (CH_2), 50.8 (CH_2); IR (thin film): 2864, 2112, 1704 cm^{-1}; LRMS (ESI) 441 (100, $[M+H]^+$); HRMS (ES^+) calcd for $C_{22}H_{25}N_4O_6$ $[M+H]^+$ 441.1747, observed 441.1762.

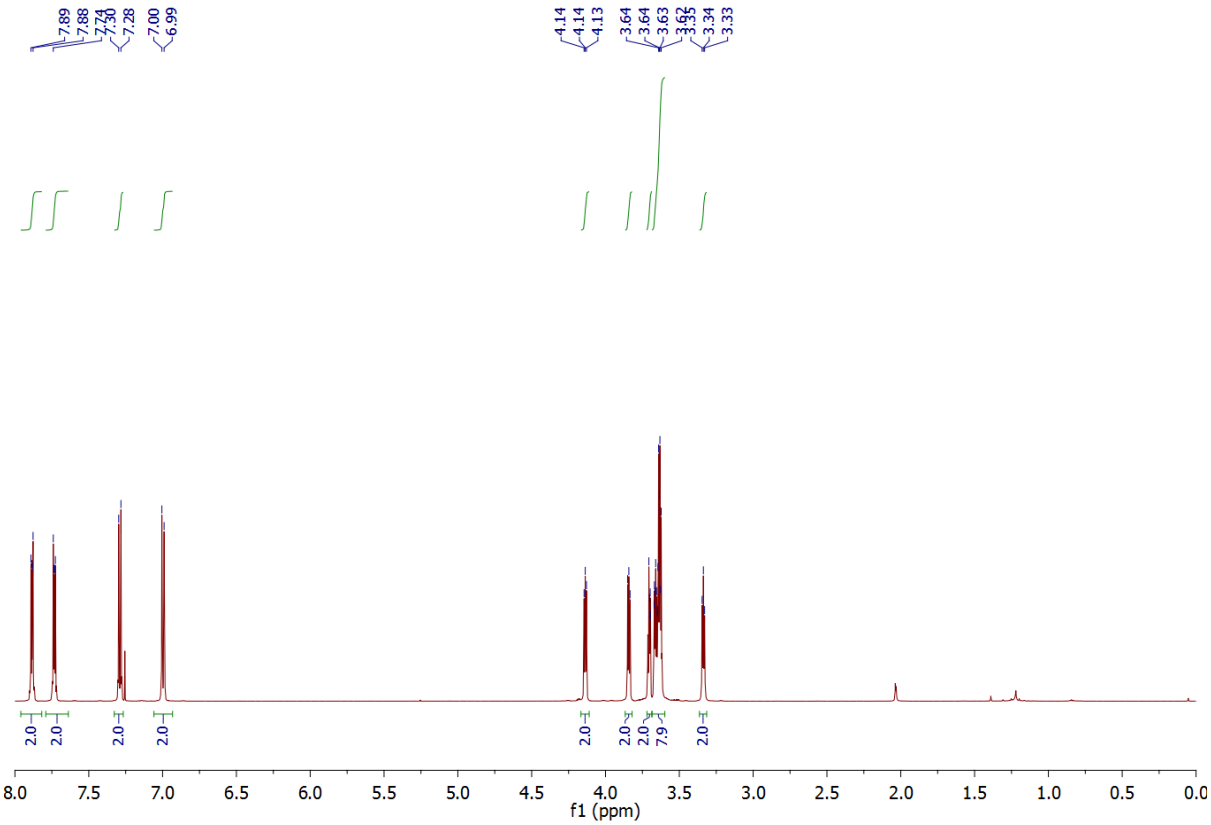
7.89
7.88
7.74
7.30
7.28
7.00
6.99
4.14
4.14
4.13
3.64
3.64
3.63
3.62
3.35
3.34
3.33
2.0
2.0
2.0
2.0
2.0
2.0
2.0
7.9
2.0
f1 (ppm)

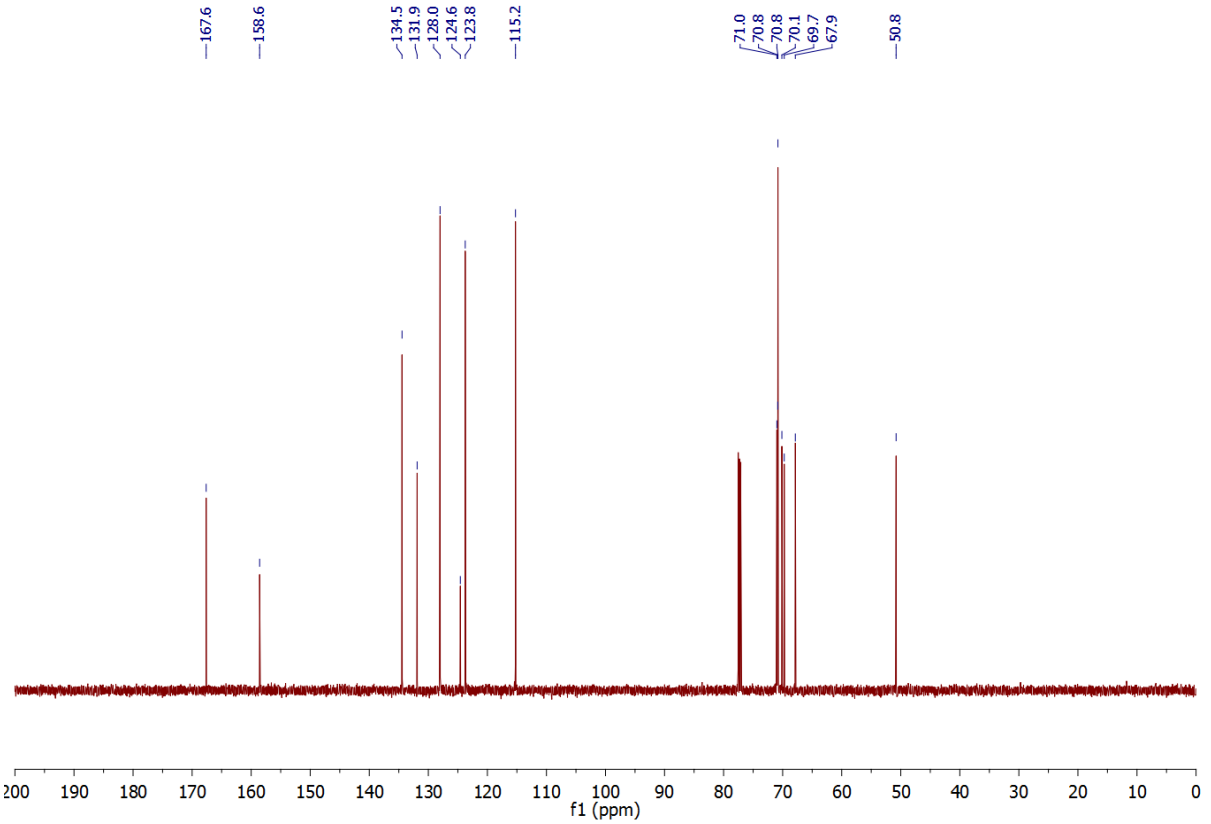
167.6
158.6
134.5
131.9
128.0
124.6
123.8
115.2
71.0
70.8
70.8
70.1
69.7
67.9
50.8
f1 (ppm)

4-(2-(2-(2-(2-Azidoethoxy)ethoxy)ethoxy)ethoxy)aniline 220 – Procedure provided by Mr A. Wall

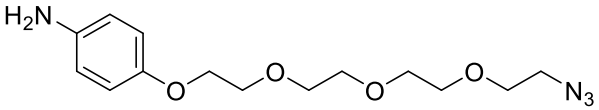

220

To 2-(4-(2-(2-(2-(2-azidoethoxy)ethoxy)ethoxy)ethoxy)phenyl)isoindoline-1,3-dione **S14** (141 mg, 0.32 mmol) in THF (10 mL) was added hydrazine monohydrate (330 µL, 60% solution). The reaction was then stirred for 2 h at 21 °C. The reaction mixture was diluted with water (30 mL) and the product was extracted with EtOAc (3 × 30 mL), washed with brine (20 mL), and dried ($MgSO_4$). The solvent was removed *in vacuo* and the crude residue was purified by flash column chromatography (20% to 100% EtOAc/petrol) to afford 4-(2-(2-(2-(2-azidoethoxy)ethoxy)ethoxy)ethoxy)aniline **220** as a brown oil (73 mg, 0.23 mmol, 73%).^{1}H NMR (600 MHz, $CDCl_3$) δ 6.74–6.73 (m, 2H), 6.62–6.60 (m, 2H), 4.06– 4.03 (m, 2H), 3.80–3.79 (m, 2H), 3.70–3.69 (m, 2H), 3.69–3.64 (m, 8H), 3.43 (s, 2H), 3.36 (t, *J* = 5.1 Hz, 2H); ^{13}C NMR (150 MHz, $CDCl_3$) δ 152.0 (C), 140.4 (C), 116.4 (CH), 116.0 (CH), 70.9 (CH_2), 70.8 (CH_2), 70.8 (CH_2), 70.8 (CH_2), 70.1 (CH_2), 70.0 (CH_2), 50.8 (CH_2); IR (thin film); 3430, 3356, 2869, 2098 cm^{-1}; LRMS (ESI) 311 (100, $[M+H]^+$); HRMS (ES^+) calcd for $C_{14}H_{22}N_4O_4$ $[M+H]^+$ 311.1733, observed 311.1719.

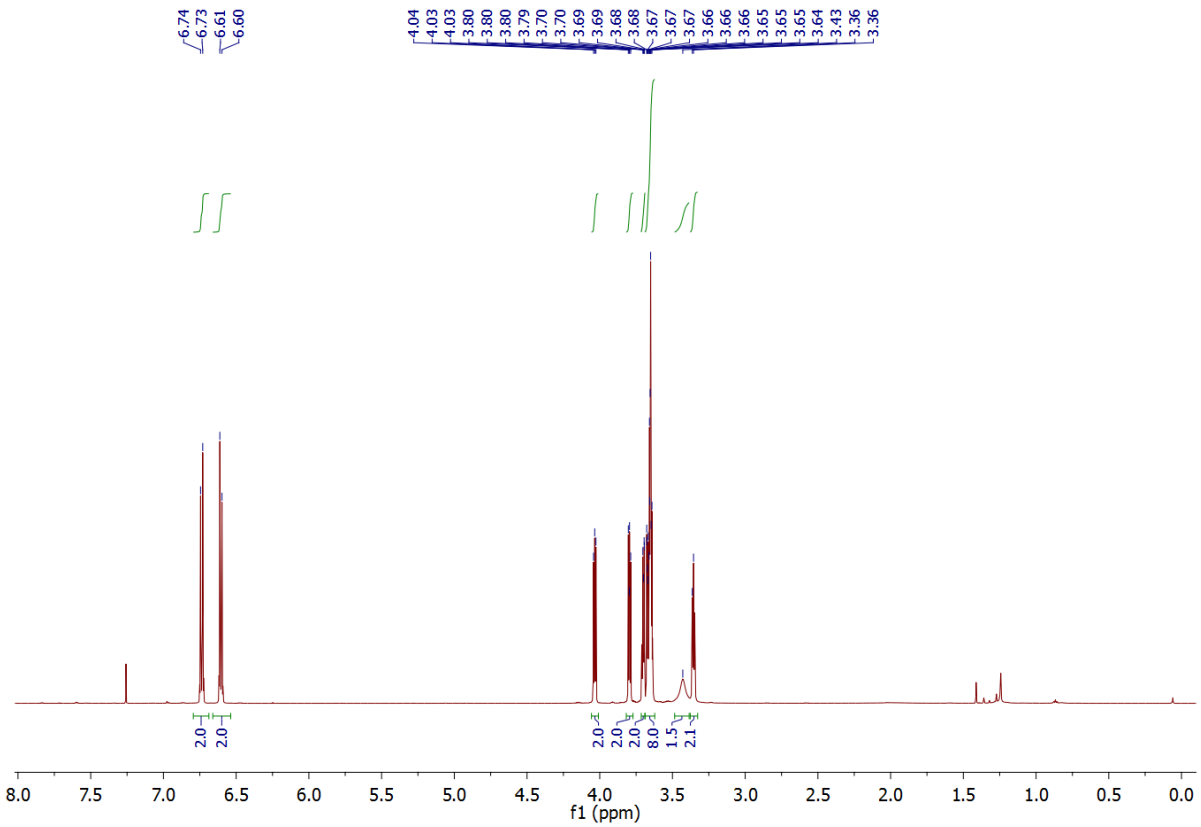
6.74
6.73
6.61
6.60
4.04
4.03
4.03
3.80
3.80
3.80
3.79
3.70
3.70
3.69
3.69
3.68
3.68
3.67
3.67
3.67
3.66
3.66
3.66
3.65
3.65
3.65
3.64
3.43
3.36
3.36
2.0
2.0
2.0
2.0
2.0
8.0
1.5
2.1
8.0
7.5
7.0
6.5
6.0
5.5
5.0
4.5
4.0
3.5
3.0
2.5
2.0
1.5
1.0
0.5
0.0
f1 (ppm)

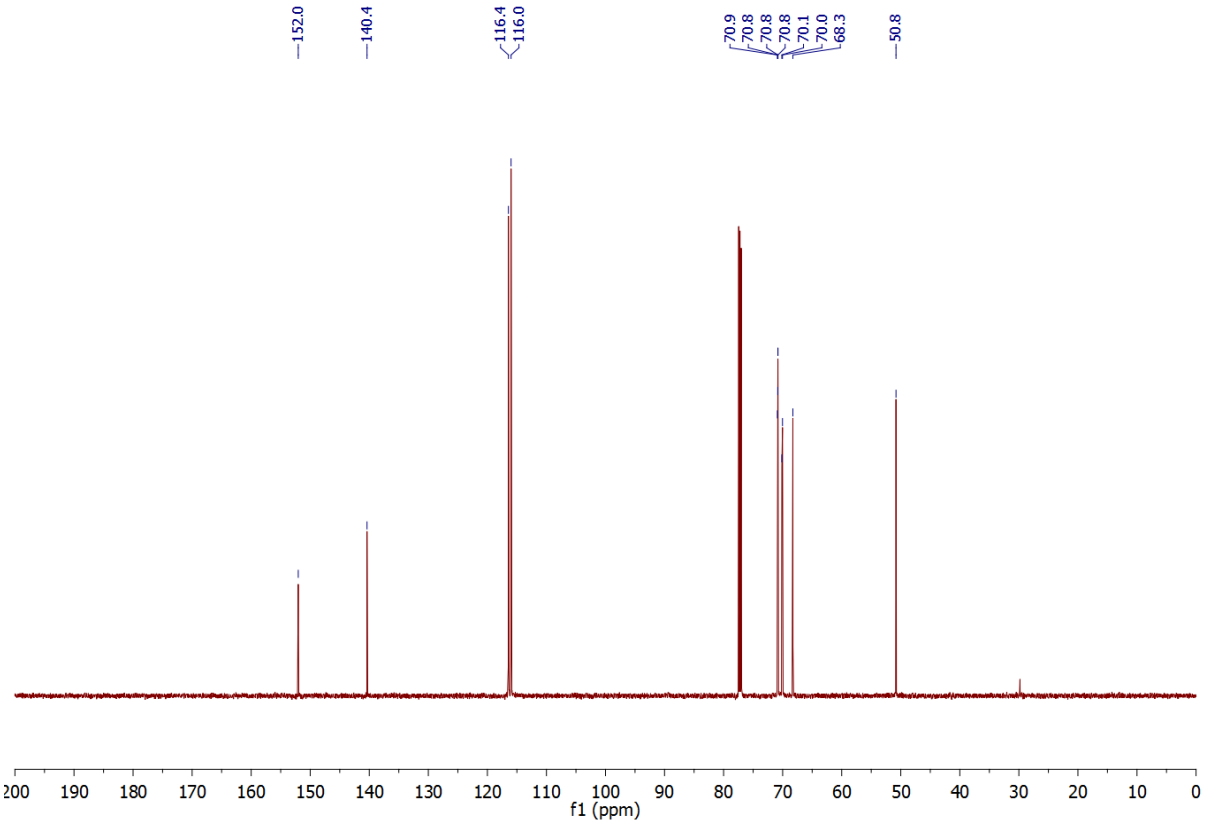
152.0
140.4
116.4
116.0
70.9
70.8
70.8
70.8
70.1
70.0
68.3
50.8
200
190
180
170
160
150
140
130
120
110
100
90
80
70
60
50
40
30
20
10
0
f1 (ppm)

Chemical Biology

Solid Phase Peptide Synthesis (SPPS) (FEKGC peptide 218) – Procedure provided by Dr R. J. Spears

Peptides were synthesised *via* manual solid phase peptide synthesis (SPPS) using an *in situ* neutralisation/HCTU activation procedure for Fmoc chemistry on an H-Cys(Trt)-2-ClTrt resin (Sigma) using Fmoc protected amino acids as described below:

Preloaded resin preparation: The preloaded 2-chlorotrityl resin was weighed out into a 5 mL SPPS cartridge fitted with a Polytetrafluoroethylene (PTFE) stopcock, swollen in DMF for 30 min and then filtered.

Amino acid coupling: DIPEA (11.0 eq.) was added to a solution of amino acid (5.0 eq.) and HCTU (5.0 eq.) dissolved in the minimum volume of DMF and the solution added to the resin. The reaction mixture was gently agitated by rotation for 1 h, and the resin filtered off and washed with DMF (3 × 2 min with rotation).

Fmoc deprotection: A solution of 20% piperidine in DMF was added to the resin and gently agitated by rotation for 2 minutes. The resin was filtered off and repeated four more times, followed by washes with DMF (5 × 2 min with rotation).

Cleavage and Isolation: Resins containing full synthesised peptides were washed with DCM (3 × 2 min with rotation) and MeOH (3 × 2 min with rotation). The resin was dried on a vacuum manifold and further dried on a high vacuum line overnight. A solution of cleavage cocktail 95:2.5:2.5 (v/v) TFA:H_2O:triisopropylsilane was then added to the resin, and the resulting mixture was gently agitated by rotation for 60 min. The reaction mixture was drained into ice-cold Et_2O and centrifuged at 6000 rpm at 4 °C until pelleted (*ca*. 5-10 min). The supernatant was carefully decanted and subsequently resuspended, centrifuged and supernatant decanted three more times. The precipitated peptide pellet was then either dissolved 10% MeCN or in 10% aq. AcOH and lyophilised. Lyophilised peptides were then stored at -20 ^oC until required.

Observed masses (LCMS Method 1): 583 Da

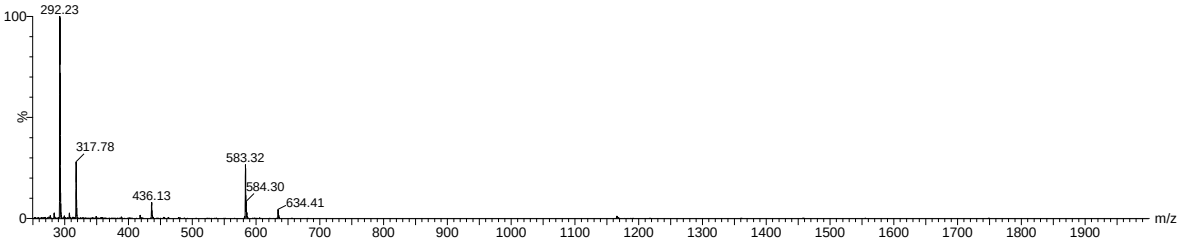

Cysteine Mutant Green Fluorescent Protein (GFPS147C) 48[211]

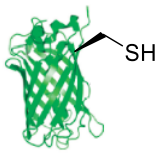

48

GFPS147C 48 was expressed in competent *E. coli* BL21(DE3) cells as described previously.[211] The two step purification (His-Tag and SEC) were carried out as follows:

The cell pellets were re-suspended in 30ml binding buffer (100mM Sodium Phosphate, 25mM imidazole, pH 8) and stored overnight at -20 °C. Cells were lysed in the presence of two tablets of a cocktail of EDTA-free Complete Protease Inhibitors (Roche) by sonication on ice, for 6 x 30 sec bursts with 1 min cooling intervals using a stud probe on the Sonicator 400 at amplitude 10. The resultant cell lysate was centrifuged at 35,000g for 30min at 4 °C and the supernatant 0.22 µm syringe filtered before loading onto a 5 mL HisTrap HP column (GE Healthcare) equilibrated in binding buffer. Bound material was eluted with a 25-500 mM imidazole gradient and fractions analysed by SDS-PAGE for pooling.

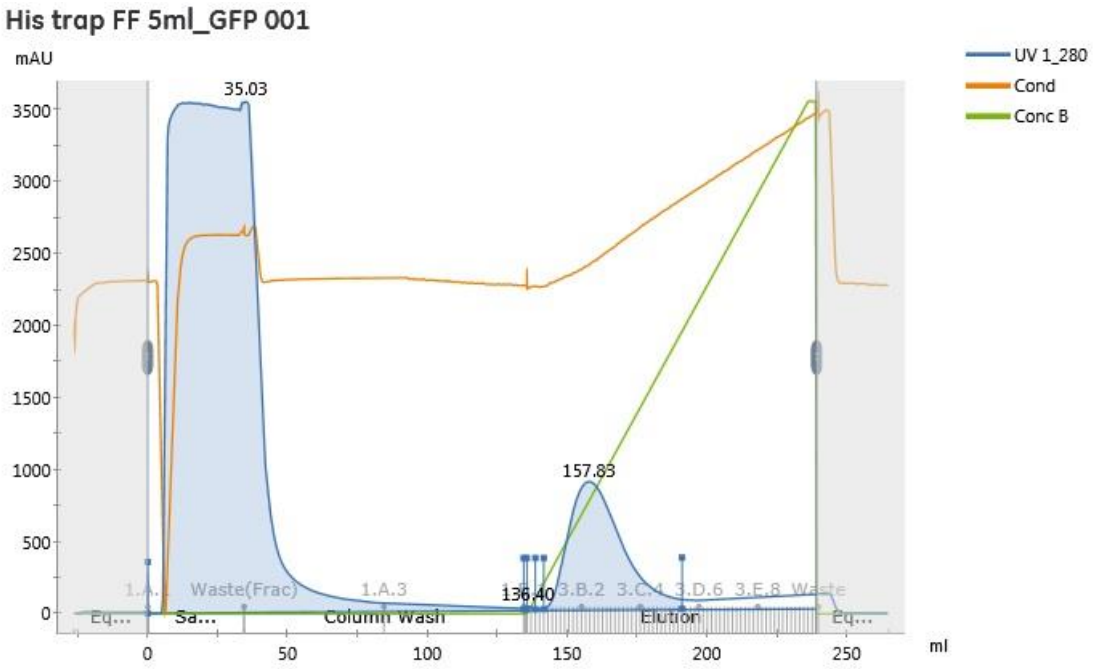

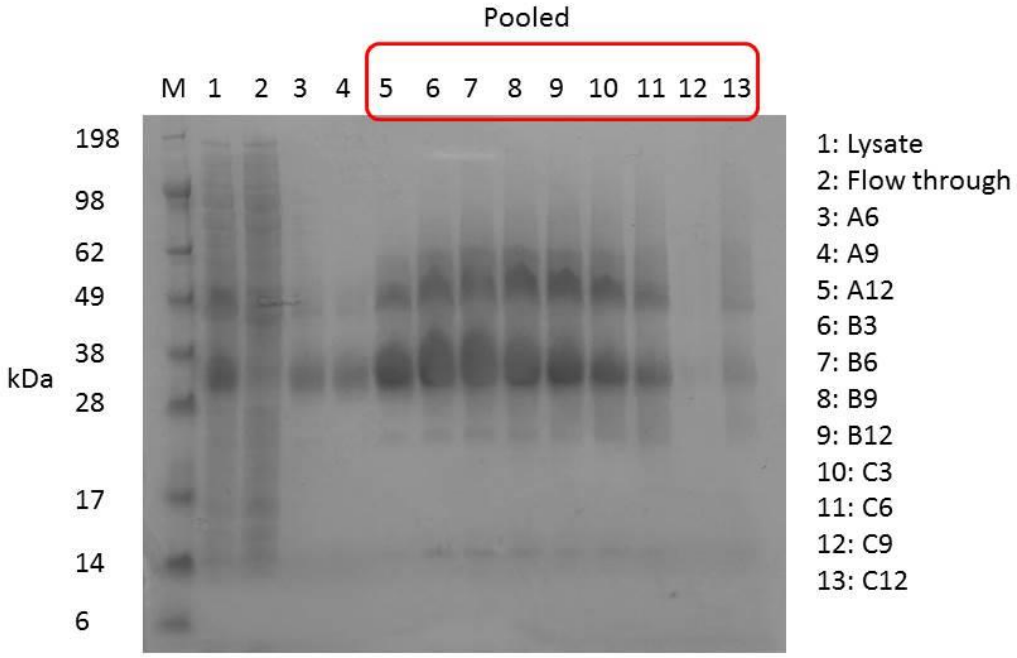

The buffer was exchanged by dialysis at 4 °C into 100mM Sodium Phosphate, pH 7.4 using MWCO 12,000-14,000 porous membrane tubing (Spectra/Por). Sample was loaded onto a Superdex 75 10/300 column (GE Healthcare) equilibrated in 100mM Sodium Phosphate, pH 7.4 and eluted fractions pooled appropriately as indicated by SDS-PAGE. Formation of the correct product was confirmed by electrospray mass spectrometry.

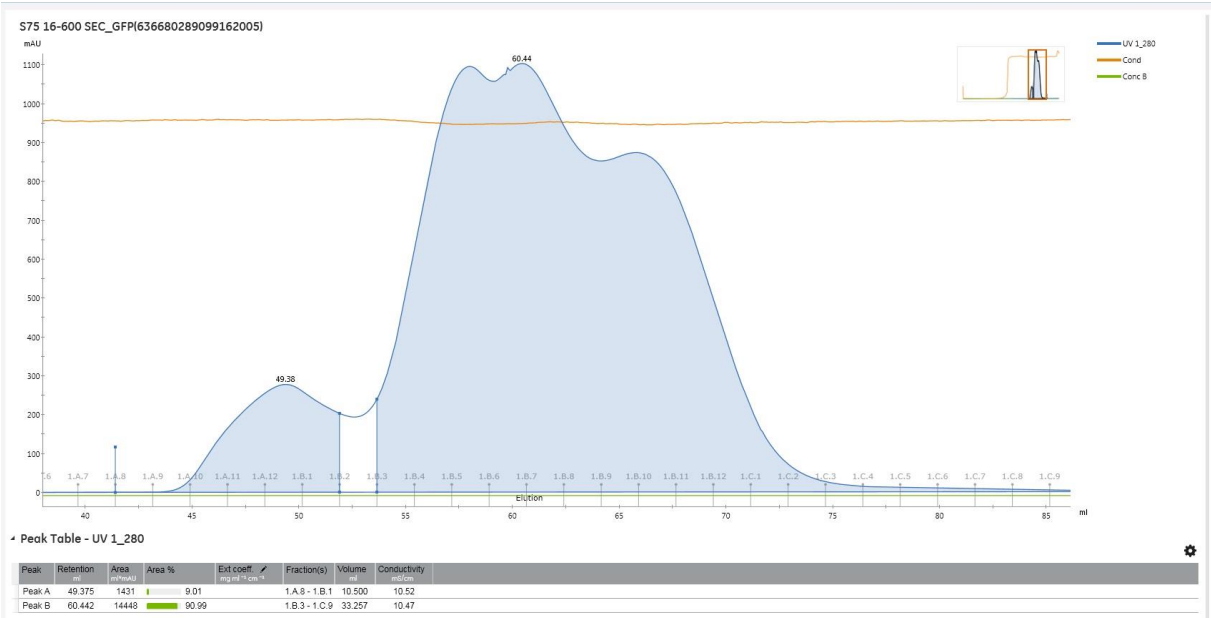

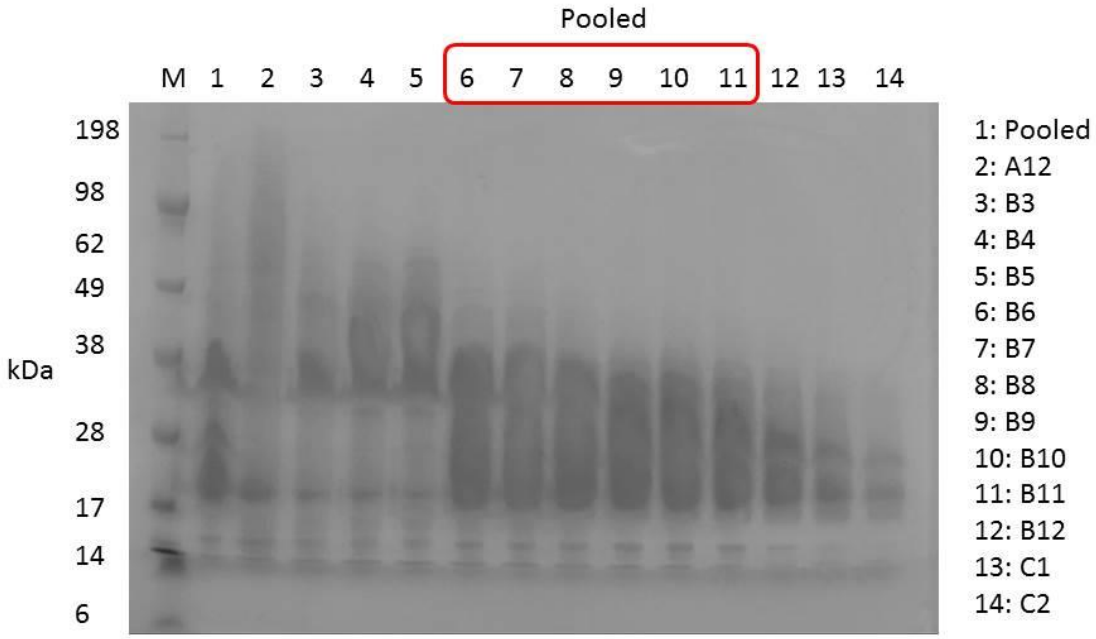

Due to the presence of a small amount of dimer species, GFPS147C **48** was then reduced prior to conjugation and characterised as below:

TCEP (31.3 µL, 20 mM in deionised water, 25 eq.) was added to a solution of GFPS147C **48** (500 µL, 50 µM) in PBS (pH 7.4, 5 mM EDTA) and the solution was incubated at 37 °C for 90 min. Excess reagents were removed by ultrafiltration (6 × 10000 MWCO, VivaSpin®, GE Healthcare) into PBS (pH 7.4, 5 mM EDTA) for further experiments. Samples were desalted (7000 MWCO, ZebaSpin®, Thermo Scientific) prior to LCMS analysis. Concentration was determined photometrically using ε_{280} = 20,500 $M^{-1}\,cm^{-1}$. Observed masses (LCMS Method 1): 29355 Da, 29538 Da.

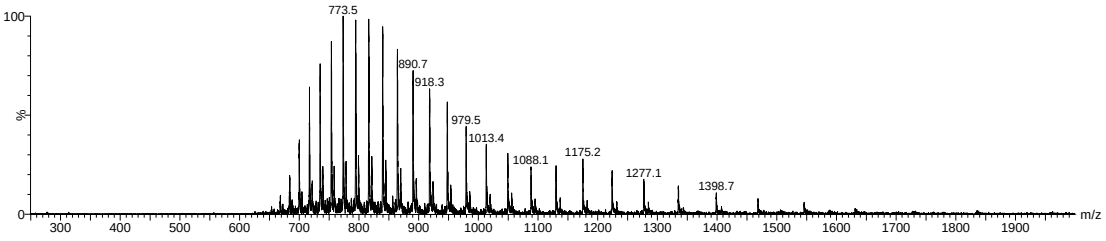

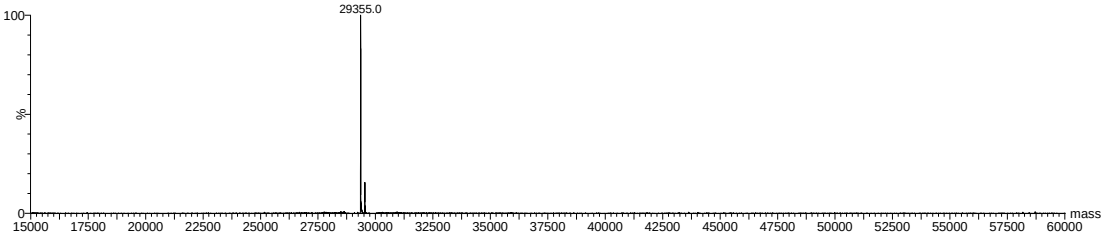

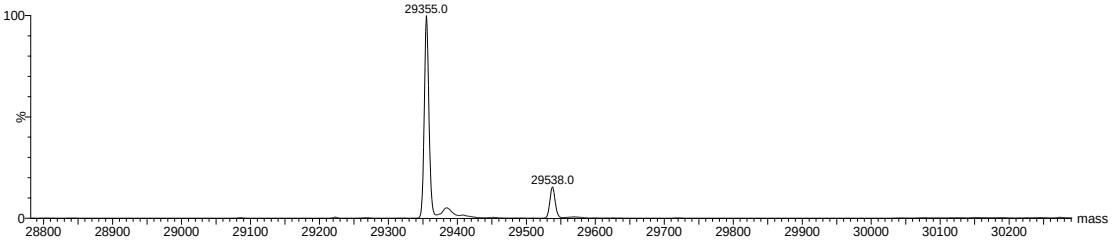

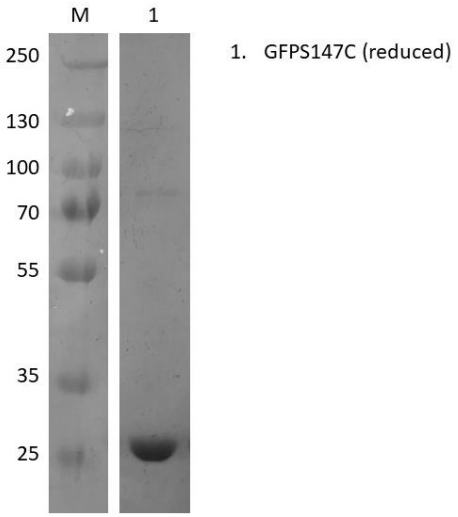

1. GFPS147C (reduced)

GFPS147C–PD (191-194, 196, 197) Bioconjugations

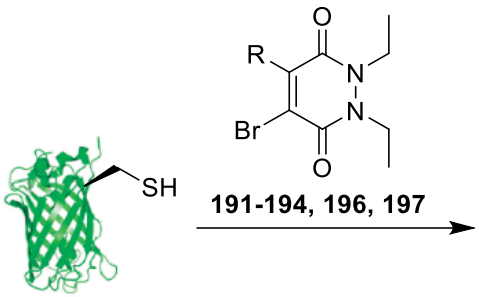

48

To a solution of reduced GFPS147C **48** (100 µL, 50 µM in PBS pH 7.4, 5 mM EDTA) was added Pyridazinedione species **191-194, 196, 197** (5 µL, 20 mM in DMSO, 20 eq., 1 mM final concentration) and the solution was incubated at 37 °C for 4 h. Excess reagents were removed using desalting columns (7000 MWCO, ZebaSpin®, Thermo Scientific) prior to LCMS analysis.

N,N'-Diethyl-Br-Hexylamine PD **191** Expected masses: 29605 Da. Observed masses (LCMS Method 3): 29340, 58680 Da.

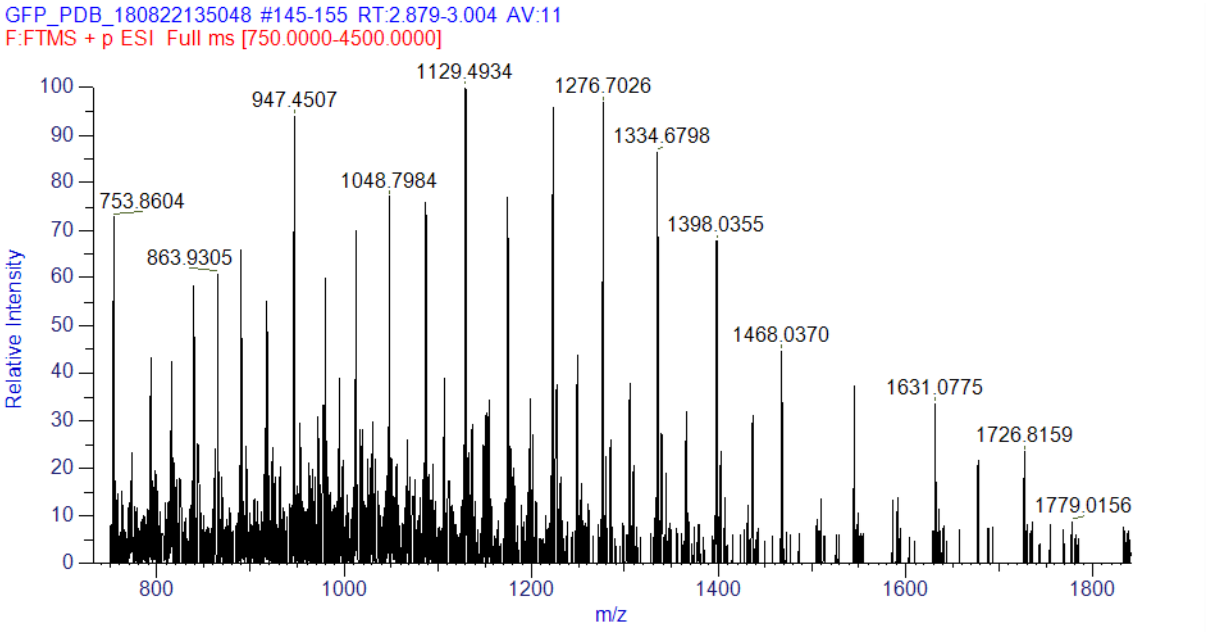

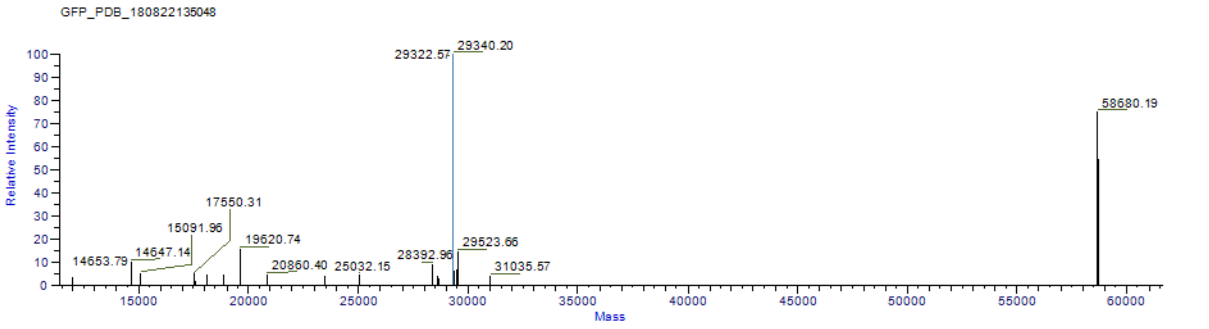

N,N'-Diethyl-Br-Hexanethiol PD **192** Expected masses: 29622 Da. Observed masses (LCMS Method 3): 29622 Da.

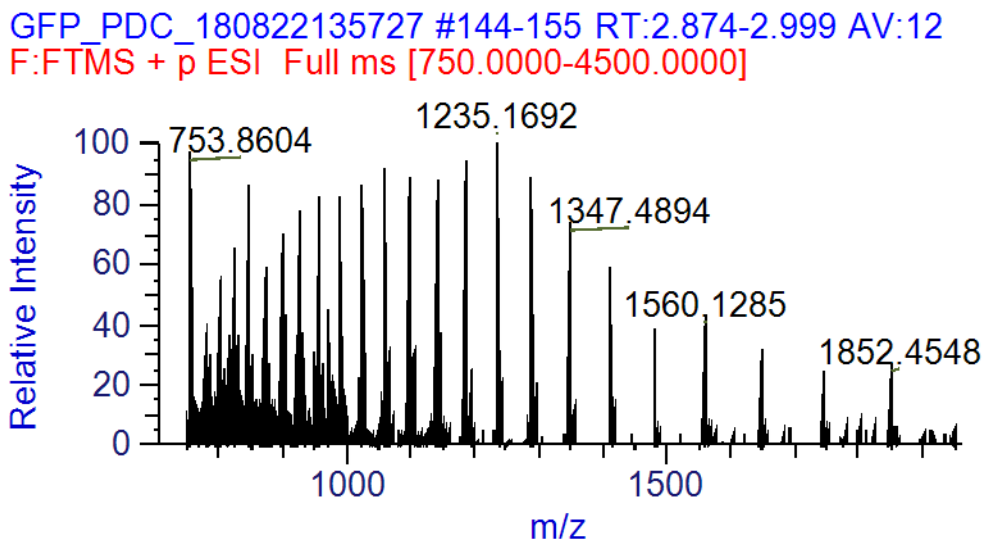

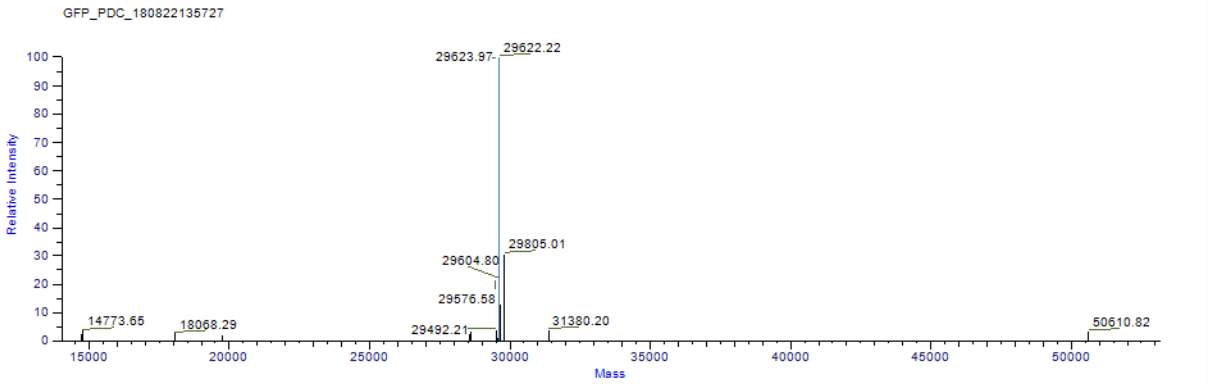

N,N'-Diethyl-Br-2-Mercaptoethanol PD **193** Expected masses: 29582 Da. Observed masses (LCMS Method 3): 29582 Da.

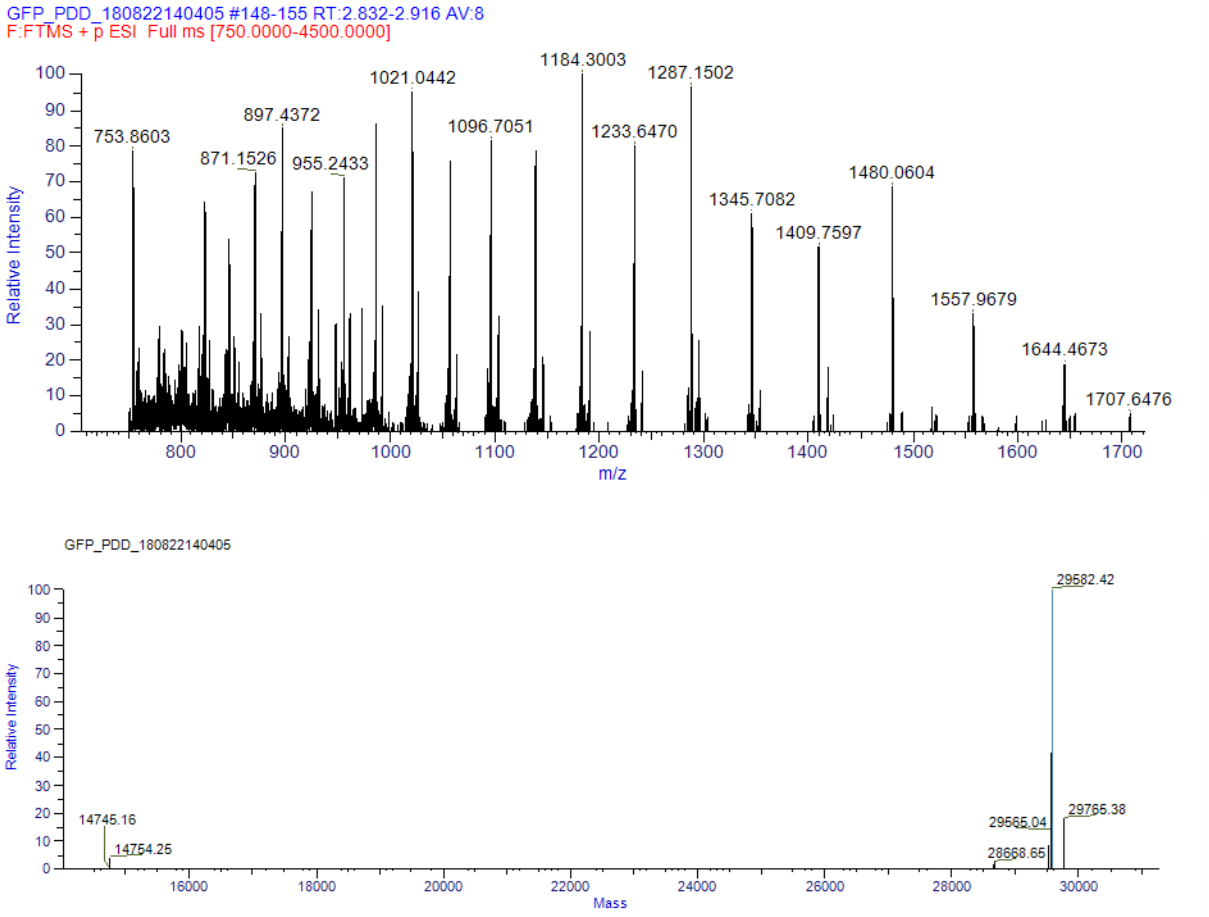

N,N'-Diethyl-Br-3-Mercaptopropanoic acid PD **194** Expected masses: 29610 Da. Observed masses (LCMS Method 3): 29610 Da.

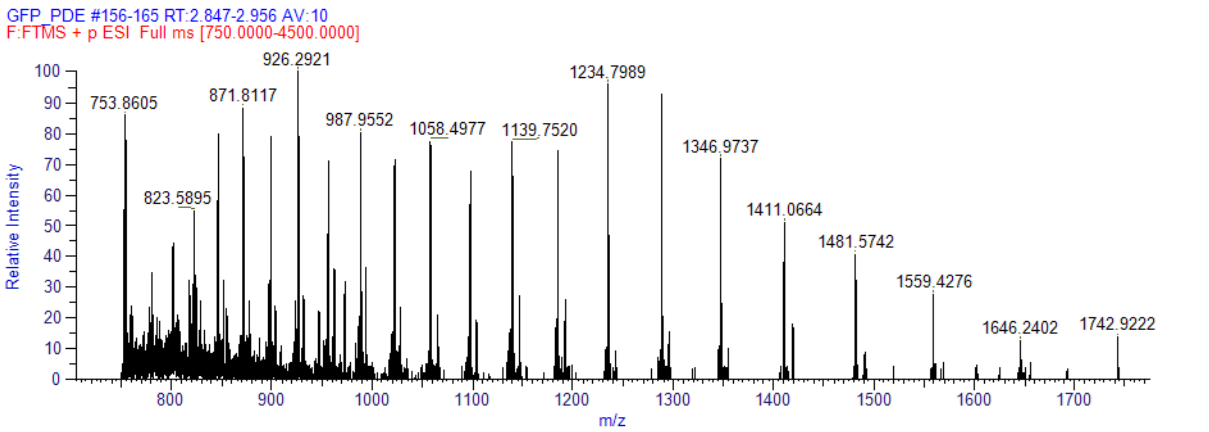

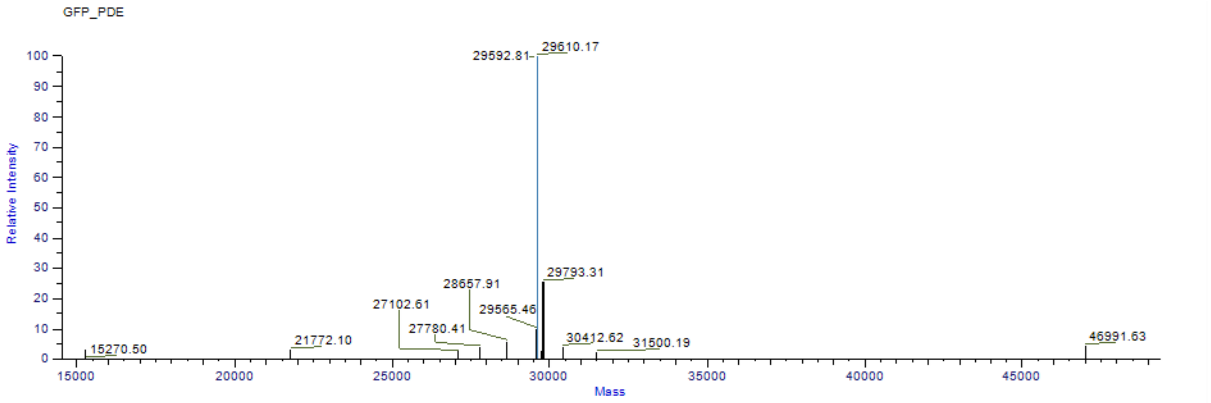

N,N'-Diethyl-Br-Azide PD **196** Expected masses: 29547 Da. Observed masses (LCMS Method 3): 29584 Da.

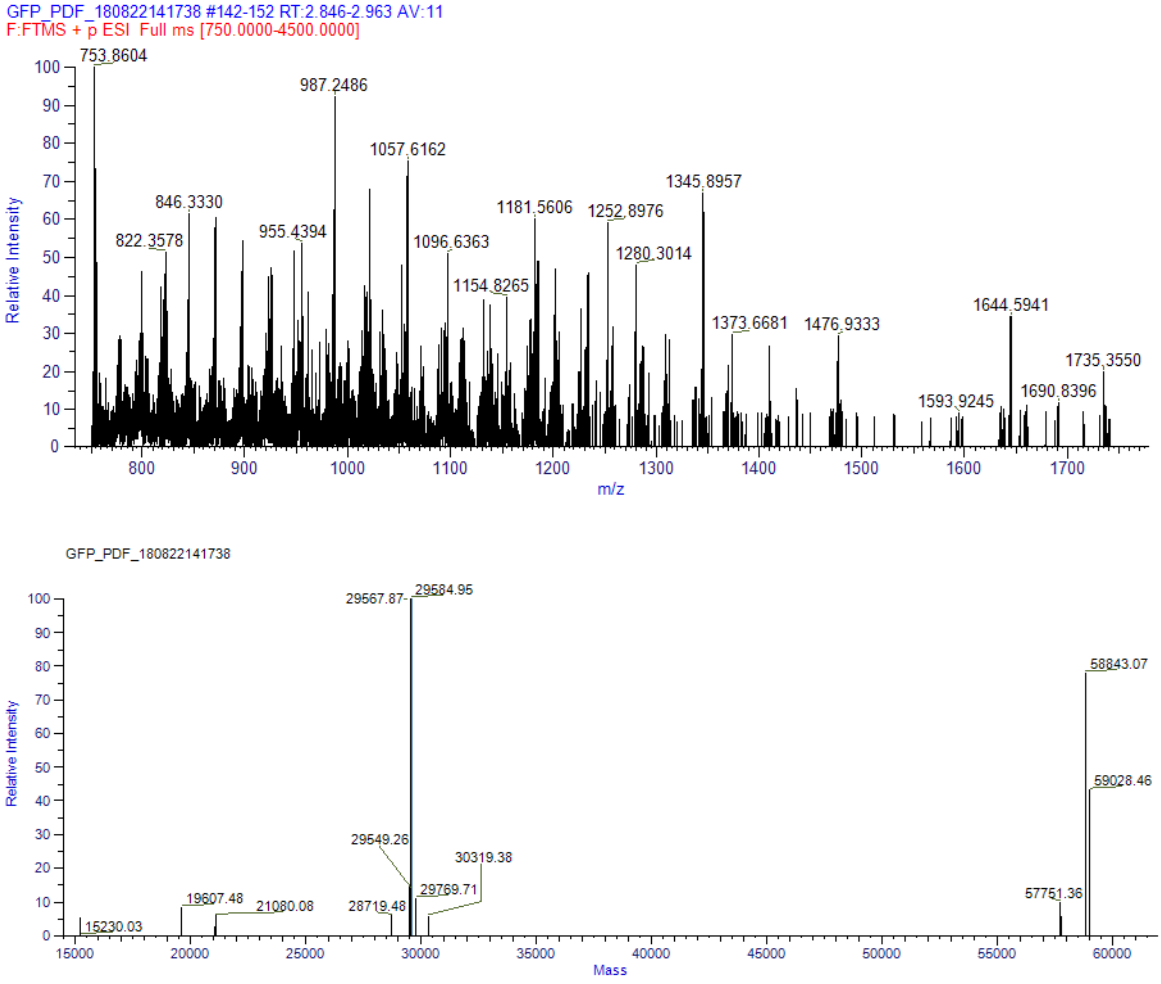

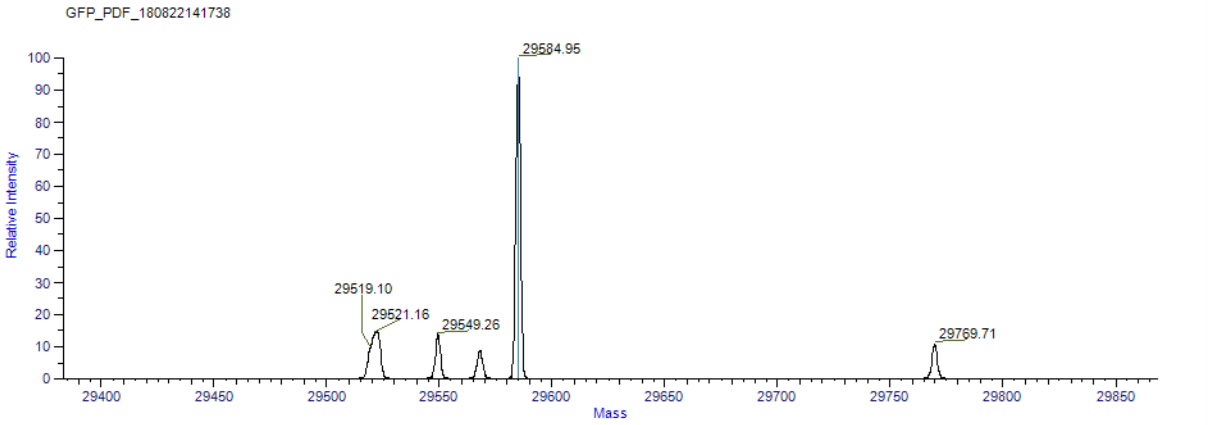

N,N'-Diethyl-Diazide PD **197** Expected masses: 29547 Da. Observed masses (LCMS Method 3): 29339 Da.

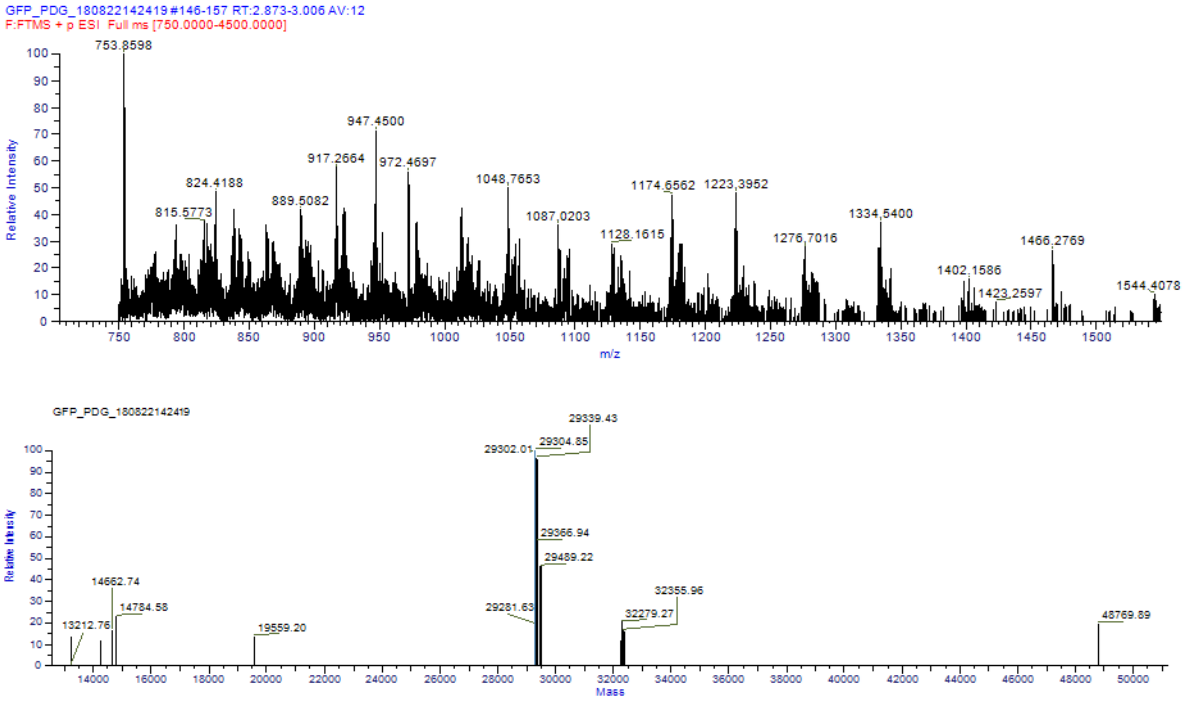

GFPS147C–PD (*N,N'*-diethyl)–Br 201

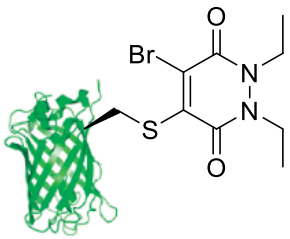

201

To a solution of reduced GFPS147C **48** (500 µL, 50 µM in PBS pH 7.4, 5 mM EDTA) was added *N,N*-diethyl dibromo pyridazinedione **136** (25 µL, 20 mM in DMSO, 20 eq., 1 mM final concentration) and the solution was incubated at 37 °C for 4 h. Excess reagents were removed using desalting columns (7000 MWCO, ZebaSpin®, Thermo Scientific) prior to LCMS analysis. Expected masses: 29586 Da. Observed masses (LCMS Method 2): 29586 Da.

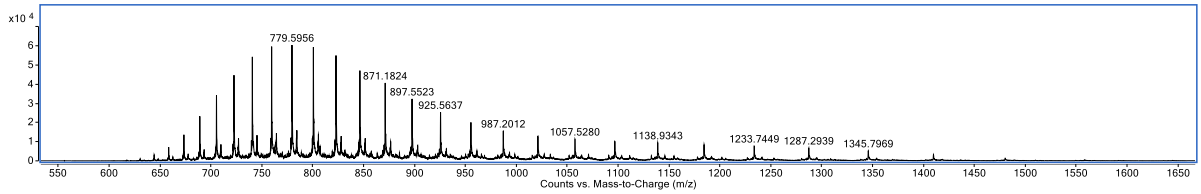

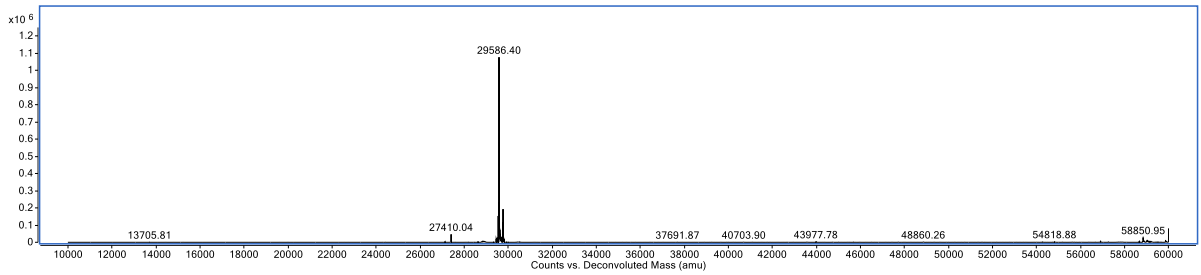

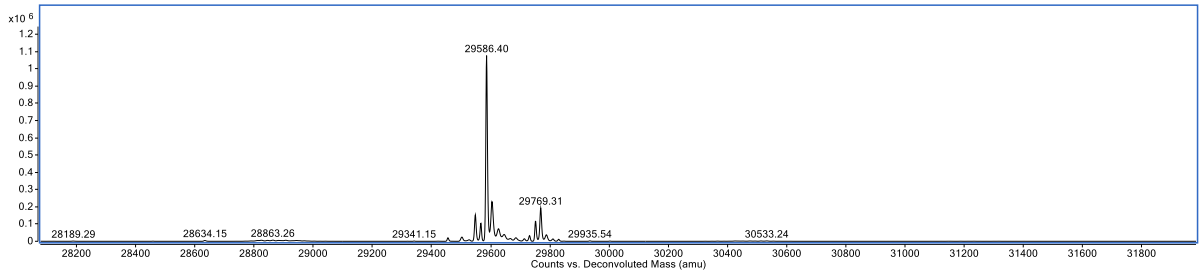

GFPS147C–PD (*N,N'*-diethyl)–Hexane thiol 206

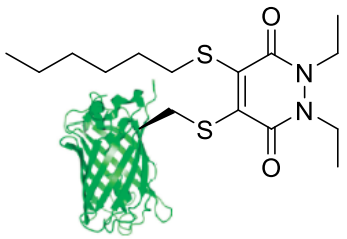

206

To a solution of GFPS147C–PD (N,N'-diethyl)–Br **201** (50 µL, 50 µM in BBS pH 8.0, 5 mM EDTA) was added *n*-hexane thiol (2.5 µL, 20 mM in DMSO, 20 eq., 1 mM final concentration) and the solution was incubated at 37 °C for 16 h. Excess reagents were removed using desalting columns (7000 MWCO, ZebaSpin®, Thermo Scientific) prior to LCMS analysis. Expected masses: 29624 Da. Observed masses (LCMS Method 2): 29624 Da.

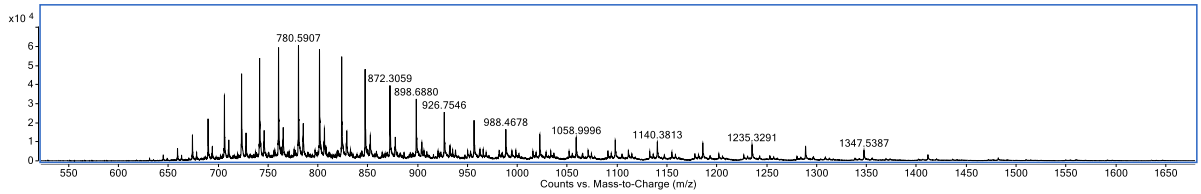

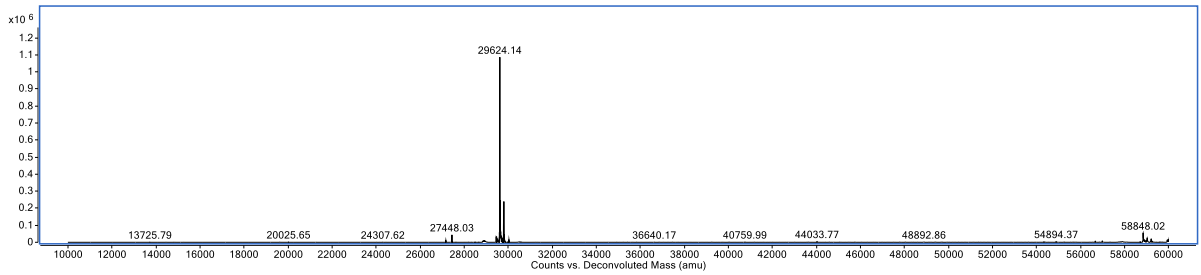

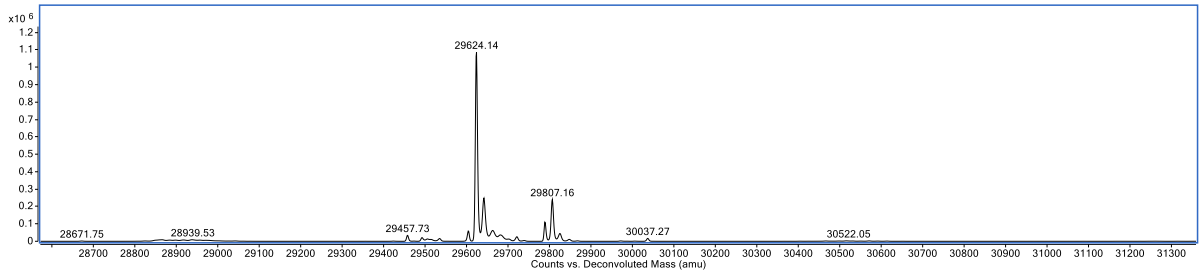

GFPS147C–PD (*N,N'*-diethyl)–FEKGC 207

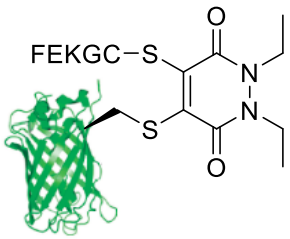

207

To a solution of GFPS147C–PD (N,N'-diethyl)–Br **201** (50 µL, 50 µM in BBS pH 8.0, 5 mM EDTA) was added peptide FEKGC (2.5 µL, 20 mM in DMSO, 20 eq., 1 mM final concentration) and the solution was incubated at 37 °C for 16 h. Excess reagents were removed using desalting columns (7000 MWCO, ZebaSpin®, Thermo Scientific) prior to LCMS analysis. Expected masses: 30088 Da. Observed masses (LCMS Method 2): 30088 Da.

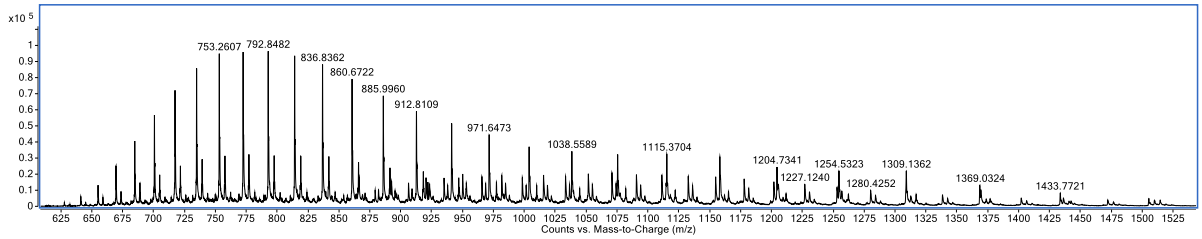

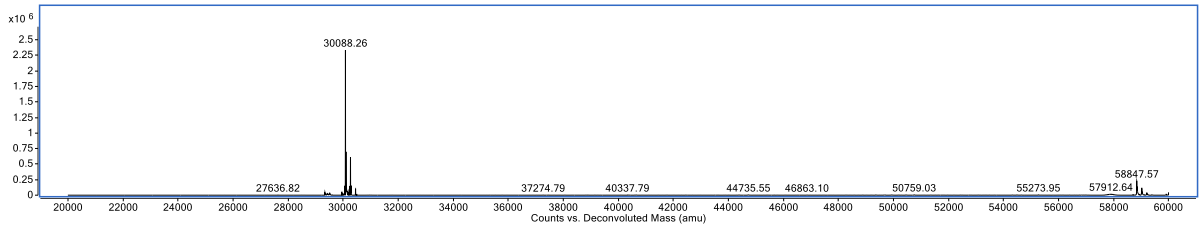

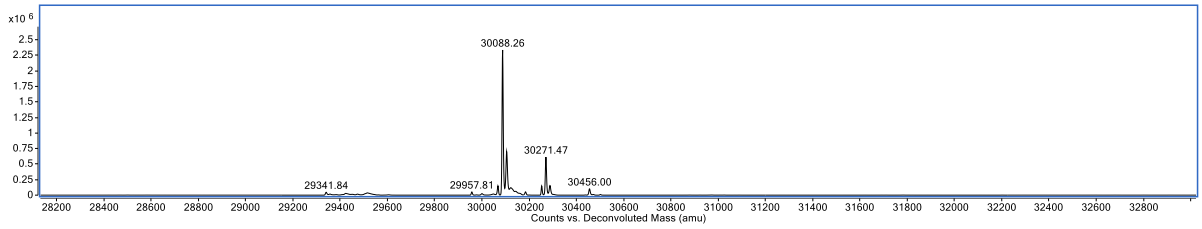

GFPS147C–PD (*N,N'*-diethyl)–*p*-Anisidine 208

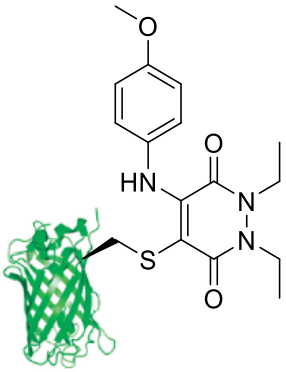

208

To a solution of GFPS147C–PD (N,N'-diethyl)–Br **201** (50 µL, 50 µM in BBS pH 8.0, 5 mM EDTA) was added *p*-anisidine (2.5 µL, 1 M in DMSO, 1000 eq., 50 mM final concentration) and the solution was incubated at 37 °C for 16 h. Excess reagents were removed using desalting columns (7000 MWCO, ZebaSpin®, Thermo Scientific) prior to LCMS analysis. Expected masses: 29629 Da. Observed masses (LCMS Method 2): 29628 Da.

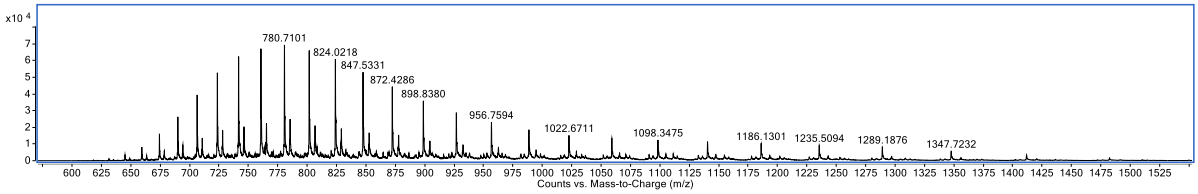

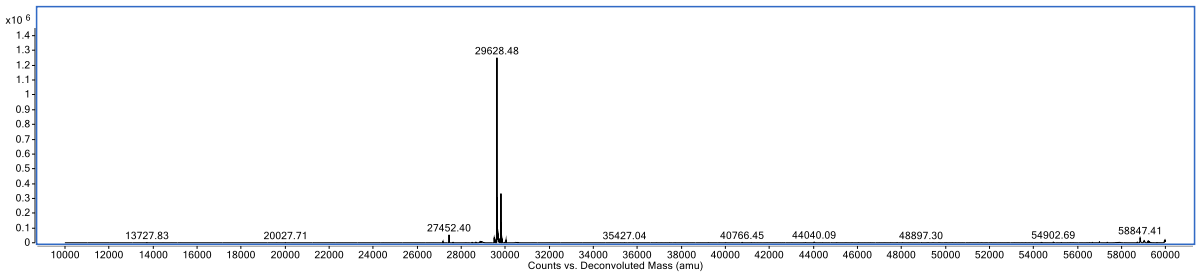

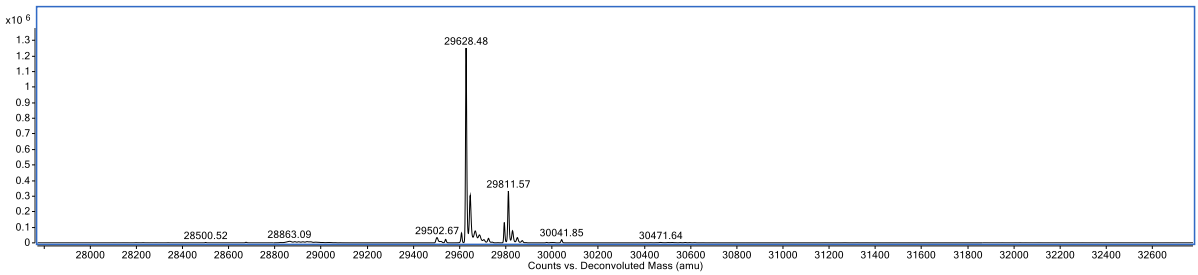

GFPS147C–PD (*N,N'*-diethyl)–Aniline Azide 209

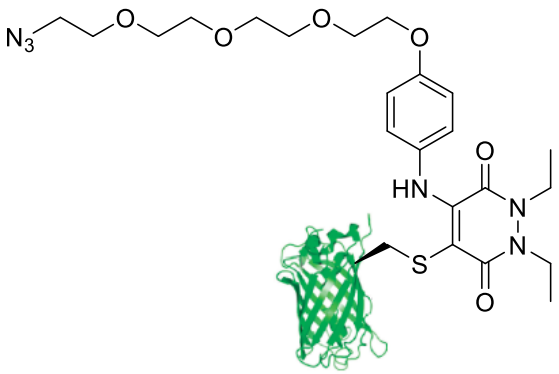

209

To a solution of GFPS147C–PD (N,N'-diethyl)–Br **201** (50 µL, 50 µM in BBS pH 8.0, 5 mM EDTA) was added aniline azide (2.5 µL, 1 M in DMSO, 1000 eq., 50 mM final concentration) and the solution was incubated at 37 °C for 16 h. Excess reagents were removed using desalting columns (7000 MWCO, ZebaSpin®, Thermo Scientific) prior to LCMS analysis. Expected masses: 29816 Da. Observed masses (LCMS Method 2): 29816 Da.

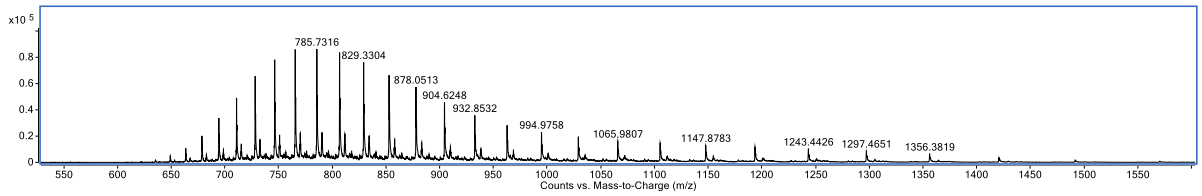

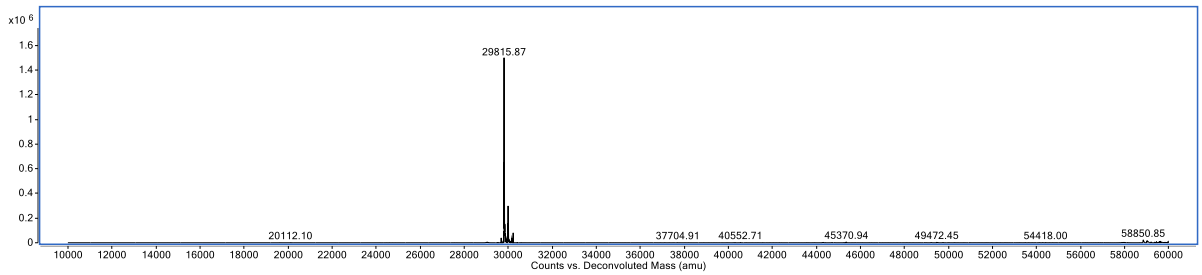

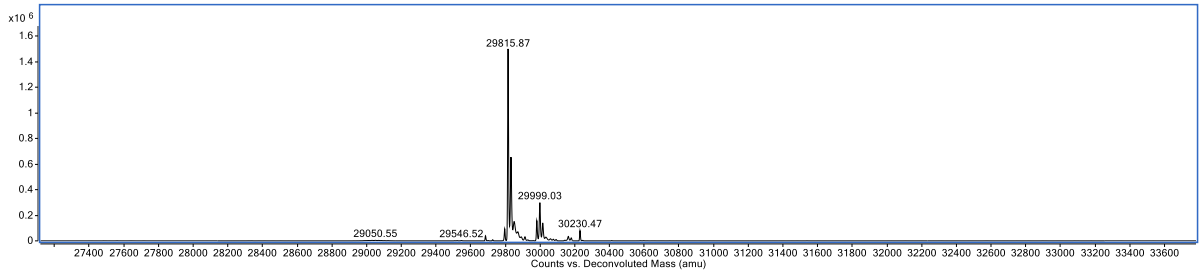

GFPS147C–PD (*N*-methyl, *N'*-BCN (AF-488))–Hexane thiol 210

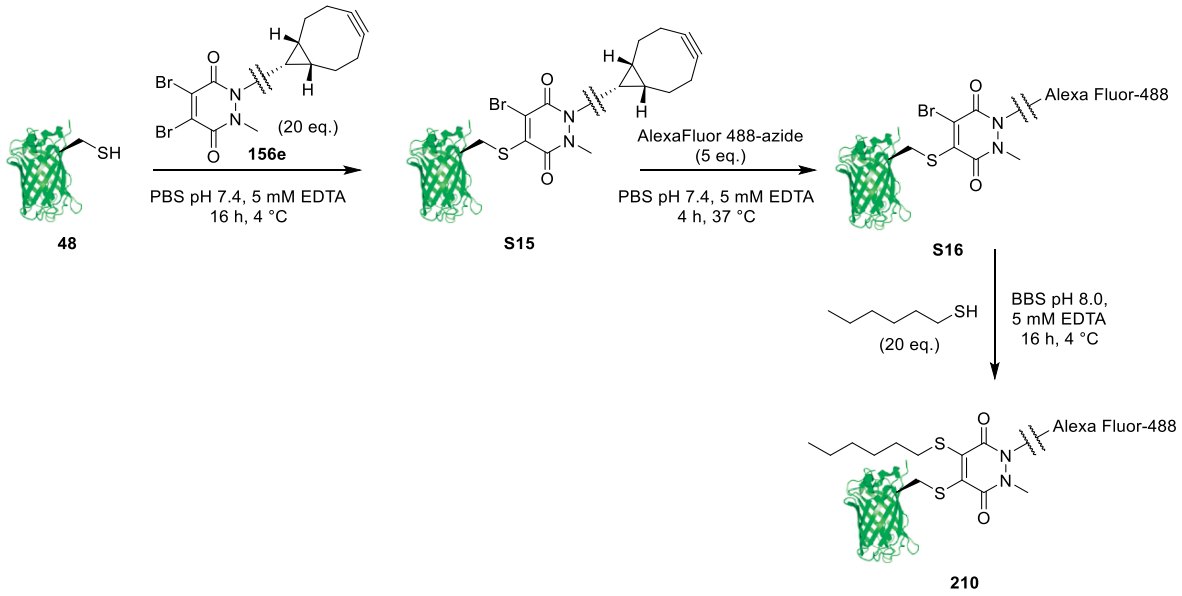

To a solution of reduced GFPS147C **48** (250 µL, 50 µM in PBS pH 7.4, 5 mM EDTA), was added *N*-methyl, *N'*-BCN dibromo PD **156e** (12.5 µL, 20 mM in DMSO, 20 eq., 1 mM final concentration) and the solution was incubated at 4 °C for 16 h. After this time excess reagents were removed using desalting columns (7000 MWCO, ZebaSpin®, Thermo Scientific) to elute the conjugate into PBS (pH 7.4, 5 mM EDTA). Alexa fluor-488 azide (6.25 µL, 10 mM in DMSO, 5 eq., 250 µM final concentration) was added and the reaction was incubated for 4 h at 37 °C. Excess reagents were removed using desalting columns (7000 MWCO, ZebaSpin®, Thermo Scientific) to elute the conjugate into BBS (pH 8.0, 5 mM EDTA). To this solution, was added *n*-hexane thiol (12.5 µL, 20 mM in DMSO, 20 eq., 1 mM final concentration) and the reaction was incubated for a further 16 h at 4 °C. Excess reagents and buffer were removed using desalting columns (7000 MWCO, ZebaSpin®, Thermo Scientific) prior to LCMS analysis. Expected masses: 30619 Da, Observed masses (LCMS Method 2): 30621 Da.

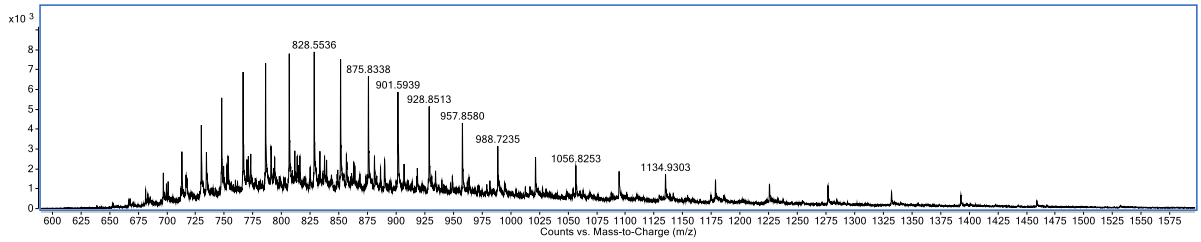

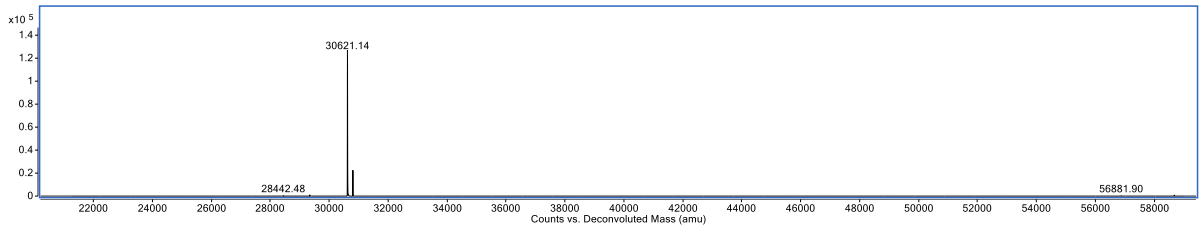
x10 5
1.4
1.2
1
0.8
0.6
0.4
0.2
0
30621.14
28442.48
56881.90
22000 24000 26000 28000 30000 32000 34000 36000 38000 40000 42000 44000 46000 48000 50000 52000 54000 56000 58000
Counts vs. Deconvoluted Mass (amu)

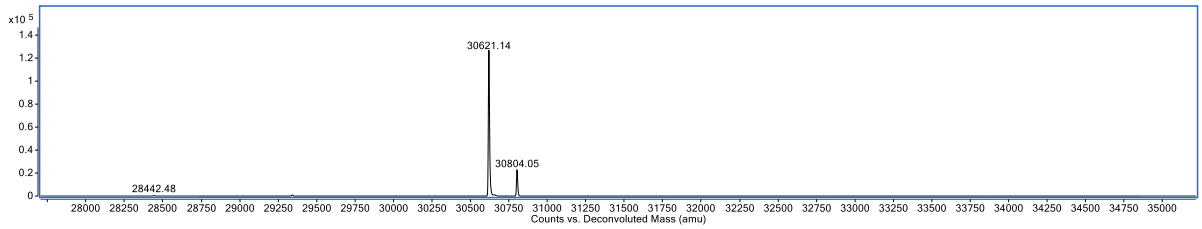
x10 5
1.4
1.2
1
0.8
0.6
0.4
0.2
0
30621.14
30804.05
28442.48
28000 28250 28500 28750 29000 29250 29500 29750 30000 30250 30500 30750 31000 31250 31500 31750 32000 32250 32500 32750 33000 33250 33500 33750 34000 34250 34500 34750 35000
Counts vs. Deconvoluted Mass (amu)

GFPS147C–PD (*N*-methyl, *N'*-BCN (AF-488)–*p*-anisidine 211

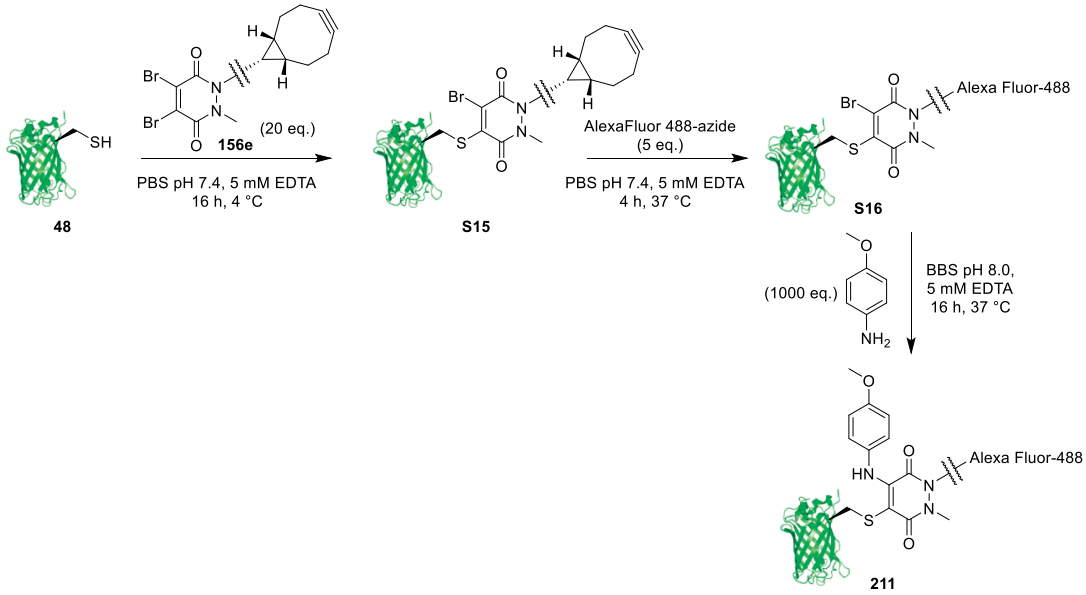

To a solution of reduced GFPS147C **48** (250 µL, 50 µM in PBS pH 7.4, 5 mM EDTA), was added *N*-methyl, *N'*-BCN dibromo PD **156e** (12.5 µL, 20 mM in DMSO, 20 eq., 1 mM final concentration) and the solution was incubated at 4 °C for 16 h. After this time excess reagents were removed using desalting columns (7000 MWCO, ZebaSpin®, Thermo Scientific) to elute the conjugate into PBS (pH 7.4, 5 mM EDTA). Alexa fluor-488 azide (6.25 µL, 10 mM in DMSO, 5 eq., 250 µM final concentration) was added and the reaction was incubated for 4 h at 37 °C. Excess reagents were removed using desalting columns (7000 MWCO, ZebaSpin®, Thermo Scientific) to elute the conjugate into BBS (pH 8.0, 5 mM EDTA). To this solution, was added *p*-anisidine (12.5 µL, 1 M in DMSO, 1000 eq., 50 mM final concentration) and the reaction was incubated for a further 16 h at 37 °C. Excess reagents and buffer were removed using desalting columns (7000 MWCO, ZebaSpin®, Thermo Scientific) prior to LCMS analysis. Expected masses: 30624 Da. Observed masses (LCMS Method 2): 30626 Da.

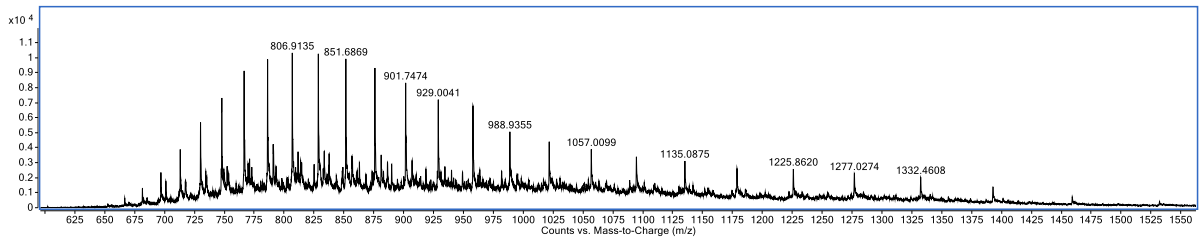

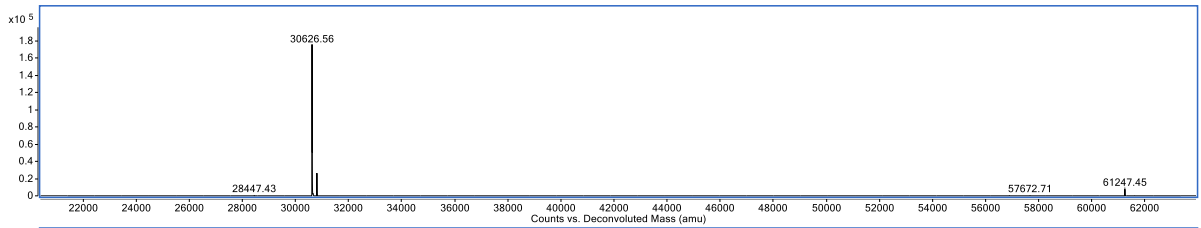
x10 5
1.8
1.6
1.4
1.2
1
0.8
0.6
0.4
0.2
0
30626.56
28447.43
57672.71
61247.45
22000 24000 26000 28000 30000 32000 34000 36000 38000 40000 42000 44000 46000 48000 50000 52000 54000 56000 58000 60000 62000
Counts vs. Deconvoluted Mass (amu)

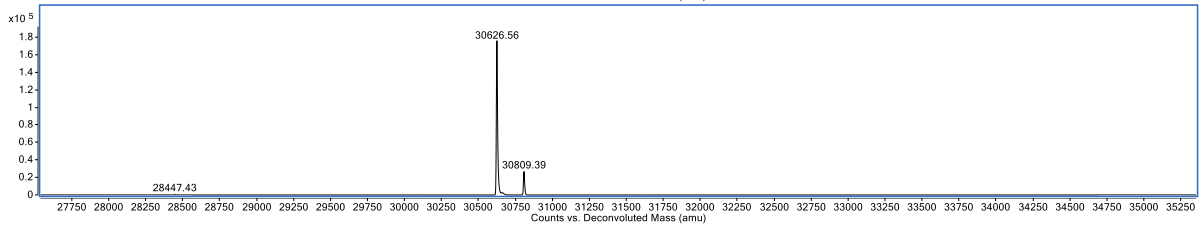
x10 5
1.8
1.6
1.4
1.2
1
0.8
0.6
0.4
0.2
0
30626.56
30809.39
28447.43
27750 28000 28250 28500 28750 29000 29250 29500 29750 30000 30250 30500 30750 31000 31250 31500 31750 32000 32250 32500 32750 33000 33250 33500 33750 34000 34250 34500 34750 35000 35250
Counts vs. Deconvoluted Mass (amu)

GFPS147C–PD (*N*-tetrazine, *N'*-azide)–Br 214

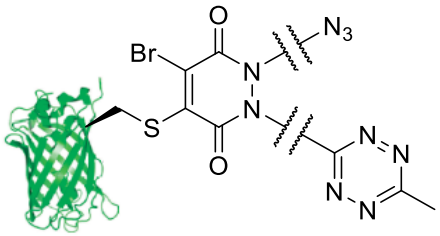

214

To a solution of reduced GFPS147C **48** (500 µL, 50 µM in PBS pH 7.4, 5 mM EDTA) was added *N*-tetrazine, *N'*-azide dibromo pyridazinedione **213** (25 µL, 20 mM in DMSO, 20 eq., 1 mM final concentration) and the solution was incubated at 37 °C for 4 h. Excess reagents were removed using desalting columns (7000 MWCO, ZebaSpin®, Thermo Scientific) prior to LCMS analysis. Expected masses: 30371 Da. Observed masses (LCMS Method 1): 30376 Da.

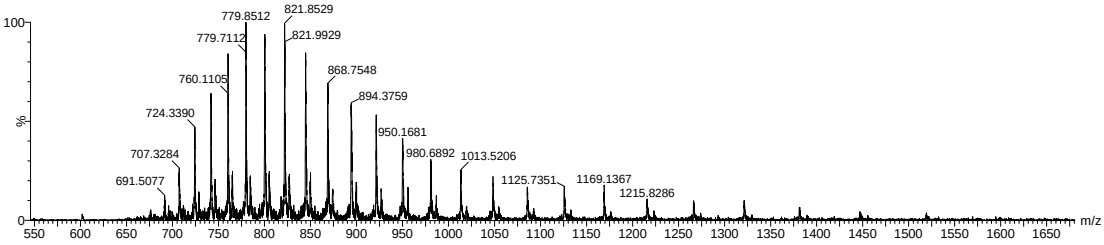

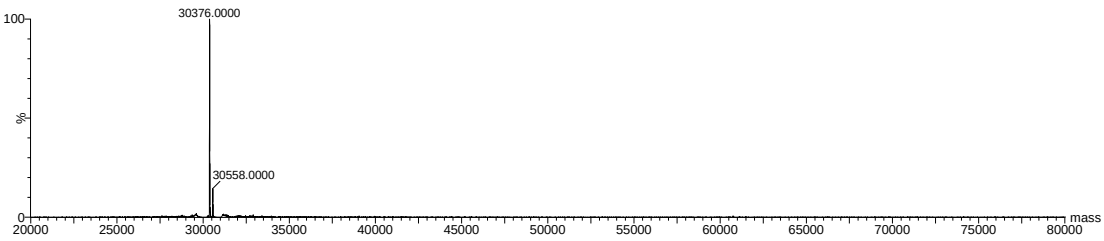

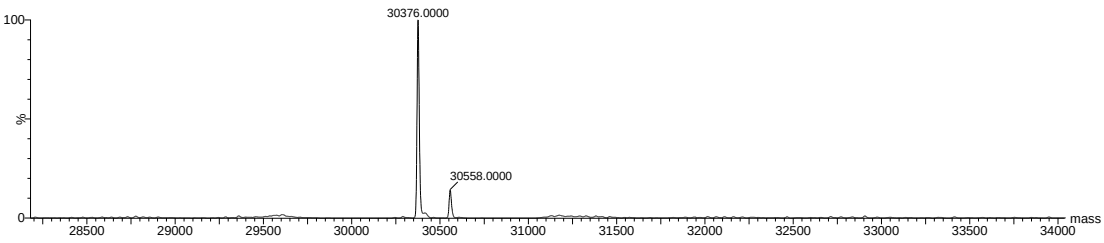

GFPS147C–PD (*N*-tetrazine (BCN fluorescein), *N'*-azide (DBCO biotin))–Br 217

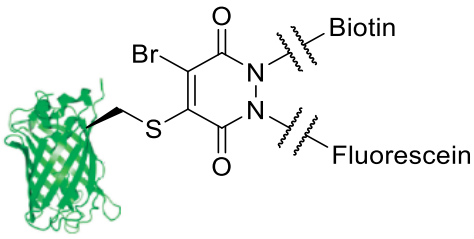

217

To a solution of GFPS147C–PD (*N*-tetrazine, *N'*-azide)–Br **214** (200 µL, 50 µM in PBS pH 7.4, 5 mM EDTA) were added BCN-Fluorescein **215** (4 µL, 5 mM in DMSO, 2 eq., 100 µM final concentration) and DBCO-biotin **216** (5 µL, 20 mM in DMSO, 10 eq., 500 µM), and the solution was incubated at 37 °C for 4 h. Excess reagents were removed using desalting columns (7000 MWCO, ZebaSpin®, Thermo Scientific) prior to LCMS analysis. Expected masses: 31806 Da. Observed masses (LCMS Method 1): 31806 Da.

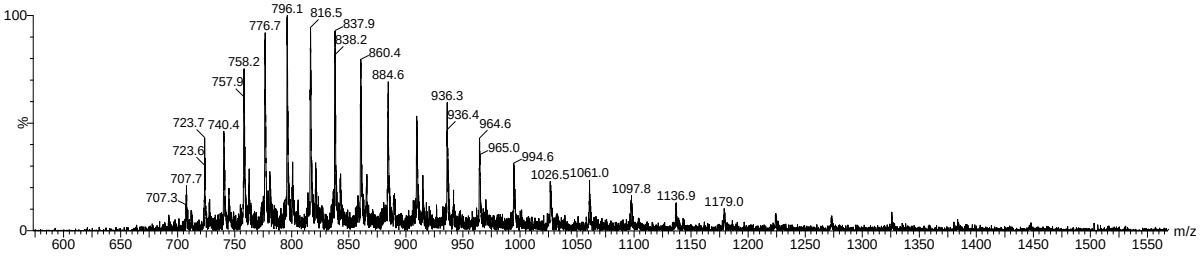

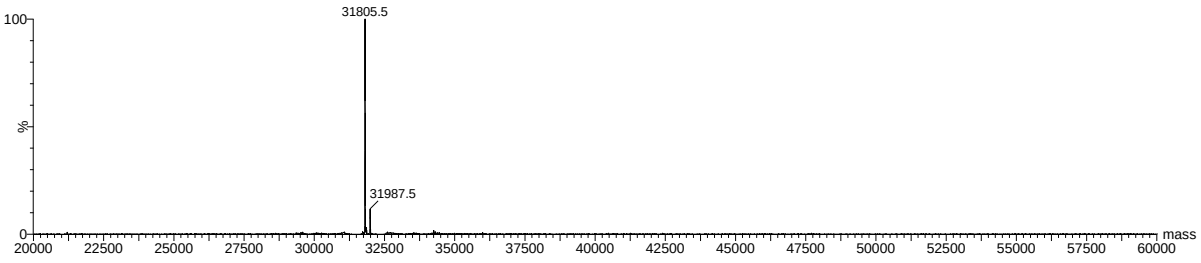

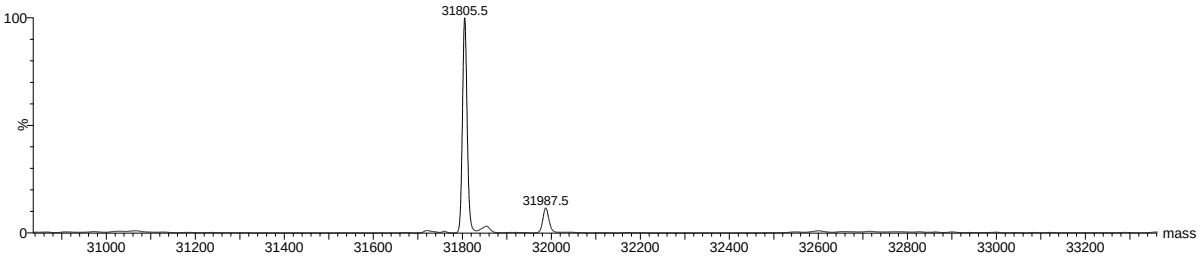

GFPS147C–PD (*N*-tetrazine(BCN fluorescein), *N'*-azide(DBCO biotin))–Peptide (FEKGC) 219

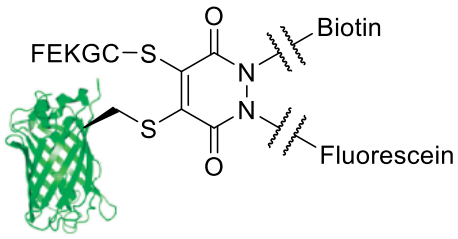

219

To a solution of GFPS147C–PD (*N*-tetrazine (BCN fluorescein), *N'*-azide (DBCO biotin))–Br **217** (50 µL, 50 µM in BBS pH 8.0, 5 mM EDTA), was added peptide FEKGC **218** (2.5 µL, 20 mM in DMSO, 20 eq., 1 mM final concentration) and the reaction was incubated at 4 °C for 16 h. Excess reagents were removed using desalting columns (7000 MWCO, ZebaSpin®, Thermo Scientific) prior to LCMS analysis. Expected masses: 32309 Da. Observed masses (LCMS Method 1): 32308 Da.

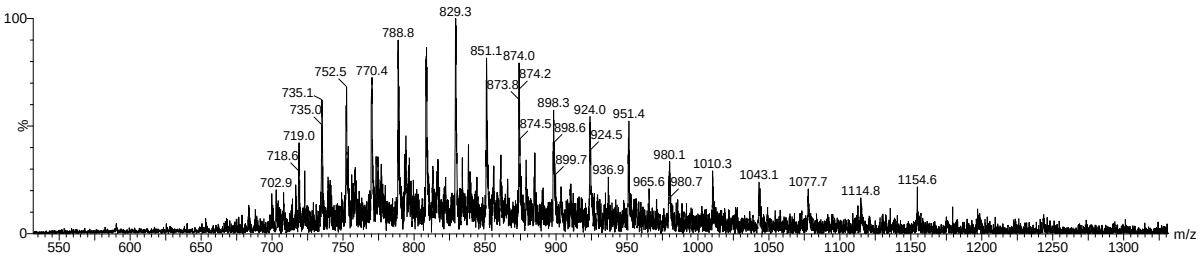

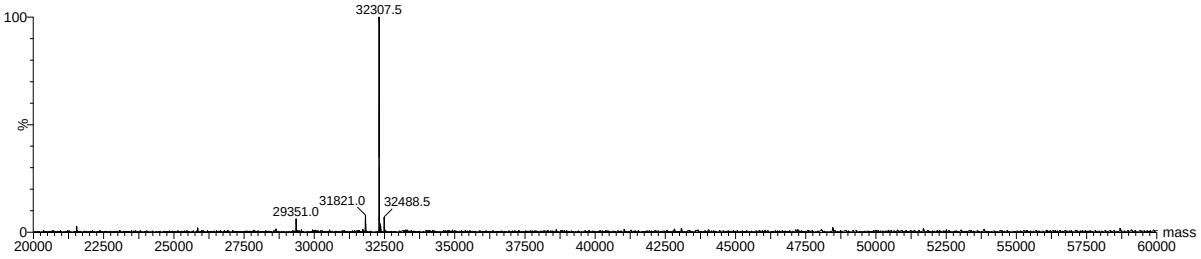

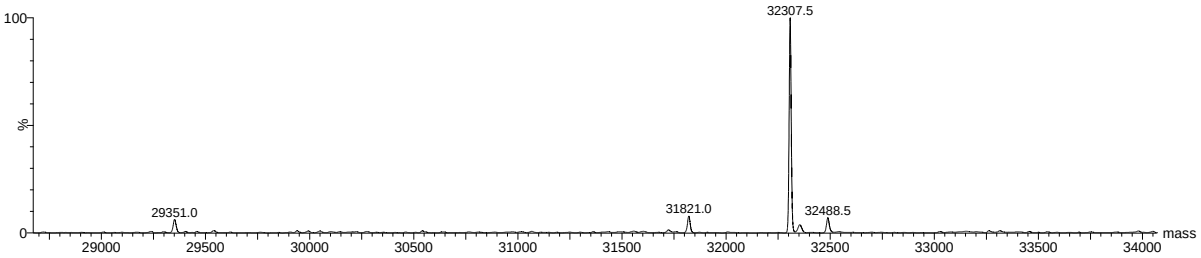

GFPS147C–PD (*N*-tetrazine(BCN fluorescein), *N'*-azide(DBCO biotin))–*p*-azido(PEG$_4$)aniline 221

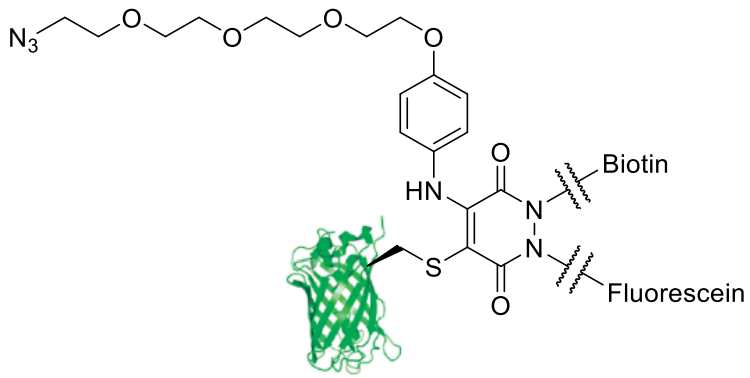

221

To a solution of GFPS147C–PD (*N*-tetrazine (BCN fluorescein), *N'*-azide (DBCO biotin))–Br **217** (50 µL, 50 µM in BBS pH 8.0, 5 mM EDTA) was added aniline azide **220** (2.5 µL, 1 M in DMSO, 1000 eq., final concentration 50 mM) and the reaction was incubated at 37 °C for 16 h. Excess reagents were removed using desalting columns (7000 MWCO, ZebaSpin®, Thermo Scientific) prior to LCMS analysis. Expected masses: 32036 Da. Observed masses (LCMS Method 1): 32035 Da

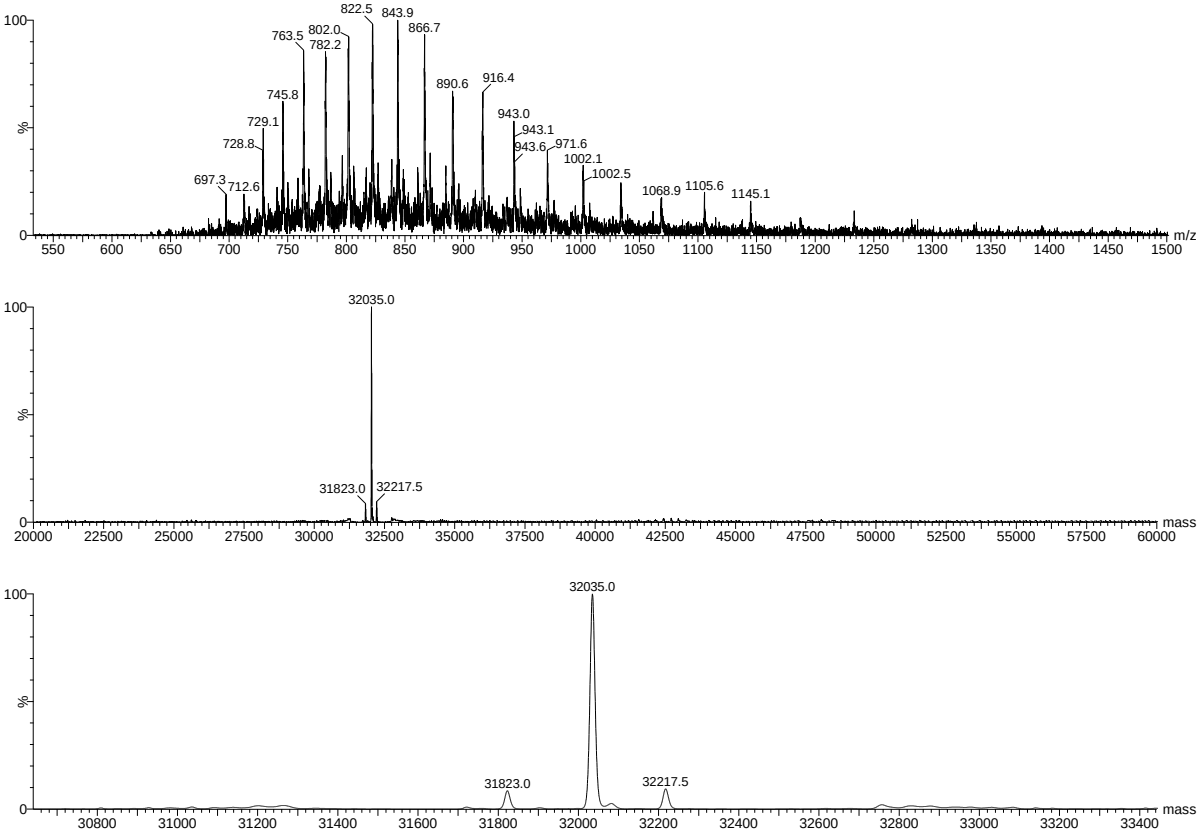
100
%
0
822.5
843.9
866.7
763.5
802.0
782.2
890.6
916.4
745.8
943.0
729.1
943.1
728.8
971.6
943.6
1002.1
697.3
712.6
1002.5
1068.9
1105.6
1145.1
550 600 650 700 750 800 850 900 950 1000 1050 1100 1150 1200 1250 1300 1350 1400 1450 1500
m/z
100
%
0
32035.0
31823.0
32217.5
20000 22500 25000 27500 30000 32500 35000 37500 40000 42500 45000 47500 50000 52500 55000 57500 60000
mass
100
%
0
32035.0
31823.0
32217.5
30800 31000 31200 31400 31600 31800 32000 32200 32400 32600 32800 33000 33200 33400
mass

GFPS147C–PD (*N*-tetrazine(BCN fluorescein), *N'*-azide(DBCO biotin))–*p*-PEG$_{12}$(PEG$_4$)aniline 223

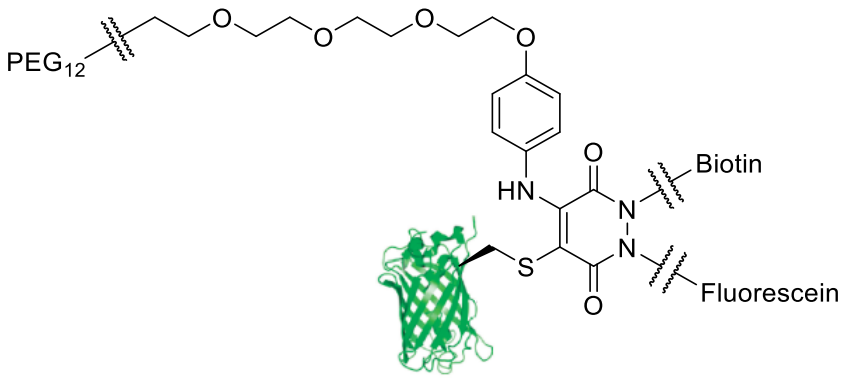

223

To a solution of GFPS147C–PD (N-tetrazine(BCN fluorescein), N'-azide(DBCO biotin))–*p*-azido(PEG$_4$)aniline **221** (50 µL, 50 µM in BBS pH 8.0, 5 mM EDTA) was added DBCO-PEG$_{12}$ **222** (2.5 µL, 20 mM in DMSO, 20 eq., 1 mM final concentration) and the reaction was incubated at 37 °C for 4 h. Excess reagents were removed using desalting columns (7000 MWCO, ZebaSpin®, Thermo Scientific) prior to LCMS analysis. Expected masses: 32897 Da. Observed masses (LCMS Method 1): 32895 Da

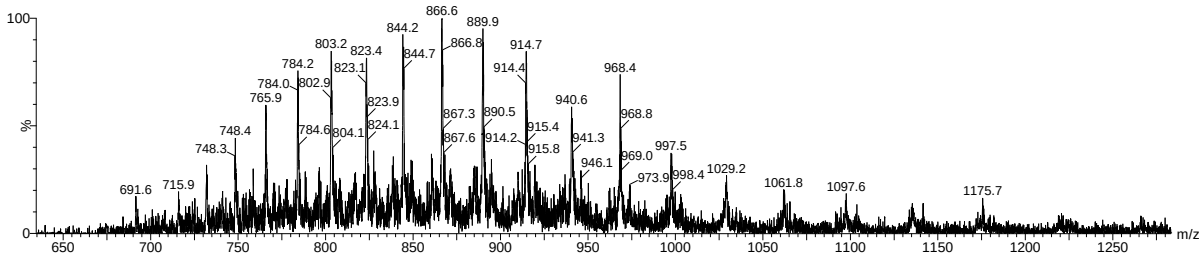

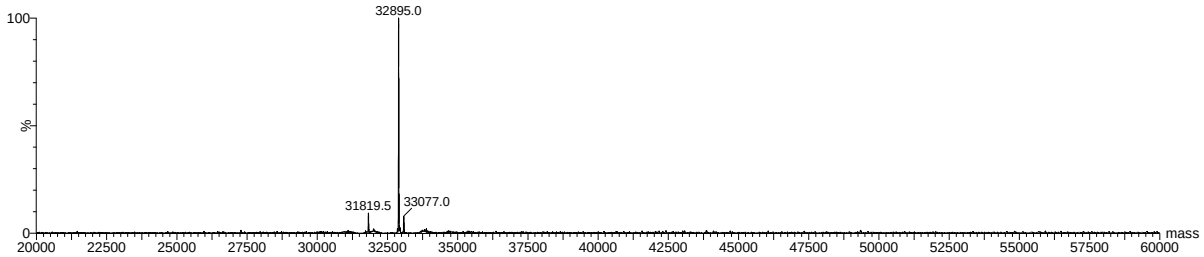

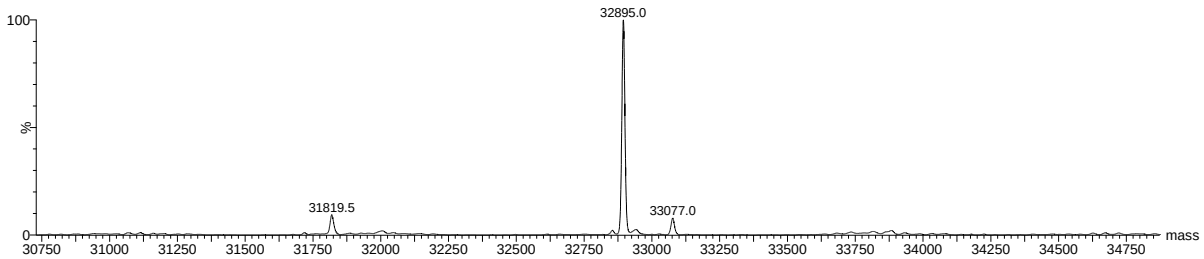

Blood-Like Glutathione (GSH) Cleavage Study

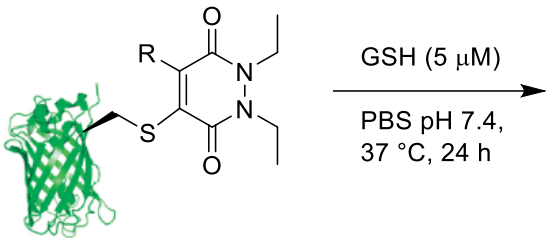

R = 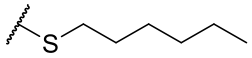 **206**

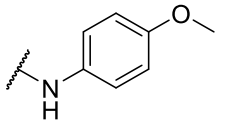 **208**

GFPS147C conjugates **206** and **208** (50 µL, 6.8 µM) were buffer exchanged using desalting columns (7000 MWCO, ZebaSpin®, Thermo Scientific) into GSH containing buffer (5 µM GSH, in PBS pH 7.4) and maintained at 37 °C for 24 h. Excess reagents were removed using desalting columns (7000 MWCO, ZebaSpin®, Thermo Scientific) prior to LCMS analysis.

GFPS147C–PD (*N*,*N*'-diethyl)–*n*-Hexane thiol **206**: Expected masses: 29342 Da (reduced GFPS147C), 29624 Da

0 h: Observed masses (LCMS Method 2): 29624 Da.

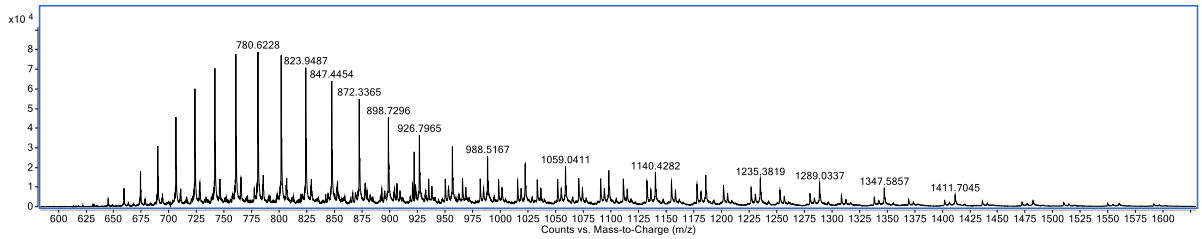

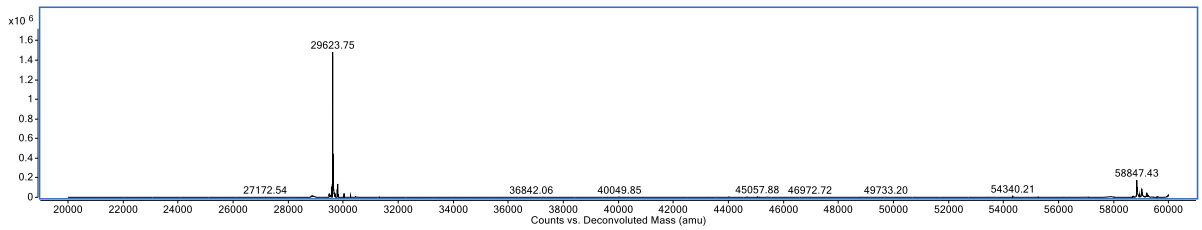

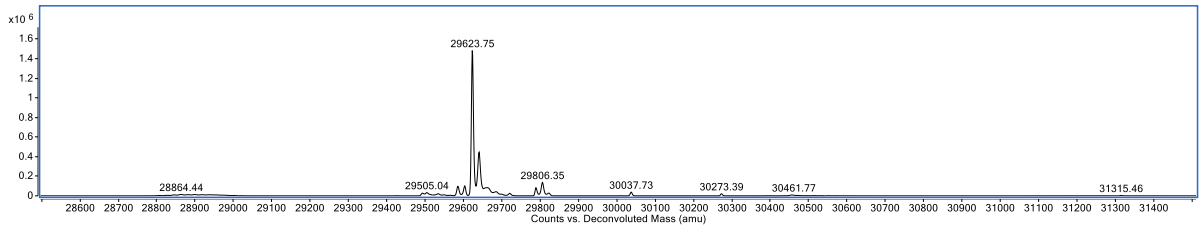

24 h: Observed mass (LCMS Method 2): 29624 Da

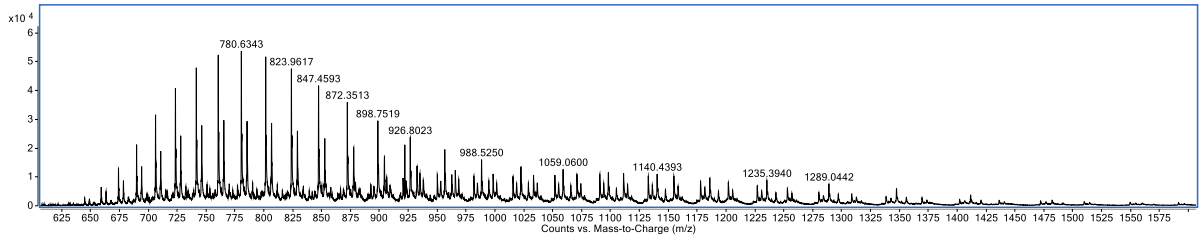

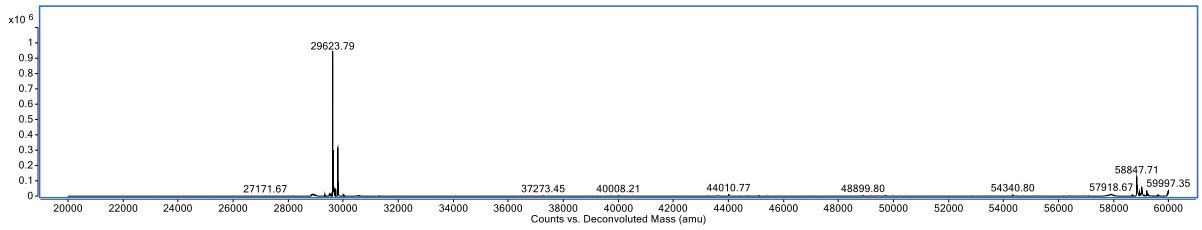

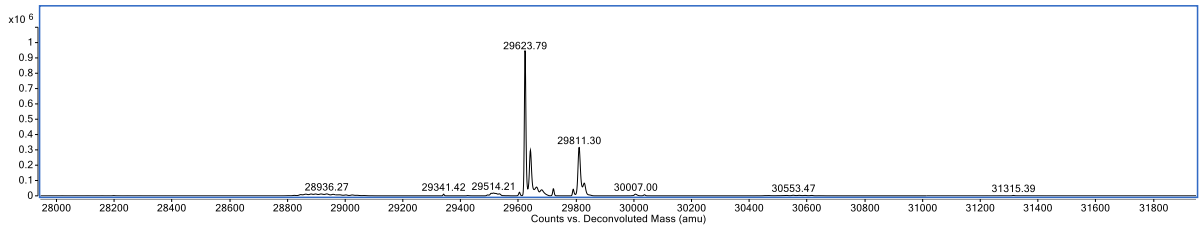

GFPS147C–PD (*N*,*N*'-diethyl)–p-Anisidine **208** – GSH cleavage: Expected masses: 29341 Da (reduced GFPS147C), 29629 Da.

0 h: Observed masses (LCMS Method 2): 29629 Da

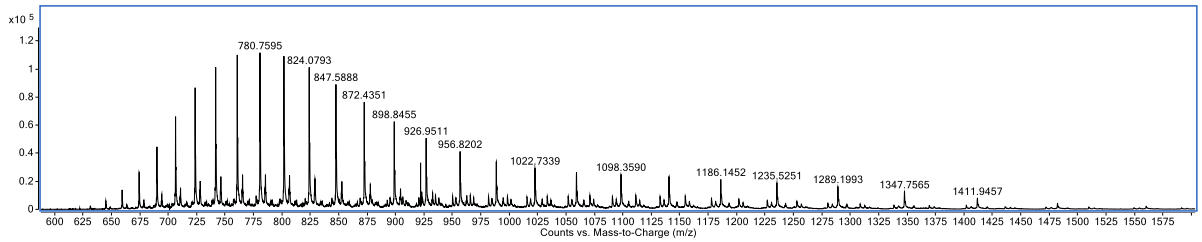

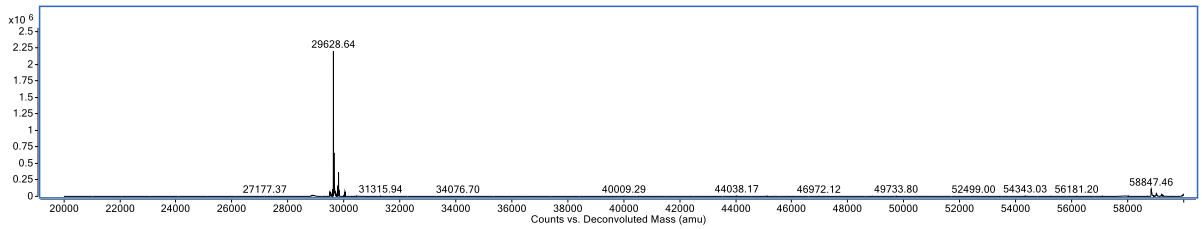

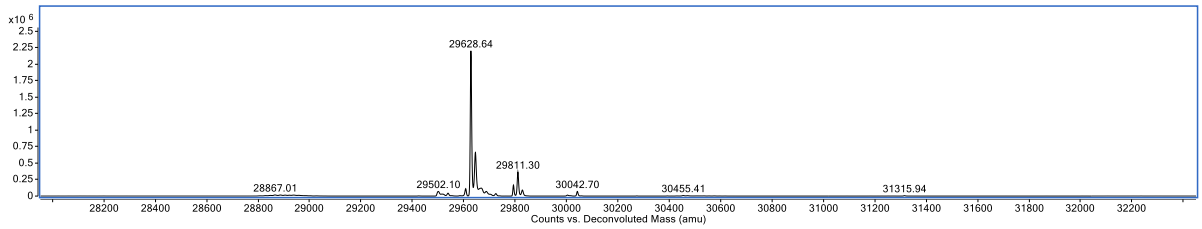

24 h: Observed masses (LCMS Method 2): 29629 Da

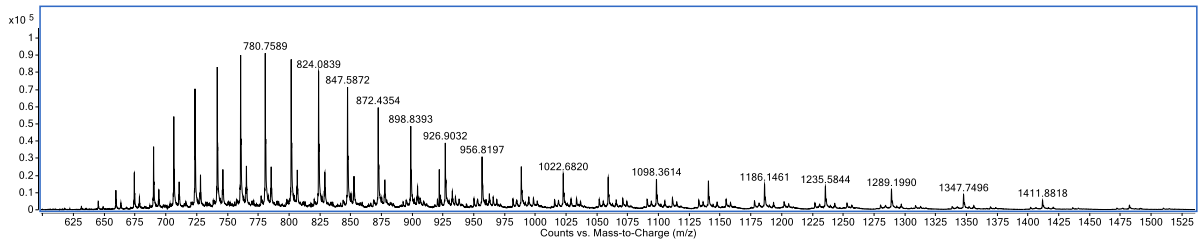

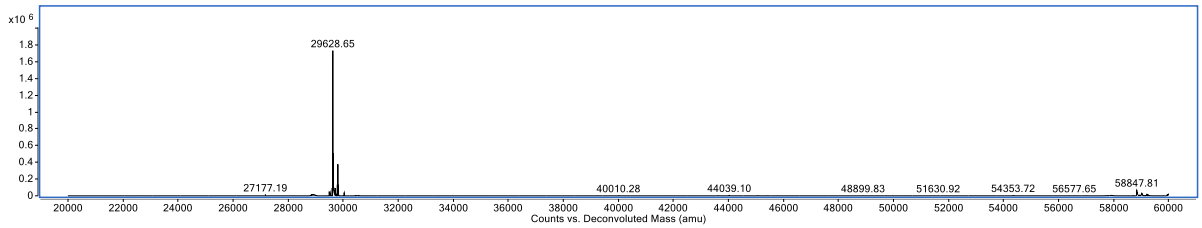

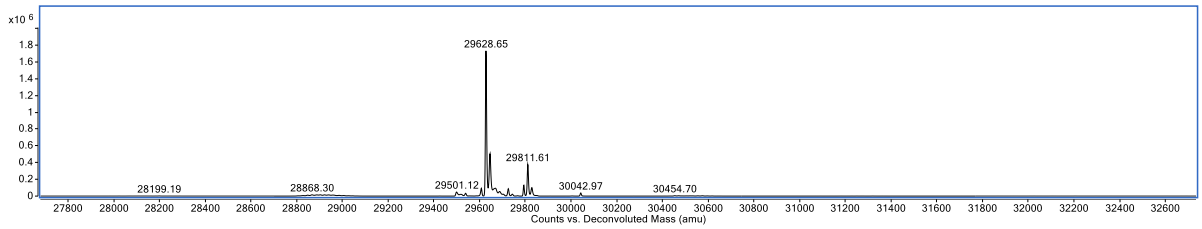
x10 6
1.8
1.6
1.4
1.2
1
0.8
0.6
0.4
0.2
0
29628.65
29811.61
28199.19
28868.30
29501.12
30042.97
30454.70
27800 28000 28200 28400 28600 28800 29000 29200 29400 29600 29800 30000 30200 30400 30600 30800 31000 31200 31400 31600 31800 32000 32200 32400 32600
Counts vs. Deconvoluted Mass (amu)

Cell-Like Glutathione (GSH) Cleavage Study

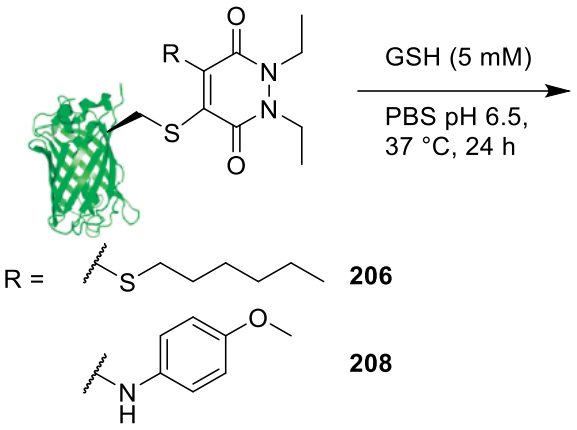

GFPS147C conjugates **206** and **208** (50 µL, 6.8 µM) were buffer exchanged using desalting columns (7000 MWCO, ZebaSpin®, Thermo Scientific) into GSH containing buffer (5 mM GSH, in PBS pH 6.5) and maintained at 37 °C for 24 h. Samples were taken at 2, 4, 8 and 24 h timepoints where excess reagents were removed using desalting columns (7000 MWCO, ZebaSpin®, Thermo Scientific) prior to LCMS analysis.

GFPS147C–PD (*N*,*N*'-diethyl)–*n*-Hexane thiol **206**: Expected masses: 29342 Da (reduced GFPS147C), 29624 Da

0 h: Expected masses: 29624 Da. Observed masses (LCMS Method 2): 29624 Da.

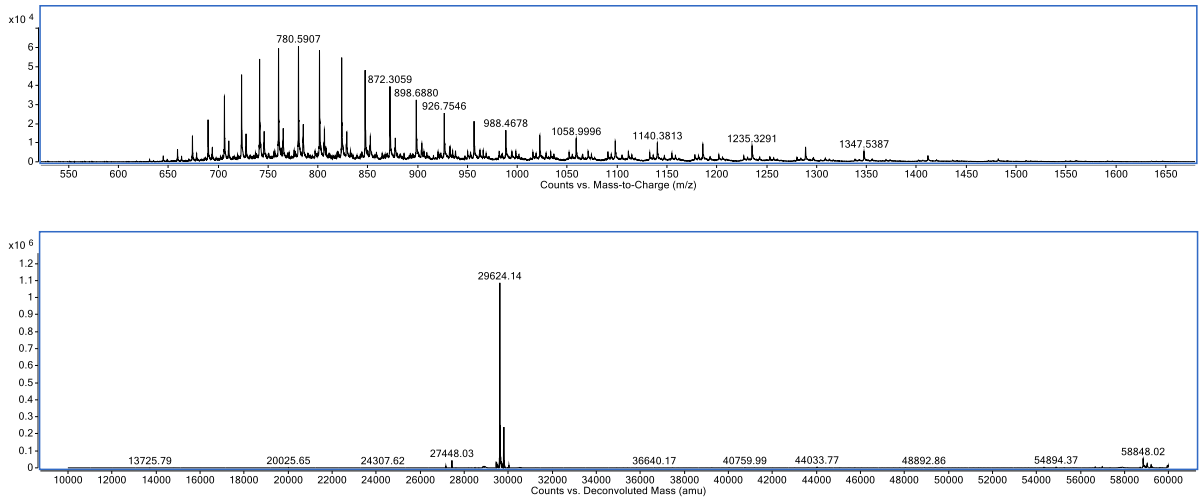

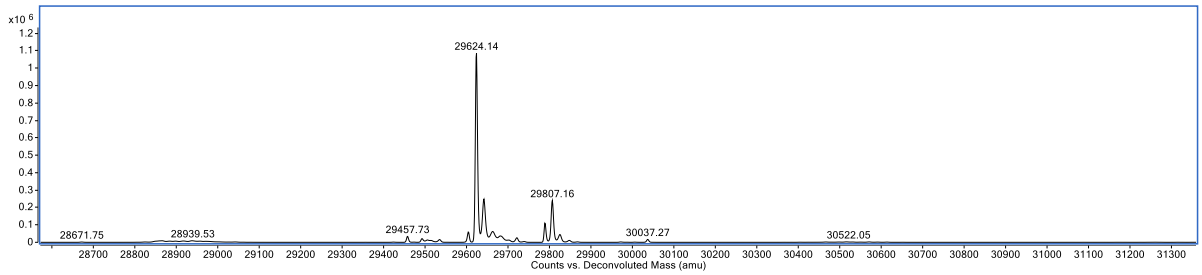

2 h: Observed masses (LCMS Method 2): 29341 Da (reduced GFPS147C), 29646 Da (GFPS147C-GSH).

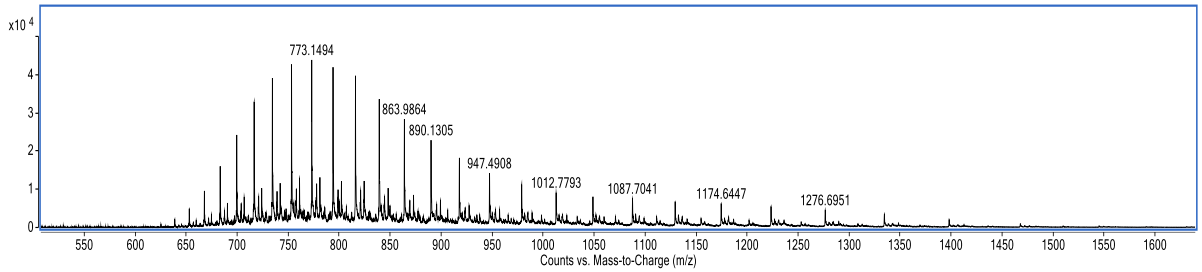

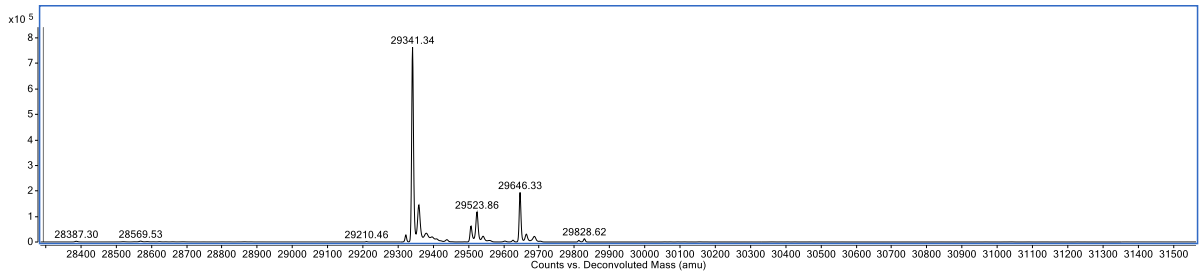

4 h: Observed masses (LCMS Method 2): 29341 Da (reduced GFPS147C), 29646 Da (GFPS147C-GSH).

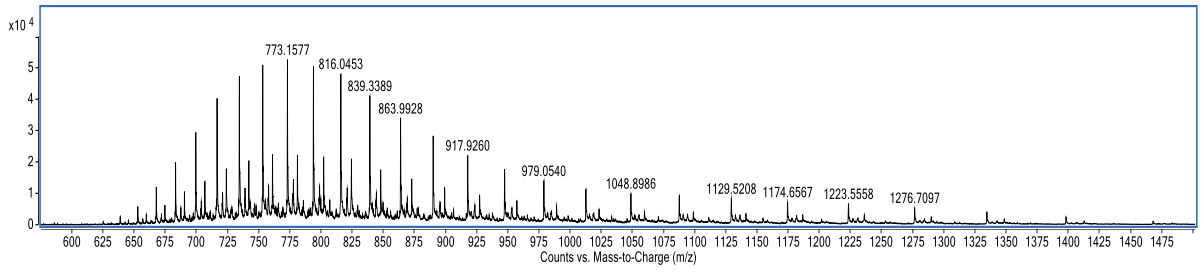

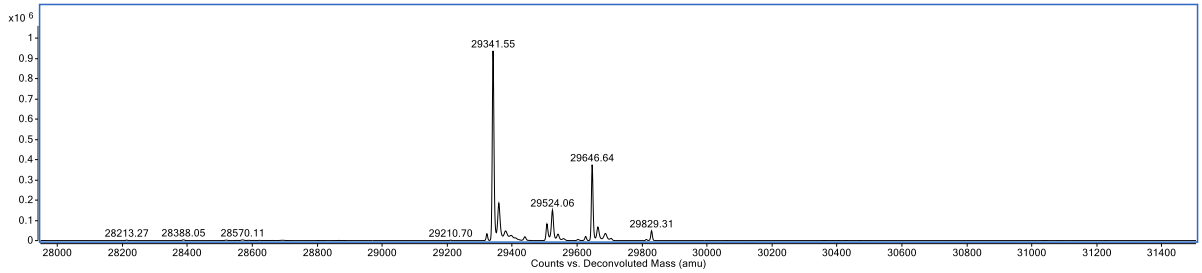

8 h: Observed masses (LCMS Method 2): 29341 Da (reduced GFPS147C), 29646 Da (GFPS147C-GSH).

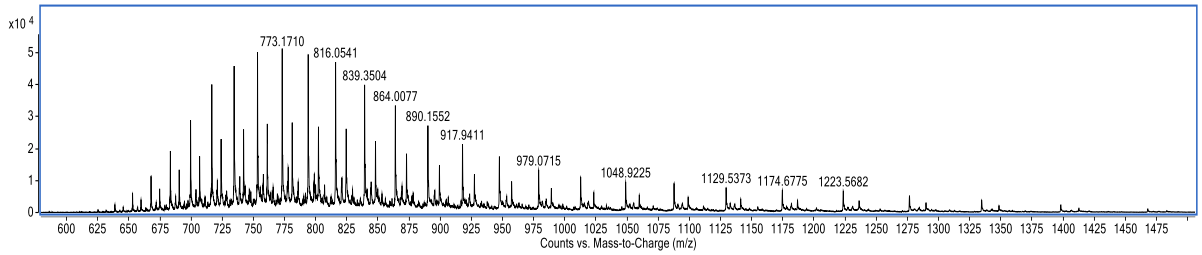

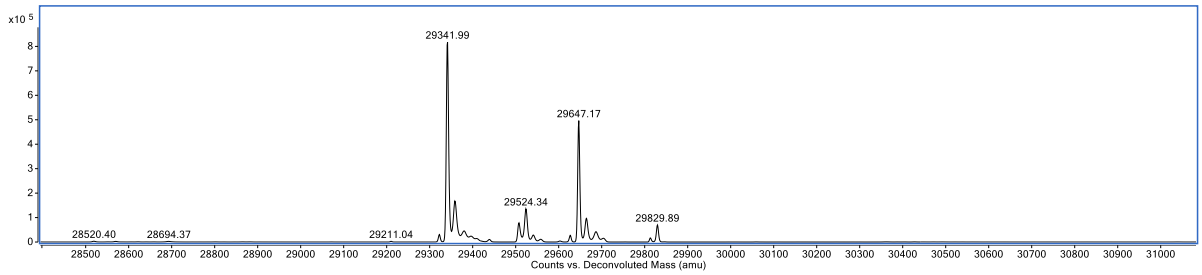

24 h: Observed masses (LCMS Method 2): 29646 Da (GFPS147C-GSH).

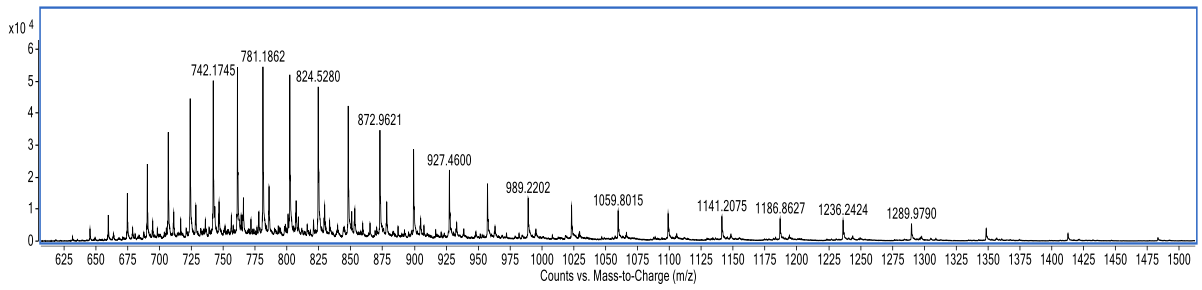

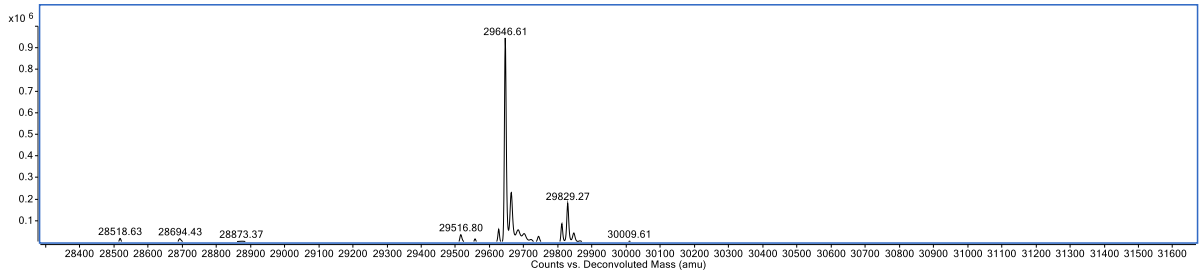

GFPS147C–PD (*N*,*N*'-diethyl)–p-Anisidine **208** – GSH cleavage: Expected masses: 29341 Da (reduced GFPS147C), 29629 Da.

0 h: Expected masses: 29629 Da. Observed masses (LCMS Method 2): 29628 Da.

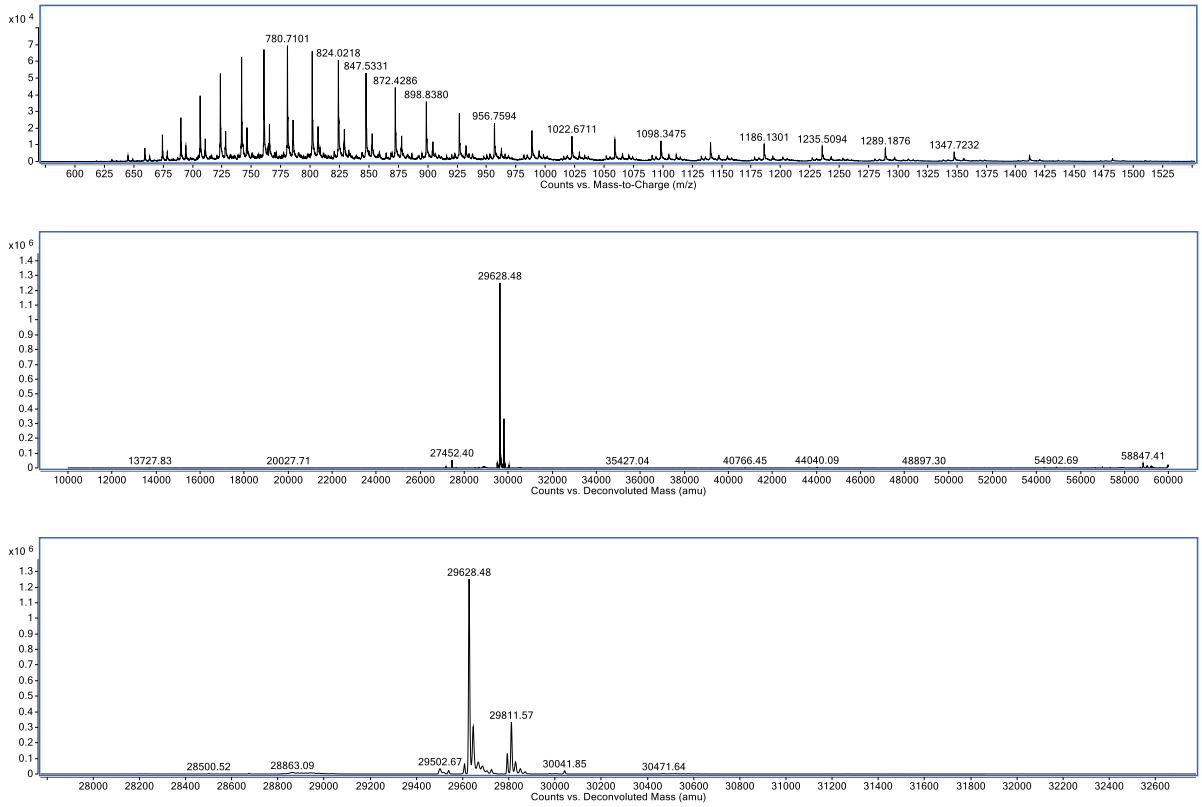

2 h: Observed masses (LCMS Method 2): 29628 Da (GFPS147C–PD (*N*,*N*'-diethyl)–p-Anisidine), 29645 GFPS147C–PD (*N*,*N*'-diethyl)–p-Anisidine + [O])

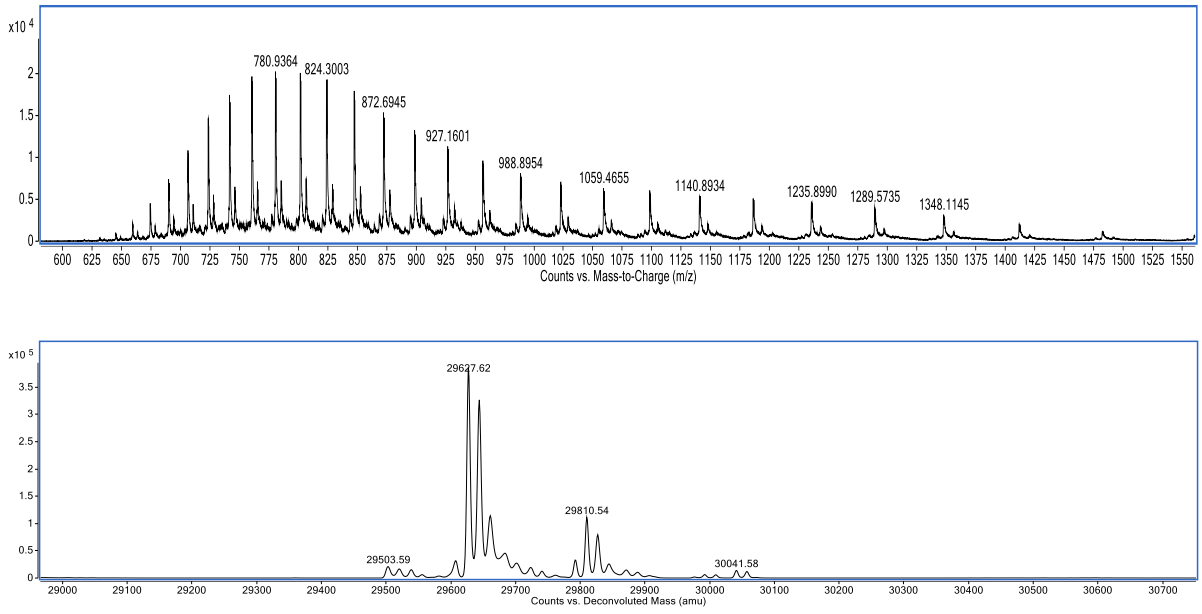

4 h: Observed masses (LCMS Method 2): 29627 Da (GFPS147C–PD (*N,N'*-diethyl)–p-Anisidine), 29645 GFPS147C–PD (*N,N'*-diethyl)–p-Anisidine + [O])

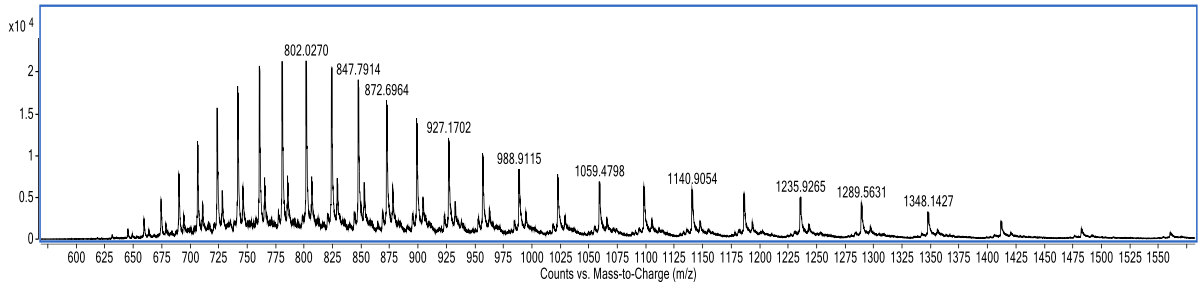

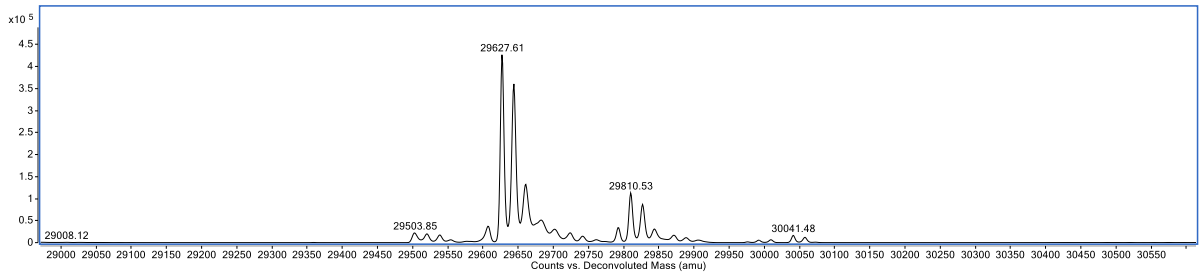

8 h: Observed masses (LCMS Method 2): 29628 Da (GFPS147C–PD (*N,N'*-diethyl)–p-Anisidine), 29645 GFPS147C–PD (*N,N'*-diethyl)–p-Anisidine + [O])

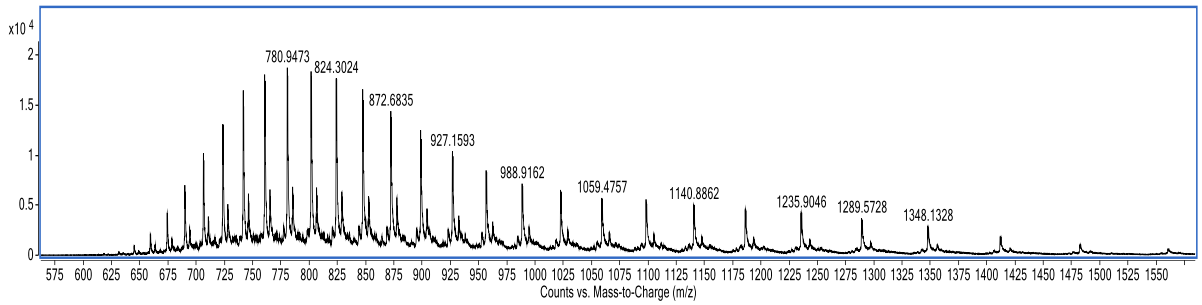

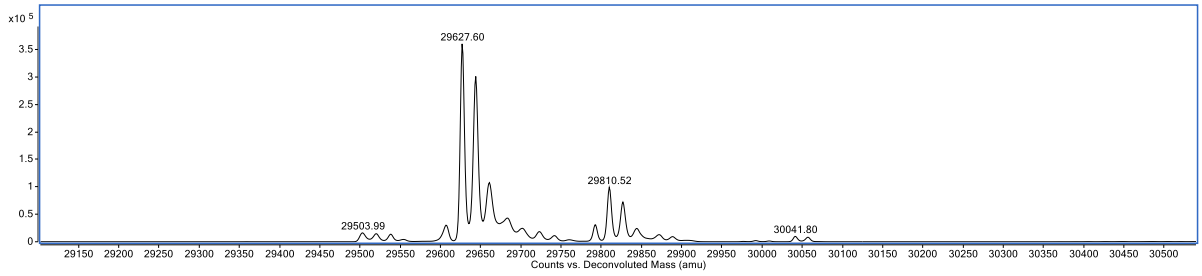

24 h: Observed masses (LCMS Method 2): 29628 Da (GFPS147C–PD (*N,N'*-diethyl)–p-Anisidine), 29645 GFPS147C–PD (*N,N'*-diethyl)–p-Anisidine + [O])

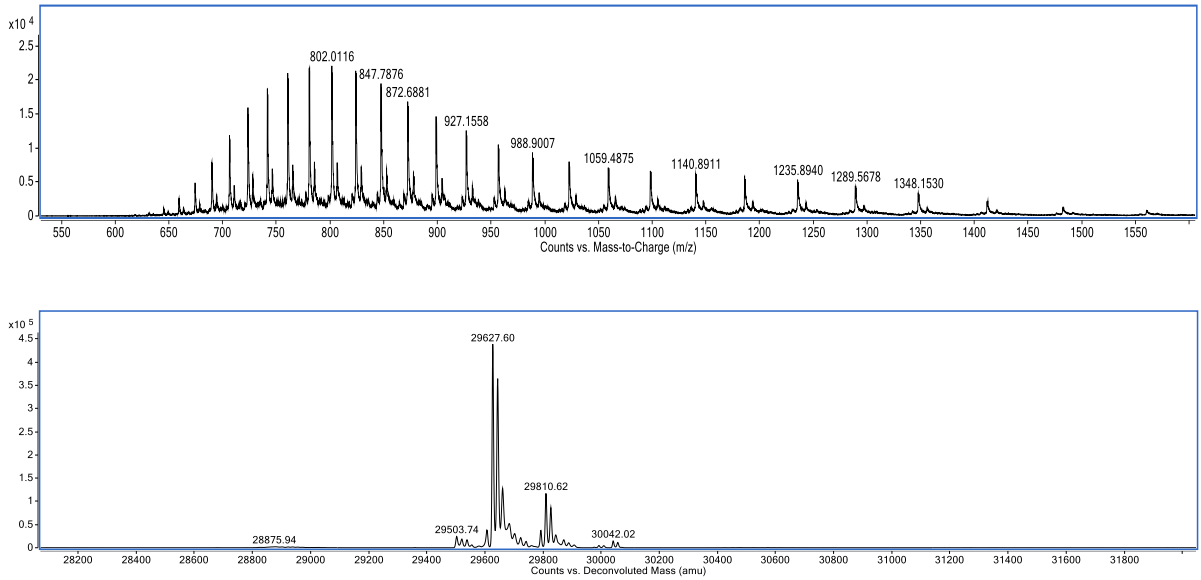

Serum Stability Study[152] – Procedure conducted in collaboration with Ms F. Javaid

GFPS147C–PD (*N*-methyl, *N*'-BCN (AF-488)–conjugates **210** and **211** were prepared as 0.2 mg/mL solutions in PBS 140 mM sodium chloride 12 mM sodium phosphates and 2 mM sodium azide at pH 7.4. The conjugates were diluted with 50 % of human blood serum to give a final a concentration of 0.1 mg/mL of 5 or 12 and 1 mM of sodium azide. One aliquot (50 µL) for each conjugate was taken, flash frozen and stored at −20 °C. The remaining solution was incubated at 37 °C under mild shaking (300 rpm) and covered from light. Aliquots (50 µL) were taken at 1, 3, 5 and 7 days, flash frozen and stored at −20 °C. Aliquots were thawed, spin-filtered (0.22 µm filter) and diluted 100× with elution buffer. Samples (20 µL) of diluted aliquots were analysed by SEC-HPLC on a TSK gel G3000SWXL (7.8 mm x 30 cm) column connected to an Agilent 1200 HPLC system equipped with a 1200 series diode array detector and a fluorescence detector. Samples were eluted using PBS 140 mM NaCl, 100 mM sodium phosphates and 0.02 % sodium azide at pH 7.0 as mobile phase at a flow rate of 0.5 mL/min. over 30 min. Fluorescence was detected with an excitation wavelength of 495 nm and emission wavelength of 525 nm.

GFPS147C–PD (*N*-methyl, *N*'-BCN (AF-488)–*n*-Hexane thiol **210**:

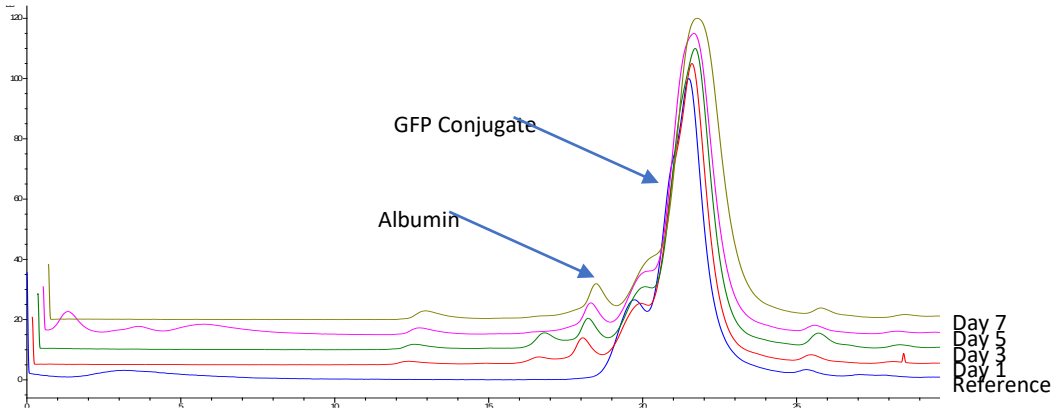

GFPS147C–PD (*N*-methyl, *N*'-BCN (AF-488)–*p*-Anisidine **211**:

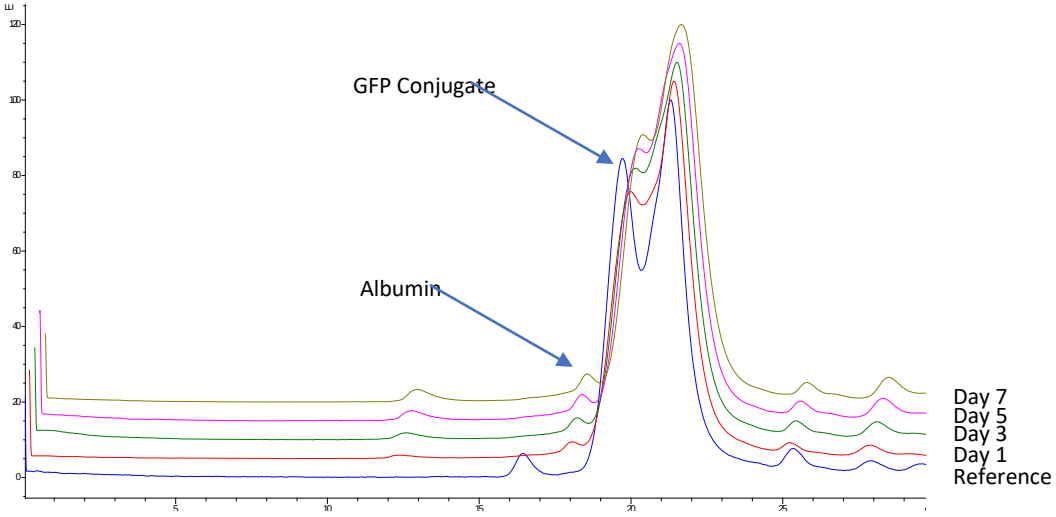

Experimental for Chapter 5

1,2-Diethyl-1,2-dihydropyridazine-3,6-dione 232[71] – Procedure provided by Dr R. J. Spears

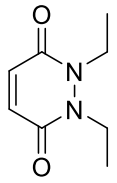

232

To a solution of maleic anhydride (0.51 g, 5.20 mmol) in glacial AcOH (20 mL) was added di-*tert*-butyl 1,2-diethylhydrazine-1,2-dicarboxylate (1.00 g, 3.46 mmol). The reaction mixture was then heated under reflux with stirring overnight. After this time, the reaction mixture was allowed to cool to 21 °C, and the solvent was removed *in vacuo* with toluene co-evaporation (3 x 20 mL, as an azeotrope). Residual toluene was subsequently removed *in vacuo* with chloroform co-evaporation (3 x 20 mL, as an azeotrope). The crude residue was then purified by flash column chromatography (20% to 80% EtOAc/petrol), yielding 1,2-diethyl-1,2-dihydropyridazine-3,6-dione **232** (0.32 g, 1.90 mmol, 55%) as a white solid. ^{1}H NMR (600 MHz, $CDCl_3$) δ 6.87 (s, 2H), 4.13 (q, *J* = 7.1 Hz, 4H), 1.26 (t, *J* = 7.1 Hz, 6H); ^{13}C NMR (150 MHz, $CDCl_3$) δ 157.6 (C), 134.7 (CH), 40.3 (CH_2), 13.3 (CH_3); IR (solid) 2981, 1620, 1452 cm^{-1}.

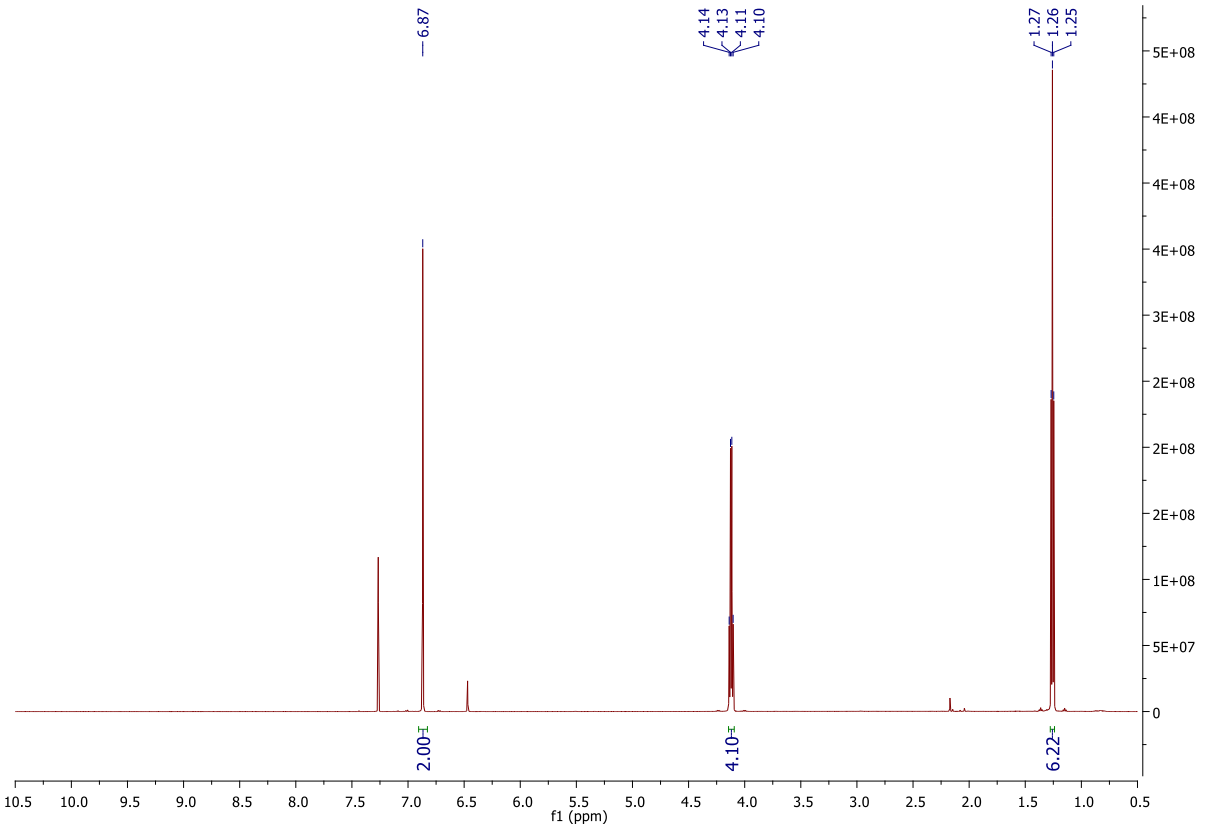
6.87
4.14
4.13
4.11
4.10
1.27
1.26
1.25
2.00
4.10
6.22
f1 (ppm)

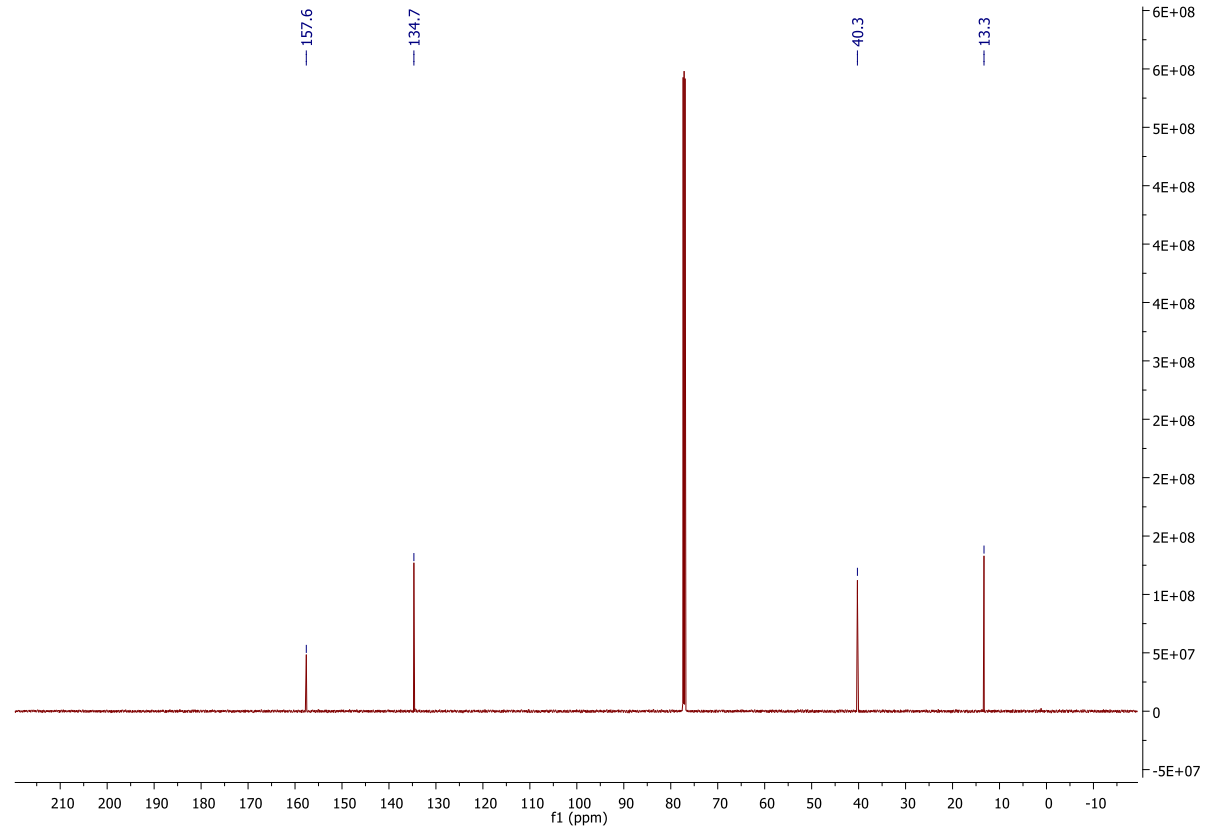
157.6
134.7
40.3
13.3
f1 (ppm)

Methyl *N*-(tert-butoxycarbonyl)-(1,2-diethyl-3,6-dioxohexahydropyridazin-4-yl)-L-cysteinate 233 – Procedure provided by Dr R. J. Spears

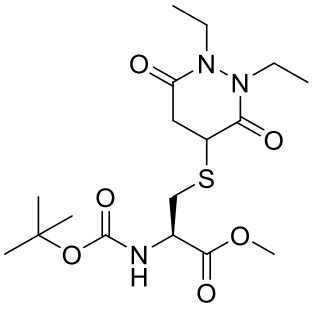

233

To a solution of *N*-(*tert*-butoxycarbonyl)-L-cysteine methyl ester **231** (122 µL, 140 mg, 0.594 mmol) in MeOH (6 mL) was added 1,2-diethyl-1,2-dihydropyridazine-3,6-dione **232** (100 mg, 0.594 mmol) and sodium acetate (146 mg, 1.78 mmol). The reaction mixture was then stirred at 21 °C for 1 h. After this time, the solvent was removed *in vacuo*, and the crude residue was purified by flash column chromatography (20% to 80% EtOAc/petrol) to give methyl *N*-(*tert*-butoxycarbonyl)-(1,2-diethyl-3,6-dioxohexahydropyridazin-4-yl)-L-cysteinate **233** as a colourless oil (128 mg, 0.317 mmol, 54%) as a mixture of diastereoisomers. ^{1}H NMR (700 MHz, $CDCl_3$, diastereomers, rotamers) δ 5.57-5.44 (m, 1H), 4.62-4.55 (m, 1H), 4.10-4.09 (m, 2H), 3.77-3.75 (m, 3H), 3.74-3.73 (m, 0.5 H), 3.71-3.69 (m, 0.5 H) 3.40-3.39 (m, 2H), 3.21-3.18 (m, 0.5 H), 3.14-3.07, (m, 1H), 2.98-2.96, (m, 0.5 H), 2.93-2.89 (m, 1H), 2.62-2.58 (m, 1H), 1.45-1.44 (m, 9H), 1.16-1.15 (m, 3H), 1.13-1.11 (m, 3H); ^{13}C NMR (175 MHz, $CDCl_3$, diastereomers, rotamers) δ 171.4 (C), 171.3 (C), 167.5 (C), 167.3 (C), 166.4 (C), 166.3 (C), 155.4 (C), 155.3 (C), 80.4 (C), 53.7 (CH), 52.9 (CH), 52.9 (CH_3), 41.4 (CH), 41.3 (CH), 38.7 (CH_2), 38.7 (CH_2), 38.6 (CH_2), 35.0 (CH_2), 35.0 (CH_2), 34.2 (CH_2), 33.8 (CH_2), 28.4 (CH_3), 12.2 (CH_3), 11.7 (CH_3), 11.7 (CH_3); IR (thin film) 3018, 2979, 2937, 1743 cm^{-1}; LRMS (ESI) 404 (100, M+H]$^{+}$); HRMS (ESI) calcd for $C_{17}H_{29}NaN_3O_6S$ [M+Na]$^{+}$ 426.1659, observed 426.1687.

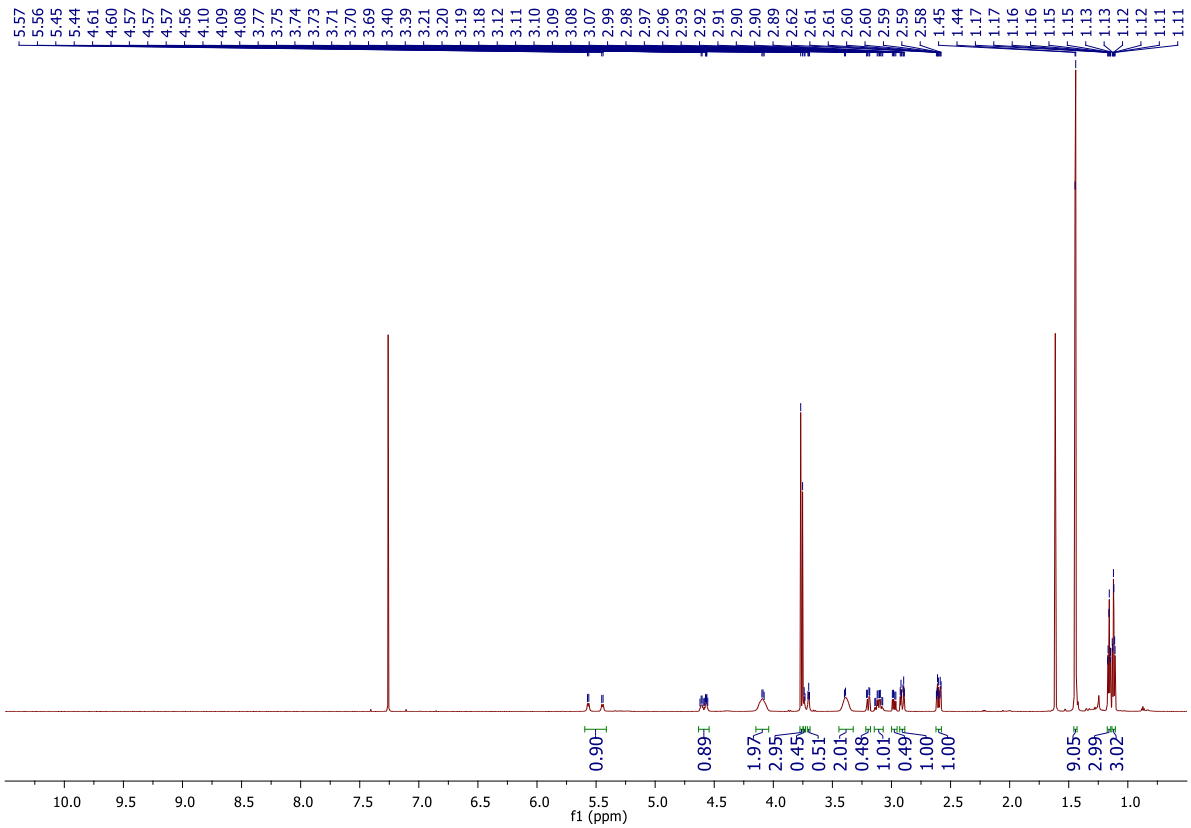
5.57 5.56 5.45 5.44 4.61 4.60 4.57 4.57 4.57 4.56 4.10 4.09 4.08 3.77 3.75 3.74 3.73 3.71 3.70 3.69 3.40 3.39 3.21 3.20 3.19 3.18 3.12 3.11 3.10 3.09 3.08 3.07 2.99 2.98 2.97 2.96 2.93 2.92 2.91 2.90 2.90 2.89 2.62 2.61 2.61 2.60 2.60 2.59 2.59 2.58 1.45 1.44 1.17 1.17 1.16 1.16 1.15 1.15 1.13 1.13 1.12 1.12 1.11 1.11
0.90 0.89 1.97 2.95 0.45 0.51 2.01 0.48 1.01 0.49 1.00 1.00 9.05 2.99 3.02
10.0 9.5 9.0 8.5 8.0 7.5 7.0 6.5 6.0 5.5 5.0 4.5 4.0 3.5 3.0 2.5 2.0 1.5 1.0
f1 (ppm)

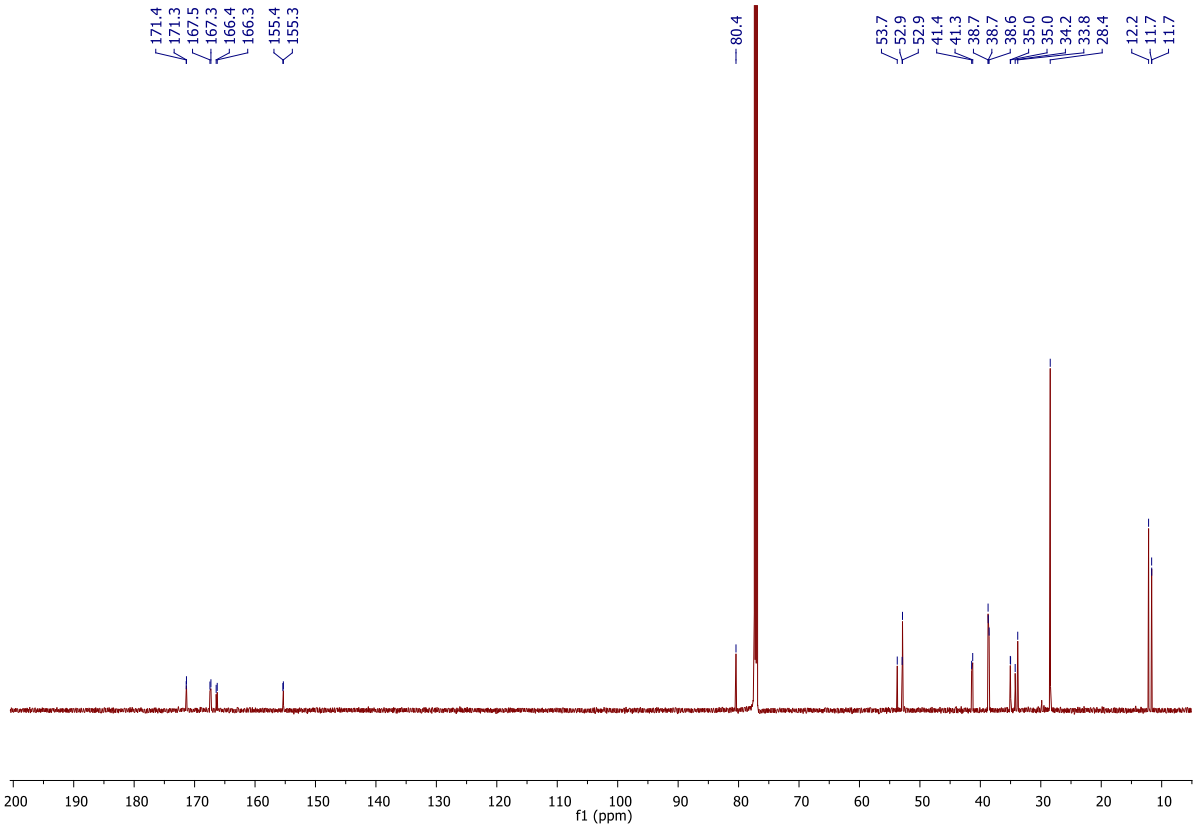
171.4 171.3 167.5 167.3 166.4 166.3 155.4 155.3
80.4
53.7 52.9 52.9 41.4 41.3 38.7 38.7 38.6 35.0 35.0 34.2 33.8 28.4 12.2 11.7 11.7
200 190 180 170 160 150 140 130 120 110 100 90 80 70 60 50 40 30 20 10
f1 (ppm)

3-(Bromo-2-methyl-3,6-dioxo-3,6-dihydropyridazin-1(2*H*)-yl)-*N*-(prop-2-yn-1-yl)propanamide 157d

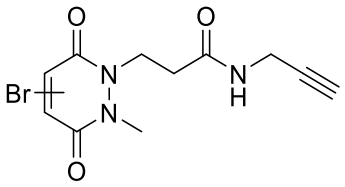

157d

3-(Bromo-2-methyl-3,6-dioxo-3,6-dihydropyridazin-1(2*H*)-yl)-*N*-(prop-2-yn-1-yl)propanamide **157d** was synthesised as described in experimental for chapter 2.

Retro-Michael Deconjugation Analysis (NMR) – Procedure provided by Dr R. J. Spears

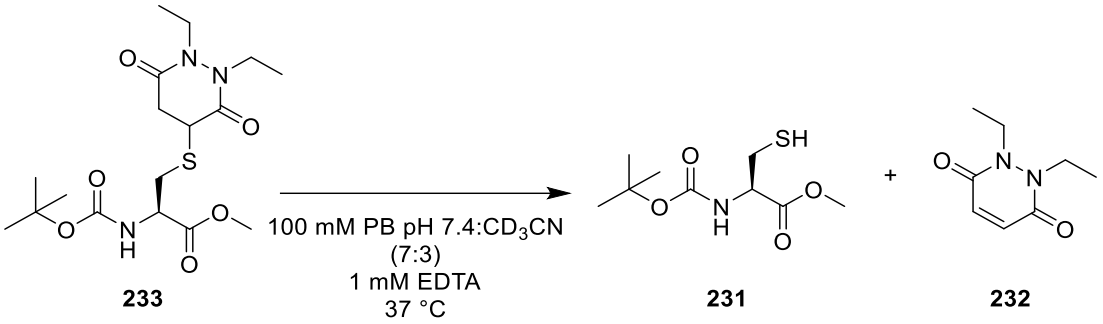

233 **231** **232**

Retro-Michael mediated deconjugation of methyl *N*-(*tert*-butoxycarbonyl)-(1,2-diethyl-3,6-dioxohexahydropyridazin-4-yl)-L-cysteinate **233** to give *N*-(*tert*-butoxycarbonyl)-L-cysteine methyl ester **231** and 1,2-diethyl-1,2-dihydropyridazine-3,6-dione **232** was performed in a solvent system of 7:3 100 mM PB pH 7.4:CD_3CN containing 1 mM EDTA. Deconjugation was monitored by ^1H NMR, and deconjugation was assessed using integrations of the appearing alkene CH protons of 1,2-diethyl-1,2-dihydropyridazine-3,6-dione **232** (relative to the integrations of protons corresponding to methyl *N*-(*tert*-butoxycarbonyl)-*S*-(1,2-diethyl-3,6-dioxohexahydropyridazin-4-yl)-L-cysteinate **231**).

Example of analysis for deconjugation (timepoint at 24 h)

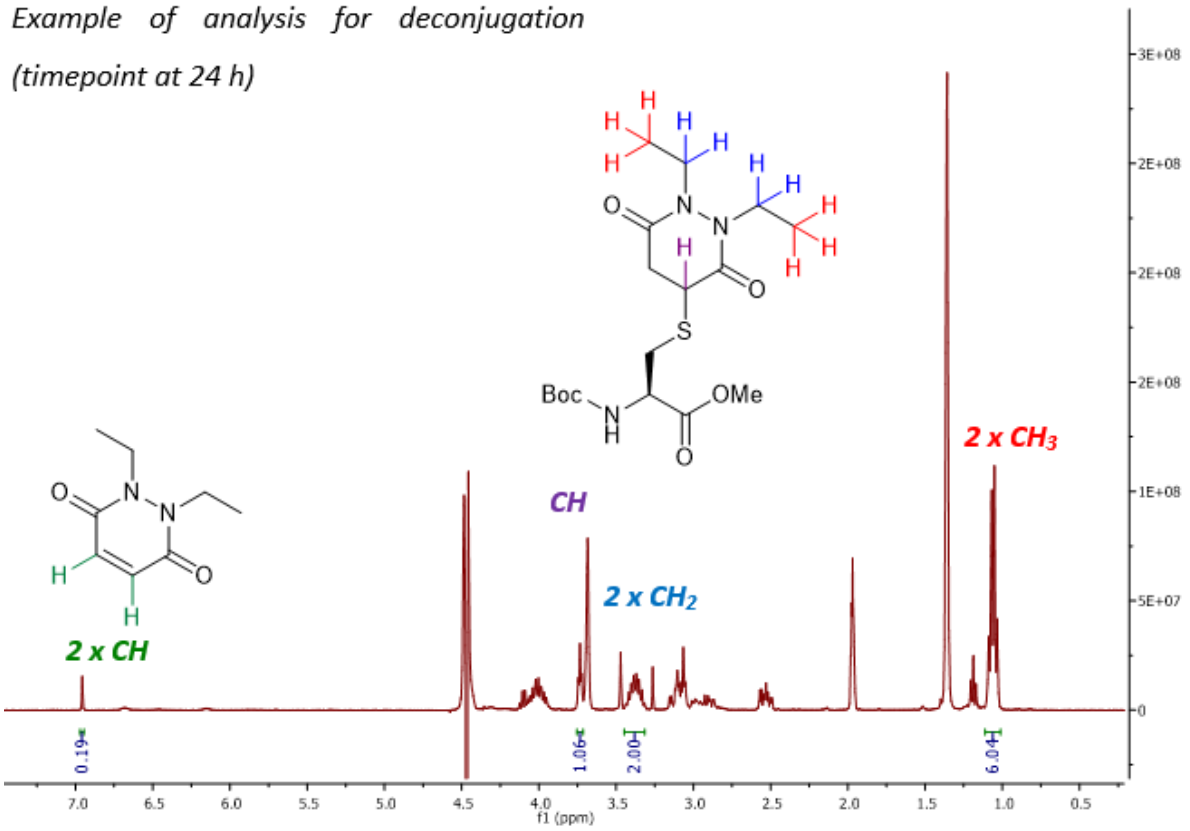

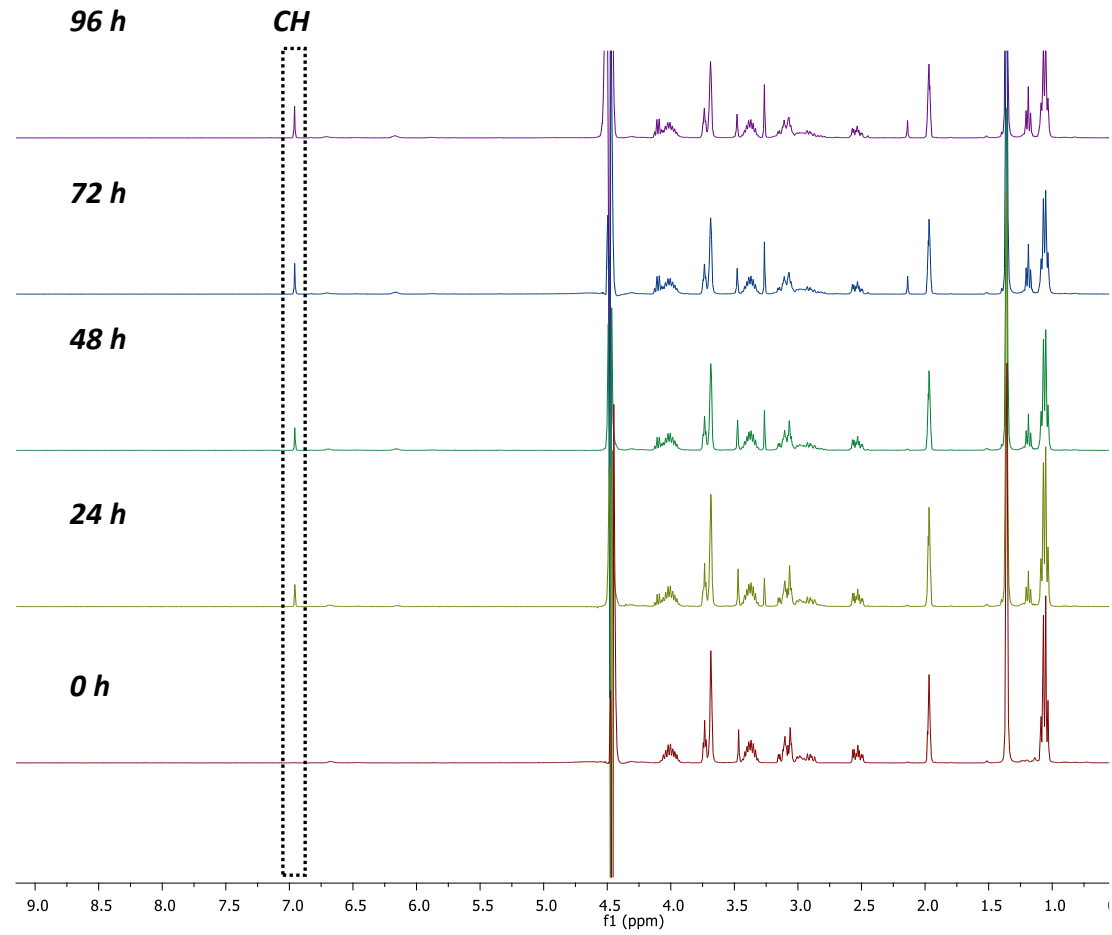

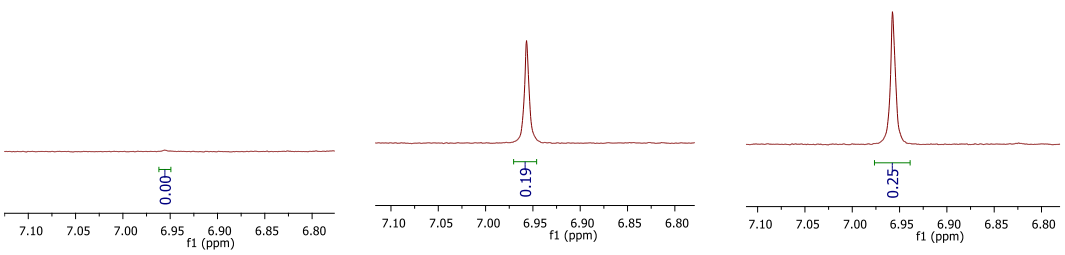

0 h ***24 h*** ***48 h***

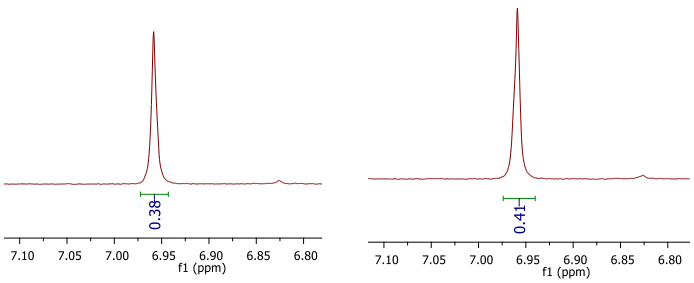

72 h ***96 h***

Small molecule Ellman's test – Procedure provided by Dr R. J. Spears

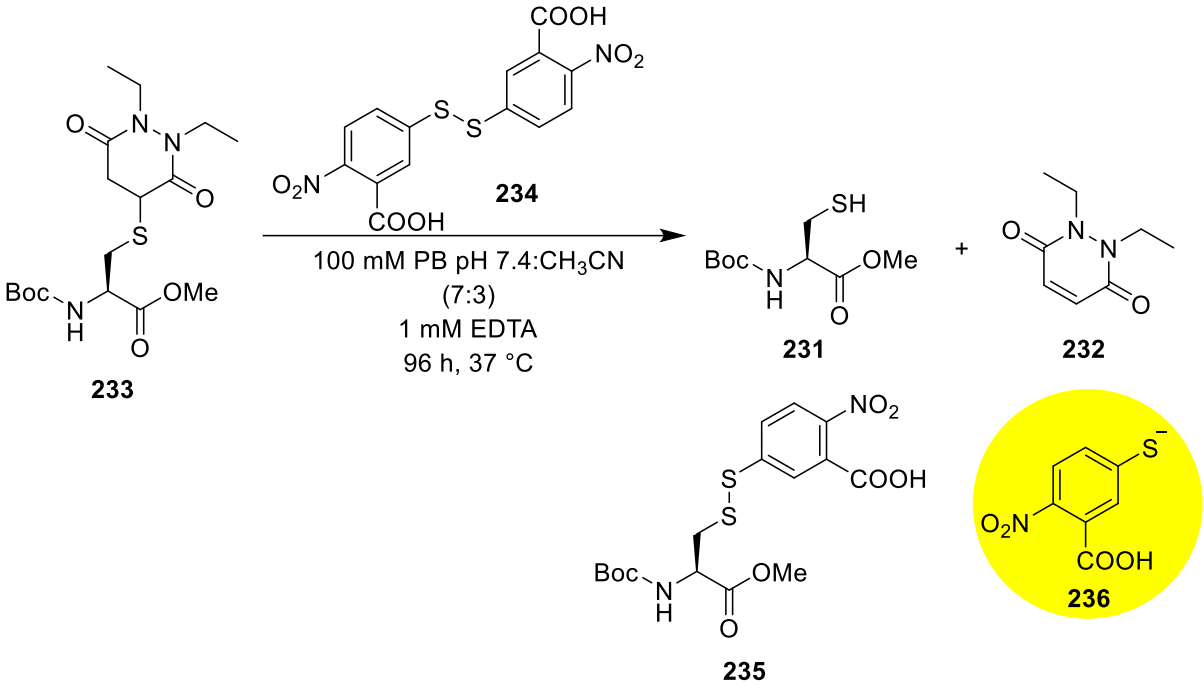

Trapping of *N*-(*tert*-butoxycarbonyl)-L-cysteine methyl ester **231** (resulting from the retro-Michael-mediated deconjugation of *methyl N-(tert*-butoxycarbonyl)-(1,2-diethyl-3,6-dioxohexahydropyridazin-4-yl)-L-cysteinate **233**) with Ellman's reagent **234** was performed thus: CH_3CN (476 µL) was added to 100 mM PB pH 7.4, 1 mM EDTA buffer (1112 µL). To this solution was added methyl *N*-(*tert*-butoxycarbonyl)-*S*-(1,2-diethyl-3,6-dioxohexahydropyridazin-4-yl)-L-cysteinate **233** (28 µL, 5 mM in CH_3CN, 1 eq.), followed by addition of Ellman's reagent **234** (57 µL, 3 mM, 1.2 eq.), resulting in a final reaction mixture of 140 µM methyl *N*-(tert-butoxycarbonyl)-(1,2-diethyl-3,6-dioxohexahydropyridazin-4-yl)-*L*-cysteinate **233** and 170 µM Ellman's reagent **234** in 100 mM PB pH 7.4, 1 mM EDTA buffer: CH_3CN (7:3). The reaction mixture was then allowed to incubate at 37 °C with shaking. An additional control reaction was also performed, wherein 170 µM Ellman's reagent **234** was incubated in 100 mM PB pH 7.4, 1 mM EDTA buffer:CH_3CN (7:3) at 37 °C with shaking. A_{412} of the reaction mixtures were monitored at time points of 24 h, 48 h, 72 h, and 96 h (using 100 mM PB pH 7.4:CH_3CN (7:3), 1 mM EDTA as a blank). Estimated free thiol content (and therefore amount of deconjugation that had occurred) at the given time points was estimated using the equation below.

$$\frac{[TNB_{Trap}] - [TNB_{Control}]}{[CysPD_{Initial}]} \times 100 = \% \text{ estimated deconjugation} \quad (1)$$

Where: TNB_{Trap} = Calculated TNB **236** concentration in trapping reaction, $TNB_{Control}$ = Calculated TNB **234** concentration in control, and $CysPD_{Initial}$ = Initial concentration of **233**

Time point (h)	A_{412}	Estimated conc^n of free TNB 236 (µM)
0	0.026	2
24	0.139	10
48	0.167	12
72	0.153	11
96	0.208	15

Time point (h)	A_{412}	Estimated conc^n of free TNB 236 (µM)	Corrected estimated 9 deconjugated (µM)	Corrected estimated 9 deconjugated (%)
0	0.012	1	0	0
24	0.452	33	23	16
48	0.687	50	38	27
72	0.797	58	47	34
96	0.908	66	51	36

Cysteine Mutant Green Fluorescent Protein (GFPS147C) 48:

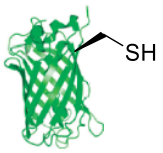

48

GFPS147C **48** was synthesised as described in chapter 4. Observed masses (LCMS Method 1): 29355 Da, 29538 Da.

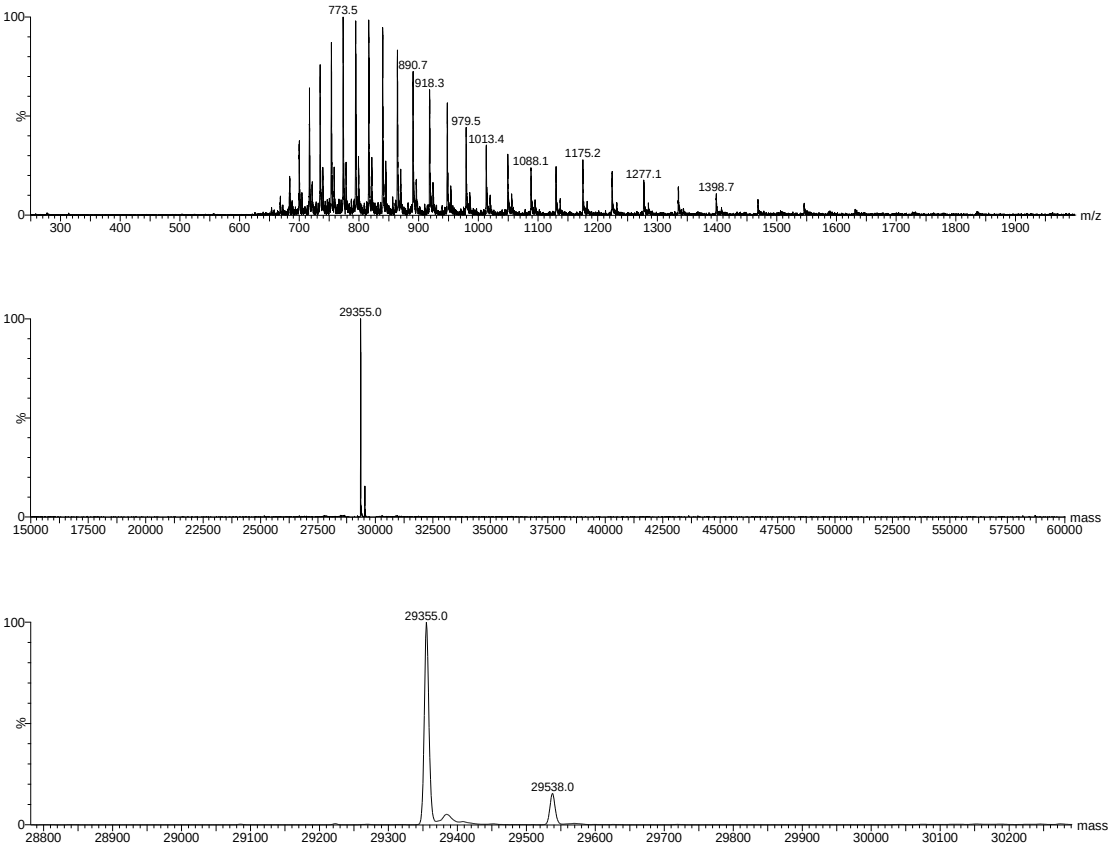

Trastuzumab Fab 116[158]

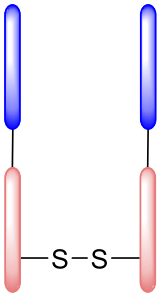

116

Trastuzumab Fab **116** was obtained through pepsin/papain digestion of trastuzumab as described previously.[158] Concentration was determined photometrically using ε_{280} = 68,590 $M^{-1}\,cm^{-1}$. Observed mass 47662 Da.

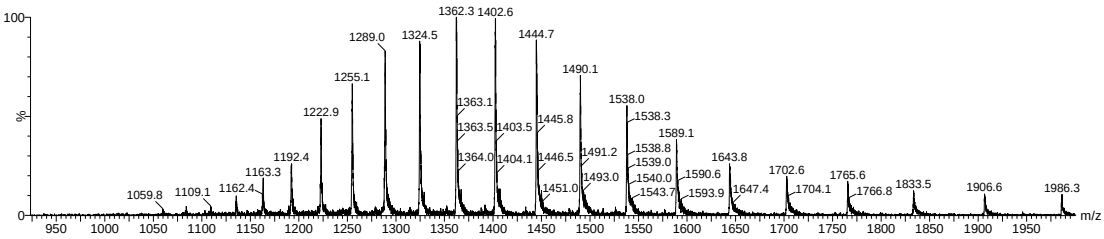

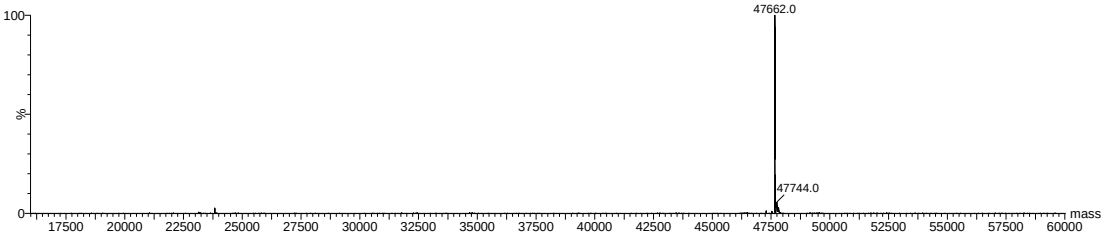

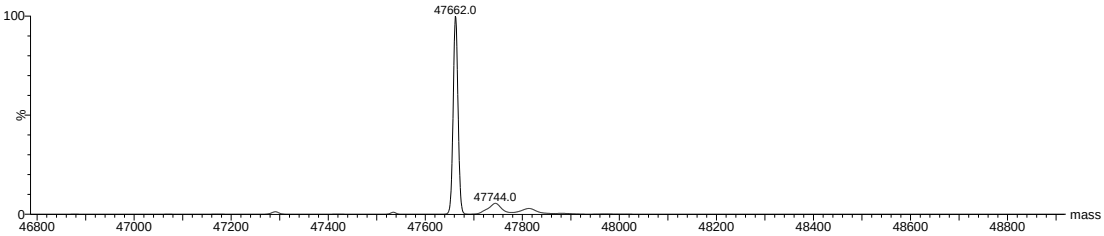

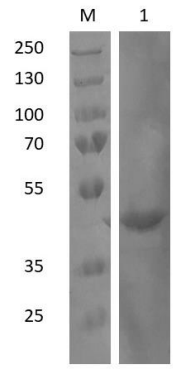

1. Trastuzumab Fab

GFPS147C 48 conjugation with *N,N*-diethyl pyridazinedione 232 (pH 7.4, 200 eq. of PD)

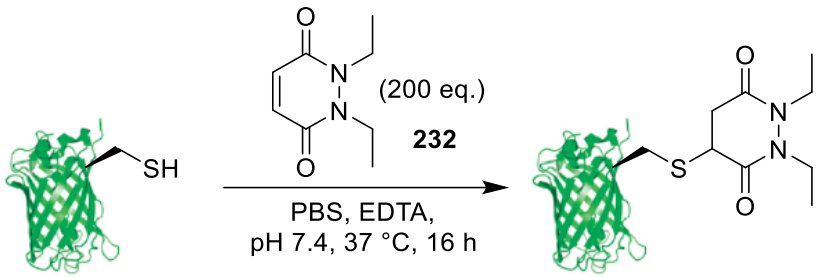

48 **237**

N,N-Diethyl pyridazinedione **232** (25 µL, 200 mM in DMSO, 200 eq.) was added to reduced GFPS147C **48** (500 µL, 50 µM in PBS pH 7.4, 5 mM EDTA) and the solution was incubated at 37 °C for 16 h. Excess reagents were removed using desalting columns (7000 MWCO, ZebaSpin®, Thermo Scientific) prior to LCMS analysis. Expected masses: 29524 Da, 29707 Da. Observed masses (LCMS Method 1): 29529 Da, 29711 Da.

GFPS147C 48 conjugation with *N,N*-diethyl pyridazinedione 232 (pH 8.0, 50 eq. of PD)

N,N-Diethyl pyridazinedione **232** (25 µL, 50 mM in DMSO, 50 eq.) was added to reduced GFPS147C **48** (500 µL, 50 µM in BBS pH 8.0, 5 mM EDTA) and the solution was incubated at 37 °C for 16 h. Excess reagents were removed using desalting columns (7000 MWCO, ZebaSpin®, Thermo Scientific) prior to LCMS analysis. Expected masses: 29524 Da, 29707 Da. Observed masses (LCMS Method 1): 29529 Da, 29711 Da.

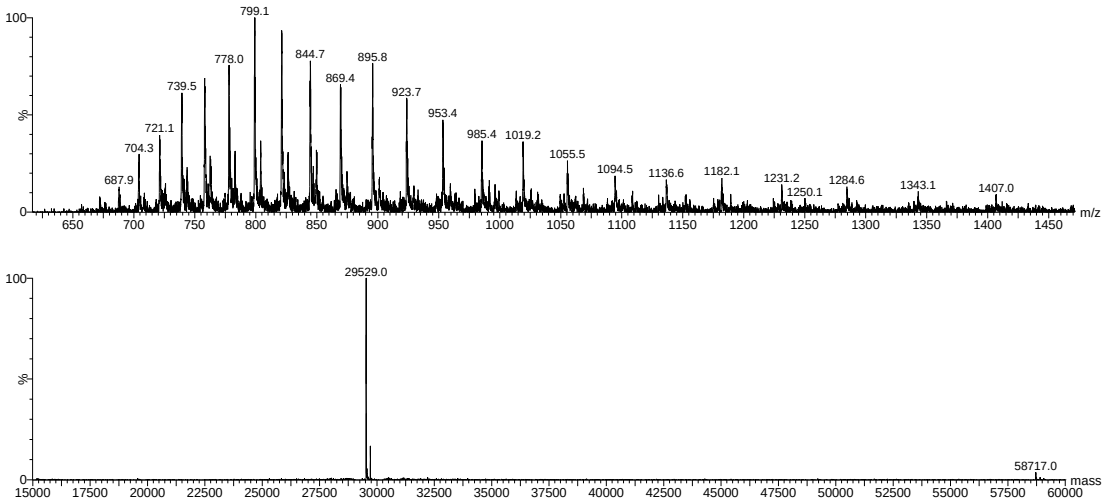

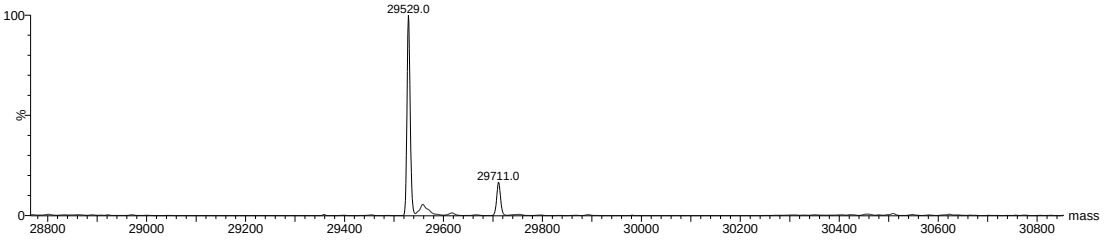
100
%
0
29529.0
29711.0
28800
29000
29200
29400
29600
29800
30000
30200
30400
30600
30800
mass

GFPS147C 48 conjugation with *N*-methyl maleimide 238

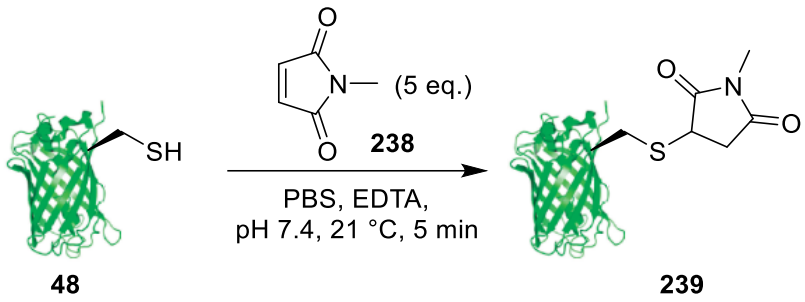

N-Methyl maleimide **238** (15 µL, 5 mM in DMSO, 5 eq.) was added to reduced GFPS147C **48** (300 µL, 50 µM in PBS pH 7.4, 5 mM EDTA) and the solution was incubated at 21 °C for 5 min. Excess reagents were removed using desalting columns (7000 MWCO, ZebaSpin®, Thermo Scientific) prior to LCMS analysis. Expected masses: 29467 Da, 29650 Da. Observed masses (LCMS Method 1): 29469 Da, 29652 Da.

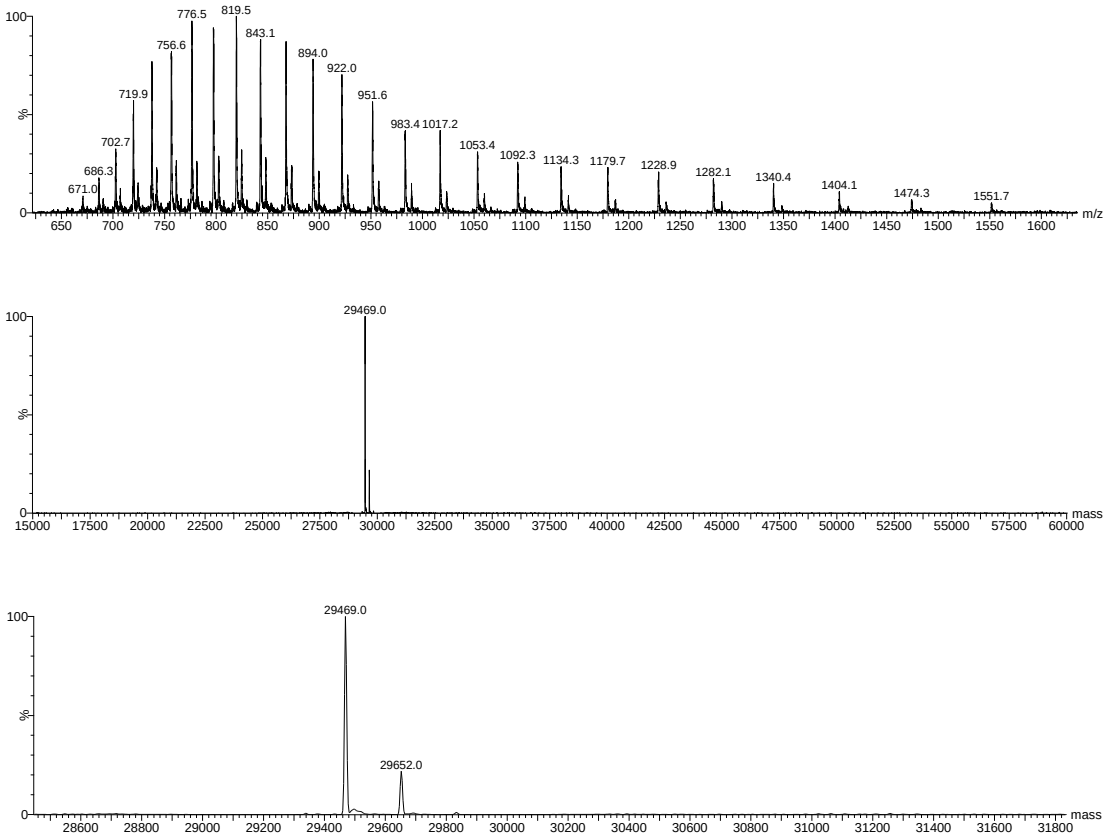

GFPS147C 48 conjugation with monoBr *N,N*-methyl propargyl pyridazinedione 157d

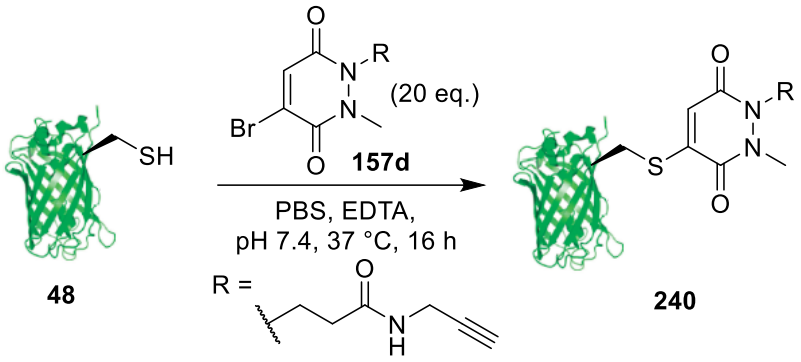

MonoBr *N,N*-methyl propargyl pyridazinedione **157d** (15 µL, 20 mM in DMSO, 20 eq.) was added to reduced GFPS147C **48** (300 µL, 50 µM in PBS pH 7.4, 5 mM EDTA) and the solution was incubated at 37 °C for 16 h. Excess reagents were removed using desalting columns (7000 MWCO, ZebaSpin®, Thermo Scientific) prior to LCMS analysis. Expected masses: 29589 Da, 29772 Da. Observed masses (LCMS Method 1): 29592 Da, 29774 Da.

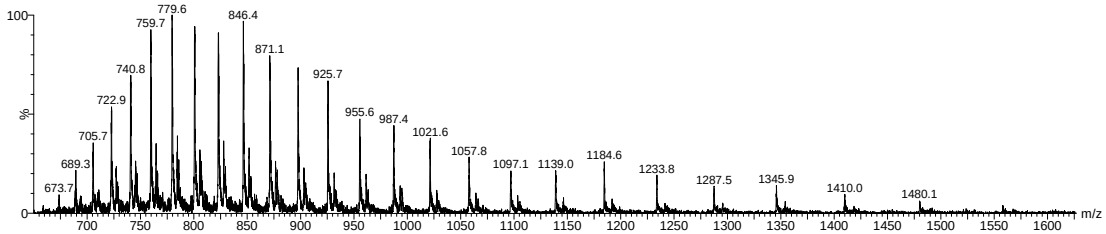

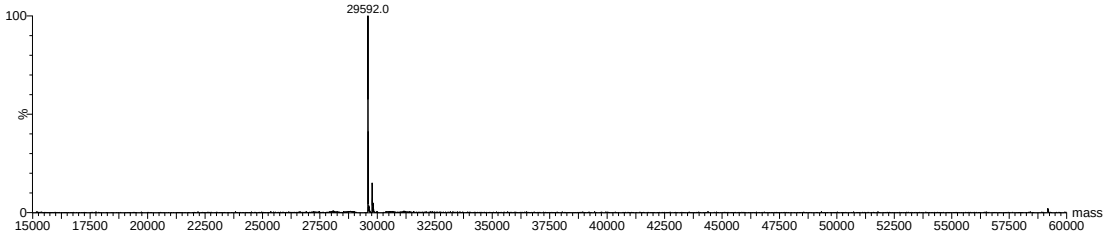

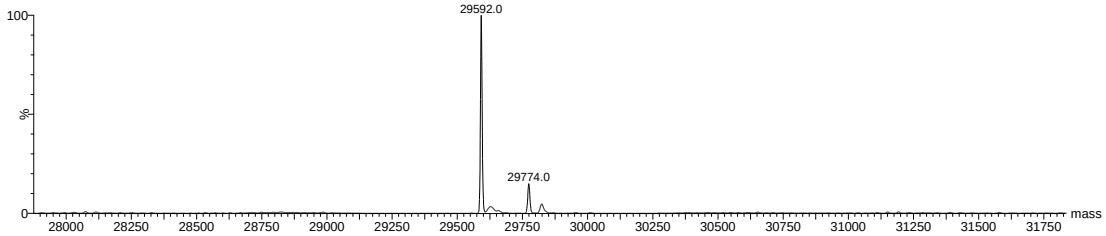

Incubation of GFPS147C-PD conjugate 237

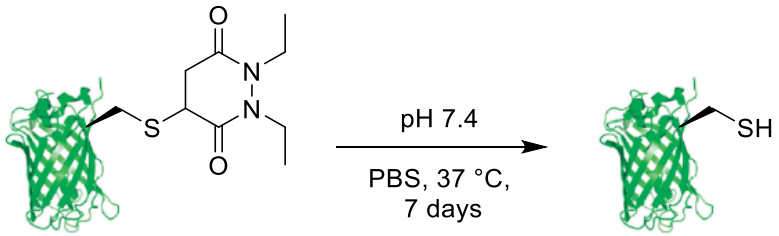

237 **48**

GFPS147C-PD conjugate **237** (200 µL, 50 µM) was buffer exchanged (7000 MWCO, ZebaSpin®, Thermo Scientific) into PBS (pH 7.4). The GFPS147C-PD conjugate **237** was then incubated at 37 °C for a total of 7 days. Samples were desalted (7000 MWCO, ZebaSpin®, Thermo Scientific) before LCMS analysis. Expected masses: 29355 Da, 29529 Da, 29538 Da, 29711 Da, Observed masses (LCMS Method 1): 29365 Da, 29538, 29717.

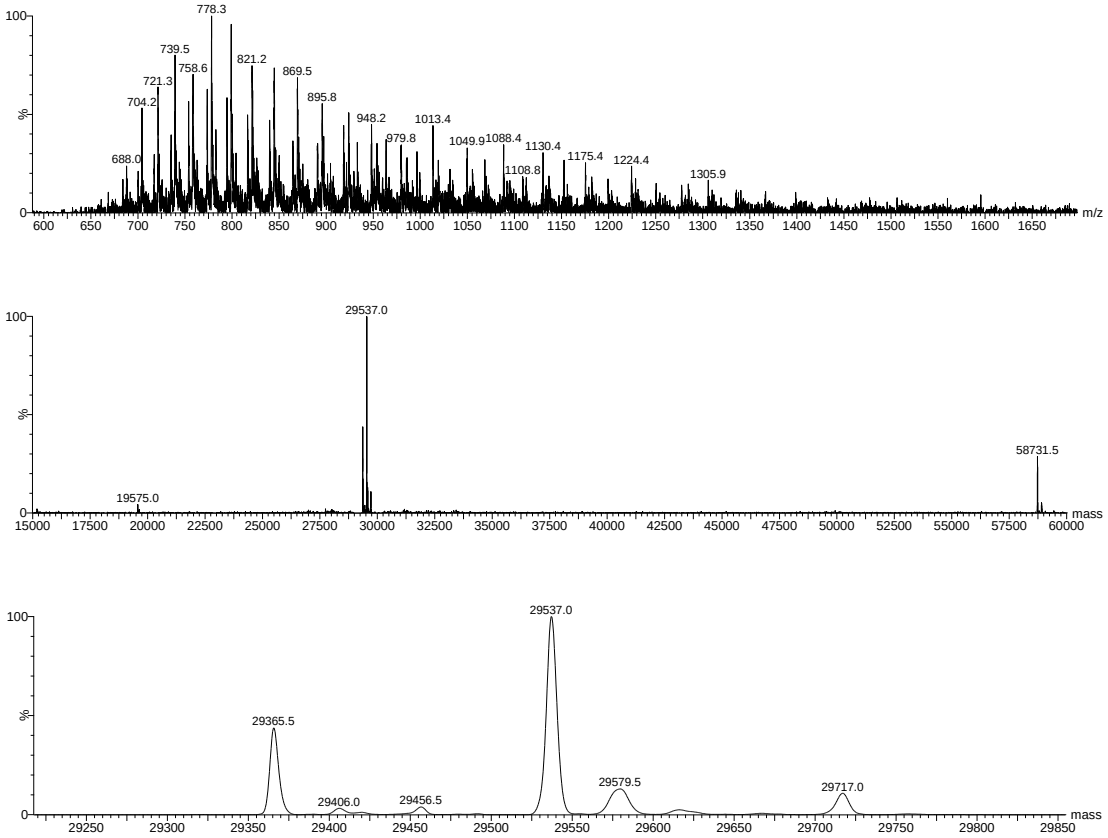

Reaction of GFPS147C-PD conjugate 237 with monoBr *N,N*-methyl propargyl pyridazinedione 157d

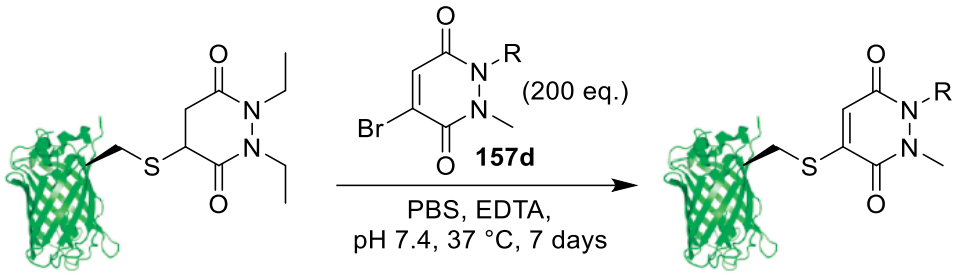

237 **240**

MonoBr *N,N*-methyl propargyl pyridazinedione **157d** (5.0 µL, 200 mM in DMSO, 200 eq.) was added to a solution of GFPS147C-PD conjugate **237** (100 µL, 50 µM in PBS pH 7.4, 5 mM EDTA) and the solution was incubated at 37 °C for 7 days. Excess reagents were removed using desalting columns (7000 MWCO, ZebaSpin®, Thermo Scientific) prior to LCMS analysis. Expected masses: 29589 Da, 29772 Da. Observed masses (LCMS Method 1): 29582 Da 29776 Da.

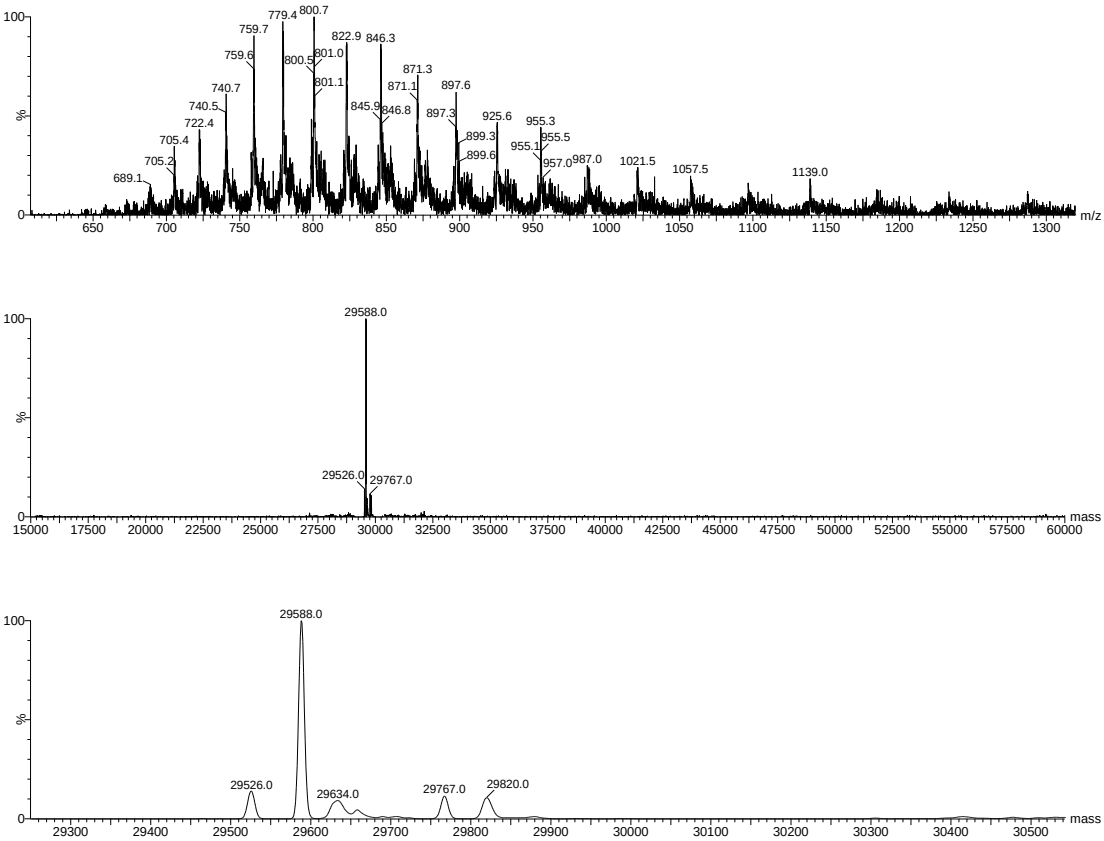

Control: Reaction of GFPS147C-PD conjugate 240 with *N,N*-diethyl pyridazinedione 232

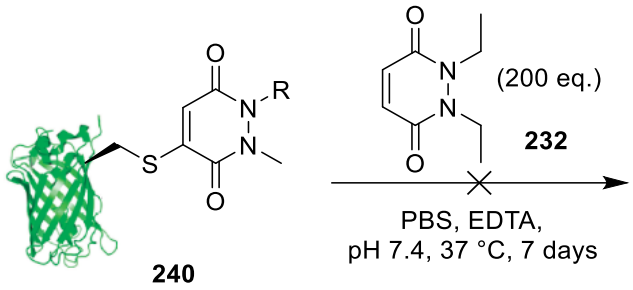

N,N-Diethyl pyridazinedione **232** (5.0 µL, 200 mM in DMSO, 200 eq.) was added to a solution of GFPS147C-PD conjugate **240** (100 µL, 50 µM in PBS = pH 7.4, 5 mM EDTA) and the solution was incubated at 37 °C for 7 days. Excess reagents were removed using desalting columns (7000 MWCO, ZebaSpin®, Thermo Scientific) prior to LCMS analysis. Expected masses: 29589 Da, 29772 Da. Observed masses (LCMS Method 1): 29596 Da, 29777 Da.

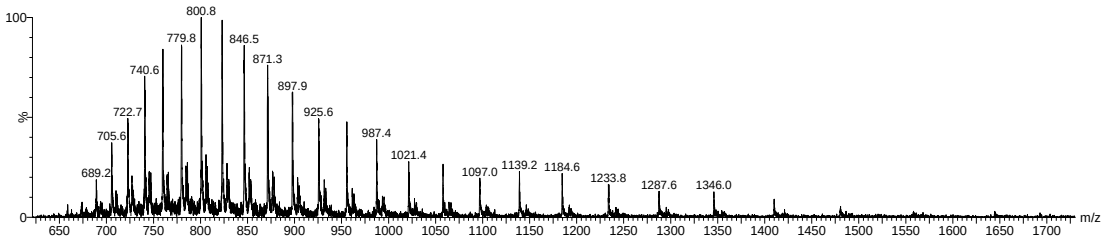

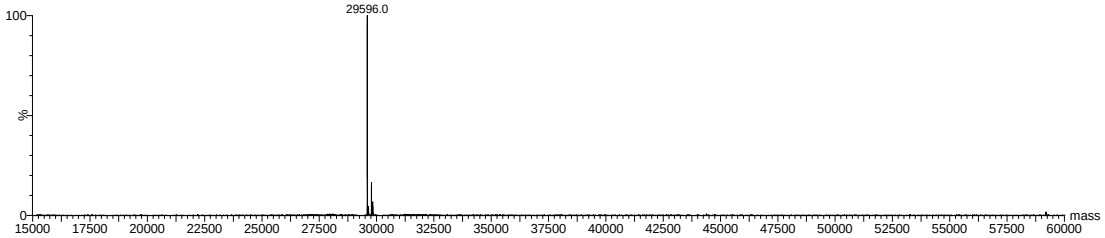

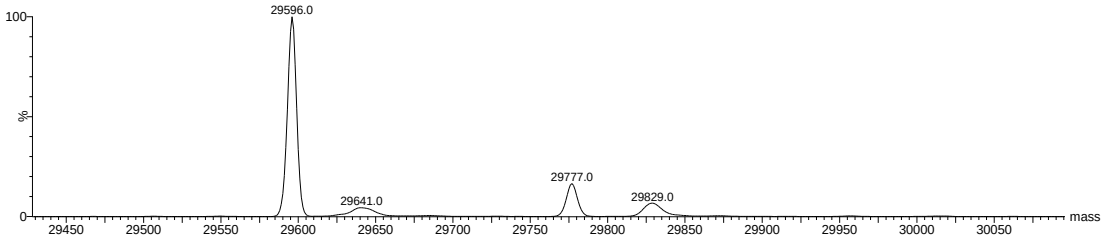

Incubation of GFPS147C-maleimide conjugate 239

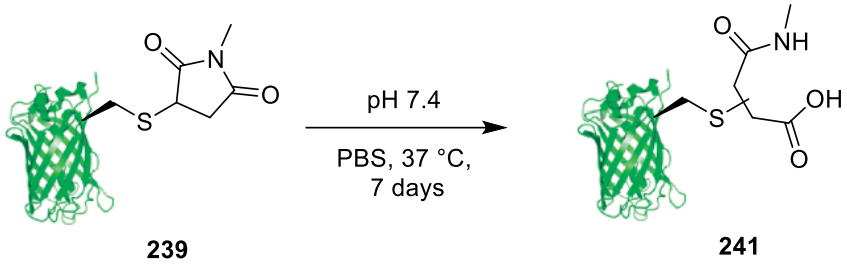

239 **241**

GFPS147C-maleimide conjugate **239** (200 µL, 50 µM) was buffer exchanged (7000 MWCO, ZebaSpin®, Thermo Scientific) into PBS (pH 7.4). The GFPS147C-maleimide conjugate **239** was then incubated at 37 °C for a total of 7 days. Samples were desalted (7000 MWCO, ZebaSpin®, Thermo Scientific) before LCMS analysis. Expected masses: 29485 Da, 29668 Da, Observed masses (LCMS Method 1): 29481 Da, 29665 Da.

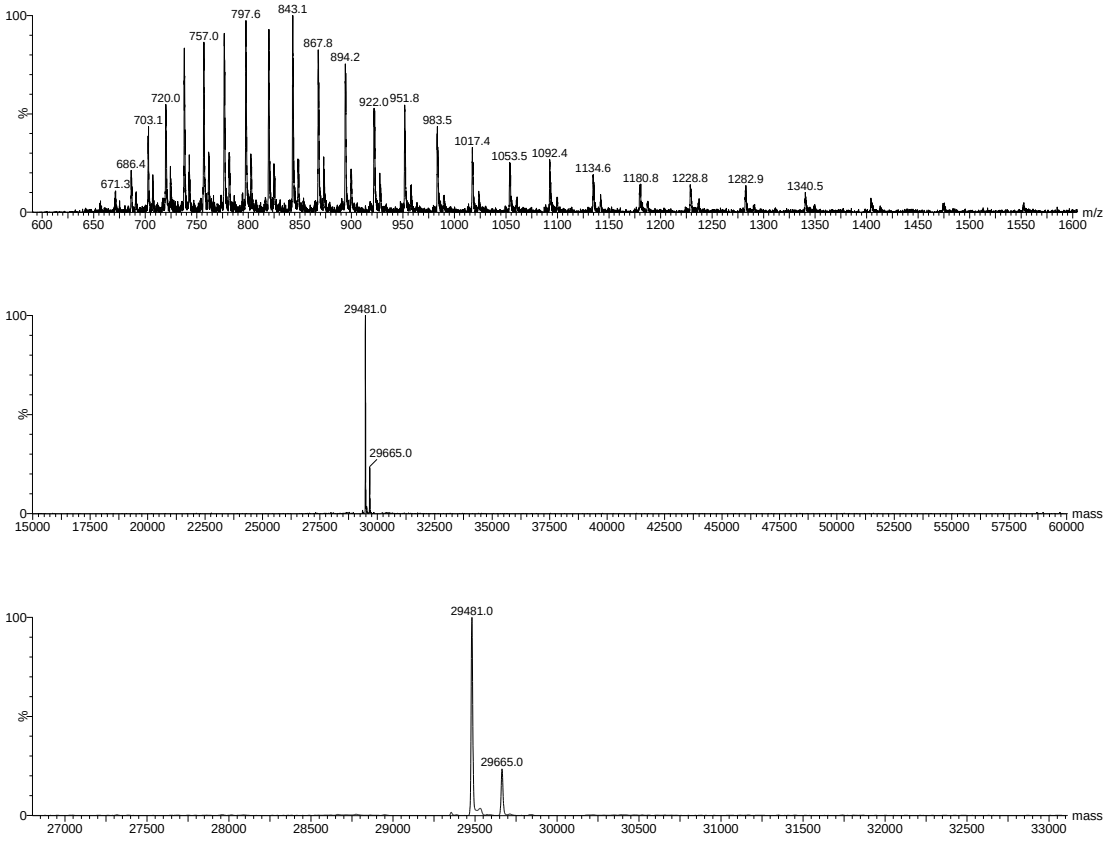

Reaction of GFPS147C-Mal 239 conjugate with monoBr *N,N*-methyl propargyl pyridazinedione 157d

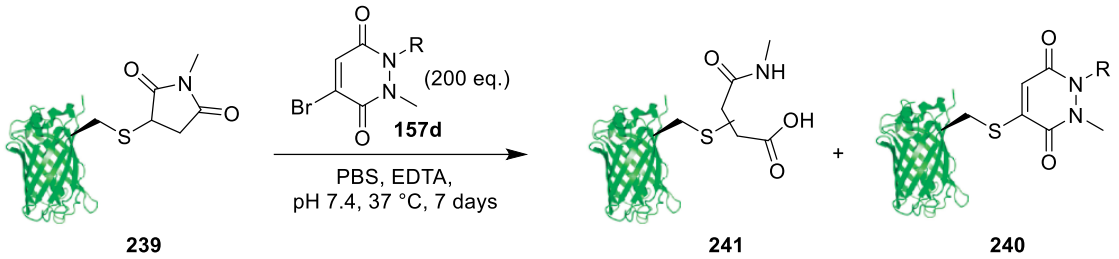

MonoBr *N,N*-methyl propargyl pyridazinedione **157d** (5.0 µL, 200 mM in DMSO, 200 eq.) was added to a solution of GFPS147C-maleimide conjugate **239** (100 µL, 50 µM in PBS pH 7.4, 5 mM EDTA) and the solution was incubated at 37 °C for 7 days. Excess reagents were removed using desalting columns (7000 MWCO, ZebaSpin®, Thermo Scientific) prior to LCMS analysis. Expected masses: 29485 Da, 29589 Da, 29668, 29772. Observed masses (LCMS Method 1): 29481 Da, 29596 Da, 29663 Da

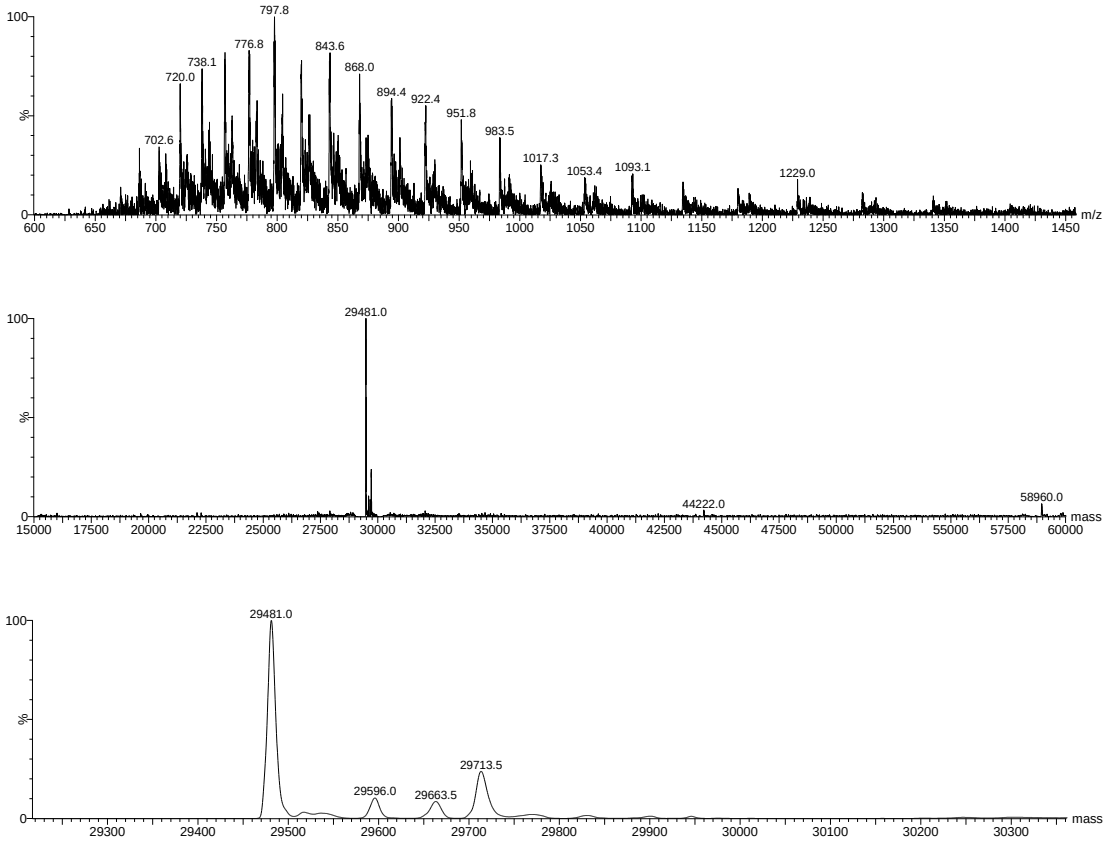

Kinetics: Reaction of GFPS147C conjugates 237 and 239 with DTNB 234

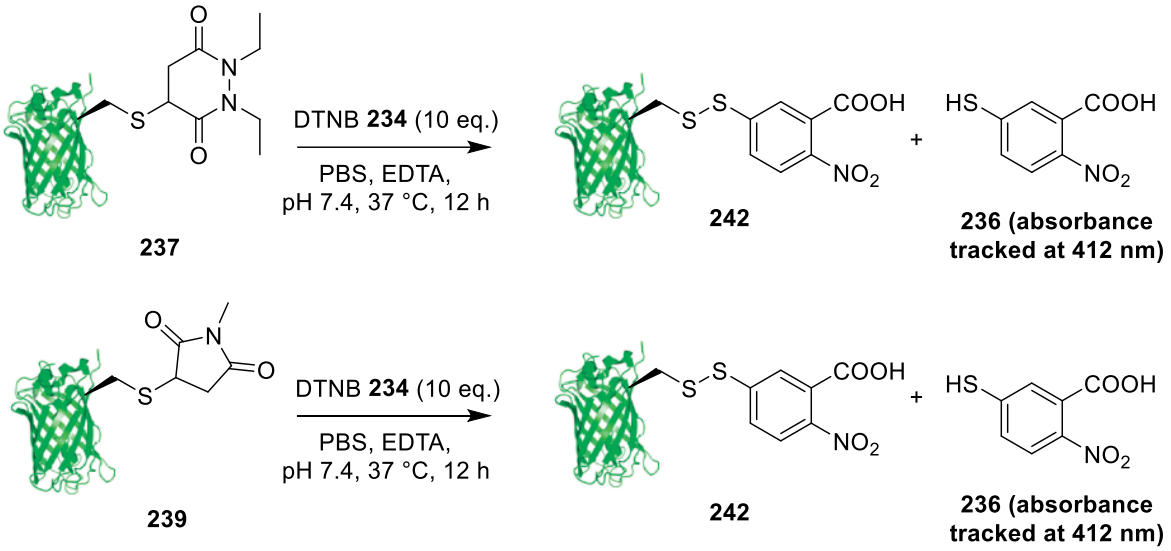

DTNB **234** (5.0 µL, 50 mM in DMSO) was added to GFPS147C-PD **237** (1000 µL, 14.4 µM in PBS pH 7.4, 5 mM EDTA), GFPS147C-maleimide **239** (1000 µL, 12.7 µM in PBS pH 7.4, 5 mM EDTA) and to PBS only (pH 7.4, 5 mM EDTA) as a control. The solutions were incubated in a 1 mL cuvette with stirring at 37 °C for 12 h. UV measurements were taken at 280 nm, 412 nm and 490 nm at 2 min intervals. A_{412} control readings for DTNB **234** only experiments were subtracted from all timepoints for GFP conjugates **237** and **239**. A_{412} for initial readings (t=180 s) were also subtracted from all timepoints for GFP conjugates **237** and **239** to plot ΔA_{412} *vs* time (seconds). ΔA_{412} values were converted into Δ[TNB **236**] values using ε_{280} = 14,150 $M^{-1}\,cm^{-1}$ for TNB **236**. Δ[TNB **236**] values were converted into Δ[GFP-TNB **242**] and subtracted from initial GFP conjugate concentrations (calculated using ε_{490} = 55,000 $M^{-1}\,cm^{-1}$) to form a plot of Δ[GFP-PD **237**] or Δ[GFP-maleimide **239**] vs time. The natural logarithm of Δ[GFP-PD **237**] and Δ[GFP-maleimide **239**] was calculated and plotted against time (seconds). Linear regression was plotted using GraphPad Prism software and pseudo order rate constants were calculated using the equation below:

$$\ln([\text{GFP conjugate } \mathbf{237} \text{ or } \mathbf{239}]) = -kt + \ln([\text{GFP conjugate}]_0)$$

Data	*GFP-PD conjugate **237***	*GFP-maleimide conjugate **239***
Linear Regression	$y = -2.292\times10^{-5}\,x - 11.07$	$y = -2.342\times10^{-5}x - 11.26$
Rate constant K (s^{-1})	2.29×10^{-5}	2.342×10^{-5}
R^2	0.9906	0.9983

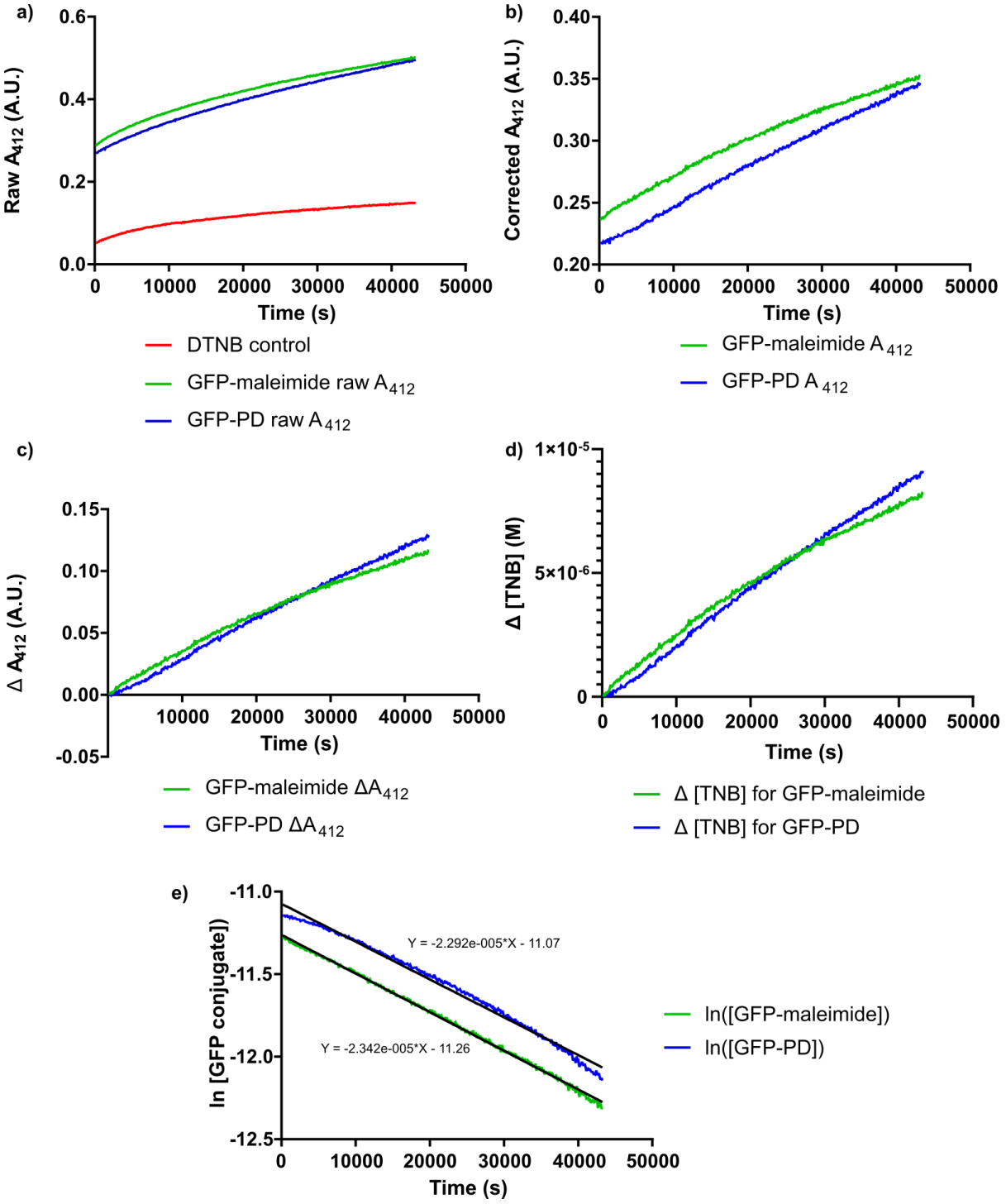
a)
Raw A412 (A.U.)
0.6
0.4
0.2
0.0
0
10000
20000
30000
40000
50000
Time (s)
DTNB control
GFP-maleimide raw A412
GFP-PD raw A412
b)
Corrected A412 (A.U.)
0.40
0.35
0.30
0.25
0.20
Time (s)
GFP-maleimide A412
GFP-PD A412
c)
Δ A412 (A.U.)
0.15
0.10
0.05
0.00
-0.05
Time (s)
GFP-maleimide ΔA412
GFP-PD ΔA412
d)
Δ [TNB] (M)
1×10-5
5×10-6
0
Time (s)
Δ [TNB] for GFP-maleimide
Δ [TNB] for GFP-PD
e)
ln [GFP conjugate])
-11.0
-11.5
-12.0
-12.5
Y = -2.292e-005*X - 11.07
Y = -2.342e-005*X - 11.26
Time (s)
ln([GFP-maleimide])
ln([GFP-PD])

Conjugation of Trastuzumab Fab 116 with *N,N*-Diethyl Pyridazinedione 232

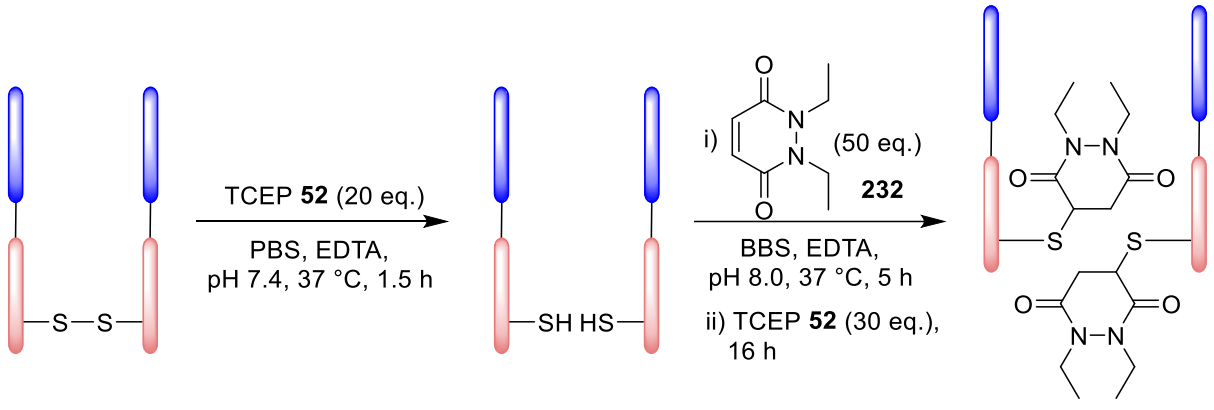

116 **243** **244**

TCEP **52** (10.0 µL, 20 mM in deionised water, 20 eq.) was added to a solution of trastuzumab Fab **116** (500 µL, 20 µM) in PBS (pH 7.4) and the solution was incubated at 37 °C for 90 min. Excess TCEP was removed by ultrafiltration (6 × 10000 MWCO, VivaSpin®, GE Healthcare) into PBS (pH 8.0, 5 mM EDTA). DiEt PD **232** (10.0 µL, 50 mM in DMSO, 50 eq.) was added to the solution of reduced trastuzumab Fab **116** and the solution was incubated at 37 °C for 5 h. After this time, additional TCEP **52** (15.0 µL, 20 mM in deionised water, 30 eq.) was added and the solution was incubated at 37 °C for a further 16 h. Excess reagents were removed by ultrafiltration (6 × 10000 MWCO, VivaSpin®, GE Healthcare) into deionised water prior to LCMS analysis. Expected masses: 23621 Da, 24382 Da. Observed masses (LCMS Method 1): 23620 Da, 24382 Da.

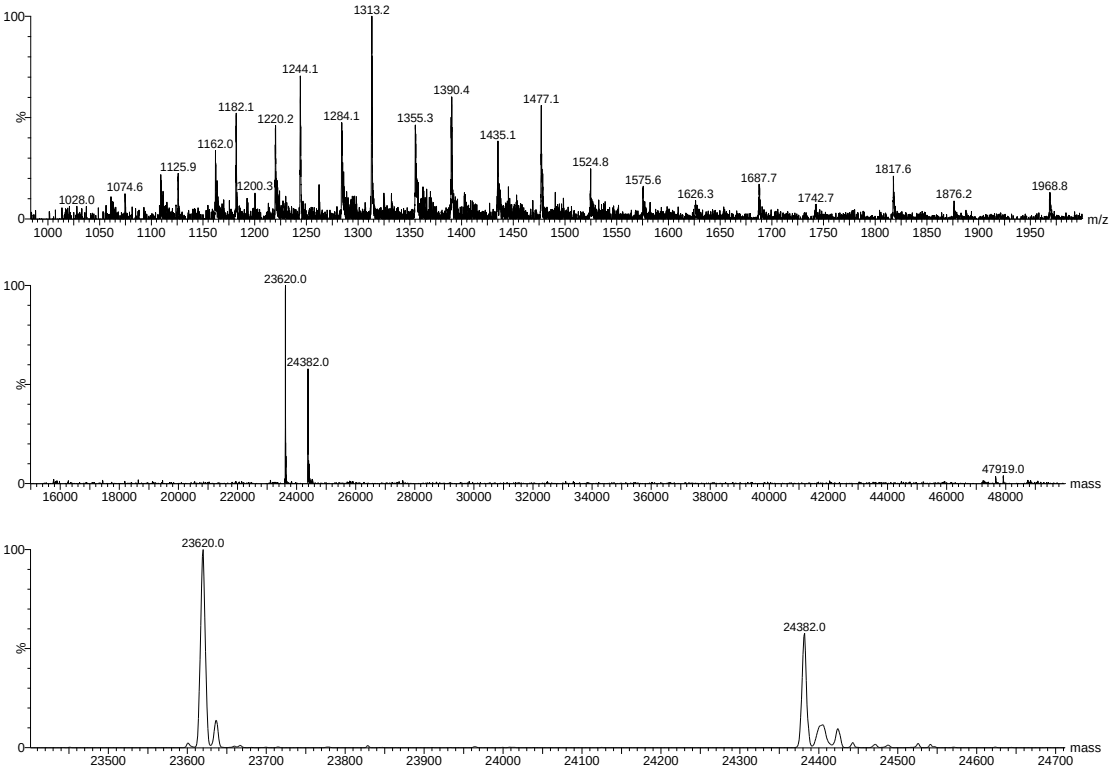
100
%
0
1313.2
1244.1
1390.4
1182.1
1220.2
1284.1
1355.3
1477.1
1435.1
1162.0
1524.8
1125.9
1575.6
1687.7
1817.6
1626.3
1742.7
1876.2
1968.8
1028.0
1074.6
1200.3
1000 1050 1100 1150 1200 1250 1300 1350 1400 1450 1500 1550 1600 1650 1700 1750 1800 1850 1900 1950
m/z
100
%
0
23620.0
24382.0
47919.0
16000 18000 20000 22000 24000 26000 28000 30000 32000 34000 36000 38000 40000 42000 44000 46000 48000
mass
100
%
0
23620.0
24382.0
23500 23600 23700 23800 23900 24000 24100 24200 24300 24400 24500 24600 24700
mass

Conjugation of Trastuzumab Fab 116 with *N*-methyl maleimide 238

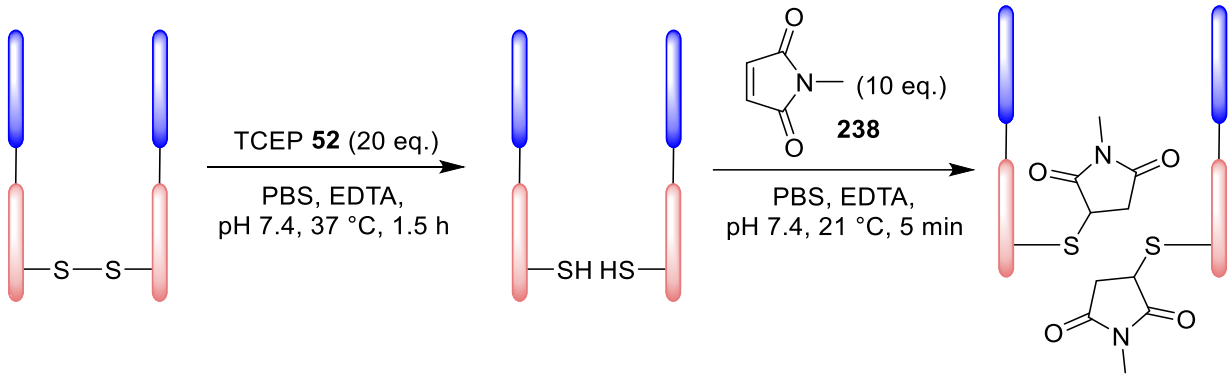

116 **243** **245**

TCEP **52** (10.0 µL, 20 mM in deionised water, 20 eq.) was added to a solution of trastuzumab Fab **116** (500 µL, 20 µM) in PBS (pH 7.4) and the solution was incubated at 37 °C for 90 min. Excess TCEP was removed by ultrafiltration (6 × 10000 MWCO, VivaSpin®, GE Healthcare) into PBS (pH 7.4, 5 mM EDTA). *N*-methyl maleimide **238** (5.0 µL, 20 mM in DMSO, 10 eq.) was added to the solution of reduced trastuzumab Fab **243** and the solution was incubated at 21 °C for 5 min. Excess reagents were removed by ultrafiltration (6 × 10000 MWCO, VivaSpin®, GE Healthcare) into deionised water prior to LCMS analysis. Expected masses: 23564 Da, 24325 Da. Observed masses (LCMS Method 1): 23561 Da, 24323 Da.

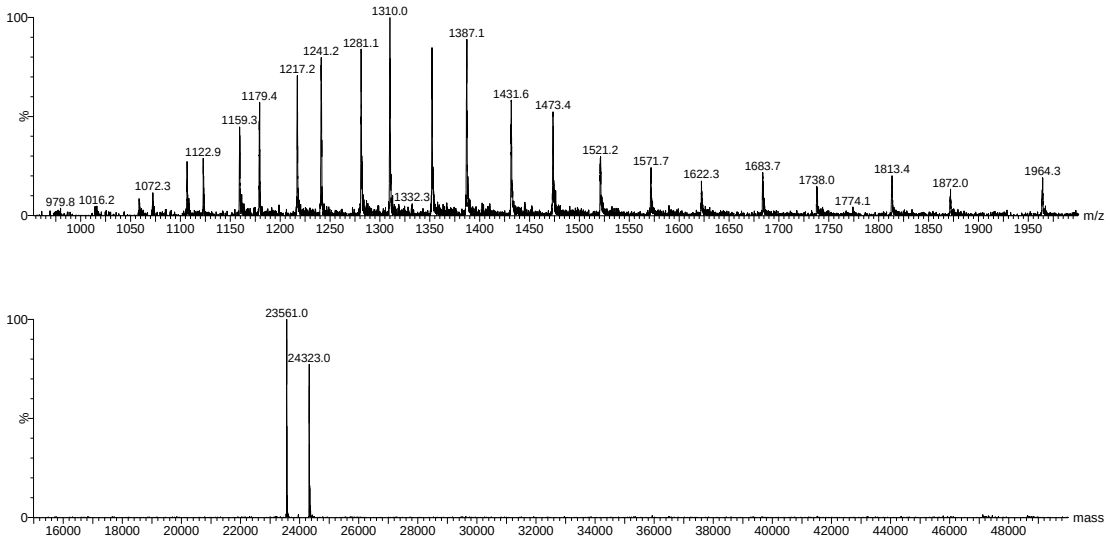

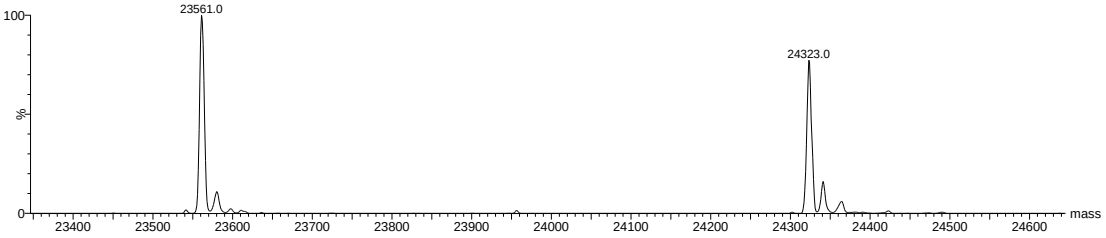
100
%
0
23561.0
24323.0
23400
23500
23600
23700
23800
23900
24000
24100
24200
24300
24400
24500
24600
mass

Release of *N,N*-Diethyl PD 232 from Trastuzumab Fab-PD conjugate 237

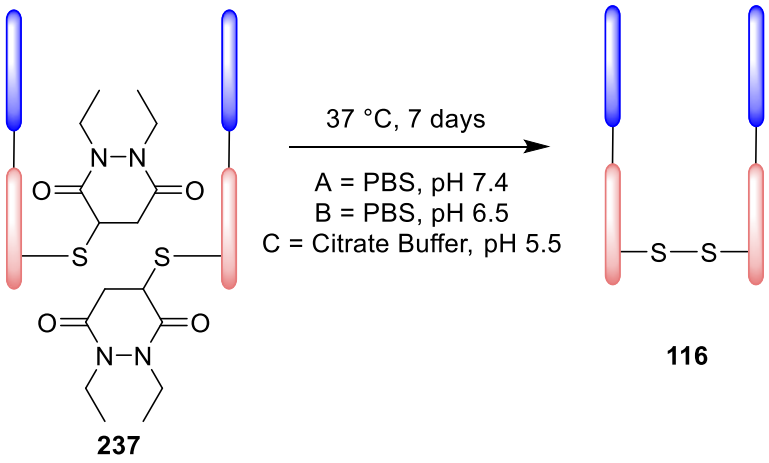

Trastuzumab Fab-PD conjugate **237** (200 µL, 20 µM) was buffer exchanged (7000 MWCO, ZebaSpin®, Thermo Scientific) into PBS (pH 7.4 and pH 6.5) or citrate buffer (pH 5.5). The trastuzumab conjugates were then incubated at 37 °C for a total of 7 days. Samples were desalted (7000 MWCO, ZebaSpin®, Thermo Scientific) before LCMS analysis. Expected masses: 23452 Da, 23621 Da, 24213 Da, 24384 Da, 47663 Da. Observed masses (LCMS Method 1): 23453 Da, 23622 Da, 23832, 24217 Da, 24385 Da, 47669 Da.

pH 5.5

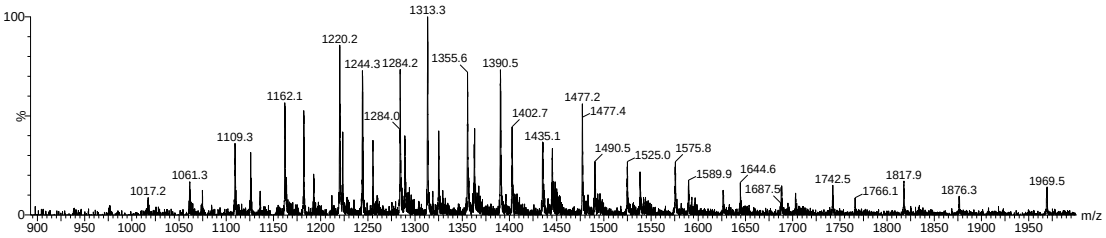

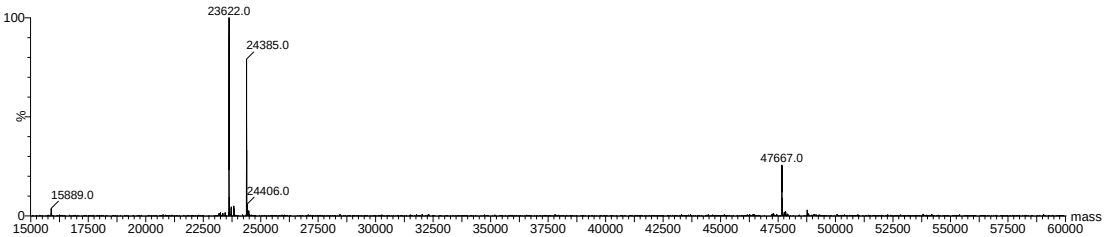

pH 6.5

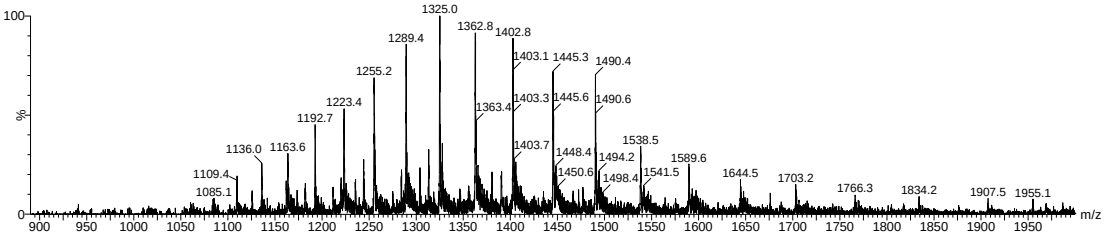
100
%
0
1325.0
1362.8
1289.4
1402.8
1403.1
1445.3
1490.4
1255.2
1403.3
1445.6
1490.6
1223.4
1363.4
1192.7
1403.7
1538.5
1136.0
1163.6
1448.4
1494.2
1589.6
1109.4
1450.6
1541.5
1644.5
1703.2
1085.1
1498.4
1766.3
1834.2
1907.5
1955.1
900 950 1000 1050 1100 1150 1200 1250 1300 1350 1400 1450 1500 1550 1600 1650 1700 1750 1800 1850 1900 1950
m/z

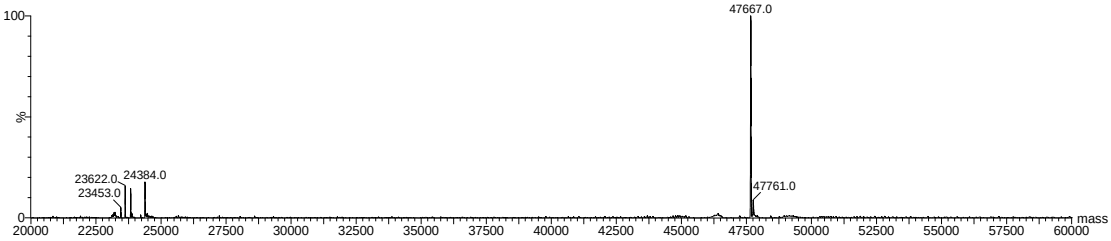
100
%
0
47667.0
23622.0
24384.0
23453.0
47761.0
20000 22500 25000 27500 30000 32500 35000 37500 40000 42500 45000 47500 50000 52500 55000 57500 60000
mass

pH 7.4

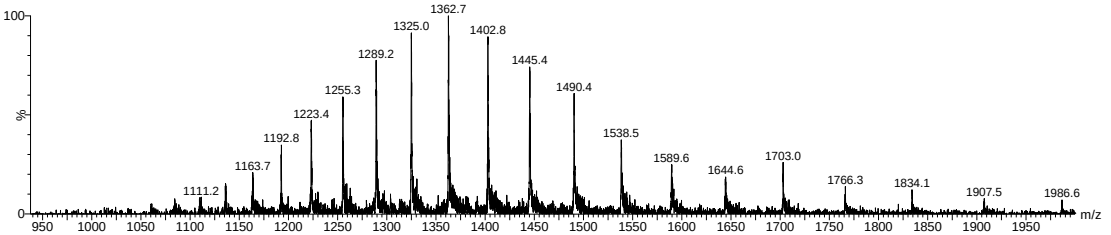
100
%
0
1362.7
1325.0
1402.8
1289.2
1445.4
1255.3
1490.4
1223.4
1538.5
1192.8
1589.6
1644.6
1703.0
1163.7
1766.3
1834.1
1111.2
1907.5
1986.6
950 1000 1050 1100 1150 1200 1250 1300 1350 1400 1450 1500 1550 1600 1650 1700 1750 1800 1850 1900 1950
m/z

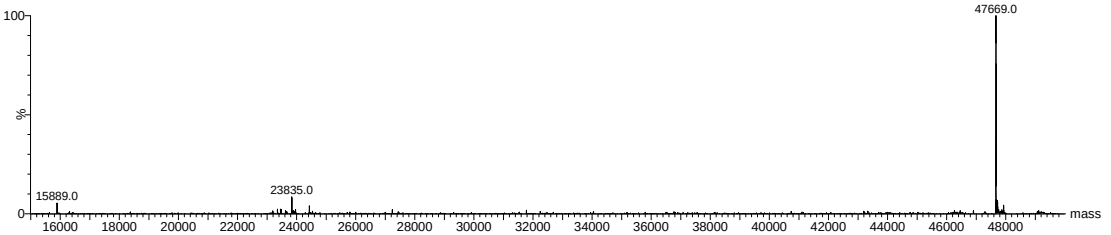
100
%
0
47669.0
15889.0
23835.0
16000 18000 20000 22000 24000 26000 28000 30000 32000 34000 36000 38000 40000 42000 44000 46000 48000
mass

Stability of Trastuzumab-PD conjugate 244 to glutathione

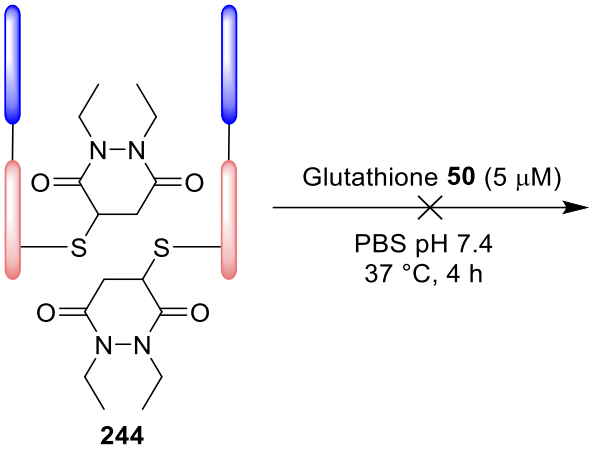

244

Glutathione **50** (1.0 µL, 500 µM in PBS adjusted to pH 7.4) was added to the solution of trastuzumab Fab-PD conjugate **244** (100 µL, 20 µM in PBS = pH 7.4) and the solution was incubated at 37 °C for 4 h. Excess reagents were removed using desalting columns (7000 MWCO, ZebaSpin®, Thermo Scientific) prior to LCMS analysis. Expected masses: 23620 Da, 24385 Da. Observed masses (LCMS Method 1): 23622 Da, 24384 Da.

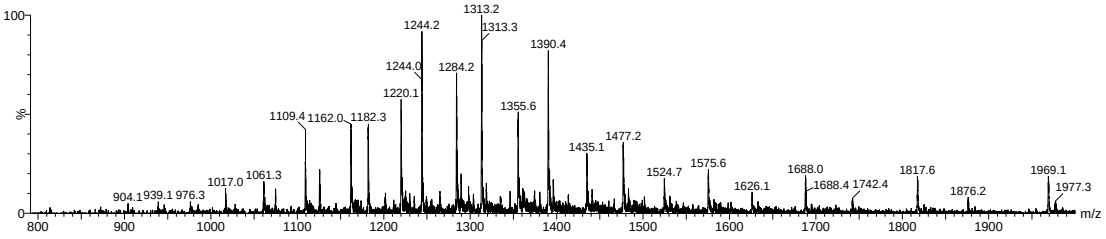

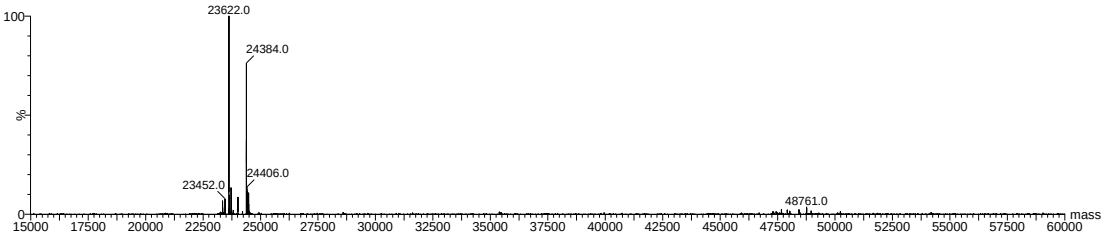

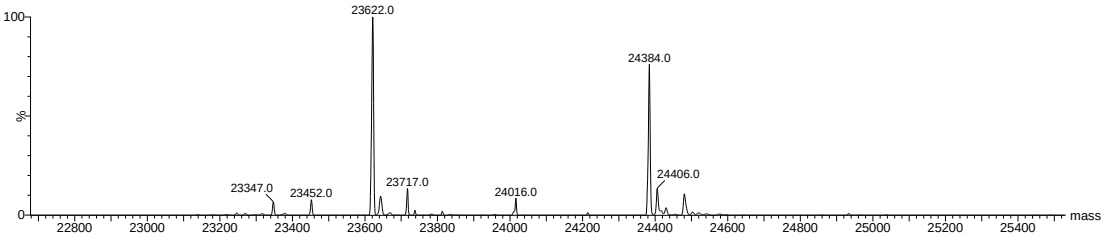

Incubation of Trastuzumab Fab-Maleimide conjugate 245

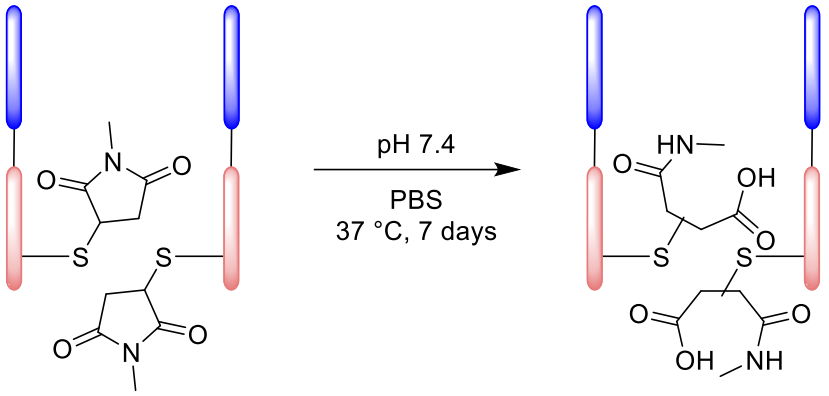

245 **246**

Trastuzumab Fab-Maleimide conjugate **245** (200 µL, 20 µM) was buffer exchanged (7000 MWCO, ZebaSpin®, Thermo Scientific) into PBS (pH 7.4). The trastuzumab conjugate was then incubated at 37 °C for a total of 7 days. Samples were desalted (7000 MWCO, ZebaSpin®, Thermo Scientific) before LCMS analysis. Expected masses: 23582 Da, 24343 Da. Observed masses (LCMS Method 1): 23580 Da, 24342 Da.

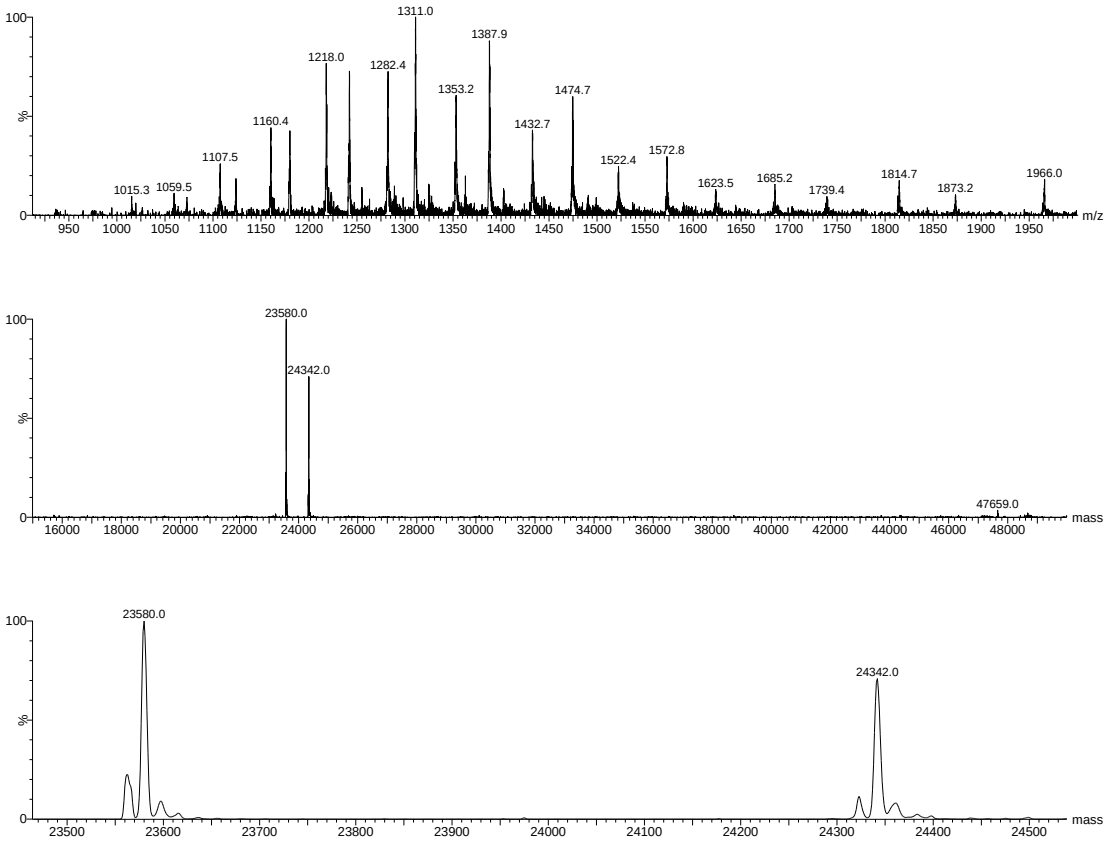

Control: Reoxidation of reduced Trastuzumab Fab 243

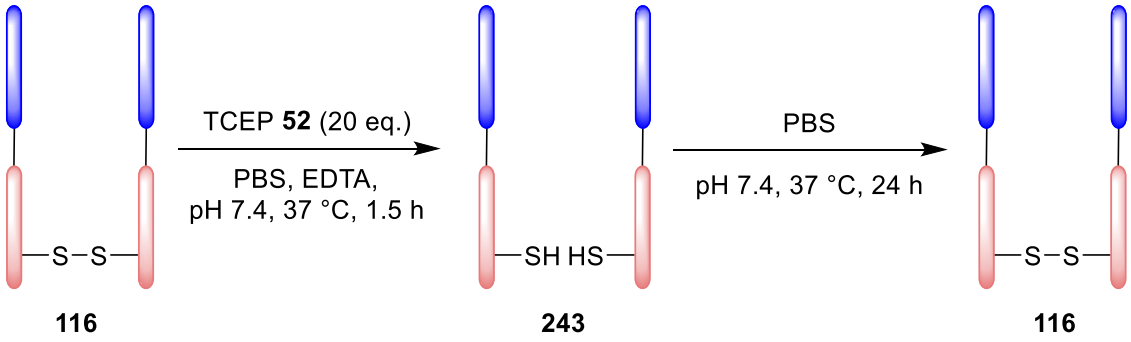

TCEP **52** (2.0 µL, 20 mM in deionised water, 20 eq.) was added to a solution of trastuzumab Fab **116** (100 µL, 20 µM) in PBS = pH 7.4, 5 mM EDTA) and the solution was incubated at 37 °C for 90 min. Excess TCEP was removed by ultrafiltration (6 × 10000 MWCO, VivaSpin®,GE Healthcare) into PBS (pH = 7.4). Reduced trastuzumab Fab **243** was then incubated at 37 °C for 24 h. Samples were desalted (7000 MWCO, ZebaSpin®, Thermo Scientific) before LCMS analysis. Expected masses: 47663 Da. Observed masses (LCMS Method 1): 23832 Da, 47663 Da.

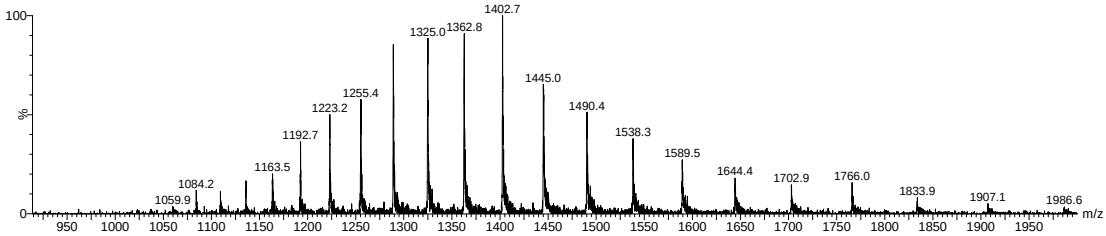

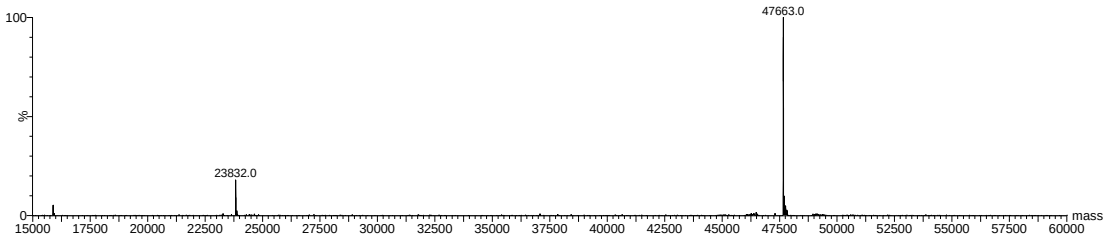

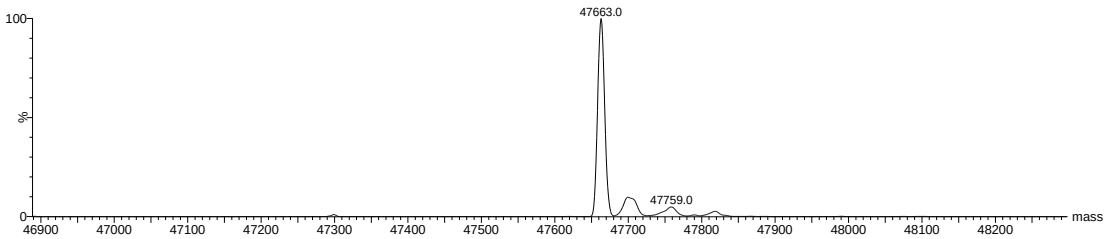

Human Serum Albumin 27

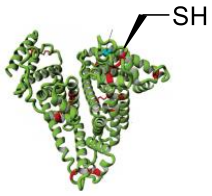

27

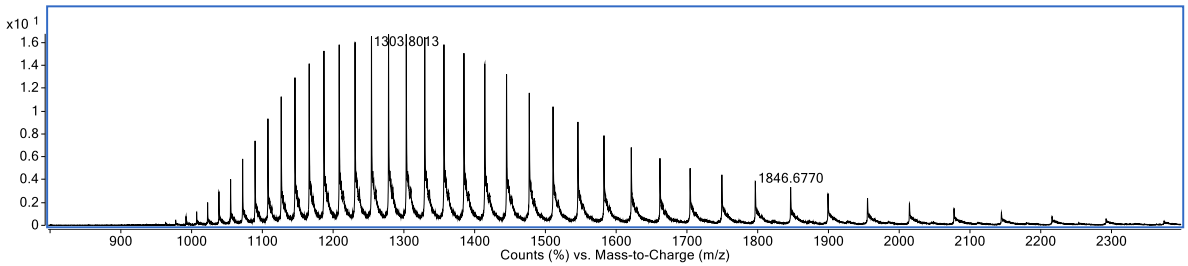

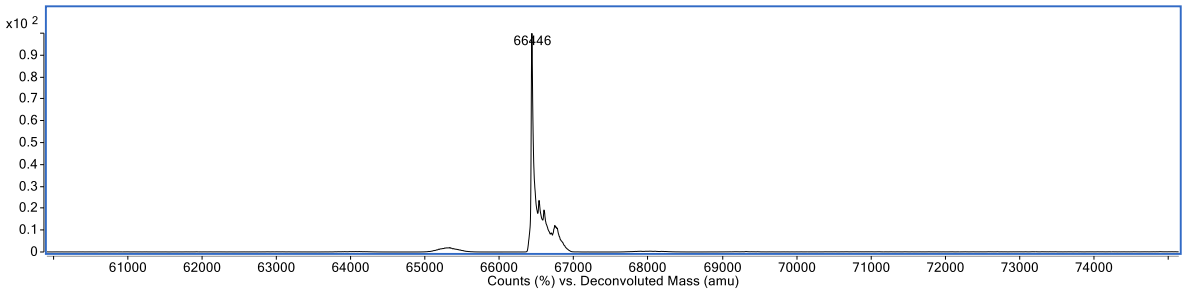

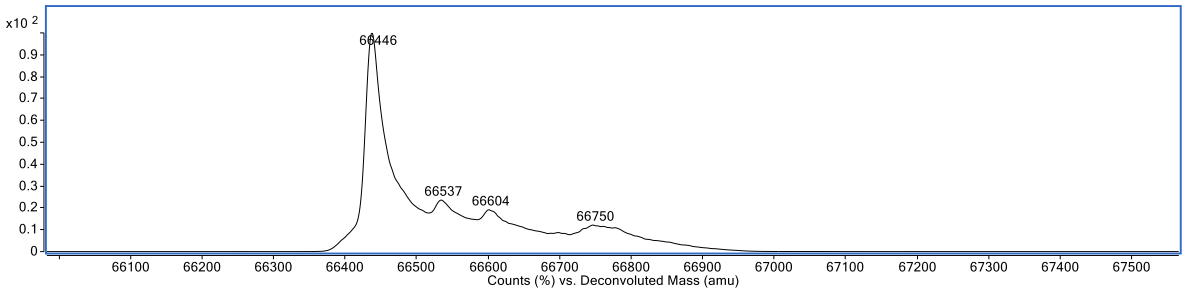

Reaction of human serum albumin 27 and *N,N*-diethyl pyridazinedione 232

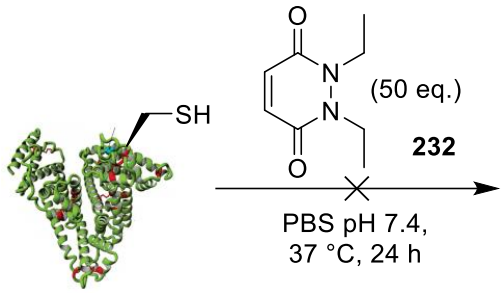

27

N,N-Diethyl pyridazinedione **232** (1.25 µL, 200 mM in DMSO, 50 eq.) was added to a solution of human serum albumin **27** (100 µL, 50 µM in PBS pH 7.4) and the solution was incubated at 37 °C for 24 h. Excess reagents were removed using desalting columns (7000 MWCO, ZebaSpin®, Thermo Scientific) prior to LCMS analysis. Expected mass: 66449 Da. Observed mass (LCMS Method 2): 66447 Da.

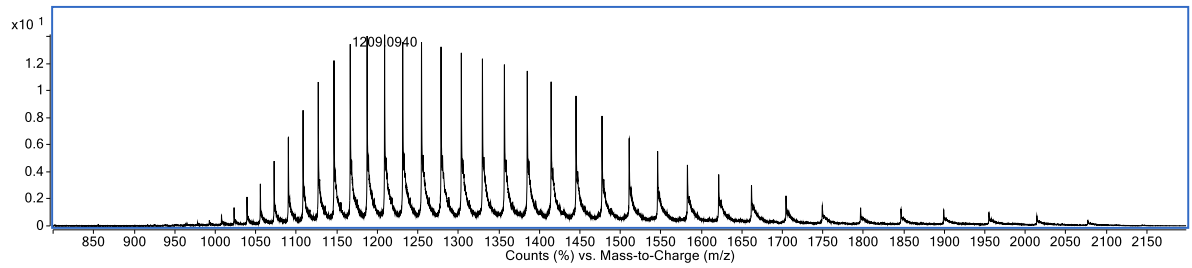

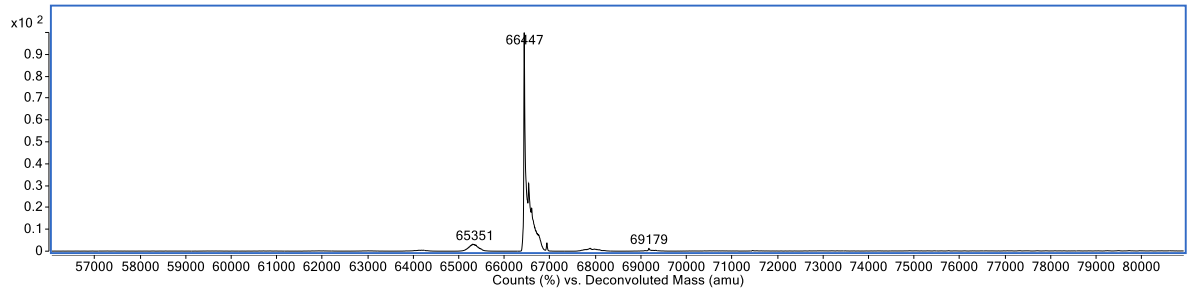

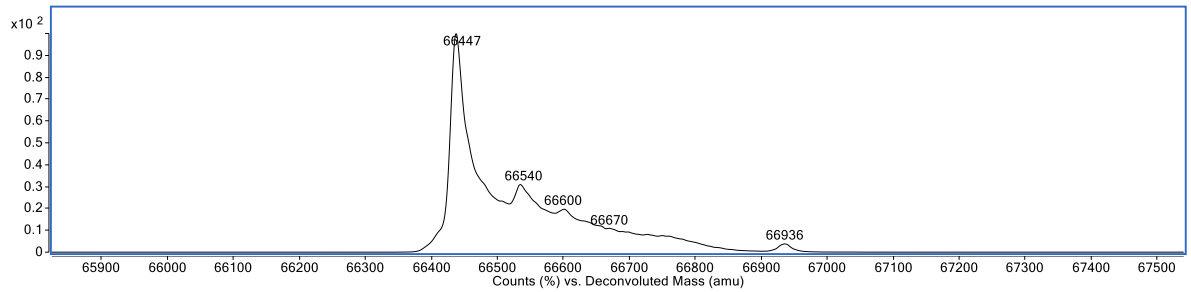

Reaction of human serum albumin 27 and Trastuzumab Fab-PD conjugate 237

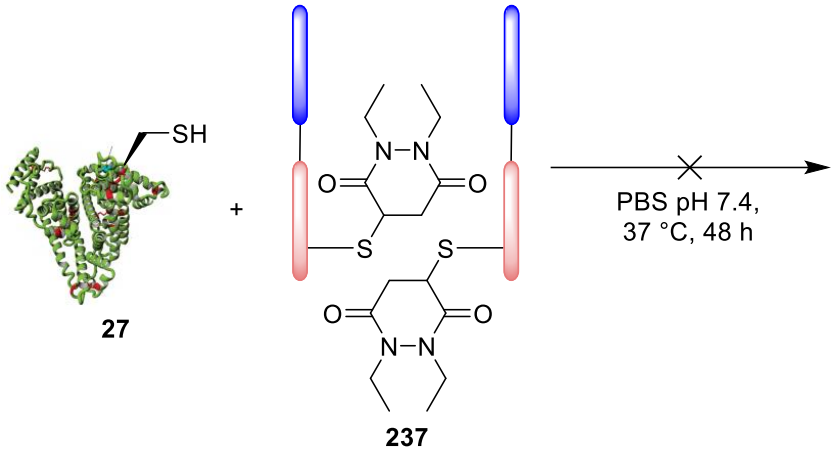

Human serum albumin **27** (25 µL, 100 µM in PBS pH 7.4) was added to a solution of trastuzumab Fab-PD conjugate **237** (100 µL, 25 µM in PBS pH 7.4) to form a 1:1 solution (125 µL, 20 µM in PBS pH 7.4). The solution was incubated at 37 °C for 48 h. Samples were desalted using desalting columns (7000 MWCO, ZebaSpin®, Thermo Scientific) prior to LCMS analysis. Expected masses: 66449 Da. Observed mass (LCMS Method 2): 66450 Da.

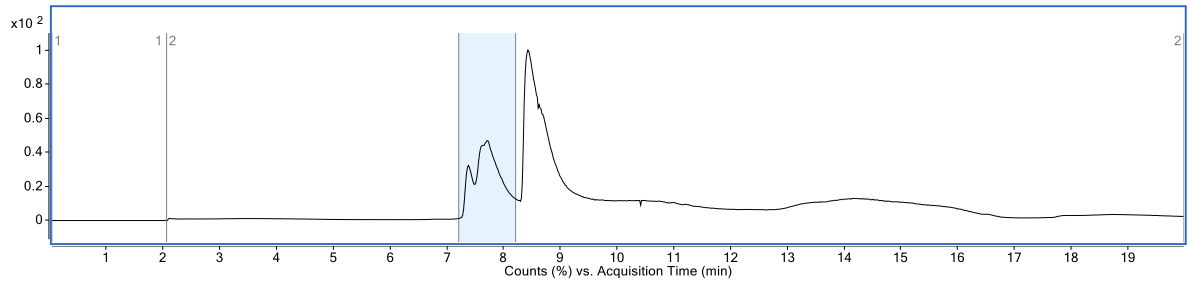

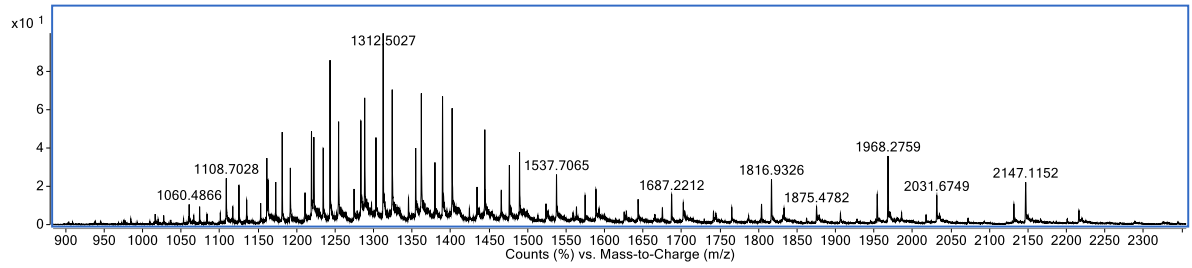

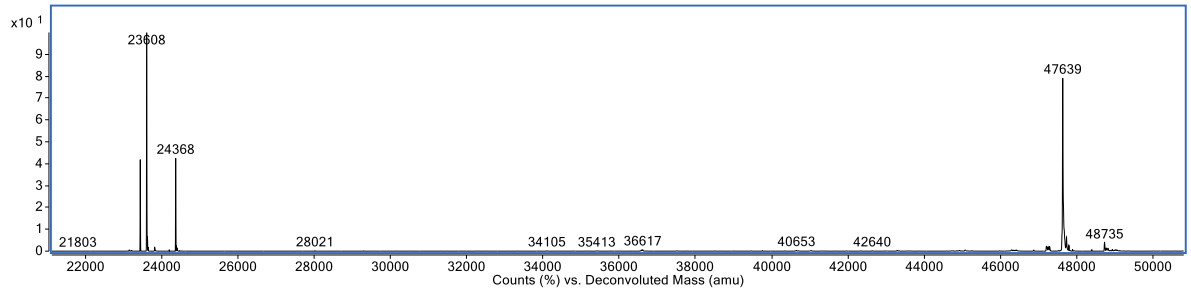

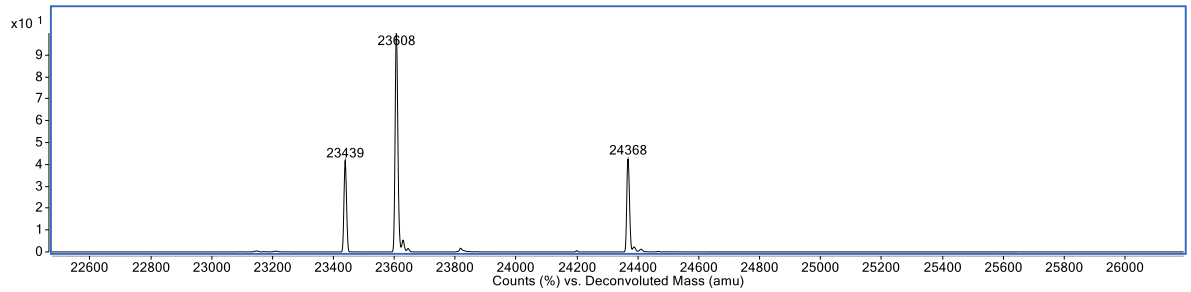
x10 1
23608
23439
24368
Counts (%) vs. Deconvoluted Mass (amu)

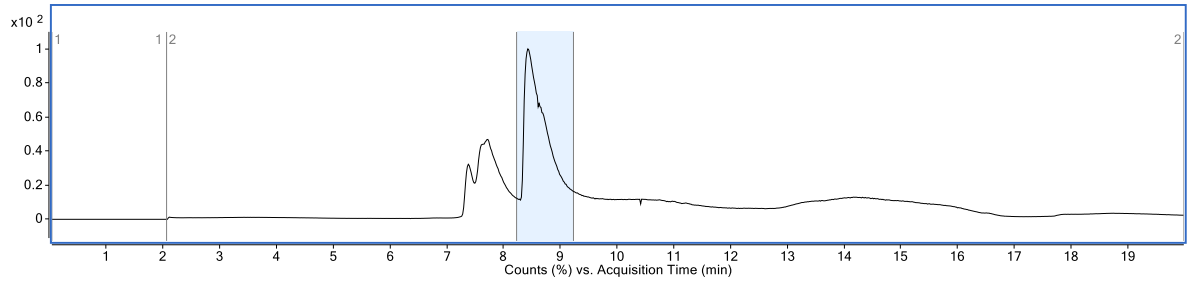
x10 2
Counts (%) vs. Acquisition Time (min)

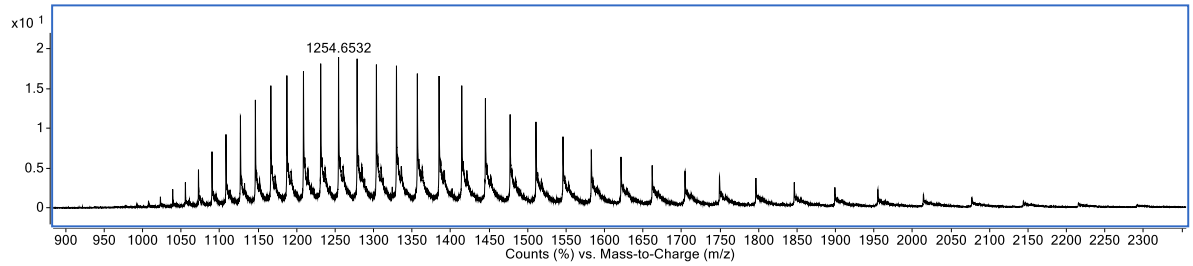
x10 1
1254.6532
Counts (%) vs. Mass-to-Charge (m/z)

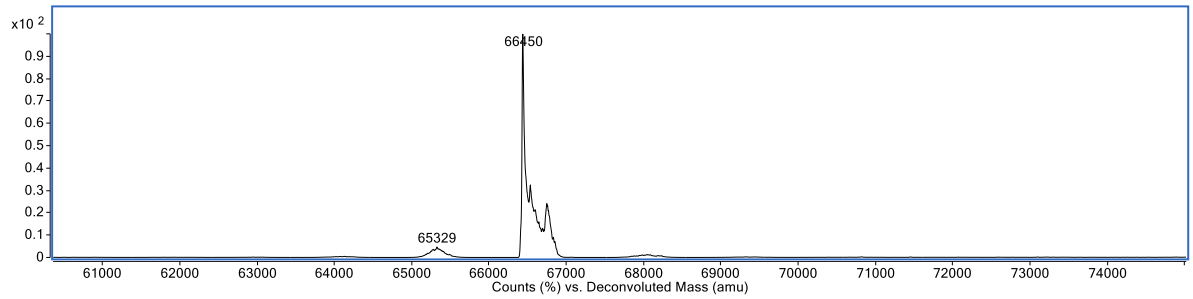
x10 2
66450
65329
Counts (%) vs. Deconvoluted Mass (amu)

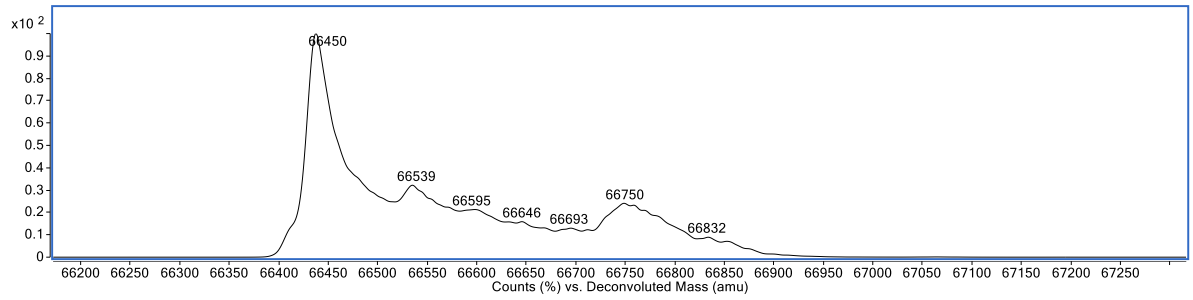
x10 2
66450
66539
66595
66646
66693
66750
66832
Counts (%) vs. Deconvoluted Mass (amu)

Reaction of human serum albumin 27 and Trastuzumab Fab-maleimide conjugate 245

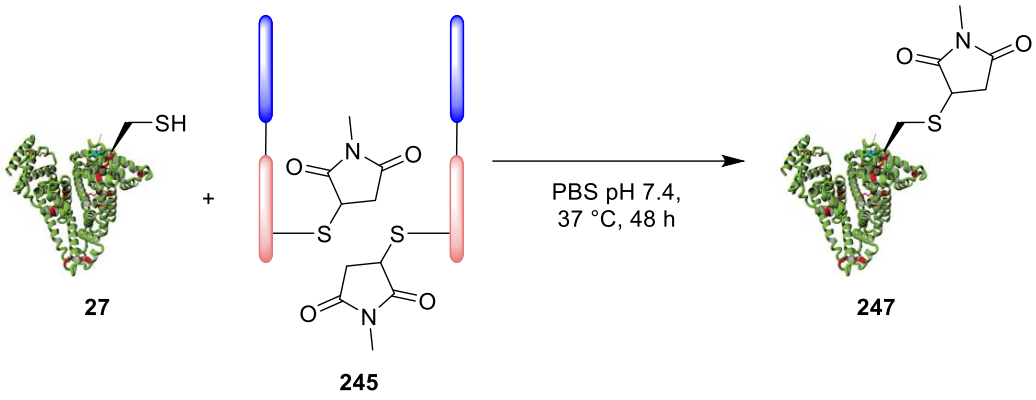

Human serum albumin **27** (25 µL, 100 µM in PBS pH 7.4) was added to a solution of trastuzumab Fab-maleimide conjugate **245** (100 µL, 25 µM in PBS ph 7.4) to form a 1:1 solution (125 µL, 20 µM in PBS pH 7.4). The solution was incubated at 37 °C for 48 h. Samples were desalted using desalting columns (7000 MWCO, ZebaSpin®, Thermo Scientific) prior to LCMS analysis. Expected mass: 66560 Da. Observed mass (LCMS Method 2): 66559 Da.

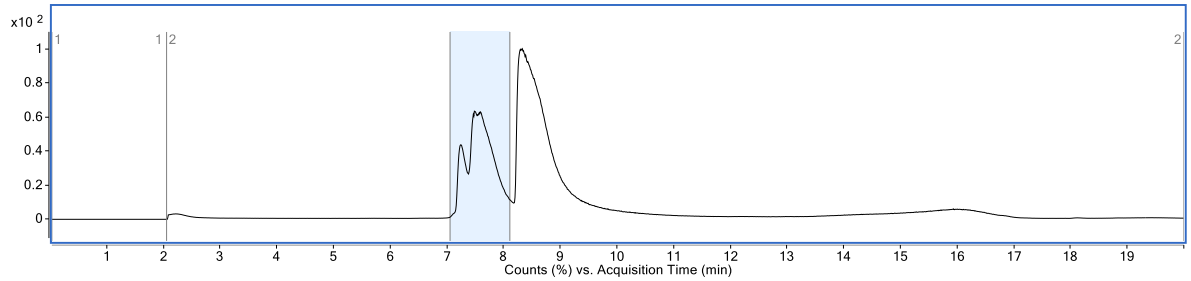

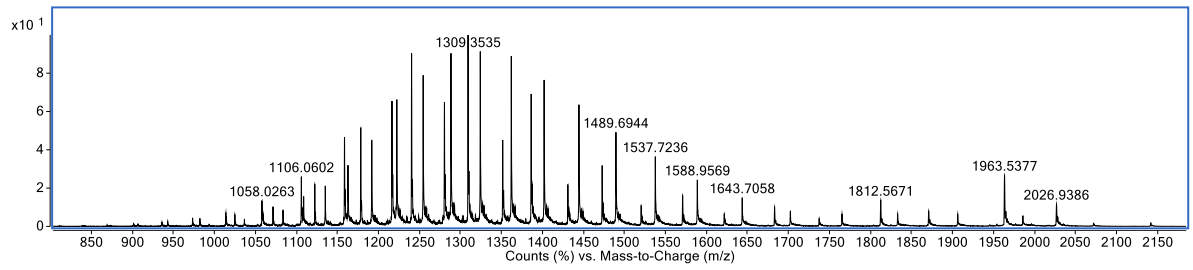

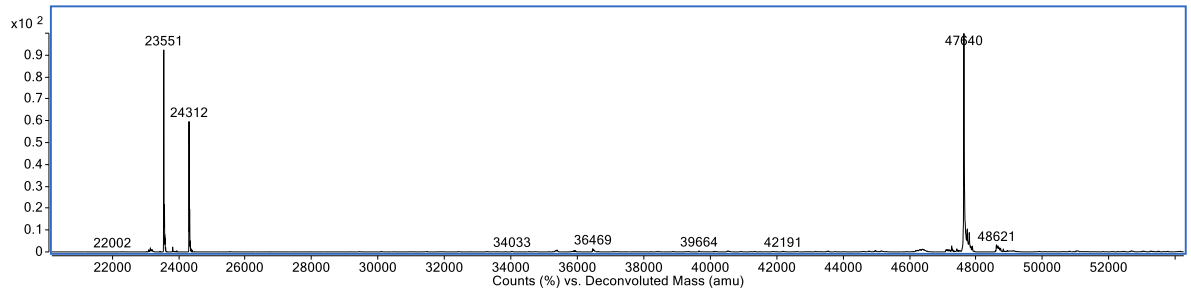

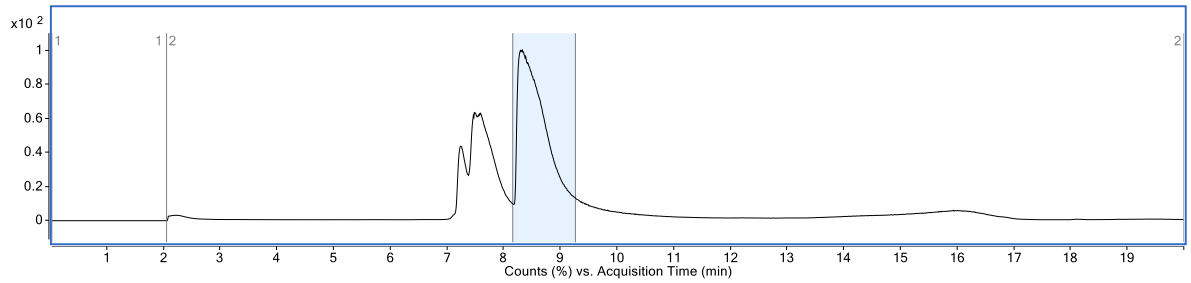
x10 2
1
0.8
0.6
0.4
0.2
0
1 2
2
1 2 3 4 5 6 7 8 9 10 11 12 13 14 15 16 17 18 19
Counts (%) vs. Acquisition Time (min)

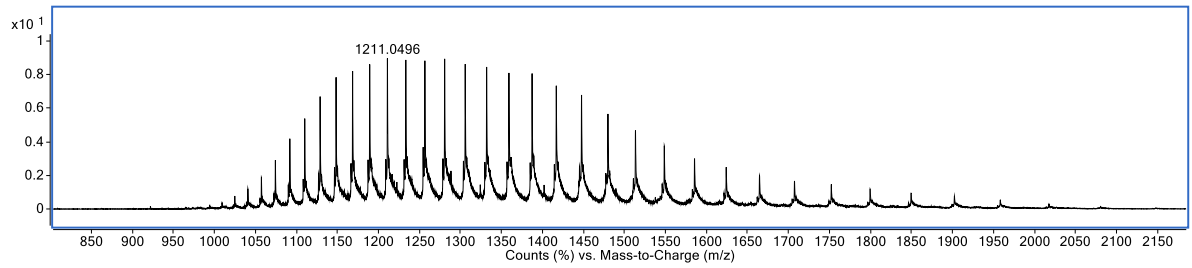
x10 1
1
0.8
0.6
0.4
0.2
0
1211.0496
850 900 950 1000 1050 1100 1150 1200 1250 1300 1350 1400 1450 1500 1550 1600 1650 1700 1750 1800 1850 1900 1950 2000 2050 2100 2150
Counts (%) vs. Mass-to-Charge (m/z)

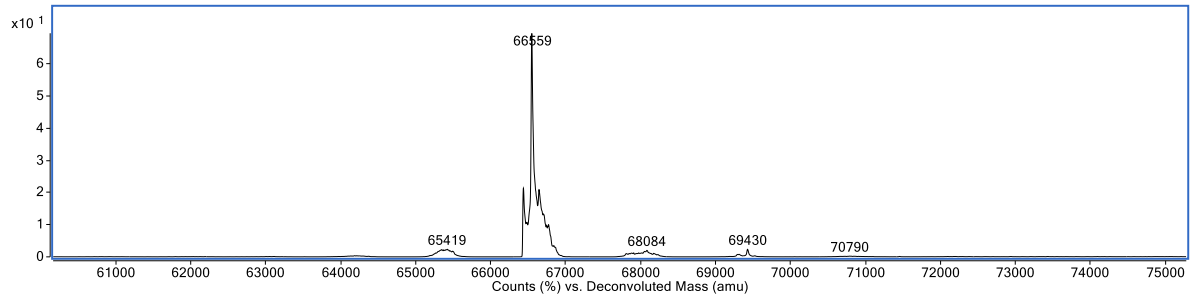
x10 1
6
5
4
3
2
1
0
66559
65419
68084
69430
70790
61000 62000 63000 64000 65000 66000 67000 68000 69000 70000 71000 72000 73000 74000 75000
Counts (%) vs. Deconvoluted Mass (amu)

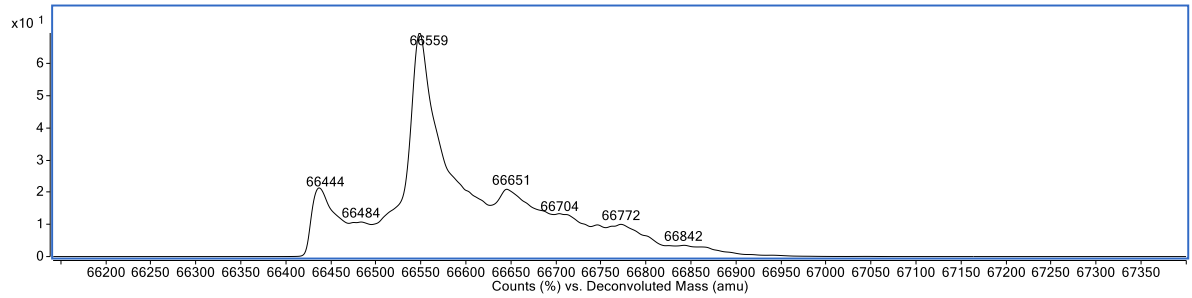
x10 1
6
5
4
3
2
1
0
66559
66444
66484
66651
66704
66772
66842
66200 66250 66300 66350 66400 66450 66500 66550 66600 66650 66700 66750 66800 66850 66900 66950 67000 67050 67100 67150 67200 67250 67300 67350
Counts (%) vs. Deconvoluted Mass (amu)

Reaction of glutathione 50 and *N,N*-diethyl pyridazinedione 232

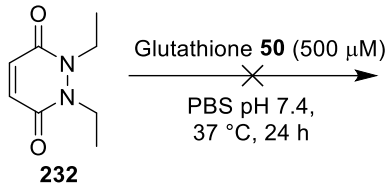

232

N,N-Diethyl pyridazinedione **232** (5 µL, 20 mM in MeCN, 1 eq.) was added to a solution of glutathione **50** (200 µL, 500 µM in PBS pH 7.4) and the solution was incubated at 37 °C for 24 h. Results were obtained directly from the reaction mixture through LCMS analysis. Expected mass: 166 Da (PD **232**), 307 Da (GSH **50**), 477 Da (GSH-PD), 612 Da (GSH-GSH). Observed mass (LCMS Method 1): 169 Da, 307 Da, 612 Da.

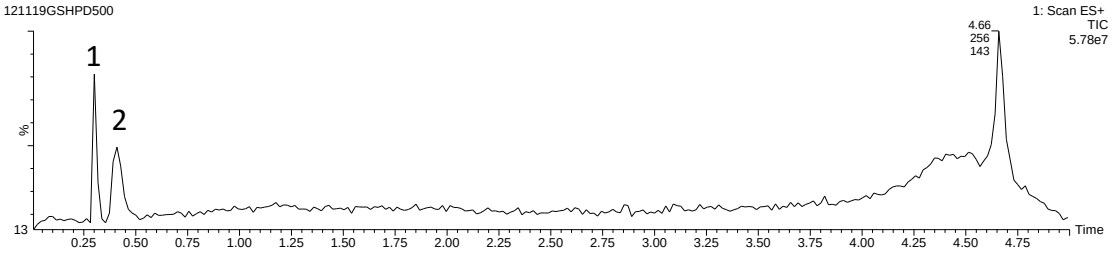

Peak 1

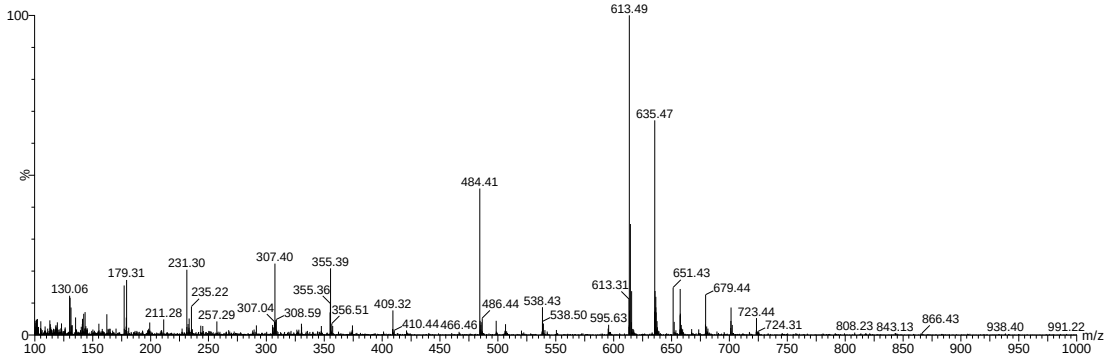

Peak 2

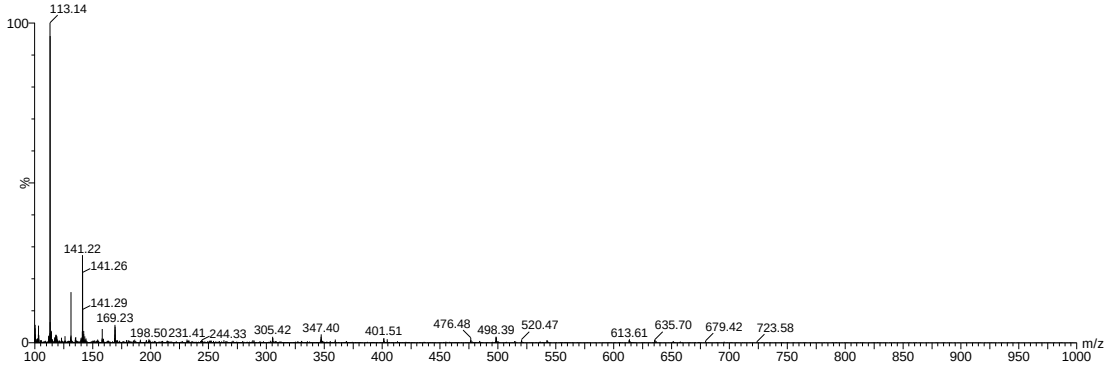

Entire Spectrum

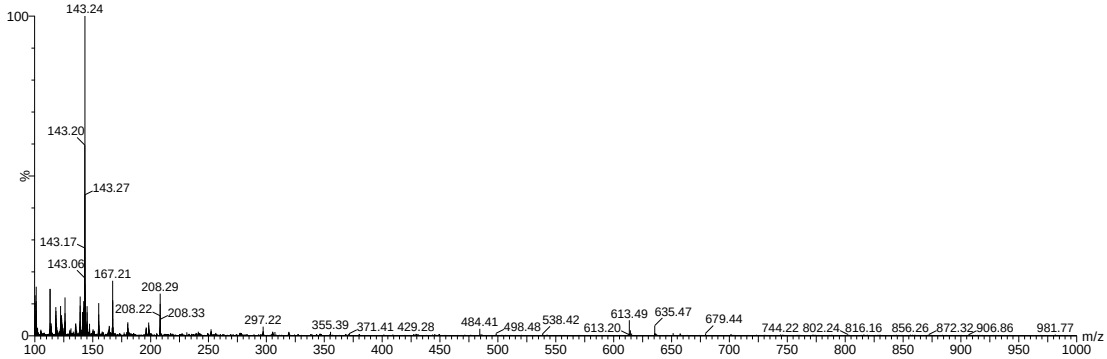

Glutathione reference:

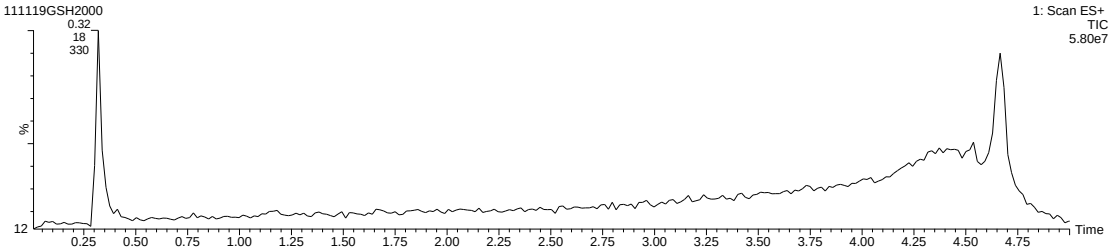

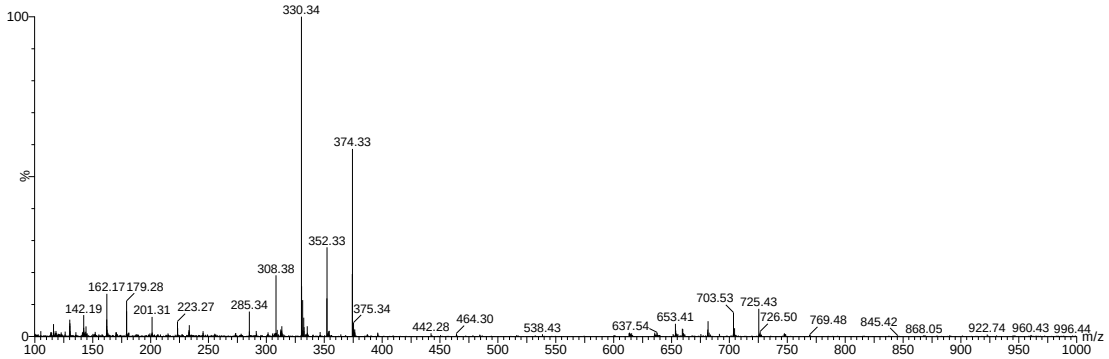

Glutathione control (24 h, 37 °C)

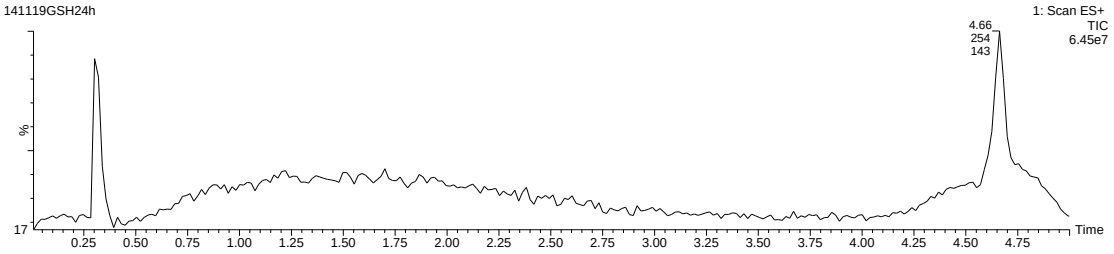

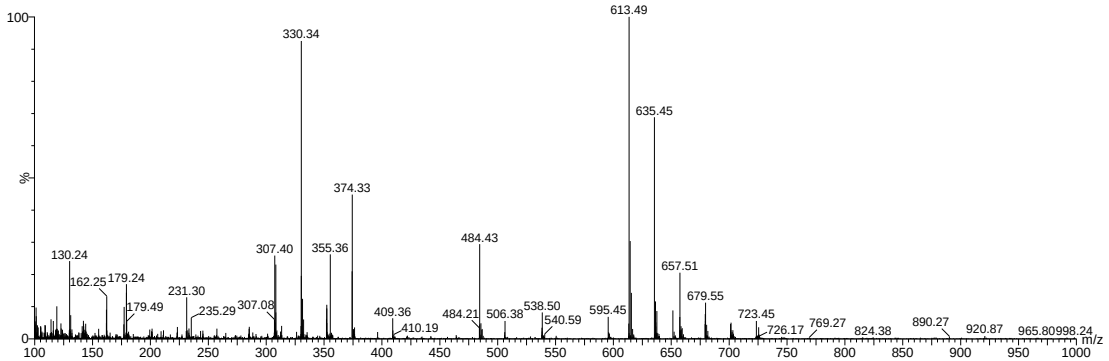

N,N-diethyl pyridazinedione **232** reference

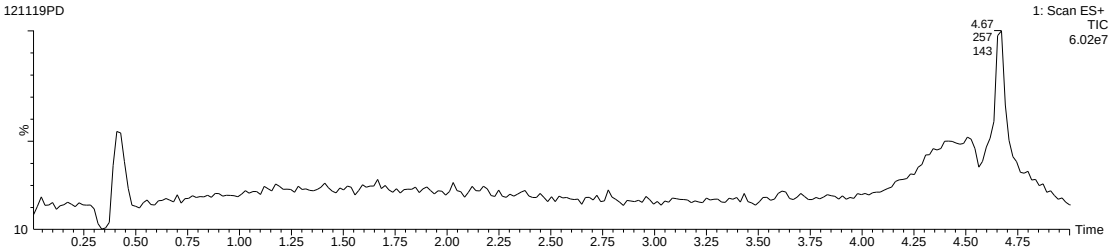

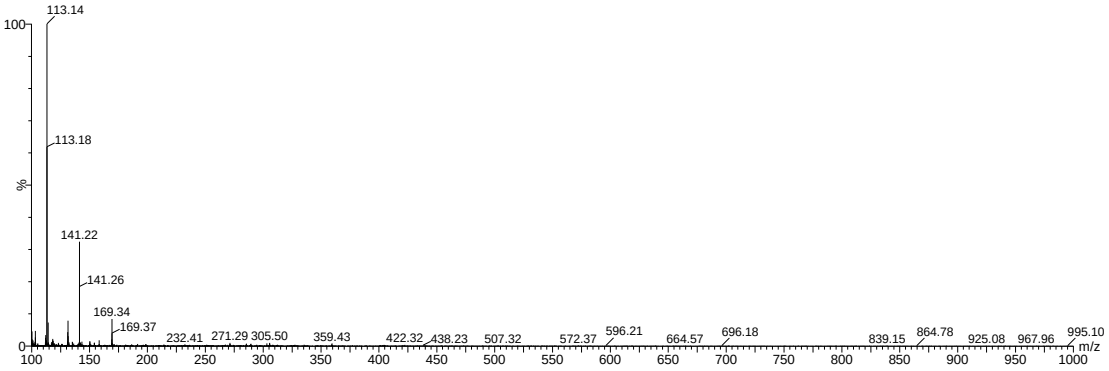
113.14
100
113.18
%
141.22
141.26
169.34
169.37
232.41
271.29
305.50
359.43
422.32
438.23
507.32
572.37
596.21
664.57
696.18
839.15
864.78
925.08
967.96
995.10
0
m/z
100
150
200
250
300
350
400
450
500
550
600
650
700
750
800
850
900
950
1000

ELISA for Trastuzumab Fab conjugates 244 and 245

Binding affinity to HER2 receptor was determined by ELISA. A 96-well plate was coated overnight at 4 °C with HER2 (Human HER2/ErbB2 Protein (His Tag) from Sino Biological) (100 µL of a 0.25 µg·mL^{-1} solution in PBS), including coating one row of wells with PBS only for negative controls. Next, the coating solutions were removed and each well washed with PBS twice. Then, the wells were coated with a 2% BSA solution in PBS (200 µL) for 1 h at 21 °C. Next, the wells were washed with PBST (0.1% Tween 20 in PBS) twice and with PBS three times. Solutions of trastuzumab Fab and trastuzumab Fab conjugates (in 0.2% BSA, PBST) were prepared with the following dilution series: 100 nm, 33 nM, 11 nM, 3.7 nM, 1.24 nM, 0.41 nM and 0.14 nM. Wells were coated with the dilution series solutions in triplicate, including a PBS only at 100 nM in the absence of HER2 as negative controls, and incubated for 2 h at 21 °C. Then, the solutions were removed and the wells washed with PBST twice and with PBS three times. Detection antibody (100 µL of anti-human IgG, Fab-specific-HRP solution, prepared by taking 4 µL of a 1:5000 diluted solution and further diluting with 20mL of 0.2% BSA in PBST) was then added and incubated for 1 h at 21 °C. Then, the solutions were removed and the wells washed with PBST twice and with PBS three times. OPD solution (100 µL of 10 mg/20 mL OPD in phosphate-citrate buffer with sodium perborate, prepared by dissolving 1 capsule in 100 mL water) was added to each well. After 30 s the reaction was stopped through addition of 4 M HCl (50 µL). The absorption was measured at 450 nm and corrected by subtracting the average of negative controls. The results obtained were analysed with GraphPad Prism using a regression with variable slope (four parameters).

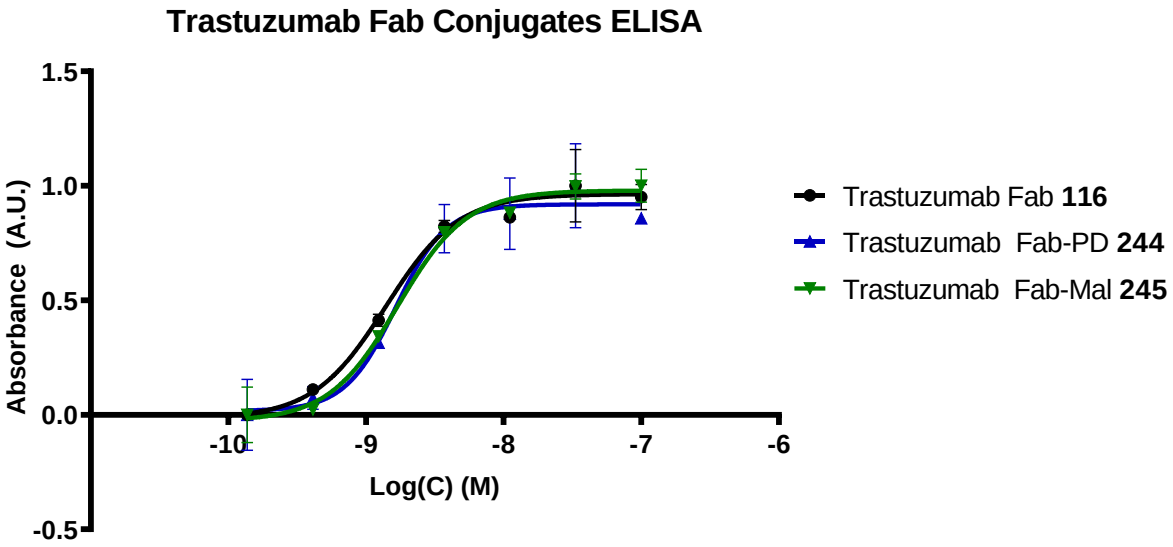

Conjugate	IC_{50} (M)
Trastuzumab Fab **116**	**1.397×10^{-9}**
Trastuzumab Fab-PD **244**	**1.830×10^{-9}**
Trastuzumab Fab-Mal **245**	**1.703×10^{-9}**

Publications

1. **C. Bahou**, D. A. Richards, A. Maruani, E. A. Love, F. Javaid, S. Caddick, J. R. Baker* and V. Chudasama*, *Org. Biomol. Chem.*, 2018, **16**, 1359–1366.

   – Publication derived from work presented in Chapter 2

2. P. A. Szijj, **C. Bahou** and V. Chudasama*, *Drug Discov. Today*, 2018, **30**, 27–34.

3. **C. Bahou**, E. A. Love, S. Leonard, R. J. Spears, A. Maruani, K. Armour, J. R. Baker* and V. Chudasama*, *Bioconjugate Chem.*, 2019, **30**, 1048–1054.

   – Publication derived from work presented in Chapter 3

4. **C. Bahou**, R. J. Spears, A. E. Aliev, A. Maruani, M. Fernández, F. Javaid, P. A. Szijj, J. R. Baker* and V. Chudasama*, *Chem. Commun.*, 2019, **55**, 14829–14832.

   – Publication derived from work presented in Chapter 5

5. A. Maruani, P. A. Szijj, **C. Bahou**, J. C. F. Nogueira, S. Caddick, J. R. Baker* and V. Chudasama*, Bioconjugate Chem., 2020, **31**, 520–529

6. A. Wall, A. G. Wills, N. Forte, **C. Bahou**, L. Bonin, K. Nicholls, M. T. Ma, V. Chudasama* and J. R. Baker*, *Chem. Sci.*, 2020, DOI:10.1039/d0sc05128d.

7. **C. Bahou**, P. A. Szijj, E. A. Love, A. Wall, F. Javaid, J. R. Baker* and V. Chudasama*, Manuscript in preparation.

   – Publication derived from work presented in Chapter 4

References

1 O. N. Jensen, *Curr. Opin. Chem. Biol.*, 2004, **8**, 33–41.

2 I. S. Carrico, *Chem. Soc. Rev.*, 2008, **37**, 1423–1431.

3 N. Stephanopoulos and M. B. Francis, *Nat. Chem. Biol.*, 2011, **7**, 876–884.

4 J. A. Prescher, D. H. Dube and C. R. Bertozzi, *Nature*, 2004, **430**, 873–877.

5 H. Cho, T. Daniel, Y. J. Buechler, D. C. Litzinger, Z. Maio, A.-M. H. Putnam, V. S. Kraynov, B.-C. Sim, S. Bussell, T. Javahishvili, S. Kaphle, G. Viramontes, M. Ong, S. Chu, B. GC, R. Lieu, N. Knudsen, P. Castiglioni, T. C. Norman, D. W. Axelrod, A. R. Hoffman, P. G. Schultz, R. D. DiMarchi and B. E. Kimmel, *Proc. Natl. Acad. Sci.*, 2011, **108**, 9060–9065.

6 L. Schofield, M. C. Hewittt, K. Evans, M. A. Slomos and P. H. Seeberger, *Nature*, 2002, **418**, 785–789.

7 J. J. Day, B. V. Marquez, H. E. Beck, T. A. Aweda, P. D. Gawande and C. F. Meares, *Curr. Opin. Chem. Biol.*, 2010, **14**, 803–809.

8 C. D. Spicer and B. G. Davis, *Nat. Commun.*, 2014, **5**, 4740.

9 I. Dovgan, S. Kolodych, O. Koniev and A. Wagner, *Sci. Rep.*, 2016, **6**, 30835.

10 W. R. Strohl, *BioDrugs*, 2015, **29**, 215–239.

11 S. C. Alley, N. M. Okeley and P. D. Senter, *Curr. Opin. Chem. Biol.*, 2010, **14**, 529–537.

12 B. Elsadek and F. Kratz, *J. Control. Release*, 2012, **157**, 4–28.

13 A. Beck and J. M. Reichert, *MAbs*, 2011, **3**, 415–416.

14 P. Caliceti and F. M. Veronese, *Adv. Drug Deliv. Rev.*, 2003, **55**, 1261–1277.

15 J. Kim, W. L. Hayton, J. M. Robinson and C. L. Anderson, *Clin. Immunol.*, 2007, **122**, 146–155.

16 V. Pechtner, C. A. Karanikas, L. E. Garcia-Perez and W. Glaesner, *Prim. Health Care*, 2017, **7**, 1.

17 M. Cavaco, M. A. R. B. Castanho and V. Neves, *Pept. Sci.*, 2018, **110**, e23095.

18 H. Marotte and R. Cimaz, *Expert Opin. Biol. Ther.*, 2014, **14**, 569–572.

19 A. Philippidis, *Genet. Eng. Biotechnol. News*, 2019, **39**, 16–17.

20 F. Winau, O. Westphal and R. Winau, *Microbes Infect.*, 2004, **6**, 786–789.

21 M. Paulik, P. Grieco, C. Kim, H.-G. Maxeiner, H.-P. Grunert, H. Zeichhardt, D. M. Morré and D. J. Morré, *Biochem. Pharmacol.*, 1999, **58**, 1781–1790.

22 M. Fernández, F. Javaid and V. Chudasama, *Chem. Sci.*, 2018, **9**, 790–810.

23 M. Srinivasarao and P. S. Low, *Chem. Rev.*, 2017, **117**, 12133–12164.

24 M. Srinivasarao, C. V. Galliford and P. S. Low, *Nat. Rev. Drug Discov.*, 2015, **14**, 203–219.

25 O. Boutureira and G. J. L. Bernardes, *Chem. Rev.*, 2015, **115**, 2174–2195.

26 P. Strop, S. H. Liu, M. Dorywalska, K. Delaria, R. G. Dushin, T. T. Tran, W. H. Ho, S. Farias, M. G. Casas, Y. Abdiche, D. Zhou, R. Chandrasekaran, C. Samain, C. Loo, A. Rossi, M. Rickert, S. Krimm, T. Wong, S. M. Chin, J. Yu, J. Dilley, J. Chaparro-Riggers, G. F. Filzen, C. J. O'Donnell, F. Wang, J. S. Myers, J. Pons, D. L. Shelton and A. Rajpal, *Chem. Biol.*, 2013, **20**, 161–167.

27 K. J. Hamblett, P. D. Senter, D. F. Chace, M. M. C. Sun, J. Lenox, C. G. Cerveny, K. M. Kissler, S. X. Bernhardt, A. K. Kopcha, R. F. Zabinski, D. L. Meyer and J. A. Francisco, *Clin. Cancer Res.*, 2004, **10**, 7063–7070.

28 A. C. Stan, D. L. Radu, S. Casares, C. A. Bona and T. D. Brumeanu, *Cancer Res.*, 1999, **59**, 115–121.

29 J. Lu, F. Jiang, A. Lu and G. Zhang, *Int. J. Mol. Sci.*, 2016, **17**, 561.

30 S. C. Alley, D. R. Benjamin, S. C. Jeffrey, N. M. Okeley, D. L. Meyer, R. J. Sanderson and P. D. Senter, *Bioconjug. Chem.*, 2008, **19**, 759–765.

31 Z. Elgundi, M. Reslan, E. Cruz, V. Sifniotis and V. Kayser, *Adv. Drug Deliv. Rev.*, 2017, **122**, 2–19.

32 S. Andris, M. Wendeler, X. Wang and J. Hubbuch, *J. Biotechnol.*, 2018, **278**, 48–55.

33 D. Rösner, T. Schneider, D. Schneider, M. Scheffner and A. Marx, *Nat. Protoc.*, 2015, **10**, 1594–1611.

34 J. W. Chin, *Nature*, 2017, **550**, 53–60.

35 W. Liu, A. Brock, S. Chen, S. Chen and P. G. Schultz, *Nat. Methods*, 2007, **4**, 239–244.

36 F. Agostini, J. S. Völler, B. Koksch, C. G. Acevedo-Rocha, V. Kubyshkin and N. Budisa, *Angew. Chemie - Int. Ed.*, 2017, **56**, 9680–9703.

37 M. G. Hoesl, C. G. Acevedo-Rocha, S. Nehring, M. Royter, C. Wolschner, B. Wiltschi, N. Budisa and G. Antranikian, *ChemCatChem*, 2011, **3**, 213–221.

38 A. R. Goerke and J. R. Swartz, *Biotechnol. Bioeng.*, 2009, **102**, 400–416.

39 K. Tanaka, K. Fukase and S. Katsumura, *Synlett*, 2011, **2011**, 2115–2139.

40 R. a Bednar, *Biochemistry*, 1990, **29**, 3684–3690.

41 J. A. Gerrard, S. J. Meade, A. G. Miller, P. K. Brown, S. B. M. Yasir, K. H. Sutton and M. P. Newberry, *Ann. N. Y. Acad. Sci.*, 2005, **1043**, 97–103.

42 G. E. Means and R. E. Feeney, *Bioconjug. Chem.*, 1990, **1**, 2–12.

43 M. T. Kim, Y. Chen, J. Marhoul and F. Jacobson, *Bioconjug. Chem.*, 2014, **25**, 1223–1232.

44 V. Chudasama, A. Maruani and S. Caddick, *Nat. Chem.*, 2016, **8**, 114–119.

45 N. C. Yoder, C. Bai, D. Tavares, W. C. Widdison, K. R. Whiteman, A. Wilhelm, S. D. Wilhelm, M. A. McShea, E. K. Maloney, O. Ab, L. Wang, S. Jin, H. K. Erickson, T. A.

Keating and J. M. Lambert, *Mol. Pharm.*, 2019, **16**, 3926–3937.

46 M. T. Petersen, P. H. Jonson and S. B. Petersen, *Protein Eng.*, 1999, **12**, 535–548.

47 R. Bhattacharya, D. Pal and P. Chakrabarti, *Protein Eng. Des. Sel.*, 2004, **17**, 795–808.

48 A. Denicolaseoane and B. M. Anderson, *J. Biol. Chem.*, 1990, **265**, 3691–3696.

49 M. Esmann, P. C. Sar, K. Hideg and D. Marsh, *Anal. Biochem.*, 1993, **213**, 336–348.

50 M. M. C. Sun, K. S. Beam, C. G. Cerveny, K. J. Hamblett, R. S. Blackmore, M. Y. Torgov, F. G. M. Handley, N. C. Ihle, P. D. Senter and S. C. Alley, *Bioconjug. Chem.*, 2005, **16**, 1282–1290.

51 C. S. Sevier and C. a Kaiser, *Nat. Rev. Mol. Cell Biol.*, 2002, **3**, 836–47.

52 L. Zhang, C. P. Chou and M. Moo-Young, *Biotechnol. Adv.*, 2011, **29**, 923–929.

53 S. Brocchini, A. Godwin, S. Balan, J. Choi, M. Zloh and S. Shaunak, *Adv. Drug Deliv. Rev.*, 2008, **60**, 3–12.

54 J. R. Junutula, S. Bhakta, H. Raab, K. E. Ervin, C. Eigenbrot, R. Vandlen, R. H. Scheller and H. B. Lowman, *J. Immunol. Methods*, 2008, **332**, 41–52.

55 E. Y. Chi, S. Krishnan, T. W. Randolph and J. F. Carpenter, *Pharm. Res.*, 2003, **20**, 1325–1336.

56 J. M. Chalker, G. J. L. Bernardes, Y. A. Lin and B. G. Davis, *Chem. - An Asian J.*, 2009, **4**, 630–640.

57 M. B. Francis and I. S. Carrico, *Curr. Opin. Chem. Biol.*, 2010, **14**, 771–773.

58 H. Chen, R. Huang, Z. Li, W. Zhu, J. Chen, Y. Zhan and B. Jiang, *Org. Biomol. Chem.*, 2017, **15**, 7339–7345.

59 P. M. S. D. Cal, J. B. Vicente, E. Pires, A. V. Coelho, L. F. Veiros, C. Cordeiro and P. M. P. Gois, *J. Am. Chem. Soc.*, 2012, **134**, 10299–10305.

60 J. Tuls, L. Geren and F. Millett, *J. Biol. Chem.*, 1989, **264**, 16421–16425.

61 I. Dovgan, S. Ursuegui, S. Erb, C. Michel, S. Kolodych, S. Cianférani and A. Wagner, *Bioconjug. Chem.*, 2017, **28**, 1452–1457.

62 M. J. Matos, B. L. Oliveira, N. Martínez-Sáez, A. Guerreiro, P. M. S. D. Cal, J. Bertoldo, M. Maneiro, E. Perkins, J. Howard, M. J. Deery, J. M. Chalker, F. Corzana, G. Jiménez-Osés and G. J. L. Bernardes, *J. Am. Chem. Soc.*, 2018, **140**, 4004–4017.

63 S. G. Tajc, B. S. Tolbert, R. Basavappa and B. L. Miller, *J. Am. Chem. Soc.*, 2004, **126**, 10508–10509.

64 J. M. Chalker, L. Lercher, N. R. Rose, C. J. Schofield and B. G. Davis, *Angew. Chemie - Int. Ed.*, 2012, **51**, 1835–1839.

65 T. P. Kogan, *Synth. Commun.*, 1992, **22**, 2417–2424.

66 J. Messens and J.-F. Collet, *Antioxid. Redox Signal.*, 2013, **18**, 1594–1596.

67 S. Ariyasu, H. Hayashi, B. Xing and S. Chiba, *Bioconjug. Chem.*, 2017, **28**, 897–902.

68 P. A. Jackson, J. C. Widen, D. A. Harki and K. M. Brummond, *J. Med. Chem.*, 2017, **60**, 839–885.

69 M. E. B. Smith, M. B. Caspersen, E. Robinson, M. Morais, A. Maruani, J. P. M. Nunes, K. Nicholls, M. J. Saxton, S. Caddick, J. R. Baker and V. Chudasama, *Org. Biomol. Chem.*, 2015, **13**, 7946–7949.

70 P. A. Szijj, C. Bahou and V. Chudasama, *Drug Discov. Today Technol.*, 2018, **30**, 27–34.

71 V. Chudasama, M. E. B. Smith, F. F. Schumacher, D. Papaioannou, G. Waksman, J. R. Baker and S. Caddick, *Chem. Commun.*, 2011, **47**, 8781.

72 A. Wall, K. Nicholls, M. B. Caspersen, S. Skrivergaard, K. A. Howard, K. Karu, V. Chudasama and J. R. Baker, *Org. Biomol. Chem.*, 2019, **17**, 7870–7873.

73 A. Maruani, S. Alom, P. Canavelli, M. T. W. Lee, R. E. Morgan, V. Chudasama and S. Caddick, *Chem. Commun.*, 2015, **51**, 5279–5282.

74 A. Maruani, M. E. B. Smith, E. Miranda, K. A. Chester, V. Chudasama and S. Caddick,

Nat. Commun., 2015, **6**, 6645.

75 S. L. Kuan, T. Wang and T. Weil, *Chem. Eur. J.*, 2016, **22**, 17112–17129.

76 M. E. B. Smith, F. F. Schumacher, C. P. Ryan, L. M. Tedaldi, D. Papaioannou, G. Waksman, S. Caddick and J. R. Baker, *J. Am. Chem. Soc.*, 2010, **132**, 1960–1965.

77 S. J. Walsh, S. Omarjee, W. R. J. D. Galloway, T. T. L. Kwan, H. F. Sore, J. S. Parker, M. Hyvonen, J. S. Carrol and D. R. Spring, *Chem. Sci.*, 2019, **10**, 694–700.

78 P. Wilson, A. Anastasaki, M. R. Owen, K. Kempe, D. M. Haddleton, S. K. Mann, A. P. R. Johnston, J. F. Quinn, M. R. Whittaker, P. J. Hogg and T. P. Davis, *J. Am. Chem. Soc.*, 2015, **137**, 4215–4222.

79 N. Griebenow, A. M. Dilmaç, S. Greven and S. Bräse, *Bioconjug. Chem.*, 2016, **27**, 911–917.

80 M. Morais, J. P. M. M. Nunes, K. Karu, N. Forte, I. Benni, M. E. B. B. Smith, S. Caddick, V. Chudasama and J. R. Baker, *Org. Biomol. Chem.*, 2017, **15**, 2947–2952.

81 H. C. Kolb, M. G. Finn and K. B. Sharpless, *Angew. Chemie Int. Ed.*, 2001, **40**, 2004–2021.

82 A. E. Speers and B. F. Cravatt, *Chem. Biol.*, 2004, **11**, 535–546.

83 K. E. Beatty, F. Xie, Q. Wang and D. A. Tirrell, *J. Am. Chem. Soc.*, 2005, **127**, 14150–14151.

84 S. I. Presolski, V. P. Hong and M. G. Finn, *Curr. Protoc. Chem. Biol.*, 2011, **3**, 153–162.

85 V. Hong, S. I. Presolski, C. Ma and M. â. G. Finn, *Angew. Chemie Int. Ed.*, 2009, **48**, 9879–9883.

86 N. J. Agard, J. A. Prescher and C. R. Bertozzi, *J. Am. Chem. Soc.*, 2004, **126**, 15046–15047.

87 X. Ning, J. Guo, M. A. Wolfert and G.-J. Boons, *Angew. Chemie Int. Ed.*, 2008, **47**, 2253–2255.

88 J. Dommerholt, O. van Rooijen, A. Borrmann, C. F. Guerra, F. M. Bickelhaupt and F. L. van Delft, *Nat. Commun.*, 2014, **5**, 5378.

89 D. M. Ecker, S. D. Jones and H. L. Levine, *MAbs*, 2015, **7**, 9–14.

90 G. Vidarsson, G. Dekkers and T. Rispens, *Front. Immunol.*, 2014, **5**, 1–17.

91 D. Cameron, M. J. Piccart-Gebhart, R. D. Gelber, M. Procter, A. Goldhirsch, E. de Azambuja, G. Castro, M. Untch, I. Smith, L. Gianni, J. Baselga, N. Al-Sakaff, S. Lauer, E. McFadden, B. Leyland-Jones, R. Bell, M. Dowsett and C. Jackisch, *Lancet*, 2017, **389**, 1195–1205.

92 H. W. Schroeder and L. Cavacini, *J. Allergy Clin. Immunol.*, 2010, **125**, S41–S52.

93 B. J. Underdown and J. M. Schiff, *Annu. Rev. Immunol.*, 1986, **4**, 389–417.

94 K. Chen, W. Xu, M. Wilson, B. He, N. W. Miller, E. Bengtén, E.-S. Edholm, P. A. Santini, P. Rath, A. Chiu, M. Cattalini, J. Litzman, J. B Bussel, B. Huang, A. Meini, K. Riesbeck, C. Cunningham-Rundles, A. Plebani and A. Cerutti, *Nat. Immunol.*, 2009, **10**, 889–898.

95 H. Turner and J.-P. Kinet, *Nature*, 1999, **402**, 24–30..

96 R. Geisberger, M. Lamers and G. Achatz, *Immunology*, 2006, **118**, 429–437

97 M. L. Chiu, D. R. Goulet, A. Teplyakov and G. L. Gilliland, *Antibodies*, 2019, **8**, 55.

98 E. Maverakis, K. Kim, M. Shimoda, M. E. Gershwin, F. Patel, R. Wilken, S. Raychaudhuri, L. R. Ruhaak and C. B. Lebrilla, *J. Autoimmun.*, 2015, **57**, 1–13.

99 T. Li, D. J. DiLillo, S. Bournazos, J. P. Giddens, J. V. Ravetch and L.-X. Wang, *Proc. Natl. Acad. Sci.*, 2017, **114**, 3485–3490.

100 D. N. Forthal, *Antibodies for Infectious Diseases*, American Society of Microbiology, 2015, 25–48.

101 P. Holliger and P. J. Hudson, *Nat. Biotechnol.*, 2005, **23**, 1126–1136.

102 A. L. Nelson and J. M. Reichert, *Nat. Biotechnol.*, 2009, **27**, 331–337.

103 R. K. Jain, *Cancer Res.*, 1990, **50**, 814–819.

104 T. Yokota, D. E. Milenic, M. Whitlow and J. Schlom, *Cancer Res.*, 1992, **52**, 3402–3408.

105 A. L. Nelson, *Landes Biosci.*, 2010, **2**, 77–83.

106 A. J. Cumber, E. S. Ward, G. Winter, G. D. Parnell and E. J. Wawrzynczak, *J. Immunol.*, 1992, **149**, 120–126.

107 L. J. Holt, A. Basran, K. Jones, J. Chorlton, L. S. Jespers, N. D. Brewis and I. M. Tomlinson, *Protein Eng. Des. Sel.*, 2008, **21**, 283–288.

108 J. Milton Harris and R. B. Chess, *Nat. Rev. Drug Discov.*, 2003, **2**, 214–221.

109 A. Jain and S. K. Jain, *Crit. Rev. Ther. Drug Carrier Syst.*, 2008, **25**, 403–47.

110 C. Hamers-Casterman, T. Atarhouch, S. Muyldermans, G. Robinson, C. Hammers, E. B. Songa, N. Bendahman and R. Hammers, *Nature*, 1993, **363**, 446–448.

111 E. Dolk, C. van Vliet, J. M. J. Perez, G. Vriend, H. Darbon, G. Ferrat, C. Cambillau, L. G. J. Frenken and T. Verrips, *Proteins Struct. Funct. Bioinforma.*, 2005, **59**, 555–564.

112 M. M. Harmsen and H. J. De Haard, *Appl. Microbiol. Biotechnol.*, 2007, **77**, 13–22.

113 M. Dumoulin, K. Conrath, A. Van Meirhaeghe, F. Meersman, K. Heremans, L. G. J. Frenken, S. Muyldermans, L. Wyns and A. Matagne, *Protein Sci.*, 2009, **11**, 500–515.

114 S. Oliveira, R. Heukers, J. Sornkom, R. J. Kok and P. M. P. Van Bergen En Henegouwen, *J. Control. Release*, 2013, **172**, 607–617.

115 U. Rothbauer, K. Zolghadr, S. Tillib, D. Nowak, L. Schermelleh, A. Gahl, N. Backmann, K. Conrath, S. Muyldermans, M. C. Cardoso and H. Leonhardt, *Nat. Methods*, 2006, **3**, 887–889.

116 G. Caljon, V. Caveliers, T. Lahoutte, B. Stijlemans, G. H. Ghassabeh, J. Van Den Abbeele, I. Smolders, P. De Baetselier, Y. Michotte, S. Muyldermans, S. Magez and R. Clinckers, *Br. J. Pharmacol.*, 2012, **165**, 2341–2353.

117 J. J. Gemmete and S. K. Mukherji, *Am. J. Neuroradiol.*, 2011, **32**, 1373–1374.

118 N. Diamantis and U. Banerji, *Br. J. Cancer*, 2016, **114**, 362–367.

119 H. Yao, F. Jiang, A. Lu and G. Zhang, *Int. J. Mol. Sci.*, 2016, **17**, 194.

120 S. O. Doronina, B. E. Toki, M. Y. Torgov, B. a Mendelsohn, C. G. Cerveny, D. F. Chace, R. L. DeBlanc, R. P. Gearing, T. D. Bovee, C. B. Siegall, J. a Francisco, A. F. Wahl, D. L. Meyer and P. D. Senter, *Nat. Biotech.*, 2003, **21**, 778–784.

121 P. R. Hamann, L. M. Hinman, I. Hollander, C. F. Beyer, D. Lindh, R. Holcomb, W. Hallett, H.-R. Tsou, J. Upeslacis, D. Shochat, A. Mountain, D. A. Flowers and I. Bernstein, *Bioconjug. Chem.*, 2002, **13**, 47–58.

122 Q. Jiang, B. Patel, X. Jin, D. Di Grandi, E. Bortell, B. Czapkowski, T. F. Lerch, D. Meyer, S. Patel, J. Pegg, A. Arbuckle, J. Lagliva, V. Sriskanda, L. Letendre, H. Li, E. Thomas and D. Nadkarni, *ACS Omega*, 2019, **4**, 6468–6475.

123 J. Katz, J. E. Janik and A. Younes, *Clin. Cancer Res.*, 2011, **17**, 6428–6436.

124 G. D. Lewis Phillips, G. Li, D. L. Dugger, L. M. Crocker, K. L. Parsons, E. Mai, W. A. Blattler, J. M. Lambert, R. V. J. Chari, R. J. Lutz, W. L. T. Wong, F. S. Jacobson, H. Koeppen, R. H. Schwall, S. R. Kenkare-Mitra, S. D. Spencer and M. X. Sliwkowski, *Cancer Res.*, 2008, **68**, 9280–9290.

125 Y. N. Lamb, *Drugs*, 2017, **77**, 1603–1610.

126 E. Bourbon and G. Salles, *Expert Opin. Investig. Drugs*, 2020, **29**, 1079–1088.

127 P. M. Challita-Eid, D. Satpayev, P. Yang, Z. An, K. Morrison, Y. Shostak, A. Raitano, R. Nadell, W. Liu, D. R. Lortie, L. Capo, A. Verlinsky, M. Leavitt, F. Malik, H. Avina, C. I. Guevara, N. Dinh, S. Karki, B. S. Anand, D. S. Pereira, I. B. J. Joseph, F. Donate, K. Morrison and D. R. Stover, *Cancer Res.*, 2016, **76**, 3003–3013.

128 Y. Ogitani, T. Aida, K. Hagihara, J. Yamaguchi, C. Ishii, N. Harada, M. Soma, H. Okamoto, M. Oitate, S. Arakawa, T. Hirai, R. Atsumi, T. Nakada, I. Hayakawa, Y. Abe and T. Agatsuma, *Clin. Cancer Res.*, 2016, **22**, 5097–5108.

129 D. M. Goldenberg, T. M. Cardillo, S. V. Govindan, E. A. Rossi and R. M. Sharkey, *Oncotarget*, 2015, **6**, 22496–22512.

130 S. K. Wootton and D. Yoo, *J. Virol.*, 2003, **77**, 4546–4557.

131 J. R. Junutula, H. Raab, S. Clark, S. Bhakta, D. D. Leipold, S. Weir, Y. Chen, M. Simpson, S. P. Tsai, M. S. Dennis, Y. Lu, Y. G. Meng, C. Ng, J. Yang, C. C. Lee, E. Duenas, J. Gorrell, V. Katta, A. Kim, K. McDorman, K. Flagella, R. Venook, S. Ross, S. D. Spencer, W. Lee Wong, H. B. Lowman, R. Vandlen, M. X. Sliwkowski, R. H. Scheller, P. Polakis and W. Mallet, *Nat. Biotechnol.*, 2008, **26**, 925–932.

132 J. Y. Axup, K. M. Bajjuri, M. Ritland, B. M. Hutchins, C. H. Kim, S. A. Kazane, R. Halder, J. S. Forsyth, A. F. Santidrian, K. Stafin, Y. Lu, H. Tran, A. J. Seller, S. L. Biroc, A. Szydlik, J. K. Pinkstaff, F. Tian, S. C. Sinha, B. Felding-Habermann, V. V. Smider and P. G. Schultz, *Proc. Natl. Acad. Sci.*, 2012, **109**, 16101–16106.

133 E. S. Zimmerman, T. H. Heibeck, A. Gill, X. Li, C. J. Murray, M. R. Madlansacay, C. Tran, N. T. Uter, G. Yin, P. J. Rivers, A. Y. Yam, W. D. Wang, A. R. Steiner, S. U. Bajad, K. Penta, W. Yang, T. J. Hallam, C. D. Thanos and A. K. Sato, *Bioconjug. Chem.*, 2014, **25**, 351–361.

134 M. Mann and O. N. Jensen, *Nat. Biotechnol.*, 2003, **21**, 255–261.

135 P. R. Hamann, L. M. Hinman, C. F. Beyer, L. M. Greenberger, C. Lin, D. Lindh, A. T. Menendez, R. Wallace, F. E. Durr and J. Upeslacis, *Bioconjug. Chem.*, 2005, **16**, 346–353.

136 W. Wang, J. Vlasak, Y. Li, P. Pristatsky, Y. Fang, T. Pittman, J. Roman, Y. Wang, T. Prueksaritanont and R. Ionescu, *Mol. Immunol.*, 2011, **48**, 860–866.

137 Q. Zhou, J. E. Stefano, C. Manning, J. Kyazike, B. Chen, D. A. Gianolio, A. Park, M. Busch, J. Bird, X. Zheng, H. Simonds-Mannes, J. Kim, R. C. Gregory, R. J. Miller, W. H. Brondyk, P. K. Dhal and C. Q. Pan, *Bioconjug. Chem.*, 2014, **25**, 510–520.

138 A. M. Sochaj, K. W. Świderska and J. Otlewski, *Biotechnol. Adv.*, 2015, **33**, 775–784.

139 T. Kanaji, H. Ozaki, T. Takao, H. Kawajiri, H. Ide, M. Motoki and Y. Shimonishi, *J. Biol. Chem.*, 1993, **268**, 11565–11572.

140 T. Kashiwagi, K. Yokoyama, K. Ishikawa, K. Ono, D. Ejima, H. Matsui and E. Suzuki, *J. Biol. Chem.*, 2002, **277**, 44252–44260.

141 S. Jeger, K. Zimmermann, A. Blanc, J. Grünberg, M. Honer, P. Hunziker, H. Struthers and R. Schibli, *Angew. Chemie Int. Ed.*, 2010, **49**, 9995–9997.

142 P. Wu, W. Shui, B. L. Carlson, N. Hu, D. Rabuka, J. Lee and C. R. Bertozzi, *Proc. Natl. Acad. Sci.*, 2009, **106**, 3000–3005.

143 P. M. Drake, A. E. Albers, J. Baker, S. Banas, R. M. Barfield, A. S. Bhat, G. W. de Hart, A. W. Garofalo, P. Holder, L. C. Jones, R. Kudirka, J. McFarland, W. Zmolek and D. Rabuka, *Bioconjug. Chem.*, 2014, **25**, 1331–1341.

144 D. Rabuka, J. S. Rush, G. W. DeHart, P. Wu and C. R. Bertozzi, *Nat. Protoc.*, 2012, **7**, 1052–1067.

145 G. Badescu, P. Bryant, M. Bird, K. Henseleit, J. Swierkosz, V. Parekh, R. Tommasi, E. Pawlisz, K. Jurlewicz, M. Farys, N. Camper, X. Sheng, M. Fisher, R. Grygorash, A. Kyle, A. Abhilash, M. Frigerio, J. Edwards and A. Godwin, *Bioconjug. Chem.*, 2014, **25**, 1124–1136.

146 F. F. Schumacher, J. P. M. Nunes, A. Maruani, V. Chudasama, M. E. B. Smith, K. A. Chester, J. R. Baker and S. Caddick, *Org. Biomol. Chem.*, 2014, **12**, 7261–7269.

147 F. F. Schumacher, V. A. Sanchania, B. Tolner, Z. V. F. Wright, C. P. Ryan, M. E. B. Smith, J. M. Ward, S. Caddick, C. W. M. Kay, G. Aeppli, K. A. Chester and J. R. Baker, *Sci. Rep.*, 2013, **3**, 1525–1534.

148 J. P. M. Nunes, M. Morais, V. Vassileva, E. Robinson, V. S. Rajkumar, M. E. B. Smith, R. B. Pedley, S. Caddick, J. R. Baker and V. Chudasama, *Chem. Commun.*, 2015, **51**, 10624–10627.

149 E. A. Hull, M. Livanos, E. Miranda, M. E. B. Smith, K. A. Chester and J. R. Baker,

Bioconjug. Chem., 2014, **25**, 1395–1401.

150 C. Marculescu, H. Kossen, R. E. Morgan, P. Mayer, S. A. Fletcher, B. Tolner, K. A. Chester, L. H. Jones and J. R. Baker, *Chem. Commun.*, 2014, **50**, 7139–7142.

151 S. A. Fletcher, P. K. B. Sin, M. Nobles, E. Årstad, A. Tinker and J. R. Baker, *Org. Biomol. Chem.*, 2015, **13**, 9559–9563.

152 E. Robinson, J. P. M. Nunes, V. Vassileva, A. Maruani, J. C. F. Nogueira, M. E. B. Smith, R. B. Pedley, S. Caddick, J. R. Baker and V. Chudasama, *RSC Adv.*, 2017, **7**, 9073–9077.

153 M. T. W. Lee, A. Maruani, J. R. Baker, S. Caddick and V. Chudasama, *Chem. Sci.*, 2016, **7**, 799–802.

154 M. T. W. Lee, A. Maruani, D. A. Richards, J. R. Baker, S. Caddick and V. Chudasama, *Chem. Sci.*, 2017, **8**, 2056–2060.

155 N. Forte, I. Benni, K. Karu, V. Chudasama and J. R. Baker, *Chem. Sci.*, 2019, **10**, 10919–10924.

156 L. Castañeda, Z. V. F. Wright, C. Marculescu, T. M. Tran, V. Chudasama, A. Maruani, E. A. Hull, J. P. M. Nunes, R. J. Fitzmaurice, M. E. B. Smith, L. H. Jones, S. Caddick and J. R. Baker, *Tetrahedron Lett.*, 2013, **54**, 3493–3495.

157 A. Maruani, H. Savoie, F. Bryden, S. Caddick, R. Boyle and V. Chudasama, *Chem. Commun.*, 2015, **51**, 15304–15307.

158 M. K. Greene, D. A. Richards, J. C. F. Nogueira, K. Campbell, P. Smyth, M. Fernández, C. J. Scott and V. Chudasama, *Chem. Sci.*, 2018, **9**, 79–87.

159 E. R. Lacy, M. Baker and M. Brigham-Burke, *Anal. Biochem.*, 2008, **382**, 66–68.

160 S. D. Gillies and J. S. Wesolowski, *Hum. Antibodies*, 1990, **1**, 47–54.

161 P. M. Hogarth, *Immunol. Rev.*, 2015, **268**, 1–5.

162 T. T. Kuo, K. Baker, M. Yoshida, S. W. Qiao, V. G. Aveson, W. I. Lencer and R. S. Blumberg, *J. Clin. Immunol.*, 2010, **30**, 777–789.

163 S. Nagarajan, K. Venkiteswaran, M. Anderson, U. Sayed, C. Zhu and P. Selvaraj, *Blood*, 2000, **95**, 1069–77.

164 P. M. LoRusso, D. Weiss, E. Guardino, S. Girish and M. X. Sliwkowski, *Clin. Cancer Res.*, 2011, **17**, 6437–6447.

165 S. J. Keam, *Drugs*, 2020, **80**, 501–508.

166 B. Petricevic, J. Laengle, J. Singer, M. Sachet, J. Fazekas, G. Steger, R. Bartsch, E. Jensen-Jarolim and M. Bergmann, *J. Transl. Med.*, 2013, **11**, 307.

167 S. M. Ansell, *Blood*, 2014, **124**, 3197–3200.

168 L. H. Sehn, A. F. Herrera, C. R. Flowers, M. K. Kamdar, A. McMillan, M. Hertzberg, S. Assouline, T. M. Kim, W. S. Kim, M. Ozcan, J. Hirata, E. Penuel, J. N. Paulson, J. Cheng, G. Ku and M. J. Matasar, *J. Clin. Oncol.*, 2020, **38**, 155–165.

169 C. Bahou, D. A. Richards, A. Maruani, E. A. Love, F. Javaid, S. Caddick, J. R. Baker and V. Chudasama, *Org. Biomol. Chem.*, 2018, **16**, 1359–1366.

170 R. L. Rich and D. G. Myszka, *Anal. Biochem.*, 2007, **361**, 1–6.

171 P. Dakshinamurthy, P. Mukunda, B. Prasad Kodaganti, B. R. Shenoy, B. Natarajan, A. Maliwalave, V. Halan, S. Murugesan and S. Maity, *Biologicals*, 2017, **46**, 46–56.

172 J. B. Stavenhagen, S. Gorlatov, N. Tuaillon, C. T. Rankin, H. Li, S. Burke, L. Huang, S. Johnson, E. Bonvini and S. Koenig, *Cancer Res.*, 2007, **67**, 8882–8890.

173 M.-C. Lo, A. Aulabaugh, G. Jin, R. Cowling, J. Bard, M. Malamas and G. Ellestad, *Anal. Biochem.*, 2004, **332**, 153–159.

174 E. A. Hoyt, P. M. S. D. S. D. Cal, B. L. Oliveira and G. J. L. L. Bernardes, *Nat. Rev. Chem.*, 2019, **3**, 147–171.

175 C. R. Behrens, E. H. Ha, L. L. Chinn, S. Bowers, G. Probst, M. Fitch-Bruhns, J. Monteon, A. Valdiosera, A. Bermudez, S. Liao-Chan, T. Wong, J. Melnick, J.-W. Theunissen, M. R. Flory, D. Houser, K. Venstrom, Z. Levashova, P. Sauer, T.-S. Migone, E. H. van der

Horst, R. L. Halcomb and D. Y. Jackson, *Mol. Pharm.*, 2015, **12**, 3986–3998.

176 D. Banerjee, A. P. Liu, N. R. Voss, S. L. Schmid and M. G. Finn, *ChemBioChem*, 2010, **11**, 1273–1279.

177 N. Stephanopoulos, G. J. Tong, S. C. Hsiao and M. B. Francis, *ACS Nano*, 2010, **4**, 6014–6020.

178 I. K. Oh, H. Mok and T. G. Park, *Bioconjug. Chem.*, 2006, **17**, 721–727.

179 J. C. F. Nogueira, M. K. Greene, D. A. Richards, A. O. Furby, J. Steven, A. Porter, C. Barelle, C. J. Scott and V. Chudasama, *Chem. Commun.*, 2019, **55**, 7671–7674.

180 S. Massa, C. Xavier, J. De Vos, V. Caveliers, T. Lahoutte, S. Muyldermans and N. Devoogdt, *Bioconjug. Chem.*, 2014, **25**, 979–988.

181 S. B. Nielsen, A. Lapierre, J. U. Andersen, U. V. Pedersen, S. Tomita and L. H. Andersen, *Phys. Rev. Lett.*, 2001, **87**, 228102.

182 B. Kallies and R. Mitzner, *J. Phys. Chem. B*, 1997, **101**, 2959–2967.

183 A. Wall, A. G. Wills, N. Forte, C. Bahou, L. Bonin, K. Nicholls, M. T. Ma, V. Chudasama and J. R. Baker, *Chem. Sci.*, 2020, Advanced Article

184 L. Yang, J. Zheng, Z. Zou, H. Cai, P. Qi, Z. Qing, Q. Yan, L. Qiu, W. Tan and R. Yang, *Chem. Commun.*, 2020, **56**, 1843–1846.

185 F. Kratz, A. Warnecke, K. Scheuermann, C. Stockmar, J. Schwab, P. Lazar, P. Drückes, N. Esser, J. Drevs, D. Rognan, C. Bissantz, C. Hinderling, G. Folkers, I. Fichtner and C. Unger, *J. Med. Chem.*, 2002, **45**, 5523–5533.

186 S. Santra, C. Kaittanis, O. J. Santiesteban and J. M. Perez, *J. Am. Chem. Soc.*, 2011, **133**, 16680–16688.

187 J. Zalevsky, A. K. Chamberlain, H. M. Horton, S. Karki, I. W. L. Leung, T. J. Sproule, G. A. Lazar, D. C. Roopenian and J. R. Desjarlais, *Nat. Biotechnol.*, 2010, **28**, 157–159.

188 Y.-B. Hu, E. B. Dammer, R.-J. Ren and G. Wang, *Transl. Neurodegener.*, 2015, **4**, 18.

189 W. Chen, D. Wang, C. Dai, D. Hamelberg and B. Wang, *Chem. Commun.*, 2012, **48**, 1736–1738.

190 A. D. Baldwin and K. L. Kiick, *Bioconjug. Chem.*, 2011, **22**, 1946–1953.

191 H. Wu, P. J. Levalley, T. Luo, A. M. Kloxin and K. L. Kiick, *Bioconjug. Chem.*, 2018, **29**, 3595–3605.

192 I. M. Serafimova, M. A. Pufall, S. Krishnan, K. Duda, M. S. Cohen, R. L. Maglathlin, J. M. McFarland, R. M. Miller, M. Frödin and J. Taunton, *Nat. Chem. Biol.*, 2012, **8**, 471–476.

193 A. D. Baldwin and K. L. Kiick, *Bioconjug. Chem.*, 2011, **22**, 1946–1953.

194 S. Krishnan, R. M. Miller, B. Tian, R. D. Mullins, M. P. Jacobson and J. Taunton, *J. Am. Chem. Soc.*, 2014, **136**, 12624–12630.

195 J. M. J. M. J. M. Ravasco, H. Faustino, A. Trindade and P. M. P. P. Gois, *Chem. – A Eur. J.*, 2019, **25**, 43–59.

196 C. M. B. Holloway, D. A. Scollard, C. B. Caldwell, L. Ehrlich, H. J. Kahn and R. M. Reilly, *Nucl. Med. Biol.*, 2013, **40**, 630–637.

197 L. J. Chan, D. B. Ascher, R. Yadav, J. B. Bulitta, C. C. Williams, C. J. H. Porter, C. B. Landersdorfer and L. M. Kaminskas, *Mol. Pharm.*, 2016, **13**, 1229–1241.

198 L. Y. Kwon, D. A. Scollard and R. M. Reilly, *Mol. Pharm.*, 2017, **14**, 492–501.

199 S. Matsui and H. Aida, *J. Chem. Soc. Perkin Trans. 2*, 1978, 1277-1280.

200 B.-Q. Q. Shen, K. Xu, L. Liu, H. Raab, S. Bhakta, M. Kenrick, K. L. Parsons-Reponte, J. Tien, S.-F. F. Yu, E. Mai, D. Li, J. Tibbitts, J. Baudys, O. M. Saad, S. J. Scales, P. J. McDonald, P. E. Hass, C. Eigenbrot, T. Nguyen, W. A. Solis, R. N. Fuji, K. M. Flagella, D. Patel, S. D. Spencer, L. A. Khawli, A. Ebens, W. L. Wong, R. Vandlen, S. Kaur, M. X. Sliwkowski, R. H. Scheller, P. Polakis and J. R. Junutula, *Nat. Biotechnol.*, 2012, **30**, 184–189.

201 G. Hao, Z. P. Xu and L. Li, *RSC Adv.*, 2018, **8**, 22182–22192.

202 J. C. Slootweg, S. Van Der Wal, H. C. Quarles Van Ufford, E. Breukink, R. M. J. Liskamp and D. T. S. Rijkers, *Bioconjug. Chem.*, 2013, **24**, 2058–2066.

203 B. Kemper, M. von Gröning, V. Lewe, D. Spitzer, T. Otremba, N. Stergiou, D. Schollmeyer, E. Schmitt, B. J. Ravoo and P. Besenius, *Chem. - A Eur. J.*, 2017, **23**, 6048–6055.

204 K. Blomberg, C. Granberg, I. Hemmilä and T. Lövgren, *J. Immunol. Methods*, 1986, **86**, 225–229.

205 K. Lang, L. Davis, S. Wallace, M. Mahesh, D. J. Cox, M. L. Blackman, J. M. Fox and J. W. Chin, *J. Am. Chem. Soc.*, 2012, **134**, 10317–10320.

206 J. Hernández-Gil, M. Braga, B. I. Harriss, L. S. Carroll, C. H. Leow, M.-X. Tang, E. O. Aboagye and N. J. Long, *Chem. Sci.*, 2019, **10**, 5603–5615.

207 L. K. Rasmussen, *J. Org. Chem.*, 2006, **71**, 3627–3629.

208 K. Zhang, J. Liu, S. Ohashi, X. Liu, Z. Han and H. Ishida, *J. Polym. Sci. Part A Polym. Chem.*, 2015, **53**, 1330–1338.

209 K. M. Bonger, R. J. B. H. N. van den Berg, L. H. Heitman, A. P. IJzerman, J. Oosterom, C. M. Timmers, H. S. Overkleeft and G. A. van der Marel, *Bioorg. Med. Chem.*, 2007, **15**, 4841–4856.

210 X. Yue, Y. Feng and Y. B. Yu, *J. Fluor. Chem.*, 2013, **152**, 173–181.

211 P. Moody, M. E. B. Smith, C. P. Ryan, V. Chudasama, J. R. Baker, J. Molloy and S. Caddick, *ChemBioChem*, 2012, **13**, 39–41.